Contents

10.0 Hazard Calculations and Results 10.1
10.1 Hazard Software and Hazard Runs 10.1
10.1.1 Hazard Calculations and Quality Assurance of Hazard Calculations 10.5
10.2 Seismic Hazard Results and Sensitivity at Priority Sites 10.5
10.2.1 200-East Area (Site A) 10.6
10.2.2 Columbia Generating Station (Site C) 10.11
10.2.3 200-West Area (Site B) 10.15
10.2.4 100BC Area (Site D) 10.16
10.2.5 300 Area (Site E) 10.17
10.3 Comparison Between Sites 10.17
10.4 Comparison of UHRS with Response Spectra for Representative Earthquake Scenarios 10.18
10.5 Recommendations for Application of Baserock Hazard Results 10.19
10.6 References 10.20

Figures

10.1 Comparison of the mean hazard computed for the YFTB zone using multiple rupture orientations or single rupture orientation and one ground motion model. 10.39

10.2 Maps showing locations of hazard calculation sites relative to the Hanford Site boundary and fault sources 10.40

10.3 Total mean seismic hazard at Site A and percentiles: a) PGA; b) T 0.02-sec; c) T 0.03-sec; d) T 0.04-sec; e) T 0.05-sec; f) T 0.07-sec; g) T 0.10-sec; h) T 0.15-sec; i) T 0.20-sec; j) T 0.30-sec; k) T 0.40-sec; l) T 0.50-sec; m) T 0.75-sec; n) T 1.0-sec; o) T 1.5-sec; p) T 2.0-sec; q) T 3.0-sec; r) T 5.0-sec; s) T 7.5-sec; t) T 10-sec spectral acceleration..... 10.41

10.4 Comparison between the total mean seismic hazard at Site A and the contribution of crustal source zones, faults, the Cascadia interface, and Cascadia intraslab source: a) PGA; b) T 0.02-sec; c) T 0.03-sec; d) T 0.04-sec; e) T 0.05-sec; f) T 0.07-sec; g) T 0.10-sec; h) T 0.15-sec; i) T 0.20-sec; j) T 0.30-sec; k) T 0.40-sec; l) T 0.50-sec; m) T 0.75-sec; n) T 1.0-sec; o) T 1.5-sec; p) T 2.0-sec; q) T 3.0-sec; r) T 5.0-sec; s) T 7.5-sec; t) T 10-sec spectral acceleration. 10.51

10.5 Uniform hazard response spectra at AFEs of 10^{-2}, 10^{-3}, 5×10^{-4}, 4×10^{-4}, 10^{-4}, 5×10^{-5}, 10^{-6}, 10^{-7} for: a) mean hazard; b) 50th percentile hazard; c) 84th percentile hazard..... 10.62

10.6 Deaggregation histogram showing magnitude-distance contributions to the total mean hazard at Site A for peak ground acceleration and AFEs of: a) 10^{-2}; b) 10^{-3}; c) 5×10^{-4}; d) 4×10^{-4}; e) 10^{-4}; f) 10^{-5}; g) 10^{-6}; h) 10^{-7}. 10.64

10.7 Deaggregation histogram showing magnitude-distance contributions to the total mean hazard at Site A for T 0.1-sec spectral acceleration and AFEs of: a) 10^{-2}; b) 10^{-3}; c) 5×10^{-4}; d) 4×10^{-4}; e) 10^{-4}; f) 10^{-5}; g) 10^{-6}; h) 10^{-7}. 10.68

10.8 Deaggregation histogram showing magnitude-distance contributions to the total mean hazard at Site A for T 1.0-sec spectral acceleration and AFEs of: a) 10^{-2}; b) 10^{-3}; c) 5×10^{-4}; d) 4×10^{-4}; e) 10^{-4}; f) 10^{-5}; g) 10^{-6}; h) 10^{-7}. 10.72

10.9 Deaggregation histogram showing magnitude-distance contributions to the total mean hazard at Site A for T 10-sec spectral acceleration and AFEs of: a) 10^{-2}; b) 10^{-3}; c) 5×10^{-4}; d) 4×10^{-4}; e) 10^{-4}; f) 10^{-5}; g) 10^{-6}; h) 10^{-7}. 10.76

10.10 Comparison between the mean hazard curves at Site A obtained for each individual source 10.80

10.11 Comparison between the total mean crustal sources seismic hazard at Site A and the individual contributions at shallow thickness, medium thickness, and deep thickness for T 0.1-sec and T 1.0-sec spectral accelerations 10.82

10.12 Comparison between the total mean CSZ extension seismic hazard at Site A and the individual contributions at shallow thickness, medium thickness, and deep thickness for T 1.0-sec and T 10-sec spectral accelerations. 10.83

10.13 Comparison between the total mean JDF extension seismic hazard at Site A and the individual contributions at 80 km, 90 km, and 100 km for T 1.0-sec and T 10-sec spectral accelerations..... 10.84

10.14 Comparison between the total mean crustal sources seismic hazard at Site A and the individual start time of deformation contributions at 6 Ma for all faults, 6 Ma and 10 Ma, and 10 Ma for all faults for T 0.1-sec and T 1.0-sec spectral accelerations..... 10.85

10.15 Comparison between the total mean crustal sources seismic hazard at Site A and the individual basis for fault dip contributions at maximum polygon width, average polygon width, and 60% of average polygon width for T 0.1-sec and T 1.0-sec spectral accelerations 10.86

10.16 Comparison between the total mean crustal sources seismic hazard at Site A and the five individual temporal model-scale factor contributions for T 0.1-sec and T 1.0-sec spectral accelerations 10.87

10.17 Comparison between alternative catalogs and declustering techniques for the YFTB source zone at Site A: a) for T 0.1-sec; b) for T 1.0-sec spectral accelerations 10.88

10.18 Comparison between alternative smoothing techniques for the YFTB source zone at Site A: a) for T 0.1-sec; b) for T 1.0-sec spectral accelerations 10.89

10.19 Comparison between the total mean Rattlesnake Mountain fault source seismic hazard at Site A and the individual contribution of approach to assessing slip rate via use of structural relief or quaternary data for T 0.1-sec and T 1.0-sec spectral accelerations 10.90

10.20 Sensitivity analysis for the Ahtanum Ridge-Rattlesnake Hills fault at Site A for T 0.1-sec and T 1-sec spectral accelerations 10.91

10.21 Sensitivity analysis for the Toppenish Ridge fault at Site A for T 0.1-sec and T 1-sec spectral accelerations 10.92

10.22 Sensitivity analysis for the RAW fault at Site A for T 0.1-sec and T 1-sec spectral accelerations 10.93

10.23 Comparison between the total mean crustal sources seismic hazard at Site A and the individual contribution from ground motion distribution shape represented by red curve for lognormal model and blue curve for mixture model, for the peak ground acceleration, T 0.1-sec, T 1.0-sec, and T 10-sec spectral accelerations 10.94

10.24 Comparison between the total mean subduction sources seismic hazard at Site A and the individual contribution from ground motion distribution shape represented by red curve for lognormal model and blue curve for mixture model, for the peak ground acceleration, T 0.1-sec, T 1.0-sec, and T 10-sec spectral accelerations 10.95

10.25 Comparison between the total mean crustal sources seismic hazard at Site A and the individual contribution from the seven different Vs-kappa adjustment factors, for the peak ground acceleration, T 0.1-sec, T 1.0-sec, and T 10-sec spectral accelerations 10.96

10.26 Comparison between the total mean crustal sources seismic hazard at Site A and the individual contribution from the nine different inherent uncertainty in backbone adjustments, for the peak ground acceleration, T 0.1-sec, T 1.0-sec, and T 10-sec spectral accelerations 10.97

10.27 Comparison between the total mean subduction sources seismic hazard at Site A and the individual contribution from the four different host-to-target Vs adjustment factors, for the peak ground acceleration, T 0.1-sec, T 1.0-sec, and T 10-sec spectral accelerations 10.98

10.28 Comparison between the total mean subduction sources seismic hazard at Site A and the individual contribution from the three different epistemic uncertainty in median factors for the peak ground acceleration, T 0.1-sec, T 1.0-sec, and T 10-sec spectral accelerations 10.99

10.29 Variance contribution histogram at the 10^{-3}, 10^{-4}, 10^{-5}, 10^{-6}, and 10^{-7} annual frequencies of exceedance for peak ground acceleration and Site A 10.100

10.30 Variance contribution histogram at the 10^{-3}, 10^{-4}, 10^{-5}, 10^{-6}, and 10^{-7} annual frequencies of exceedance for T 0.1-sec spectral acceleration and Site A. 10.101

10.31 Variance contribution histogram at the 10^{-3}, 10^{-4}, 10^{-5}, 10^{-6}, and 10^{-7} annual frequencies of exceedance for T 1.0-sec spectral acceleration and Site A. 10.102

10.32 Variance contribution histogram at the 10^{-3}, 10^{-4}, 10^{-5}, 10^{-6}, and 10^{-7} annual frequencies of exceedance for T 10-sec spectral acceleration and Site A. 10.103

10.33 Tornado plots for Site A and peak ground acceleration at AFEs of: a) 10^{-3}; b) 10^{-4}; c) 10^{-5}; d) 10^{-6}; e) 10^{-7} 10.104

10.34 Tornado plots for Site A and T 0.1-sec spectral acceleration at AFEs of: a) 10^{-3}; b) 10^{-4}; c) 10^{-5}; d) 10^{-6}; e) 10^{-7} 10.107

10.35 Tornado plots for Site A and T 1.0-sec spectral acceleration at AFEs of: a) 10^{-3}; b) 10^{-4}; c) 10^{-5}; d) 10^{-6}; e) 10^{-7} 10.110

10.36 Tornado plots for Site A and T 10-sec spectral acceleration at AFEs of: a) 10^{-3}; b) 10^{-4}; c) 10^{-5}; d) 10^{-6}; e) 10^{-7} 10.113

10.37 Total mean seismic hazard at Site C and percentiles: a) PGA; b) T 0.02-sec; c) T 0.03-sec; d) T 0.04-sec; e) T 0.05-sec; f) T 0.07-sec; g) T 0.10-sec; h) T 0.15-sec; i) T 0.20-sec; j) T 0.30-sec; k) T 0.40-sec; l) T 0.50-sec; m) T 0.75-sec; n) T 1.0-sec; o) T 1.5-sec; p) T 2.0-sec; q) T 3.0-sec; r) T 5.0-sec; s) T 7.5-sec; t) T 10-sec spectral acceleration. 10.116

10.38 Comparison between the total mean seismic hazard at Site C and the contribution of crustal source zones, faults, the Cascadia interface, and Cascadia intraslab source: a) PGA; b) T 0.02-sec; c) T 0.03-sec; d) T 0.04-sec; e) T 0.05-sec; f) T 0.07-sec; g) T 0.10-sec; h) T 0.15-sec; i) T 0.20-sec; j) T 0.30-sec; k) T 0.40-sec; l) T 0.50-sec; m) T 0.75-sec; n) T 1.0-sec; o) T 1.5-sec; p) T 2.0-sec; q) T 3.0-sec; r) T 5.0-sec; s) T 7.5-sec; t) T 10-sec spectral acceleration. 10.126

10.39 Uniform hazard response spectra at AFEs of 10^{-2}, 10^{-3}, 5×10^{-4}, 4×10^{-4}, 10^{-4}, 5×10^{-5}, 10^{-6}, 10^{-7} for: a) mean hazard; b) 50th percentile hazard; c) 84th percentile hazard. 10.136

10.40 Deaggregation histogram showing magnitude-distance contributions to the total mean hazard at Site C for peak ground acceleration and AFEs of: a) 10^{-2}; b) 10^{-3}; c) 5×10^{-4}; d) 4×10^{-4}; e) 10^{-4}; f) 10^{-5}; g) 10^{-6}; h) 10^{-7}. 10.138

10.41 Deaggregation histogram showing magnitude-distance contributions to the total mean hazard at Site C for T 0.1-sec spectral acceleration and AFEs of: a) 10^{-2}; b) 10^{-3}; c) 5×10^{-4}; d) 4×10^{-4}; e) 10^{-4}; f) 10^{-5}; g) 10^{-6}; h) 10^{-7}. 10.142

10.42 Deaggregation histogram showing magnitude-distance contributions to the total mean hazard at Site C for T 1.0-sec spectral acceleration and AFEs of: a) 10^{-2}; b) 10^{-3}; c) 5×10^{-4}; d) 4×10^{-4}; e) 10^{-4}; f) 10^{-5}; g) 10^{-6}; h) 10^{-7}. 10.146

10.43 Deaggregation histogram showing magnitude-distance contributions to the total mean hazard at Site C for T 10-sec spectral acceleration and AFEs of: a) 10^{-2}; b) 10^{-3}; c) 5×10^{-4}; d) 4×10^{-4}; e) 10^{-4}; f) 10^{-5}; g) 10^{-6}; h) 10^{-7}. 10.150

10.44 Comparison between the mean hazard curves at Site C obtained for each individual source: subduction sources are shown by dotted star curves; crustal sources by dotted circle curves; and fault sources by solid curves: a) peak ground acceleration; b) T 0.1-sec; c) T 1-sec; d) T 10-sec spectral acceleration. Acronyms used in figures are listed in Table 10.13. ..... 10.154

10.45 Comparison between the total mean crustal sources seismic hazard at Site C and the individual contributions at shallow thickness, medium thickness, and deep thickness for T 0.1-sec and T 1.0-sec spectral accelerations 10.156

10.46 Comparison between the total mean CSZ extension seismic hazard at Site C and the individual contributions at shallow thickness, medium thickness, and deep thickness for T 1.0-sec and T 10-sec spectral accelerations. 10.156

10.47 Comparison between the total mean JDF extension seismic hazard at Site C and the individual contributions at 80 km, 90 km, and 100 km for T 1.0-sec and T 10-sec spectral accelerations..... 10.157

10.48 Comparison between the total mean crustal sources seismic hazard at Site C and the individual start time of deformation contributions at 6 Ma for all faults, 6 Ma and 10 Ma, and 10 Ma for all faults for T 0.1-sec and T 1.0-sec spectral accelerations..... 10.157

10.49 Comparison between the total mean crustal sources seismic hazard at Site C and the individual basis for fault dip contributions at maximum polygon width, average polygon width, and 60% of average polygon width for T 0.1-sec and T 1.0-sec spectral accelerations..... 10.158

10.50 Comparison between the total mean crustal sources seismic hazard at Site C and the five individual temporal model-scale factor contributions for T 0.1-sec and T 1.0-sec spectral accelerations..... 10.158

10.51 Comparison between alternative catalogs and declustering techniques for the YFTB source zone at Site C: a) for T 0.1-sec; b) for T 1.0-sec spectral accelerations 10.159

10.52 Comparison between alternative smoothing techniques for the YFTB source zone at Site C: a) for T 0.1-sec; b) for T 1.0-sec spectral accelerations 10.159

10.53 Comparison between the total mean Rattlesnake Mountain fault source seismic hazard at Site C and the individual contribution of approach to assessing slip rate via use of structural relief or quaternary data for T 0.1-sec and T 1.0-sec spectral accelerations..... 10.160

10.54 Sensitivity analysis for the Ahtanum Ridge-Rattlesnake Hills fault at Site C for T 0.1-sec and T 1-sec spectral accelerations..... 10.160

10.55 Sensitivity analysis for the Toppenish Ridge fault at Site C for T 0.1-sec and T 1-sec spectral accelerations 10.161

10.56 Sensitivity analysis for the RAW fault at Site C for T 0.1-sec and T 1-sec spectral accelerations..... 10.161

10.57 Comparison between the total mean crustal sources seismic hazard at Site C and the individual contribution from ground motion distribution shape represented by red curve for lognormal model and blue curve for mixture model, for the peak ground acceleration, T 0.1-sec, T 1.0-sec, and T 10-sec spectral accelerations 10.162

10.58 Comparison between the total mean subduction sources seismic hazard at Site C and the individual contribution from ground motion distribution shape represented by red curve for lognormal model and blue curve for mixture model, for the peak ground acceleration, T 0.1-sec, T 1.0-sec, and T 10-sec spectral accelerations 10.162

10.59 Comparison between the total mean crustal sources seismic hazard at Site C and the individual contribution from the seven different Vs-kappa adjustment factors, for the peak ground acceleration, T 0.1-sec, T 1.0-sec, and T 10-sec spectral accelerations..... 10.163

10.60 Comparison between the total mean crustal sources seismic hazard at Site C and the individual contribution from the nine different inherent uncertainty in backbone adjustments, for the peak ground acceleration, T 0.1-sec, T 1.0-sec, and T 10-sec spectral accelerations..... 10.163

10.61 Comparison between the total mean subduction sources seismic hazard at Site C and the individual contribution from the four different host-to-target Vs adjustment factors, for the peak ground acceleration, T 0.1-sec, T 1.0-sec, and T 10-sec spectral accelerations 10.164

10.62 Comparison between the total mean subduction sources seismic hazard at Site C and the individual contribution from the three different epistemic uncertainty in median factors for the peak ground acceleration, T 0.1-sec, T 1.0-sec, and T 10-sec spectral accelerations 10.164

10.63 Variance contribution histogram at the 10^{-3}, 10^{-4}, 10^{-5}, 10^{-6}, and 10^{-7} annual frequencies of exceedance for peak ground acceleration and Site C. 10.165

10.64 Variance contribution histogram at the 10^{-3}, 10^{-4}, 10^{-5}, 10^{-6}, and 10^{-7} annual frequencies of exceedance for T 0.1-sec spectral acceleration and Site C. 10.166

10.65 Variance contribution histogram at the 10^{-3}, 10^{-4}, 10^{-5}, 10^{-6}, and 10^{-7} annual frequencies of exceedance for T 1.0-sec spectral acceleration and Site C. 10.167

10.66 Variance contribution histogram at the 10^{-3}, 10^{-4}, 10^{-5}, 10^{-6}, and 10^{-7} annual frequencies of exceedance for T 10-sec spectral acceleration and Site C. 10.168

10.67 Tornado plots for Site C and peak ground acceleration at AFEs of: a) 10^{-3}; b) 10^{-4}; c) 10^{-5}; d) 10^{-6}; e) 10^{-7} 10.169

10.68 Tornado plots for Site C and T 0.1-sec spectral acceleration at AFEs of: a) 10^{-3}; b) 10^{-4}; c) 10^{-5}; d) 10^{-6}; e) 10^{-7} 10.172

10.69 Tornado plots for Site C and T 1.0-sec spectral acceleration at AFEs of: a) 10^{-3}; b) 10^{-4}; c) 10^{-5}; d) 10^{-6}; e) 10^{-7} 10.175

10.70 Tornado plot for Site C and T 10-sec spectral acceleration at AFEs of: a) 10^{-3}; b) 10^{-4}; c) 10^{-5}; d) 10^{-6}; e) 10^{-7} 10.178

10.71 Total mean seismic hazard at Site B and percentiles: a) PGA; b) T 0.02-sec; c) T 0.03-sec; d) T 0.04-sec; e) T 0.05-sec; f) T 0.07-sec; g) T 0.10-sec; h) T 0.15-sec; i) T 0.20-sec; j) T 0.30-sec; k) T 0.40-sec; l) T 0.50-sec; m) T 0.75-sec; n) T 1.0-sec; o) T 1.5-sec; p) T 2.0-sec; q) T 3.0-sec; r) T 5.0-sec; s) T 7.5-sec; t) T 10-sec spectral acceleration. 10.181

10.72 Comparison between the total mean seismic hazard at Site B and the contribution of crustal source zones, faults, the Cascadia interface, and Cascadia intraslab source: a) PGA; b) T 0.02-sec; c) T 0.03-sec; d) T 0.04-sec; e) T 0.05-sec; f) T 0.07-sec; g) T 0.10-sec; h) T 0.15-sec; i) T 0.20-sec; j) T 0.30-sec; k) T 0.40-sec; l) T 0.50-sec; m) T 0.75-sec; n) T 1.0-sec; o) T 1.5-sec; p) T 2.0-sec; q) T 3.0-sec; r) T 5.0-sec; s) T 7.5-sec; t) T 10-sec spectral acceleration. 10.191

10.73 Uniform hazard response spectra at AFEs of 10^{-2}, 10^{-3}, 5×10^{-4}, 4×10^{-4}, 10^{-4}, 5×10^{-5}, 10^{-6}, 10^{-7} for: a) mean hazard; b) 50th percentile hazard; c) 84th percentile hazard. 10.201

10.74 Comparison between the mean hazard curves at Site B obtained for each individual source 10.203

10.75 Total mean seismic hazard at Site D and percentiles: a) PGA; b) T 0.02-sec; c) T 0.03-sec; d) T 0.04-sec; e) T 0.05-sec; f) T 0.07-sec; g) T 0.10-sec; h) T 0.15-sec; i) T 0.20-sec; j) T 0.30-sec; k) T 0.40-sec; l) T 0.50-sec; m) T 0.75-sec; n) T 1.0-sec; o) T 1.5-sec; p) T 2.0-sec; q) T 3.0-sec; r) T 5.0-sec; s) T 7.5-sec; t) T 10-sec spectral acceleration. 10.205

10.76 Comparison between the total mean seismic hazard at Site D and the contribution of crustal source zones, faults, the Cascadia interface, and Cascadia intraslab source: a) PGA; b) T 0.02-sec; c) T 0.03-sec; d) T 0.04-sec; e) T 0.05-sec; f) T 0.07-sec; g) T 0.10-sec; h) T 0.15-sec; i) T 0.20-sec; j) T 0.30-sec; k) T 0.40-sec; l) T 0.50-sec; m) T 0.75-sec; n) T 1.0-sec; o) T 1.5-sec; p) T 2.0-sec; q) T 3.0-sec; r) T 5.0-sec; s) T 7.5-sec; t) T 10-sec spectral acceleration. 10.215

10.77 Uniform hazard response spectra at AFEs of 10^{-2}, 10^{-3}, 5×10^{-4}, 4×10^{-4}, 10^{-4}, 5×10^{-5}, 10^{-6}, 10^{-7} for: a) mean hazard; b) 50th percentile hazard; c) 84th percentile hazard..... 10.225

10.78 Comparison between the mean hazard curves at Site D obtained for each individual source 10.227

10.79 Total mean seismic hazard at Site E and percentiles: a) PGA; b) T 0.02-sec; c) T 0.03-sec; d) T 0.04-sec; e) T 0.05-sec; f) T 0.07-sec; g) T 0.10-sec; h) T 0.15-sec; i) T 0.20-sec; j) T 0.30-sec; k) T 0.40-sec; l) T 0.50-sec; m) T 0.75-sec; n) T 1.0-sec; o) T 1.5-sec; p) T 2.0-sec; q) T 3.0-sec; r) T 5.0-sec; s) T 7.5-sec; t) T 10-sec spectral acceleration. 10.229

10.80 Comparison between the total mean seismic hazard at Site E and the contribution of crustal source zones, faults, the Cascadia interface, and Cascadia intraslab source: a) PGA; b) T 0.02-sec; c) T 0.03-sec; d) T 0.04-sec; e) T 0.05-sec; f) T 0.07-sec; g) T 0.10-sec; h) T 0.15-sec; i) T 0.20-sec; j) T 0.30-sec; k) T 0.40-sec; l) T 0.50-sec; m) T 0.75-sec; n) T 1.0-sec; o) T 1.5-sec; p) T 2.0-sec; q) T 3.0-sec; r) T 5.0-sec; s) T 7.5-sec; t) T 10-sec spectral acceleration. 10.239

10.81 Uniform hazard response spectra at AFEs of 10^{-2}, 10^{-3}, 5×10^{-4}, 4×10^{-4}, 10^{-4}, 5×10^{-5}, 10^{-6}, 10^{-7} for: a) mean hazard; b) 50th percentile hazard; c) 84th percentile hazard..... 10.249

10.82 Comparison between the mean hazard curves at Site E obtained for each individual source 10.251

10.83 Comparison between the mean UHRS at Sites A, B, C, D, and E: a) 10^{-2} AFE; b) 10^{-4} AFE; c) 10^{-6} AFE. 10.253

10.84 Comparison between the mean UHRS at Site A and weighted median response spectra for scenarios representing the mean magnitude and distance for earthquakes contribution to the hazard at periods of 0.01, 0.1, 1, and 10 s: a) 10^{-2} AFE; b) 10^{-4} AFE; c) 10^{-6} AFE. Weighted median spectra are based on logic-tree weights and deaggregation weights..... 10.255

10.85 Comparison between the mean UHRS at Site C and weighted median response spectra for scenarios representing the mean magnitude and distance for earthquakes contribution to the hazard at periods of 0.01, 0.1, 1, and 10 s: a) 10^{-2} AFE; b) 10^{-4} AFE; c) 10^{-6} AFE. Weighted median spectra are based on logic-tree weights and deaggregation weights..... 10.258

Tables

10.1 Distance increment in km used for computing the distribution of downdip locations for fault ruptures. 10.21

10.2 Values of the initial smoothing distance *h* used for the crustal background sources and each of four declustered catalogs. 10.21

10.3 Values of the initial smoothing distance *h* used for the alternative geometries of the Juan de Fuca slab source, two alternative catalogs each declustered applying four alternative methods. 10.22

10.4 Simplified strike and dip model for the YFTB source zone used in the hazard calculations. 10.22

10.5 Percent differences between the PGA calculated with multiple rupture orientations and with single rupture orientation model for the YFTB zone at Site A. 10.22

10.6 Input data for example variance calculation. 10.22

10.7 Site coordinates. 10.22

10.8 Uniform Hazard Response Spectra for Site A for annual frequencies of exceedance of 10^{-2}, 10^{-3}, 5×10^{-4}, 4×10^{-4}, 10^{-4}, 5×10^{-5}, 10^{-5}, 10^{-6}, and 10^{-7}. 10.23

10.9 Uniform Hazard Response Spectra for Site C for annual frequencies of exceedance of 10^{-2}, 10^{-3}, 5×10^{-4}, 4×10^{-4}, 10^{-4}, 5×10^{-5}, 10^{-5}, 10^{-6}, and 10^{-7}. 10.26

10.10 Uniform Hazard Response Spectra for Site B for annual frequencies of exceedance of 10^{-2}, 10^{-3}, 5×10^{-4}, 4×10^{-4}, 10^{-4}, 5×10^{-5}, 10^{-5}, 10^{-6}, and 10^{-7}. 10.29

10.11 Uniform Hazard Response Spectra for Site D for annual frequencies of exceedance of 10^{-2}, 10^{-3}, 5×10^{-4}, 4×10^{-4}, 10^{-4}, 5×10^{-5}, 10^{-5}, 10^{-6}, and 10^{-7}. 10.32

10.12 Uniform Hazard Response Spectra for Site E for annual frequencies of exceedance of 10^{-2}, 10^{-3}, 5×10^{-4}, 4×10^{-4}, 10^{-4}, 5×10^{-5}, 10^{-5}, 10^{-6}, and 10^{-7}. 10.35

10.13 Acronyms for seismic sources used in Chapter 10 figures. 10.38

10.0 Hazard Calculations and Results

This section provides and describes the seismic hazard calculations resulting from the implementation of the comprehensive seismic hazard model described in the previous chapters, and it presents the results of seismic hazard sensitivity analyses at five sites: Site A in the 200-East Area, Site B in the 200-West Area, Site C, the Columbia Generating Station, Site D in the 100 BC Area, and Site E in the 300 Area (Figure 1.1).[1] As discussed in Sections 7.2.5 and 9.1.1, the baserock elevation for the hazard calculations was selected as being the top of the Wanapum Basalt (minus the ~4-m flowtop of the uppermost Lolo flow), which is encountered at depths of between 332 and 446 m at hazard calculation Sites A through E. The results shown in this chapter are based on 20 structural periods (peak ground acceleration [PGA] and T 0.02-, 0.03-, 0.04-, 0.05-, 0.07-, 0.1-, 0.15-, 0.20-, 0.30-, 0.40-, 0.50-, 0.75-, 1.0-, 1.5-, 2.0-, 3.0-, 5.0-, 7.5- and 10-sec spectral acceleration) and extend from annual frequencies of exceedance (AFEs) of 10^{-2} to 10^{-8}. In addition, sensitivity analyses of various elements of the ground motion characterization (GMC) and seismic source characterization (SSC) inputs are shown for Sites A and C based on results at PGA, and T 0.1-, 1.0-, and 10-sec spectral accelerations. In the interest of presenting only a reasonable number of figures in this chapter, comparable sensitivity analyses for the other sites were not included in the report. The contribution of individual faults and source zones is shown for all five sites at the four spectral periods listed above. Tables and figures cited in the narrative are provided in sequence at the end of the Section 10.5. A discussion of all hazard calculations conducted for the Hanford Probabilistic Seismic Hazard Analysis (PSHA) is included in Appendix J and the results of these calculations are provided in digital form in the associated folders.

10.1 Hazard Software and Hazard Runs

In probabilistic terms, seismic hazard is defined as the likelihood that various levels of ground motion will be exceeded at a site during a specified time period. It is commonly assumed that the occurrence of individual main shocks can be represented as a Poisson process. Following the approach developed by Cornell and Van Marke (1969) and Cornell (1971), the probability that at a given site a ground motion parameter, Z, will exceed a specified level, z, during a specified time period, T, is given by the following expression:

$$P(Z > z) = 1 - \exp\{-\nu(z)T\} \leq \nu(z)T \tag{10.1}$$

where $\nu(z)$ is the average frequency during time period T at which the level of ground motion parameter Z exceeds level z at the site resulting from earthquakes on all sources in the region. The inequality at the right of Equation (10.1) is valid regardless of the appropriate probability model for earthquake occurrence, and $\nu(z)T$ provides an accurate and slightly conservative estimate of the hazard for probabilities of 0.1 or less, provided $\nu(z)$ is the appropriate value for the time period of interest.

The frequency of exceedance, $\nu(z)$, is a function of the uncertainty in the time, size, and location of future earthquakes and the uncertainty in the level of ground motions they may produce at the site. It is computed by the following expression:

[1] First tables then figures cited in the text are grouped in numerical order at the end of the narrative portion of this chapter.

$$\nu(z) = \sum_{n=1}^{N} \alpha_n\left(m^0\right) \int_{m=m^0}^{m^u} f_n(m)\left[\int_{r=0}^{\infty} f_n(r|m) \cdot P(Z > z|m,r)dr\right]dm \tag{10.2}$$

where $\alpha_n(m^0)$ = is the frequency of earthquakes on source n above a minimum magnitude of engineering significance, m^0;

$f_n(m)$ = the probability density function for event size on source n between m^0 and a maximum event size for the source, m^u;

$f_n(r|m)$ = the probability density function for distance to earthquake rupture on source n, which is usually conditional on the earthquake size; and

$P(Z>z|m,r)$ = the probability that, given a magnitude m earthquake at a distance r from the site, the ground motion exceeds level z.

The PSHA calculations were performed using AMEC software programs, which are validated, installed, and controlled as prescribed in the PSHA project quality assurance procedures for software control. Validation was performed in part by AMEC running test cases following the installation of software to assure that results of the test matched expected results and verification of results with alternative calculations.

In the AMEC computer codes, the double integral in Equation (10.2) is replaced by a double summation with the density functions $f_n(m)$ and $f_n(r|m)$ replaced by discretizations of their corresponding cumulative functions in the following expression:

$$\nu(z) = \sum_{n=1}^{N} \sum_{m_i=m^0}^{m_i=m^u} \lambda_n(m_i) \cdot \left[\sum_{r_j=r_{\min}}^{r_j=r_{\max}} P\,(R = r_j|m_i) \cdot P(Z > z|m_i, r_j)\right] \tag{10.3}$$

where $\lambda_n(m_i)$ = is the frequency of earthquakes of magnitude i on source n; and

$P(R=r_j|m_i)$ = the probability that a given magnitude m_i will occur at distance j.

The relative frequency of various magnitude earthquakes is allowed to take on a number of forms for the complementary cumulative function $N(m)$, the frequency of events with magnitude $\geq m$. The forms used in the Hanford seismic hazard model are described in the earthquake recurrence sections of Chapter 8.0. The minimum magnitude m^0 is set to magnitude 5 in the hazard calculations.

The conditional probability distribution for distance from the earthquake rupture to the site, $P(R=r_j \mid m_i)$, is computed numerically. The basic computational procedure is to construct earthquake rupture polygons and place them on the earthquake source. At each rupture location the program calculates the distance used by the ground motion prediction equation (GMPE). Details about the calculation of $P(R=r_j \mid m_i)$ for the types of sources in the Hanford probabilistic seismic hazard model are given below.

Fault sources are modeled as segmented planar surfaces. Earthquake ruptures are modeled as rectangular shapes. Following the discussion in Section 8.3.2.6 and in the SSC hazard input document (HID; Appendix D), the relationship between the logarithm of rupture area (RA) and magnitude is defined as follows:

$$\ln(RA) = C_{3a} + C_{4a}m \quad \text{for } m \le m_c$$
$$\ln(RA) = C_{3b} + C_{4b}m \quad \text{for } m > m_c \tag{10.4}$$

and the relationship between magnitude and the logarithm of aspect ratio as follows:

$$\log_{10}(AR) = ar_1\left[\max(m-4,0)\right]^{ar_2} \tag{10.5}$$

where aspect ratio (*AR*) is defined as rupture length (*RL*) divided by rupture width (*RW*). The program limits ruptures to the defined fault plane: if the calculated value for *RW* exceeds the fault width, it is set equal to the fault width and the value of *RL* is computed by dividing the *RA* from Equation (10.4) by the fault width. The resulting value of *RL* is limited to the total length of the fault. In the hazard calculations, earthquake ruptures are moved along the fault plane surface using a 1-km increment, and ruptures are assumed to have equal probability of location along the strike of the fault. For each earthquake magnitude, a distribution for the downdip location of ruptures is computed by convolving a distribution for focal depth with a distribution for location of the hypocenter within the ruptures. In the Hanford PSHA, the Seattle fault source, which lies at a large distance from the Hanford Site and, therefore, is not defined by individual segments, is modeled as described above.

As described in Section 8.4.2, most of the fault sources are defined to consist of multiple fault segments. The hazard fault model provides for the case where segment boundaries are not boundaries to ruptures, but represent changes in the slip rate and/or dip of the fault along the fault length. The difference from the previous simpler model is that each fault panel is characterized by a slip-rate factor, which is used to adjust the relative likelihood of ruptures at each location, so that segments with higher slip rates will have more likelihood of ruptures than segments with lower slip rates. The fault is again represented by a series of trapezoid panels, with the top and bottom edges parallel to the ground surface but the panels may have differing dips, and thus differing widths. The fault surface is divided into quadrilateral rupture cells of approximately equal area. Each earthquake rupture is composed of the number of cells for which the sum of the cell area most closely matches the *RA* given by Equation (10.4). Rupture locations are again incrementally placed along the length of the fault, and at each location along strike, the slip-rate factor and fault width are averaged over the *RL*. The product of these two values is a measure of the relative moment release rate at that rupture location. The process is repeated at each possible location along strike and the resulting values are normalized to sum to 1.0 to provide the distribution for rupture location along strike. The distribution for downdip location is computed as described above, using a different distance increment for nearby and distant sources (Table 10.1). In the Hanford PSHA the fault model with variable dip and slip rate is applied to all the faults in the Yakima Fold Belt (YFB).

The calculation of $P(R=r_j \mid m_i)$ for the crustal source zones and for the Juan de Fuca slab source zone uses a grid of equally spaced points. For each source zone, the fraction of earthquake ruptures that occur at each grid point is specified along the reference depth for the grid point as either a uniform spatial density or a kernel density, according to the directions provided in the HID (Appendix D). The kernel density is specified using a Gaussian density function with relative shape parameters specified in each case. The technique applied in this project is the adaptive kernel smoothing presented by Stock and Smith (2002), in which the kernel size is adjusted throughout the region so that the smoothing distance *h* is small in areas of higher seismicity and large in areas of sparse seismicity. The starting value of *h* was selected

based on the optimum kernel size determined from seismicity data (e.g., Silverman [1986]). The starting values of *h* for each combination of source zone and earthquake catalog are summarized in Table 10.2 for the crustal zones and Table 10.3 for the Juan de Fuca slab. As discussed in Chapter 6.0, the crustal earthquake catalog is declustered using four alternative methods, so for each of the source zones that require smoothing, four grids are produced. For the Juan de Fuca slab there are two possible subduction catalogs (see discussion in Chapter 6.0): one that contains only earthquakes with a known focal depth that occurred near or below the top of the slab, and one that also contains all of the earthquakes with unknown or fixed depths. Each of these two catalogs is declustered using four algorithms; therefore, for each possible geometry of the Juan de Fuca source, eight alternative grids are produced. In the hazard calculations, the smoothed grids are paired to the recurrence rates obtained using the same declustered catalog.

The distributions for the strike and dip of ruptures and a focal depth distribution are discussed in Section 8.3.3. Because of the size of the model the computational time required to run the specified aleatory distribution of rupture orientations for the Yakima Fold and Thrust Belt (YFTB) background source zone would have been too long. The model was simplified to use only one strike and one dip for each style of faulting, as shown in Table 10.4. The values selected represent the strike and dip with the highest aleatory frequency in Table 2 of the SSC HID (Appendix D.1). Note that although Table 2 of the SSC HID lists two strikes with equal frequency for strike-slip faults, only one value was used. Given the negligible effect of this element of the model on the hazard (discussed below) use of either strike would produce similar results.

A sample calculation was conducted to show that the effect of this simplification is very small. Figure 10.1 compares the mean hazard curve obtained for the YFTB background zone using one ground motion model (i.e., one branch of the GMC logic tree) and multiple rupture orientations (in blue), and the corresponding mean hazard curve obtained using the simplified model from Table 10.4 (red, dashed curve). The simplified model produces hazard results that are smaller than the hazard results from using multiple rupture orientations by approximately 0.09 percent at AFE of 10^{-3}, up to approximately 2 percent at the 10^{-6} AFE level. Preliminary Hanford PSHA results indicate that the crustal sources (i.e., active faults and background source zones combined) dominate the total mean hazard for PGA. Therefore, to evaluate the impact on the total hazard of using the single rupture orientation model versus the multiple rupture orientations model, the hazard from the YFTB source zone for each case was combined with those of all other crustal sources, and results were compared at five AFEs: 10^{-3}, 10^{-4}, 10^{-5}, 10^{-6}, and 10^{-7}. Table 10.5 shows the corresponding PGA values and the percent differences between the models: the simplified rupture orientation model produces PGA values that are consistently less than 1% lower than the values calculated with multiple rupture orientations. These results confirm that the use of the simplified model for strike and dip has negligible impact on the total hazard.

The Cascadia interface is a large curved surface that does not have constant depth at the top or bottom. This surface is represented by a set of contiguous quadrilaterals, and is then divided into a grid of approximately 1-km^2 cells. Earthquake ruptures are modeled as quasi-rectangular areas by combining sufficient cells to closely approximate the target magnitude-dependent *RA* as a function of magnitude and approximately represent the target magnitude-dependent *AR*. The relative likelihood of ruptures at each location is computed from the ratio of the average interface width along the *RL* compared to the overall average *RW*. This approximates the assumption of uniform likelihood over the area of the interface, with wider locations along strike having more likelihood of ruptures than narrower locations. The closest distance to the site is obtained as the minimum value for the cells that make up the rupture.

10.1.1 Hazard Calculations and Quality Assurance of Hazard Calculations

Final hazard calculations for Sites A, B, D, and E were performed using Pacific Northwest National Laboratory (PNNL) Institutional Computing at PNNL. Final hazard calculations for Site C were conducted using PNNL Institutional Computing at PNNL and local machines at AMEC. Final hazard calculations were conducted following procedures for acquisition, development, modification, control, and use of software in accordance with U.S. Department of Energy (DOE) Order 414.1D (DOE 2011). The Hanford PSHA calculations were performed using AMEC software programs, which were validated, installed, and controlled as prescribed in the Hanford PSHA project quality assurance procedures for software control. Validation was performed in part by AMEC running test cases following the installation of software to assure that results of the test matched expected results and verification of results with alternative calculations.

10.2 Seismic Hazard Results and Sensitivity at Priority Sites

This section describes the seismic hazard results and the results of the sensitivity analyses. The results of the sensitivity analyses will be shown only for Sites A and C and four spectral periods to provide the reader with an understanding of the key results and sensitivities; the results for the other sites are comparable to those given for nearby sites.

For each site, results are shown in terms of seismic hazard curves showing the mean total hazard and the contribution of groups of sources (e.g., background zones, faults, intraslab, and interface sources) to the total hazard. Individual source contribution plots are shown to help identify the zone(s) and fault(s) that contribute the most to the hazard. Uniform hazard response spectra (UHRS) are shown for the mean, 5, 16, 50, 84, and 95 percent fractile levels at AFEs of 10^{-2}, 10^{-3}, 5×10^{-4}, 4×10^{-4}, 10^{-4}, 5×10^{-5}, 10^{-5}, 10^{-6}, and 10^{-7}. Deaggregation analysis is used to identify the combination of magnitude and distance pairs that contribute the most to the total seismic hazard at the site. Results of the deaggregation are represented by histograms and are calculated at the same AFE as the UHRS. Deaggregation results for Sites B, D, and E have been calculated and are provided in Appendix J for subsequent use. Variance contribution histograms are used to show the relative contribution to the total epistemic variance in the AFE introduced by each element of the seismic hazard model logic tree. This is performed via a simple calculation with the parameters listed in Table 10.6. The calculation consists of a logic tree with two levels: level 1 has two branches, one with weight of 0.4 and one with weight of 0.6. At level 2 of the logic tree, the lowest weighted branch has only one possible alternative (i.e., weight of 1), while the highest weighted branch has three possible alternatives (i.e., weights of 0.3, 0.2, or 0.5). In total, the logic tree has four branches (with individual weights w_i – see Table 10.6); the hazard values produced by each branch (x_i) are listed in Table 10.6. The total mean and total variance for this example can be calculated using:

$$E[x] = \sum_i w_i x_i \tag{10.6}$$

$$Var[x] = \sum_i w_i\, x_i^2 - E[x]^2 \tag{10.7}$$

yielding *E[x]*=0.019 and *Var[x]*=1.18E-04, respectively. The variance contributions of the two levels of the logic tree are obtained by using Equations (10.6) and (10.7) to compute the conditional means and variances at each node and the weighted average of these values for each level. The calculation proceeds

from the highest level of the logic tree to the lowest level as follows. Branch L1-A of level 1 contains only one possible alternative at level 2, branch L2-A. The conditional mean and variance at the level 2 node on this branch are $E[x_1]$=0.017 and $Var[x_1]$=0, respectively. Branch L1-B of level 1 has three possible alternatives at level 2, branches L2-B, L2-C, and L2-D. The conditional mean and variance at the level 2 node on this branch are $E[x_{2,3,4}]$=0.020 and $Var[x_{2,3,4}]$=1.93E-04, respectively. The variance contribution from level 2 of the logic tree is the weighted average of the conditional variances at the two nodes: $Var[x_{lvl2}]$=0.4*0.0+0.6*1.93E-04=1.16E-04. The process is repeated for level 1 of the logic tree by applying Equations (10.6) and (10.7) to the conditional mean values on each of the level 1 branches, $E[x_1]$ and $E[x_{2,3,4}]$. The resulting variance for level 1 is $Var[x_{lvl1}]$=1.59E-06. The sum of variances for levels 1 and 2 equals the total variance: 1.59E-06+1.16E-04=1.18E-04. The contribution of the variance from each level of the logic tree to the total variance is calculated by dividing the variance at each level by the total. For this simple example, level 1 contributes 1.4 percent of the total and level 2 contributes 98.6 percent. This type of information is and conveniently represented by histograms of percent contributions.

Tornado plots are used to summarize the results of sensitivity analyses: the plots show the effects of major seismic hazard model components (listed on the vertical axis) on the total mean hazard specified in terms of ground motion at a given AFE (represented by a vertical line). For each key element of the seismic hazard model, sensitivity analyses are performed by assigning weight of 1.0 to one of the possible epistemic alternatives for that element of the seismic hazard model. For example, the Vs-kappa adjustment for crustal GMPEs is a key element of the logic tree that is modeled by seven alternative factors. To generate the tornado plot, the total mean hazard is re-calculated by assigning full weight alternatively to each of the seven Vs-kappa adjustments. The resulting seven values are represented in the figures by a square whose size is proportional to the actual logic-tree weight assigned to each of the seven alternative values of Vs-kappa adjustments. The process is repeated for all the key elements of the seismic hazard model and their epistemic alternatives. Then, the results are ranked based on the variability that they produce in terms of total mean hazard at the specified AFE. The variability is calculated for each key element of the seismic hazard model as the maximum difference between results of the sensitivity analysis. The key components of the seismic hazard model are ranked from the largest variability (plotted at the top) to the smallest (plotted at the bottom).

The two types of plots convey somewhat different information. The tornado plots show the sensitivity of the hazard to the range of a particular parameter included in the model. The variance contribution plots show the combined effect of the range in hazard and the weights assigned to the various alternatives. For these plots, a particular level can have a small contribution to the total variance because the hazard is not sensitive to the parameter range used, or the assigned weights heavily favor one of the alternatives and give little weight to the others. Thus, the variance contribution and tornado plots complement each other to provide a more complete picture of the contributions to the epistemic uncertainty in the hazard.

10.2.1 200-East Area (Site A)

This site is located in the 200-East Area and is hosted within the YFTB background zone (see Figure 10.2). The coordinates of the site are listed in Table 10.7. Figure 10.3a through Figure 10.3t show the total mean and the 5th, 16th, 50th, 84th, and 95th percentile seismic hazard curves for Site A and 20 spectral periods. Figure 10.4a through Figure 10.4t compare the total mean hazard at 20 spectral periods

with the mean hazard produced by the crustal background sources (green curve), faults (blue curve), Cascadia interface (magenta curve), and Cascadia intraslab source (red curve). The crustal background sources control the high-frequency hazard (PGA and spectral periods up to 1.0 sec). The Cascadia interface contribution becomes noticeable starting at spectral periods of 0.3 sec, and is predominant for spectral periods greater than 1 sec. At these spectral periods the faults are contributing significantly to the hazard at AFE of 10^{-3} or less. Table 10.8 contains the values of the total mean hazard at Site A and the 5th, 16th, 50th, 84th, and 95th percentile of the total hazard at AFEs of 10^{-2}, 10^{-3}, 5×10^{-4}, 4×10^{-4}, 10^{-4}, 5×10^{-5}, 10^{-5}, 10^{-6}, and 10^{-7} (corresponding to return periods of 100, 1,000, 2,000, 2,500, 10,000, 20,000, 100,000, 1 million, and 10 million years). The values in Table 10.8 are the UHRS; the mean, 50th and 84th percentiles are shown in Figure 10.5a, Figure 10.5b, and Figure 10.5c, respectively.

Deaggregation of the total mean seismic hazard is shown in Figure 10.6 through Figure 10.9. Each figure contains histograms representing the percent contribution to the total mean seismic hazard from different magnitude-distance bins. Each histogram represents one AFE level: 10^{-2}, 10^{-3}, 5×10^{-4}, 4×10^{-4}, 10^{-4}, 10^{-5}, 10^{-6}, 10^{-7}. Consistent with the seismic hazard curves, the deaggregation plots for PGA and T 0.1-sec spectral acceleration are similar; at the 10^{-2} and 10^{-3} AFE levels the contribution of the background source (small magnitudes at distance of less than 50 km) and of the nearby faults (magnitudes of about 7 at distance of 15 to 20 km) is evident. The histograms also show contributions from both distant interface events (magnitude 9 at 300 to 400 km) and from the Seattle fault (magnitude of about 7.5 and distance of 200 km). At AFE of 5×10^{-4}, 4×10^{-4}, 10^{-4}, and 10^{-5} the interface contribution is negligible, while the background seismicity and the contribution from faults within 50 km of Site A are predominant. At AFE of 10^{-6} and 10^{-7}, the seismic hazard is dominated by nearby faults (within 15 km of Site A). The deaggregation plots for T 1.0 sec show a much larger contribution from the interface earthquakes that dominate the hazard at the 10^{-3} AFE level, then diminishes at lower AFEs where the hazard is again controlled by nearby faults with very little contribution from the background seismicity. Interface earthquakes dominate the seismic hazard at 10-sec spectral acceleration; at the 10^{-2} AFE level, the Seattle fault source contributes about 4 percent to the total hazard, but its contribution diminishes with decreasing AFE and it is negligible at AFE of 10^{-4} and lower.

10.2.1.1 Individual Source Contributions

Figure 10.10a through Figure 10.10d compare the mean seismic hazard curves for each of the seismic sources described in Chapter 8.0. The main contributors to the total hazard among the crustal zones are the YFTB background zone, and the Rattlesnake Mountain, Umtanum Ridge, Yakima Ridge, Horse Heaven Hills, Saddle Mountain, Ahtanum-Rattlesnake Hills faults, and the Seattle fault. Among the subduction sources, the Cascadia interface source (CSZ) is the predominant contributor, particularly for low-frequency ground motions. Zones B and D contribute only for AFEs greater than 10^{-3}.

10.2.1.2 Sensitivity Analyses

This section presents a series of seismic hazard curves that illustrate the effect of individual branches of the logic tree on the seismic hazard. For a particular node of the logic tree, the sensitivity analyses are conducted by assigning full weight alternatively to each of the branches that represent epistemic uncertainty. The elements of the SSC model that were tested include the crustal thickness, start time of the deformation, basis for calculating the fault dips, and temporal model-scale factors. In addition to these, some sensitivity analyses were conducted for individual sources; i.e., the use of alternative catalogs and declustering techniques in the YFTB source zone, the use of a uniform spatial earthquake distribution

or kernel smoothing in YFTB source zone, the use of Quaternary or long-term slip rates for the Rattlesnake Mountain fault, the use of recurrence intervals or slip rates for Ahtanum-Rattlesnake Hills fault, Rattlesnake-Wallula (RAW) fault, and Toppenish Ridge fault sources; the downdip extension of the Cascadia interface; and the downdip extension of the Juan de Fuca slab. For the GMC model, sensitivity analyses were conducted for both crustal and subduction ground motion models and comparisons were made for use of lognormal versus mixture model in the sigma model; the uncertainty in the backbone adjustments for crustal ground motion models; the epistemic uncertainty in the mean for subduction ground motions; the V_s-k adjustment factors; and the host-to-target V_s adjustment factor.

10.2.1.2.1 Elements of the SSC Model

This section describes the hazard sensitivity at Site A that is related to various elements of the SSC model. Figure 10.11 compares the mean hazard curve for all crustal sources (black curve) with the mean hazard curves obtained assigning full weight to each of the three seismogenic crustal thicknesses. Results are shown for 0.1-sec and 1.0-sec spectral accelerations and are not significantly different. At AFEs smaller than 10^{-3} the hazard is dominated by the nearby faults, and smaller seismogenic thickness produces a higher hazard than larger thickness because the fault dips are less steep and the slip rates are higher to accommodate the observed structural relief. At AFEs between 10^{-1} and 10^{-3} this effect is reversed for two reasons. First, the hazard has a larger contribution from Zone B and the distant parts of the YFTB source zone. The crustal earthquake ground motion characterization developed in Chapter 9.0 predicts increasing ground motions with increasing depth, and a thicker crust allows for deeper earthquakes without significantly changing the source-to-site distance for the majority of earthquakes contributing to the hazard. Second, there is a significant contribution from the Seattle fault for which a thicker seismogenic thickness implies higher moment rate and, therefore, more frequent earthquakes. The next two figures (Figure 10.12 and Figure 10.13) illustrate the effect of alternative models for the downdip extension of the CSZ and of the Juan de Fuca slab for 1-sec and 10-sec spectral accelerations. A deeper downdip extension of the CSZ produces a higher seismic hazard because it brings the earthquakes closer to the site. However, the effect of deepening the slab is negligible because the spatial distribution of earthquake recurrence rates for the slab are based on the spatial distribution of observed seismicity, which is more frequent (i.e., higher spatial density of earthquakes) at shallower depths.

The next three figures test elements of the model applicable to the faults in the YFB: the start time of deformation (Figure 10.14), the basis for assessing the fault dip (Figure 10.15), and the temporal model-scale factors (Figure 10.16). Sensitivity analyses are done comparing the mean total hazard for the crustal sources, with the mean hazard obtained assigning full weight alternatively to each of the branches. Results are shown for 0.1- and 1-sec spectral accelerations. In Figure 10.14 the mean hazard computed assuming a start time of 6 Ma for all faults is higher than the other two models (10 Ma, and 6 Ma except for faults Horse Heaven Hills, Horn Rapids, Rattlesnake Mountain, RAW, and Wallula Fault that have 10 Ma). Differences between the models are generally small. Figure 10.15 shows sensitivity to the alternative models used to assess the fault dip. Using the maximum width of the structural relief polygon results in higher seismic hazard than the alternative models because it produces smaller dip angles, which in turn, results in larger slip rates. Lastly, the temporal model-scale factors are used to represent a renewal process. The five alternative factors are multipliers on the mean Poisson rate; therefore, the larger the value, the higher the seismic hazard. This is shown in Figure 10.16, where the effect is noticeable particularly in the 10^{-3} to 10^{-5} AFE range.

Figure 10.17 and Figure 10.18 test elements of the model that apply to the YFTB background zone (e.g., the earthquake catalog and its declustering techniques) and the spatial distribution of earthquakes within the zone. Following the discussion in Section 8.3.3.4, earthquake recurrence for the YFTB zone is assessed in one of two ways: the first is to assign the observed seismicity within "capture zones" (see Figure 8.95) to the faults; the second is to assign all of the observed seismicity to YFTB zone. This is done by creating two separate catalogs for zone YFTB and each catalog is then declustered using four alternative techniques as described in Chapter 6.0. Figure 10.17 shows that differences are larger at AFEs of 10^{-3} or greater, where the contribution of the small magnitude earthquakes is dominant, and that the declustering technique number 3 (i.e., that of Uhrhammer [1986]) produces the highest hazard results. Chapter 6.0 indicates that this technique removes significantly fewer earthquakes than the other three declustering methods used and, therefore, produces higher seismicity rates. In addition, Chapter 6.0 reports that the largest differences between the alternative declustering methods are observed for small magnitude earthquakes. Figure 10.18 compares the hazard for the YFTB zone calculated using a uniform spatial density of earthquake ruptures within the zone, or a kernel density. For Site A, the kernel density model produces higher hazard than the uniform model because the site is close to a cluster of seismicity. In the kernel smoothing, areas with more earthquakes are assigned a greater fraction of future earthquake ruptures; therefore, the density of earthquakes is locally higher than the one modeled by a uniform spatial density.

Figure 10.19 compares the mean seismic hazard curve for the Rattlesnake Mountain fault (solid black curve is the mean hazard) to the mean hazard curves obtained assigning full weight to each of the alternative approaches to assessing recurrence. The hazard curve produced using the long-term recurrence rates based on structural relief is shown by the solid blue line, while the hazard curve produced using the Quaternary rates (combination of five models) is shown by the solid red line. The hazard curves obtained with the five alternative Quaternary rates are shown by the dotted lines. In general, the Quaternary rates produce a lower seismic hazard than the rates obtained from the structural relief; only the highest Quaternary rate (Q5 in Figure 10.19) is comparable to the rates based on structural relief.

Figure 10.20, Figure 10.21, and Figure 10.22 compare the hazard curves obtained using recurrence rates based on slip rates with hazard curves obtained using paleoseismic recurrence intervals, respectively for Ahtanum-Rattlesnake Hills, Toppenish Ridge, and RAW faults. In each figure, the black line is the mean hazard curve for the fault, the red line is the hazard curve obtained using recurrence intervals, and the green line is the hazard curve obtained using the slip rates. The figures contain three subplots; the first two are seismic hazard curves for T 0.1- and T 1.0-sec spectral accelerations, and the third shows the recurrence curves calculated in the magnitude range of interest for hazard calculations, that is E[**M**] greater than 5.0. Consistent with the recurrence curves, the slip-rates approach produces lower hazard for Ahtanum-Rattlesnake Hills and RAW faults, and higher hazard for the Toppenish Ridge fault. In the case of Ahtanum-Rattlesnake Hills, the difference between the results obtained with the recurrence intervals and those obtained with slip rates is higher for low AFEs. This effect is explained by the fact that in the recurrence interval approach the frequency of earthquakes does not change for the characteristic magnitudes, while it decreases with increasing characteristic magnitude in the slip-rate approach.

10.2.1.2.2 Elements of the GMC Model

This section describes the hazard sensitivity at Site A related to various elements of the GMC model. Figure 10.23 and Figure 10.24 show comparisons of the alternative shapes of the sigma model distribution for the crustal and subduction ground motion models, respectively. For crustal ground

motions, the differences are negligible and the curves appear superimposed. For subduction ground motions the curves differ at AFEs smaller than 10^{-5}, with the mixture model producing slightly higher results than the lognormal. The reason for the small difference in hazard produced by the two distribution forms is that the average values of the number of standard deviations are generally less than 3 such that motions from the extreme tails of the ground motion distribution do not have a large contribution to the hazard.

The sensitivity to different Vs-k adjustment factors for crustal motions is shown in Figure 10.25. The curves obtained with each of the seven adjustment factors are compared to the total mean hazard curve for all crustal zones. As expected, Vs-k adjustments are largest for the high-frequency ground motions, as shown by the PGA and 0.1-sec spectral acceleration plots. Figure 10.26 shows the sensitivity to the nine branches representing the inherent uncertainty in the adjustments to the backbone model. The variability between the models is significant at all spectral levels and particularly for 10-sec spectral accelerations. The hazard results are consistent with those presented in Figure 9.72, which shows the range of mean residuals against ground motion data: models 2 and 9 have the highest mean residuals and consistently produce the lowest hazard.

The subduction backbone model is adjusted to local site conditions using four alternative adjustments. Figure 10.27 shows that the seismic hazard from all subduction sources is not particularly sensitive to these four adjustments. Figure 10.28 compares the mean hazard curve from all subduction sources (black curve) with the three alternative models representing the epistemic uncertainty in the median motion. The effect of the scaling is significant at all frequency levels.

10.2.1.3 Variance Contribution and Tornado Plots

Variance contribution histograms, which show the relative contribution that various input uncertainties make to the total variance in the hazard results, were produced for PGA and T 0.1-, 1-, and 10-sec spectral accelerations and are shown in Figure 10.29 through Figure 10.32. Each figure contains histograms of the total variance calculated at four AFEs: 10^{-3}, 10^{-4}, 10^{-5}, 10^{-6}, and 10^{-7}. The figures show that for PGA and T 0.1-sec spectral acceleration most of the total variance comes from the Vs-k adjustments in the crustal ground motions (labeled “crustal Vsk” in the figures). Other significant contributions to the total variance come from the crustal backbone adjustment model and the epistemic uncertainty on the median subduction model, which are grouped in one histogram bin (labeled “median scaling” in the figures) because they appear at the same level of the logic tree used in the hazard calculations; the host-to-target adjustment factors for crustal ground motions (labeled “host to target”); and the sigma model (labeled “sigma”) for both crustal and subduction ground motion (these are also grouped in one histogram because they appear at the same level of the logic trees). Among the elements of the SSC model, the largest contribution to the total variance is given by the alternative b-values, style of faulting, and maximum magnitude (labeled “Mmax”). For spectral periods of 1 sec or more, the largest contributions to the total variance come from elements of the GMC model, such as the scaling on the anelastic attenuation term for subduction ground motions (labeled “subd anelastic attenuation (theta6)” in the figures), the uncertainty in the median backbone models, and the host-to-target adjustments. The SSC elements that contribute the most to the total variance are the maximum magnitude and the recurrence model used for the faults: these include both the choice of recurrence intervals vs structural relief (labeled “Rec. interval vs Struct. Relief appr.” in the figures), and the uncertainty on the recurrence interval s (labeled “Rec. Interval unc.”). Note that the use of alternative earthquake catalogs (both for

zone YFTB and for the subduction intraslab source JDF) and alternative declustering techniques have negligible impact on the total hazard at the site.

Tornado plots are used to show how each alternative element of the SSC and GMC models scales the total mean seismic hazard up or down, and to rank each element based on the relative effect on the hazard. Figure 10.33 through Figure 10.36 show tornado plots for PGA and T 0.1-, 1.0- and 10-sec spectral accelerations, respectively, and for AFEs of 10^{-3}, 10^{-4}, 10^{-5}, 10^{-6}, and 10^{-7} (corresponding to return periods of 1,000, 10,000, 100,000, 1,000,000, and 10,000,000 years). The figures show that the crustal Vs-k adjustments dominate PGA and T 0.1-sec spectral acceleration at all AFEs. The second largest contribution comes from the uncertainty in the median crustal backbone model, whereas the epistemic uncertainty on the median subduction model has very little impact on the seismic hazard. Elements of the SSC model for faults such as the basis for fault dip, start time of the deformation, and temporal model-scale factor, and crustal thickness have a non-negligible impact on the total seismic hazard. At T 1-sec spectral acceleration, the predominant effect on the total hazard is given by the uncertainty in the adjustment to the backbone model for crustal sources and the epistemic uncertainty on the median for subduction sources. Among the elements of the SSC model, the temporal model-scale factor, start time of deformation, and crustal thickness have the largest effect on the total mean hazard. At T 10-sec spectral acceleration, Figure 10.9 shows that the Cascadia interface dominates the hazard at the 10^{-3} AFE level, while at lower AFEs the hazard is controlled by nearby faults. Consistently, the tornado plots show that the epistemic uncertainty on the median ground motion for subduction introduces the largest variability in the seismic hazard at AFEs between 10^{-3} and 10^{-5}, followed by the scaling of the median crustal backbone. In this AFE range, the SSC elements that have the largest effect on the hazard are the eastern boundary of the Cascadia interface and the temporal model-scale factor applied to the faults. At lower AFEs (10^{-6} and 10^{-7}), the faults are again dominating the hazard, so the scaling of the median crustal backbone shows the largest variability, followed by the epistemic uncertainty on the median subduction ground motions.

10.2.2 Columbia Generating Station (Site C)

This site is located within the YFTB background zone (see Figure 10.2); the site coordinates are listed in Table 10.7. Figure 10.37a through Figure 10.37t show the total mean and the 5th, 16th 50th, 84th, and 95th percentile seismic hazard curves for Site C and 20 spectral periods. Figure 10.38a through Figure 10.38t compare the total mean hazard at 20 spectral periods, with the mean hazard produced by the crustal background sources (green curve), faults (blue curve), Cascadia interface (magenta curve), and Cascadia intraslab source (red curve). The hazard is similar to that observed for Site A: for PGA and T 0.1-sec spectral acceleration (Figure 10.38a and Figure 10.38g) the crustal sources, particularly the background zone, control the hazard. At T 1.0 sec, the crustal sources still control the hazard, with a significant contribution of the subduction sources at 10^{-3} to 10^{-4}AFEs (Figure 10.38n); at T 10 sec, the seismic hazard is dominated by the subduction sources (Figure 10.38t). Table 10.9 contains the values of the total mean hazard at Site C and the 5th, 16th, 50th, 84th, and 95th percentile of the total hazard at AFEs of 10^{-2}, 10^{-3}, 5×10^{-4}, 4×10^{-4}, 10^{-4}, 5×10^{-5}, 10^{-5}, 10^{-6}, and 10^{-7} (corresponding to return periods of 100, 1,000, 2,000, 2,500, 10,000, 20,000, 100,000, 1 million, and 10 million years). The values in Table 10.9 are the UHRS: the mean, 50th, and 84th percentiles are shown in Figure 10.39a, Figure 10.39b, and Figure 10.39c, respectively.

Deaggregation of the total mean seismic hazard is shown in Figure 10.40 through Figure 10.43. As in the previous section, each figure contains histograms representing the percent contribution to the total mean seismic hazard from different magnitude-distance bins. Histograms are presented for AFEs of 10^{-3}, 10^{-4}, 10^{-5}, 10^{-6}, and 10^{-7}. Similar to what was observed for Site A, the deaggregation plot for PGA at the 10^{-2} and 10^{-3} AFE level show the contribution of the source zones (small magnitudes at distances of less than 100 km). The Seattle fault (magnitude of about 7.5 at a distance of about 200 km) and distant interface events (magnitude 9 at a distance of 300 to 400 km) contribute at the 10^{-2} AFE level, while the nearby faults (magnitudes of about 7.5 at a distance of 15 to 50 km) contribute at the 10^{-3} AFE level. Compared to Site A, the contribution of small earthquakes at a distance of 30 to 50 km is higher, while the contribution of the interface earthquakes is lower. For longer return periods (10^{-4} to 10^{-7} AFEs) the interface contribution is negligible, while the contribution from nearby faults and source zones remains predominant. The deaggregation plots for the T 0.1-sec spectral accelerations (Figure 10.40a through Figure 10.40h) are similar to those for PGA: in both cases at an AFE of 10^{-6} the dominant contributor to the seismic hazard are small background earthquakes at very close distances. The deaggregation plots for T 1.0-sec and T 10-sec spectral accelerations (Figure 10.42 and Figure 10.43) show large contributions from the interface earthquakes, particularly at T 10-sec spectral acceleration, and contributions from nearby faults located within 20 km of Site C.

10.2.2.1 Individual Source Contributions

Figure 10.44a through Figure 10.44d compare the mean seismic hazard curves for each of the seismic sources described in the previous chapters. The main contributors to the total hazard for PGA and T 0.1-sec spectral acceleration (Figure 10.44a and Figure 10.44b) are the YFTB background zone, and the Rattlesnake Mountain, Umtanum Ridge, Horse Heaven Hill, Horns Rapid, Yakima Ridge, and Seattle faults. Among the subduction sources, the CSZ is the predominant contributor, particularly for low-frequency ground motions. The background Zones B, C, and D contribute to the seismic hazard only at AFEs of 10^{-3} and higher. For T 1.0-sec and 10-sec spectral accelerations (shown in Figure 10.44c and Figure 10.44d) the hazard is dominated by the Cascadia interface; a lesser contribution comes from the crustal sources Zones YFTB, B, and D, and the Rattlesnake Mountain, Umtanum Ridge, Horse Heaven Hill, Yakima Ridge, and Seattle faults. The Saddle Mountain, Horns Rapid, Ahtanum-Rattlesnake Hills, RAW, and Toppenish Ridge faults also contribute to the total hazard at AFEs of 10^{-5} or less.

10.2.2.2 Sensitivity Analyses

The sensitivity analyses presented in this section test the effect of different elements of the SSC and GMC models on the hazard at Site C. The sensitivity tests are the same as those presented for Site A and include the following

- seismogenic crustal thickness
- start time of the deformation
- basis for calculating the fault dips
- temporal model-scale factors
- the use of Quaternary rates or long-term slip rates for Rattlesnake Mountain
- the use of alternative catalogs and declustering techniques in the YFTB zone

- the use of uniform spatial earthquake distribution or kernel smoothing in the YFTB zone
- the use of recurrence intervals or slip rates for Ahtanum-Rattlesnake Hills fault, RAW, and Toppenish Ridge faults
- the downdip extension of the Cascadia interface
- the downdip extension of the JDF slab
- use of lognormal versus mixture model in the sigma model
- the uncertainty in the backbone adjustments for crustal ground motion models
- the epistemic uncertainty in the mean for subduction ground motions
- the V_s-k adjustment factors; and the host-to-target V_s adjustment factor for subduction ground motions.

The sensitivity to elements of the SSC model are presented first, followed by sensitivity to elements of the GMC model.

10.2.2.2.1 Elements of the SSC Model

This section describes the hazard sensitivity at Site C that is related to various elements of the SSC model. Figure 10.45 compares the mean hazard curve for all crustal sources (black curve) with the mean hazard curves obtained assigning full weight to each of the three seismogenic crustal thicknesses. Results are shown for 0.1-sec and 1.0-sec spectral accelerations and are not significantly different, and the effects are similar to those shown for Site A. The reason for the small differences is given in Section 10.2.1.2.1.

The effect of alternative models for the downdip extension of the CSZ and of the JDF slab are shown in Figure 10.46 and Figure 10.47, respectively. Similar to what is shown in Figure 10.12 and Figure 10.13 for Site A, the deeper downdip extension of CSZ produces a higher hazard because it brings the earthquakes closer to the site, but the differences between the three alternative models are small. As noted before, extending the JDF slab to the 100-km contour line does not add more seismicity to the slab because most of the earthquakes occur near the coast well to the west of the site; therefore, the earthquake recurrence rates and consequently the hazard results are not significantly different between the three alternative models.

Figure 10.48, Figure 10.49, and Figure 10.50 present the results of sensitivity analysis to the start time of deformation, the basis for assessing the fault dip, and the temporal model-scale factors, respectively. As shown for Site A (Figure 10.14 through Figure 10.16) the alternative models differ for AFEs smaller than 10^{-3}: selecting a start time of 6 Ma for all faults or using the maximum structural relief to assess the fault dip produces higher hazard than their alternatives because these models determine higher slip rates. The highest temporal model-scale factor produces higher results because it is a multiplier on the mean Poisson rate.

Figure 10.51 and Figure 10.52 test the effect of using alternative earthquake catalogs and declustering techniques for the YFTB zone, and different spatial distributions of earthquakes within the zone (see Section 10.2.1.2.1). Similar to Figure 10.17, differences between alternative declustering methods are larger at AFEs of 10^{-3} or greater, with the declustering technique number 3 (Uhrhammer 1986) producing

the highest hazard results. The effect of the alternative spatial distribution is also similar to what is shown in Figure 10.18 for Site A: the kernel density model produces higher hazard than the uniform model because the site is close to a cluster of seismicity.

Figure 10.53 compares the mean seismic hazard curve for the RM fault (black curve) to the mean hazard curves obtained assigning full weight to each of the alternative recurrence approaches. The hazard curve produced using the recurrence rates based on structural relief is shown by the solid blue line, while the hazard curve produced using the Quaternary rates (combination of five models) is shown by the solid red line. The hazard curves obtained using the five alternative Quaternary rates are shown by dotted lines. Consistent with Site A, the Quaternary rates produce lower seismic hazard than the rates obtained from the structural relief; only the highest Quaternary rate (model Q5 in Figure 10.53) is comparable to the structural relief rates.

Figure 10.54 through Figure 10.56 compare the hazard curves obtained using recurrence rates based on slip rates with hazard curves obtained using recurrence intervals, respectively, for ARH, TR, and RAW faults. In each figure the black line is the mean hazard curve for the fault, the red line is the hazard curve obtained using recurrence intervals, and the green line is the hazard curve obtained using the slip rates. The seismic hazard curves calculated for T 0.1- and T 1.0-sec spectral accelerations (first two subplots) are compared to the recurrence curves calculated in the magnitude range of interest for hazard calculations, that is E[**M**] greater than 5.0 (third subplot). Consistent with the recurrence curves, the slip-rates approach produces lower hazard for faults ARH and RAW, and higher hazard for fault TR.

10.2.2.2.2 Elements of the GMC Model

This section describes the hazard sensitivity at Site C related to various elements of the GMC model. Figure 10.57 and Figure 10.58 show comparisons of the alternative shapes of the sigma model distribution for the crustal and subduction ground motion models, respectively. Differences between the hazard results are undetectable or very minor. For subduction ground motions the curves differ at very low AFEs (less than 10^{-5}); the mixture model produces slightly higher results than the lognormal.

The sensitivity to different Vs-k adjustment factors for crustal motions is shown in Figure 10.59. The curves obtained with each of the seven adjustment factors are compared to the total mean hazard curve for all crustal zones. As shown in Figure 10.25 for Site A, V_s-k adjustments are significant for the high-frequency ground motion. Figure 10.60 shows the sensitivity to the nine branches representing the inherent uncertainty in the adjustments to the backbone model. The variability between the models is significant at all spectral levels and particularly for 10-sec spectral accelerations.

The host-to-target V_s adjustments for the subduction backbone model and the epistemic uncertainty on the median model are presented in Figure 10.61 and Figure 10.62, respectively. As shown for Site A (Figure 10.27 and Figure 10.28), the alternative V_s adjustments produce very similar hazard results, whereas the effect of scaling the median background model is significant at all frequency levels.

10.2.2.3 Variance Contribution and Tornado Plots

Variance contribution histograms, which show the relative contribution that various input uncertainties make to the total variance in the hazard results, for PGA and T 0.1-, 1-, and 10-sec spectral accelerations and are shown in Figure 10.63 through Figure 10.66. Each figure compares histograms of

contributions to the total variance calculated at four AFEs: 10^{-3}, 10^{-4}, 10^{-5}, 10^{-6}, and 10^{-7}. The figures show that for PGA and T 0.1-sec spectral acceleration the largest contributions to the total variance are generated by the V_s-k adjustments in the crustal ground motions and the b-value. Additional elements of the GMC logic tree, such as the median ground motion scaling factors (labeled "median scaling" in the figures), the host-to-target adjustments, and the sigma model (labeled "sigma" in the figures) also contribute approximately 10 to 20 percent (depending on the AFE). In addition, the style of faulting can contribute up to 10 percent to the total variance, depending on the AFE. For spectral periods of 1 and 10 sec, the uncertainty in the median backbone model (combined between the crustal and subduction models, labeled "median scaling" in the figures) and the scaling on the anelastic attenuation term in the subduction ground motion (labeled "subd anelastic attenuation (theta6)" in the figures) contribute most to the total variance in the hazard. Among the elements of the SSC logic tree, the b-value, maximum magnitude, and the fault recurrence models contribute most to the total variance. Fault recurrence models include both the choice of recurrence intervals or rates based on structural relief (labeled "Rec. interval vs Struct. Relief appr." in the figures), and the uncertainty on the recurrence interval s (labeled "Rec. Interval unc."). As observed in Section 10.2.1.3 the use of alternative earthquake catalogs and alternative declustering techniques has negligible effect on the total hazard at the site.

Tornado plots are shown in Figure 10.67 through Figure 10.70 for PGA and T 0.1-, 1.0-, and 10-sec spectral accelerations, respectively, and for AFEs of 10^{-3}, 10^{-4}, 10^{-5}, 10^{-6}, and 10^{-7} (corresponding to return periods of 1,000, 10,000, 100,000, 1,000,000, and 10,000,000 years). For PGA and T 0.1-sec spectral acceleration, the crustal V_s-k adjustments determine the largest variability in ground motions at all AFEs, followed by the uncertainty in the median crustal backbone model. The basis for fault dip, temporal model adjustment, start time, and seismogenic crustal thickness (at AFEs of 10^{-5} or lower) of the deformation produce less variability, whereas elements of the subduction model have little or no effect. At T 1.0-sec spectral accelerations the predominant effect on the total hazard is given by the uncertainty in the adjustment to the backbone model for crustal sources, the crustal Vs-k adjustments, and the epistemic uncertainty on the median subduction model. Among the elements of the SSC the largest variability in ground motions is produced by the temporal model-scale factor, the eastern extension of the Cascadia interface (mainly at AFEs between 10^{-3} and 10^{-5}), the start time of the deformation, and the crustal thickness (at AFEs of 10^{-5} or lower). At T 10-sec spectral acceleration the epistemic uncertainty on the median for subduction sources generates the most significant variability in results, followed by the uncertainty in the adjustment to the backbone model for crustal sources, and the eastern extension of the Cascadia interface.

10.2.3 200-West Area (Site B)

This site is located within the YFTB background zone (see Figure 10.2); the site coordinates are listed in Table 10.7. Figure 10.71a through Figure 10.71t show the total mean and the 5th, 16th, 50th, 84th, and 95th percentile seismic hazard curves for Site B and 20 spectral periods. Figure 10.72a through Figure 10.72t compare the total mean hazard at 20 spectral periods, with the mean hazard produced by the crustal background sources (green curve), faults (blue curve), Cascadia interface (magenta curve), and Cascadia intraslab source (red curve). The hazard is similar to that observed for Site A, although due to the close proximity between Site B and the three main faults crossing the Hanford Site (Umtanum Ridge, Yakima Ridge, and Rattlesnake Mountain) the hazard from the faults is dominant at AFEs in the 10^{-4} to 10^{-7} range for PGA and spectral accelerations up to T 0.75-sec spectral acceleration (Figure 10.72a through Figure 10.72m); and at AFEs in the 10^{-3} to 10^{-7} range for spectral periods between 1.0 and 10 sec (Figure 10.72n

through Figure 10.72t). Table 10.10 contains the values of the total mean hazard at Site B and the 5th, 16th, 50th, 84th, and 95th percentile of the total hazard at AFEs of 10^{-2}, 10^{-3}, 5×10^{-4}, 4×10^{-4}, 10^{-4}, 5×10^{-5}, 10^{-5}, 10^{-6}, and 10^{-7} (corresponding to return periods of 100, 1,000, 2,000, 2,500, 10,000, 20,000, 100,000, 1 million, and 10 million years). The mean, 50th, and 84th percentile UHRS are shown in Figure 10.73a, Figure 10.73b, and Figure 10.73c, respectively.

10.2.3.1 Individual Source Contributions

Figure 10.74a through Figure 10.74d compare the mean seismic hazard curves at Site B for each of the seismic sources described in the previous chapters. Among the source zones, the main contributors to the total hazard for PGA and T 0.1-sec spectral acceleration (Figure 10.74a and Figure 10.74b) are the YFTB zone and Zone B. The interface (CSZ) and the Seattle fault also contribute, mostly at the 10^{-2} and 10^{-3} AFE levels. Among the local faults, the largest contributors are the Rattlesnake Mountain, Umtanum Ridge, Yakima Ridge, Ahtanum-Rattlesnake Hills, Saddle Mountain, and Horse Heaven Hill faults. For T 1.0-sec and 10-sec spectral accelerations (shown in Figure 10.74c and Figure 10.74d) the hazard is dominated by the Cascadia interface and by the Yakima Ridge and Ahtanum-Rattlesnake Hills faults. Other important contributions to the total hazard come from the Umtanum Ridge and Rattlesnake Mountain faults, and from the Toppenish Ridge fault at AFEs of 10^{-6} or smaller. At AFEs of 10^{-2} and 10^{-3} the hazard is controlled by the background sources YFTB, Zone B and Zone D, and by the distant Seattle fault.

10.2.4 100BC Area (Site D)

Site D is located within the YFTB background zone (see Figure 10.2), directly above the Umtanum Ridge fault; the site coordinates are listed in Table 10.7. Figure 10.75a through Figure 10.75t show the total mean and the 5th, 16th, 50th, 84th, and 95th percentile seismic hazard curves for Site D and 20 spectral periods. Figure 10.76a through Figure 10.76t compare the total mean hazard at 20 spectral periods, with the mean hazard produced by the crustal background sources (green curve), faults (blue curve), Cascadia interface (magenta curve), and Cascadia intraslab source (red curve). Due to the proximity of Site D to the Umtanum Ridge fault, the hazard at AFEs in the 10^{-4} to 10^{-7} range is dominated by the faults; the Cascadia interface is a significant contributor at spectral periods between 1 and 10 sec. Table 10.11 contains the values of the total mean hazard at Site D and the 5th, 16th, 50th, 84th, and 95th percentile of the total hazard at AFEs of 10^{-2}, 10^{-3}, 5×10^{-4}, 4×10^{-4}, 10^{-4}, 5×10^{-5}, 10^{-5}, 10^{-6}, and 10^{-7} (corresponding to return periods of 100, 1,000, 2,000, 2,500, 10,000, 20,000, 100,000, 1 million, and 10 million years). The mean, 50th, and 84th percentile UHRS are shown in Figure 10.77a, Figure 10.77b, and Figure 10.77c, respectively.

10.2.4.1 Individual Source Contributions

Figure 10.78a through Figure 10.78d compare the mean seismic hazard curves at Site D for each of the seismic sources described in the previous chapters. At all spectral periods shown, the hazard at AFEs of 10^{-4} and lower is clearly dominated by the Umtanum Ridge fault. Figure 10.78a and Figure 10.78b show the hazard at PGA and T 0.1-sec spectral acceleration: at AFEs between 10^{-2} and 10^{-4}, the crustal background YFTB zone and Zone B, the Seattle fault, and the Cascadia interface contribute to the hazard. For lower AFEs (10^{-4} and smaller), the dominant contributors to the total hazard are the Umtanum Ridge fault and the YFTB zone. At T 1-sec spectral acceleration (Figure 10.78c) the contribution from the

Cascadia interface increases between 10^{-2} and 10^{-3} AFEs; at T 10-sec spectral acceleration, the Cascadia interface dominates the hazard in the 10^{-3} to 10^{-5} AFE level, while the Umtanum Ridge fault controls the hazard at lower AFEs.

10.2.5 300 Area (Site E)

This site is located within the YFTB background zone (see Figure 10.2); the site coordinates are listed in Table 10.7. Figure 10.79a through Figure 10.79t show the total mean and the 5th, 16th, 50th, 84th, and 95th percentile seismic hazard curves for Site E and 20 spectral periods. Figure 10.80a through Figure 10.80t compare the total mean hazard at 20 spectral periods, with the mean hazard produced by the crustal seismic source zones (green curve), faults (blue curve), Cascadia interface (magenta curve), and Cascadia intraslab source (red curve). The hazard is dominated by the crustal source zones and only at periods greater than 1-sec and AFEs in the 10^{-4} to 10^{-7} range do the Cascadia interface and the faults produce significant contributions to the total mean hazard. Table 10.12 contains the values of the total mean hazard at Site E and the 5th, 16th, 50th, 84th, and 95th percentile of the total hazard at AFEs of 10^{-2}, 10^{-3}, 5×10^{-4}, 4×10^{-4}, 10^{-4}, 5×10^{-5}, 10^{-5}, 10^{-6}, and 10^{-7} (corresponding to return periods of 100, 1,000, 2,000, 2,500, 10,000, 20,000, 100,000, 1 million, and 10 million years). The mean, 50th, and 84th percentile UHRS are shown in Figure 10.81a, Figure10.81b, and Figure10.81c, respectively.

10.2.5.1 Individual Source Contributions

Figure 10.82a through Figure 10.82d compare the mean seismic hazard curves for each of the seismic sources described in the previous chapters. Among the source zones, the main contributors to the total hazard for PGA and T 0.1-sec spectral acceleration (Figure 10.82a and Figure10.82b) are the YFTB source zone and Zone B. The interface (CSZ) and the Seattle fault also contribute mostly at the 10^{-2} and 10^{-3} AFE levels. Among the local faults, the largest contributors are the Rattlesnake Mountain, Horse Heaven Hill, RAW, and Horn Rapid faults. At T 1.0-sec and 10-sec spectral accelerations, shown in Figure 10.82c and Figure 10.82d, the Cascadia interface becomes dominant particularly at AFEs of 10^{-4} or less. Other important contributions to the total hazard come from the Yakima Ridge and Umtanum Ridge faults at AFEs of 10^{-5} or smaller.

10.3 Comparison Between Sites

This section compares the hazard results obtained at the five sites and described individually in Section 10.2. Figure 10.83 compares the UHRS calculated for each of the five sites at three AFE levels: 10^{-2} (Figure 10.83a), 10^{-4} (Figure 10.83b), and 10^{-6} (Figure 10.83c). At an AFE of 10^{-2}, the hazard at the five sites is similar for all spectral periods, because the sites are all influenced by small magnitude earthquakes from the nearest source zones (including the host YFTB background zone), and, to a much lesser extent, by the distant Seattle fault zone.

At an AFE of 10^{-4} (Figure 10.83b) and for spectral periods greater than T 0.05-sec, the hazard at Sites B and D has similar characteristics: as discussed in Sections 10.2.3 and 10.2.4, these two sites are located within 5 to 10 km of fault sources (see Figure 10.2), which dominate the hazard at AFEs of 10^{-4} and lower. The hazard at Sites C and E also exhibits similar characteristics: these two sites are located in the southeastern part of the Hanford Site and further away from the faults (within 10 to 20 km, see Figure 10.2). Sections 10.2.2 and 10.2.5 illustrate that the crustal sources are the largest contributors to

the total hazard up to spectral periods of about 1 sec, then the Cascadia interface is predominant for longer period motions and AFEs of 10^{-4} or lower. The hazard at Site A is similar to that of Sites B and D. For PGA and spectral periods smaller than T 0.05 sec, the hazard at Sites C and E is higher than the hazard at sites A, B, and D. By comparing the individual source contribution figure for PGA, Site C (Figure 10.44a), and Site E (Figure 10.82a) with the corresponding figures for Sites A, B, and D (Figure 10.10a, Figure 10.74a, and Figure 10.78a) the difference is caused by the contribution to hazard from the YFTB zone, that produces a higher contribution to PGA at sites C and E than at Sites A, B, and D due to a higher spatial density of observed seismicity and the use of a spatial smoothing approach for the YFTB source zone.

At AFEs of 10^{-6} (Figure 10.83c) the UHRS of the five sites are more spread apart: from T 0.03 sec to T 10 sec Site D has the highest hazard due to its proximity to the Umtanum Ridge fault. In the same spectral range, Site E has the lowest hazard because it is the most distant site from the faults. In general, Sites C and E are shifted toward high-frequency motions: their UHRS peak at spectral periods of about T 0.05 sec, because the hazard is dominated by the background source zones. The hazard at Sites A, B, and D is controlled by the faults and the UHRS peak at spectral periods of about T 0.1 sec.

10.4 Comparison of UHRS with Response Spectra for Representative Earthquake Scenarios

The UHRS presented in Figure 10.83 represent the combined effects of multiple earthquake scenarios that contribute to the hazard. The relative contribution of these scenarios varies with period and AFE, as illustrated in the deaggregation plots (e.g., Figure 10.6 through Figure 10.9). Therefore, the shape of the UHRS will not correspond to that of a single earthquake scenario. Nevertheless, comparisons between the UHRS and response spectra for representative earthquake scenarios are useful in evaluating the consistency of the hazard results.

Figure 10.84 and Figure 10.85 compare the 10^{-2}, 10^{-4}, and 10^{-6} UHRS for Sites A and C, respectively, with weighted median response spectra for representative earthquake scenarios. The selected scenarios are mean magnitude and distance of shallow crustal earthquakes contributing to the hazard at periods of 0.01, 0.1, 1, and 10 sec, and the mean magnitude and distance of Cascadia interface earthquakes. Each figure contains two plots. The upper plot shows the weighted median ground motion response spectra derived using all of the model adjustments and associated logic-tree weights for the alternative crustal and subduction models developed in Chapter 9. The lower plot shows weighted median spectra using deaggregation weights as defined in Equation 6 of Carlton and Abrahamson (2014) that capture the fact that the higher amplitude ground motion alternatives have a greater contribution to mean hazard than the lower amplitude alternatives. The deaggregation weights can vary substantially from the logic-tree weights, especially at the smaller values of AFE. As shown in the figures, the deaggregation weighted median spectra have shapes that, in general, represent the UHRS shape as the mean magnitude and distance varies across the period range.

In general, the UHRS have substantially different shapes than the response spectra for the Cascadia interface scenario. This reflects the fact that the hazard is generally dominated by contributions from crustal earthquakes except at the longer periods. The influence of the Cascadia source ground motions can be seen in the upward flaring of the 10^{-4} and 10^{-6} UHRS at periods greater than 2 sec. The Cascadia scenario has little effect on the 10^{-2} UHRS as the mean frequency of Cascadia interface earthquakes is approximately 0.6×10^{-2}.

The weighted median spectra for the Cascadia interface scenarios also show that the site adjustment factors combined with extending the model to large distances results in a slight sag in the ground motion predictions in the period range of 0.02 to 0.075 sec. These results are unphysical in that high-frequency PSA values should not be lower than PGA. This effect has been seen in other GMPEs. For example both Campbell and Bozorgnia (2014) and Chiou and Youngs (2014) state in their implementation guidance that ground motion predictions for periods smaller than about 0.3 sec should not be lower than PGA. The weighted median Cascadia scenario response spectra at large distances show values of PSA at 0.04 sec that are about 10 percent lower than PGA. The impact of this on the site hazard was evaluated by recomputing the mean hazard at a period of 0.04 sec imposing a 20 percent increase in the predicted ground motions, twice the deficit in the existing model. The effect was a less than 1 percent increase in the mean hazard near an AFE of 10^{-2} that quickly diminished with decreasing AFE. Thus, the small deficiency in the high-frequency portion of the subduction interface GMPE has negligible effect on the site hazard.

10.5 Recommendations for Application of Baserock Hazard Results

The seismic hazard results presented in this chapter (and digitally in Appendix J) represent the hazard at the baserock horizon defined to be at the top of the Wanapum basalts (minus the ~4-m flowtop of the uppermost Lolo flow), which is encountered at depths of between 332 and 446 m at the hazard calculation Sites A−E (see Section 9.1.1). Development of design ground motions for facilities at the Hanford site will require the development of appropriate site amplification functions to translate the baserock hazard to the desired site horizon. Development of the site amplification functions will require specification of the dynamic properties of the materials above the baserock horizon. This report contains the necessary dynamic properties for the Saddle Mountains basalts and the Ellensburg Formation interbeds, as well as for the Lolo flowtop. These properties are described in Section 9.6 and are contained digitally in Appendix J. The development of appropriate properties for the supra-basalt sediments will require appropriate site-specific investigations at each facility or area.

As discussed in Section 9.5, aleatory variability in the baserock ground motions is modeled using single-station sigma. Single-station sigma is based on the concept that the repeatable component of site ground motions is known (within epistemic uncertainty) and the appropriate aleatory variability to use in baserock PSHA calculations is the variability in motions at a specific site about this known repeatable site effect. As indicated in Section 9.5.1, use of single-station-sigma imposes on the user of the results the requirements that the median value of the repeatable value of the site term and its epistemic uncertainty must be properly incorporated in the analysis. Because the Hanford sites do not have sets of recorded ground motions to provide empirical data for assessing site-specific amplification terms, the assessment of site-specific amplifications must rely on site response analyses. The epistemic uncertainty in the shear-wave velocity and damping (including kappa effect) for the Saddle Mountains basalts and Ellensburg Formation interbeds has been captured through the uncertainty in the baserock motions, and through the alternative sets of dynamic properties presented in Section 9.6 and contained digitally in Appendix J.

As discussed in Sections 9.1.1 and 9.5.6, site response analyses, particularly 1-dimensional site response analyses, will not be able capture variability in site response at periods much longer that the fundamental period of the analysis profile. In addition, the potential presence of shallow basin effects at intermediate periods near 1 s introduces an additional component of variability that would not be captured by 1-dimensional site response analyses. To address these issues, the GMC TI Team identified in Section

9.5.6 a minimum level of uncertainty that should be applied in developing surface and near-surface motions from the baserock hazard. As discussed in Section 9.6.5, this uncertainty should be incorporated into the probabilistic convolution of the baserock motions to the surface in order to develop probabilistic soil hazard results consistent with the rock hazard and the uncertainty in site amplification. It is the GMC TI Team's assessment that the most appropriate method to achieve this is by applying Approach 3 as defined in McGuire et al. (2001) and illustrated in Bazzurro and Cornell (2004), and this is the approach recommended for application at the Hanford sites. An example of the application of Approach 3 to develop surface soil hazard curves is presented in Appendix K.

10.6 References

Bazzurro, P., and C.A. Cornell. 2004. Nonlinear Soil-Site Effects in Probabilistic Seismic-Hazard Analysis, *Bulletin of the Seismological Society of America*, v. 94, p. 2110–2123.

Campbell KW and Y Bozorgnia. 2014. NGA-West2 Ground Motion Model for the Average Horizontal Components of PGA, PGV, and 5%-Damped Linear Acceleration Response Spectra. *Earthquake Spectra* 30(3): 1087-1115.

Carlton, B., and N. Abrahamson, 2014, Issues and approaches for implementing conditional mean spectra in practice. *Bulletin of the Seismological Society of America*, v. 104, p. 503-512.

Chiou BS-J and RR Youngs. 2014. Update of the Chiou and Youngs NGA Ground Motion Model for Average Horizontal Component of Peak Ground Motion and Response Spectra. *Earthquake Spectra* 30(3):1117-1153.

Cornell CA. 1971. "Probabilistic analysis of damage to structures under seismic loads." In *Dynamic Waves in Civil Engineering*, DA Howells, IP Haigh, and C Taylor (eds.), John Wiley, London.

Cornell CA and EH Van Marke. 1969. The major influences on seismic risk. *Proceedings of the Third World Conference on Earthquake Engineering*, Santiago Chile, A-1:69−93.

DOE (U.S. Department of Energy). 2011. *Quality Assurance*. DOE Order 414.1D, Washington, D.C.

McGuire RK, WJ Silva, and CJ Costantino. 2001. *Technical Basis for Revision of Regulatory Guidance on Design Ground Motions: Hazard- and Risk-Consistent Ground Motion Spectra Guidelines*. NUREG/CR-6728, U.S. Nuclear Regulatory Commission, Washington, D.C.

Stock C and EG Smith. 2002. Adaptive kernel estimation and continuous probability representation of historical earthquake catalogs. *Bulletin of the Seismological Society of America* 92(3):904−912.

Silverman BW. 1986. *Density Estimation for Statistics and Data Analysis*. Chapman and Hall, London, England.

Uhrhammer RA. 1986. Characteristics of northern and central California seismicity (abs.). *Earthquake Notes* 57:21.

Table 10.1. Distance increment (dR) in km used for computing the distribution of downdip locations for fault ruptures.

Fault	dR [km]
Ahtanum Ridge-Rattlesnake Hills	0.5
Arlington	1.0
Cleman Mountain	1.0
Columbia Hills	1.0
Frenchman Hills	1.0
Horn Rapids Fault	0.5
Horse Heaven Hills	1.0
Laurel	1.0
Luna Butte	1.0
Manastash Ridge	1.0
Maupin	1.0
Rattles of the Rattlesnake-Wallula Alignment	0.5
Rattlesnake Mountain	0.5
Saddle Mountain	0.5
Seattle Fault	1.0
Selah Butte	1.0
Toppenish Ridge	1.0
Umtanum Ridge	0.5
Wallula Fault	1.0
Yakima Ridge	0.5

Table 10.2. Values of the initial smoothing distance *h* used for the crustal background sources and each of four declustered catalogs.

Source Zone and Catalog	Initial Smoothing Distance (*h*)
Zone B catalog 1	10
Zone B catalog 2	10
Zone B catalog 3	10
Zone B catalog 4	10
Zone D catalog 1	15
Zone D catalog 2	10
Zone D catalog 3	10
Zone D catalog 4	10
Zone YFTB catalog 1	15
Zone YFTB catalog 2	15
Zone YFTB catalog 3	10
Zone YFTB catalog 4	15

Table 10.3. Values of the initial smoothing distance *h* used for the alternative geometries of the Juan de Fuca slab source, two alternative catalogs each declustered applying four alternative methods.

Geometry	Catalog 1	Catalog 2	Catalog 3	Catalog 4	Alternative Catalog 1	Alternative Catalog 2	Alternative Catalog 3	Alternative Catalog 4
JPSE	30	30	30	30	30	30	30	30
JPSC	30	30	30	30	30	30	30	30
JPSW	30	30	30	30	30	25	20	20
JPDE80	15	15	15	15	20	20	15	20
JPDE90	15	15	15	15	15	15	15	20
JPDE00	15	15	15	15	15	15	15	20
JPDC80	20	20	20	20	20	20	20	20
JPDC90	20	20	20	20	20	20	20	20
JPDC00	20	20	20	20	20	20	20	20
JPDW80	20	20	20	20	25	20	20	25
JPDW90	20	20	20	20	20	20	20	20
JPDW00	20	20	20	20	20	20	20	20

Table 10.4. Simplified strike and dip model for the YFTB source zone used in the hazard calculations.

Style of Faulting	Strike	Dip	Dip Direction
Reverse	90˚ (100%)	50˚ (100%)	Random
Normal	90˚ (100%)	60˚ (100%)	Random
Strike Slip	60˚ (100%)	90˚ (100%)	Not applicable

Table 10.5. Percent differences between the PGA (in g) calculated with multiple rupture orientations and with single rupture orientation model for the YFTB zone at Site A.

AFE	Multiple Orientations	Single Orientation	% Difference
10^{-3}	0.0356	0.0355	-0.28%
10^{-4}	0.1454	0.1451	-0.21%
10^{-5}	0.3345	0.3339	-0.18%
10^{-6}	0.5774	0.5756	-0.31%
10^{-7}	0.8828	0.8779	-0.56%

Table 10.6. Input data for example variance calculation.

Level 1		Level 2		Overall Logic Tree		
Branch	Weight	Branch	Weight	Branch	Weight, w_i	Value, x_i
L1-A	0.4	L2-A	1.0	1	0.40	0.017
		L2-B	0.3	2	0.18	0.041
L1-B	0.6	L2-C	0.2	3	0.12	0.008
		L2-D	0.5	4	0.30	0.015

Table 10.7. Site coordinates.

Acronym	Site	Latitude	Longitude
A	200-East Area	46.554848	-119.517907
C	Columbia Generating Station	46.471667	-119.332778
B	200-West Area	46.552066	-119.625063
D	100BC Area	46.630378	-119.647486
E	300 Area	46.368604	-119.277461

Table 10.8. Uniform Hazard Response Spectra (UHRS) for Site A for annual frequencies of exceedance of 10^{-2}, 10^{-3}, 5×10^{-4}, 4×10^{-4}, 10^{-4}, 5×10^{-5}, 10^{-5}, 10^{-6}, and 10^{-7} (corresponding to return periods of 100, 1,000, 2,000, 2,500, 10,000, 20,000, 100,000, 1 million, and 10 million years).

Site A − Mean UHRS									
Period	10^{-2}	10^{-3}	5×10^{-4}	4×10^{-4}	10^{-4}	5×10^{-5}	10^{-5}	10^{-6}	10^{-7}
0.01	1.79E-02	1.17E-01	1.88E-01	2.17E-01	4.86E-01	6.91E-01	1.39E+00	3.12E+00	5.76E+00
0.02	2.20E-02	1.48E-01	2.42E-01	2.81E-01	6.39E-01	9.13E-01	1.81E+00	3.83E+00	6.96E+00
0.03	2.44E-02	1.69E-01	2.76E-01	3.20E-01	7.21E-01	1.02E+00	1.96E+00	3.99E+00	7.14E+00
0.04	2.60E-02	1.83E-01	2.98E-01	3.43E-01	7.63E-01	1.06E+00	2.01E+00	4.01E+00	7.12E+00
0.05	2.67E-02	1.91E-01	3.10E-01	3.56E-01	7.82E-01	1.07E+00	2.02E+00	3.99E+00	7.04E+00
0.075	2.69E-02	1.99E-01	3.21E-01	3.68E-01	7.91E-01	1.08E+00	1.98E+00	3.85E+00	6.75E+00
0.1	2.73E-02	2.00E-01	3.20E-01	3.66E-01	7.79E-01	1.06E+00	1.91E+00	3.70E+00	6.47E+00
0.15	2.72E-02	1.86E-01	2.97E-01	3.38E-01	7.04E-01	9.51E-01	1.70E+00	3.27E+00	5.66E+00
0.2	2.72E-02	1.74E-01	2.74E-01	3.13E-01	6.42E-01	8.67E-01	1.55E+00	2.98E+00	5.14E+00
0.3	2.53E-02	1.49E-01	2.31E-01	2.63E-01	5.35E-01	7.21E-01	1.28E+00	2.47E+00	4.26E+00
0.4	2.18E-02	1.24E-01	1.90E-01	2.16E-01	4.38E-01	5.92E-01	1.07E+00	2.07E+00	3.56E+00
0.5	1.87E-02	1.05E-01	1.58E-01	1.80E-01	3.65E-01	5.00E-01	9.02E-01	1.74E+00	3.06E+00
0.75	1.28E-02	7.08E-02	1.08E-01	1.22E-01	2.48E-01	3.36E-01	6.15E-01	1.20E+00	2.12E+00
1	9.52E-03	5.37E-02	8.01E-02	9.10E-02	1.81E-01	2.45E-01	4.46E-01	8.80E-01	1.51E+00
1.5	6.16E-03	3.69E-02	5.50E-02	6.15E-02	1.19E-01	1.57E-01	2.84E-01	5.51E-01	9.58E-01
2	4.49E-03	2.89E-02	4.26E-02	4.81E-02	9.04E-02	1.18E-01	2.10E-01	4.02E-01	7.00E-01
3	2.59E-03	1.92E-02	2.84E-02	3.18E-02	5.79E-02	7.49E-02	1.28E-01	2.44E-01	4.16E-01
5	1.33E-03	1.20E-02	1.80E-02	2.04E-02	3.67E-02	4.77E-02	8.04E-02	1.49E-01	2.54E-01
7.5	7.13E-04	8.11E-03	1.18E-02	1.31E-02	2.40E-02	3.10E-02	5.19E-02	9.76E-02	1.67E-01
10	4.38E-04	6.04E-03	8.95E-03	1.00E-02	1.77E-02	2.28E-02	3.78E-02	7.10E-02	1.21E-01
Site A − 5th percentile UHRS									
Period	10^{-2}	10^{-3}	5×10^{-4}	4×10^{-4}	10^{-4}	5×10^{-5}	10^{-5}	10^{-6}	10^{-7}
0.01	6.12E-03	3.57E-02	5.49E-02	6.23E-02	1.19E-01	1.54E-01	2.54E-01	4.29E-01	6.63E-01
0.02	6.18E-03	3.63E-02	5.56E-02	6.31E-02	1.20E-01	1.56E-01	2.59E-01	4.40E-01	6.79E-01
0.03	6.26E-03	3.76E-02	5.81E-02	6.62E-02	1.26E-01	1.66E-01	2.76E-01	4.72E-01	7.34E-01
0.04	6.64E-03	4.09E-02	6.30E-02	7.18E-02	1.37E-01	1.82E-01	3.03E-01	5.21E-01	8.09E-01
0.05	7.14E-03	4.49E-02	6.99E-02	7.96E-02	1.52E-01	2.05E-01	3.33E-01	5.80E-01	9.09E-01
0.075	8.87E-03	5.64E-02	8.88E-02	1.02E-01	2.04E-01	2.65E-01	4.42E-01	7.79E-01	1.22E+00
0.1	1.04E-02	6.79E-02	1.08E-01	1.22E-01	2.47E-01	3.27E-01	5.48E-01	9.60E-01	1.52E+00
0.15	1.27E-02	8.20E-02	1.29E-01	1.47E-01	3.03E-01	3.93E-01	6.64E-01	1.17E+00	1.85E+00
0.2	1.38E-02	8.62E-02	1.34E-01	1.53E-01	3.14E-01	4.11E-01	6.99E-01	1.23E+00	1.95E+00
0.3	1.37E-02	7.94E-02	1.23E-01	1.40E-01	2.90E-01	3.81E-01	6.51E-01	1.15E+00	1.81E+00
0.4	1.22E-02	6.72E-02	1.04E-01	1.18E-01	2.48E-01	3.31E-01	5.65E-01	1.01E+00	1.59E+00
0.5	1.08E-02	5.69E-02	8.79E-02	1.01E-01	2.12E-01	2.86E-01	4.92E-01	8.73E-01	1.35E+00
0.75	7.58E-03	3.89E-02	5.95E-02	6.78E-02	1.41E-01	1.98E-01	3.41E-01	6.17E-01	9.83E-01
1	5.52E-03	2.91E-02	4.38E-02	4.99E-02	1.05E-01	1.40E-01	2.52E-01	4.53E-01	7.18E-01
1.5	3.53E-03	1.94E-02	2.89E-02	3.27E-02	6.64E-02	9.11E-02	1.57E-01	2.89E-01	4.52E-01
2	2.50E-03	1.47E-02	2.19E-02	2.47E-02	5.00E-02	6.58E-02	1.16E-01	2.13E-01	3.33E-01
3	1.36E-03	9.58E-03	1.39E-02	1.56E-02	3.09E-02	4.08E-02	6.93E-02	1.25E-01	2.01E-01
5	6.37E-04	5.85E-03	8.52E-03	9.53E-03	1.80E-02	2.38E-02	4.04E-02	7.30E-02	1.14E-01
7.5	2.92E-04	3.67E-03	5.40E-03	6.01E-03	1.10E-02	1.41E-02	2.40E-02	4.26E-02	6.78E-02
10	1.59E-04	2.71E-03	3.90E-03	4.35E-03	7.89E-03	1.01E-02	1.65E-02	2.97E-02	4.65E-02

Table 10.8. (contd)

Site A − 16th percentile UHRS									
Period	10^{-2}	10^{-3}	5×10^{-4}	4×10^{-4}	10^{-4}	5×10^{-5}	10^{-5}	10^{-6}	10^{-7}
0.01	8.28E-03	4.70E-02	7.20E-02	8.16E-02	1.56E-01	2.08E-01	3.36E-01	5.75E-01	8.93E-01
0.02	8.48E-03	4.85E-02	7.41E-02	8.37E-02	1.59E-01	2.11E-01	3.43E-01	5.91E-01	9.21E-01
0.03	8.87E-03	5.15E-02	7.91E-02	8.98E-02	1.74E-01	2.29E-01	3.74E-01	6.52E-01	1.03E+00
0.04	9.75E-03	5.72E-02	8.85E-02	1.01E-01	2.00E-01	2.59E-01	4.26E-01	7.50E-01	1.16E+00
0.05	1.06E-02	6.52E-02	1.01E-01	1.14E-01	2.25E-01	2.98E-01	4.93E-01	8.57E-01	1.33E+00
0.075	1.27E-02	8.20E-02	1.28E-01	1.46E-01	3.00E-01	3.88E-01	6.52E-01	1.15E+00	1.83E+00
0.1	1.45E-02	9.66E-02	1.50E-01	1.73E-01	3.48E-01	4.60E-01	7.78E-01	1.37E+00	2.18E+00
0.15	1.66E-02	1.08E-01	1.70E-01	1.96E-01	3.91E-01	5.25E-01	8.83E-01	1.57E+00	2.48E+00
0.2	1.78E-02	1.09E-01	1.70E-01	1.96E-01	3.95E-01	5.29E-01	8.93E-01	1.58E+00	2.50E+00
0.3	1.72E-02	1.00E-01	1.53E-01	1.76E-01	3.53E-01	4.72E-01	8.05E-01	1.44E+00	2.28E+00
0.4	1.49E-02	8.31E-02	1.28E-01	1.46E-01	3.03E-01	3.98E-01	6.89E-01	1.23E+00	1.97E+00
0.5	1.29E-02	6.92E-02	1.07E-01	1.21E-01	2.55E-01	3.41E-01	5.90E-01	1.06E+00	1.69E+00
0.75	9.20E-03	4.71E-02	7.18E-02	8.21E-02	1.72E-01	2.34E-01	4.09E-01	7.54E-01	1.19E+00
1	6.71E-03	3.51E-02	5.34E-02	6.05E-02	1.24E-01	1.70E-01	3.04E-01	5.49E-01	8.79E-01
1.5	4.32E-03	2.35E-02	3.50E-02	3.96E-02	8.00E-02	1.09E-01	1.92E-01	3.46E-01	5.53E-01
2	3.14E-03	1.79E-02	2.65E-02	2.99E-02	5.90E-02	7.92E-02	1.38E-01	2.55E-01	4.04E-01
3	1.71E-03	1.15E-02	1.68E-02	1.90E-02	3.65E-02	4.91E-02	8.35E-02	1.50E-01	2.44E-01
5	8.41E-04	7.18E-03	1.04E-02	1.16E-02	2.17E-02	2.87E-02	4.96E-02	8.94E-02	1.41E-01
7.5	4.09E-04	4.58E-03	6.67E-03	7.48E-03	1.33E-02	1.75E-02	3.00E-02	5.36E-02	8.60E-02
10	2.33E-04	3.40E-03	4.94E-03	5.47E-03	9.73E-03	1.23E-02	2.08E-02	3.68E-02	5.92E-02
Site A − 50th percentile UHRS									
Period	10^{-2}	10^{-3}	5×10^{-4}	4×10^{-4}	10^{-4}	5×10^{-5}	10^{-5}	10^{-6}	10^{-7}
0.01	1.34E-02	7.72E-02	1.16E-01	1.32E-01	2.61E-01	3.39E-01	5.60E-01	9.75E-01	1.49E+00
0.02	1.45E-02	8.34E-02	1.26E-01	1.43E-01	2.85E-01	3.67E-01	6.09E-01	1.06E+00	1.66E+00
0.03	1.63E-02	9.84E-02	1.50E-01	1.71E-01	3.37E-01	4.41E-01	7.40E-01	1.27E+00	2.05E+00
0.04	1.88E-02	1.18E-01	1.86E-01	2.12E-01	4.13E-01	5.45E-01	9.07E-01	1.56E+00	2.51E+00
0.05	2.10E-02	1.35E-01	2.14E-01	2.44E-01	4.89E-01	6.34E-01	1.06E+00	1.86E+00	2.99E+00
0.075	2.37E-02	1.61E-01	2.56E-01	2.95E-01	5.89E-01	7.81E-01	1.30E+00	2.31E+00	3.66E+00
0.1	2.48E-02	1.71E-01	2.75E-01	3.15E-01	6.28E-01	8.31E-01	1.40E+00	2.48E+00	3.95E+00
0.15	2.53E-02	1.67E-01	2.64E-01	3.03E-01	6.09E-01	8.10E-01	1.37E+00	2.44E+00	3.92E+00
0.2	2.57E-02	1.58E-01	2.49E-01	2.86E-01	5.72E-01	7.63E-01	1.29E+00	2.32E+00	3.74E+00
0.3	2.39E-02	1.38E-01	2.14E-01	2.43E-01	4.89E-01	6.44E-01	1.11E+00	2.02E+00	3.25E+00
0.4	2.08E-02	1.15E-01	1.74E-01	1.99E-01	4.02E-01	5.40E-01	9.32E-01	1.70E+00	2.76E+00
0.5	1.76E-02	9.70E-02	1.45E-01	1.66E-01	3.38E-01	4.54E-01	7.97E-01	1.43E+00	2.37E+00
0.75	1.22E-02	6.51E-02	9.88E-02	1.12E-01	2.29E-01	3.10E-01	5.46E-01	1.01E+00	1.64E+00
1	9.14E-03	4.86E-02	7.22E-02	8.20E-02	1.65E-01	2.25E-01	3.94E-01	7.41E-01	1.19E+00
1.5	5.91E-03	3.28E-02	4.82E-02	5.42E-02	1.08E-01	1.42E-01	2.52E-01	4.64E-01	7.60E-01
2	4.29E-03	2.50E-02	3.65E-02	4.11E-02	7.94E-02	1.07E-01	1.85E-01	3.39E-01	5.54E-01
3	2.45E-03	1.62E-02	2.37E-02	2.64E-02	5.00E-02	6.43E-02	1.11E-01	2.05E-01	3.31E-01
5	1.25E-03	1.05E-02	1.47E-02	1.64E-02	3.03E-02	3.91E-02	6.69E-02	1.20E-01	1.99E-01
7.5	6.60E-04	6.92E-03	9.90E-03	1.09E-02	1.94E-02	2.49E-02	4.15E-02	7.58E-02	1.21E-01
10	4.07E-04	5.24E-03	7.42E-03	8.18E-03	1.40E-02	1.80E-02	2.98E-02	5.31E-02	8.60E-02

Table 10.8. (contd)

Site A − 84th percentile UHRS									
Period	10^{-2}	10^{-3}	5×10^{-4}	4×10^{-4}	10^{-4}	5×10^{-5}	10^{-5}	10^{-6}	10^{-7}
0.01	2.75E-02	1.62E-01	2.54E-01	2.91E-01	5.71E-01	7.56E-01	1.21E+00	2.14E+00	3.34E+00
0.02	3.95E-02	2.43E-01	3.80E-01	4.34E-01	8.66E-01	1.12E+00	1.85E+00	3.21E+00	5.06E+00
0.03	4.51E-02	2.90E-01	4.52E-01	5.17E-01	1.02E+00	1.31E+00	2.22E+00	3.84E+00	6.07E+00
0.04	4.69E-02	3.09E-01	4.86E-01	5.52E-01	1.09E+00	1.40E+00	2.37E+00	4.12E+00	6.57E+00
0.05	4.68E-02	3.14E-01	4.93E-01	5.61E-01	1.11E+00	1.43E+00	2.43E+00	4.27E+00	6.83E+00
0.075	4.34E-02	3.05E-01	4.86E-01	5.52E-01	1.10E+00	1.45E+00	2.40E+00	4.26E+00	6.90E+00
0.1	4.14E-02	2.95E-01	4.59E-01	5.25E-01	1.06E+00	1.38E+00	2.32E+00	4.14E+00	6.77E+00
0.15	3.82E-02	2.55E-01	3.99E-01	4.58E-01	9.15E-01	1.20E+00	2.06E+00	3.68E+00	6.05E+00
0.2	3.74E-02	2.30E-01	3.58E-01	4.08E-01	8.20E-01	1.09E+00	1.86E+00	3.37E+00	5.54E+00
0.3	3.34E-02	1.94E-01	2.96E-01	3.34E-01	6.67E-01	8.91E-01	1.54E+00	2.83E+00	4.67E+00
0.4	2.83E-02	1.58E-01	2.41E-01	2.73E-01	5.47E-01	7.36E-01	1.27E+00	2.35E+00	3.88E+00
0.5	2.43E-02	1.32E-01	2.00E-01	2.26E-01	4.52E-01	6.07E-01	1.07E+00	2.02E+00	3.33E+00
0.75	1.68E-02	9.04E-02	1.34E-01	1.51E-01	3.06E-01	4.11E-01	7.44E-01	1.37E+00	2.32E+00
1	1.23E-02	6.75E-02	1.00E-01	1.12E-01	2.23E-01	3.00E-01	5.36E-01	1.01E+00	1.66E+00
1.5	8.12E-03	4.80E-02	6.80E-02	7.60E-02	1.43E-01	1.92E-01	3.36E-01	6.30E-01	1.04E+00
2	5.91E-03	3.73E-02	5.33E-02	5.89E-02	1.08E-01	1.41E-01	2.48E-01	4.63E-01	7.67E-01
3	3.52E-03	2.54E-02	3.56E-02	3.92E-02	6.83E-02	8.87E-02	1.49E-01	2.77E-01	4.56E-01
5	1.88E-03	1.62E-02	2.31E-02	2.54E-02	4.35E-02	5.57E-02	9.32E-02	1.68E-01	2.73E-01
7.5	1.04E-03	1.10E-02	1.51E-02	1.67E-02	2.88E-02	3.62E-02	5.98E-02	1.09E-01	1.78E-01
10	6.80E-04	8.35E-03	1.15E-02	1.25E-02	2.13E-02	2.68E-02	4.36E-02	7.90E-02	1.27E-01
Site A − 95th percentile UHRS									
Period	10^{-2}	10^{-3}	5×10^{-4}	4×10^{-4}	10^{-4}	5×10^{-5}	10^{-5}	10^{-6}	10^{-7}
0.01	5.30E-02	3.23E-01	5.07E-01	5.73E-01	1.12E+00	1.45E+00	2.44E+00	4.20E+00	6.60E+00
0.02	6.92E-02	4.26E-01	6.69E-01	7.67E-01	1.46E+00	1.96E+00	3.23E+00	5.61E+00	8.87E+00
0.03	7.19E-02	4.60E-01	7.19E-01	8.16E-01	1.56E+00	2.08E+00	3.41E+00	6.00E+00	9.57E+00
0.04	7.03E-02	4.60E-01	7.19E-01	8.16E-01	1.56E+00	2.08E+00	3.43E+00	6.06E+00	9.77E+00
0.05	6.70E-02	4.53E-01	7.00E-01	7.96E-01	1.52E+00	2.05E+00	3.37E+00	6.01E+00	9.77E+00
0.075	5.98E-02	4.19E-01	6.53E-01	7.48E-01	1.47E+00	1.92E+00	3.21E+00	5.75E+00	9.41E+00
0.1	5.59E-02	3.90E-01	6.09E-01	6.97E-01	1.37E+00	1.80E+00	3.06E+00	5.51E+00	9.03E+00
0.15	5.00E-02	3.32E-01	5.14E-01	5.83E-01	1.16E+00	1.54E+00	2.61E+00	4.77E+00	7.88E+00
0.2	4.78E-02	2.95E-01	4.53E-01	5.17E-01	1.03E+00	1.36E+00	2.32E+00	4.25E+00	7.07E+00
0.3	4.20E-02	2.38E-01	3.61E-01	4.10E-01	8.23E-01	1.10E+00	1.90E+00	3.51E+00	5.87E+00
0.4	3.56E-02	1.94E-01	2.92E-01	3.31E-01	6.67E-01	8.95E-01	1.57E+00	2.95E+00	4.92E+00
0.5	2.97E-02	1.62E-01	2.42E-01	2.74E-01	5.53E-01	7.51E-01	1.30E+00	2.49E+00	4.17E+00
0.75	2.04E-02	1.12E-01	1.64E-01	1.85E-01	3.67E-01	5.05E-01	9.06E-01	1.71E+00	2.91E+00
1	1.51E-02	8.50E-02	1.23E-01	1.37E-01	2.67E-01	3.59E-01	6.54E-01	1.23E+00	2.10E+00
1.5	1.00E-02	6.08E-02	8.62E-02	9.64E-02	1.76E-01	2.33E-01	4.08E-01	7.79E-01	1.29E+00
2	7.35E-03	4.93E-02	6.76E-02	7.47E-02	1.33E-01	1.74E-01	3.04E-01	5.67E-01	9.52E-01
3	4.37E-03	3.39E-02	4.74E-02	5.21E-02	8.72E-02	1.11E-01	1.85E-01	3.40E-01	5.66E-01
5	2.41E-03	2.24E-02	3.11E-02	3.39E-02	5.65E-02	7.11E-02	1.16E-01	2.12E-01	3.44E-01
7.5	1.41E-03	1.45E-02	2.08E-02	2.26E-02	3.74E-02	4.71E-02	7.69E-02	1.38E-01	2.28E-01
10	9.30E-04	1.11E-02	1.52E-02	1.69E-02	2.84E-02	3.53E-02	5.66E-02	1.02E-01	1.67E-01

Table 10.9. Uniform Hazard Response Spectra (UHRS) for Site C for annual frequencies of exceedance of 10^{-2}, 10^{-3}, 5×10^{-4}, 4×10^{-4}, 10^{-4}, 5×10^{-5}, 10^{-5}, 10^{-6}, and 10^{-7} (corresponding to return periods of 100, 1,000, 2,000, 2,500, 10,000, 20,000, 100,000, 1 million, and 10 million years).

Site C − Mean UHRS									
Period	10^{-2}	10^{-3}	5×10^{-4}	4×10^{-4}	10^{-4}	5×10^{-5}	10^{-5}	10^{-6}	10^{-7}
0.01	2.08E-02	1.45E-01	2.38E-01	2.76E-01	6.37E-01	9.18E-01	1.87E+00	4.13E+00	7.86E+00
0.02	2.56E-02	1.79E-01	2.95E-01	3.41E-01	7.82E-01	1.09E+00	2.14E+00	4.49E+00	8.23E+00
0.03	2.70E-02	1.93E-01	3.15E-01	3.64E-01	8.19E-01	1.13E+00	2.17E+00	4.47E+00	8.09E+00
0.04	2.77E-02	2.00E-01	3.25E-01	3.75E-01	8.27E-01	1.13E+00	2.15E+00	4.37E+00	7.88E+00
0.05	2.76E-02	2.02E-01	3.27E-01	3.77E-01	8.21E-01	1.12E+00	2.10E+00	4.25E+00	7.66E+00
0.075	2.68E-02	2.03E-01	3.27E-01	3.74E-01	7.98E-01	1.08E+00	2.00E+00	4.00E+00	7.19E+00
0.1	2.62E-02	1.96E-01	3.14E-01	3.58E-01	7.54E-01	1.02E+00	1.85E+00	3.69E+00	6.60E+00
0.15	2.54E-02	1.75E-01	2.80E-01	3.20E-01	6.53E-01	8.81E-01	1.59E+00	3.15E+00	5.58E+00
0.2	2.53E-02	1.62E-01	2.55E-01	2.92E-01	5.88E-01	7.93E-01	1.42E+00	2.81E+00	4.98E+00
0.3	2.34E-02	1.38E-01	2.13E-01	2.41E-01	4.83E-01	6.44E-01	1.16E+00	2.29E+00	4.05E+00
0.4	2.02E-02	1.14E-01	1.73E-01	1.97E-01	3.87E-01	5.23E-01	9.41E-01	1.87E+00	3.31E+00
0.5	1.72E-02	9.62E-02	1.43E-01	1.62E-01	3.22E-01	4.30E-01	7.80E-01	1.53E+00	2.76E+00
0.75	1.18E-02	6.47E-02	9.80E-02	1.10E-01	2.14E-01	2.86E-01	5.15E-01	1.03E+00	1.83E+00
1	8.78E-03	4.94E-02	7.19E-02	8.11E-02	1.54E-01	2.07E-01	3.64E-01	7.28E-01	1.28E+00
1.5	5.75E-03	3.39E-02	5.02E-02	5.56E-02	1.03E-01	1.32E-01	2.30E-01	4.43E-01	7.79E-01
2	4.19E-03	2.64E-02	3.85E-02	4.32E-02	7.76E-02	1.02E-01	1.70E-01	3.23E-01	5.59E-01
3	2.49E-03	1.81E-02	2.66E-02	2.99E-02	5.29E-02	6.66E-02	1.11E-01	2.05E-01	3.46E-01
5	1.29E-03	1.16E-02	1.70E-02	1.93E-02	3.40E-02	4.33E-02	7.14E-02	1.28E-01	2.17E-01
7.5	6.90E-04	7.77E-03	1.12E-02	1.24E-02	2.24E-02	2.85E-02	4.65E-02	8.45E-02	1.40E-01
10	4.21E-04	5.77E-03	8.52E-03	9.51E-03	1.65E-02	2.13E-02	3.45E-02	6.26E-02	1.05E-01
Site C − 5th percentile UHRS									
Period	10^{-2}	10^{-3}	5×10^{-4}	4×10^{-4}	10^{-4}	5×10^{-5}	10^{-5}	10^{-6}	10^{-7}
0.01	5.78E-03	3.36E-02	5.13E-02	5.78E-02	1.09E-01	1.39E-01	2.34E-01	4.12E-01	6.58E-01
0.02	5.91E-03	3.46E-02	5.26E-02	5.92E-02	1.11E-01	1.42E-01	2.39E-01	4.24E-01	6.78E-01
0.03	6.07E-03	3.65E-02	5.59E-02	6.30E-02	1.19E-01	1.54E-01	2.60E-01	4.65E-01	7.50E-01
0.04	6.44E-03	3.99E-02	6.09E-02	6.91E-02	1.30E-01	1.70E-01	2.90E-01	5.20E-01	8.35E-01
0.05	6.97E-03	4.42E-02	6.81E-02	7.76E-02	1.45E-01	1.93E-01	3.23E-01	5.84E-01	9.51E-01
0.075	8.66E-03	5.54E-02	8.64E-02	9.97E-02	1.94E-01	2.53E-01	4.28E-01	7.90E-01	1.28E+00
0.1	1.00E-02	6.54E-02	1.04E-01	1.17E-01	2.33E-01	3.07E-01	5.20E-01	9.51E-01	1.55E+00
0.15	1.19E-02	7.68E-02	1.20E-01	1.36E-01	2.73E-01	3.57E-01	6.10E-01	1.12E+00	1.83E+00
0.2	1.29E-02	7.90E-02	1.22E-01	1.39E-01	2.79E-01	3.65E-01	6.27E-01	1.15E+00	1.88E+00
0.3	1.28E-02	7.29E-02	1.12E-01	1.27E-01	2.54E-01	3.34E-01	5.71E-01	1.05E+00	1.71E+00
0.4	1.14E-02	6.12E-02	9.45E-02	1.07E-01	2.14E-01	2.84E-01	4.89E-01	8.95E-01	1.46E+00
0.5	1.00E-02	5.21E-02	7.91E-02	9.05E-02	1.79E-01	2.39E-01	4.10E-01	7.66E-01	1.23E+00
0.75	7.00E-03	3.50E-02	5.33E-02	6.00E-02	1.20E-01	1.59E-01	2.83E-01	5.21E-01	8.54E-01
1	5.20E-03	2.62E-02	3.90E-02	4.43E-02	8.76E-02	1.16E-01	2.04E-01	3.71E-01	6.08E-01
1.5	3.35E-03	1.77E-02	2.61E-02	2.95E-02	5.61E-02	7.33E-02	1.25E-01	2.31E-01	3.72E-01
2	2.30E-03	1.34E-02	1.98E-02	2.21E-02	4.19E-02	5.48E-02	9.34E-02	1.66E-01	2.70E-01
3	1.32E-03	8.95E-03	1.29E-02	1.44E-02	2.68E-02	3.45E-02	5.70E-02	1.03E-01	1.62E-01
5	6.22E-04	5.53E-03	8.02E-03	8.93E-03	1.58E-02	2.06E-02	3.34E-02	5.90E-02	9.44E-02
7.5	2.85E-04	3.48E-03	5.06E-03	5.58E-03	9.91E-03	1.23E-02	2.02E-02	3.50E-02	5.54E-02
10	1.57E-04	2.55E-03	3.64E-03	4.03E-03	7.06E-03	8.89E-03	1.39E-02	2.44E-02	3.82E-02

Table 10.9. (contd)

Site C − 16th percentile UHRS									
Period	10^{-2}	10^{-3}	5×10^{-4}	4×10^{-4}	10^{-4}	5×10^{-5}	10^{-5}	10^{-6}	10^{-7}
0.01	7.75E-03	4.50E-02	6.83E-02	7.75E-02	1.42E-01	1.88E-01	3.13E-01	5.57E-01	8.93E-01
0.02	8.09E-03	4.63E-02	7.02E-02	7.94E-02	1.47E-01	1.95E-01	3.25E-01	5.79E-01	9.32E-01
0.03	8.66E-03	5.07E-02	7.80E-02	8.80E-02	1.65E-01	2.18E-01	3.63E-01	6.56E-01	1.06E+00
0.04	9.75E-03	5.72E-02	8.85E-02	1.01E-01	1.94E-01	2.51E-01	4.21E-01	7.69E-01	1.22E+00
0.05	1.06E-02	6.52E-02	1.01E-01	1.13E-01	2.21E-01	2.92E-01	4.93E-01	8.92E-01	1.43E+00
0.075	1.25E-02	8.20E-02	1.28E-01	1.46E-01	2.94E-01	3.81E-01	6.52E-01	1.19E+00	1.96E+00
0.1	1.40E-02	9.35E-02	1.45E-01	1.66E-01	3.32E-01	4.36E-01	7.50E-01	1.37E+00	2.25E+00
0.15	1.55E-02	1.01E-01	1.57E-01	1.80E-01	3.56E-01	4.73E-01	8.13E-01	1.50E+00	2.44E+00
0.2	1.64E-02	1.03E-01	1.56E-01	1.78E-01	3.52E-01	4.68E-01	8.02E-01	1.48E+00	2.42E+00
0.3	1.58E-02	9.10E-02	1.38E-01	1.57E-01	3.14E-01	4.09E-01	7.07E-01	1.30E+00	2.16E+00
0.4	1.39E-02	7.56E-02	1.15E-01	1.30E-01	2.60E-01	3.43E-01	5.91E-01	1.10E+00	1.82E+00
0.5	1.19E-02	6.30E-02	9.73E-02	1.10E-01	2.18E-01	2.89E-01	5.03E-01	9.33E-01	1.52E+00
0.75	8.45E-03	4.26E-02	6.42E-02	7.29E-02	1.44E-01	1.96E-01	3.39E-01	6.31E-01	1.05E+00
1	6.22E-03	3.17E-02	4.74E-02	5.35E-02	1.06E-01	1.38E-01	2.43E-01	4.53E-01	7.53E-01
1.5	4.06E-03	2.14E-02	3.15E-02	3.52E-02	6.67E-02	8.92E-02	1.51E-01	2.82E-01	4.59E-01
2	2.91E-03	1.62E-02	2.37E-02	2.66E-02	5.04E-02	6.46E-02	1.11E-01	2.05E-01	3.31E-01
3	1.66E-03	1.09E-02	1.55E-02	1.73E-02	3.18E-02	4.09E-02	6.77E-02	1.23E-01	2.02E-01
5	8.12E-04	6.82E-03	9.78E-03	1.08E-02	1.92E-02	2.46E-02	4.03E-02	7.25E-02	1.15E-01
7.5	3.93E-04	4.34E-03	6.23E-03	6.93E-03	1.19E-02	1.50E-02	2.47E-02	4.33E-02	6.97E-02
10	2.28E-04	3.22E-03	4.61E-03	5.13E-03	8.73E-03	1.09E-02	1.73E-02	3.06E-02	4.86E-02
Site C − 50th percentile UHRS									
Period	10^{-2}	10^{-3}	5×10^{-4}	4×10^{-4}	10^{-4}	5×10^{-5}	10^{-5}	10^{-6}	10^{-7}
0.01	1.34E-02	7.72E-02	1.16E-01	1.30E-01	2.51E-01	3.27E-01	5.50E-01	9.94E-01	1.58E+00
0.02	1.45E-02	8.46E-02	1.26E-01	1.42E-01	2.74E-01	3.55E-01	5.98E-01	1.08E+00	1.74E+00
0.03	1.64E-02	1.03E-01	1.55E-01	1.76E-01	3.39E-01	4.42E-01	7.50E-01	1.33E+00	2.21E+00
0.04	1.93E-02	1.23E-01	1.94E-01	2.19E-01	4.16E-01	5.47E-01	9.27E-01	1.67E+00	2.76E+00
0.05	2.13E-02	1.40E-01	2.22E-01	2.51E-01	4.89E-01	6.37E-01	1.08E+00	1.98E+00	3.23E+00
0.075	2.37E-02	1.63E-01	2.60E-01	2.99E-01	5.81E-01	7.69E-01	1.30E+00	2.39E+00	3.92E+00
0.1	2.38E-02	1.66E-01	2.64E-01	3.03E-01	5.95E-01	7.89E-01	1.34E+00	2.47E+00	4.07E+00
0.15	2.37E-02	1.56E-01	2.47E-01	2.83E-01	5.55E-01	7.37E-01	1.26E+00	2.33E+00	3.86E+00
0.2	2.40E-02	1.47E-01	2.29E-01	2.61E-01	5.18E-01	6.80E-01	1.17E+00	2.18E+00	3.62E+00
0.3	2.25E-02	1.27E-01	1.95E-01	2.20E-01	4.29E-01	5.68E-01	9.92E-01	1.86E+00	3.09E+00
0.4	1.92E-02	1.05E-01	1.58E-01	1.79E-01	3.49E-01	4.64E-01	8.10E-01	1.53E+00	2.56E+00
0.5	1.62E-02	8.76E-02	1.31E-01	1.48E-01	2.94E-01	3.84E-01	6.75E-01	1.26E+00	2.15E+00
0.75	1.13E-02	5.95E-02	8.88E-02	1.01E-01	1.96E-01	2.58E-01	4.52E-01	8.61E-01	1.43E+00
1	8.41E-03	4.42E-02	6.46E-02	7.27E-02	1.39E-01	1.87E-01	3.23E-01	6.11E-01	1.03E+00
1.5	5.54E-03	3.00E-02	4.33E-02	4.87E-02	9.03E-02	1.17E-01	2.04E-01	3.75E-01	6.25E-01
2	4.02E-03	2.29E-02	3.28E-02	3.66E-02	6.67E-02	8.74E-02	1.46E-01	2.74E-01	4.50E-01
3	2.38E-03	1.52E-02	2.20E-02	2.44E-02	4.33E-02	5.54E-02	9.23E-02	1.66E-01	2.74E-01
5	1.23E-03	1.01E-02	1.39E-02	1.53E-02	2.71E-02	3.42E-02	5.59E-02	1.00E-01	1.61E-01
7.5	6.37E-04	6.58E-03	9.29E-03	1.02E-02	1.73E-02	2.19E-02	3.49E-02	6.19E-02	1.01E-01
10	3.90E-04	5.00E-03	6.95E-03	7.69E-03	1.26E-02	1.58E-02	2.53E-02	4.42E-02	7.13E-02

Table 10.9. (contd)

Site C − 84th percentile UHRS									
Period	10^{-2}	10^{-3}	5×10^{-4}	4×10^{-4}	10^{-4}	5×10^{-5}	10^{-5}	10^{-6}	10^{-7}
0.01	3.68E-02	2.27E-01	3.50E-01	3.96E-01	7.70E-01	1.00E+00	1.65E+00	3.01E+00	4.84E+00
0.02	5.10E-02	3.18E-01	4.94E-01	5.57E-01	1.07E+00	1.37E+00	2.34E+00	4.19E+00	6.78E+00
0.03	5.33E-02	3.43E-01	5.33E-01	6.03E-01	1.16E+00	1.50E+00	2.55E+00	4.62E+00	7.56E+00
0.04	5.22E-02	3.45E-01	5.40E-01	6.11E-01	1.17E+00	1.52E+00	2.60E+00	4.75E+00	7.77E+00
0.05	5.00E-02	3.38E-01	5.27E-01	5.95E-01	1.15E+00	1.49E+00	2.57E+00	4.69E+00	7.74E+00
0.075	4.33E-02	3.14E-01	4.93E-01	5.59E-01	1.09E+00	1.44E+00	2.44E+00	4.48E+00	7.50E+00
0.1	3.95E-02	2.90E-01	4.52E-01	5.17E-01	1.01E+00	1.32E+00	2.25E+00	4.16E+00	6.97E+00
0.15	3.55E-02	2.43E-01	3.78E-01	4.30E-01	8.41E-01	1.11E+00	1.92E+00	3.56E+00	5.98E+00
0.2	3.42E-02	2.18E-01	3.33E-01	3.77E-01	7.50E-01	9.92E-01	1.70E+00	3.20E+00	5.39E+00
0.3	3.10E-02	1.80E-01	2.73E-01	3.10E-01	6.01E-01	7.96E-01	1.38E+00	2.62E+00	4.45E+00
0.4	2.61E-02	1.46E-01	2.21E-01	2.49E-01	4.84E-01	6.38E-01	1.12E+00	2.14E+00	3.63E+00
0.5	2.25E-02	1.22E-01	1.82E-01	2.06E-01	3.93E-01	5.27E-01	9.29E-01	1.77E+00	3.06E+00
0.75	1.55E-02	8.24E-02	1.21E-01	1.35E-01	2.61E-01	3.45E-01	6.12E-01	1.17E+00	2.04E+00
1	1.13E-02	6.25E-02	9.07E-02	1.02E-01	1.90E-01	2.50E-01	4.34E-01	8.37E-01	1.41E+00
1.5	7.58E-03	4.39E-02	6.16E-02	6.80E-02	1.22E-01	1.58E-01	2.71E-01	5.14E-01	8.64E-01
2	5.50E-03	3.45E-02	4.89E-02	5.37E-02	9.30E-02	1.18E-01	2.01E-01	3.68E-01	6.20E-01
3	3.41E-03	2.42E-02	3.36E-02	3.67E-02	6.14E-02	7.72E-02	1.25E-01	2.29E-01	3.77E-01
5	1.82E-03	1.56E-02	2.22E-02	2.43E-02	4.01E-02	5.04E-02	7.96E-02	1.39E-01	2.29E-01
7.5	1.00E-03	1.06E-02	1.44E-02	1.58E-02	2.65E-02	3.29E-02	5.18E-02	9.13E-02	1.46E-01
10	6.55E-04	8.10E-03	1.10E-02	1.19E-02	2.00E-02	2.46E-02	3.83E-02	6.68E-02	1.08E-01
Site C − 95th percentile UHRS									
Period	10^{-2}	10^{-3}	5×10^{-4}	4×10^{-4}	10^{-4}	5×10^{-5}	10^{-5}	10^{-6}	10^{-7}
0.01	7.19E-02	4.47E-01	6.91E-01	7.86E-01	1.48E+00	1.96E+00	3.27E+00	5.87E+00	9.55E+00
0.02	8.31E-02	5.22E-01	8.02E-01	9.10E-01	1.72E+00	2.26E+00	3.75E+00	6.82E+00	1.10E+01
0.03	7.98E-02	5.22E-01	7.99E-01	9.02E-01	1.70E+00	2.24E+00	3.73E+00	6.85E+00	1.12E+01
0.04	7.50E-02	5.07E-01	7.70E-01	8.69E-01	1.64E+00	2.17E+00	3.64E+00	6.67E+00	1.10E+01
0.05	7.01E-02	4.83E-01	7.41E-01	8.37E-01	1.57E+00	2.08E+00	3.52E+00	6.49E+00	1.07E+01
0.075	6.01E-02	4.31E-01	6.72E-01	7.66E-01	1.47E+00	1.93E+00	3.27E+00	6.06E+00	1.02E+01
0.1	5.47E-02	3.87E-01	6.01E-01	6.83E-01	1.32E+00	1.74E+00	2.98E+00	5.54E+00	9.33E+00
0.15	4.65E-02	3.23E-01	5.01E-01	5.62E-01	1.09E+00	1.43E+00	2.46E+00	4.62E+00	7.82E+00
0.2	4.45E-02	2.81E-01	4.30E-01	4.92E-01	9.52E-01	1.25E+00	2.16E+00	4.06E+00	6.92E+00
0.3	3.91E-02	2.25E-01	3.40E-01	3.84E-01	7.57E-01	1.00E+00	1.73E+00	3.30E+00	5.65E+00
0.4	3.26E-02	1.80E-01	2.71E-01	3.06E-01	5.97E-01	7.98E-01	1.40E+00	2.67E+00	4.60E+00
0.5	2.77E-02	1.49E-01	2.24E-01	2.52E-01	4.89E-01	6.48E-01	1.14E+00	2.22E+00	3.81E+00
0.75	1.92E-02	1.04E-01	1.49E-01	1.67E-01	3.20E-01	4.23E-01	7.61E-01	1.45E+00	2.55E+00
1	1.41E-02	7.74E-02	1.11E-01	1.24E-01	2.30E-01	3.03E-01	5.33E-01	1.03E+00	1.78E+00
1.5	9.33E-03	5.63E-02	7.80E-02	8.67E-02	1.50E-01	1.95E-01	3.30E-01	6.25E-01	1.07E+00
2	6.90E-03	4.56E-02	6.21E-02	6.80E-02	1.16E-01	1.46E-01	2.43E-01	4.52E-01	7.68E-01
3	4.26E-03	3.27E-02	4.50E-02	4.99E-02	7.98E-02	1.01E-01	1.57E-01	2.84E-01	4.69E-01
5	2.34E-03	2.18E-02	3.03E-02	3.29E-02	5.39E-02	6.63E-02	1.03E-01	1.79E-01	2.87E-01
7.5	1.37E-03	1.41E-02	2.02E-02	2.20E-02	3.57E-02	4.39E-02	6.81E-02	1.17E-01	1.92E-01
10	8.96E-04	1.08E-02	1.47E-02	1.63E-02	2.70E-02	3.32E-02	5.11E-02	8.77E-02	1.40E-01

Table 10.10. Uniform Hazard Response Spectra (UHRS) for Site B for annual frequencies of exceedance of 10^{-2}, 10^{-3}, 5×10^{-4}, 4×10^{-4}, 10^{-4}, 5×10^{-5}, 10^{-5}, 10^{-6}, and 10^{-7} (corresponding to return periods of 100, 1,000, 2,000, 2,500, 10,000, 20,000, 100,000, 1 million, and 10 million years).

Site B − Mean UHRS									
Period	10^{-2}	10^{-3}	5×10^{-4}	4×10^{-4}	10^{-4}	5×10^{-5}	10^{-5}	10^{-6}	10^{-7}
0.01	1.75E-02	1.14E-01	1.83E-01	2.12E-01	4.75E-01	6.76E-01	1.37E+00	3.12E+00	5.79E+00
0.02	2.13E-02	1.43E-01	2.34E-01	2.72E-01	6.25E-01	9.02E-01	1.83E+00	3.93E+00	7.23E+00
0.03	2.38E-02	1.65E-01	2.71E-01	3.14E-01	7.17E-01	1.02E+00	2.00E+00	4.12E+00	7.43E+00
0.04	2.56E-02	1.80E-01	2.96E-01	3.41E-01	7.70E-01	1.07E+00	2.06E+00	4.16E+00	7.40E+00
0.05	2.65E-02	1.90E-01	3.10E-01	3.57E-01	7.96E-01	1.10E+00	2.08E+00	4.14E+00	7.33E+00
0.075	2.71E-02	2.01E-01	3.26E-01	3.75E-01	8.18E-01	1.12E+00	2.06E+00	4.03E+00	7.07E+00
0.1	2.74E-02	2.01E-01	3.25E-01	3.73E-01	8.05E-01	1.09E+00	2.00E+00	3.86E+00	6.73E+00
0.15	2.76E-02	1.90E-01	3.06E-01	3.49E-01	7.44E-01	1.01E+00	1.80E+00	3.46E+00	5.99E+00
0.2	2.79E-02	1.80E-01	2.85E-01	3.26E-01	6.84E-01	9.27E-01	1.65E+00	3.19E+00	5.50E+00
0.3	2.59E-02	1.55E-01	2.42E-01	2.78E-01	5.75E-01	7.82E-01	1.40E+00	2.71E+00	4.69E+00
0.4	2.24E-02	1.29E-01	2.01E-01	2.29E-01	4.79E-01	6.49E-01	1.18E+00	2.31E+00	4.00E+00
0.5	1.93E-02	1.09E-01	1.67E-01	1.92E-01	4.00E-01	5.50E-01	1.01E+00	2.00E+00	3.48E+00
0.75	1.32E-02	7.44E-02	1.14E-01	1.30E-01	2.75E-01	3.76E-01	7.06E-01	1.39E+00	2.49E+00
1	9.85E-03	5.63E-02	8.53E-02	9.75E-02	2.02E-01	2.77E-01	5.16E-01	1.04E+00	1.82E+00
1.5	6.35E-03	3.88E-02	5.82E-02	6.56E-02	1.30E-01	1.78E-01	3.27E-01	6.53E-01	1.14E+00
2	4.63E-03	3.04E-02	4.52E-02	5.12E-02	1.00E-01	1.32E-01	2.41E-01	4.80E-01	8.42E-01
3	2.67E-03	2.02E-02	3.01E-02	3.35E-02	6.28E-02	8.29E-02	1.45E-01	2.87E-01	5.00E-01
5	1.35E-03	1.24E-02	1.88E-02	2.12E-02	3.90E-02	5.14E-02	8.91E-02	1.72E-01	2.96E-01
7.5	7.26E-04	8.36E-03	1.22E-02	1.36E-02	2.53E-02	3.29E-02	5.68E-02	1.10E-01	1.96E-01
10	4.47E-04	6.23E-03	9.28E-03	1.04E-02	1.87E-02	2.41E-02	4.10E-02	7.96E-02	1.39E-01
Site B − 5th percentile UHRS									
Period	10^{-2}	10^{-3}	5×10^{-4}	4×10^{-4}	10^{-4}	5×10^{-5}	10^{-5}	10^{-6}	10^{-7}
0.01	6.26E-03	3.70E-02	5.73E-02	6.53E-02	1.26E-01	1.65E-01	2.71E-01	4.53E-01	6.92E-01
0.02	6.32E-03	3.76E-02	5.81E-02	6.62E-02	1.28E-01	1.67E-01	2.76E-01	4.64E-01	7.06E-01
0.03	6.40E-03	3.93E-02	6.09E-02	6.97E-02	1.34E-01	1.77E-01	2.94E-01	4.97E-01	7.61E-01
0.04	6.75E-03	4.22E-02	6.53E-02	7.48E-02	1.45E-01	1.94E-01	3.17E-01	5.39E-01	8.31E-01
0.05	7.31E-03	4.62E-02	7.29E-02	8.30E-02	1.61E-01	2.14E-01	3.49E-01	6.01E-01	9.35E-01
0.075	9.06E-03	5.83E-02	9.27E-02	1.06E-01	2.15E-01	2.82E-01	4.66E-01	8.05E-01	1.25E+00
0.1	1.07E-02	7.01E-02	1.11E-01	1.27E-01	2.62E-01	3.43E-01	5.71E-01	9.95E-01	1.55E+00
0.15	1.30E-02	8.48E-02	1.34E-01	1.54E-01	3.19E-01	4.18E-01	7.05E-01	1.22E+00	1.92E+00
0.2	1.41E-02	8.91E-02	1.41E-01	1.62E-01	3.35E-01	4.44E-01	7.50E-01	1.30E+00	2.04E+00
0.3	1.43E-02	8.37E-02	1.31E-01	1.50E-01	3.14E-01	4.13E-01	7.04E-01	1.22E+00	1.93E+00
0.4	1.25E-02	7.07E-02	1.10E-01	1.26E-01	2.71E-01	3.59E-01	6.14E-01	1.09E+00	1.71E+00
0.5	1.10E-02	5.97E-02	9.30E-02	1.07E-01	2.30E-01	3.13E-01	5.39E-01	9.59E-01	1.47E+00
0.75	7.77E-03	4.07E-02	6.28E-02	7.20E-02	1.57E-01	2.19E-01	3.81E-01	6.92E-01	1.09E+00
1	5.67E-03	3.04E-02	4.66E-02	5.33E-02	1.15E-01	1.57E-01	2.85E-01	5.14E-01	8.12E-01
1.5	3.64E-03	2.05E-02	3.08E-02	3.50E-02	7.37E-02	1.03E-01	1.82E-01	3.29E-01	5.22E-01
2	2.58E-03	1.56E-02	2.33E-02	2.64E-02	5.47E-02	7.41E-02	1.32E-01	2.44E-01	3.84E-01
3	1.40E-03	1.01E-02	1.48E-02	1.67E-02	3.36E-02	4.60E-02	7.98E-02	1.44E-01	2.33E-01
5	6.46E-04	6.04E-03	8.88E-03	9.98E-03	1.98E-02	2.63E-02	4.60E-02	8.44E-02	1.31E-01
7.5	2.96E-04	3.79E-03	5.62E-03	6.29E-03	1.18E-02	1.55E-02	2.71E-02	4.94E-02	7.84E-02
10	1.66E-04	2.79E-03	4.07E-03	4.58E-03	8.46E-03	1.10E-02	1.87E-02	3.33E-02	5.30E-02

Table 10.10. (contd)

Site B − 16th percentile UHRS									
Period	10^{-2}	10^{-3}	5×10^{-4}	4×10^{-4}	10^{-4}	5×10^{-5}	10^{-5}	10^{-6}	10^{-7}
0.01	8.48E-03	4.92E-02	7.51E-02	8.52E-02	1.66E-01	2.19E-01	3.55E-01	6.05E-01	9.31E-01
0.02	8.50E-03	5.00E-02	7.71E-02	8.75E-02	1.70E-01	2.24E-01	3.62E-01	6.20E-01	9.56E-01
0.03	8.89E-03	5.31E-02	8.27E-02	9.44E-02	1.85E-01	2.42E-01	3.95E-01	6.82E-01	1.05E+00
0.04	9.76E-03	5.84E-02	9.10E-02	1.03E-01	2.07E-01	2.70E-01	4.43E-01	7.71E-01	1.18E+00
0.05	1.06E-02	6.59E-02	1.03E-01	1.16E-01	2.35E-01	3.09E-01	5.12E-01	8.81E-01	1.35E+00
0.075	1.27E-02	8.34E-02	1.31E-01	1.50E-01	3.11E-01	4.03E-01	6.78E-01	1.18E+00	1.86E+00
0.1	1.46E-02	9.83E-02	1.54E-01	1.77E-01	3.62E-01	4.86E-01	8.07E-01	1.41E+00	2.21E+00
0.15	1.70E-02	1.11E-01	1.77E-01	2.05E-01	4.14E-01	5.53E-01	9.35E-01	1.64E+00	2.56E+00
0.2	1.82E-02	1.13E-01	1.80E-01	2.07E-01	4.22E-01	5.62E-01	9.53E-01	1.67E+00	2.62E+00
0.3	1.79E-02	1.04E-01	1.61E-01	1.86E-01	3.79E-01	5.12E-01	8.66E-01	1.54E+00	2.41E+00
0.4	1.55E-02	8.71E-02	1.35E-01	1.55E-01	3.27E-01	4.37E-01	7.59E-01	1.34E+00	2.13E+00
0.5	1.33E-02	7.29E-02	1.13E-01	1.30E-01	2.80E-01	3.74E-01	6.52E-01	1.16E+00	1.86E+00
0.75	9.39E-03	5.00E-02	7.72E-02	8.88E-02	1.93E-01	2.61E-01	4.63E-01	8.44E-01	1.32E+00
1	6.92E-03	3.71E-02	5.66E-02	6.45E-02	1.37E-01	1.94E-01	3.40E-01	6.20E-01	1.00E+00
1.5	4.51E-03	2.47E-02	3.73E-02	4.24E-02	8.96E-02	1.21E-01	2.19E-01	3.97E-01	6.37E-01
2	3.23E-03	1.89E-02	2.81E-02	3.19E-02	6.55E-02	9.08E-02	1.59E-01	2.98E-01	4.73E-01
3	1.76E-03	1.20E-02	1.78E-02	2.02E-02	4.02E-02	5.44E-02	9.75E-02	1.77E-01	2.85E-01
5	8.64E-04	7.50E-03	1.09E-02	1.21E-02	2.38E-02	3.19E-02	5.61E-02	1.03E-01	1.64E-01
7.5	4.24E-04	4.78E-03	6.98E-03	7.82E-03	1.45E-02	1.94E-02	3.35E-02	6.16E-02	1.00E-01
10	2.38E-04	3.51E-03	5.17E-03	5.73E-03	1.04E-02	1.34E-02	2.32E-02	4.22E-02	6.80E-02
Site B − 50th percentile UHRS									
Period	10^{-2}	10^{-3}	5×10^{-4}	4×10^{-4}	10^{-4}	5×10^{-5}	10^{-5}	10^{-6}	10^{-7}
0.01	1.34E-02	7.83E-02	1.19E-01	1.36E-01	2.76E-01	3.57E-01	5.89E-01	1.01E+00	1.54E+00
0.02	1.45E-02	8.46E-02	1.30E-01	1.48E-01	3.00E-01	3.86E-01	6.43E-01	1.10E+00	1.71E+00
0.03	1.63E-02	1.00E-01	1.54E-01	1.78E-01	3.55E-01	4.69E-01	7.77E-01	1.32E+00	2.11E+00
0.04	1.88E-02	1.18E-01	1.88E-01	2.16E-01	4.32E-01	5.68E-01	9.43E-01	1.61E+00	2.56E+00
0.05	2.10E-02	1.36E-01	2.18E-01	2.49E-01	5.09E-01	6.64E-01	1.09E+00	1.92E+00	3.04E+00
0.075	2.41E-02	1.65E-01	2.66E-01	3.07E-01	6.19E-01	8.22E-01	1.36E+00	2.38E+00	3.75E+00
0.1	2.48E-02	1.74E-01	2.79E-01	3.19E-01	6.55E-01	8.71E-01	1.46E+00	2.55E+00	4.03E+00
0.15	2.58E-02	1.72E-01	2.75E-01	3.15E-01	6.46E-01	8.59E-01	1.45E+00	2.55E+00	4.05E+00
0.2	2.62E-02	1.65E-01	2.60E-01	2.99E-01	6.12E-01	8.17E-01	1.38E+00	2.46E+00	3.92E+00
0.3	2.45E-02	1.44E-01	2.24E-01	2.56E-01	5.29E-01	7.03E-01	1.20E+00	2.16E+00	3.46E+00
0.4	2.12E-02	1.21E-01	1.86E-01	2.13E-01	4.38E-01	5.89E-01	1.03E+00	1.86E+00	3.01E+00
0.5	1.83E-02	1.01E-01	1.55E-01	1.78E-01	3.70E-01	5.05E-01	8.81E-01	1.59E+00	2.62E+00
0.75	1.27E-02	6.87E-02	1.06E-01	1.20E-01	2.53E-01	3.44E-01	6.17E-01	1.14E+00	1.87E+00
1	9.35E-03	5.14E-02	7.73E-02	8.82E-02	1.86E-01	2.54E-01	4.52E-01	8.45E-01	1.36E+00
1.5	6.08E-03	3.43E-02	5.13E-02	5.80E-02	1.19E-01	1.61E-01	2.91E-01	5.37E-01	8.78E-01
2	4.40E-03	2.65E-02	3.90E-02	4.40E-02	8.91E-02	1.19E-01	2.14E-01	3.94E-01	6.45E-01
3	2.51E-03	1.71E-02	2.51E-02	2.82E-02	5.43E-02	7.18E-02	1.26E-01	2.37E-01	3.86E-01
5	1.27E-03	1.09E-02	1.55E-02	1.73E-02	3.29E-02	4.35E-02	7.60E-02	1.38E-01	2.28E-01
7.5	6.69E-04	7.18E-03	1.03E-02	1.14E-02	2.09E-02	2.73E-02	4.67E-02	8.68E-02	1.40E-01
10	4.07E-04	5.37E-03	7.67E-03	8.50E-03	1.50E-02	1.97E-02	3.28E-02	6.03E-02	9.91E-02

Table 10.10. (contd)

Site B − 84th percentile UHRS									
Period	10^{-2}	10^{-3}	5×10^{-4}	4×10^{-4}	10^{-4}	5×10^{-5}	10^{-5}	10^{-6}	10^{-7}
0.01	2.58E-02	1.52E-01	2.42E-01	2.78E-01	5.58E-01	7.37E-01	1.19E+00	2.08E+00	3.21E+00
0.02	3.65E-02	2.27E-01	3.56E-01	4.09E-01	8.33E-01	1.08E+00	1.77E+00	3.09E+00	4.77E+00
0.03	4.31E-02	2.76E-01	4.37E-01	5.05E-01	1.02E+00	1.30E+00	2.20E+00	3.76E+00	5.90E+00
0.04	4.58E-02	3.04E-01	4.79E-01	5.46E-01	1.10E+00	1.41E+00	2.38E+00	4.13E+00	6.50E+00
0.05	4.58E-02	3.09E-01	4.93E-01	5.63E-01	1.13E+00	1.46E+00	2.47E+00	4.31E+00	6.81E+00
0.075	4.34E-02	3.09E-01	4.93E-01	5.63E-01	1.14E+00	1.51E+00	2.50E+00	4.40E+00	7.04E+00
0.1	4.14E-02	2.95E-01	4.71E-01	5.39E-01	1.09E+00	1.45E+00	2.42E+00	4.29E+00	6.88E+00
0.15	3.89E-02	2.59E-01	4.12E-01	4.76E-01	9.69E-01	1.28E+00	2.17E+00	3.87E+00	6.29E+00
0.2	3.82E-02	2.37E-01	3.72E-01	4.26E-01	8.75E-01	1.16E+00	2.00E+00	3.58E+00	5.84E+00
0.3	3.45E-02	2.00E-01	3.08E-01	3.50E-01	7.25E-01	9.73E-01	1.69E+00	3.08E+00	5.04E+00
0.4	2.91E-02	1.65E-01	2.54E-01	2.91E-01	5.97E-01	8.07E-01	1.42E+00	2.61E+00	4.28E+00
0.5	2.49E-02	1.38E-01	2.11E-01	2.41E-01	5.05E-01	6.80E-01	1.19E+00	2.26E+00	3.72E+00
0.75	1.72E-02	9.44E-02	1.43E-01	1.63E-01	3.41E-01	4.70E-01	8.50E-01	1.58E+00	2.67E+00
1	1.27E-02	7.12E-02	1.07E-01	1.20E-01	2.49E-01	3.39E-01	6.17E-01	1.16E+00	1.96E+00
1.5	8.31E-03	5.06E-02	7.25E-02	8.14E-02	1.59E-01	2.18E-01	3.89E-01	7.45E-01	1.22E+00
2	6.05E-03	3.92E-02	5.65E-02	6.29E-02	1.19E-01	1.60E-01	2.89E-01	5.45E-01	9.10E-01
3	3.62E-03	2.67E-02	3.76E-02	4.16E-02	7.52E-02	1.00E-01	1.72E-01	3.26E-01	5.42E-01
5	1.88E-03	1.67E-02	2.39E-02	2.64E-02	4.69E-02	6.08E-02	1.05E-01	1.98E-01	3.17E-01
7.5	1.07E-03	1.13E-02	1.56E-02	1.73E-02	3.05E-02	3.93E-02	6.73E-02	1.24E-01	2.08E-01
10	6.80E-04	8.61E-03	1.18E-02	1.30E-02	2.25E-02	2.88E-02	4.85E-02	8.95E-02	1.45E-01
Site B − 95th percentile UHRS									
Period	10^{-2}	10^{-3}	5×10^{-4}	4×10^{-4}	10^{-4}	5×10^{-5}	10^{-5}	10^{-6}	10^{-7}
0.01	4.90E-02	3.04E-01	4.79E-01	5.48E-01	1.11E+00	1.43E+00	2.40E+00	4.10E+00	6.37E+00
0.02	6.64E-02	4.17E-01	6.59E-01	7.58E-01	1.47E+00	2.00E+00	3.27E+00	5.63E+00	8.80E+00
0.03	7.03E-02	4.53E-01	7.18E-01	8.20E-01	1.59E+00	2.13E+00	3.49E+00	6.11E+00	9.62E+00
0.04	6.89E-02	4.60E-01	7.19E-01	8.23E-01	1.61E+00	2.15E+00	3.54E+00	6.20E+00	9.91E+00
0.05	6.70E-02	4.51E-01	7.09E-01	8.09E-01	1.59E+00	2.13E+00	3.50E+00	6.20E+00	9.96E+00
0.075	5.98E-02	4.24E-01	6.69E-01	7.67E-01	1.53E+00	2.02E+00	3.35E+00	5.98E+00	9.69E+00
0.1	5.59E-02	3.94E-01	6.18E-01	7.07E-01	1.42E+00	1.88E+00	3.19E+00	5.70E+00	9.25E+00
0.15	5.10E-02	3.40E-01	5.34E-01	6.07E-01	1.22E+00	1.63E+00	2.77E+00	5.05E+00	8.24E+00
0.2	4.89E-02	3.00E-01	4.72E-01	5.39E-01	1.09E+00	1.46E+00	2.50E+00	4.59E+00	7.57E+00
0.3	4.37E-02	2.47E-01	3.80E-01	4.34E-01	8.93E-01	1.19E+00	2.10E+00	3.85E+00	6.41E+00
0.4	3.63E-02	2.03E-01	3.08E-01	3.50E-01	7.33E-01	1.00E+00	1.76E+00	3.30E+00	5.48E+00
0.5	3.10E-02	1.69E-01	2.58E-01	2.95E-01	6.12E-01	8.42E-01	1.48E+00	2.86E+00	4.78E+00
0.75	2.12E-02	1.17E-01	1.73E-01	1.97E-01	4.13E-01	5.75E-01	1.05E+00	2.04E+00	3.39E+00
1	1.56E-02	8.95E-02	1.31E-01	1.47E-01	3.03E-01	4.15E-01	7.77E-01	1.46E+00	2.51E+00
1.5	1.02E-02	6.35E-02	9.10E-02	1.02E-01	1.96E-01	2.66E-01	4.88E-01	9.37E-01	1.54E+00
2	7.62E-03	5.17E-02	7.16E-02	7.95E-02	1.47E-01	1.98E-01	3.54E-01	6.82E-01	1.14E+00
3	4.49E-03	3.52E-02	4.95E-02	5.42E-02	9.46E-02	1.22E-01	2.14E-01	4.02E-01	6.77E-01
5	2.41E-03	2.28E-02	3.20E-02	3.50E-02	5.97E-02	7.69E-02	1.29E-01	2.42E-01	4.08E-01
7.5	1.44E-03	1.49E-02	2.14E-02	2.33E-02	3.94E-02	5.04E-02	8.57E-02	1.59E-01	2.64E-01
10	9.30E-04	1.14E-02	1.57E-02	1.74E-02	2.95E-02	3.73E-02	6.23E-02	1.15E-01	1.95E-01

Table 10.11. Uniform Hazard Response Spectra (UHRS) for Site D for annual frequencies of exceedance of 10^{-2}, 10^{-3}, 5×10^{-4}, 4×10^{-4}, 10^{-4}, 5×10^{-5}, 10^{-5}, 10^{-6}, and 10^{-7} (corresponding to return periods of 100, 1,000, 2,000, 2,500, 10,000, 20,000, 100,000, 1 million, and 10 million years).

Site D − Mean UHRS									
Period	10^{-2}	10^{-3}	5×10^{-4}	4×10^{-4}	10^{-4}	5×10^{-5}	10^{-5}	10^{-6}	10^{-7}
0.01	1.75E-02	1.08E-01	1.72E-01	2.00E-01	4.49E-01	6.41E-01	1.31E+00	3.10E+00	5.86E+00
0.02	2.14E-02	1.37E-01	2.22E-01	2.57E-01	5.92E-01	8.55E-01	1.79E+00	4.12E+00	7.77E+00
0.03	2.44E-02	1.60E-01	2.61E-01	3.04E-01	6.92E-01	9.93E-01	2.04E+00	4.47E+00	8.16E+00
0.04	2.68E-02	1.78E-01	2.90E-01	3.35E-01	7.59E-01	1.07E+00	2.16E+00	4.60E+00	8.24E+00
0.05	2.80E-02	1.89E-01	3.08E-01	3.54E-01	7.96E-01	1.12E+00	2.22E+00	4.66E+00	8.26E+00
0.075	2.86E-02	2.02E-01	3.26E-01	3.75E-01	8.34E-01	1.17E+00	2.26E+00	4.63E+00	8.12E+00
0.1	2.88E-02	2.02E-01	3.25E-01	3.74E-01	8.26E-01	1.15E+00	2.22E+00	4.48E+00	7.85E+00
0.15	2.89E-02	1.90E-01	3.05E-01	3.49E-01	7.66E-01	1.07E+00	2.04E+00	4.04E+00	7.06E+00
0.2	2.90E-02	1.79E-01	2.83E-01	3.25E-01	7.07E-01	9.92E-01	1.89E+00	3.74E+00	6.52E+00
0.3	2.68E-02	1.55E-01	2.41E-01	2.75E-01	5.92E-01	8.35E-01	1.62E+00	3.24E+00	5.61E+00
0.4	2.31E-02	1.29E-01	1.99E-01	2.27E-01	4.91E-01	6.96E-01	1.37E+00	2.77E+00	4.83E+00
0.5	1.99E-02	1.09E-01	1.66E-01	1.90E-01	4.10E-01	5.86E-01	1.16E+00	2.40E+00	4.18E+00
0.75	1.35E-02	7.42E-02	1.13E-01	1.29E-01	2.79E-01	4.00E-01	8.25E-01	1.69E+00	3.01E+00
1	1.01E-02	5.62E-02	8.45E-02	9.64E-02	2.04E-01	2.92E-01	5.95E-01	1.22E+00	2.19E+00
1.5	6.45E-03	3.88E-02	5.80E-02	6.52E-02	1.33E-01	1.87E-01	3.68E-01	7.71E-01	1.33E+00
2	4.71E-03	3.04E-02	4.50E-02	5.09E-02	1.01E-01	1.37E-01	2.68E-01	5.52E-01	9.72E-01
3	2.71E-03	2.02E-02	3.00E-02	3.35E-02	6.38E-02	8.60E-02	1.58E-01	3.21E-01	5.61E-01
5	1.36E-03	1.23E-02	1.86E-02	2.10E-02	3.91E-02	5.20E-02	9.27E-02	1.82E-01	3.11E-01
7.5	7.32E-04	8.32E-03	1.21E-02	1.35E-02	2.54E-02	3.31E-02	5.78E-02	1.13E-01	2.00E-01
10	4.52E-04	6.21E-03	9.25E-03	1.03E-02	1.87E-02	2.42E-02	4.12E-02	7.97E-02	1.38E-01
Site D − 5th percentile UHRS									
Period	10^{-2}	10^{-3}	5×10^{-4}	4×10^{-4}	10^{-4}	5×10^{-5}	10^{-5}	10^{-6}	10^{-7}
0.01	6.74E-03	3.84E-02	5.89E-02	6.71E-02	1.37E-01	1.90E-01	3.36E-01	5.89E-01	8.98E-01
0.02	6.85E-03	3.90E-02	6.01E-02	6.88E-02	1.40E-01	1.94E-01	3.42E-01	6.02E-01	9.22E-01
0.03	7.11E-03	4.11E-02	6.35E-02	7.27E-02	1.49E-01	2.06E-01	3.64E-01	6.47E-01	1.00E+00
0.04	7.57E-03	4.49E-02	6.99E-02	7.99E-02	1.64E-01	2.26E-01	4.00E-01	7.19E-01	1.10E+00
0.05	8.25E-03	5.00E-02	7.81E-02	8.87E-02	1.84E-01	2.51E-01	4.51E-01	8.09E-01	1.23E+00
0.075	1.02E-02	6.30E-02	1.00E-01	1.14E-01	2.42E-01	3.33E-01	6.00E-01	1.08E+00	1.68E+00
0.1	1.18E-02	7.48E-02	1.18E-01	1.35E-01	2.93E-01	4.00E-01	7.38E-01	1.32E+00	2.07E+00
0.15	1.40E-02	8.91E-02	1.40E-01	1.61E-01	3.43E-01	4.79E-01	8.82E-01	1.61E+00	2.51E+00
0.2	1.51E-02	9.21E-02	1.44E-01	1.65E-01	3.54E-01	4.95E-01	9.18E-01	1.68E+00	2.63E+00
0.3	1.49E-02	8.44E-02	1.31E-01	1.50E-01	3.24E-01	4.53E-01	8.57E-01	1.58E+00	2.47E+00
0.4	1.32E-02	7.12E-02	1.10E-01	1.26E-01	2.75E-01	3.88E-01	7.61E-01	1.41E+00	2.22E+00
0.5	1.14E-02	6.03E-02	9.32E-02	1.07E-01	2.35E-01	3.34E-01	6.55E-01	1.22E+00	2.00E+00
0.75	8.04E-03	4.08E-02	6.25E-02	7.15E-02	1.59E-01	2.30E-01	4.72E-01	9.15E-01	1.43E+00
1	5.88E-03	3.08E-02	4.62E-02	5.26E-02	1.16E-01	1.68E-01	3.43E-01	6.73E-01	1.08E+00
1.5	3.73E-03	2.08E-02	3.08E-02	3.49E-02	7.43E-02	1.07E-01	2.18E-01	4.19E-01	6.80E-01
2	2.58E-03	1.57E-02	2.33E-02	2.64E-02	5.48E-02	7.76E-02	1.54E-01	3.09E-01	5.00E-01
3	1.41E-03	1.01E-02	1.47E-02	1.66E-02	3.36E-02	4.73E-02	9.35E-02	1.79E-01	2.92E-01
5	6.60E-04	6.00E-03	8.84E-03	9.97E-03	1.96E-02	2.68E-02	5.10E-02	9.61E-02	1.50E-01
7.5	3.05E-04	3.79E-03	5.60E-03	6.25E-03	1.18E-02	1.58E-02	2.88E-02	5.30E-02	8.46E-02
10	1.66E-04	2.79E-03	4.04E-03	4.54E-03	8.50E-03	1.11E-02	1.95E-02	3.45E-02	5.51E-02

Table 10.11. (contd)

Site D − 16th percentile UHRS									
Period	10^{-2}	10^{-3}	5×10^{-4}	4×10^{-4}	10^{-4}	5×10^{-5}	10^{-5}	10^{-6}	10^{-7}
0.01	9.10E-03	5.00E-02	7.71E-02	8.75E-02	1.80E-01	2.48E-01	4.43E-01	7.84E-01	1.18E+00
0.02	9.32E-03	5.15E-02	7.93E-02	9.06E-02	1.86E-01	2.55E-01	4.56E-01	8.08E-01	1.22E+00
0.03	1.00E-02	5.55E-02	8.61E-02	9.84E-02	2.04E-01	2.79E-01	5.06E-01	8.90E-01	1.35E+00
0.04	1.08E-02	6.26E-02	9.73E-02	1.11E-01	2.32E-01	3.17E-01	5.67E-01	1.02E+00	1.55E+00
0.05	1.17E-02	7.14E-02	1.10E-01	1.25E-01	2.65E-01	3.61E-01	6.52E-01	1.16E+00	1.82E+00
0.075	1.41E-02	8.91E-02	1.41E-01	1.62E-01	3.46E-01	4.79E-01	8.66E-01	1.57E+00	2.44E+00
0.1	1.60E-02	1.03E-01	1.62E-01	1.88E-01	4.01E-01	5.57E-01	1.02E+00	1.85E+00	2.91E+00
0.15	1.82E-02	1.15E-01	1.83E-01	2.11E-01	4.49E-01	6.23E-01	1.14E+00	2.10E+00	3.31E+00
0.2	1.95E-02	1.16E-01	1.83E-01	2.10E-01	4.48E-01	6.23E-01	1.15E+00	2.13E+00	3.36E+00
0.3	1.87E-02	1.04E-01	1.61E-01	1.86E-01	3.96E-01	5.55E-01	1.05E+00	1.97E+00	3.12E+00
0.4	1.62E-02	8.73E-02	1.34E-01	1.53E-01	3.33E-01	4.72E-01	9.16E-01	1.73E+00	2.77E+00
0.5	1.37E-02	7.34E-02	1.13E-01	1.29E-01	2.85E-01	4.03E-01	7.98E-01	1.49E+00	2.44E+00
0.75	9.78E-03	5.00E-02	7.65E-02	8.78E-02	1.92E-01	2.79E-01	5.65E-01	1.10E+00	1.77E+00
1	7.07E-03	3.69E-02	5.58E-02	6.37E-02	1.40E-01	2.03E-01	4.12E-01	8.15E-01	1.28E+00
1.5	4.63E-03	2.48E-02	3.70E-02	4.21E-02	8.95E-02	1.27E-01	2.61E-01	5.10E-01	8.14E-01
2	3.29E-03	1.89E-02	2.78E-02	3.15E-02	6.58E-02	9.43E-02	1.89E-01	3.63E-01	5.89E-01
3	1.78E-03	1.21E-02	1.78E-02	2.02E-02	4.03E-02	5.61E-02	1.10E-01	2.15E-01	3.44E-01
5	8.64E-04	7.39E-03	1.07E-02	1.20E-02	2.35E-02	3.22E-02	6.10E-02	1.15E-01	1.88E-01
7.5	4.26E-04	4.78E-03	6.98E-03	7.81E-03	1.45E-02	1.96E-02	3.54E-02	6.67E-02	1.07E-01
10	2.43E-04	3.51E-03	5.17E-03	5.73E-03	1.04E-02	1.36E-02	2.41E-02	4.42E-02	7.11E-02
Site D − 50th percentile UHRS									
Period	10^{-2}	10^{-3}	5×10^{-4}	4×10^{-4}	10^{-4}	5×10^{-5}	10^{-5}	10^{-6}	10^{-7}
0.01	1.41E-02	7.94E-02	1.21E-01	1.37E-01	2.93E-01	3.98E-01	7.21E-01	1.25E+00	1.97E+00
0.02	1.54E-02	8.73E-02	1.33E-01	1.52E-01	3.23E-01	4.42E-01	7.95E-01	1.37E+00	2.18E+00
0.03	1.78E-02	1.06E-01	1.65E-01	1.91E-01	3.96E-01	5.45E-01	9.85E-01	1.72E+00	2.73E+00
0.04	2.09E-02	1.27E-01	2.03E-01	2.31E-01	4.88E-01	6.70E-01	1.17E+00	2.15E+00	3.36E+00
0.05	2.30E-02	1.45E-01	2.32E-01	2.66E-01	5.64E-01	7.79E-01	1.35E+00	2.49E+00	3.91E+00
0.075	2.57E-02	1.69E-01	2.74E-01	3.15E-01	6.68E-01	9.22E-01	1.67E+00	3.04E+00	4.78E+00
0.1	2.64E-02	1.77E-01	2.83E-01	3.24E-01	6.98E-01	9.70E-01	1.75E+00	3.19E+00	5.10E+00
0.15	2.73E-02	1.72E-01	2.75E-01	3.16E-01	6.76E-01	9.39E-01	1.73E+00	3.18E+00	5.12E+00
0.2	2.72E-02	1.65E-01	2.60E-01	2.99E-01	6.38E-01	8.90E-01	1.65E+00	3.07E+00	4.95E+00
0.3	2.54E-02	1.44E-01	2.23E-01	2.54E-01	5.42E-01	7.66E-01	1.44E+00	2.71E+00	4.38E+00
0.4	2.20E-02	1.19E-01	1.84E-01	2.10E-01	4.53E-01	6.37E-01	1.22E+00	2.34E+00	3.81E+00
0.5	1.88E-02	1.01E-01	1.54E-01	1.76E-01	3.78E-01	5.40E-01	1.06E+00	2.06E+00	3.36E+00
0.75	1.29E-02	6.83E-02	1.04E-01	1.18E-01	2.58E-01	3.70E-01	7.56E-01	1.44E+00	2.42E+00
1	9.56E-03	5.07E-02	7.63E-02	8.70E-02	1.88E-01	2.70E-01	5.45E-01	1.07E+00	1.75E+00
1.5	6.21E-03	3.43E-02	5.13E-02	5.79E-02	1.20E-01	1.70E-01	3.37E-01	6.67E-01	1.09E+00
2	4.51E-03	2.63E-02	3.85E-02	4.35E-02	8.89E-02	1.24E-01	2.44E-01	4.81E-01	7.93E-01
3	2.59E-03	1.71E-02	2.51E-02	2.82E-02	5.50E-02	7.54E-02	1.41E-01	2.81E-01	4.61E-01
5	1.29E-03	1.07E-02	1.53E-02	1.71E-02	3.28E-02	4.40E-02	8.15E-02	1.53E-01	2.50E-01
7.5	6.83E-04	7.18E-03	1.02E-02	1.13E-02	2.07E-02	2.74E-02	4.88E-02	9.23E-02	1.49E-01
10	4.09E-04	5.37E-03	7.66E-03	8.47E-03	1.49E-02	1.97E-02	3.36E-02	6.21E-02	1.02E-01

Table 10.11. (contd)

Site D − 84th percentile UHRS									
Period	10^{-2}	10^{-3}	5×10^{-4}	4×10^{-4}	10^{-4}	5×10^{-5}	10^{-5}	10^{-6}	10^{-7}
0.01	2.53E-02	1.44E-01	2.26E-01	2.58E-01	5.45E-01	7.51E-01	1.30E+00	2.37E+00	3.69E+00
0.02	3.51E-02	2.06E-01	3.26E-01	3.71E-01	7.91E-01	1.07E+00	1.97E+00	3.45E+00	5.42E+00
0.03	4.19E-02	2.55E-01	4.02E-01	4.63E-01	9.88E-01	1.32E+00	2.40E+00	4.31E+00	6.82E+00
0.04	4.51E-02	2.86E-01	4.51E-01	5.19E-01	1.08E+00	1.46E+00	2.66E+00	4.81E+00	7.59E+00
0.05	4.59E-02	3.00E-01	4.72E-01	5.39E-01	1.13E+00	1.54E+00	2.80E+00	5.07E+00	8.00E+00
0.075	4.46E-02	3.00E-01	4.78E-01	5.48E-01	1.15E+00	1.59E+00	2.88E+00	5.25E+00	8.42E+00
0.1	4.26E-02	2.90E-01	4.58E-01	5.26E-01	1.12E+00	1.54E+00	2.77E+00	5.15E+00	8.31E+00
0.15	4.00E-02	2.55E-01	4.02E-01	4.63E-01	1.00E+00	1.37E+00	2.50E+00	4.66E+00	7.66E+00
0.2	3.93E-02	2.34E-01	3.66E-01	4.20E-01	9.02E-01	1.25E+00	2.30E+00	4.32E+00	7.15E+00
0.3	3.56E-02	2.00E-01	3.04E-01	3.47E-01	7.50E-01	1.04E+00	1.97E+00	3.72E+00	6.18E+00
0.4	3.01E-02	1.63E-01	2.49E-01	2.83E-01	6.12E-01	8.67E-01	1.66E+00	3.21E+00	5.35E+00
0.5	2.54E-02	1.38E-01	2.08E-01	2.36E-01	5.12E-01	7.33E-01	1.39E+00	2.79E+00	4.66E+00
0.75	1.76E-02	9.44E-02	1.41E-01	1.60E-01	3.44E-01	5.01E-01	1.01E+00	2.00E+00	3.33E+00
1	1.29E-02	7.07E-02	1.05E-01	1.19E-01	2.53E-01	3.60E-01	7.30E-01	1.41E+00	2.45E+00
1.5	8.51E-03	5.06E-02	7.20E-02	8.07E-02	1.62E-01	2.28E-01	4.45E-01	8.94E-01	1.47E+00
2	6.20E-03	3.92E-02	5.64E-02	6.26E-02	1.20E-01	1.67E-01	3.23E-01	6.38E-01	1.08E+00
3	3.62E-03	2.67E-02	3.74E-02	4.14E-02	7.58E-02	1.02E-01	1.90E-01	3.68E-01	6.23E-01
5	1.88E-03	1.66E-02	2.38E-02	2.62E-02	4.64E-02	6.10E-02	1.08E-01	2.10E-01	3.44E-01
7.5	1.07E-03	1.11E-02	1.54E-02	1.71E-02	3.03E-02	3.91E-02	6.84E-02	1.28E-01	2.16E-01
10	6.93E-04	8.56E-03	1.17E-02	1.29E-02	2.23E-02	2.86E-02	4.89E-02	9.09E-02	1.48E-01
Site D − 95th percentile UHRS									
Period	10^{-2}	10^{-3}	5×10^{-4}	4×10^{-4}	10^{-4}	5×10^{-5}	10^{-5}	10^{-6}	10^{-7}
0.01	4.44E-02	2.64E-01	4.14E-01	4.77E-01	1.00E+00	1.35E+00	2.47E+00	4.37E+00	6.81E+00
0.02	6.25E-02	3.73E-01	5.84E-01	6.69E-01	1.39E+00	1.94E+00	3.44E+00	6.20E+00	9.79E+00
0.03	6.74E-02	4.13E-01	6.50E-01	7.48E-01	1.54E+00	2.14E+00	3.77E+00	6.85E+00	1.07E+01
0.04	6.74E-02	4.26E-01	6.69E-01	7.68E-01	1.58E+00	2.18E+00	3.86E+00	7.06E+00	1.11E+01
0.05	6.60E-02	4.24E-01	6.69E-01	7.68E-01	1.58E+00	2.18E+00	3.85E+00	7.09E+00	1.12E+01
0.075	5.95E-02	4.06E-01	6.40E-01	7.37E-01	1.53E+00	2.10E+00	3.74E+00	6.97E+00	1.12E+01
0.1	5.67E-02	3.81E-01	6.01E-01	6.88E-01	1.45E+00	2.00E+00	3.55E+00	6.66E+00	1.09E+01
0.15	5.21E-02	3.29E-01	5.21E-01	5.94E-01	1.25E+00	1.73E+00	3.14E+00	5.91E+00	9.77E+00
0.2	5.00E-02	2.95E-01	4.59E-01	5.26E-01	1.12E+00	1.56E+00	2.86E+00	5.42E+00	8.99E+00
0.3	4.39E-02	2.45E-01	3.75E-01	4.28E-01	9.19E-01	1.28E+00	2.40E+00	4.62E+00	7.77E+00
0.4	3.71E-02	2.00E-01	3.04E-01	3.46E-01	7.50E-01	1.06E+00	2.03E+00	3.92E+00	6.64E+00
0.5	3.13E-02	1.69E-01	2.53E-01	2.88E-01	6.24E-01	8.92E-01	1.72E+00	3.41E+00	5.80E+00
0.75	2.16E-02	1.17E-01	1.72E-01	1.94E-01	4.18E-01	6.03E-01	1.18E+00	2.41E+00	4.11E+00
1	1.58E-02	8.85E-02	1.29E-01	1.45E-01	3.04E-01	4.34E-01	8.73E-01	1.74E+00	3.06E+00
1.5	1.05E-02	6.35E-02	9.10E-02	1.02E-01	1.98E-01	2.75E-01	5.41E-01	1.08E+00	1.85E+00
2	7.62E-03	5.17E-02	7.16E-02	7.95E-02	1.49E-01	2.02E-01	3.84E-01	7.81E-01	1.32E+00
3	4.49E-03	3.53E-02	5.00E-02	5.47E-02	9.55E-02	1.25E-01	2.28E-01	4.49E-01	7.75E-01
5	2.45E-03	2.27E-02	3.17E-02	3.47E-02	5.95E-02	7.63E-02	1.31E-01	2.53E-01	4.34E-01
7.5	1.44E-03	1.48E-02	2.12E-02	2.32E-02	3.92E-02	5.00E-02	8.63E-02	1.63E-01	2.72E-01
10	9.62E-04	1.14E-02	1.57E-02	1.74E-02	2.93E-02	3.69E-02	6.19E-02	1.16E-01	1.97E-01

Table 10.12. Uniform Hazard Response Spectra (UHRS) for Site E for annual frequencies of exceedance of 10^{-2}, 10^{-3}, 5×10^{-4}, 4×10^{-4}, 10^{-4}, 5×10^{-5}, 10^{-5}, 10^{-6}, and 10^{-7} (corresponding to return periods of 100, 1,000, 2,000, 2,500, 10,000, 20,000, 100,000, 1 million, and 10 million years).

Site E − Mean UHRS									
Period	10^{-2}	10^{-3}	5×10^{-4}	4×10^{-4}	10^{-4}	5×10^{-5}	10^{-5}	10^{-6}	10^{-7}
0.01	1.86E-02	1.32E-01	2.15E-01	2.48E-01	5.66E-01	8.15E-01	1.64E+00	3.62E+00	6.82E+00
0.02	2.31E-02	1.65E-01	2.70E-01	3.13E-01	7.05E-01	9.92E-01	1.89E+00	3.92E+00	7.19E+00
0.03	2.50E-02	1.82E-01	2.98E-01	3.42E-01	7.55E-01	1.04E+00	1.93E+00	3.90E+00	7.05E+00
0.04	2.62E-02	1.94E-01	3.14E-01	3.60E-01	7.75E-01	1.05E+00	1.93E+00	3.84E+00	6.89E+00
0.05	2.64E-02	1.99E-01	3.20E-01	3.66E-01	7.77E-01	1.05E+00	1.90E+00	3.76E+00	6.72E+00
0.075	2.53E-02	1.96E-01	3.14E-01	3.58E-01	7.46E-01	1.00E+00	1.78E+00	3.49E+00	6.21E+00
0.1	2.44E-02	1.86E-01	2.98E-01	3.39E-01	6.91E-01	9.24E-01	1.64E+00	3.21E+00	5.67E+00
0.15	2.41E-02	1.70E-01	2.71E-01	3.10E-01	6.16E-01	8.22E-01	1.44E+00	2.81E+00	4.96E+00
0.2	2.41E-02	1.58E-01	2.47E-01	2.83E-01	5.59E-01	7.44E-01	1.30E+00	2.52E+00	4.43E+00
0.3	2.24E-02	1.34E-01	2.07E-01	2.33E-01	4.57E-01	6.04E-01	1.06E+00	2.07E+00	3.63E+00
0.4	1.93E-02	1.11E-01	1.67E-01	1.90E-01	3.68E-01	4.93E-01	8.64E-01	1.69E+00	2.99E+00
0.5	1.64E-02	9.31E-02	1.38E-01	1.56E-01	3.08E-01	4.05E-01	7.18E-01	1.39E+00	2.49E+00
0.75	1.14E-02	6.28E-02	9.46E-02	1.06E-01	2.06E-01	2.72E-01	4.78E-01	9.39E-01	1.65E+00
1	8.44E-03	4.78E-02	6.97E-02	7.85E-02	1.48E-01	1.98E-01	3.42E-01	6.65E-01	1.17E+00
1.5	5.57E-03	3.29E-02	4.87E-02	5.41E-02	1.00E-01	1.28E-01	2.19E-01	4.10E-01	7.15E-01
2	4.06E-03	2.57E-02	3.75E-02	4.20E-02	7.53E-02	9.89E-02	1.62E-01	3.04E-01	5.17E-01
3	2.38E-03	1.73E-02	2.56E-02	2.87E-02	5.12E-02	6.41E-02	1.06E-01	1.92E-01	3.21E-01
5	1.25E-03	1.13E-02	1.65E-02	1.86E-02	3.31E-02	4.19E-02	6.84E-02	1.22E-01	2.04E-01
7.5	6.66E-04	7.58E-03	1.10E-02	1.21E-02	2.18E-02	2.77E-02	4.48E-02	8.08E-02	1.33E-01
10	4.06E-04	5.64E-03	8.32E-03	9.28E-03	1.61E-02	2.08E-02	3.35E-02	6.01E-02	1.00E-01
Site E − 5th percentile UHRS									
Period	10^{-2}	10^{-3}	5×10^{-4}	4×10^{-4}	10^{-4}	5×10^{-5}	10^{-5}	10^{-6}	10^{-7}
0.01	5.78E-03	3.46E-02	5.26E-02	5.92E-02	1.11E-01	1.39E-01	2.29E-01	3.97E-01	6.32E-01
0.02	5.86E-03	3.56E-02	5.39E-02	6.07E-02	1.13E-01	1.43E-01	2.36E-01	4.09E-01	6.52E-01
0.03	6.21E-03	3.81E-02	5.83E-02	6.59E-02	1.22E-01	1.56E-01	2.59E-01	4.56E-01	7.33E-01
0.04	6.69E-03	4.22E-02	6.47E-02	7.38E-02	1.35E-01	1.77E-01	2.92E-01	5.17E-01	8.31E-01
0.05	7.27E-03	4.76E-02	7.30E-02	8.27E-02	1.53E-01	2.03E-01	3.30E-01	5.86E-01	9.51E-01
0.075	8.84E-03	5.90E-02	9.29E-02	1.06E-01	2.05E-01	2.63E-01	4.33E-01	7.85E-01	1.26E+00
0.1	1.00E-02	6.74E-02	1.06E-01	1.20E-01	2.36E-01	3.09E-01	5.12E-01	9.22E-01	1.50E+00
0.15	1.14E-02	7.73E-02	1.20E-01	1.37E-01	2.72E-01	3.51E-01	5.89E-01	1.06E+00	1.72E+00
0.2	1.24E-02	7.94E-02	1.23E-01	1.39E-01	2.77E-01	3.57E-01	5.97E-01	1.07E+00	1.75E+00
0.3	1.23E-02	7.13E-02	1.11E-01	1.25E-01	2.46E-01	3.21E-01	5.35E-01	9.67E-01	1.57E+00
0.4	1.08E-02	5.95E-02	9.18E-02	1.04E-01	2.07E-01	2.70E-01	4.53E-01	8.20E-01	1.33E+00
0.5	9.56E-03	5.07E-02	7.63E-02	8.70E-02	1.72E-01	2.29E-01	3.83E-01	6.98E-01	1.13E+00
0.75	6.69E-03	3.40E-02	5.20E-02	5.86E-02	1.17E-01	1.53E-01	2.65E-01	4.80E-01	7.83E-01
1	5.00E-03	2.54E-02	3.78E-02	4.28E-02	8.48E-02	1.12E-01	1.92E-01	3.44E-01	5.60E-01
1.5	3.21E-03	1.70E-02	2.50E-02	2.81E-02	5.45E-02	7.08E-02	1.20E-01	2.16E-01	3.44E-01
2	2.23E-03	1.30E-02	1.90E-02	2.14E-02	4.07E-02	5.34E-02	8.90E-02	1.55E-01	2.50E-01
3	1.27E-03	8.52E-03	1.23E-02	1.37E-02	2.58E-02	3.34E-02	5.47E-02	9.56E-02	1.48E-01
5	5.95E-04	5.32E-03	7.68E-03	8.55E-03	1.52E-02	2.00E-02	3.23E-02	5.54E-02	8.66E-02
7.5	2.73E-04	3.36E-03	4.88E-03	5.41E-03	9.65E-03	1.20E-02	1.95E-02	3.30E-02	5.14E-02
10	1.53E-04	2.47E-03	3.52E-03	3.91E-03	6.83E-03	8.63E-03	1.33E-02	2.30E-02	3.54E-02

Table 10.12. (contd)

Site E − 16th percentile UHRS									
Period	10^{-2}	10^{-3}	5×10^{-4}	4×10^{-4}	10^{-4}	5×10^{-5}	10^{-5}	10^{-6}	10^{-7}
0.01	7.71E-03	4.57E-02	6.93E-02	7.85E-02	1.43E-01	1.86E-01	3.05E-01	5.33E-01	8.53E-01
0.02	8.09E-03	4.77E-02	7.30E-02	8.20E-02	1.49E-01	1.97E-01	3.18E-01	5.58E-01	8.99E-01
0.03	8.84E-03	5.38E-02	8.20E-02	9.25E-02	1.72E-01	2.24E-01	3.64E-01	6.49E-01	1.05E+00
0.04	1.00E-02	6.17E-02	9.48E-02	1.07E-01	2.05E-01	2.62E-01	4.28E-01	7.69E-01	1.23E+00
0.05	1.08E-02	7.03E-02	1.07E-01	1.20E-01	2.33E-01	3.05E-01	5.00E-01	8.94E-01	1.43E+00
0.075	1.25E-02	8.59E-02	1.32E-01	1.51E-01	3.00E-01	3.83E-01	6.39E-01	1.15E+00	1.89E+00
0.1	1.35E-02	9.49E-02	1.47E-01	1.68E-01	3.29E-01	4.26E-01	7.14E-01	1.29E+00	2.12E+00
0.15	1.50E-02	1.03E-01	1.57E-01	1.81E-01	3.53E-01	4.62E-01	7.74E-01	1.39E+00	2.28E+00
0.2	1.59E-02	1.01E-01	1.55E-01	1.78E-01	3.43E-01	4.49E-01	7.59E-01	1.36E+00	2.24E+00
0.3	1.51E-02	8.96E-02	1.35E-01	1.54E-01	3.02E-01	3.89E-01	6.55E-01	1.19E+00	1.97E+00
0.4	1.33E-02	7.34E-02	1.12E-01	1.26E-01	2.50E-01	3.27E-01	5.51E-01	1.01E+00	1.66E+00
0.5	1.15E-02	6.18E-02	9.46E-02	1.07E-01	2.11E-01	2.75E-01	4.65E-01	8.50E-01	1.38E+00
0.75	8.11E-03	4.14E-02	6.23E-02	7.05E-02	1.39E-01	1.87E-01	3.18E-01	5.81E-01	9.62E-01
1	5.97E-03	3.08E-02	4.62E-02	5.22E-02	1.03E-01	1.33E-01	2.29E-01	4.16E-01	6.88E-01
1.5	3.92E-03	2.05E-02	3.04E-02	3.40E-02	6.44E-02	8.54E-02	1.43E-01	2.61E-01	4.22E-01
2	2.83E-03	1.56E-02	2.28E-02	2.56E-02	4.90E-02	6.25E-02	1.07E-01	1.91E-01	3.09E-01
3	1.57E-03	1.04E-02	1.48E-02	1.65E-02	3.08E-02	3.94E-02	6.44E-02	1.15E-01	1.84E-01
5	7.85E-04	6.49E-03	9.34E-03	1.04E-02	1.87E-02	2.39E-02	3.85E-02	6.76E-02	1.07E-01
7.5	3.90E-04	4.18E-03	6.03E-03	6.71E-03	1.16E-02	1.45E-02	2.36E-02	4.05E-02	6.40E-02
10	2.19E-04	3.14E-03	4.46E-03	4.99E-03	8.49E-03	1.06E-02	1.65E-02	2.86E-02	4.46E-02
Site E − 50th percentile UHRS									
Period	10^{-2}	10^{-3}	5×10^{-4}	4×10^{-4}	10^{-4}	5×10^{-5}	10^{-5}	10^{-6}	10^{-7}
0.01	1.30E-02	7.72E-02	1.15E-01	1.29E-01	2.45E-01	3.16E-01	5.18E-01	9.18E-01	1.46E+00
0.02	1.47E-02	8.86E-02	1.32E-01	1.49E-01	2.86E-01	3.63E-01	5.97E-01	1.06E+00	1.72E+00
0.03	1.75E-02	1.12E-01	1.71E-01	1.97E-01	3.63E-01	4.71E-01	7.78E-01	1.36E+00	2.25E+00
0.04	2.03E-02	1.34E-01	2.10E-01	2.37E-01	4.49E-01	5.79E-01	9.60E-01	1.70E+00	2.80E+00
0.05	2.20E-02	1.50E-01	2.36E-01	2.69E-01	5.13E-01	6.58E-01	1.09E+00	1.96E+00	3.20E+00
0.075	2.29E-02	1.65E-01	2.61E-01	2.99E-01	5.71E-01	7.44E-01	1.23E+00	2.23E+00	3.64E+00
0.1	2.28E-02	1.61E-01	2.56E-01	2.95E-01	5.62E-01	7.37E-01	1.22E+00	2.22E+00	3.64E+00
0.15	2.27E-02	1.54E-01	2.42E-01	2.76E-01	5.32E-01	6.93E-01	1.16E+00	2.13E+00	3.50E+00
0.2	2.27E-02	1.44E-01	2.25E-01	2.56E-01	4.95E-01	6.39E-01	1.08E+00	1.99E+00	3.28E+00
0.3	2.12E-02	1.24E-01	1.89E-01	2.14E-01	4.08E-01	5.37E-01	9.06E-01	1.68E+00	2.80E+00
0.4	1.83E-02	1.03E-01	1.53E-01	1.75E-01	3.34E-01	4.38E-01	7.45E-01	1.38E+00	2.31E+00
0.5	1.55E-02	8.50E-02	1.27E-01	1.43E-01	2.79E-01	3.63E-01	6.21E-01	1.15E+00	1.96E+00
0.75	1.08E-02	5.71E-02	8.53E-02	9.71E-02	1.87E-01	2.46E-01	4.19E-01	7.84E-01	1.30E+00
1	8.05E-03	4.30E-02	6.28E-02	7.05E-02	1.34E-01	1.77E-01	3.06E-01	5.61E-01	9.43E-01
1.5	5.33E-03	2.88E-02	4.21E-02	4.74E-02	8.78E-02	1.14E-01	1.93E-01	3.48E-01	5.76E-01
2	3.92E-03	2.21E-02	3.21E-02	3.58E-02	6.51E-02	8.47E-02	1.40E-01	2.54E-01	4.15E-01
3	2.25E-03	1.46E-02	2.11E-02	2.34E-02	4.18E-02	5.36E-02	8.71E-02	1.53E-01	2.51E-01
5	1.20E-03	9.73E-03	1.34E-02	1.49E-02	2.62E-02	3.31E-02	5.33E-02	9.34E-02	1.47E-01
7.5	6.15E-04	6.36E-03	9.00E-03	9.98E-03	1.67E-02	2.13E-02	3.36E-02	5.79E-02	9.21E-02
10	3.75E-04	4.79E-03	6.73E-03	7.48E-03	1.23E-02	1.53E-02	2.43E-02	4.13E-02	6.55E-02

Table 10.12. (contd)

Site E − 84th percentile UHRS									
Period	10^{-2}	10^{-3}	5×10^{-4}	4×10^{-4}	10^{-4}	5×10^{-5}	10^{-5}	10^{-6}	10^{-7}
0.01	3.12E-02	1.93E-01	3.00E-01	3.36E-01	6.35E-01	8.22E-01	1.31E+00	2.36E+00	3.78E+00
0.02	4.40E-02	2.81E-01	4.30E-01	4.92E-01	9.28E-01	1.17E+00	1.94E+00	3.43E+00	5.56E+00
0.03	4.77E-02	3.14E-01	4.86E-01	5.49E-01	1.04E+00	1.31E+00	2.18E+00	3.88E+00	6.32E+00
0.04	4.77E-02	3.23E-01	5.07E-01	5.69E-01	1.07E+00	1.35E+00	2.27E+00	4.05E+00	6.64E+00
0.05	4.56E-02	3.23E-01	5.01E-01	5.62E-01	1.07E+00	1.35E+00	2.27E+00	4.08E+00	6.73E+00
0.075	4.00E-02	3.00E-01	4.60E-01	5.22E-01	1.00E+00	1.28E+00	2.14E+00	3.88E+00	6.45E+00
0.1	3.60E-02	2.68E-01	4.13E-01	4.72E-01	9.03E-01	1.17E+00	1.97E+00	3.58E+00	5.98E+00
0.15	3.35E-02	2.34E-01	3.59E-01	4.07E-01	7.84E-01	1.02E+00	1.72E+00	3.18E+00	5.33E+00
0.2	3.27E-02	2.12E-01	3.23E-01	3.64E-01	7.00E-01	9.12E-01	1.55E+00	2.86E+00	4.82E+00
0.3	2.94E-02	1.74E-01	2.64E-01	2.99E-01	5.64E-01	7.44E-01	1.26E+00	2.35E+00	3.98E+00
0.4	2.50E-02	1.40E-01	2.13E-01	2.39E-01	4.56E-01	5.95E-01	1.03E+00	1.93E+00	3.28E+00
0.5	2.16E-02	1.17E-01	1.75E-01	1.99E-01	3.73E-01	4.96E-01	8.51E-01	1.59E+00	2.75E+00
0.75	1.49E-02	8.01E-02	1.17E-01	1.31E-01	2.50E-01	3.28E-01	5.66E-01	1.07E+00	1.84E+00
1	1.11E-02	6.07E-02	8.76E-02	9.85E-02	1.82E-01	2.38E-01	4.04E-01	7.67E-01	1.29E+00
1.5	7.24E-03	4.27E-02	6.03E-02	6.67E-02	1.19E-01	1.52E-01	2.56E-01	4.71E-01	7.94E-01
2	5.37E-03	3.36E-02	4.73E-02	5.22E-02	9.05E-02	1.15E-01	1.90E-01	3.43E-01	5.72E-01
3	3.25E-03	2.35E-02	3.26E-02	3.56E-02	5.92E-02	7.40E-02	1.19E-01	2.13E-01	3.47E-01
5	1.76E-03	1.51E-02	2.16E-02	2.36E-02	3.87E-02	4.86E-02	7.63E-02	1.31E-01	2.13E-01
7.5	9.66E-04	1.04E-02	1.40E-02	1.54E-02	2.58E-02	3.20E-02	5.03E-02	8.59E-02	1.36E-01
10	6.30E-04	7.93E-03	1.08E-02	1.17E-02	1.95E-02	2.39E-02	3.69E-02	6.31E-02	1.01E-01
Site E − 95th percentile UHRS									
Period	10^{-2}	10^{-3}	5×10^{-4}	4×10^{-4}	10^{-4}	5×10^{-5}	10^{-5}	10^{-6}	10^{-7}
0.01	6.32E-02	4.03E-01	6.22E-01	7.09E-01	1.30E+00	1.68E+00	2.79E+00	4.94E+00	7.96E+00
0.02	7.50E-02	4.84E-01	7.41E-01	8.33E-01	1.52E+00	2.00E+00	3.26E+00	5.81E+00	9.47E+00
0.03	7.33E-02	4.84E-01	7.41E-01	8.33E-01	1.52E+00	2.02E+00	3.29E+00	5.92E+00	9.72E+00
0.04	6.85E-02	4.76E-01	7.21E-01	8.14E-01	1.48E+00	1.95E+00	3.21E+00	5.82E+00	9.62E+00
0.05	6.50E-02	4.53E-01	6.93E-01	7.83E-01	1.43E+00	1.88E+00	3.13E+00	5.68E+00	9.44E+00
0.075	5.48E-02	4.03E-01	6.17E-01	7.01E-01	1.31E+00	1.71E+00	2.85E+00	5.24E+00	8.74E+00
0.1	4.87E-02	3.59E-01	5.52E-01	6.22E-01	1.18E+00	1.54E+00	2.56E+00	4.74E+00	7.97E+00
0.15	4.33E-02	3.08E-01	4.67E-01	5.29E-01	1.01E+00	1.30E+00	2.19E+00	4.05E+00	6.88E+00
0.2	4.14E-02	2.69E-01	4.09E-01	4.66E-01	8.83E-01	1.15E+00	1.94E+00	3.61E+00	6.15E+00
0.3	3.66E-02	2.17E-01	3.26E-01	3.66E-01	7.06E-01	9.20E-01	1.57E+00	2.96E+00	5.07E+00
0.4	3.13E-02	1.75E-01	2.61E-01	2.95E-01	5.62E-01	7.37E-01	1.26E+00	2.41E+00	4.12E+00
0.5	2.62E-02	1.44E-01	2.15E-01	2.41E-01	4.61E-01	6.05E-01	1.05E+00	2.01E+00	3.44E+00
0.75	1.83E-02	1.00E-01	1.43E-01	1.61E-01	3.05E-01	3.98E-01	6.96E-01	1.31E+00	2.30E+00
1	1.37E-02	7.54E-02	1.09E-01	1.20E-01	2.20E-01	2.87E-01	4.96E-01	9.42E-01	1.61E+00
1.5	9.09E-03	5.50E-02	7.59E-02	8.41E-02	1.45E-01	1.87E-01	3.12E-01	5.76E-01	9.80E-01
2	6.63E-03	4.44E-02	6.08E-02	6.65E-02	1.13E-01	1.41E-01	2.31E-01	4.18E-01	7.03E-01
3	4.03E-03	3.16E-02	4.33E-02	4.79E-02	7.66E-02	9.63E-02	1.49E-01	2.64E-01	4.30E-01
5	2.26E-03	2.13E-02	2.94E-02	3.20E-02	5.24E-02	6.42E-02	9.94E-02	1.68E-01	2.66E-01
7.5	1.32E-03	1.38E-02	1.98E-02	2.15E-02	3.47E-02	4.27E-02	6.59E-02	1.11E-01	1.78E-01
10	8.64E-04	1.07E-02	1.44E-02	1.59E-02	2.64E-02	3.25E-02	4.97E-02	8.39E-02	1.32E-01

Table 10.13. Acronyms for seismic sources used in Chapter 10 figures.

Identifier	Seismic Source Name
AF	Arlington
AR	Ahtanum Ridge
ARH	Ahtanum – Rattlesnake Hills
CH	Columbia Hills
CM	Cleman Mountain
CSZ	Cascadia Subduction Zone
CTZ	Coseismic transition zone
FH	Frenchman Hills
FLTS	Total contribution of faults
HHH	Horse Heaven Hills
HR	Horn Rapids Fault
JDF	Juan de Fuca slab source
LB	Luna Butte
LF	Laurel
MF	Maupin
MR	Manastash Ridge
RAW	Rattles of the Rattlesnake-Wallula Alignment
RH	Rattlesnake Hills
RM	Rattlesnake Mountain
SB	Selah Butte
SFZ	Seattle Fault
SM	Saddle Mountain
TOT	Total mean seismic hazard
TR	Toppenish Ridge
UR	Umtanum Ridge
WF	Wallula Fault
YFTB	Yakima Fold and Thrust Belt Background
YR	Yakima Ridge
Zone B	Mid-C Study Zone B
Zone C	Mid-C Study Zone C
Zone D	Zone D
Zones	Total contribution of seismic zones

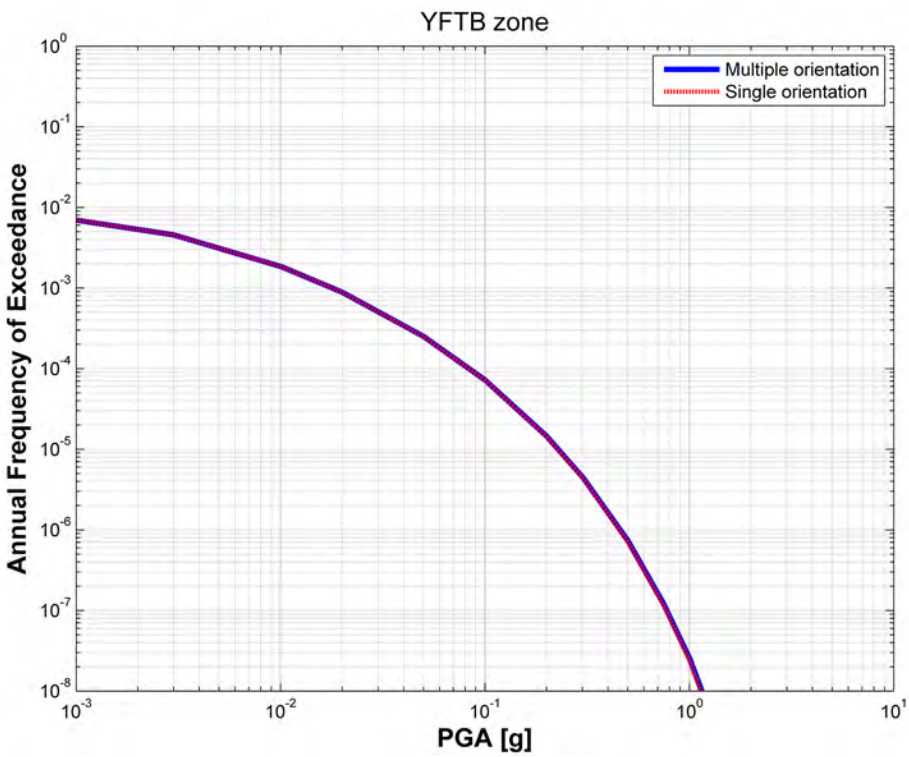

Figure 10.1. Comparison of the mean hazard computed for the YFTB zone using multiple rupture orientations (blue, solid curve) or single rupture orientation (red, dashed curve) and one ground motion model.

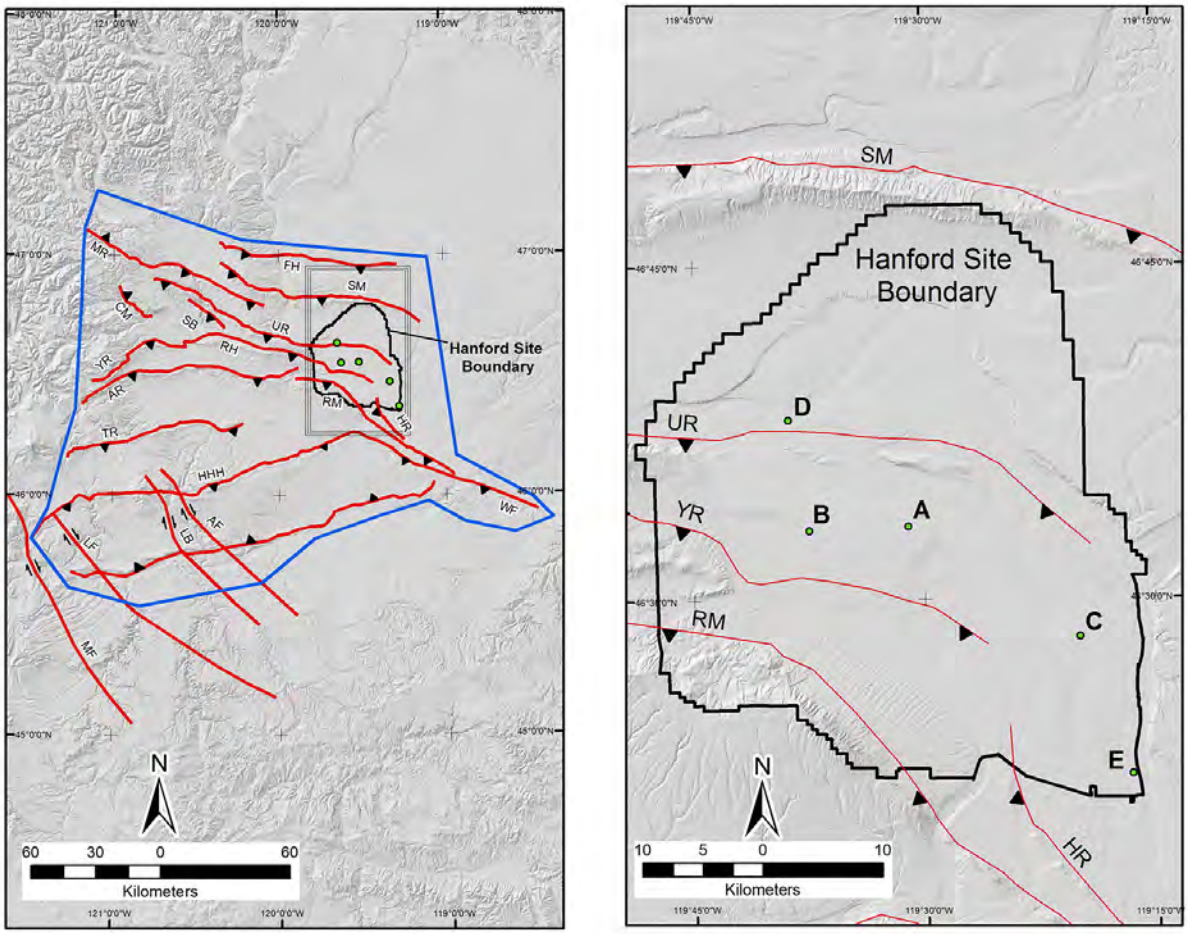

Figure 10.2. Maps showing locations of hazard calculation sites (green) relative to the Hanford Site boundary and fault sources (red). The left panel shows the YFTB Background source zone in blue. Fault sources are shown with teeth on the hanging wall. The black rectangle indicates the location of right panel. The right panel shows a detailed view of the hazard calculation sites on the Hanford Site.

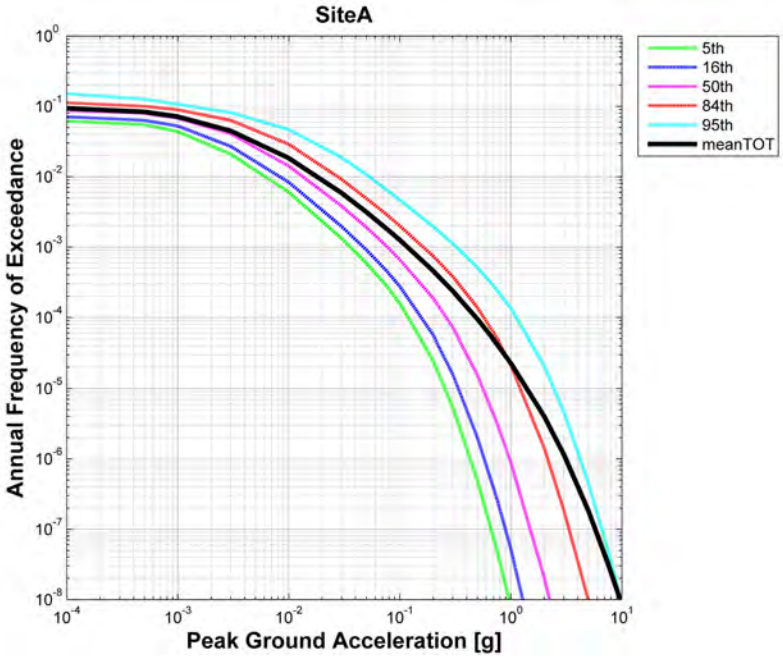

(a)

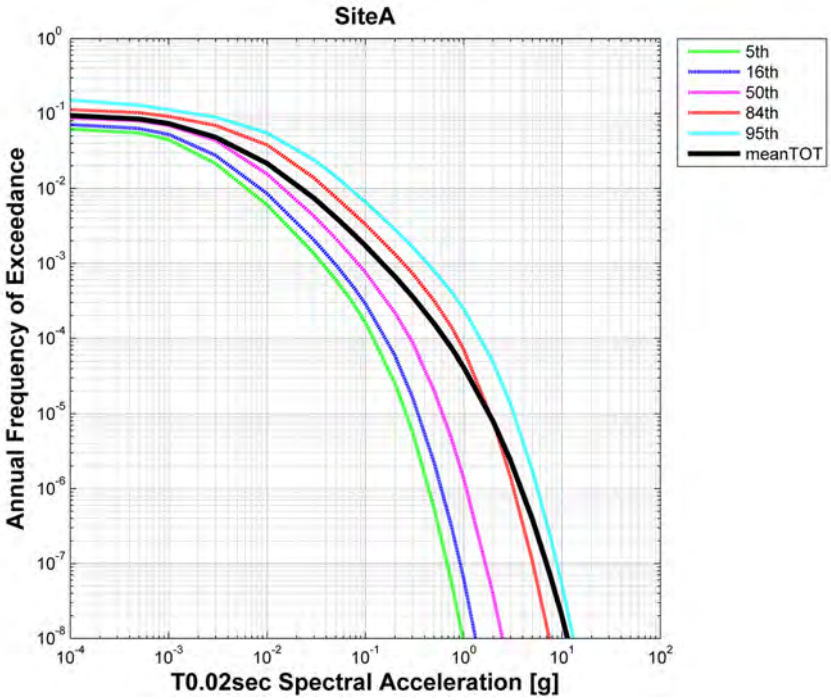

(b)

Figure 10.3. Total mean seismic hazard at Site A and percentiles: a) PGA; b) T 0.02-sec; c) T 0.03-sec; d) T 0.04-sec; e) T 0.05-sec; f) T 0.07-sec; g) T 0.10-sec; h) T 0.15-sec; i) T 0.20-sec; j) T 0.30-sec; k) T 0.40-sec; l) T 0.50-sec; m) T 0.75-sec; n) T 1.0-sec; o) T 1.5-sec; p) T 2.0-sec; q) T 3.0-sec; r) T 5.0-sec; s) T 7.5-sec; t) T 10-sec spectral acceleration.

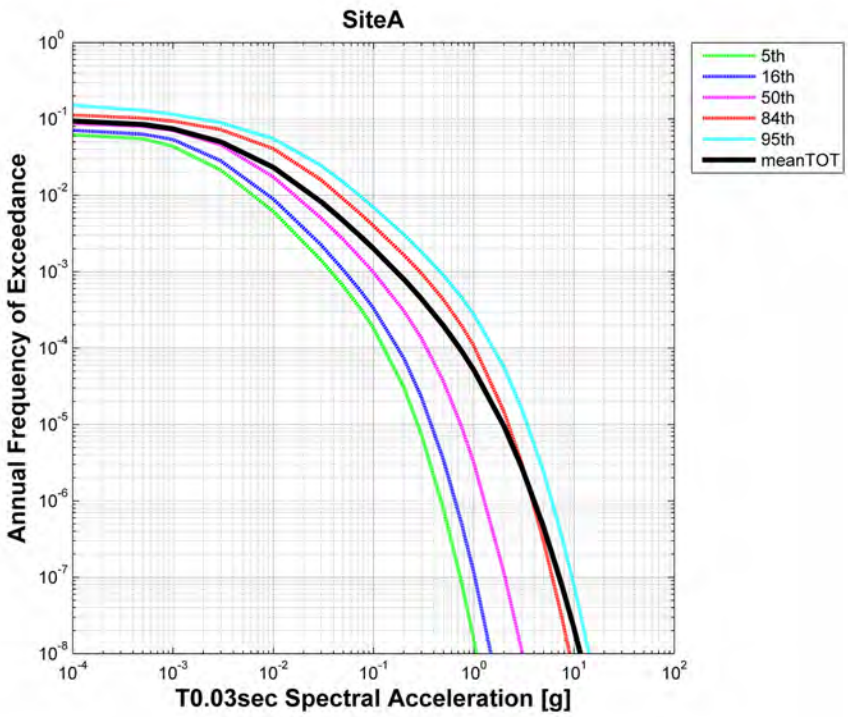

(c)

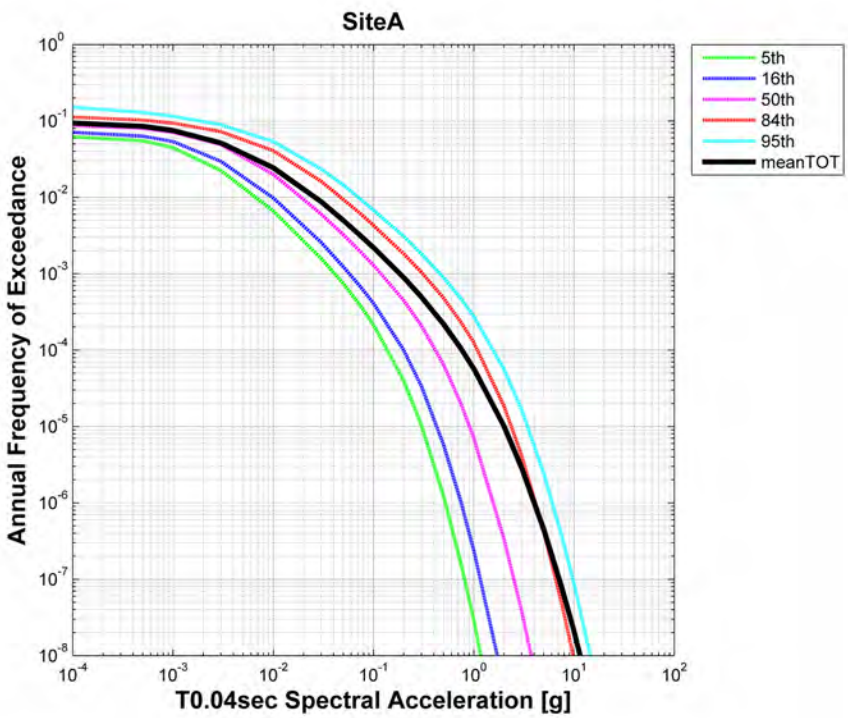

(d)

Figure 10.3. (contd)

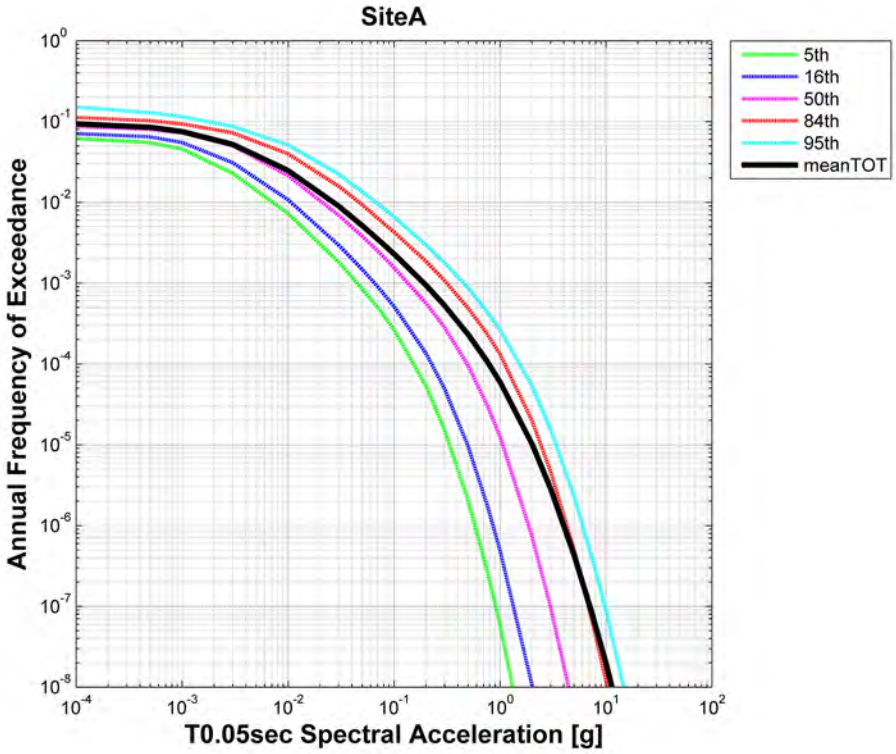

(e)

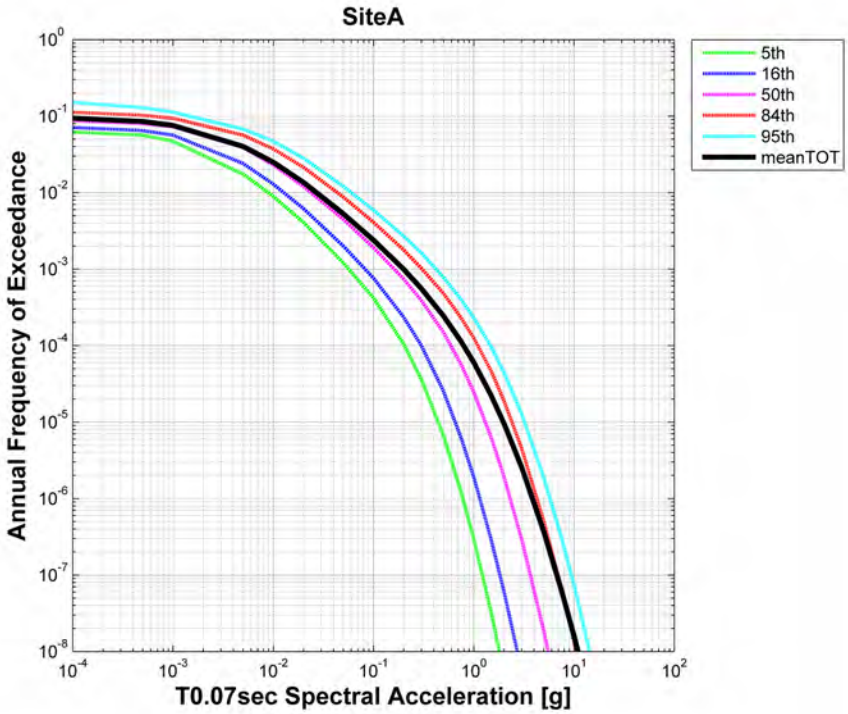

(f)

Figure 10.3. (contd)

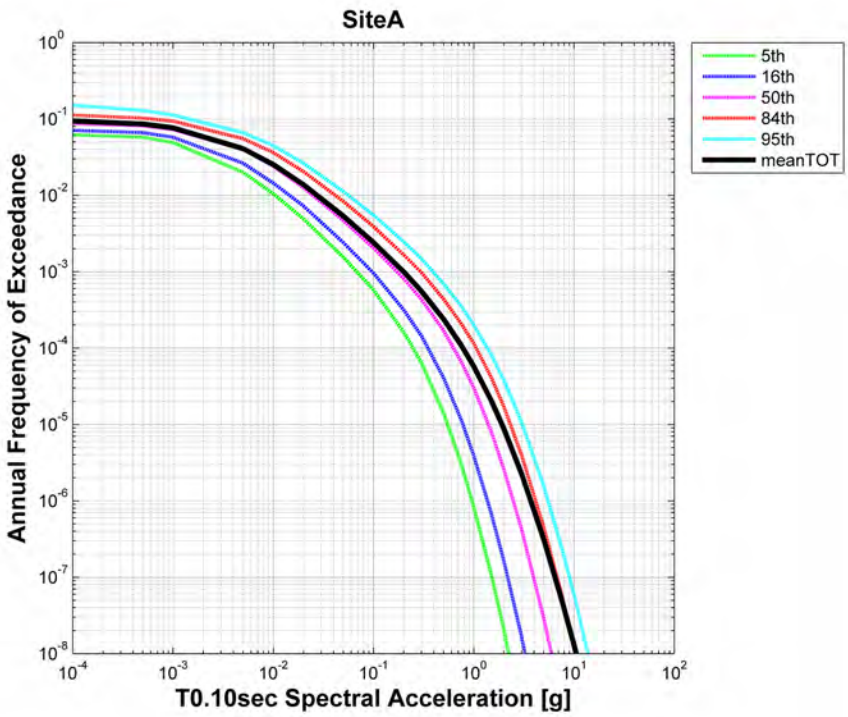

(g)

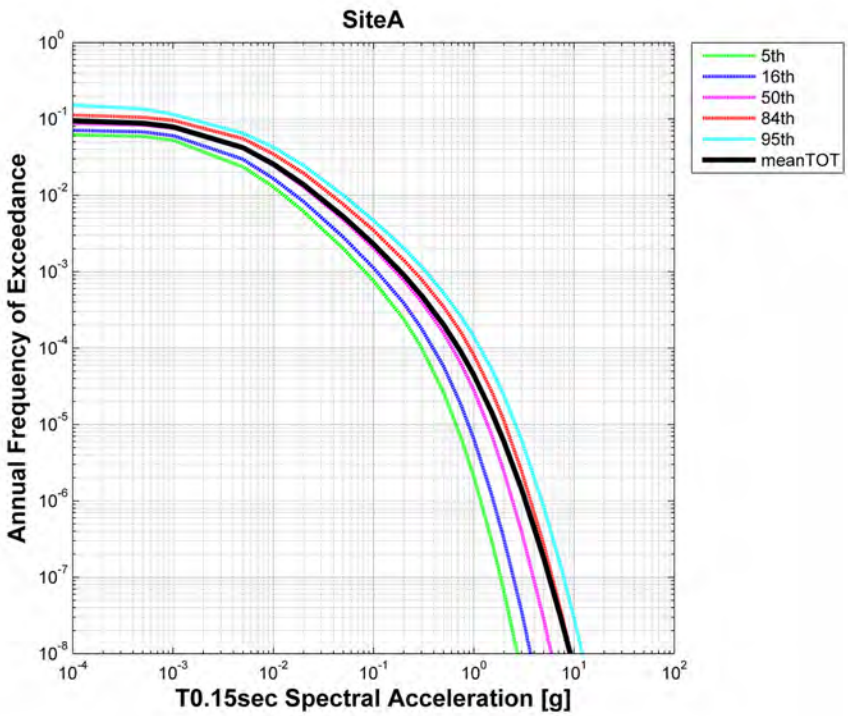

(h)

Figure 10.3. (contd)

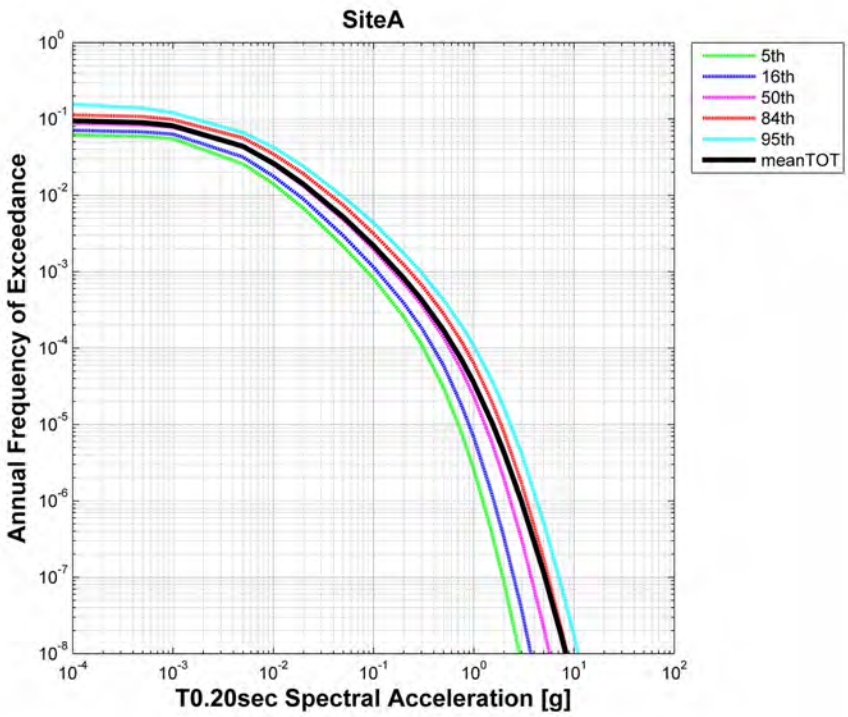

(i)

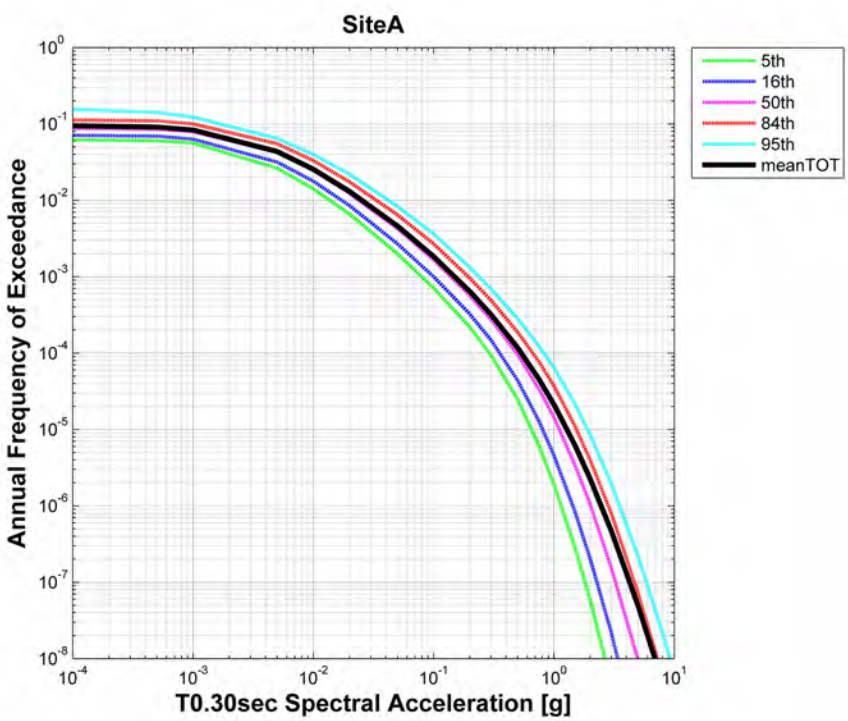

(j)

Figure 10.3. (contd)

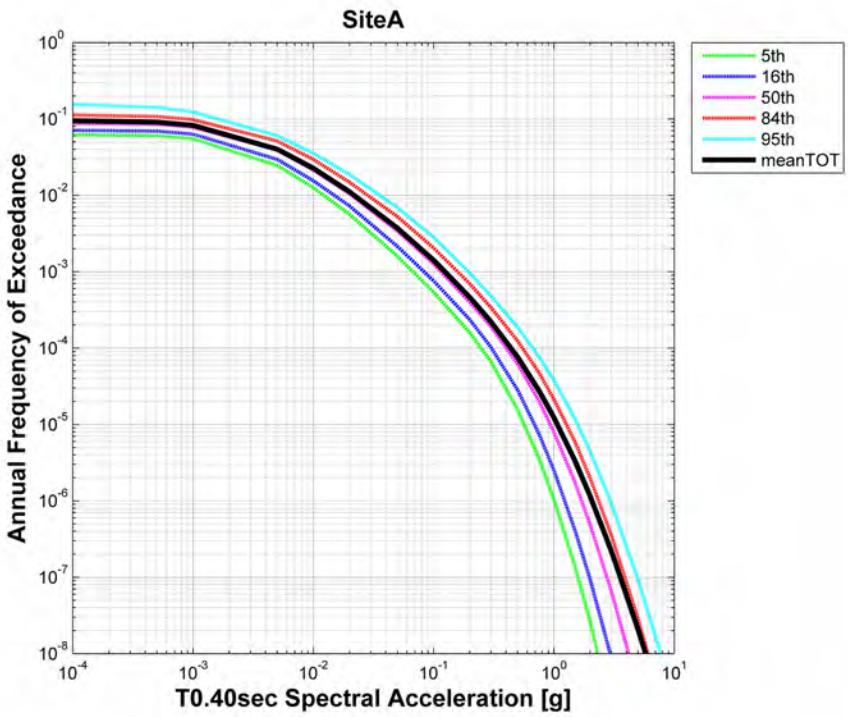

(k)

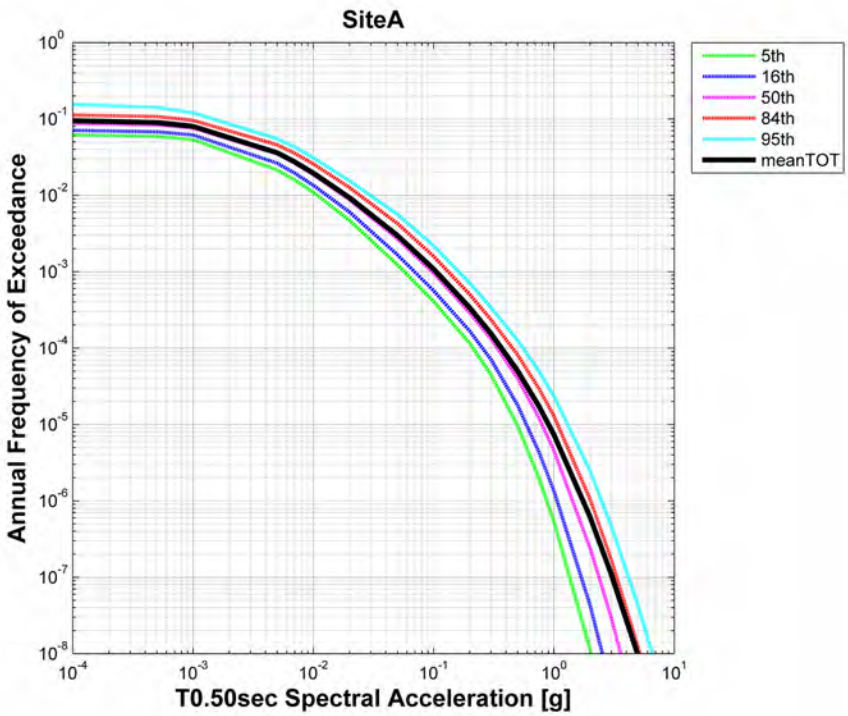

(l)

Figure 10.3. (contd)

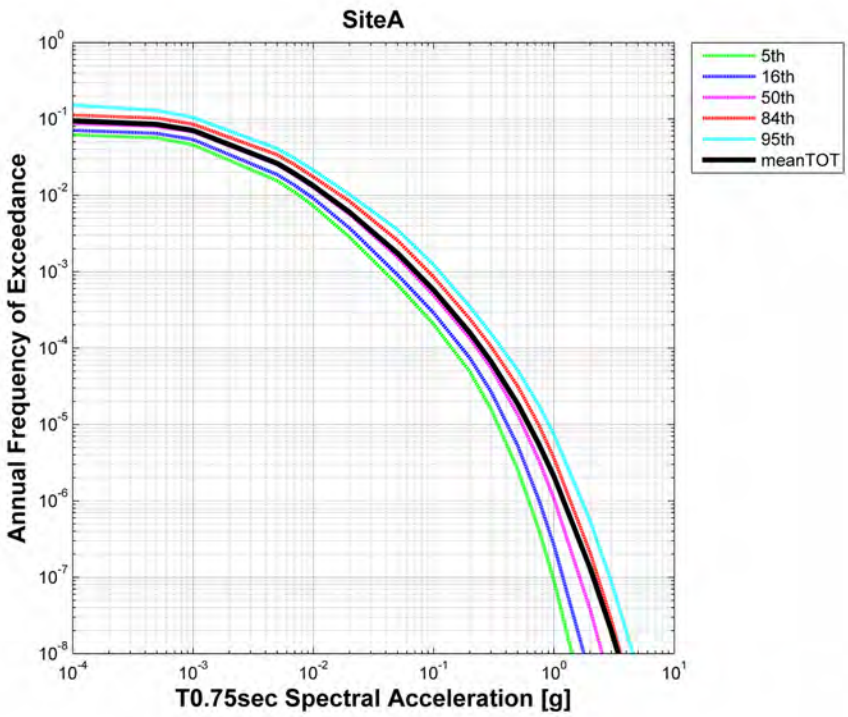

(m)

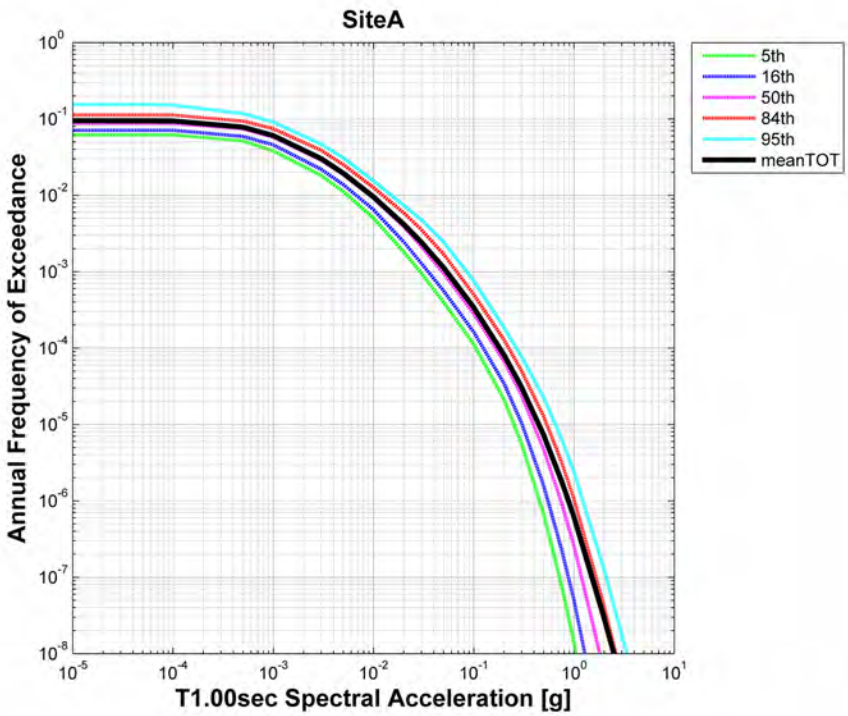

(n)

Figure 10.3. (contd)

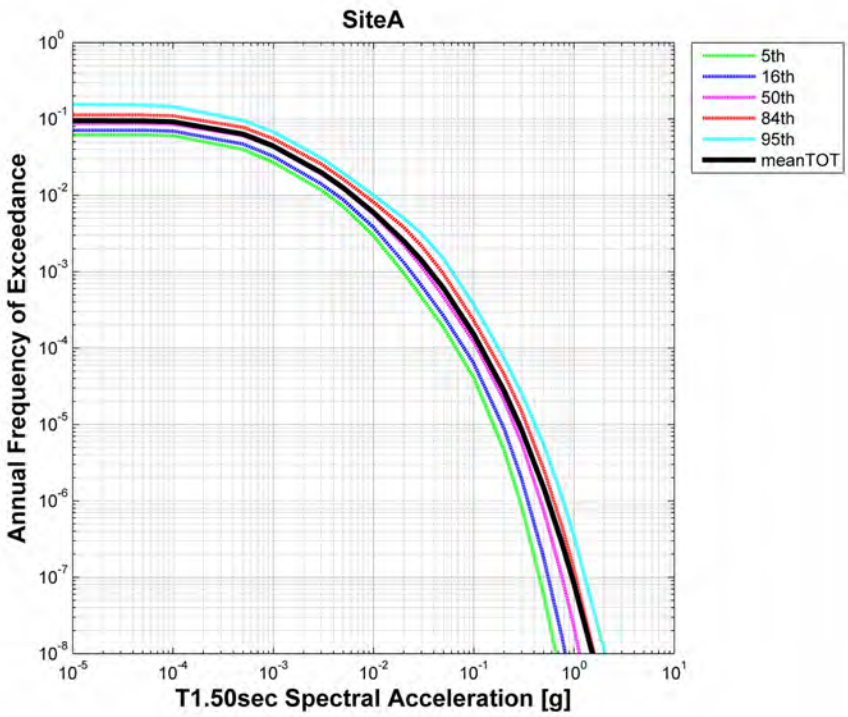

(o)

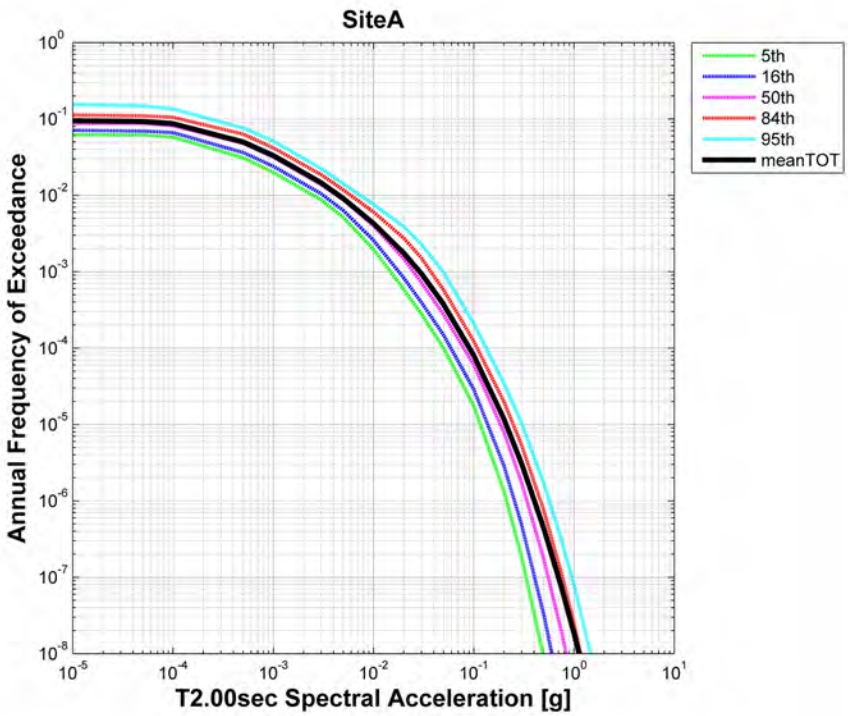

(p)

Figure 10.3. (contd)

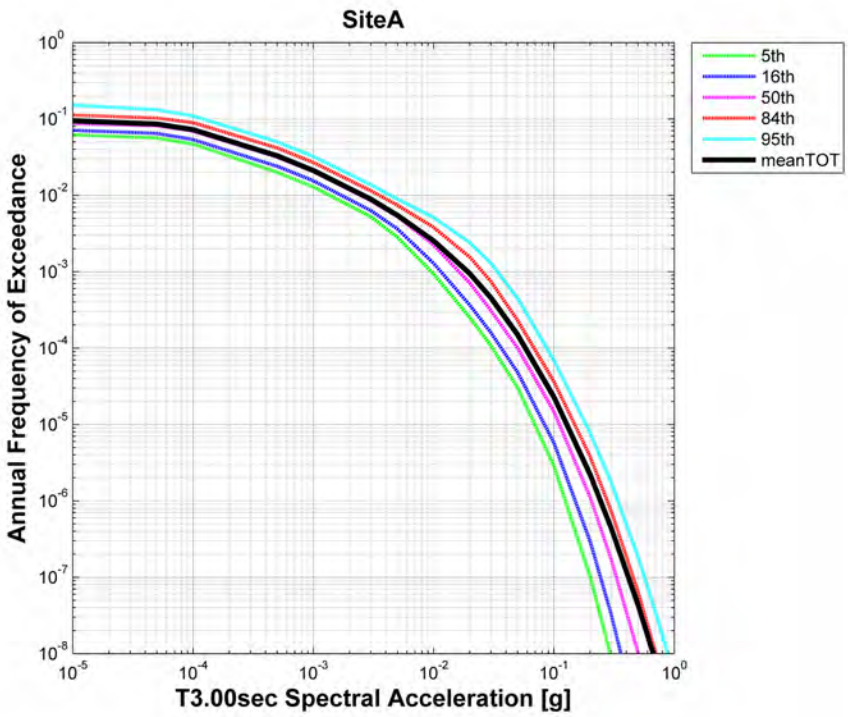

(q)

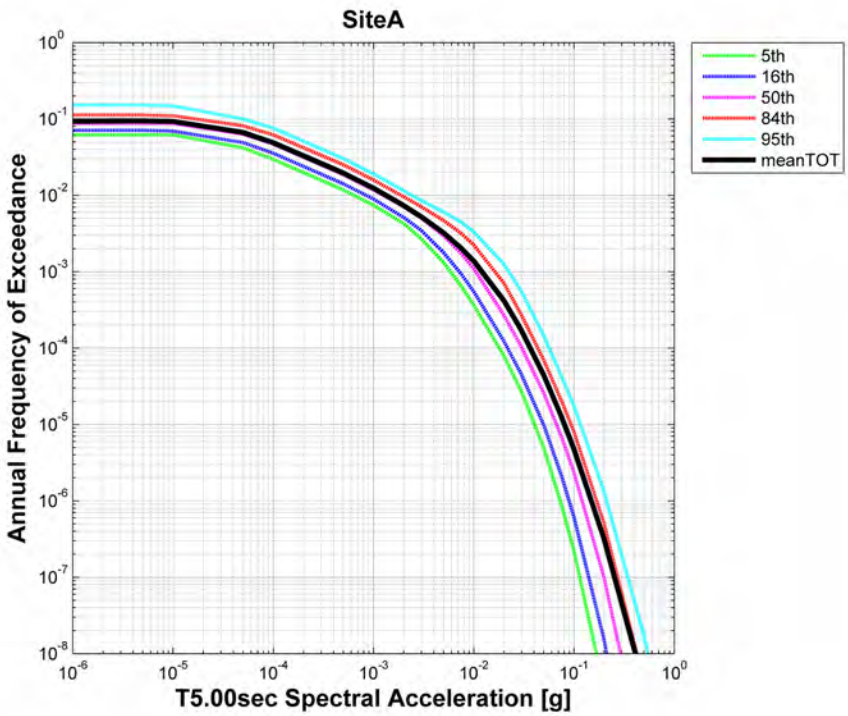

(r)

Figure 10.3. (contd)

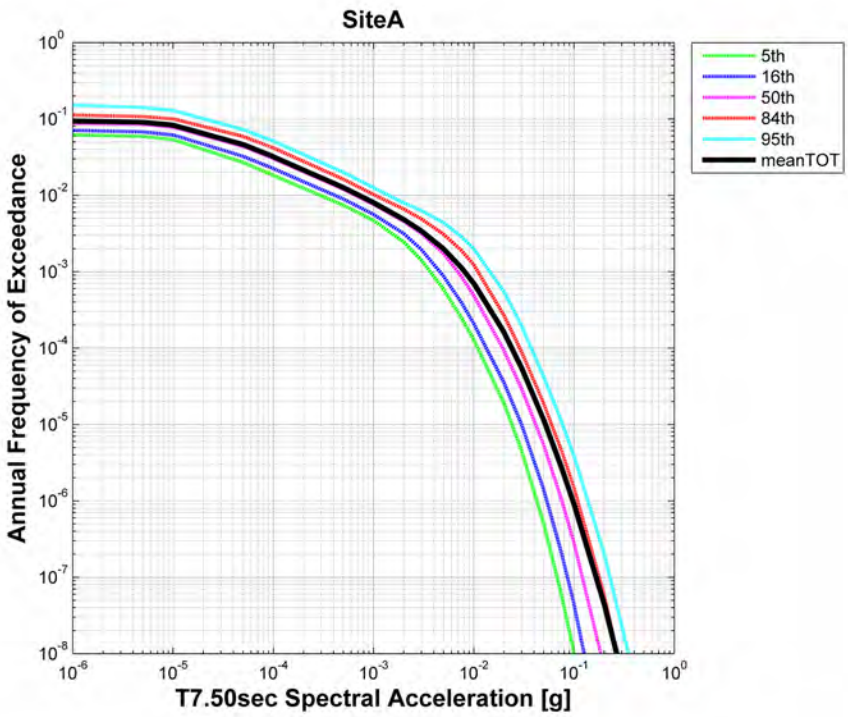

(s)

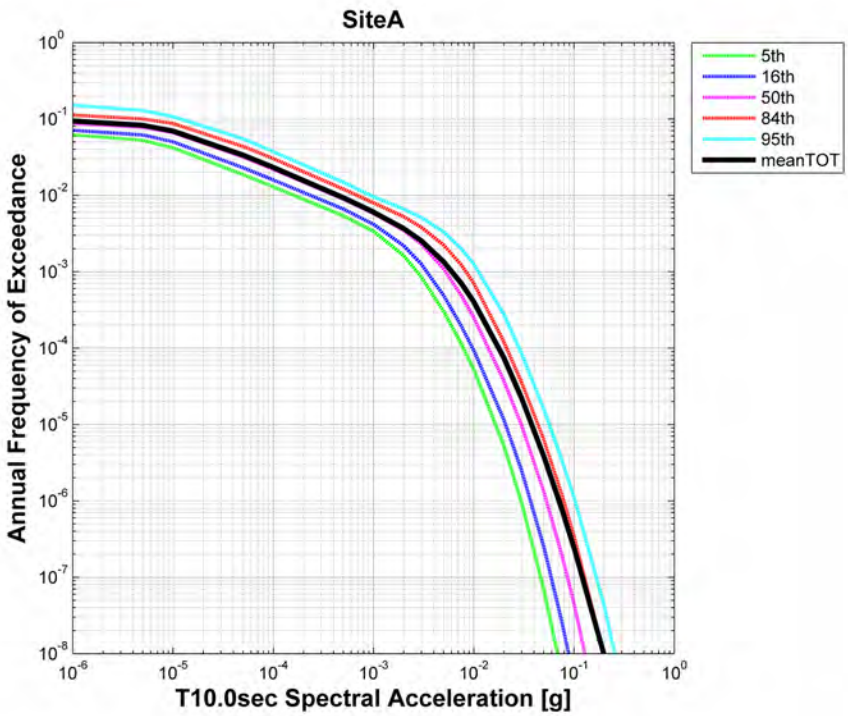

(t)

Figure 10.3. (contd)

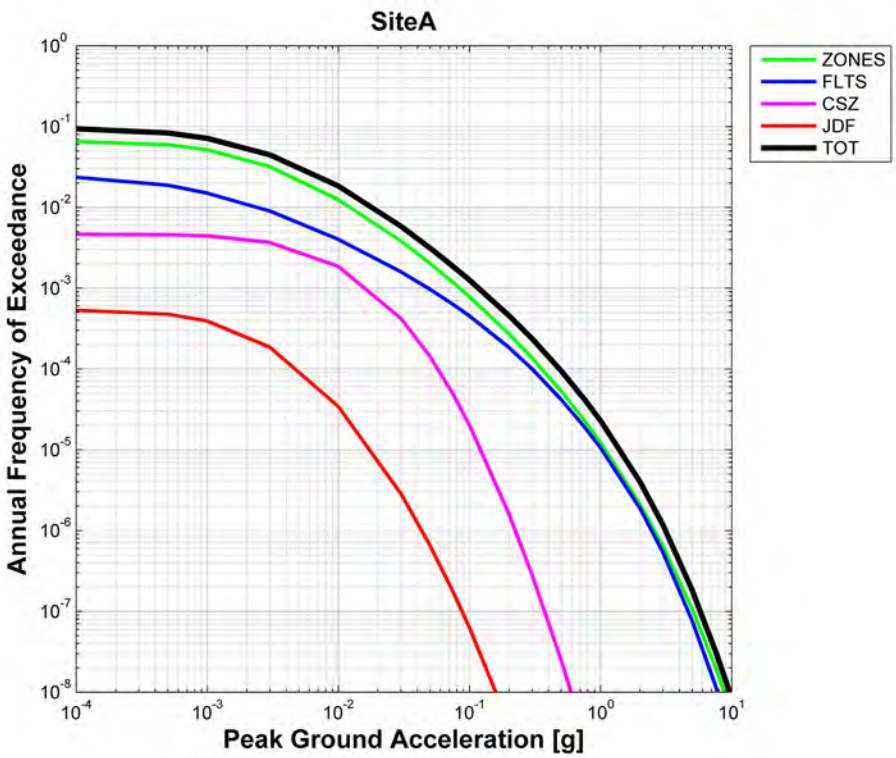

(a)

Figure 10.4. Comparison between the total mean seismic hazard at Site A (black curve) and the contribution of crustal source zones (green curve), faults (blue curve), the Cascadia interface (CSZ − magenta curve), and Cascadia intraslab source (JDF − red curve): a) PGA; b) T 0.02-sec; c) T 0.03-sec; d) T 0.04-sec; e) T 0.05-sec; f) T 0.07-sec; g) T 0.10-sec; h) T 0.15-sec; i) T 0.20-sec; j) T 0.30-sec; k) T 0.40-sec; l) T 0.50-sec; m) T 0.75-sec; n) T 1.0-sec; o) T 1.5-sec; p) T 2.0-sec; q) T 3.0-sec; r) T 5.0-sec; s) T 7.5-sec; t) T 10-sec spectral acceleration.

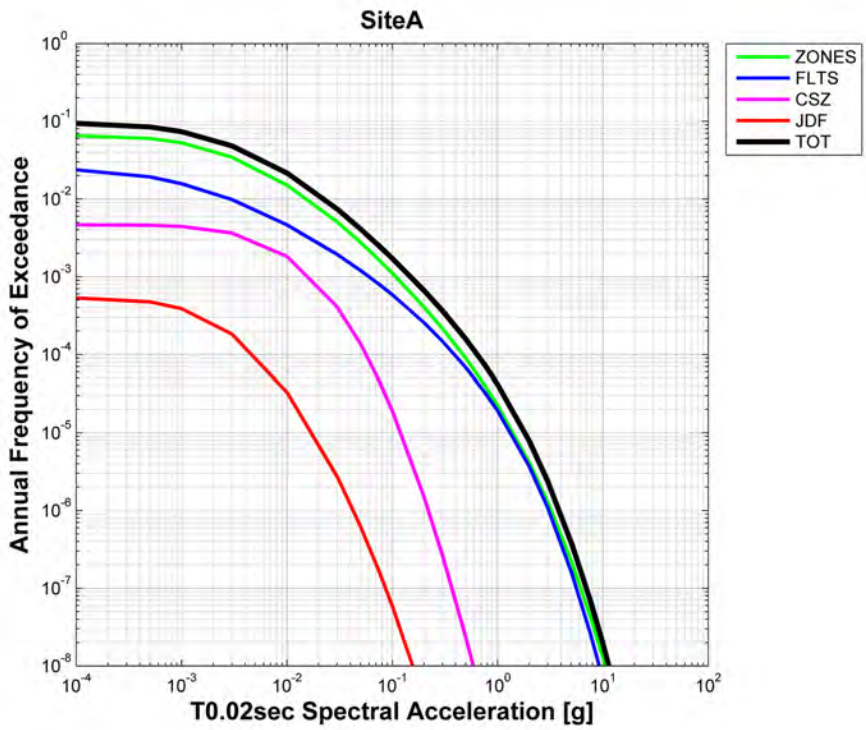

(b)

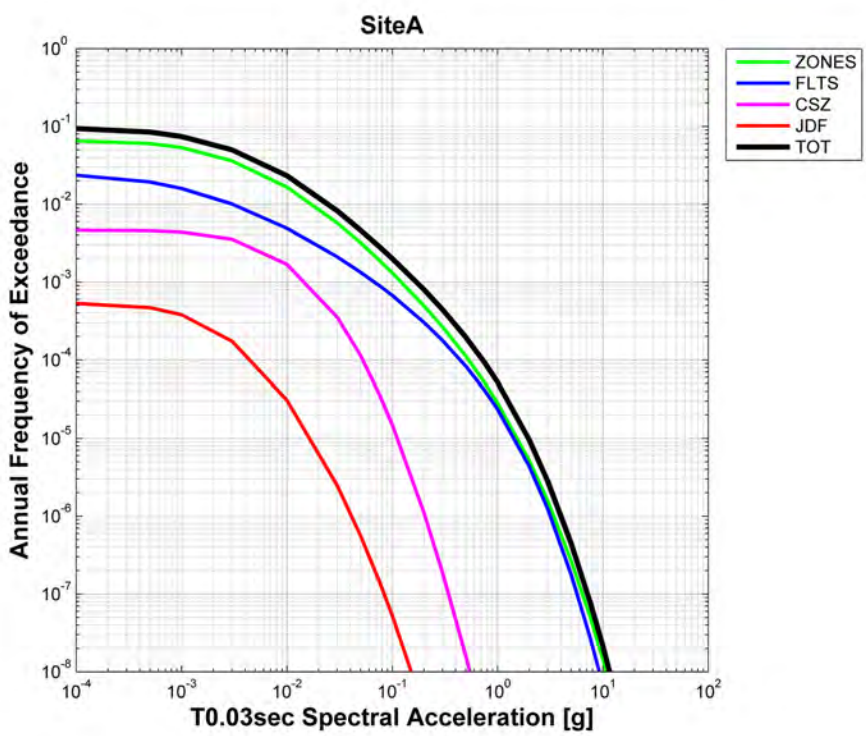

(c)

Figure 10.4. (contd)

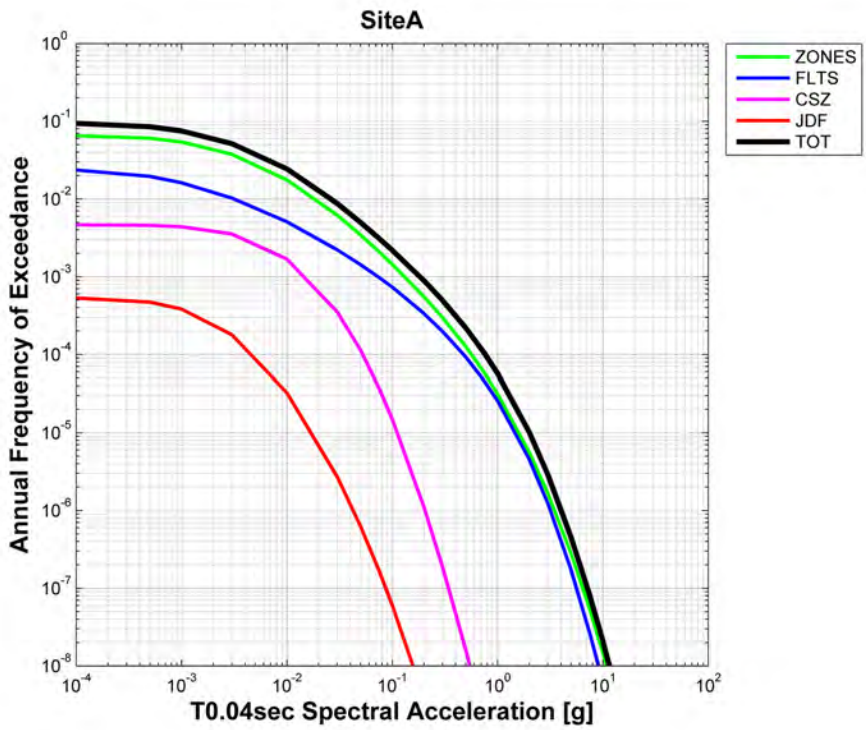

(d)

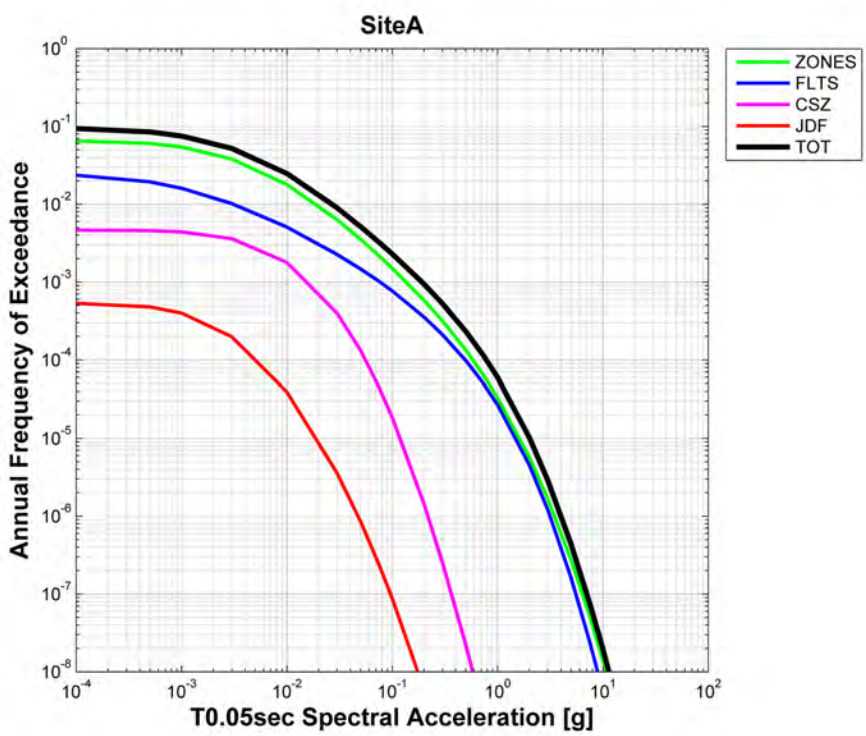

(e)

Figure 10.4. (contd)

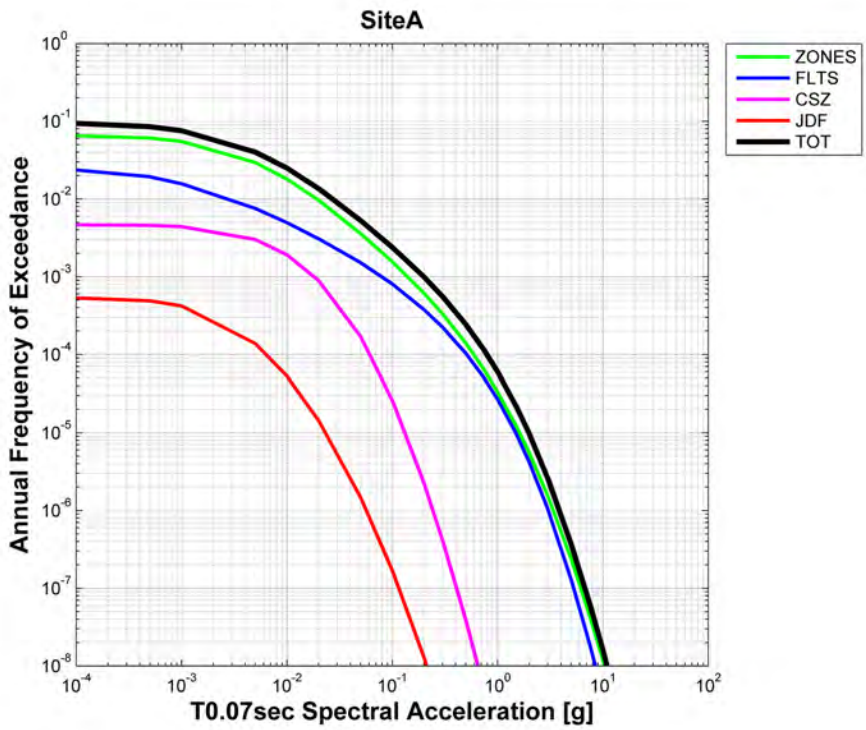

(f)

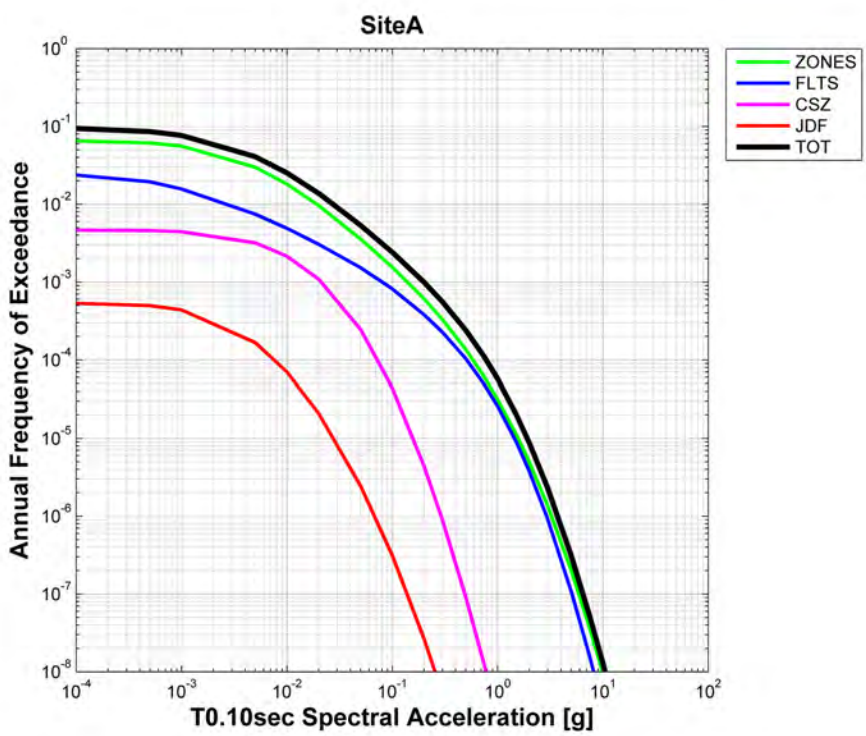

(g)

Figure 10.4. (contd)

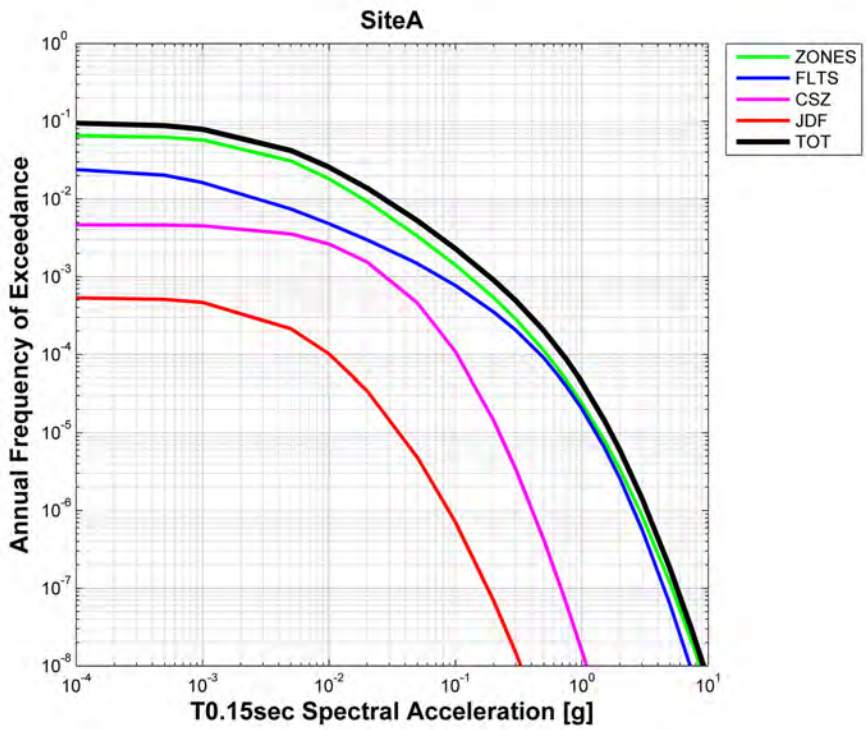

(h)

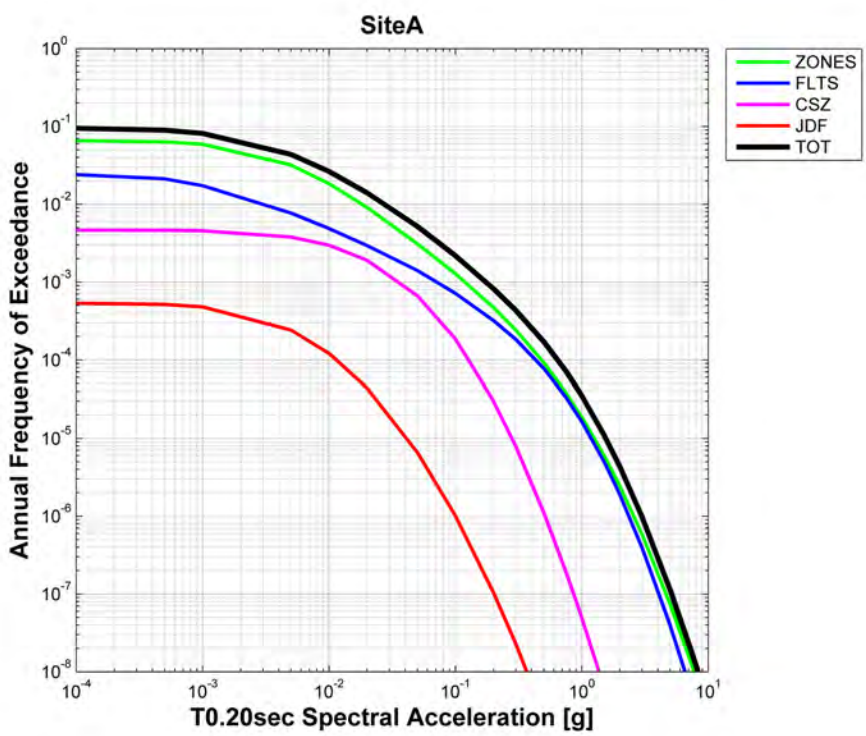

(i)

Figure 10.4. (contd)

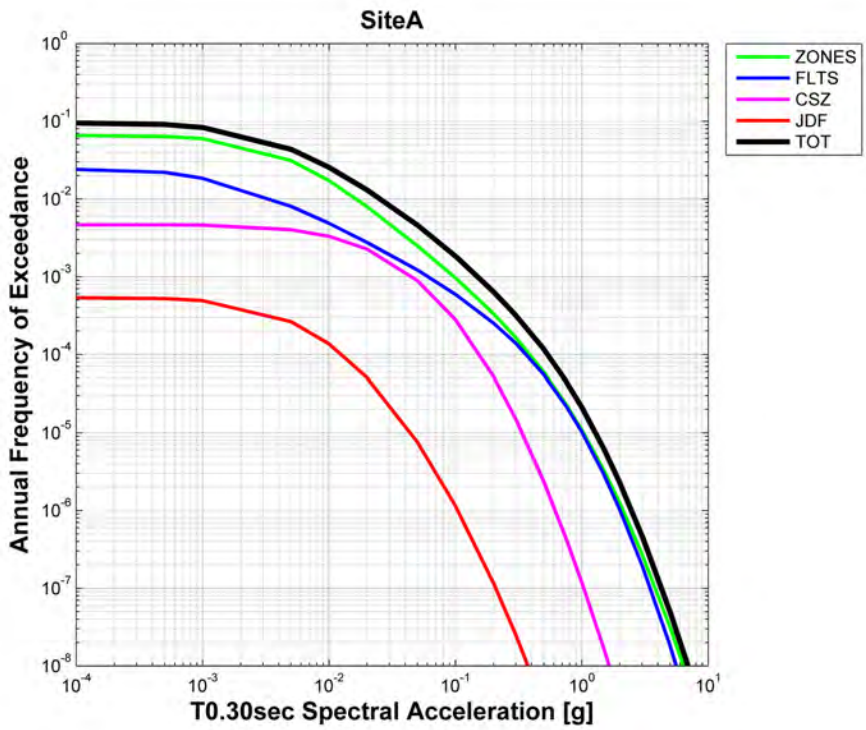

(j)

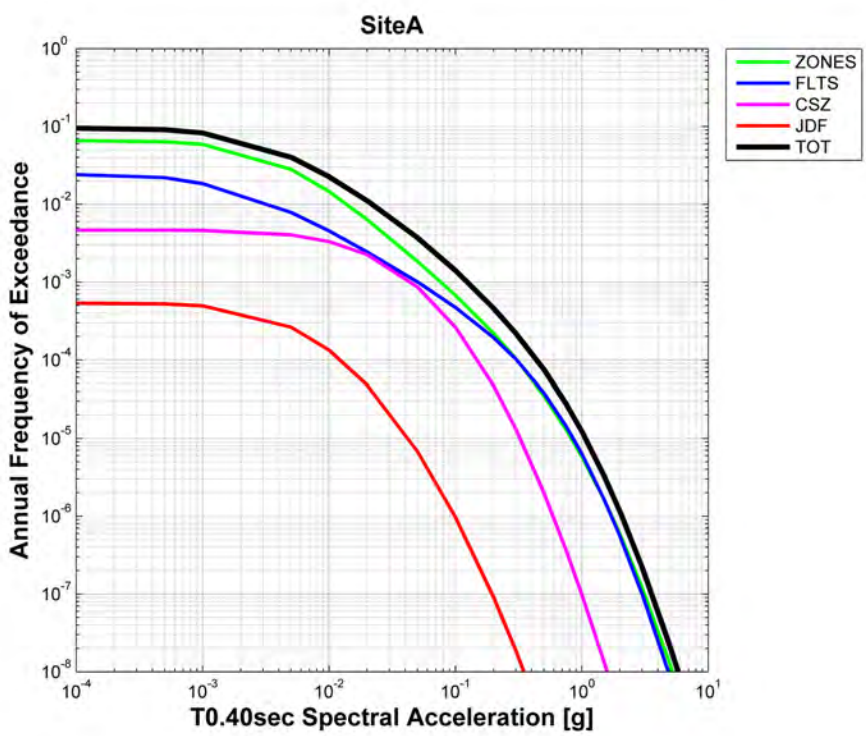

(k)

Figure 10.4. (contd)

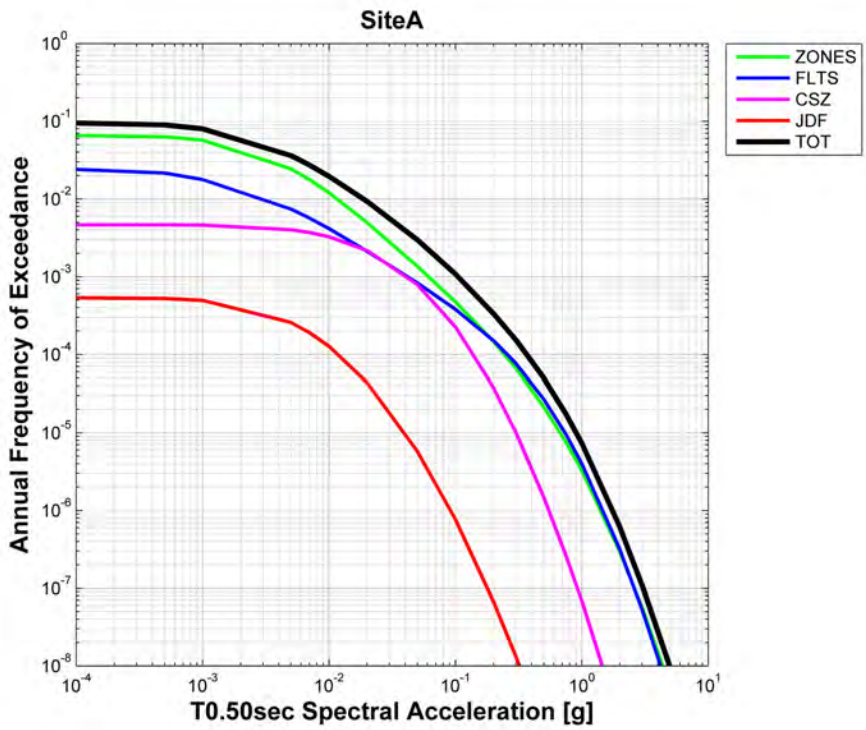

(l)

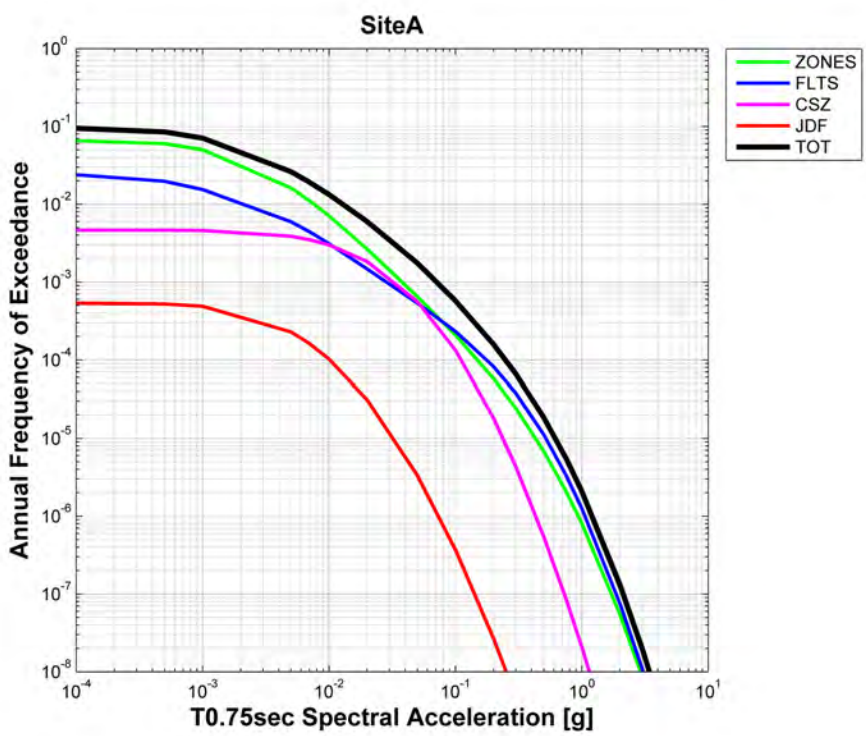

(m)

Figure 10.4. (contd)

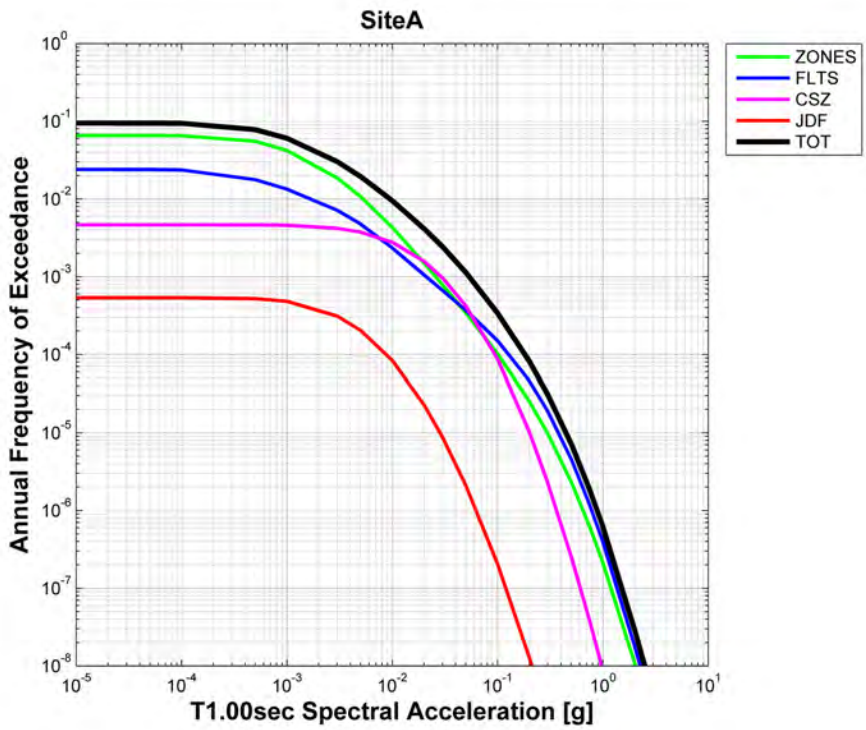

(n)

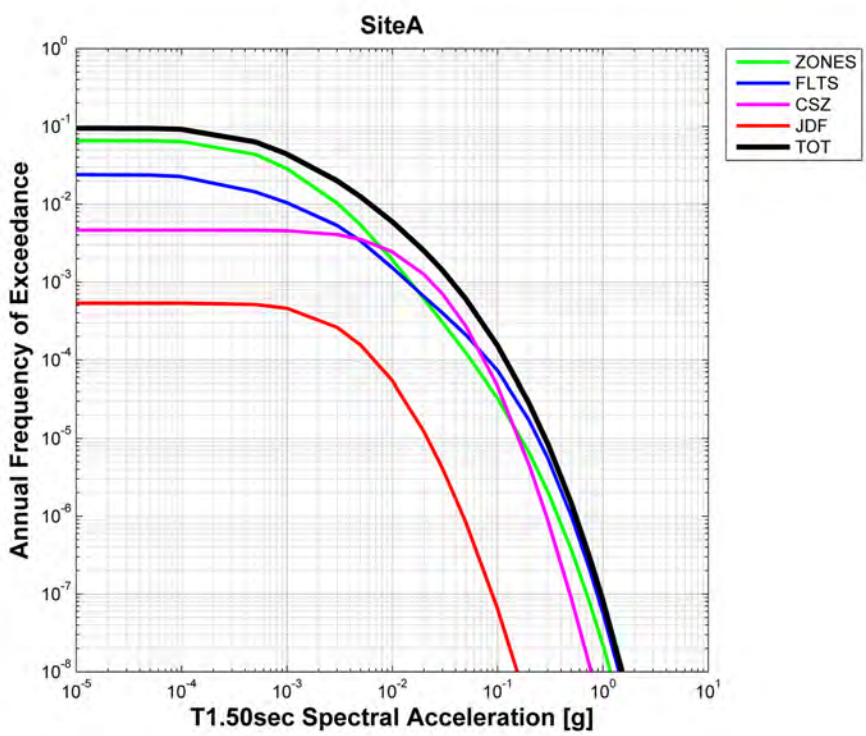

(o)

Figure 10.4. (contd)

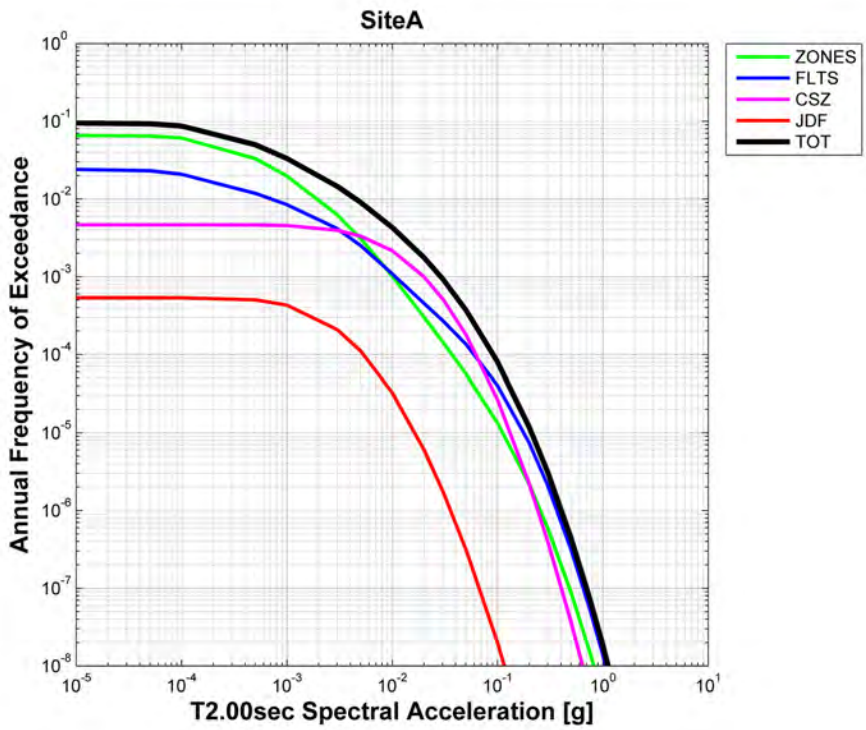

(p)

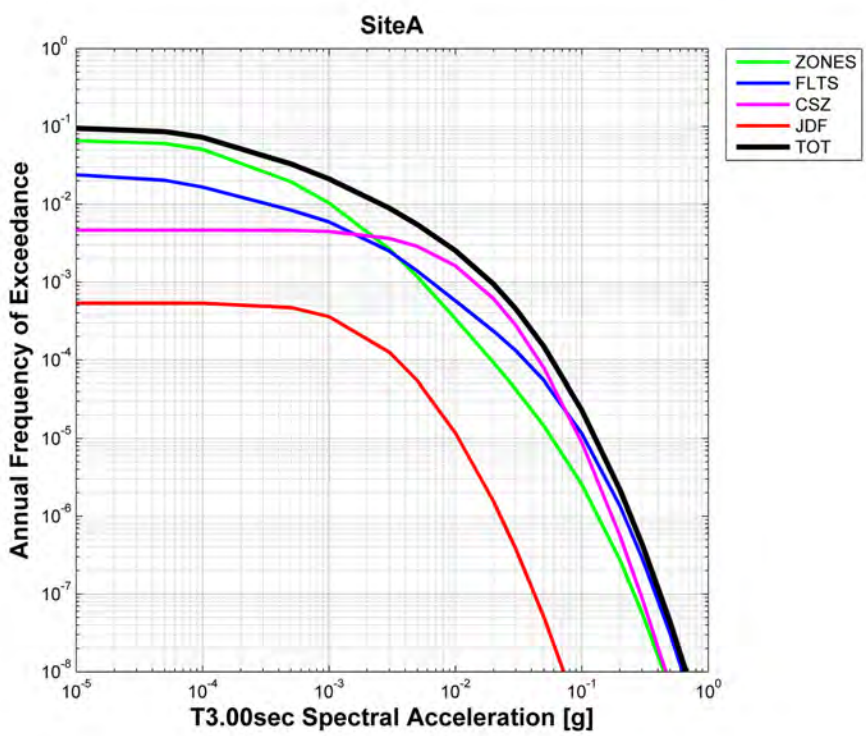

(q)

Figure 10.4. (contd)

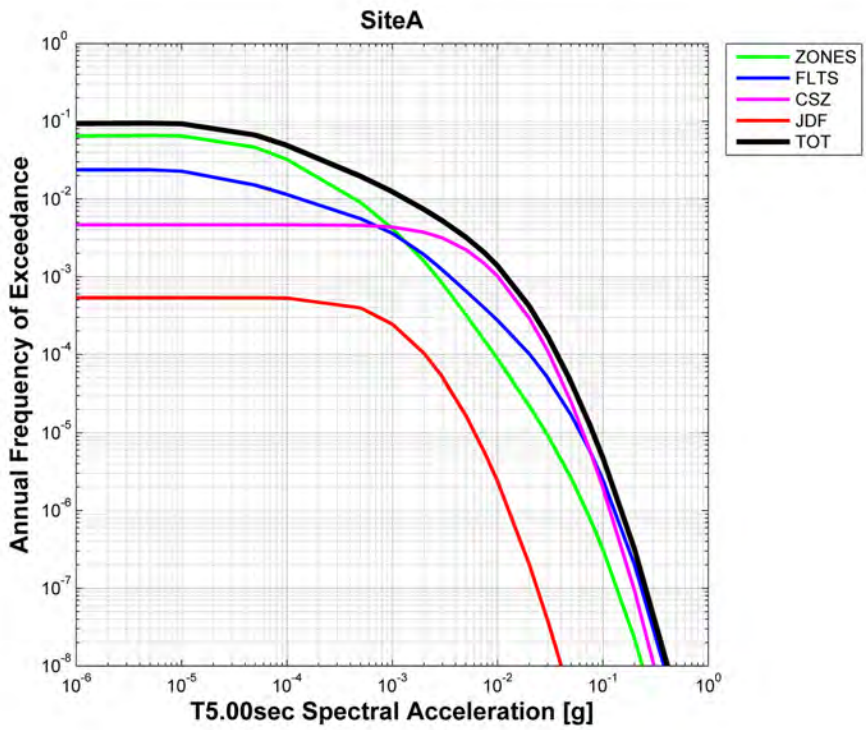

(r)

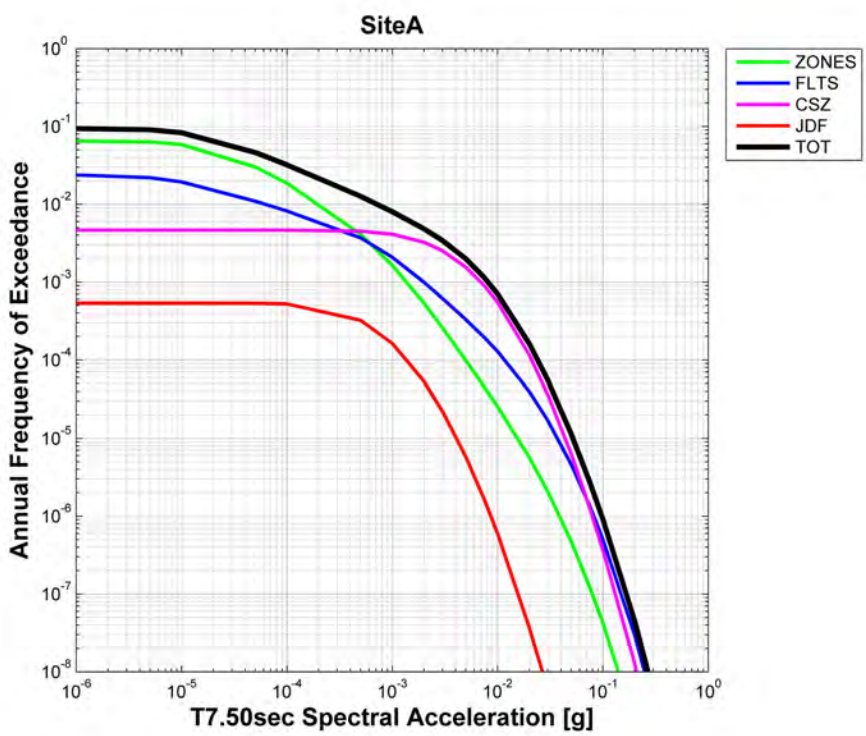

(s)

Figure 10.4. (contd)

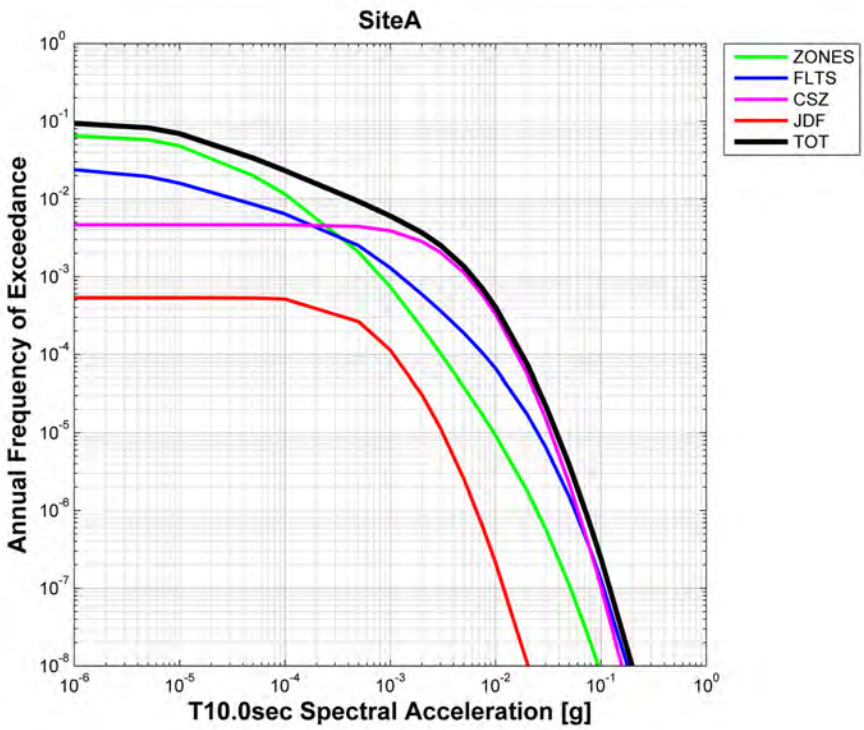

(t)

Figure 10.4. (contd)

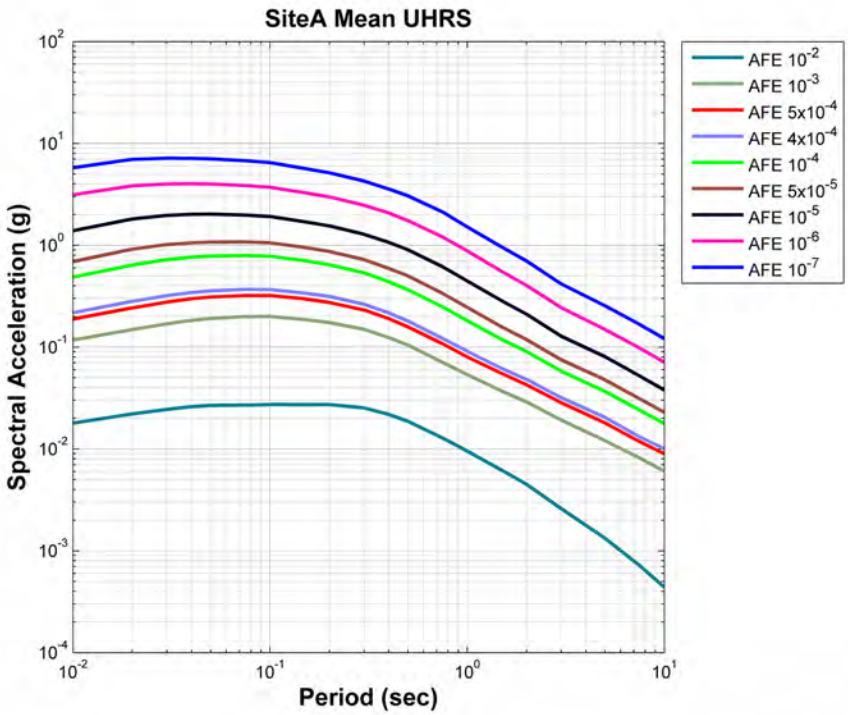

(a)

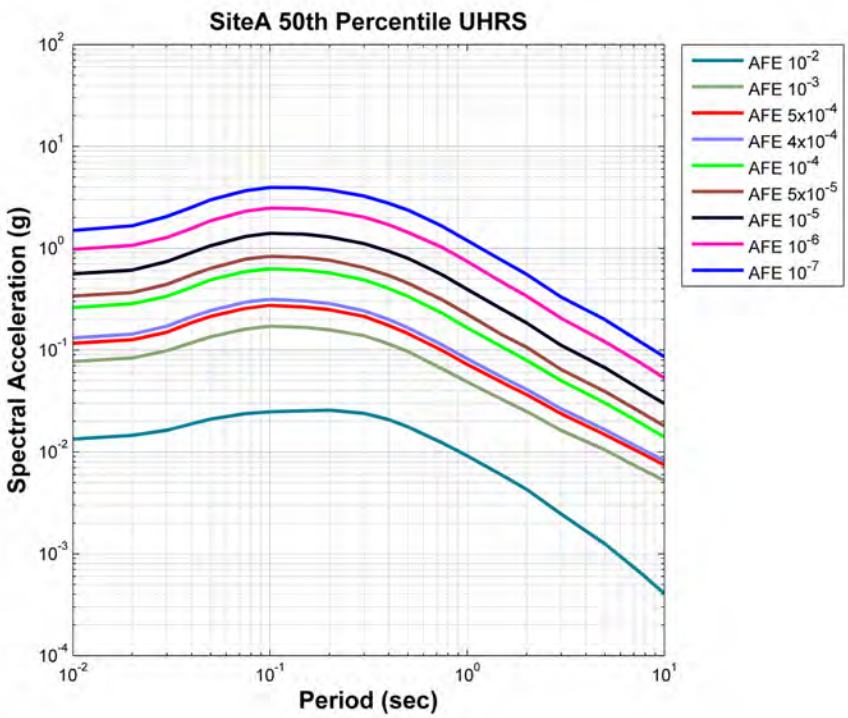

(b)

Figure 10.5. Uniform hazard response spectra at AFEs of 10^{-2}, 10^{-3}, 5×10^{-4}, 4×10^{-4}, 10^{-4}, 5×10^{-5}, 10^{-6}, 10^{-7} (return periods of 100, 1,000, 2,000, 2,500, 10,000, 20,000, 100,000, 1 million, and 10 million years) for: a) mean hazard; b) 50th percentile hazard; c) 84th percentile hazard.

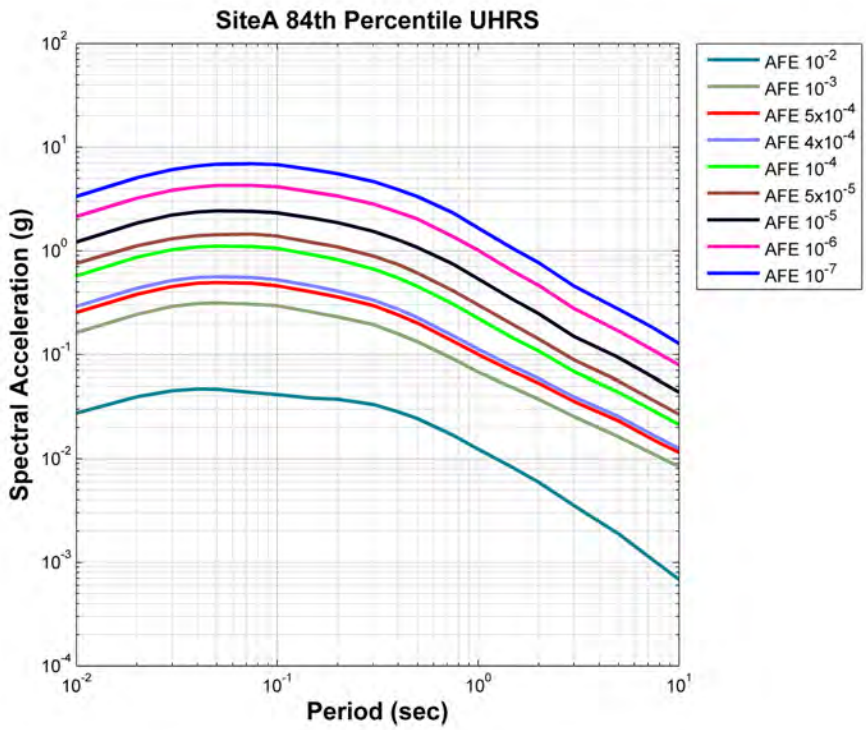

(c)

Figure 10.5. (contd)

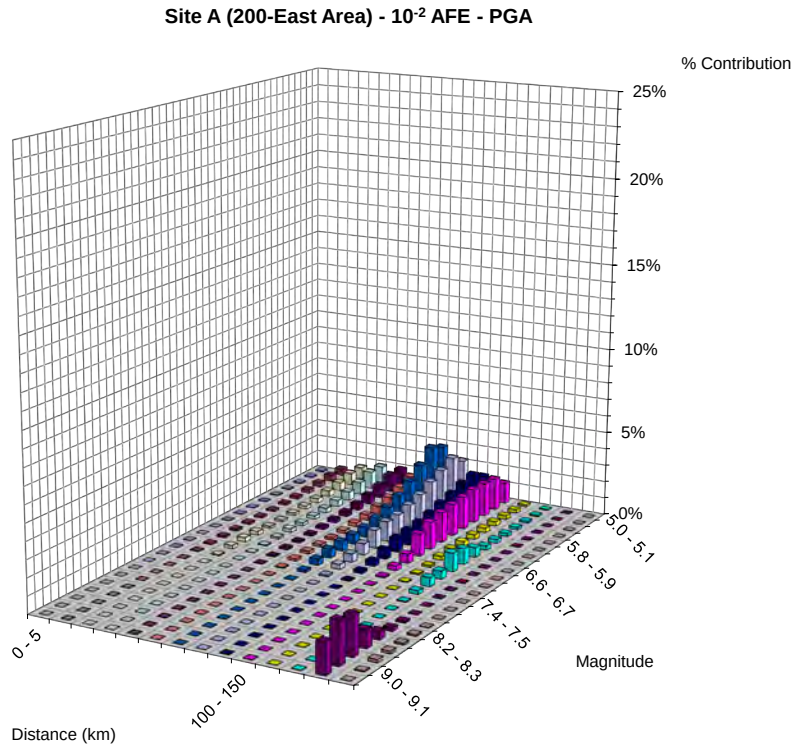

(a)

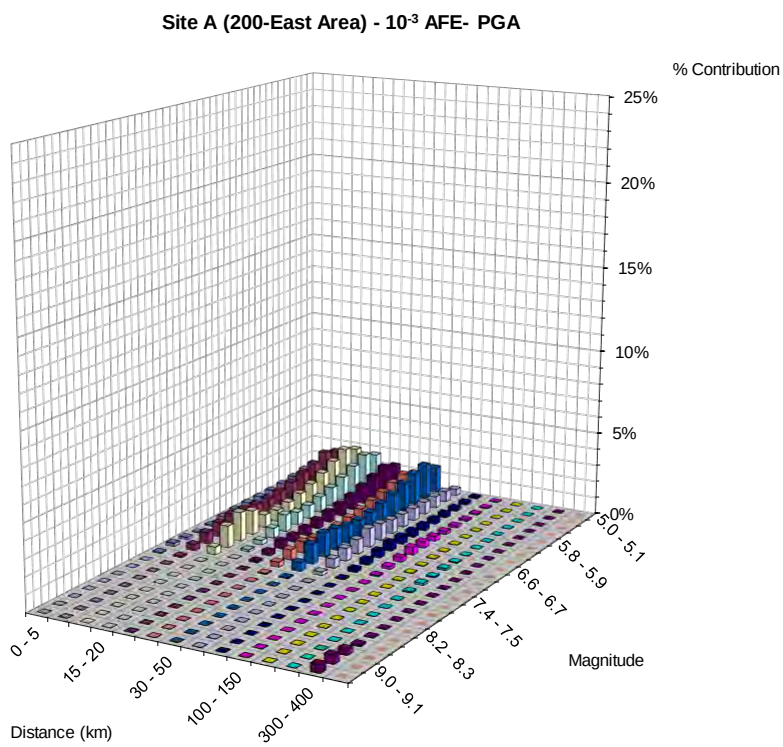

(b)

Figure 10.6. Deaggregation histogram showing magnitude-distance contributions to the total mean hazard at Site A for peak ground acceleration and AFEs of: a) 10^{-2}; b) 10^{-3}; c) 5×10^{-4}; d) 4×10^{-4}; e) 10^{-4}; f) 10^{-5}; g) 10^{-6}; h) 10^{-7}.

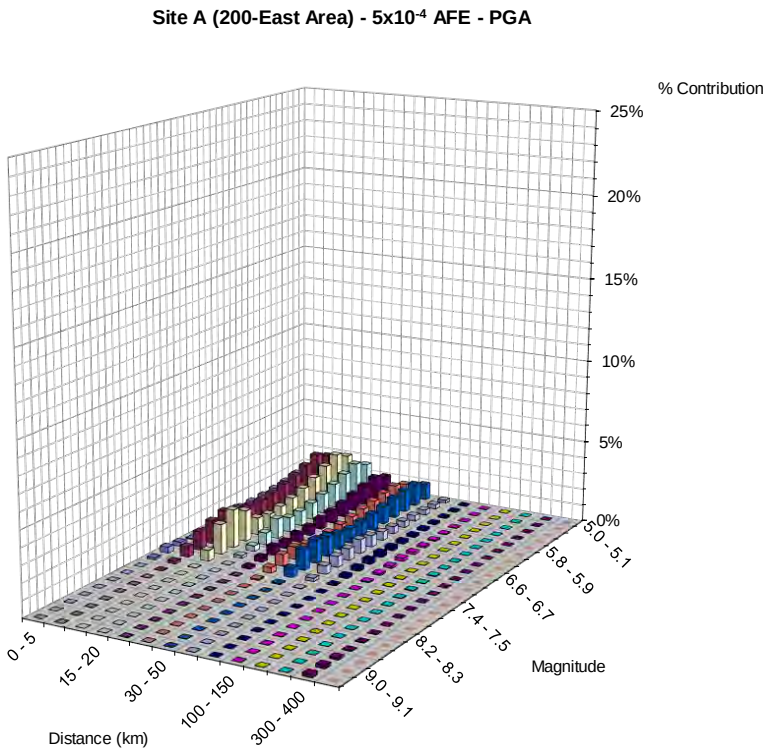

(c)

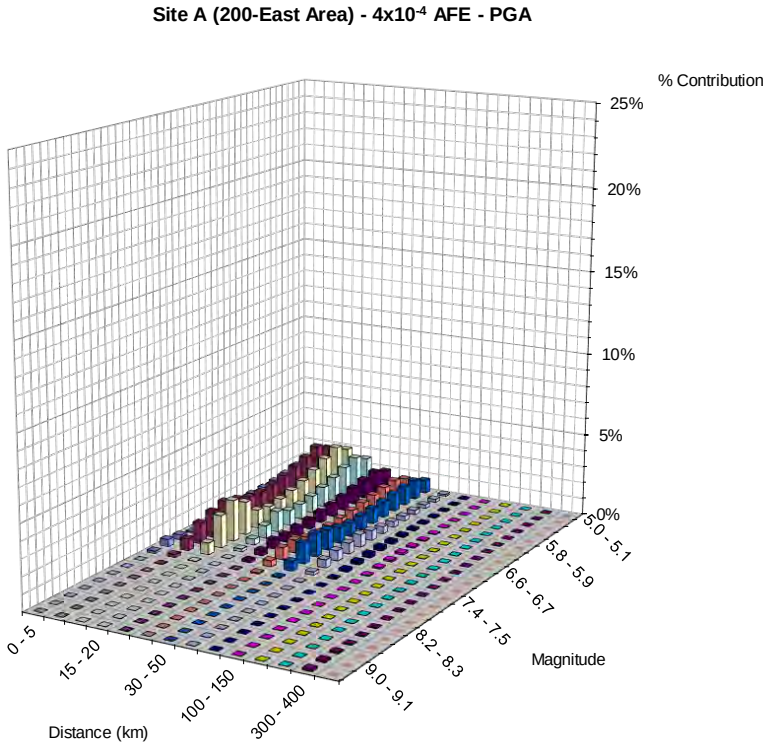

(d)

Figure 10.6. (contd)

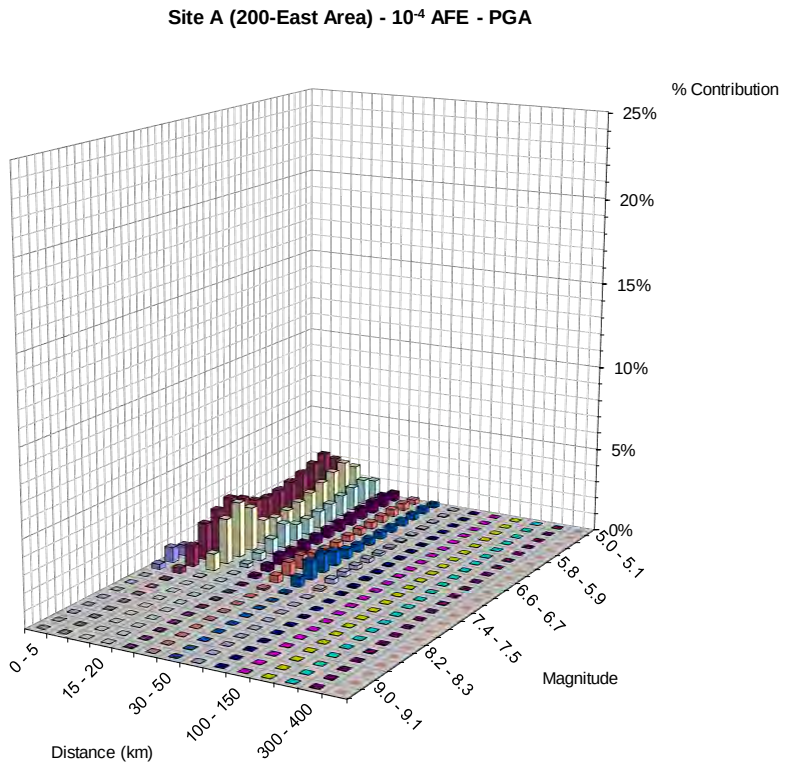

(e)

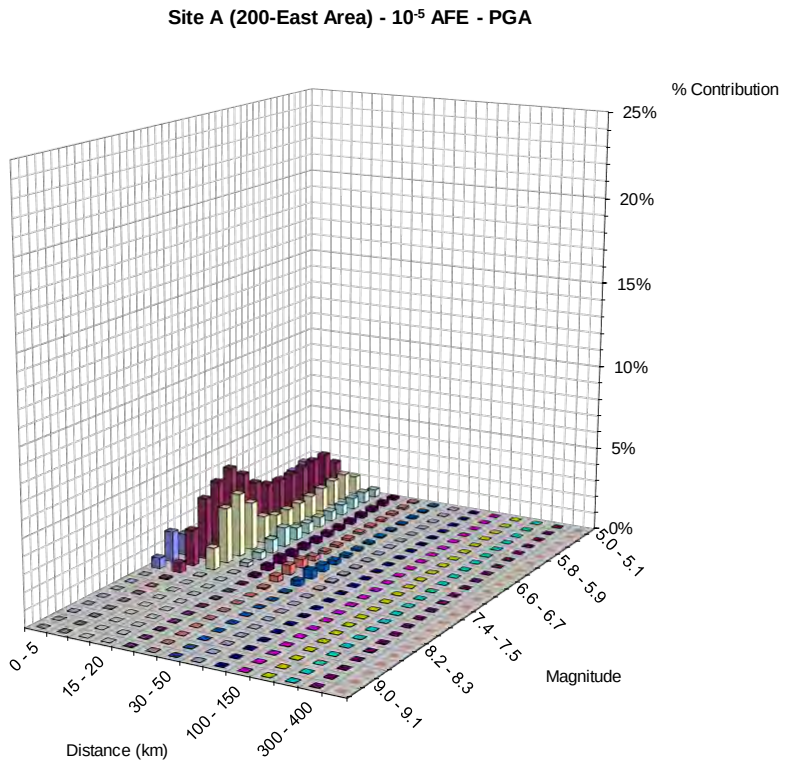

(f)

Figure 10.6. (contd)

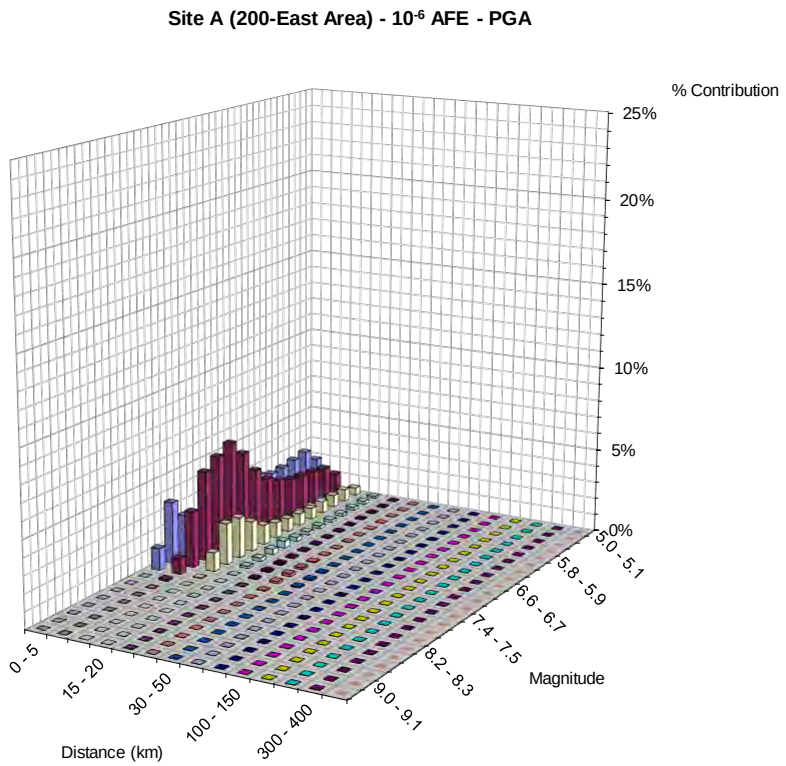

(g)

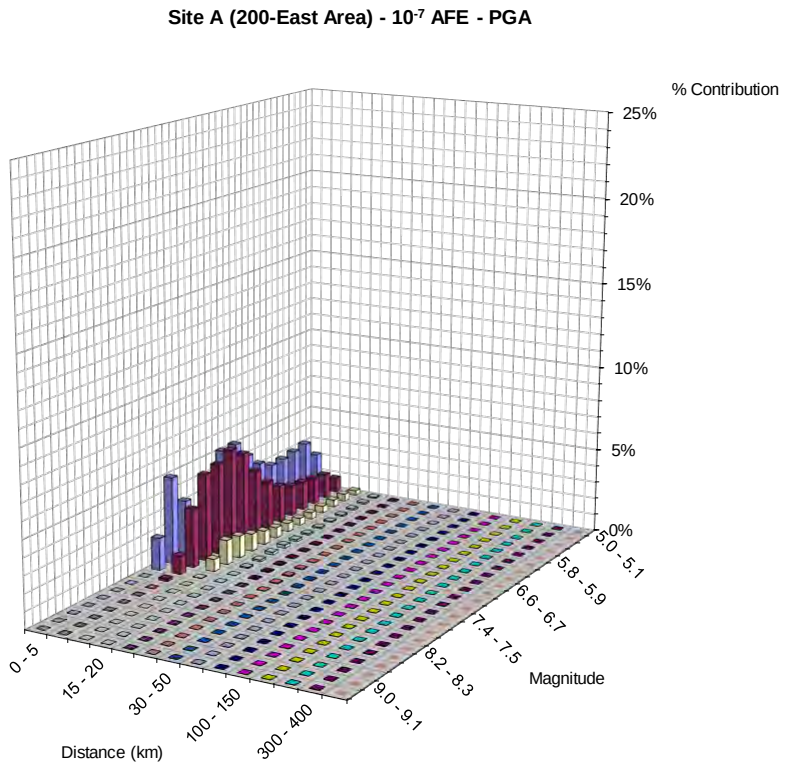

(h)

Figure 10.6. (contd)

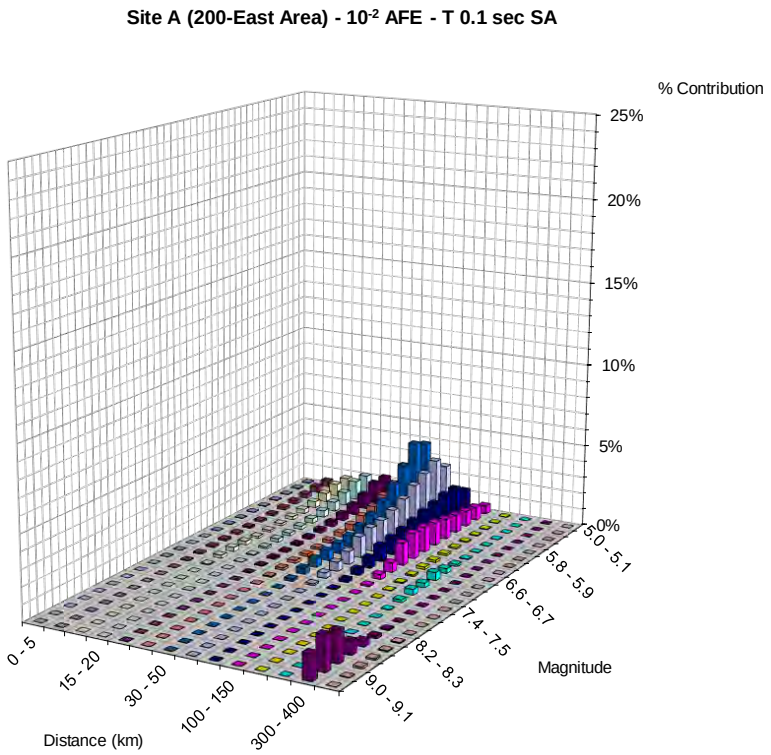

(a)

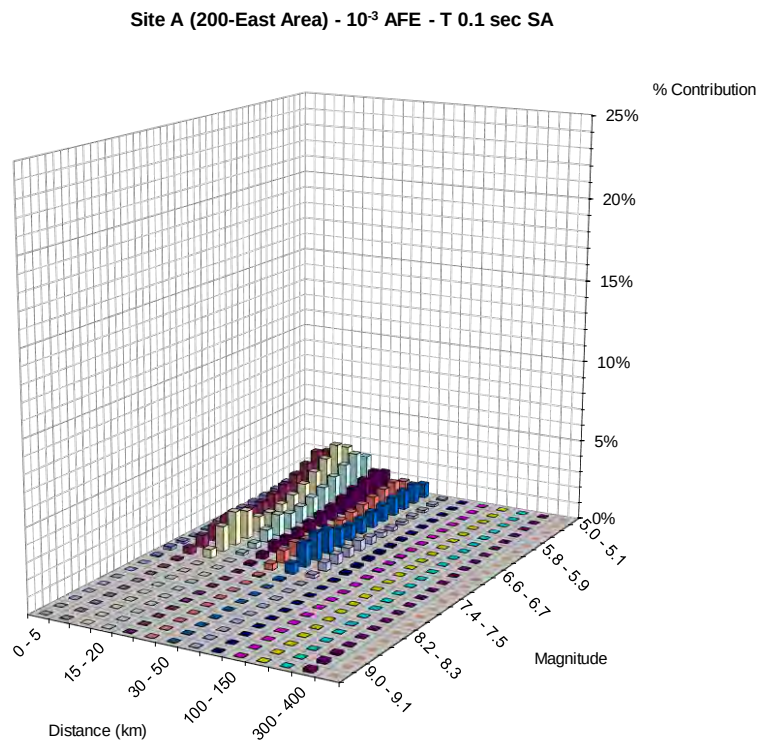

(b)

Figure 10.7. Deaggregation histogram showing magnitude-distance contributions to the total mean hazard at Site A for T 0.1-sec spectral acceleration and AFEs of: a) 10^{-2}; b) 10^{-3}; c) 5×10^{-4}; d) 4×10^{-4}; e) 10^{-4}; f) 10^{-5}; g) 10^{-6}; h) 10^{-7}.

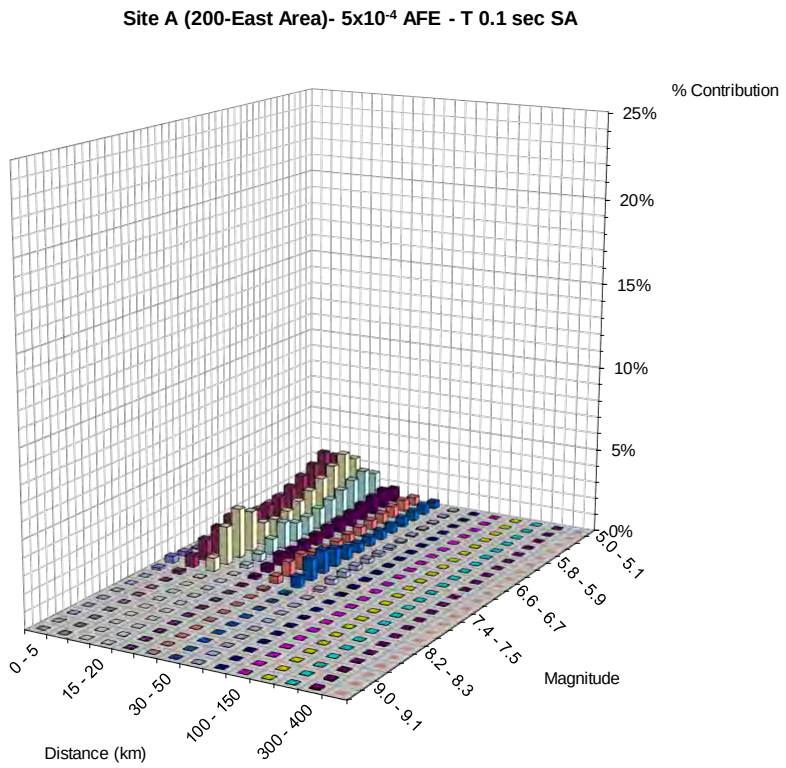

(c)

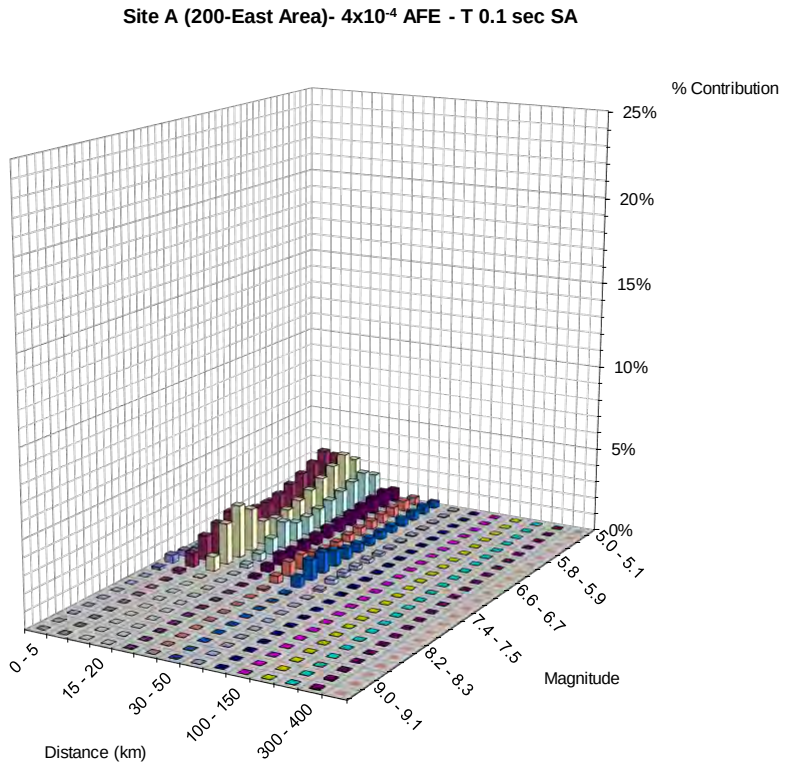

(d)

Figure 10.7. (contd)

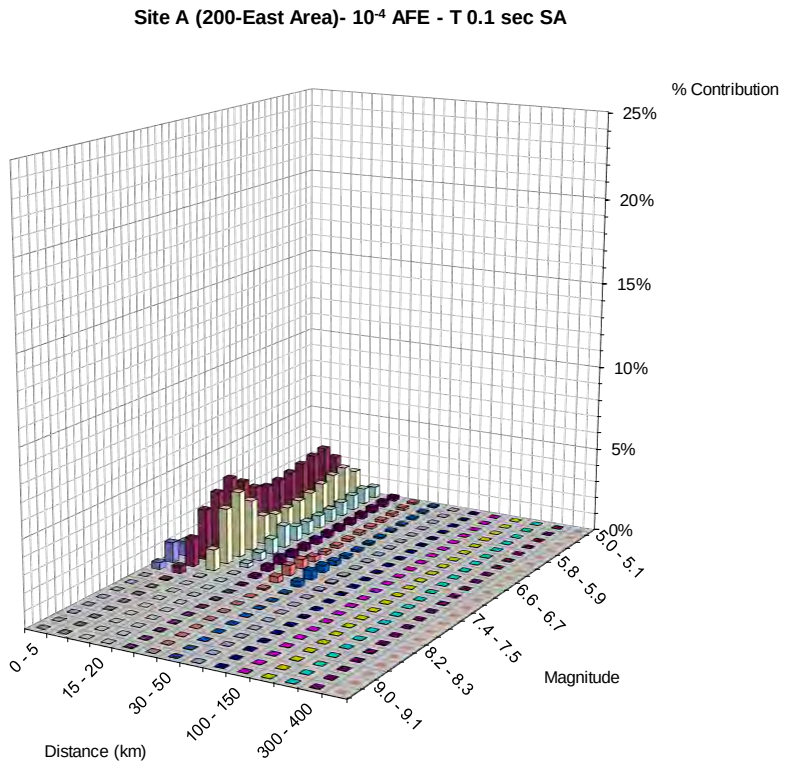

(e)

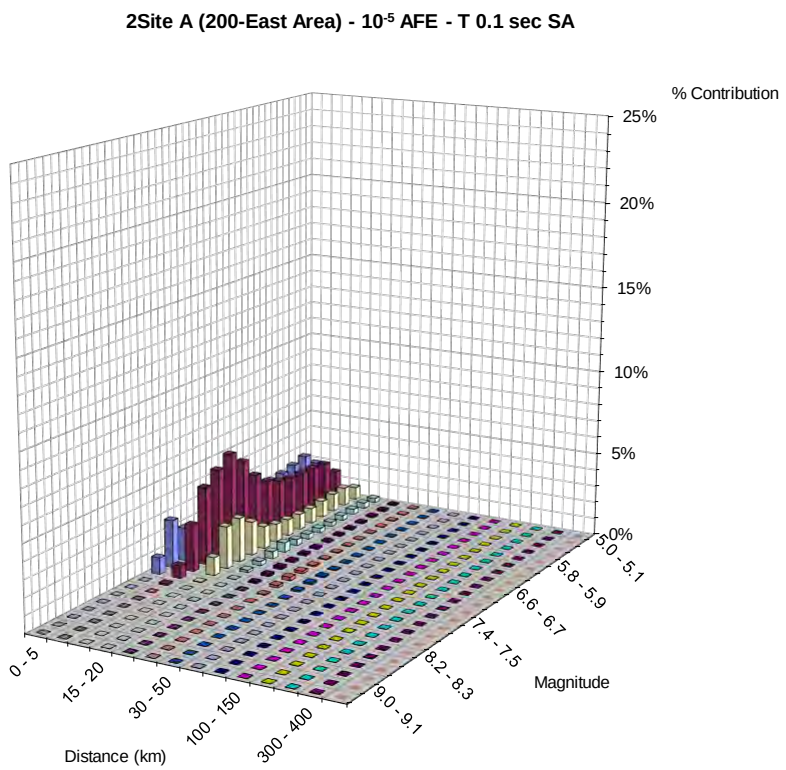

(f)

Figure 10.7. (contd)

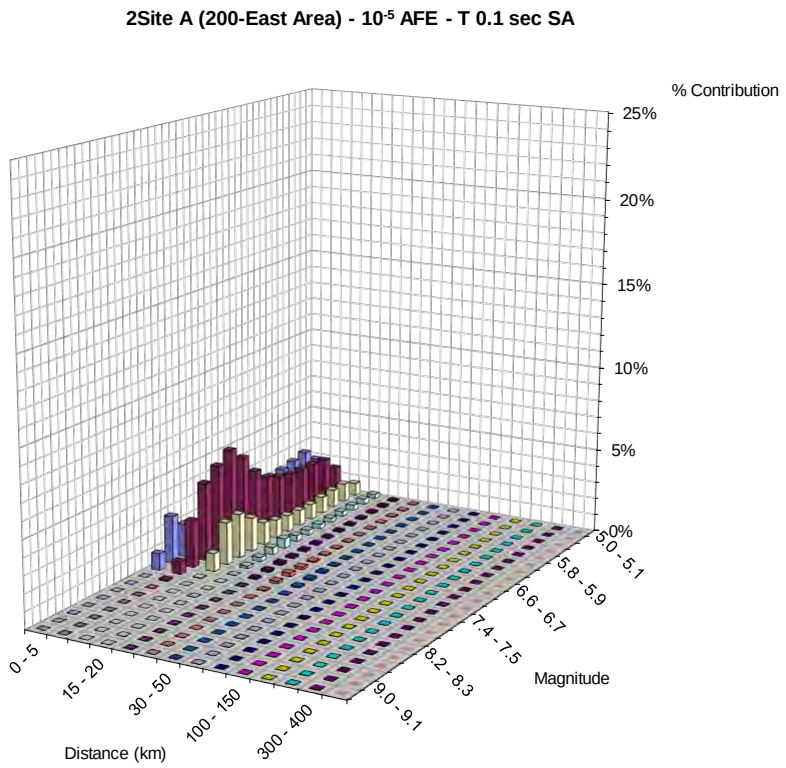

(g)

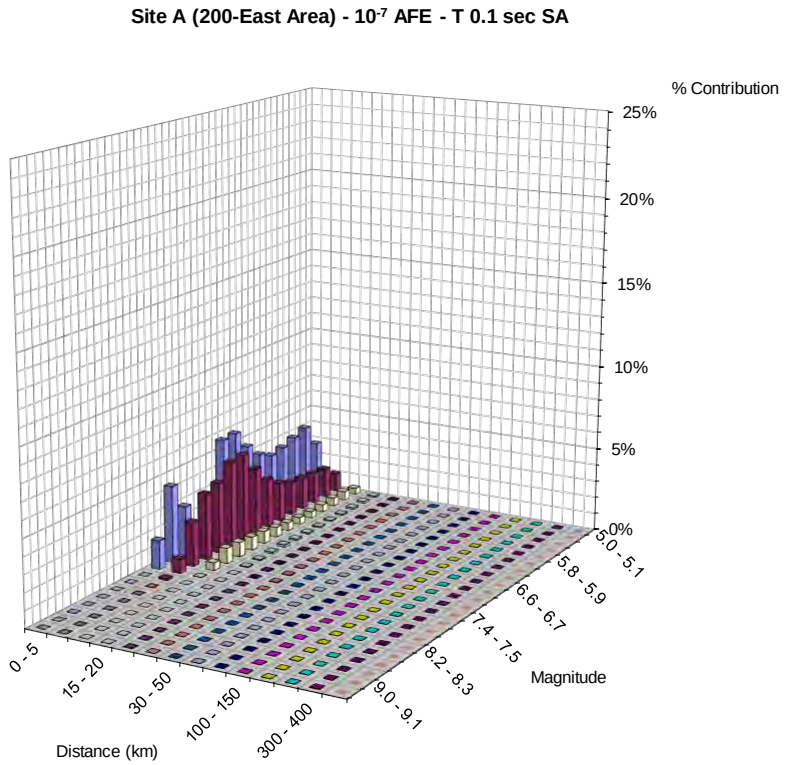

(h)

Figure 10.7. (contd)

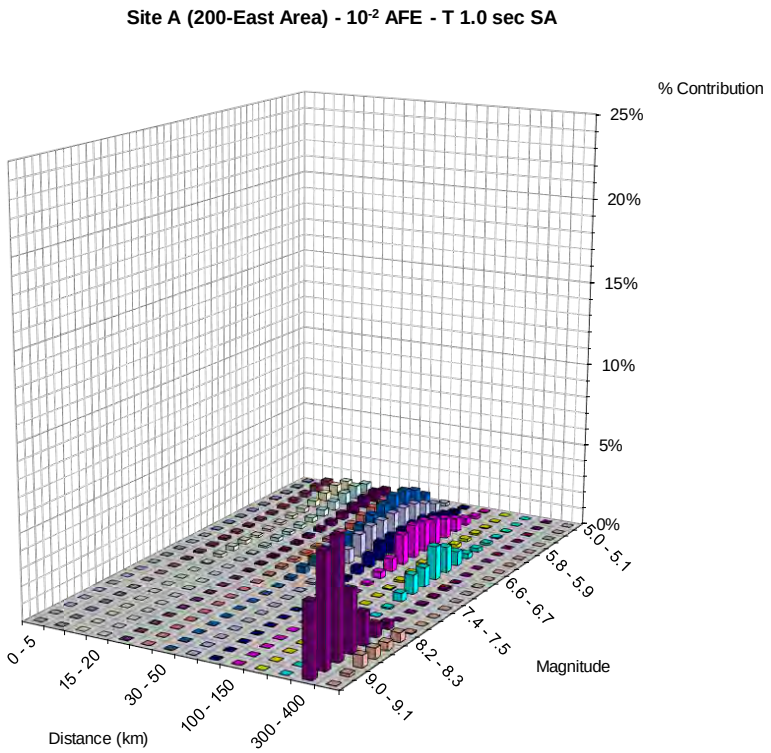

(a)

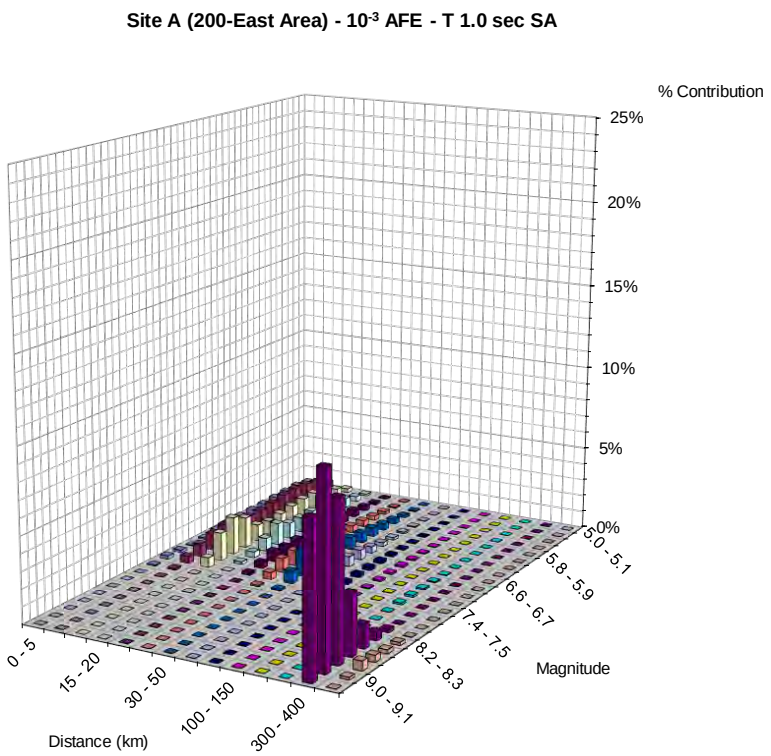

(b)

Figure 10.8. Deaggregation histogram showing magnitude-distance contributions to the total mean hazard at Site A for T 1.0-sec spectral acceleration and AFEs of: a) 10^{-2}; b) 10^{-3}; c) 5×10^{-4}; d) 4×10^{-4}; e) 10^{-4}; f) 10^{-5}; g) 10^{-6}; h) 10^{-7}.

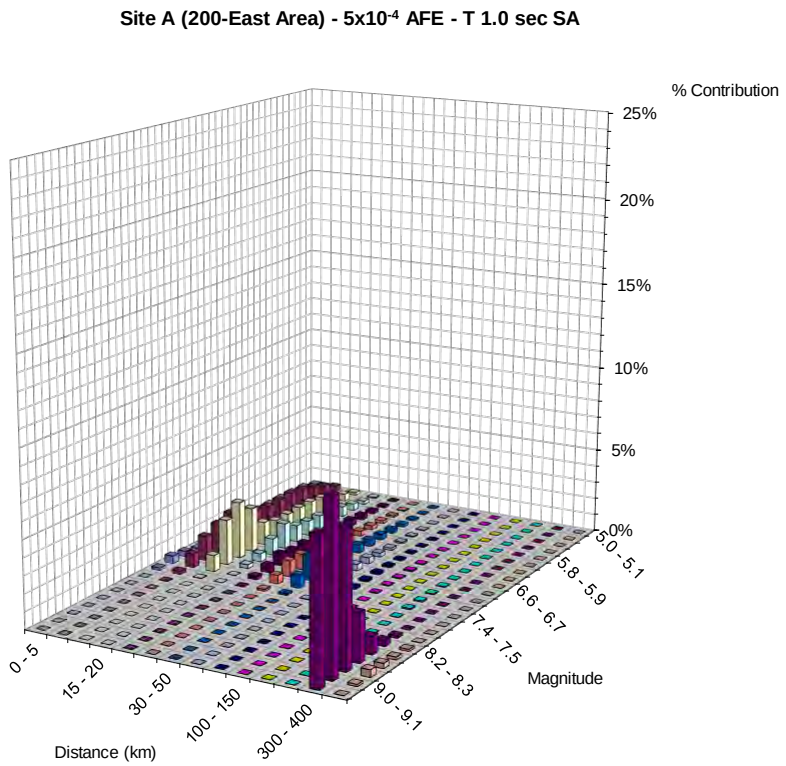

(c)

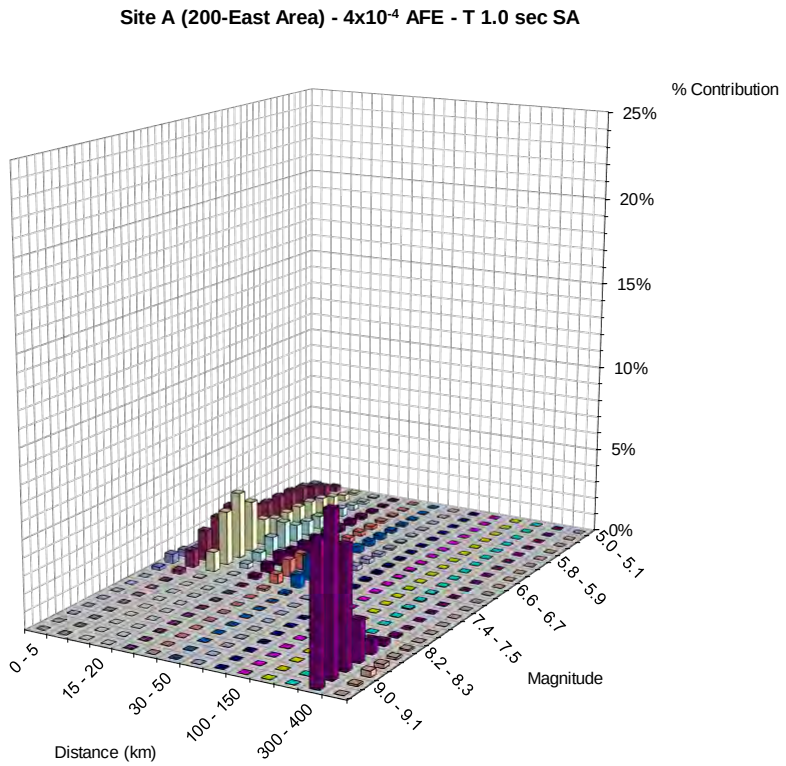

(d)

Figure 10.8. (contd)

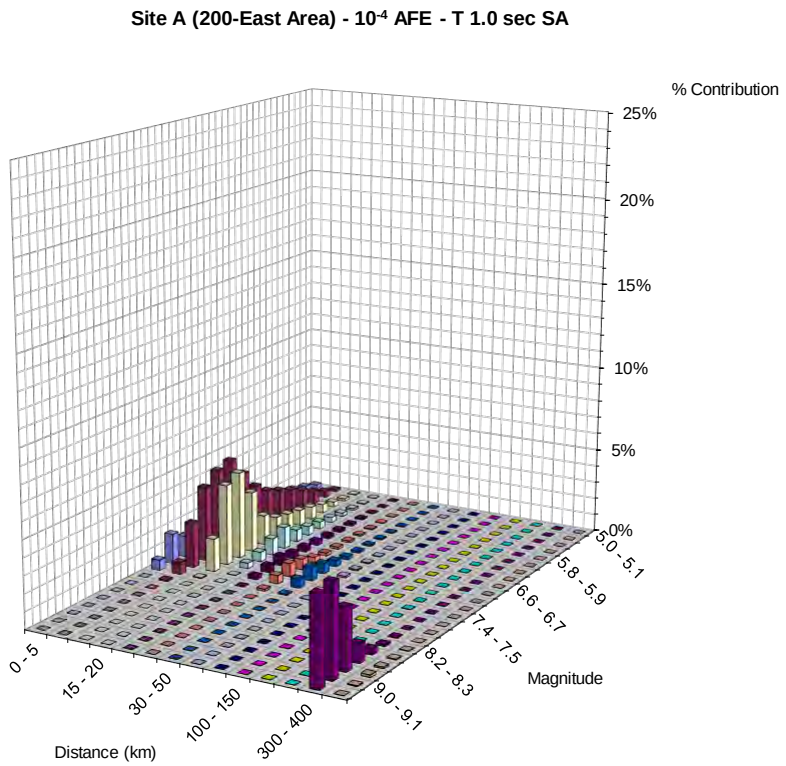

(e)

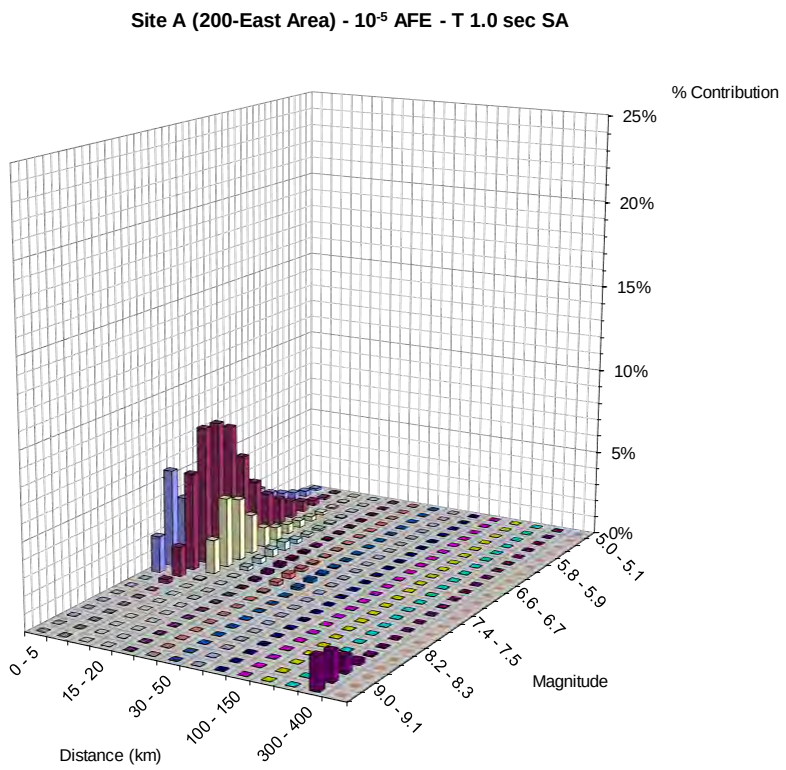

(f)

Figure 10.8. (contd)

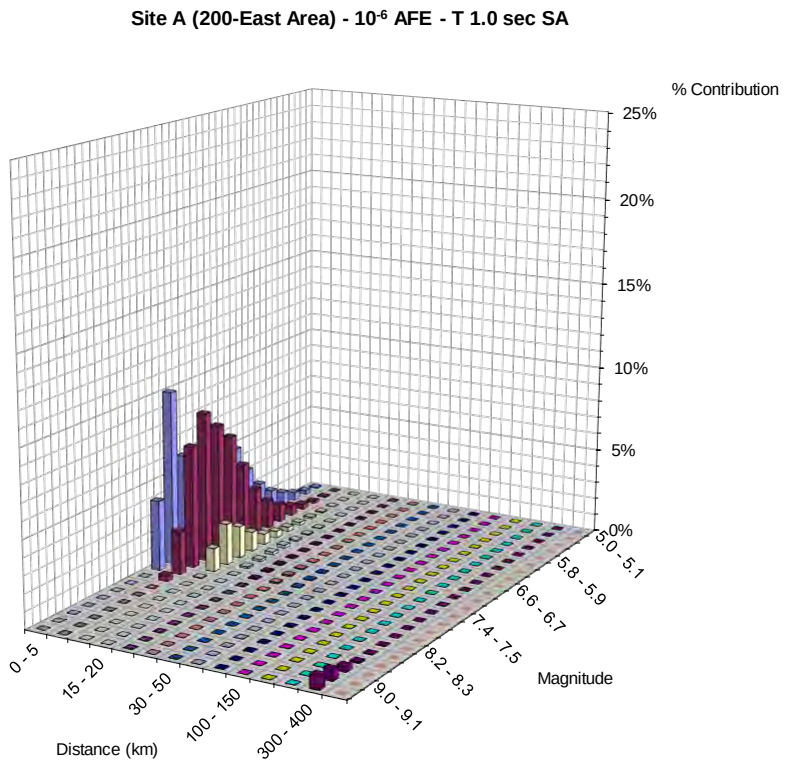

(g)

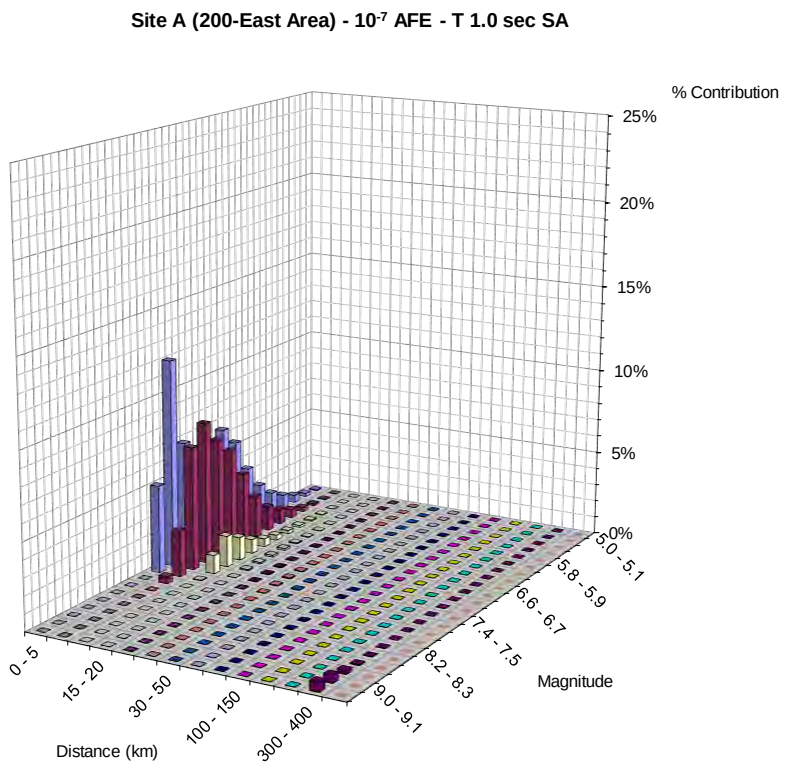

(h)

Figure 10.8. (contd)

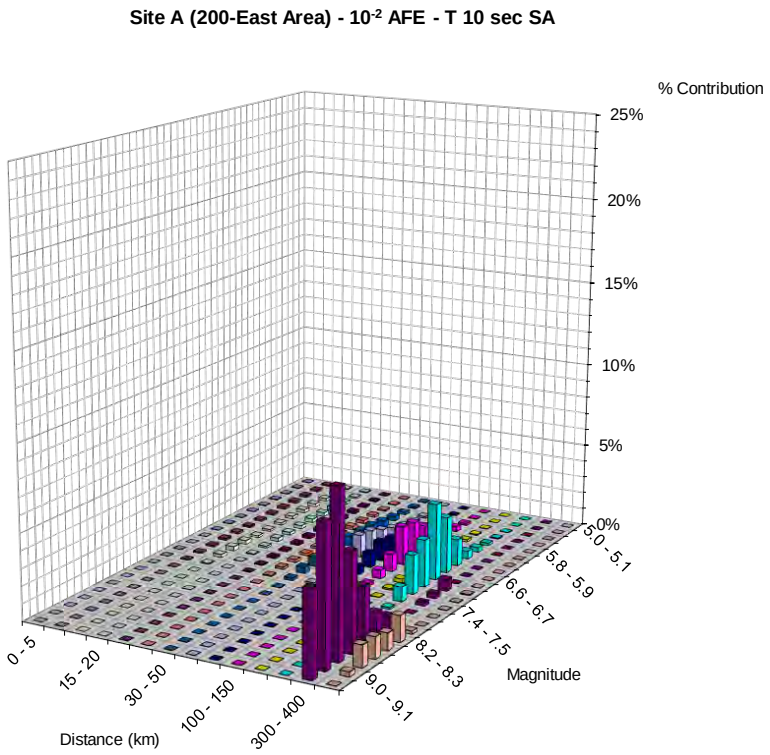

(a)

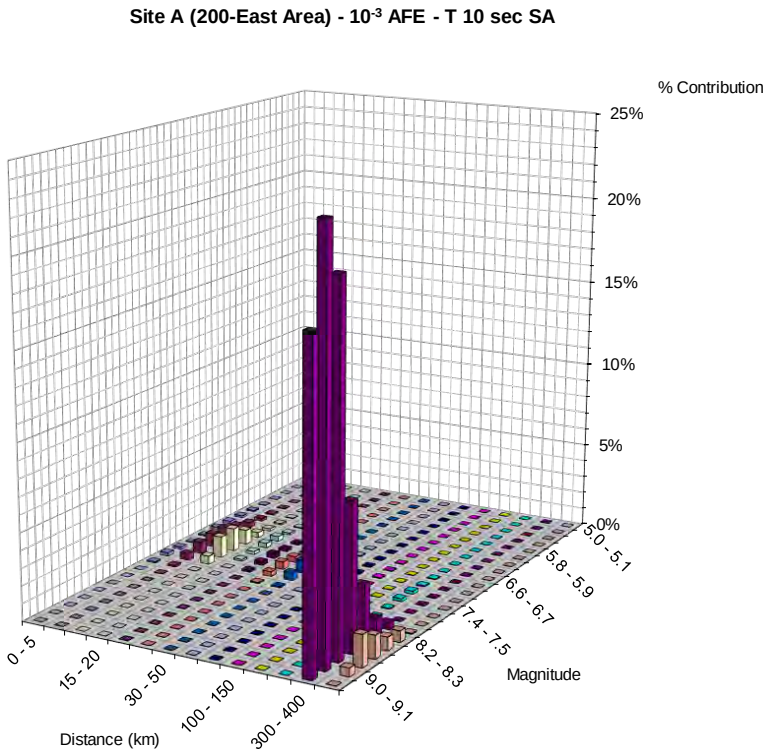

(b)

Figure 10.9. Deaggregation histogram showing magnitude-distance contributions to the total mean hazard at Site A for T 10-sec spectral acceleration and AFEs of: a) 10^{-2}; b) 10^{-3}; c) 5×10^{-4}; d) 4×10^{-4}; e) 10^{-4}; f) 10^{-5}; g) 10^{-6}; h) 10^{-7}.

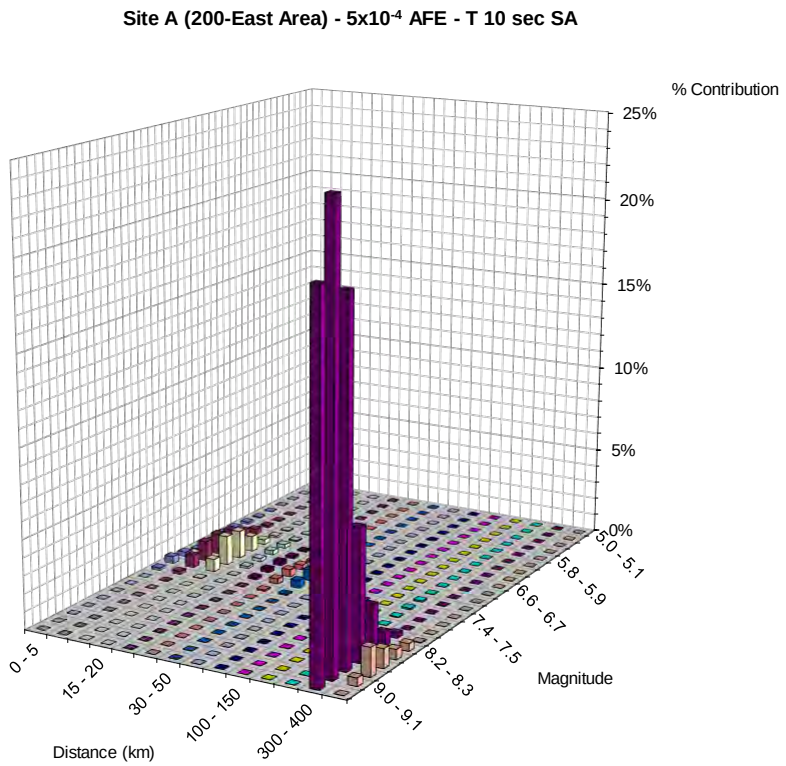

(c)

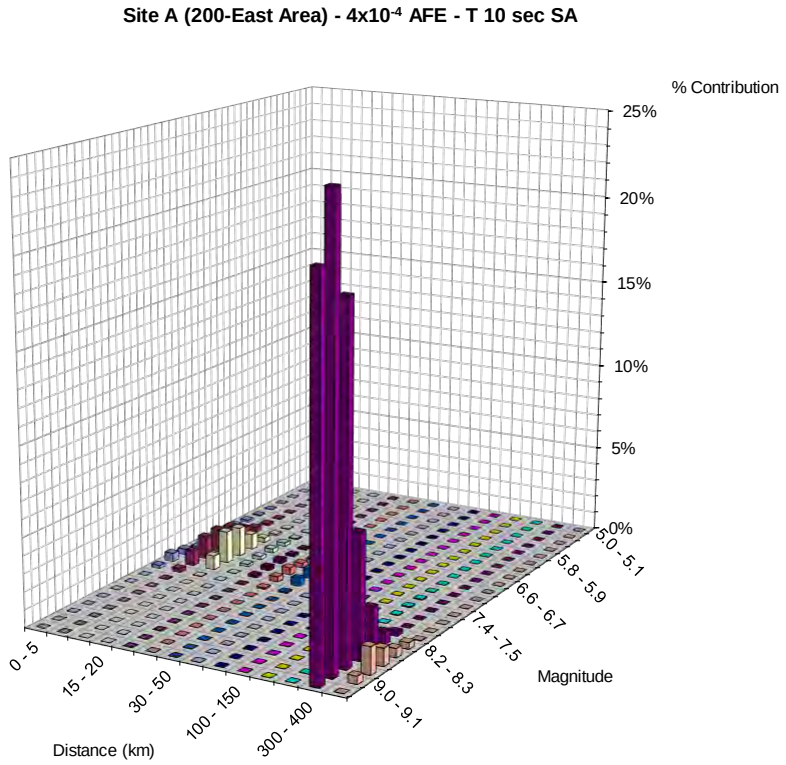

(d)

Figure 10.9. (contd)

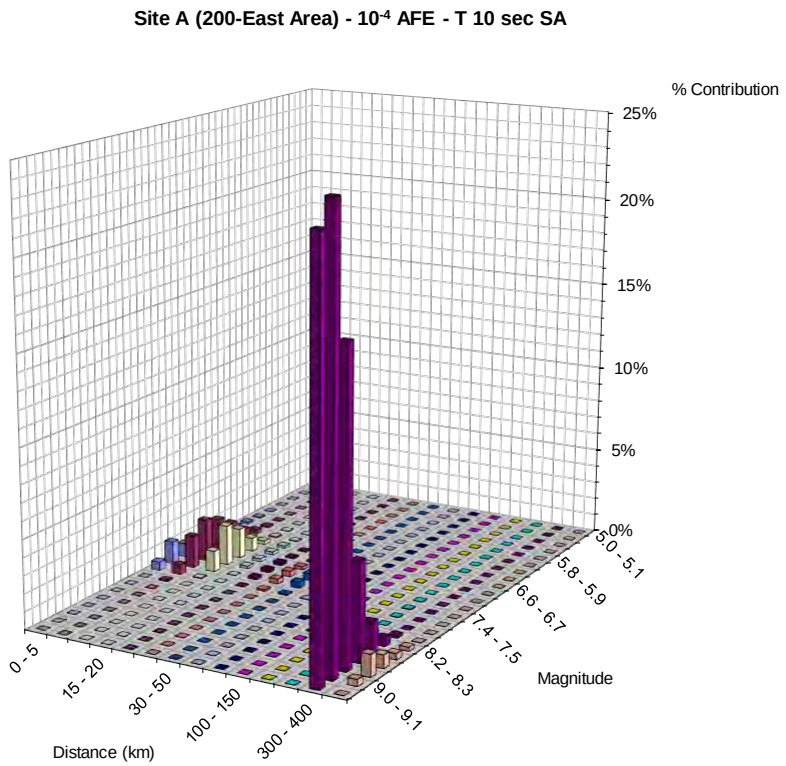

(e)

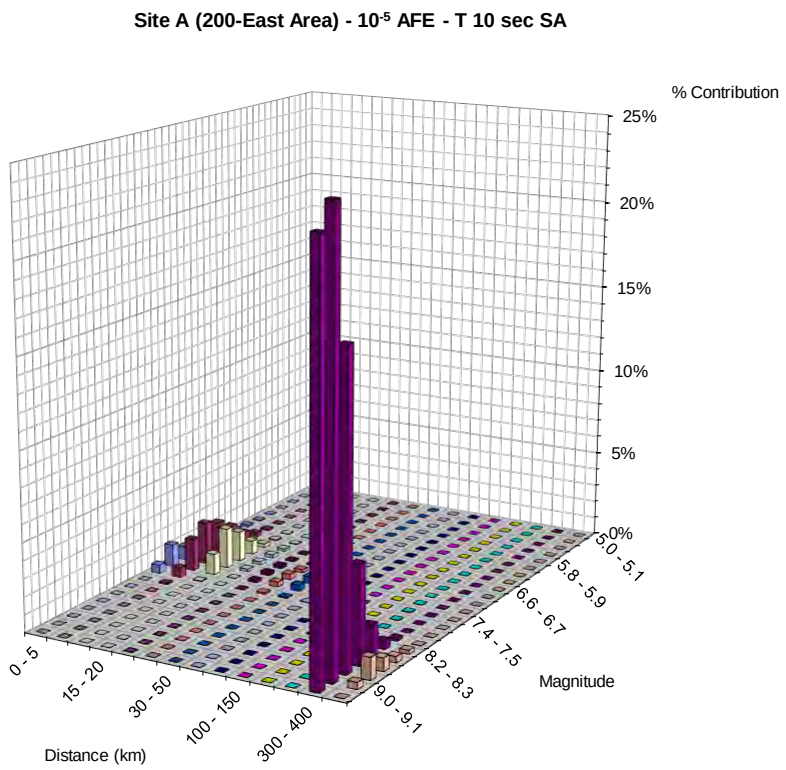

(f)

Figure 10.9. (contd)

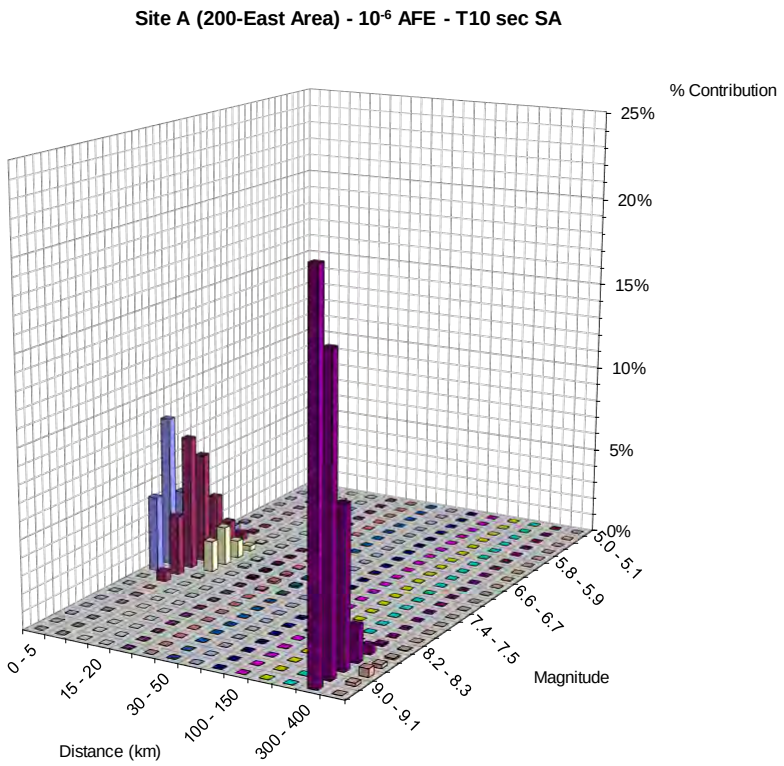

(g)

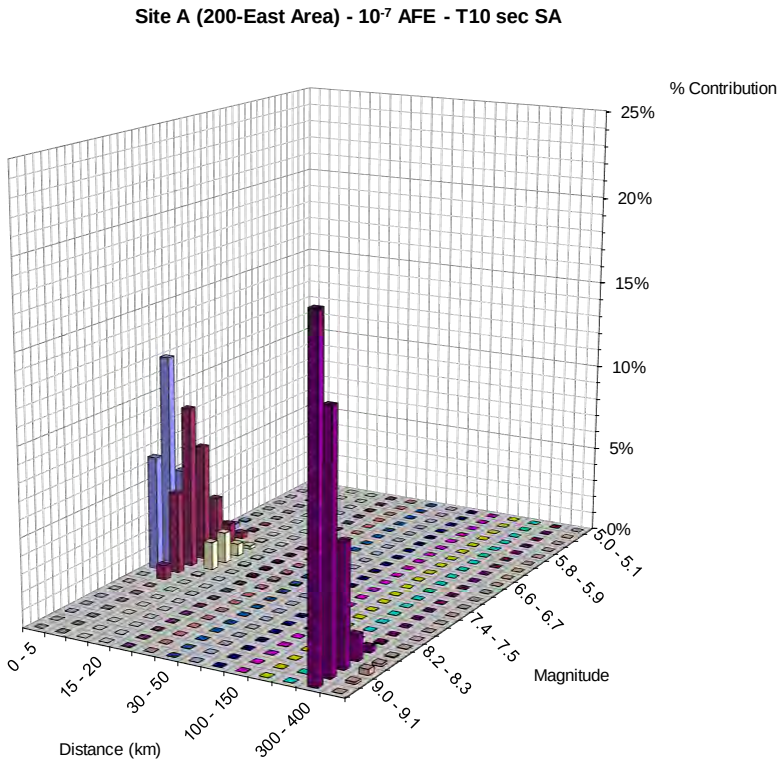

(h)

Figure 10.9. (contd)

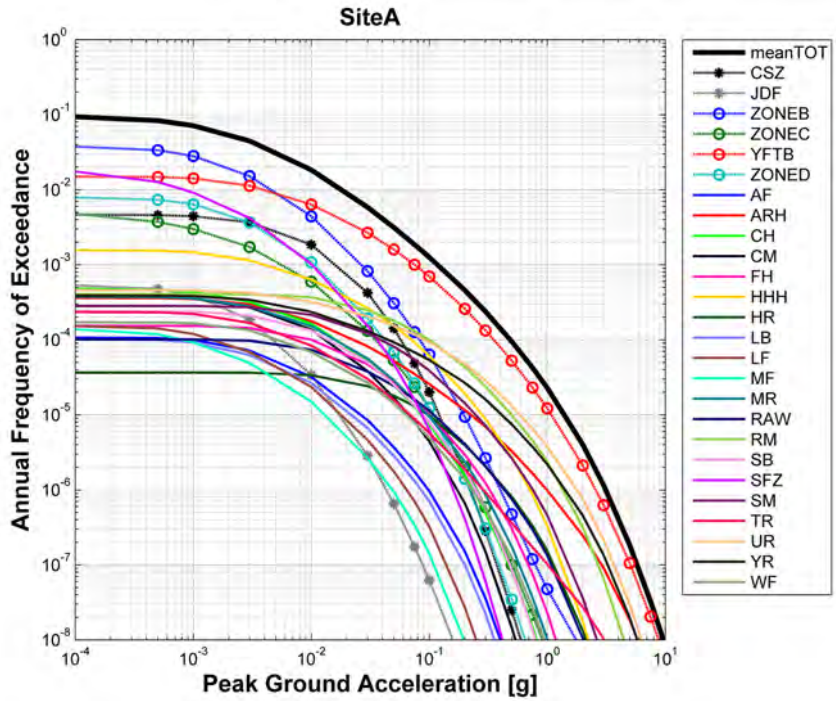

(a)

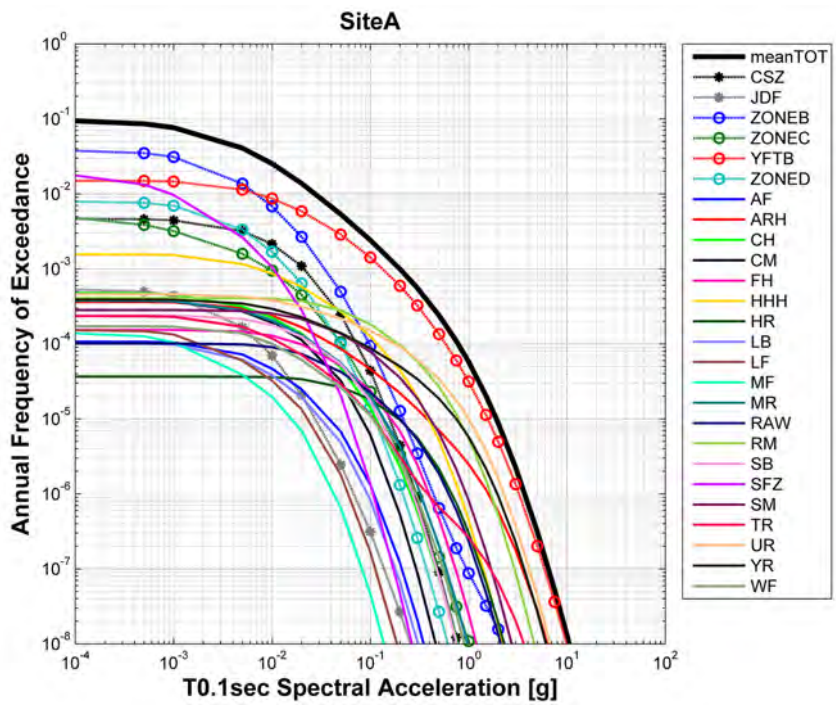

(b)

Figure 10.10. Comparison between the mean hazard curves at Site A obtained for each individual source. Subduction sources are shown by dotted star curves; crustal sources by dotted circle curves; and fault sources by solid curves: a) peak ground acceleration; b) T 0.1-sec; c) T 1-sec; d) T 10-sec spectral acceleration. Acronyms used in figures are listed in Table 10.13.

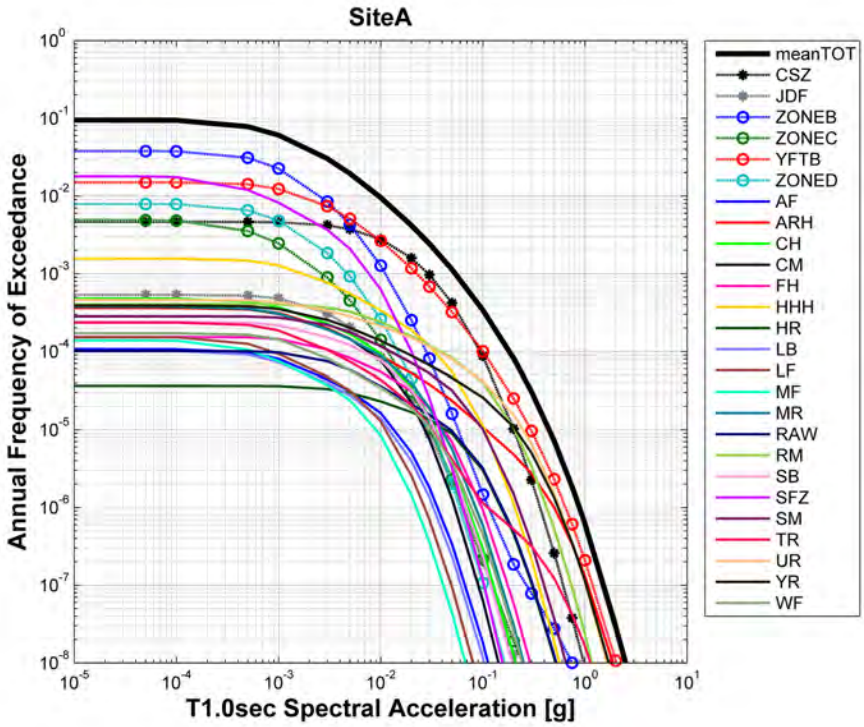

(c)

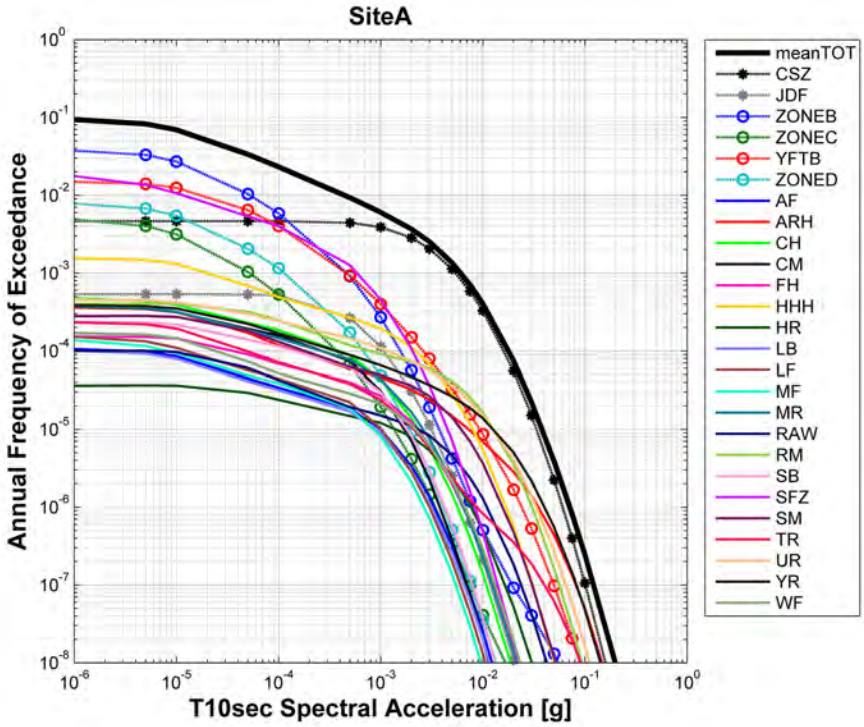

(d)

Figure 10.10. (contd)

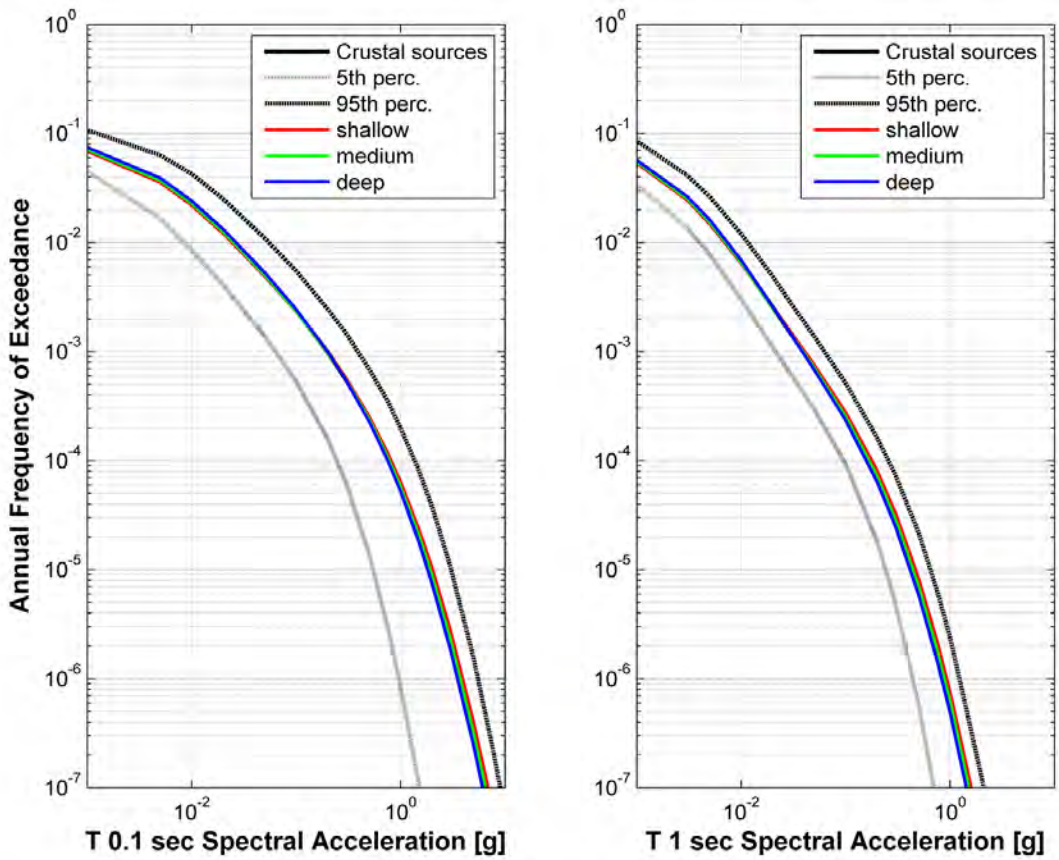

Figure 10.11. Comparison between the total mean crustal sources seismic hazard at Site A (black curve) and the individual contributions at shallow thickness (red curve), medium thickness (green curve), and deep thickness (blue curve) for T 0.1-sec and T 1.0-sec spectral accelerations. The 5th and 95th percentiles of the total crustal hazard are shown by the light and dark grey curves, respectively.

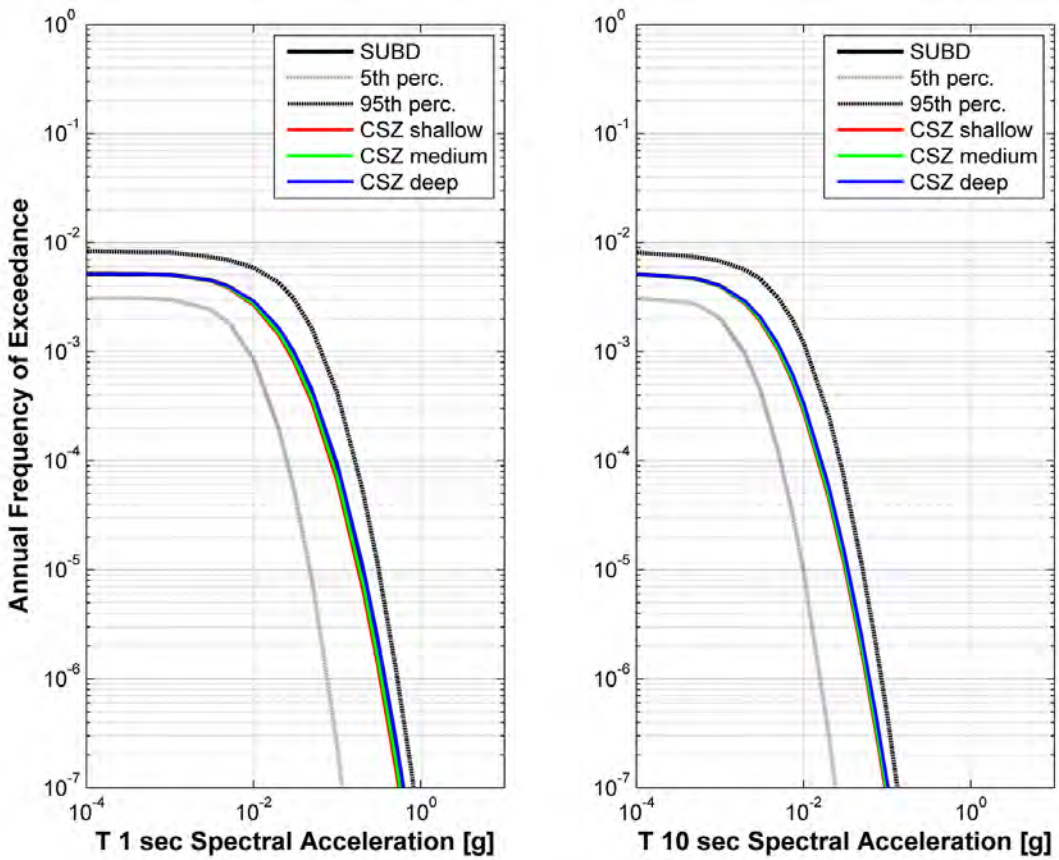

Figure 10.12. Comparison between the total mean CSZ extension seismic hazard at Site A (black curve) and the individual contributions at shallow thickness (red curve), medium thickness (green curve), and deep thickness (blue curve) for T 1.0-sec and T 10-sec spectral accelerations.

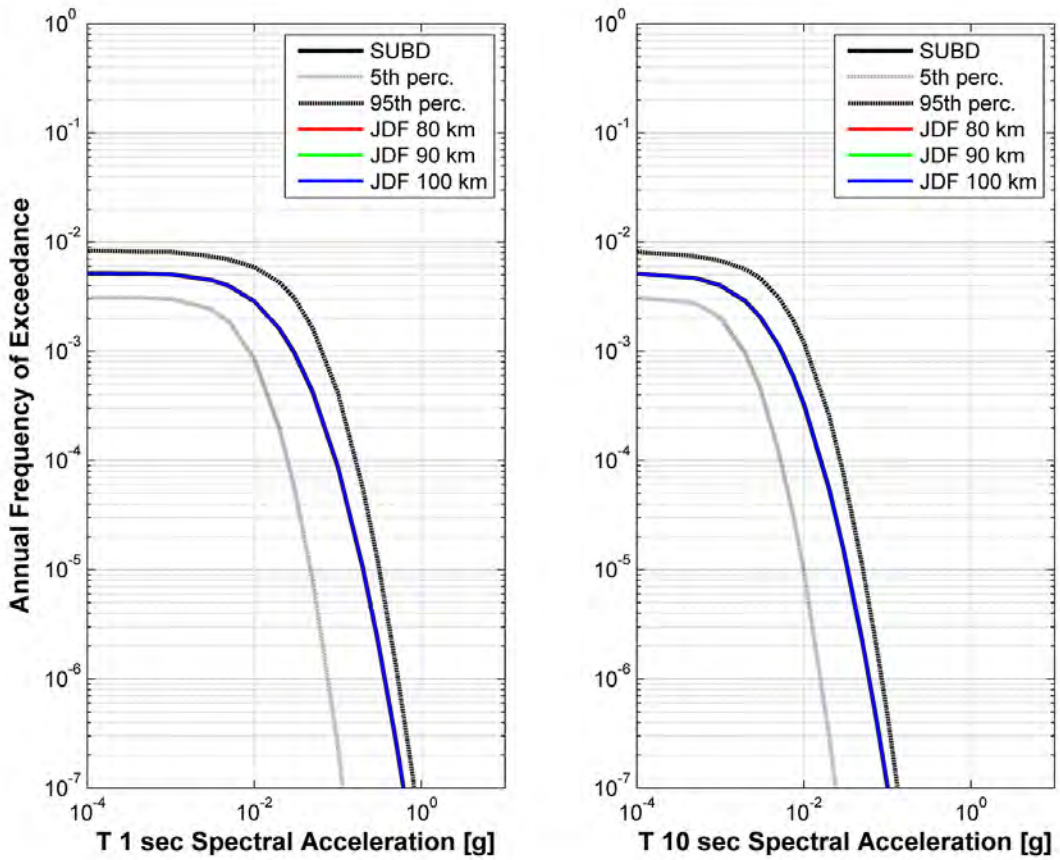

Figure 10.13. Comparison between the total mean JDF extension seismic hazard at Site A (black curve) and the individual contributions at 80 km (red curve), 90 km (green curve), and 100 km (blue curve) for T 1.0-sec and T 10-sec spectral accelerations.

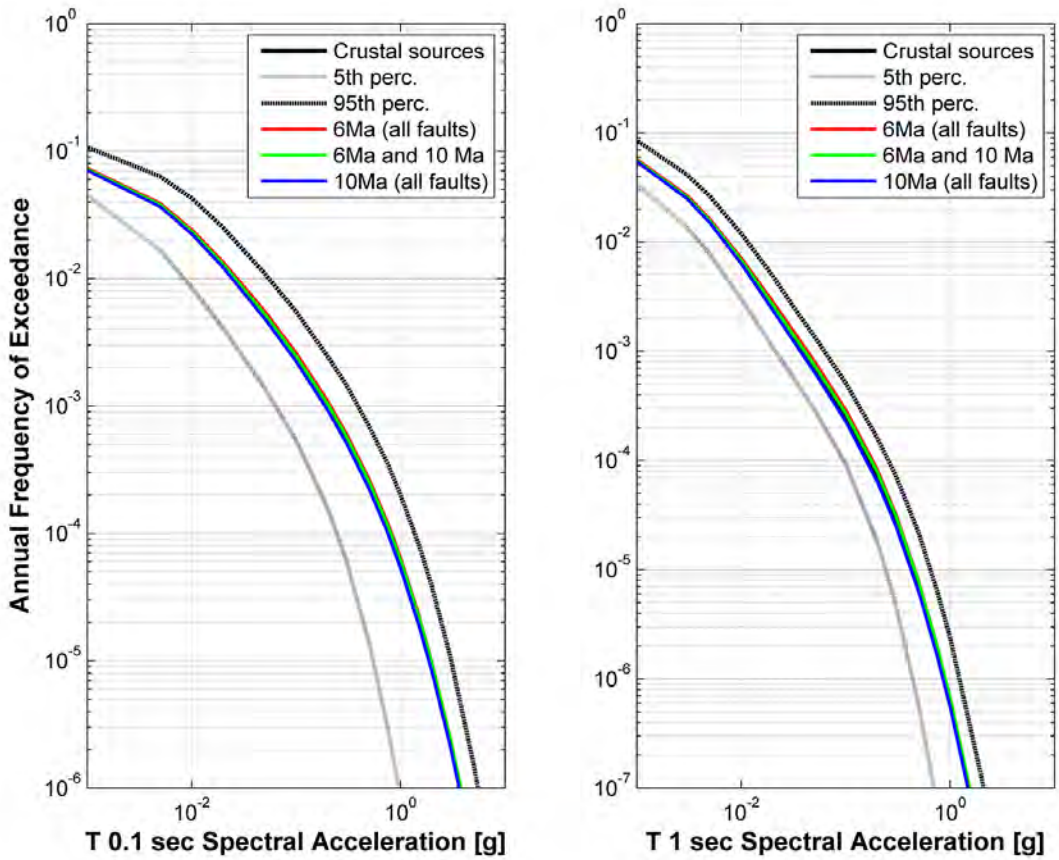

Figure 10.14. Comparison between the total mean crustal sources seismic hazard at Site A (black curve) and the individual start time of deformation contributions at 6 Ma for all faults (red curve), 6 Ma and 10 Ma (green curve), and 10 Ma for all faults (blue curve) for T 0.1-sec and T 1.0-sec spectral accelerations. The 5th and 95th percentiles of the total crustal hazard are shown by the light and dark grey curves, respectively.

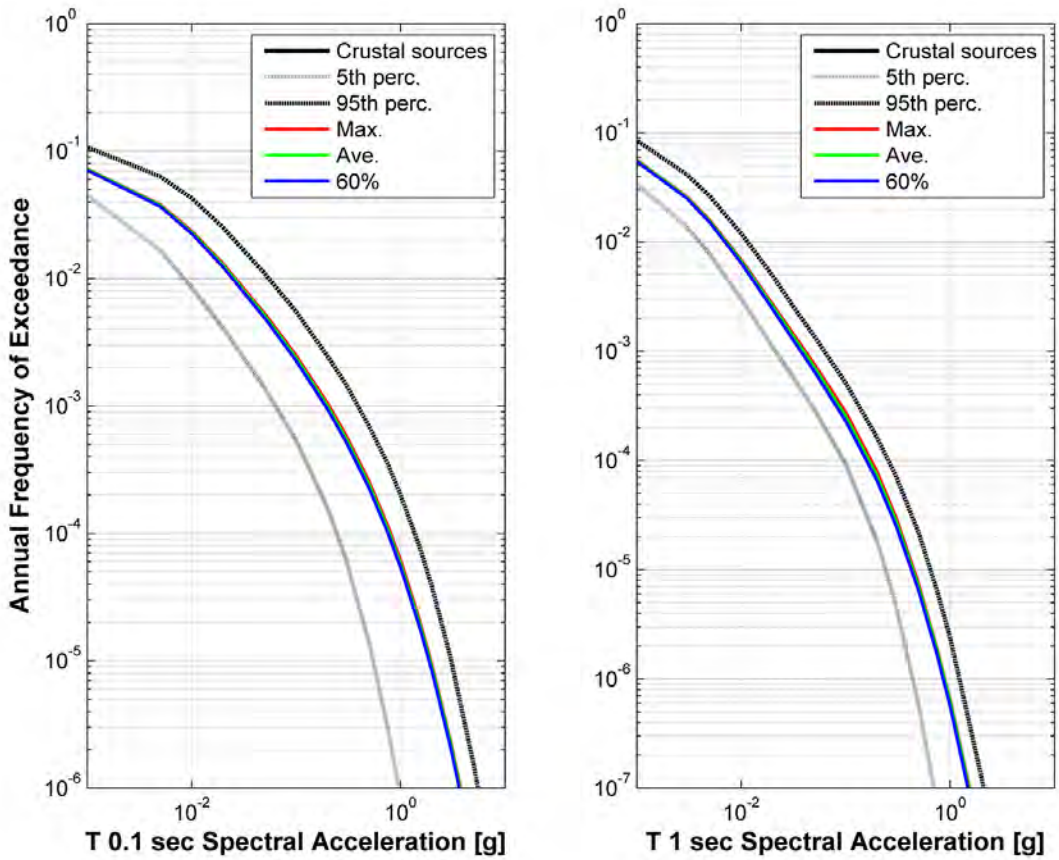

Figure 10.15. Comparison between the total mean crustal sources seismic hazard at Site A (black curve) and the individual basis for fault dip contributions at maximum polygon width (red curve), average polygon width (green curve), and 60% of average polygon width (blue curve) for T 0.1-sec and T 1.0-sec spectral accelerations. The 5th and 95th percentiles of the total crustal hazard are shown by the light and dark grey curves, respectively.

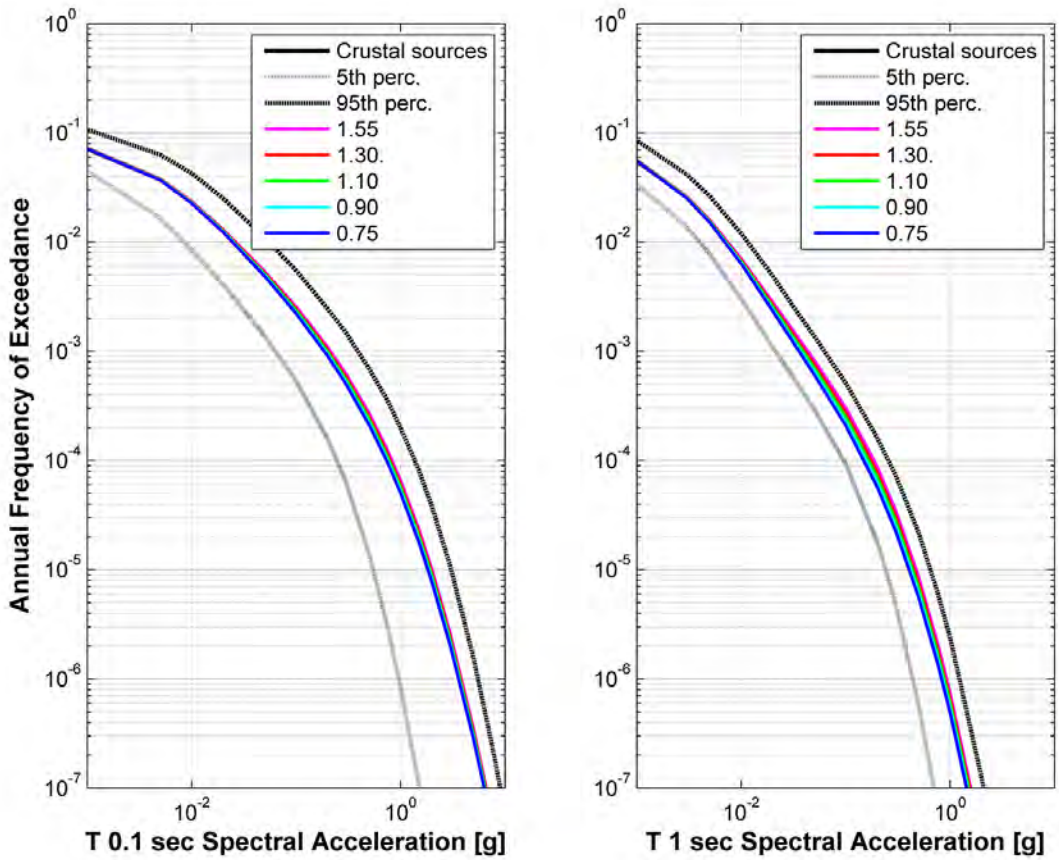

Figure 10.16. Comparison between the total mean crustal sources seismic hazard at Site A (black curve) and the five individual temporal model-scale factor contributions for T 0.1-sec and T 1.0-sec spectral accelerations. The 5th and 95th percentiles of the total crustal hazard are shown by the light and dark grey curves, respectively.

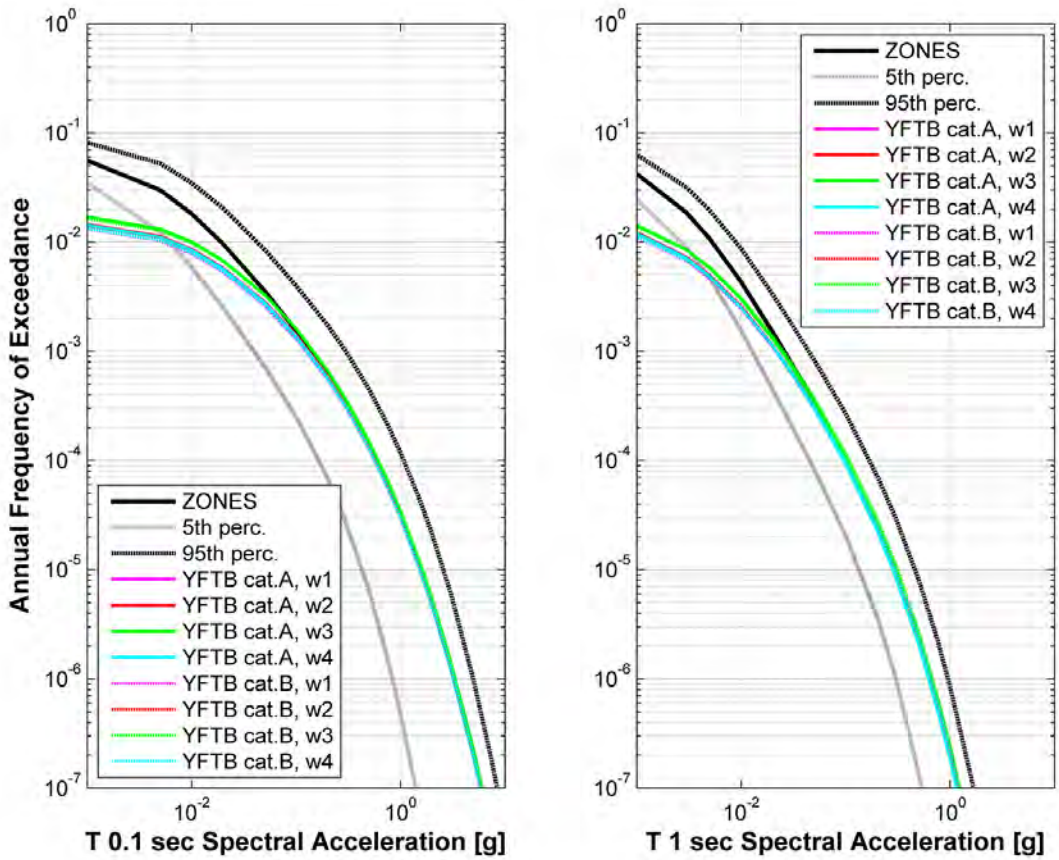

Figure 10.17. Comparison between alternative catalogs and declustering techniques for the YFTB source zone at Site A: a) for T 0.1-sec; b) for T 1.0-sec spectral accelerations. On each plot the black solid curves are the hazard computed from all the background sources (solid curve is the mean, light and dark grey curves show 5th and 95th percentiles, respectively).

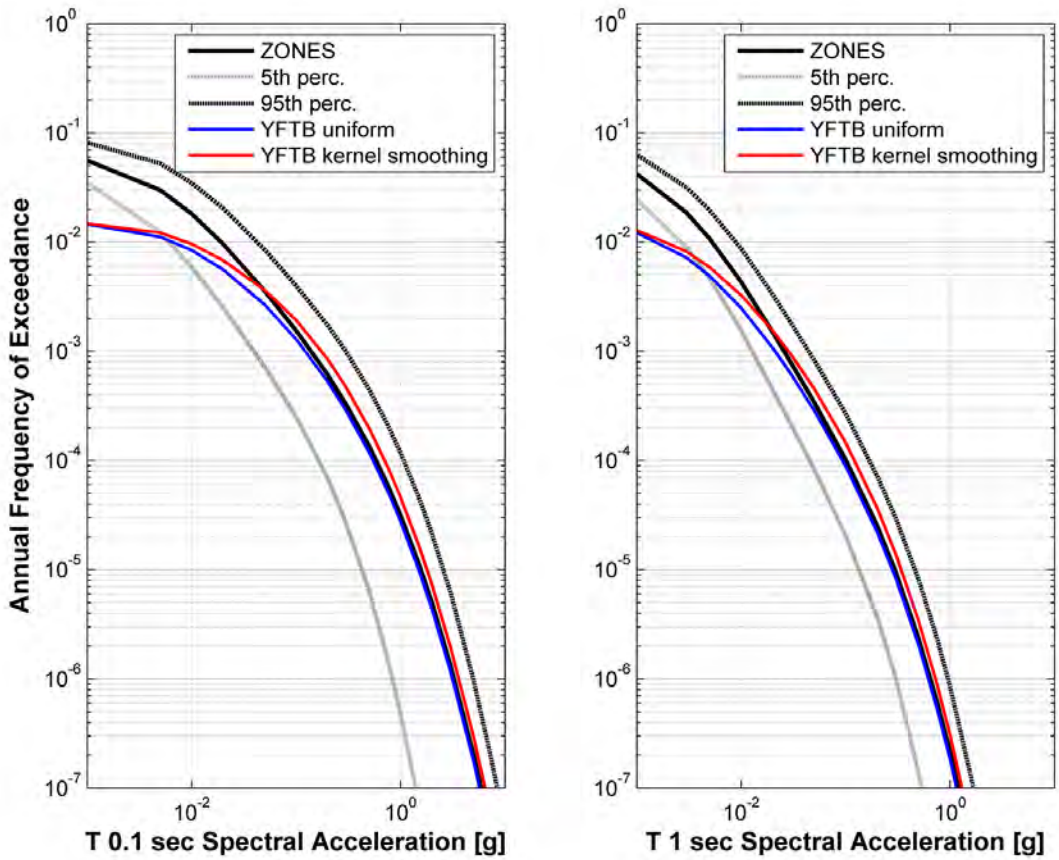

Figure 10.18. Comparison between alternative smoothing techniques for the YFTB source zone at Site A: a) for T 0.1-sec; b) for T 1.0-sec spectral accelerations. On each plot the black solid curves are the hazard computed from all the background sources (solid curve is the mean, light and dark grey curves show 5th and 95th percentiles, respectively).

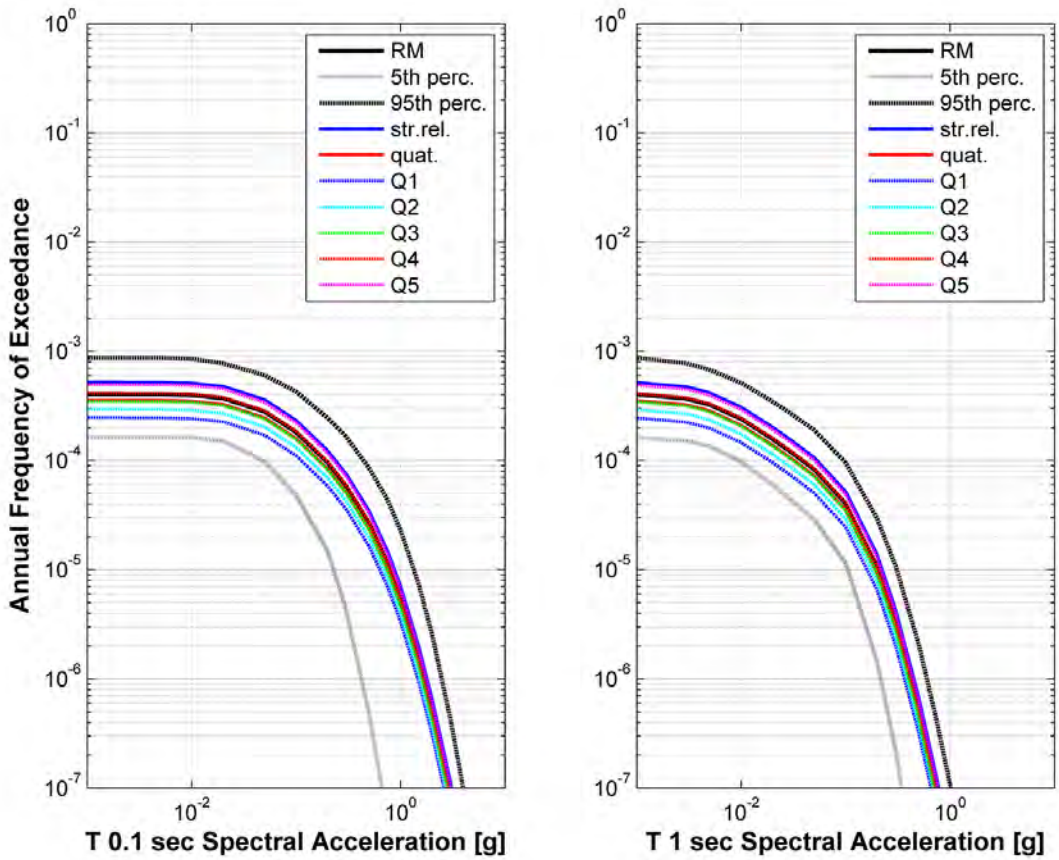

Figure 10.19. Comparison between the total mean Rattlesnake Mountain fault source seismic hazard at Site A (black curve) and the individual contribution of approach to assessing slip rate via use of structural relief (blue solid curve) or quaternary data (red solid curve) for T 0.1-sec and T 1.0-sec spectral accelerations. In addition, the five average quaternary rates are shown by dotted curves. The 5th and 95th percentiles are shown by the light and dark grey curves, respectively.

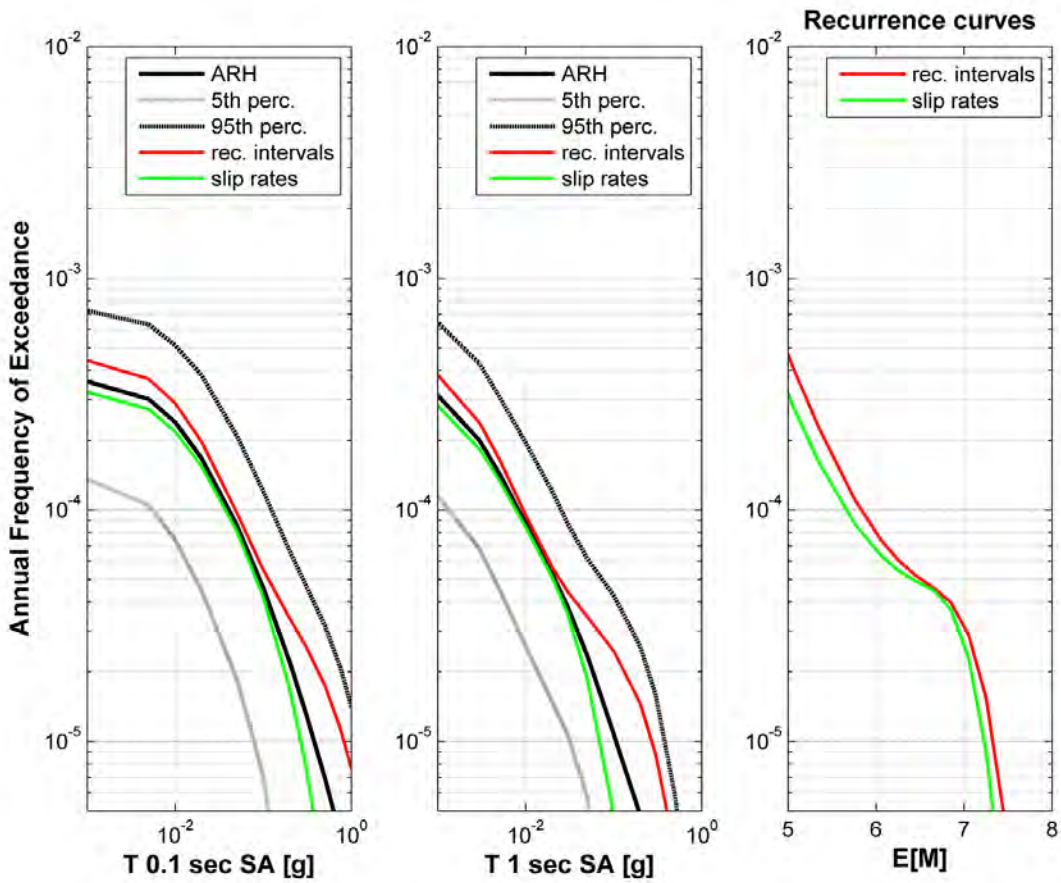

Figure 10.20. Sensitivity analysis for the Ahtanum Ridge-Rattlesnake Hills (ARH) fault at Site A for T 0.1-sec (left) and T 1-sec (middle) spectral accelerations. In both plots the mean seismic hazard for the ARH fault is shown by the black solid curve and its 5th and 95th percentiles by the light and dark grey curves, respectively. The hazard obtained using recurrence intervals is shown by the red curve and using slip rates by the green curve. The recurrence curves are shown for comparison.

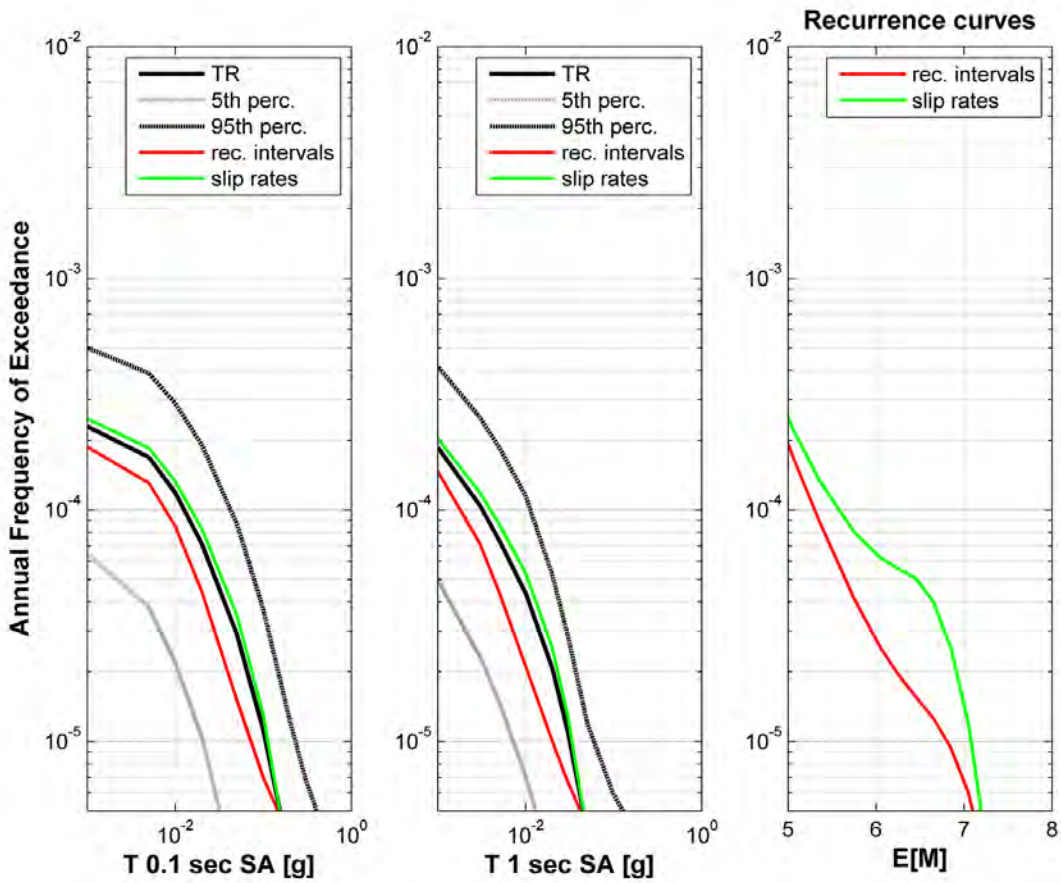

Figure 10.21. Sensitivity analysis for the Toppenish Ridge (TR) fault at Site A for T 0.1-sec (left) and T 1-sec (middle) spectral accelerations. In both plots the mean seismic hazard for the ARH fault is shown by the black solid curve and its 5th and 95th percentiles by the light and dark grey curves, respectively. The hazard obtained using recurrence intervals is shown by the red curve and using slip rates by the green curve. The recurrence curves are shown for comparison.

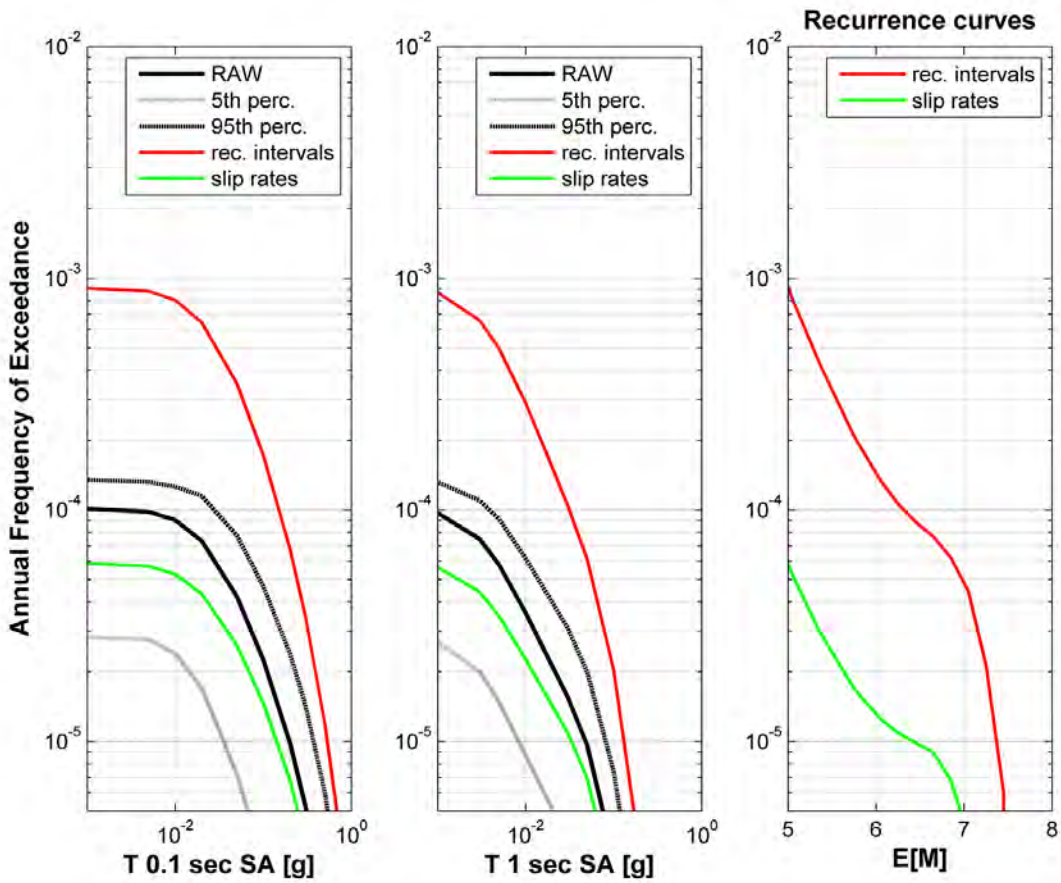

Figure 10.22. Sensitivity analysis for the RAW fault at Site A for T 0.1-sec (left) and T 1-sec (middle) spectral accelerations. In both plots the mean seismic hazard for the RAW fault is shown by the black solid curve and its 5th and 95th percentiles by the light and dark grey curves, respectively. The hazard obtained using recurrence intervals is shown by the red curve and using slip rates by the green curve. The recurrence curves are shown for comparison.

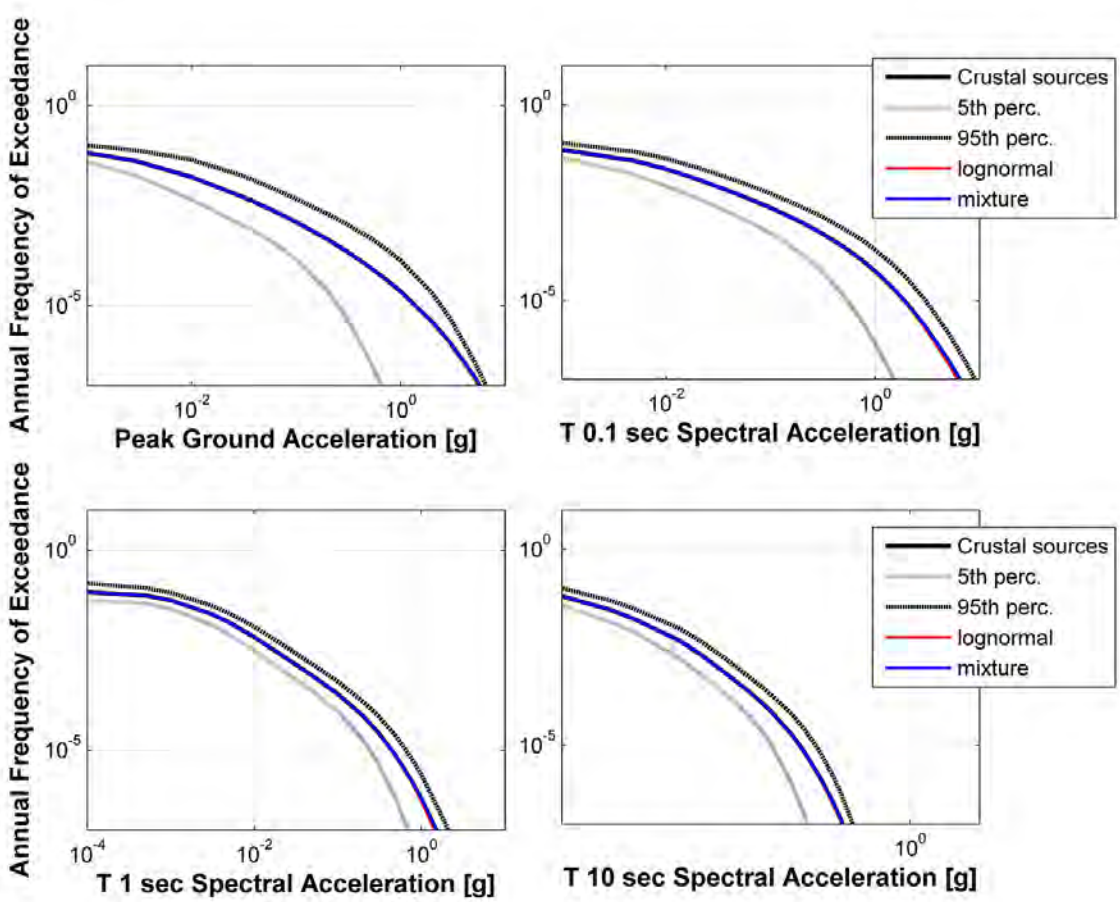

Figure 10.23. Comparison between the total mean crustal sources seismic hazard at Site A (black curve) and the individual contribution from ground motion distribution shape represented by red curve for lognormal model and blue curve for mixture model, for the peak ground acceleration, T 0.1-sec, T 1.0-sec, and T 10-sec spectral accelerations. The 5th and 95th percentiles are shown on each plot by the light and dark grey curves.

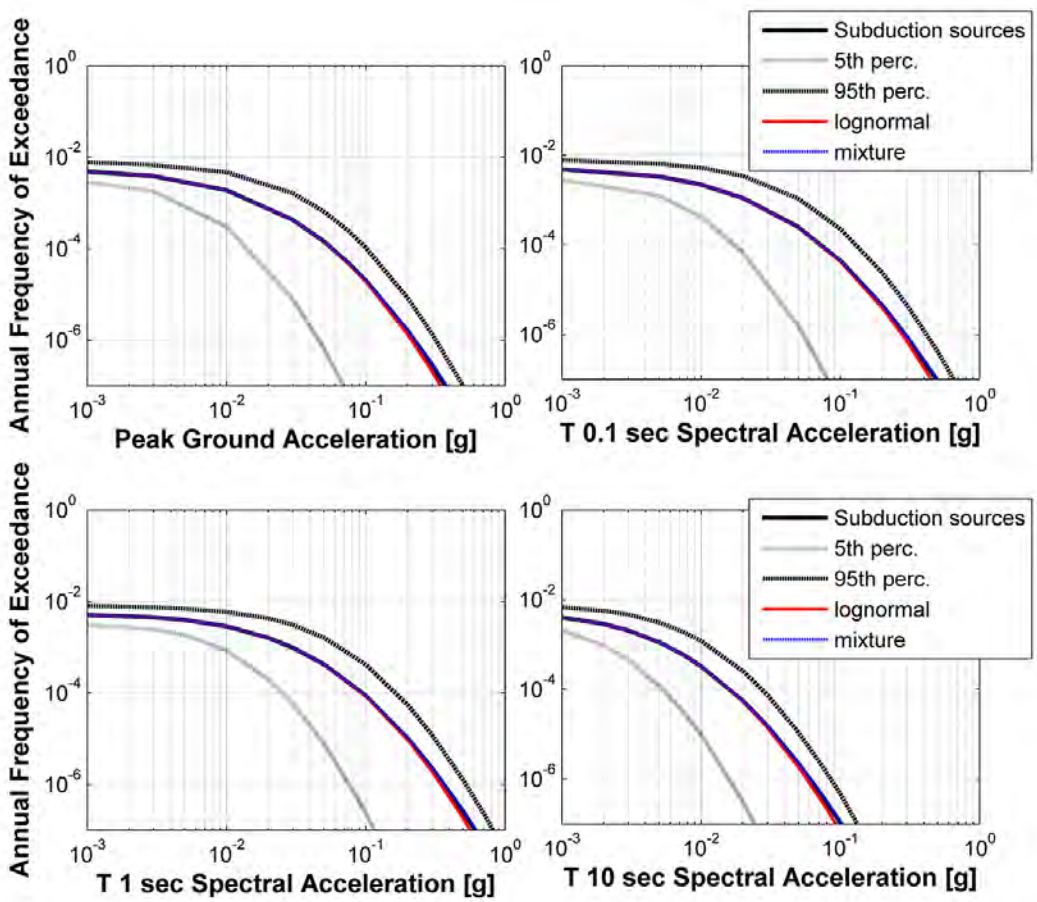

Figure 10.24. Comparison between the total mean subduction sources seismic hazard at Site A (black curve) and the individual contribution from ground motion distribution shape represented by red curve for lognormal model and blue curve for mixture model, for the peak ground acceleration, T 0.1-sec, T 1.0-sec, and T 10-sec spectral accelerations. The 5th and 95th percentiles are shown on each plot by the light and dark grey curves.

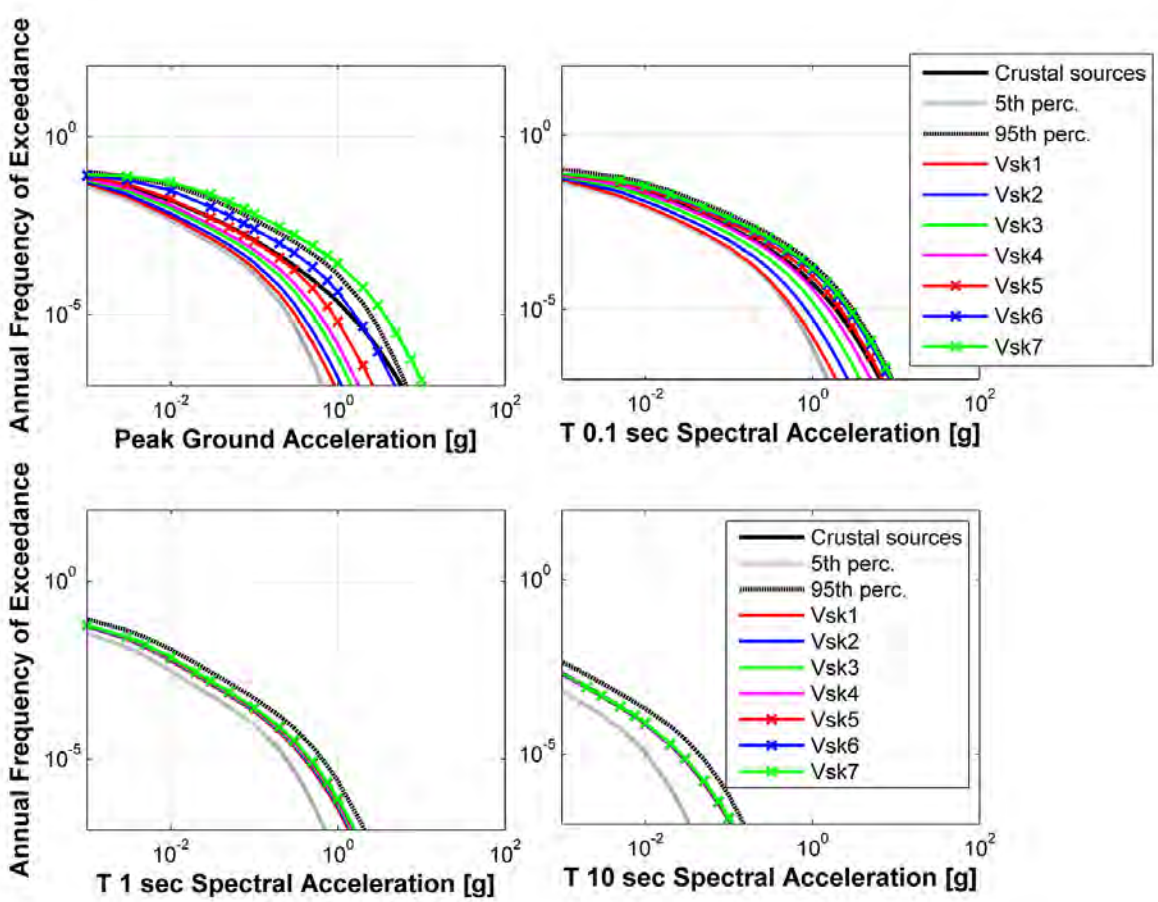

Figure 10.25. Comparison between the total mean crustal sources seismic hazard at Site A (black curve) and the individual contribution from the seven different Vs-kappa adjustment factors, for the peak ground acceleration, T 0.1-sec, T 1.0-sec, and T 10-sec spectral accelerations. The 5th and 95th percentiles are shown on each plot by the light and dark grey curves.

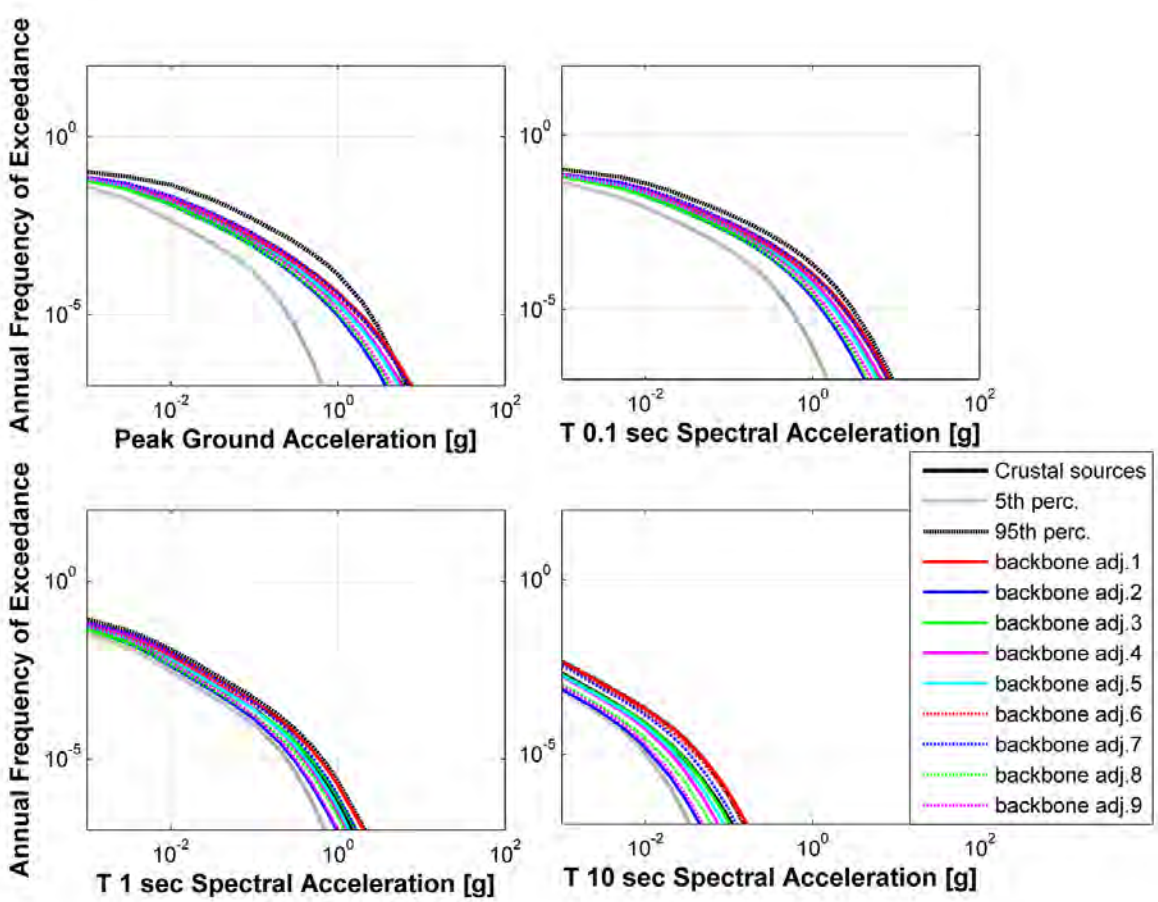

Figure 10.26. Comparison between the total mean crustal sources seismic hazard at Site A (black curve) and the individual contribution from the nine different inherent uncertainty in backbone adjustments, for the peak ground acceleration, T 0.1-sec, T 1.0-sec, and T 10-sec spectral accelerations. The 5th and 95th percentiles are shown on each plot by the light and dark grey curves.

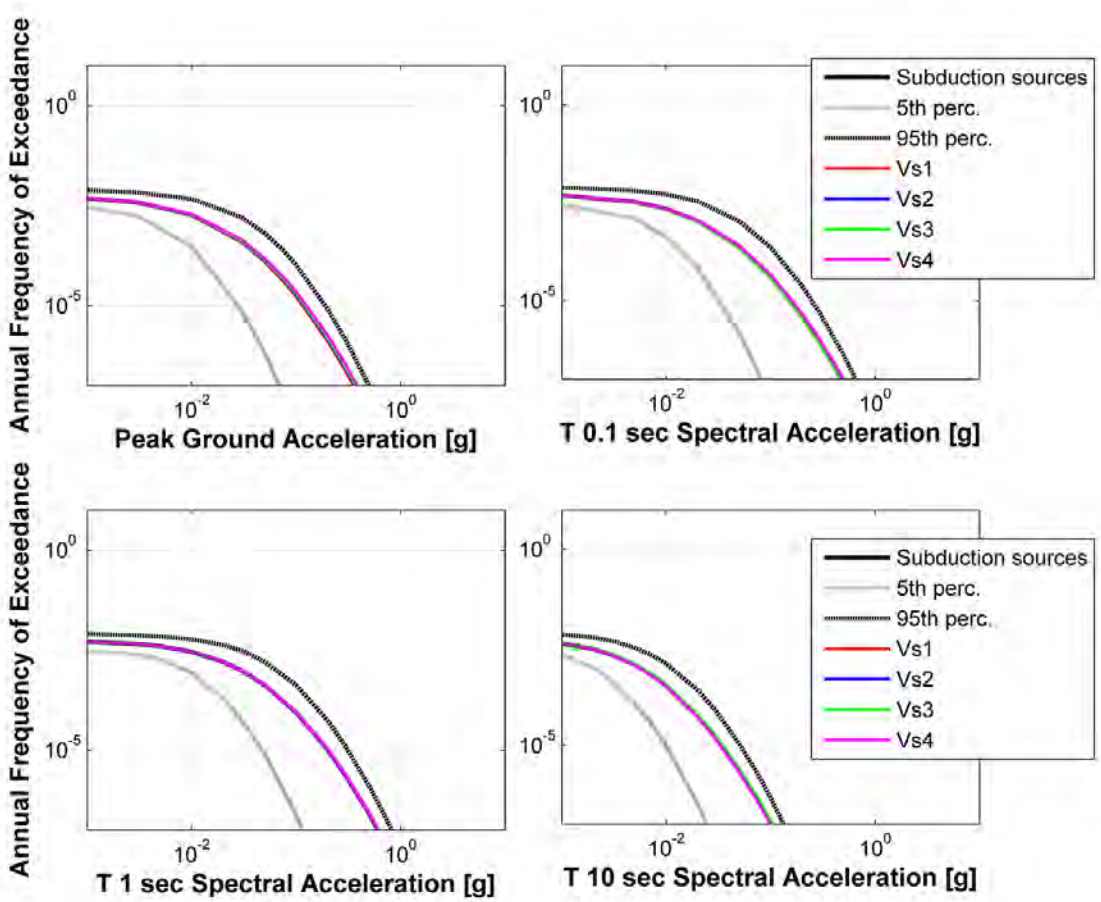

Figure 10.27. Comparison between the total mean subduction sources seismic hazard at Site A (black curve) and the individual contribution from the four different host-to-target Vs adjustment factors, for the peak ground acceleration, T 0.1-sec, T 1.0-sec, and T 10-sec spectral accelerations. The 5th and 95th percentiles are shown on each plot by the light and dark grey curves.

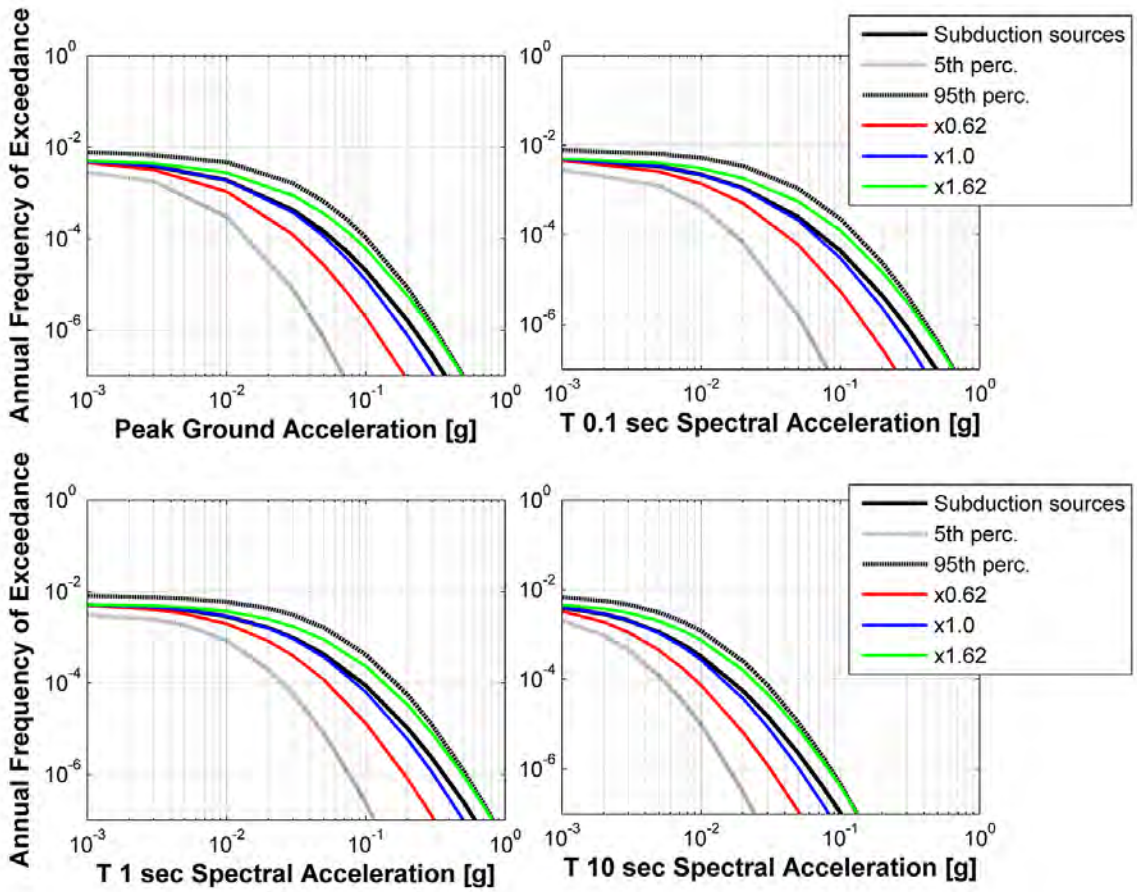

Figure 10.28. Comparison between the total mean subduction sources seismic hazard at Site A (black curve) and the individual contribution from the three different epistemic uncertainty in median factors for the peak ground acceleration, T 0.1-sec, T 1.0-sec, and T 10-sec spectral accelerations. The 5th and 95th percentiles are shown on each plot by the light and dark grey curves.

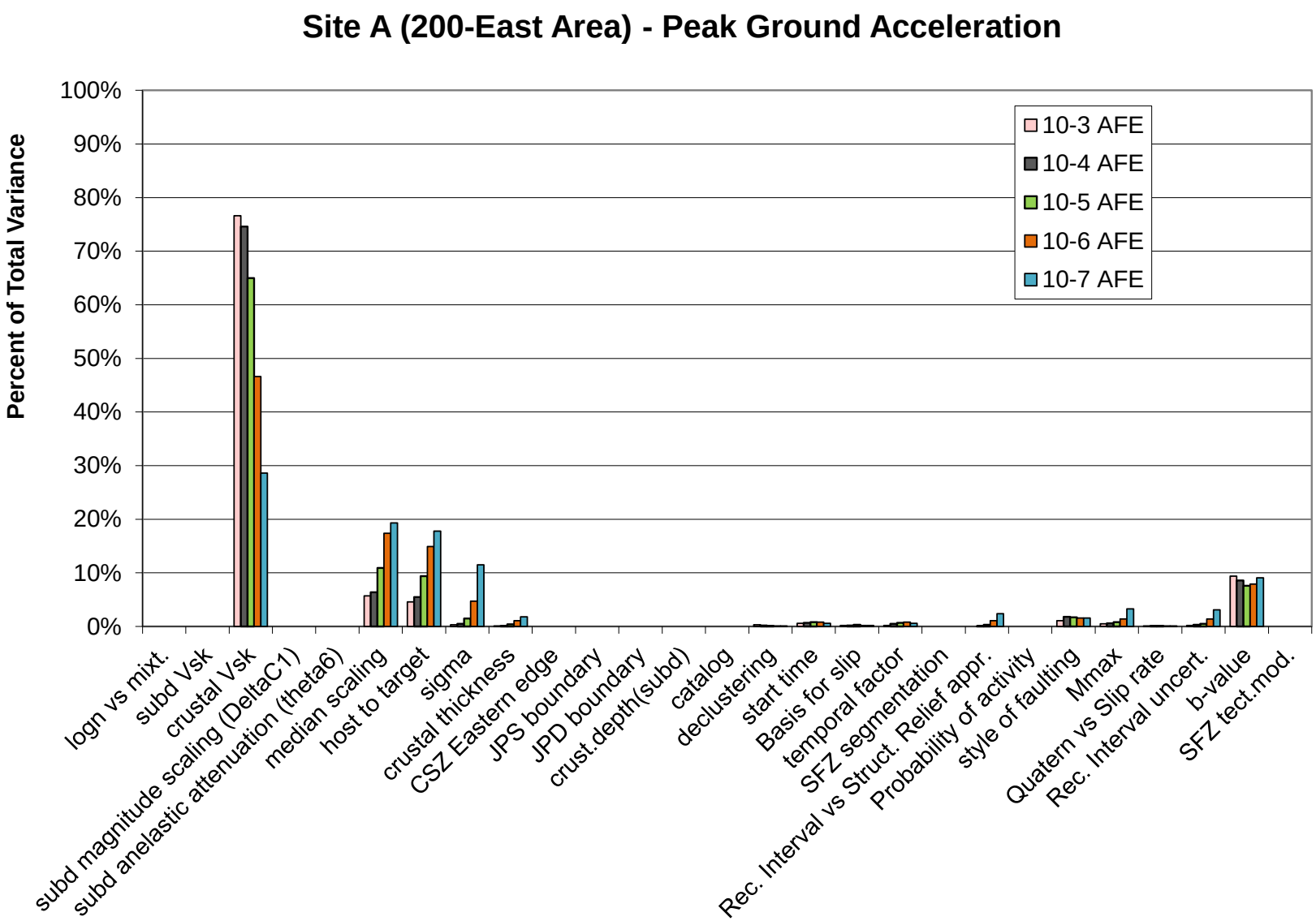

Figure 10.29. Variance contribution histogram at the 10^{-3}, 10^{-4}, 10^{-5}, 10^{-6}, and 10^{-7} annual frequencies of exceedance for peak ground acceleration and Site A.

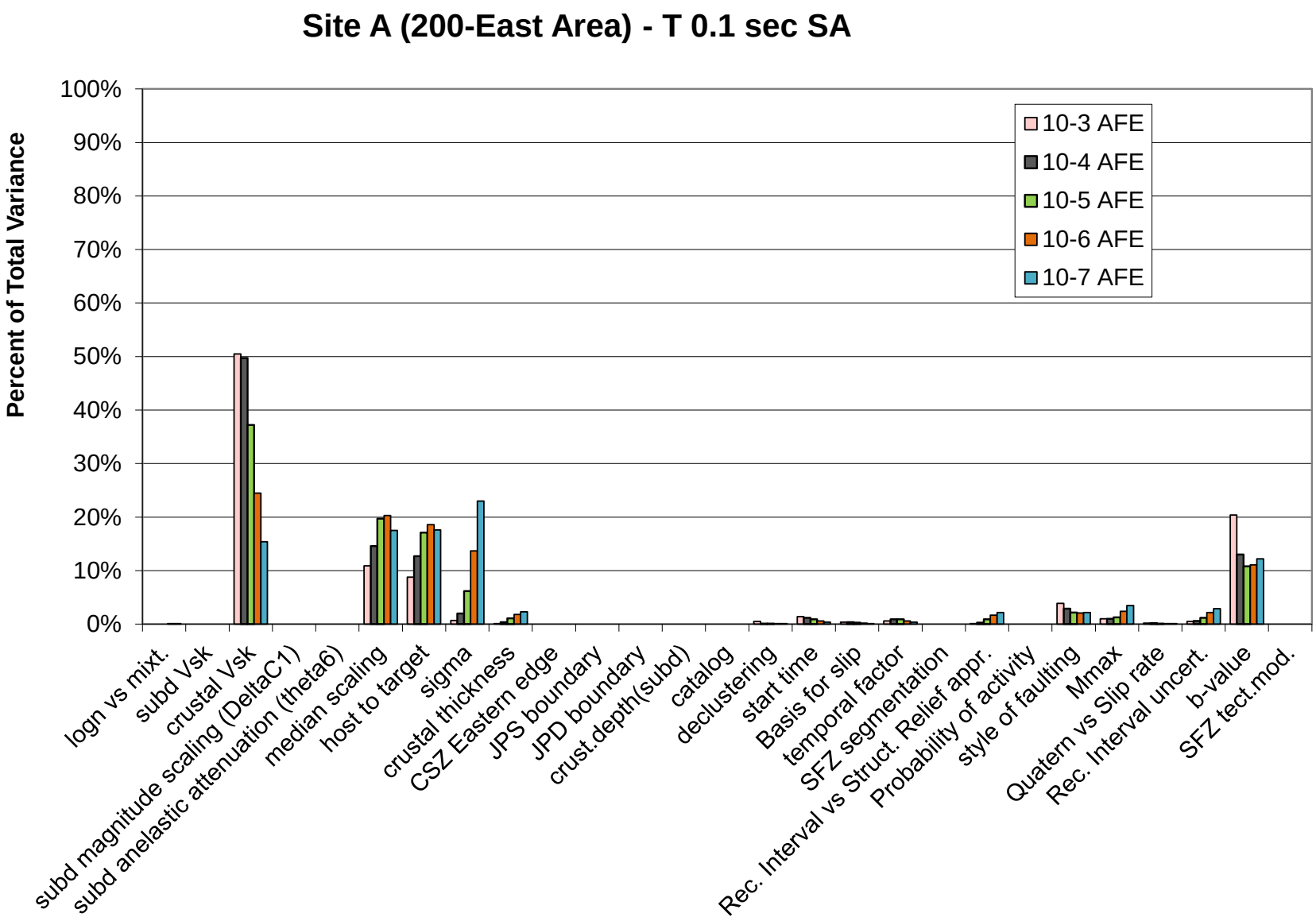

Figure 10.30. Variance contribution histogram at the 10^{-3}, 10^{-4}, 10^{-5}, 10^{-6}, and 10^{-7} annual frequencies of exceedance for T 0.1-sec spectral acceleration and Site A.

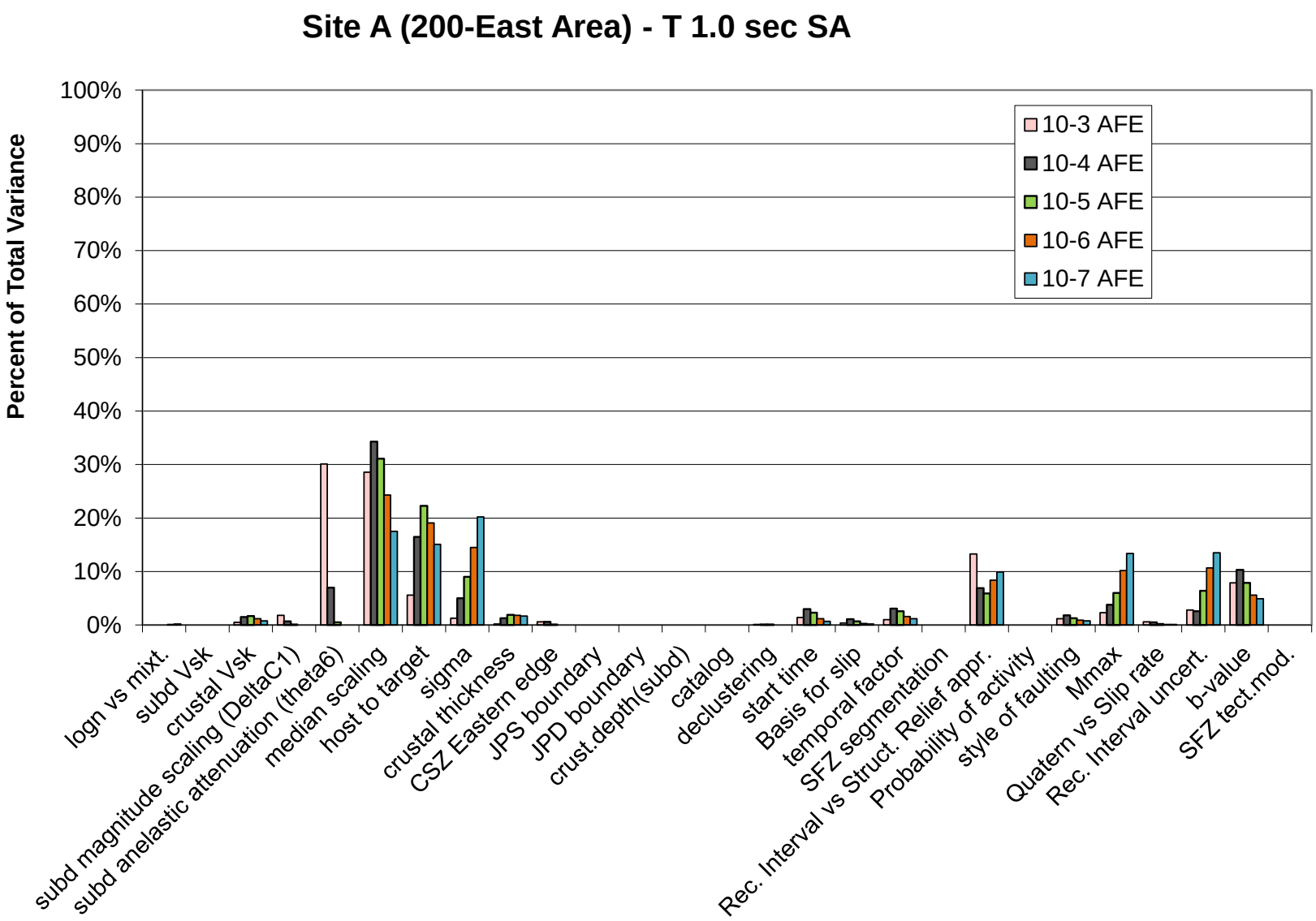

Figure 10.31. Variance contribution histogram at the 10^{-3}, 10^{-4}, 10^{-5}, 10^{-6}, and 10^{-7} annual frequencies of exceedance for T 1.0-sec spectral acceleration and Site A.

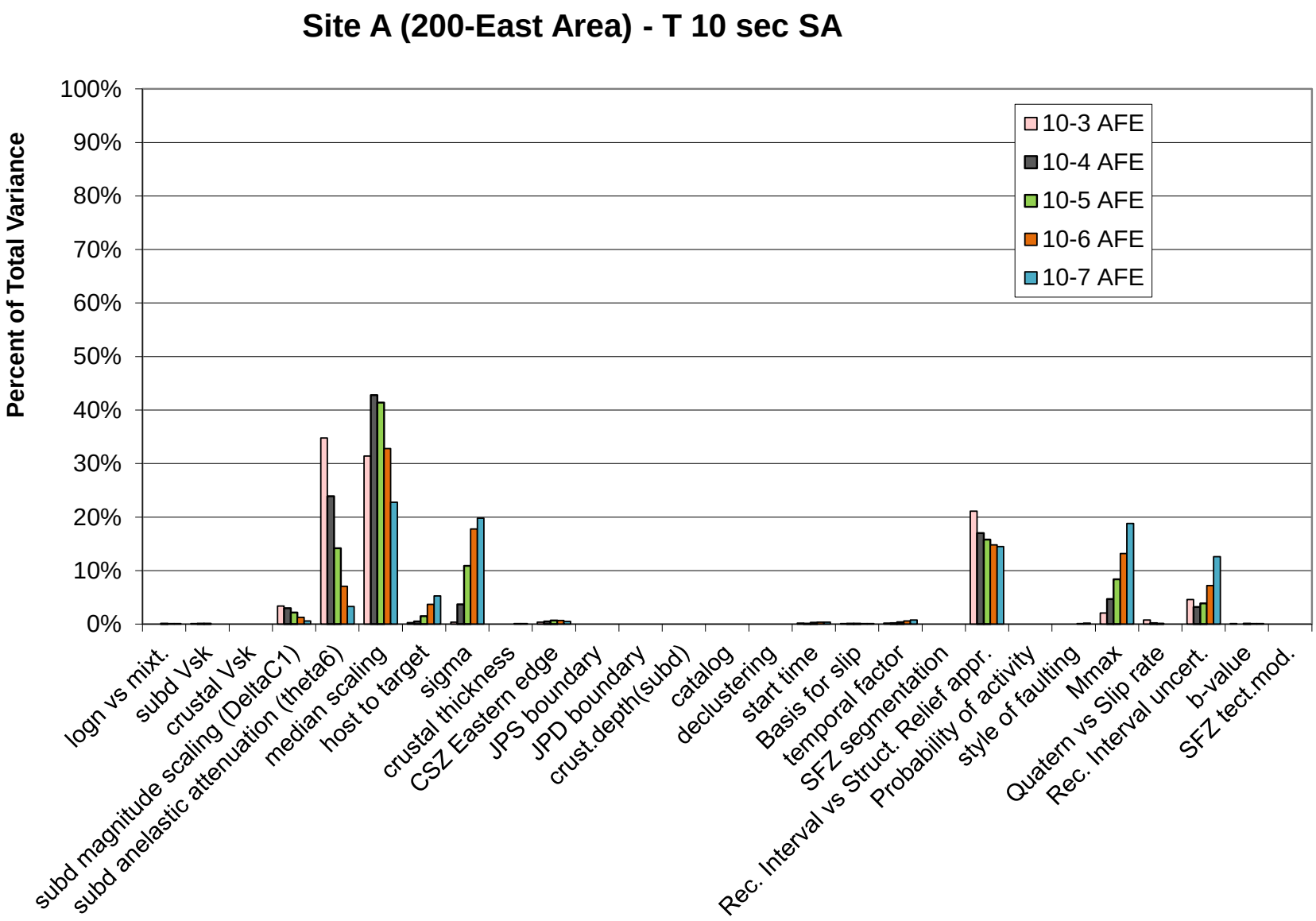

Figure 10.32. Variance contribution histogram at the 10^{-3}, 10^{-4}, 10^{-5}, 10^{-6}, and 10^{-7} annual frequencies of exceedance for T 10-sec spectral acceleration and Site A.

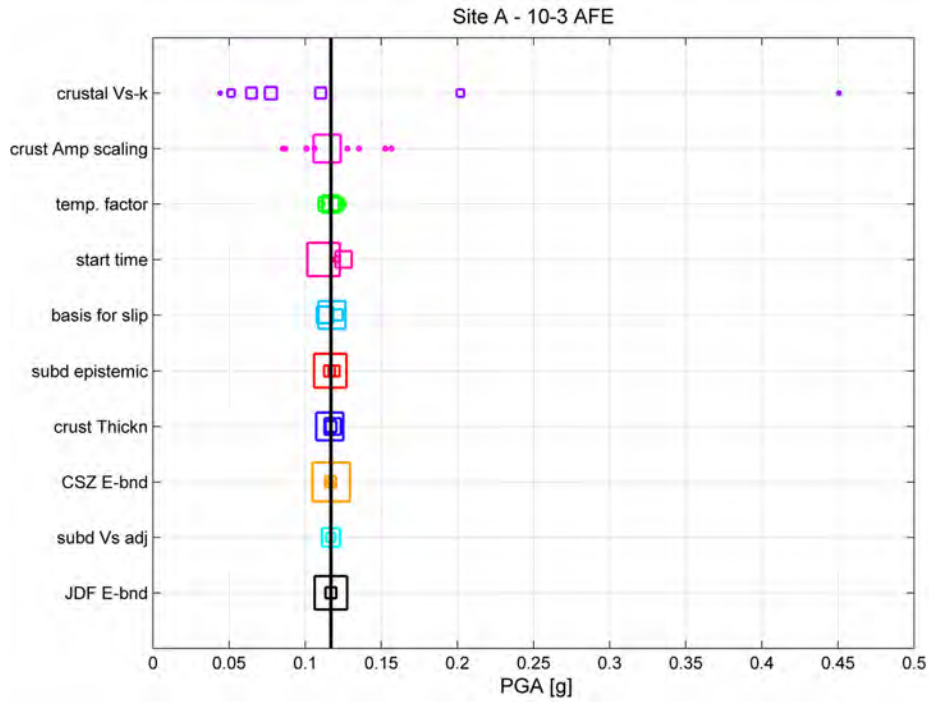

(a)

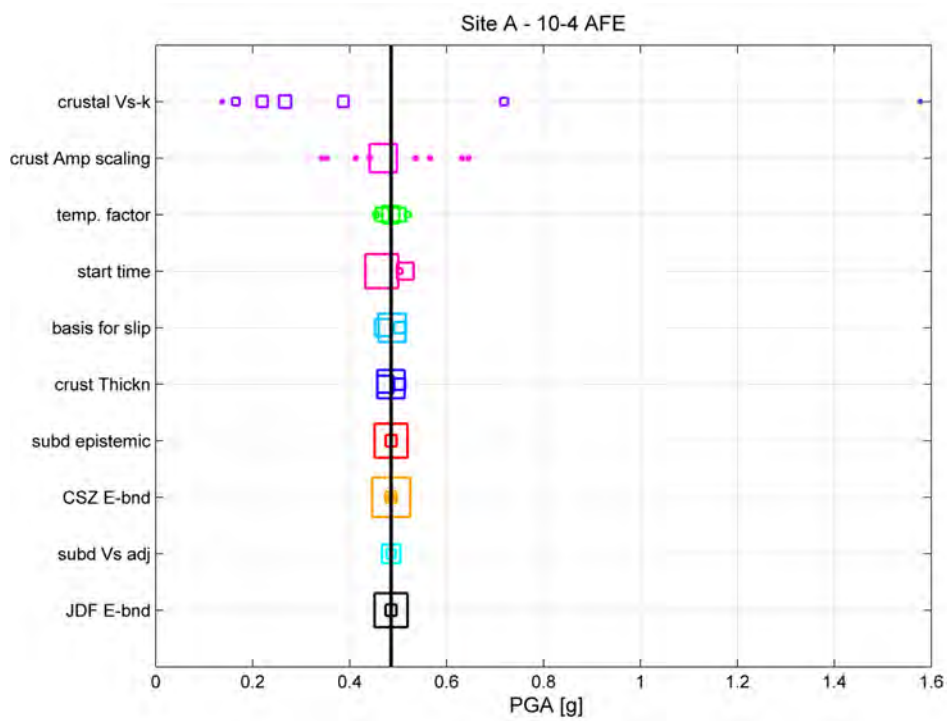

(b)

Figure 10.33. Tornado plots for Site A and peak ground acceleration at AFEs of: a) 10^{-3} (1000 years return period); b) 10^{-4} (10,000 years return period); c) 10^{-5} (100,000 years return period); d) 10^{-6} (1,000,000 years return period); e) 10^{-7} (10,000,000 years return period). The size of the symbols is proportional to the logic-tree weight assigned to each branch.

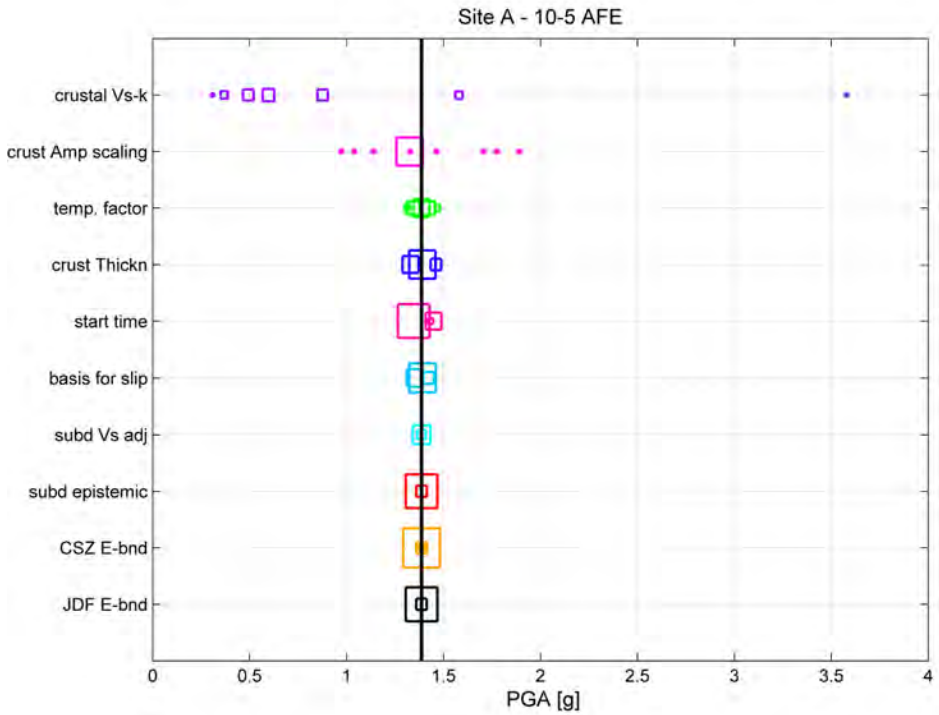

(c)

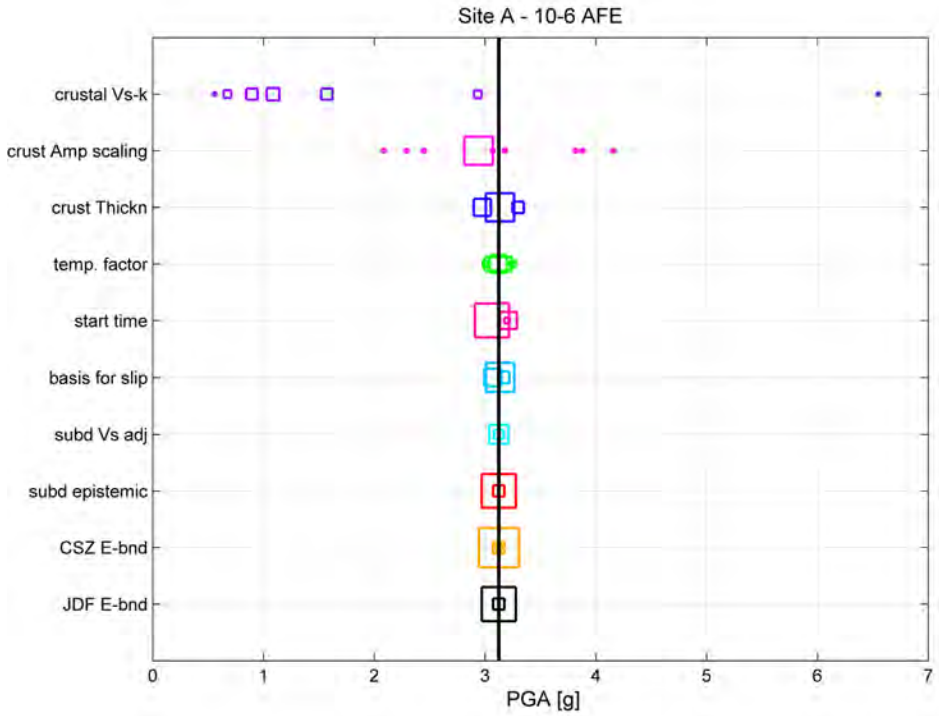

(d)

Figure 10.33. (contd)

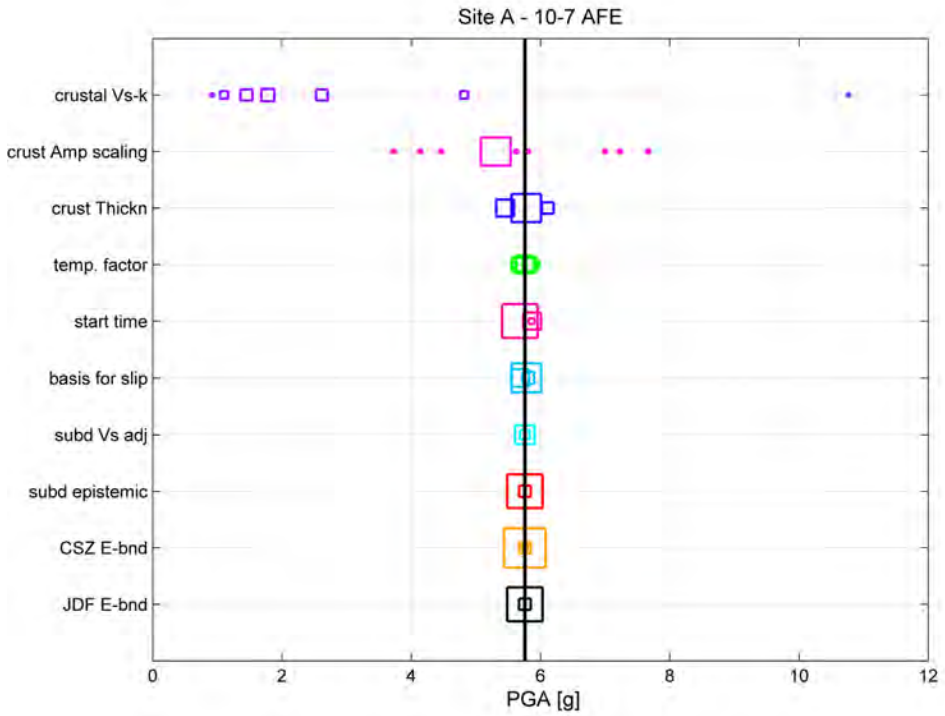

(e)

Figure 10.33. (contd)

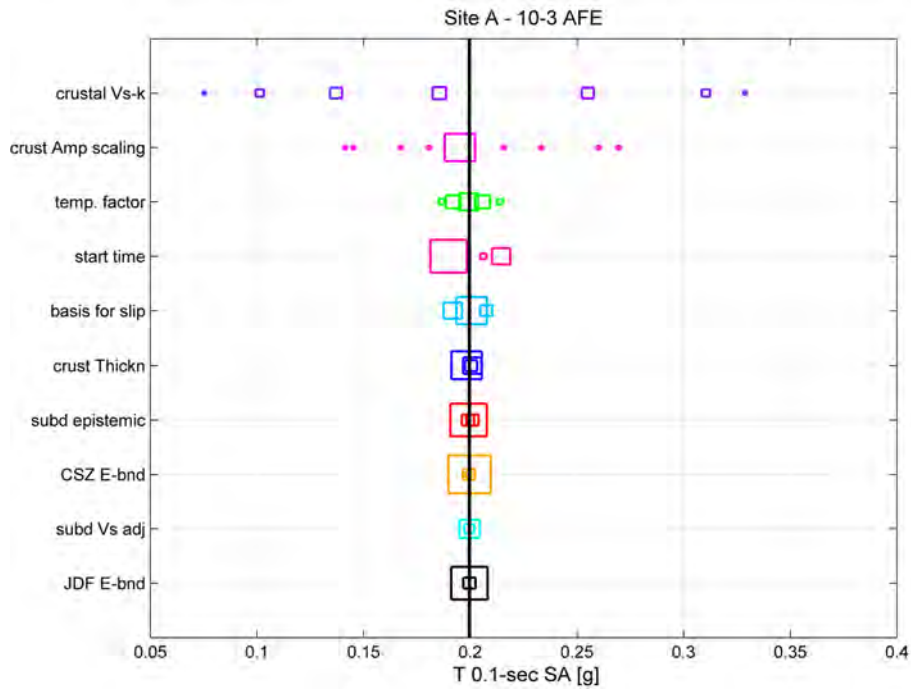

(a)

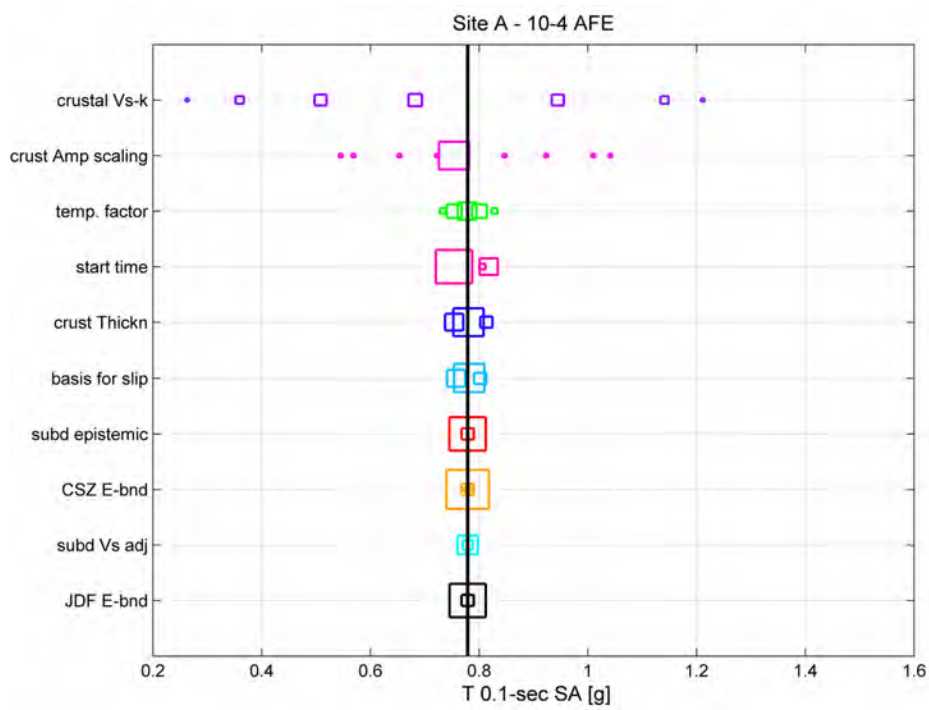

(b)

Figure 10.34. Tornado plots for Site A and T 0.1-sec spectral acceleration at AFEs of: a) 10^{-3} (1000 years return period); b) 10^{-4} (10,000 years return period); c) 10^{-5} (100,000 years return period); d) 10^{-6} (1,000,000 years return period); e) 10^{-7} (10,000,000 years return period). The size of the symbols is proportional to the logic-tree weight assigned to each branch.

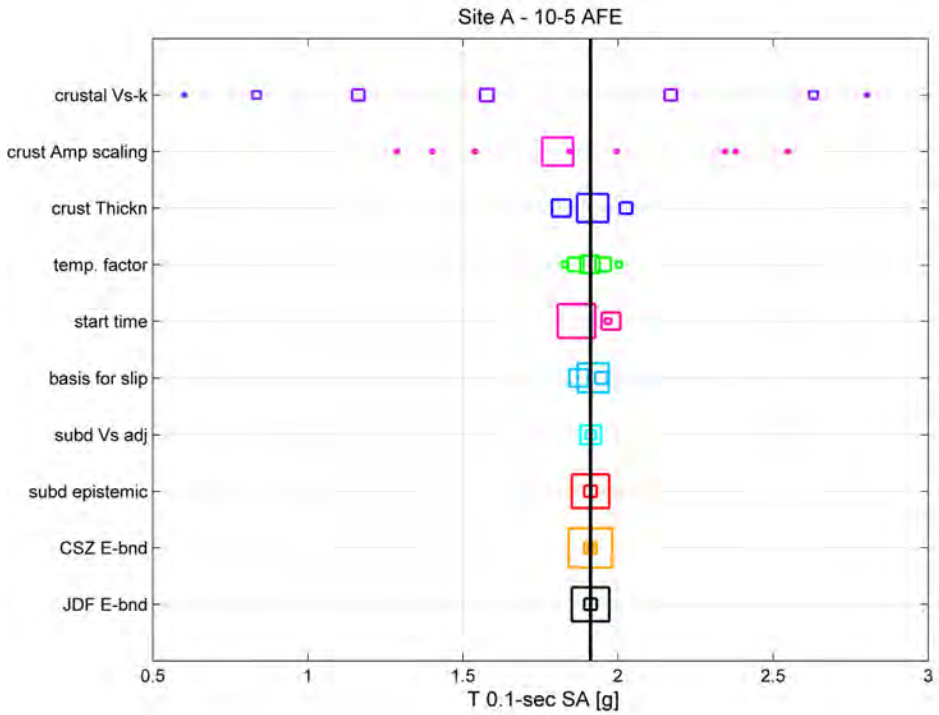

(c)

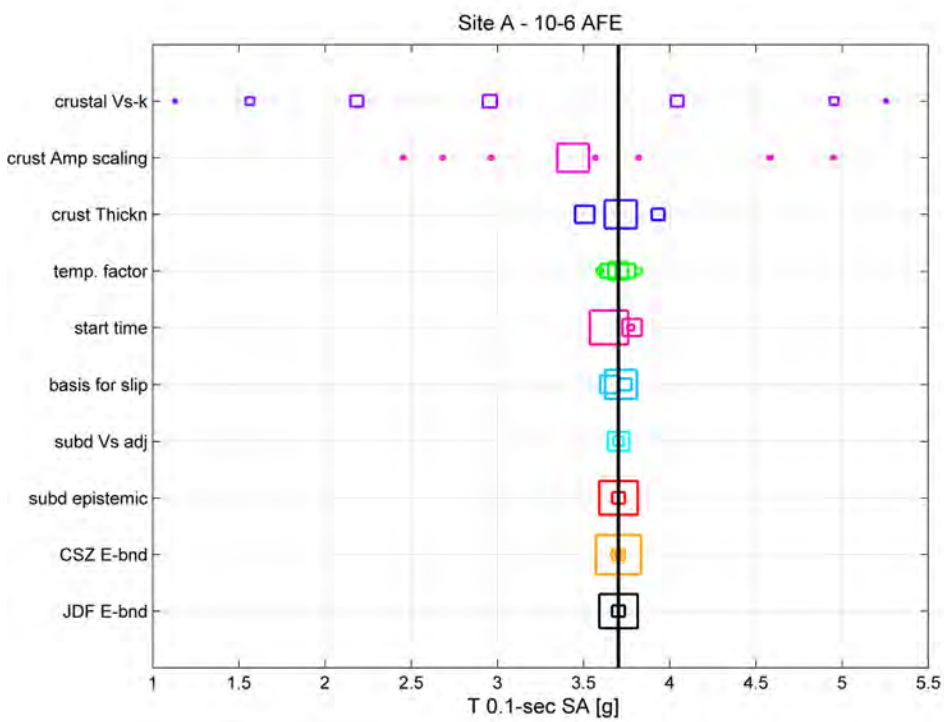

(d)

Figure 10.34. (contd)

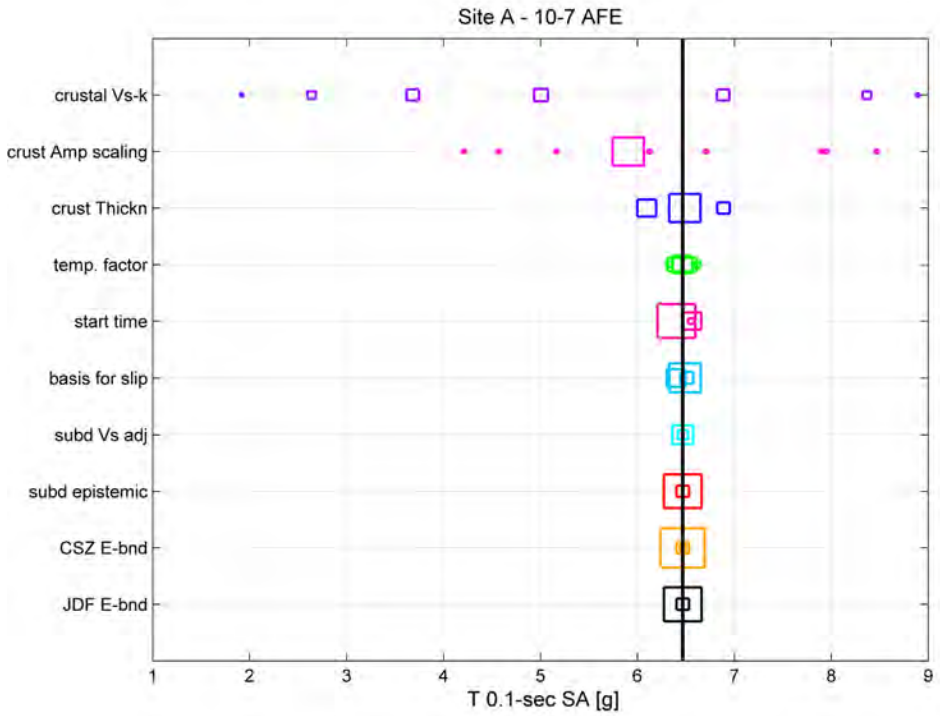

(e)

Figure 10.34. (contd)

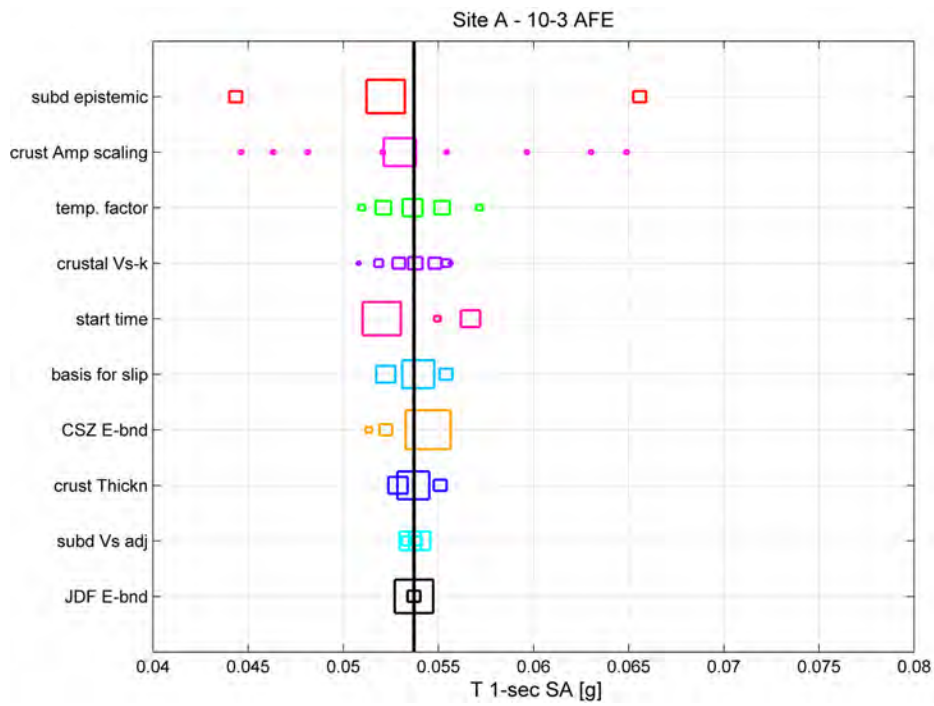

(a)

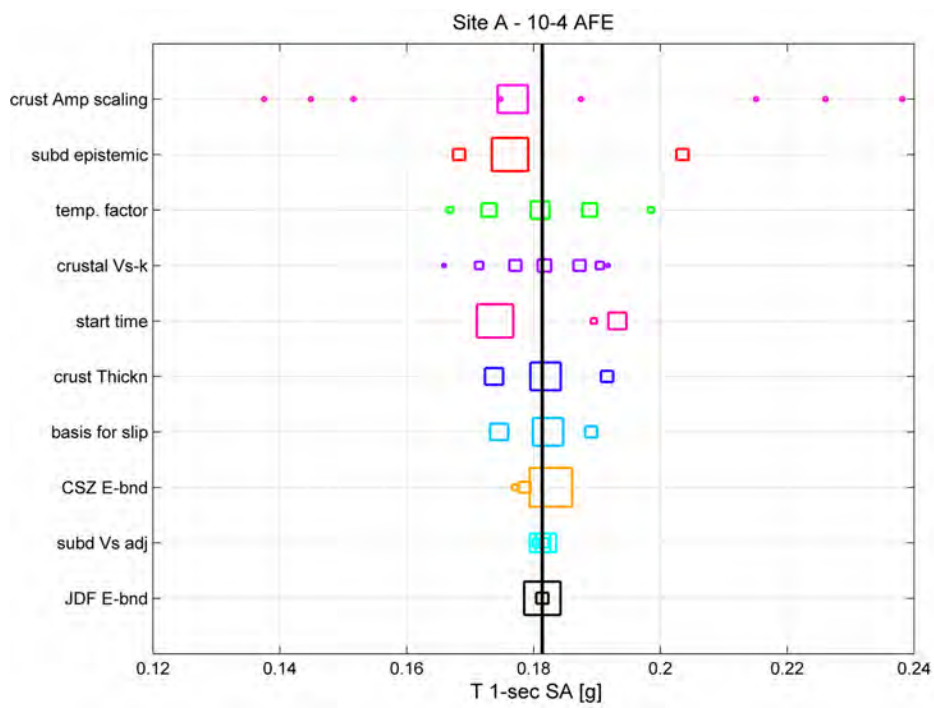

(b)

Figure 10.35. Tornado plots for Site A and T 1.0-sec spectral acceleration at AFEs of: a) 10^{-3} (1000 years return period); b) 10^{-4} (10,000 years return period); c) 10^{-5} (100,000 years return period); d) 10^{-6} (1,000,000 years return period); e) 10^{-7} (10,000,000 years return period). The size of the symbols is proportional to the logic-tree weight assigned to each branch.

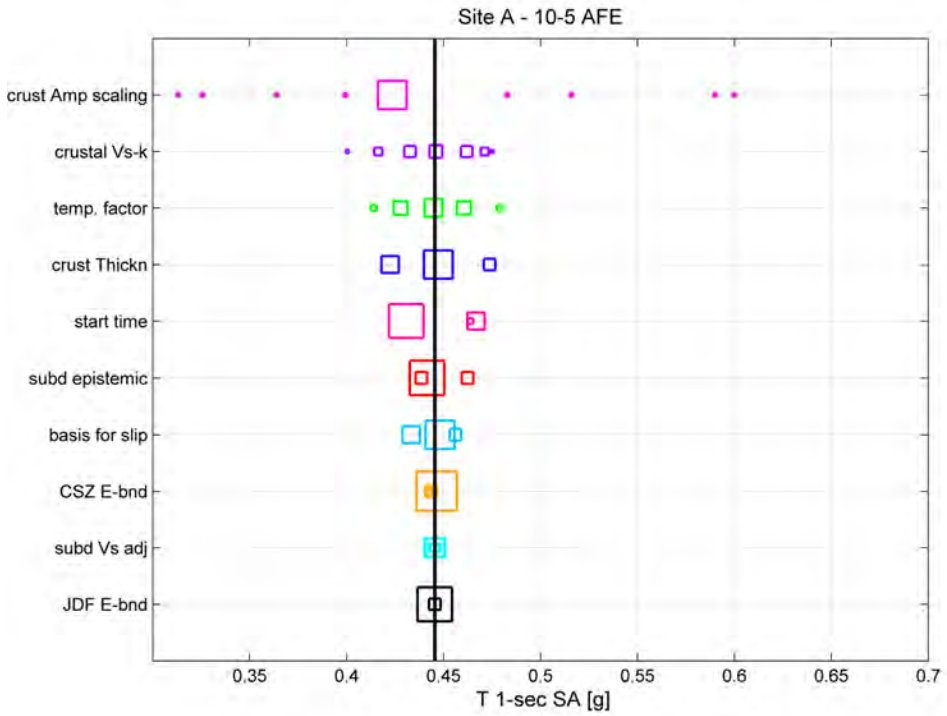

(c)

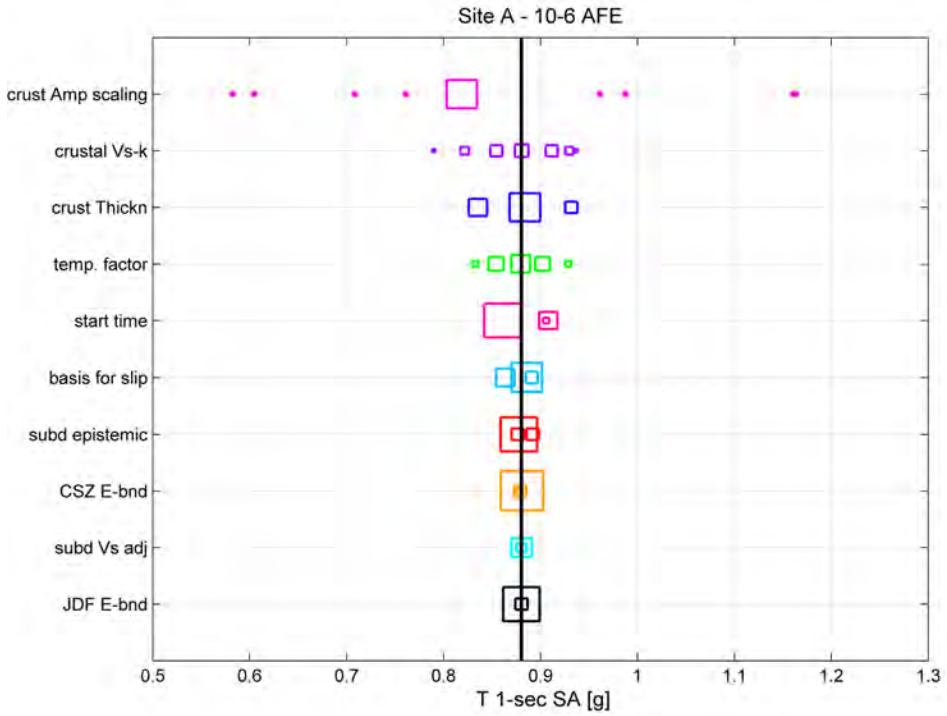

(d)

Figure 10.35. (contd)

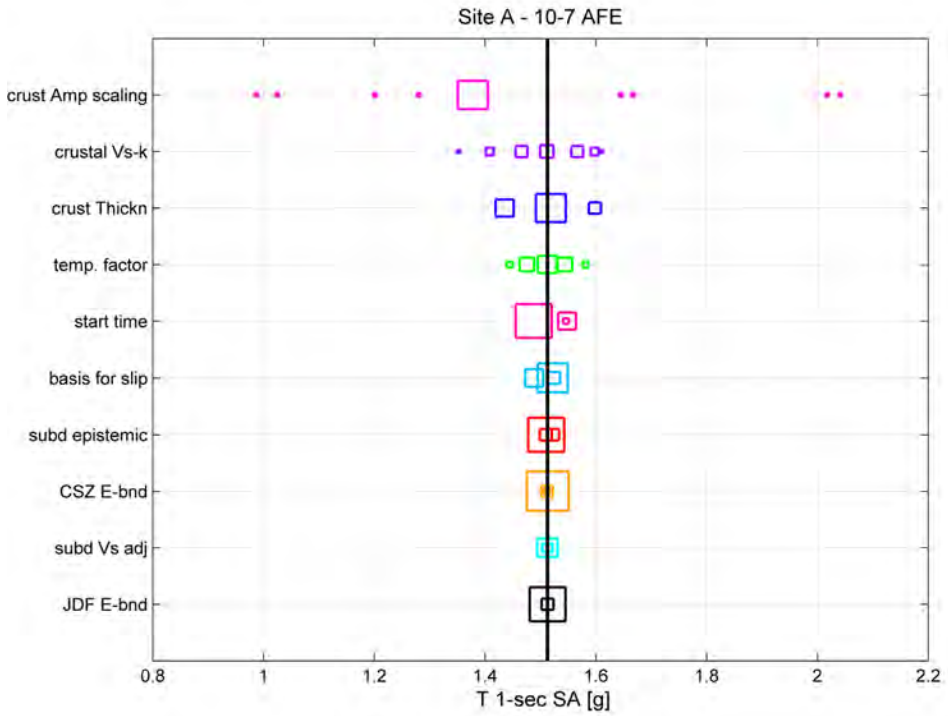

(e)

Figure 10.35. (contd)

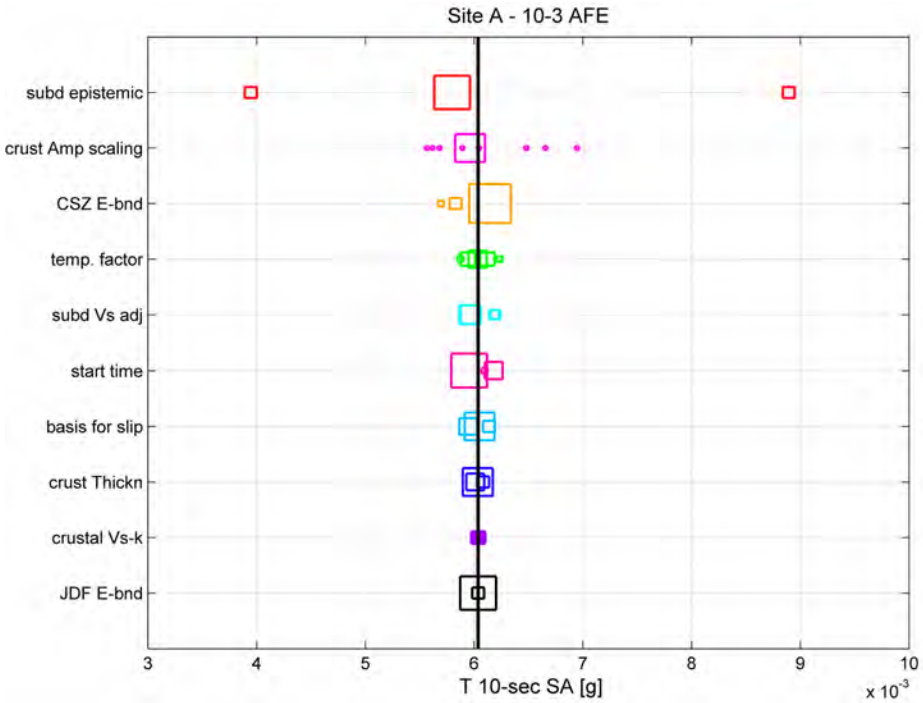

(a)

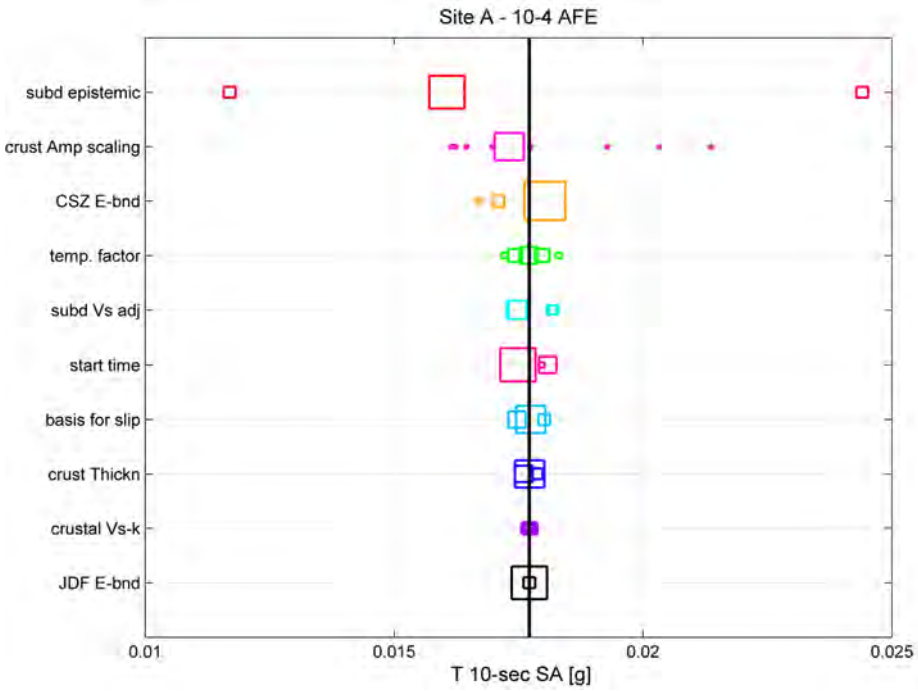

(b)

Figure 10.36. Tornado plots for Site A and T 10-sec spectral acceleration at AFEs of: a) 10^{-3} (1000 years return period); b) 10^{-4} (10,000 years return period); c) 10^{-5} (100,000 years return period); d) 10^{-6} (1,000,000 years return period); e) 10^{-7} (10,000,000 years return period). The size of the symbols is proportional to the logic-tree weight assigned to each branch.

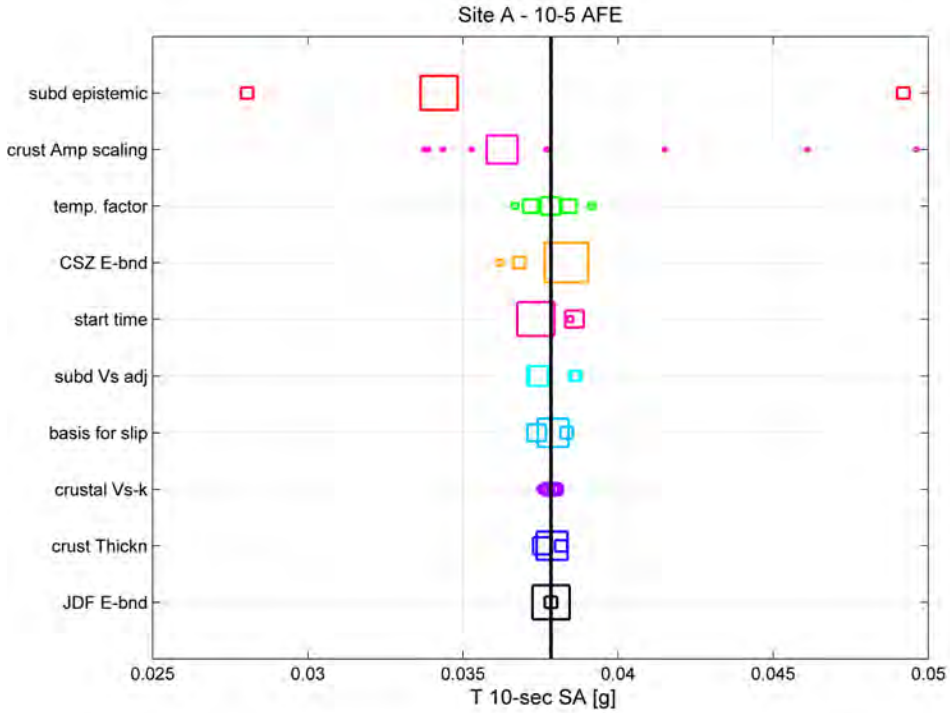

(c)

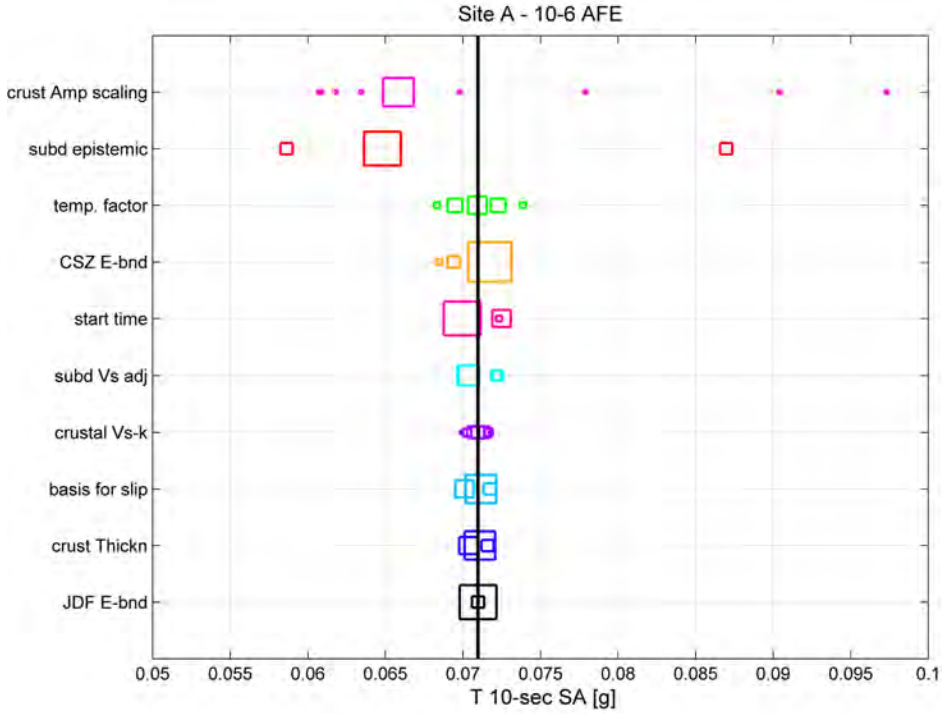

(d)

Figure 10.36. (contd)

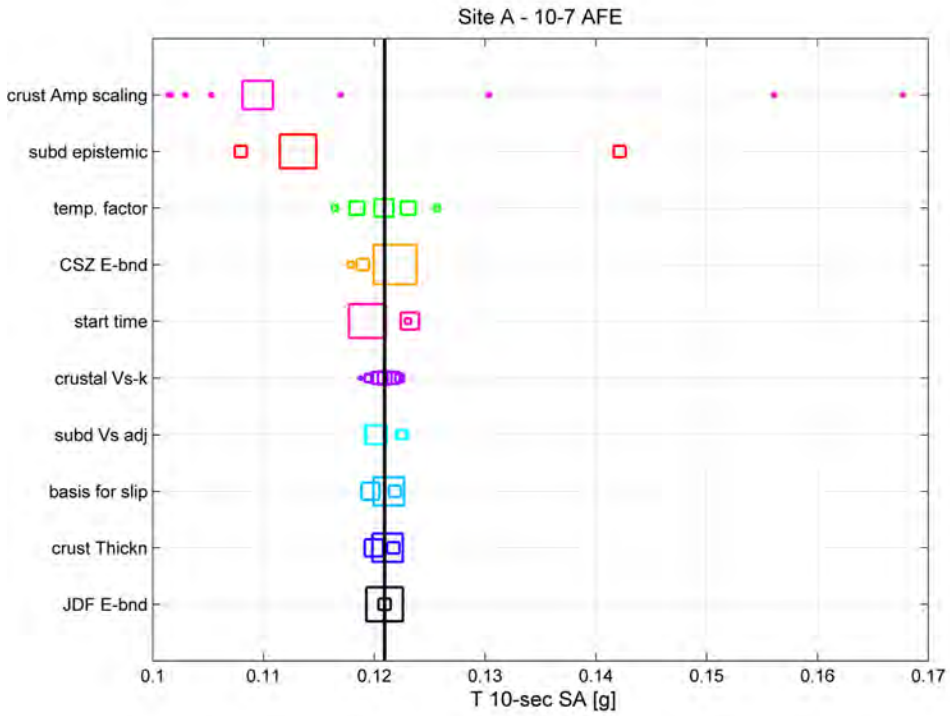

(e)

Figure 10.36. (contd)

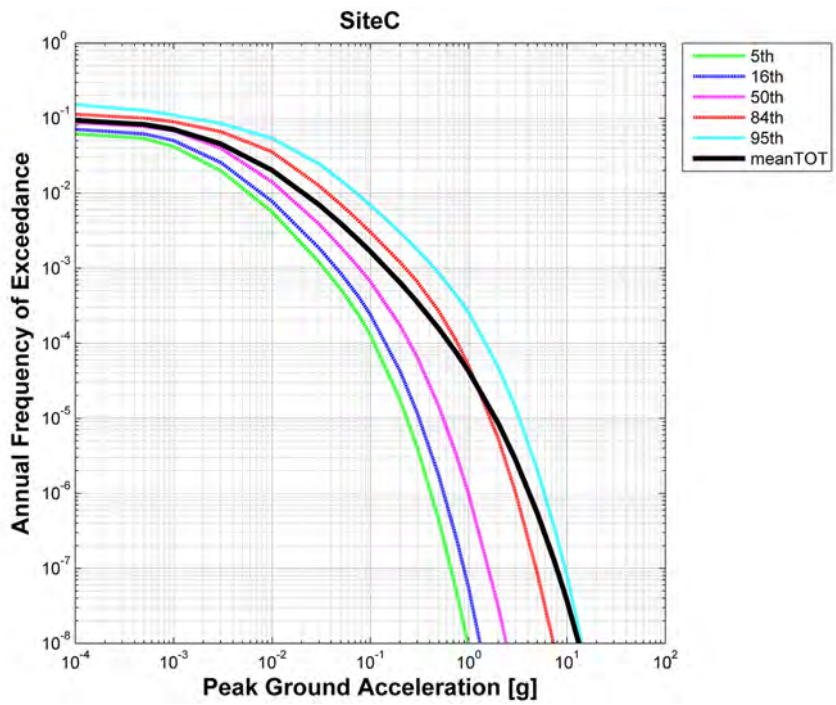

(a)

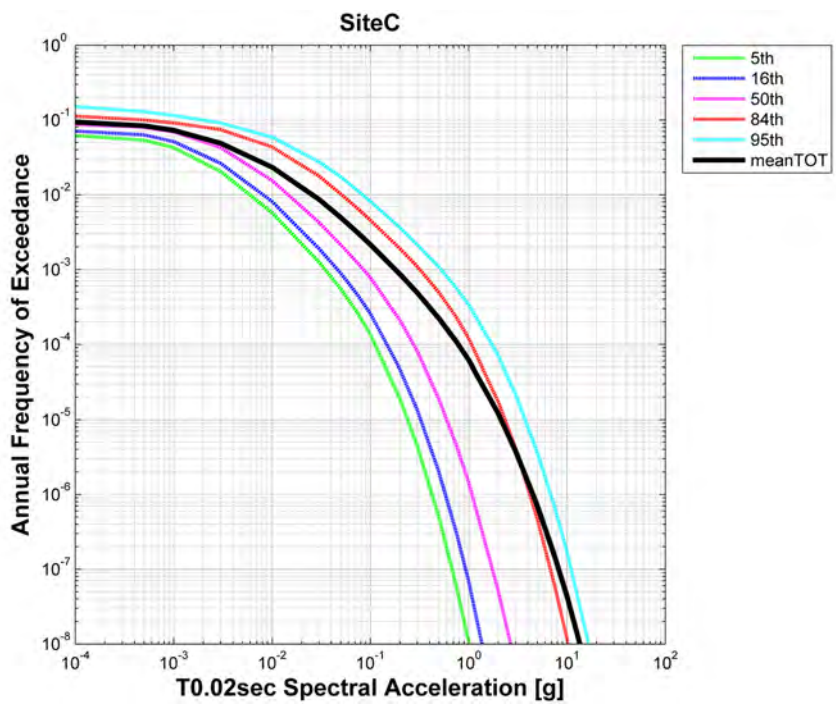

(b)

Figure 10.37. Total mean seismic hazard at Site C and percentiles: a) PGA; b) T 0.02-sec; c) T 0.03-sec; d) T 0.04-sec; e) T 0.05-sec; f) T 0.07-sec; g) T 0.10-sec; h) T 0.15-sec; i) T 0.20-sec; j) T 0.30-sec; k) T 0.40-sec; l) T 0.50-sec; m) T 0.75-sec; n) T 1.0-sec; o) T 1.5-sec; p) T 2.0-sec; q) T 3.0-sec; r) T 5.0-sec; s) T 7.5-sec; t) T 10-sec spectral acceleration.

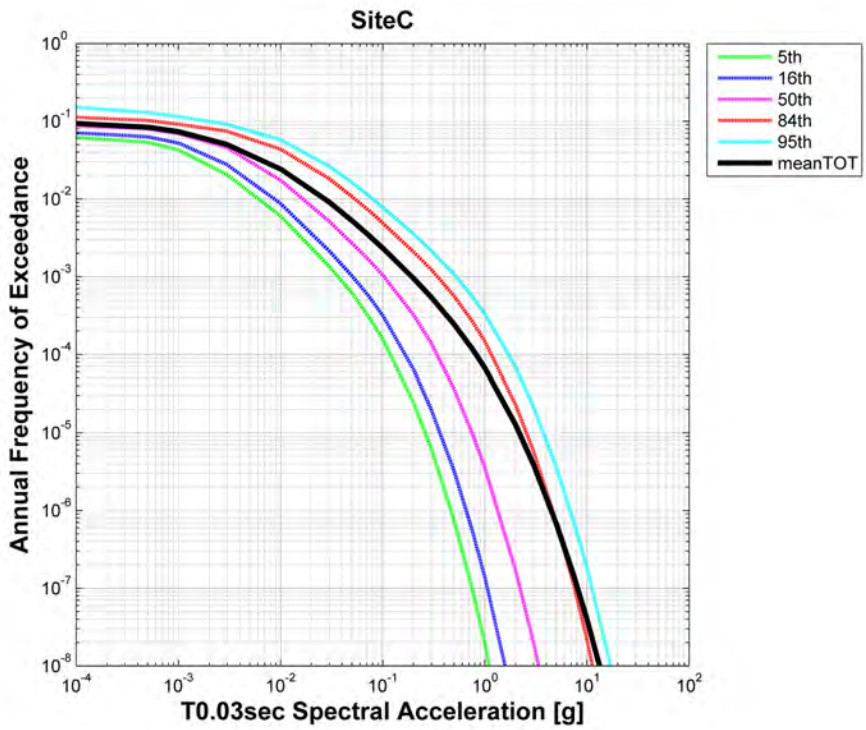

(c)

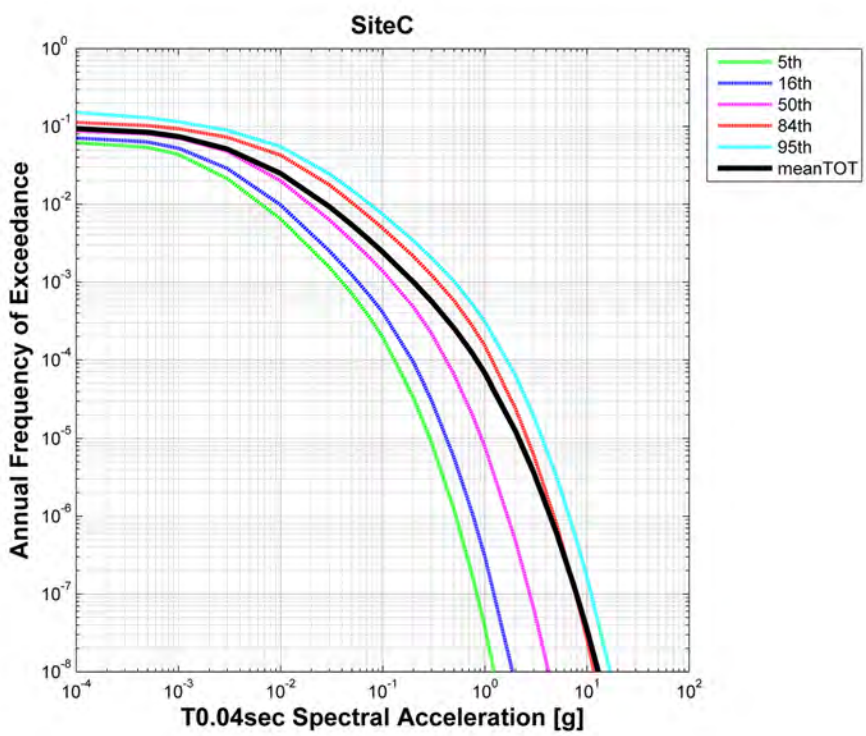

(d)

Figure 10.37. (contd)

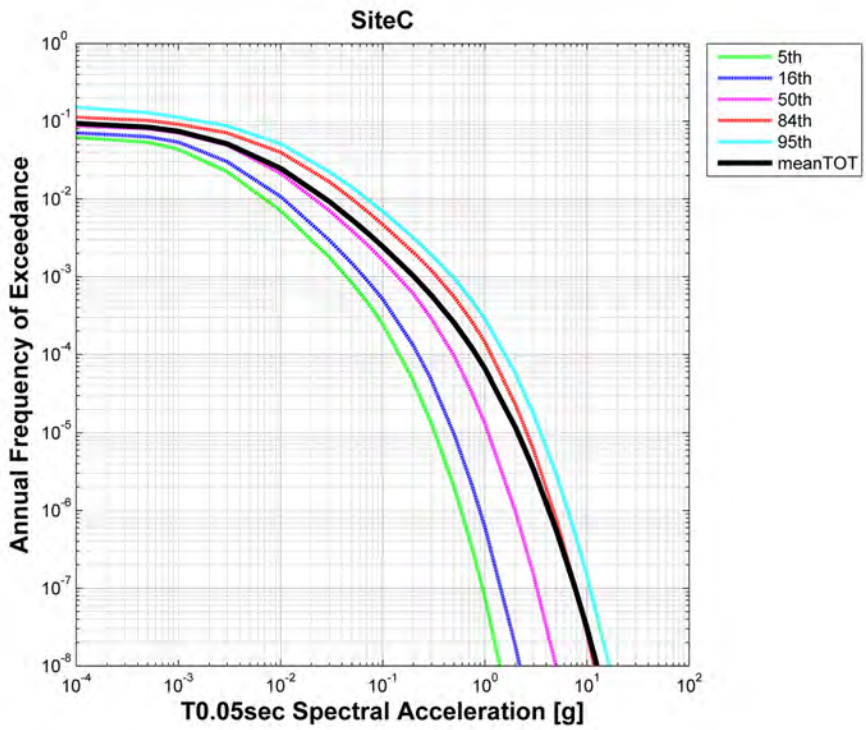

(e)

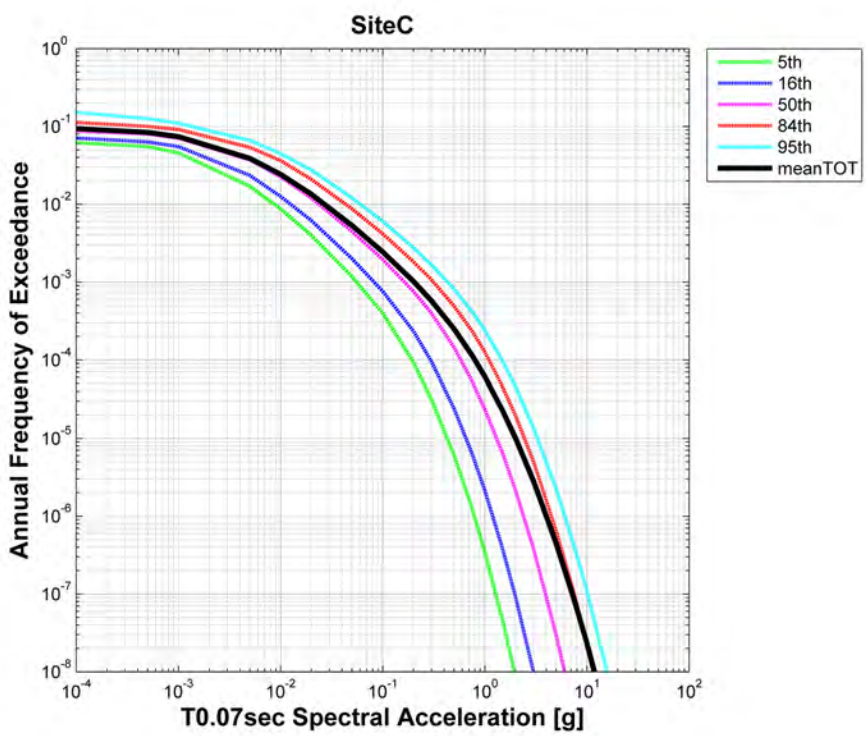

(f)

Figure 10.37. (contd)

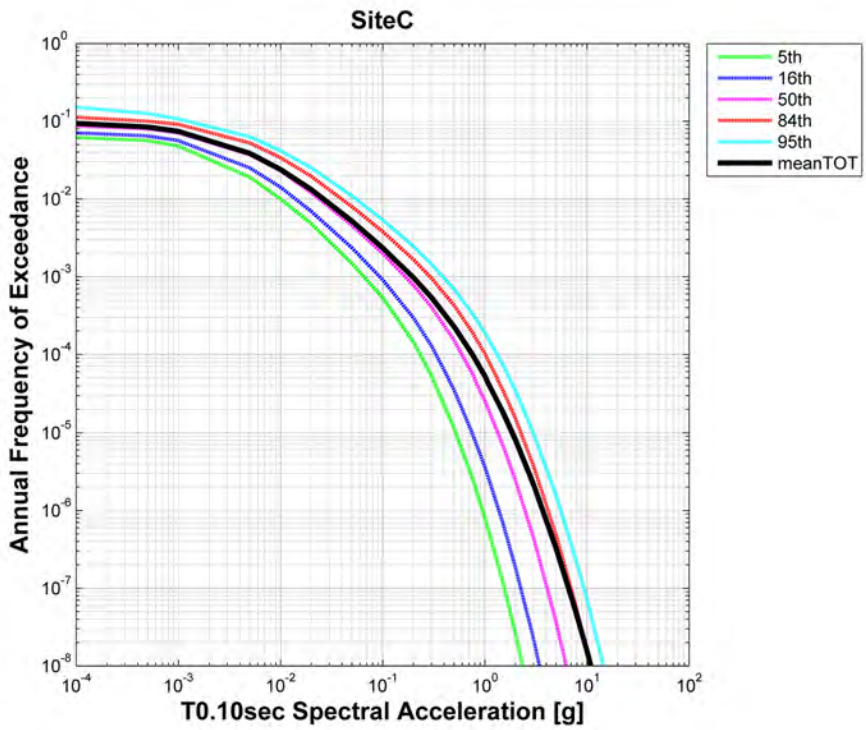

(g)

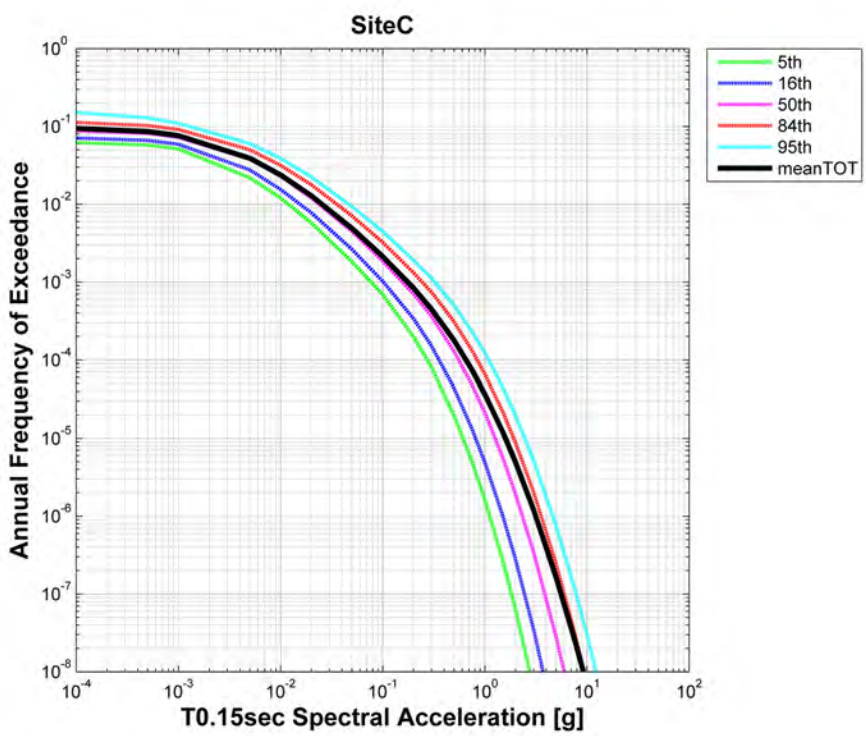

(h)

Figure 10.37. (contd)

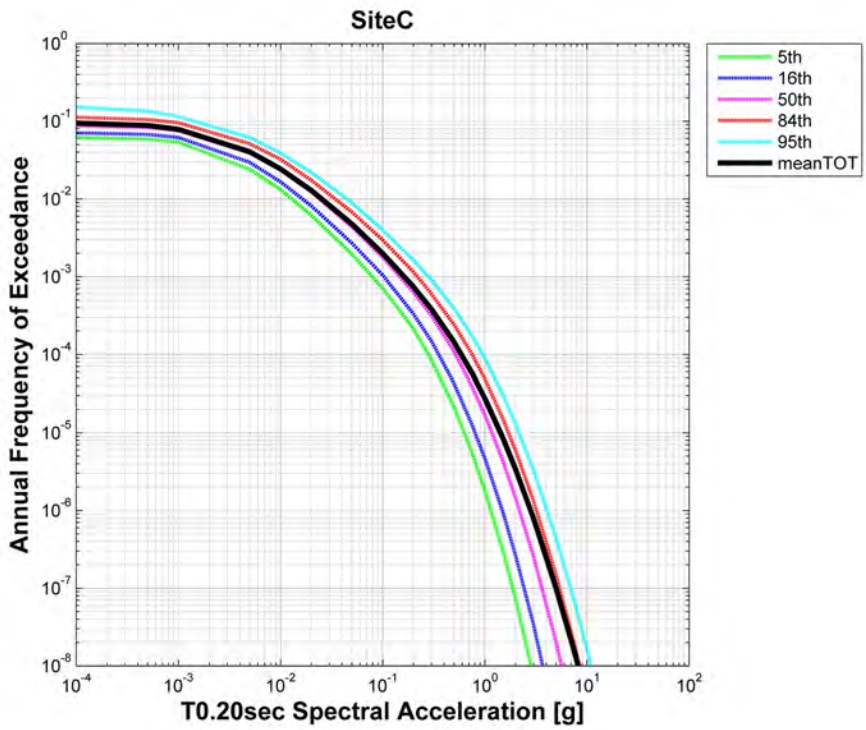

(i)

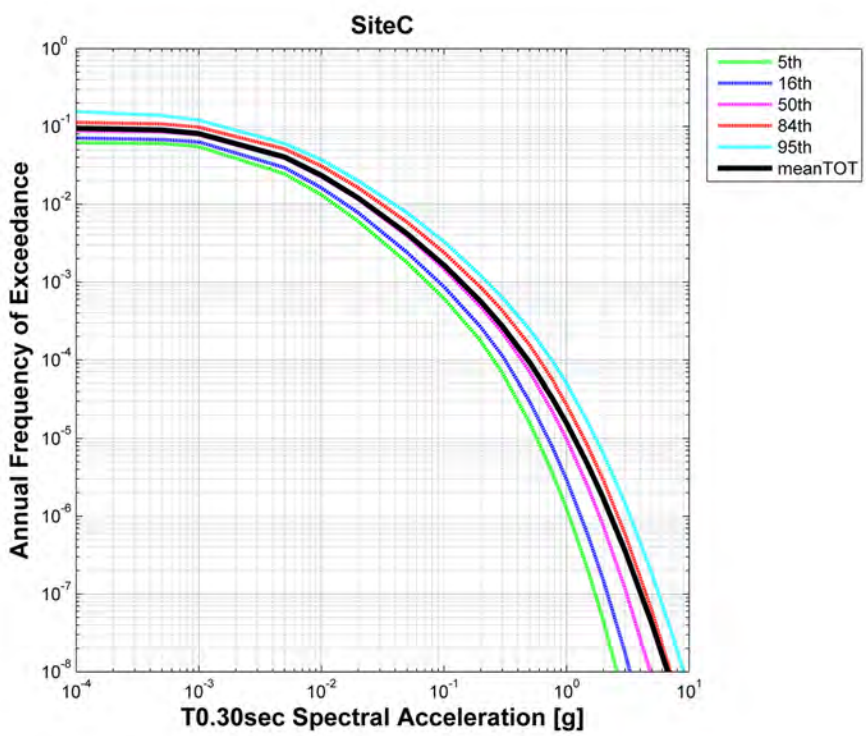

(j)

Figure 10.37. (contd)

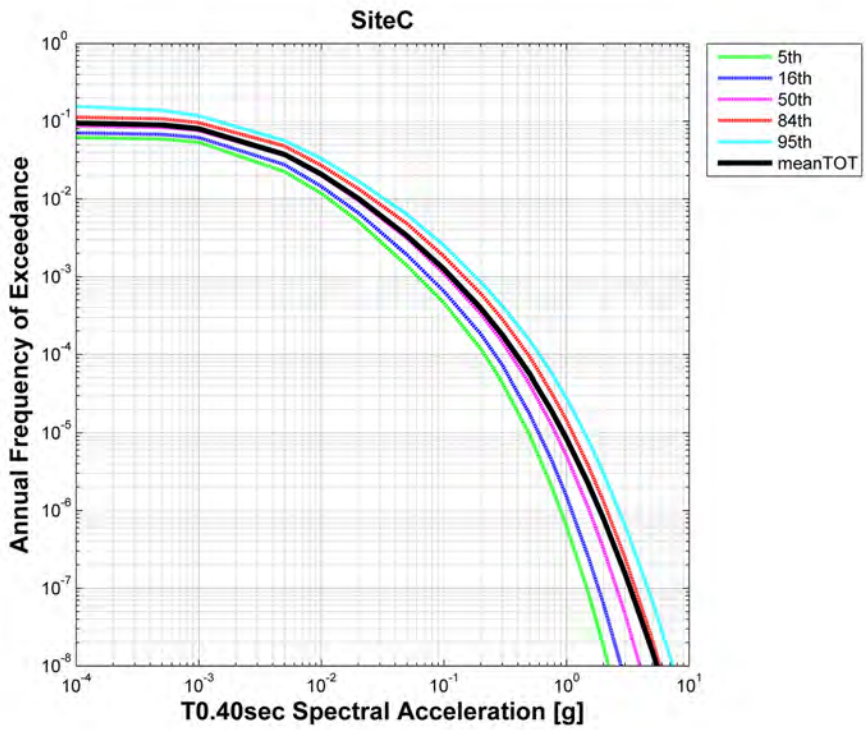

(k)

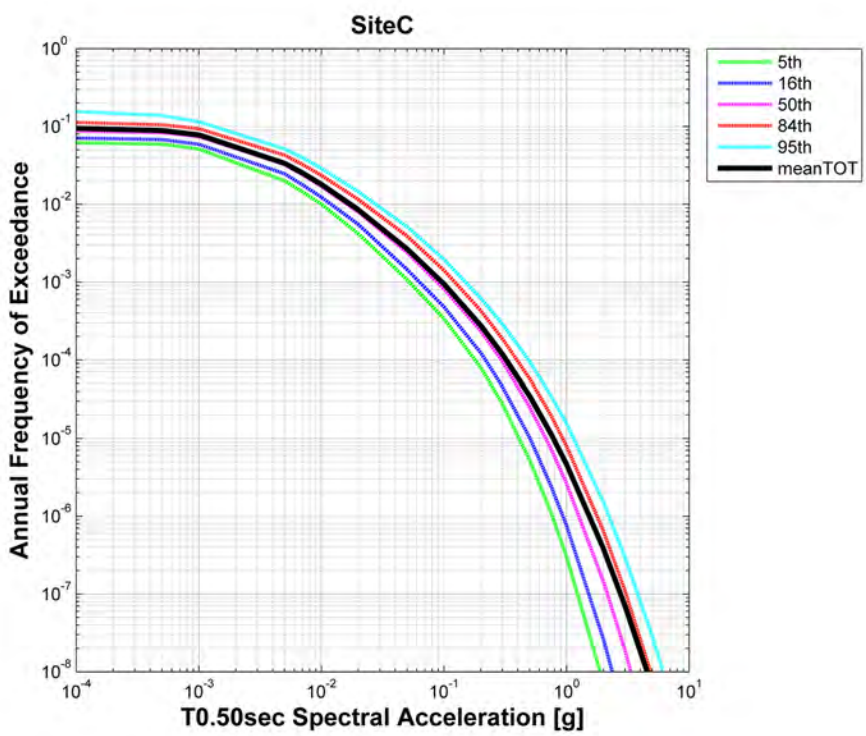

(l)

Figure 10.37. (contd)

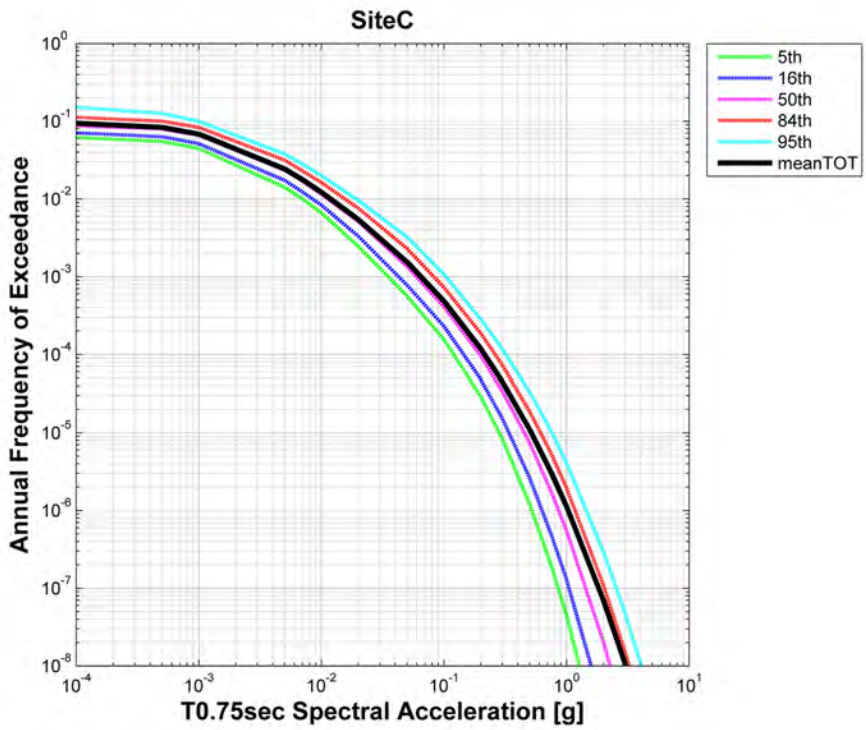

(m)

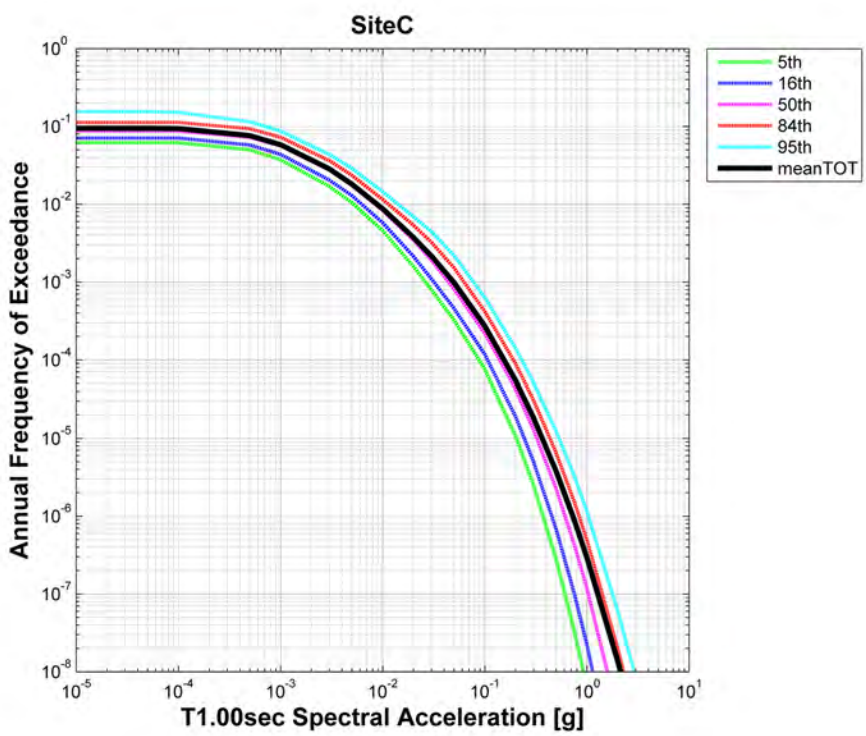

(n)

Figure 10.37. (contd)

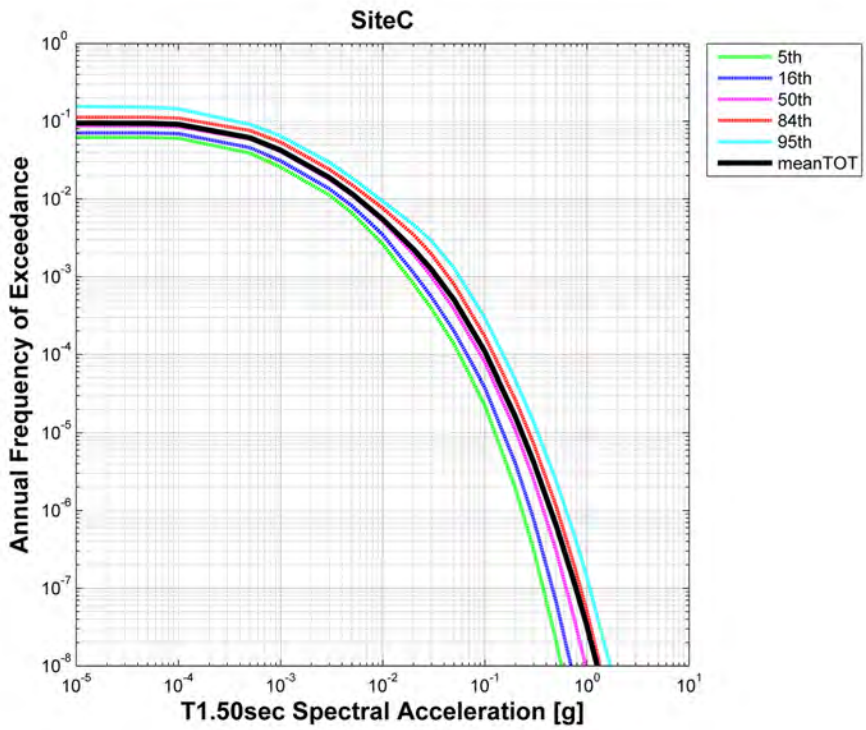

(o)

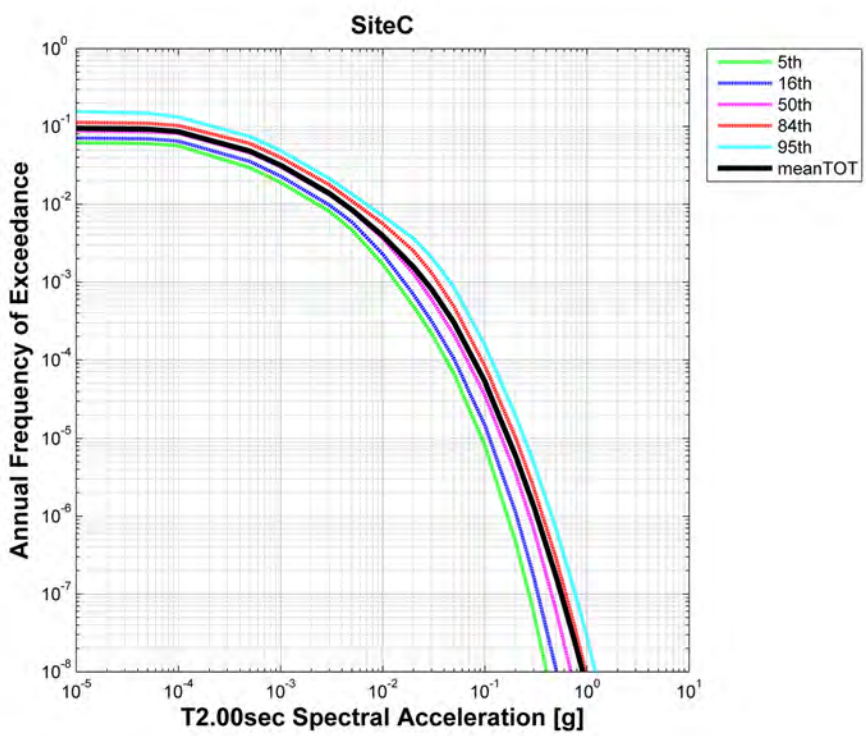

(p)

Figure 10.37. (contd)

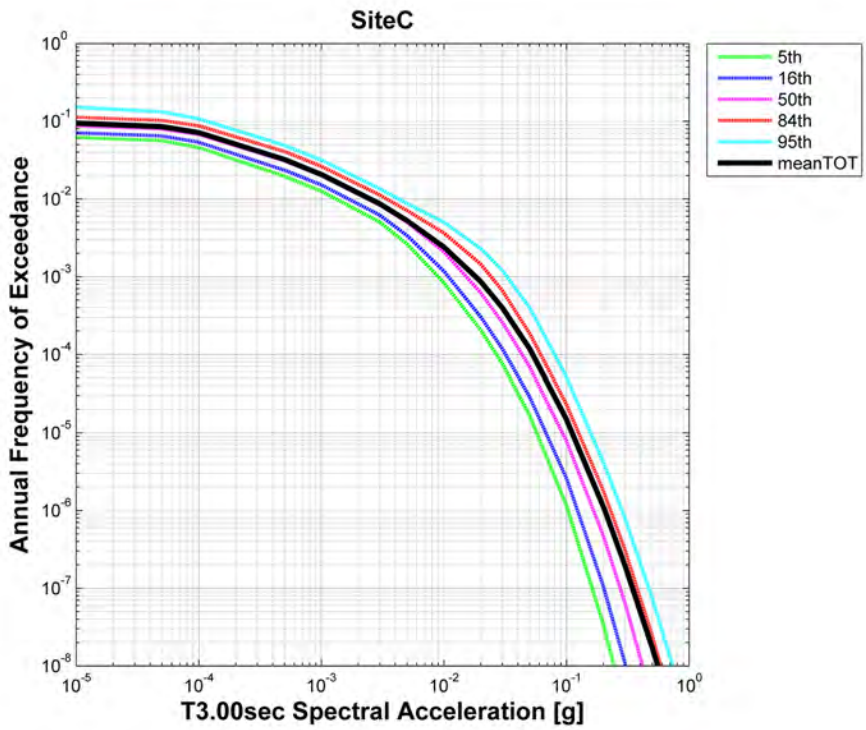

(q)

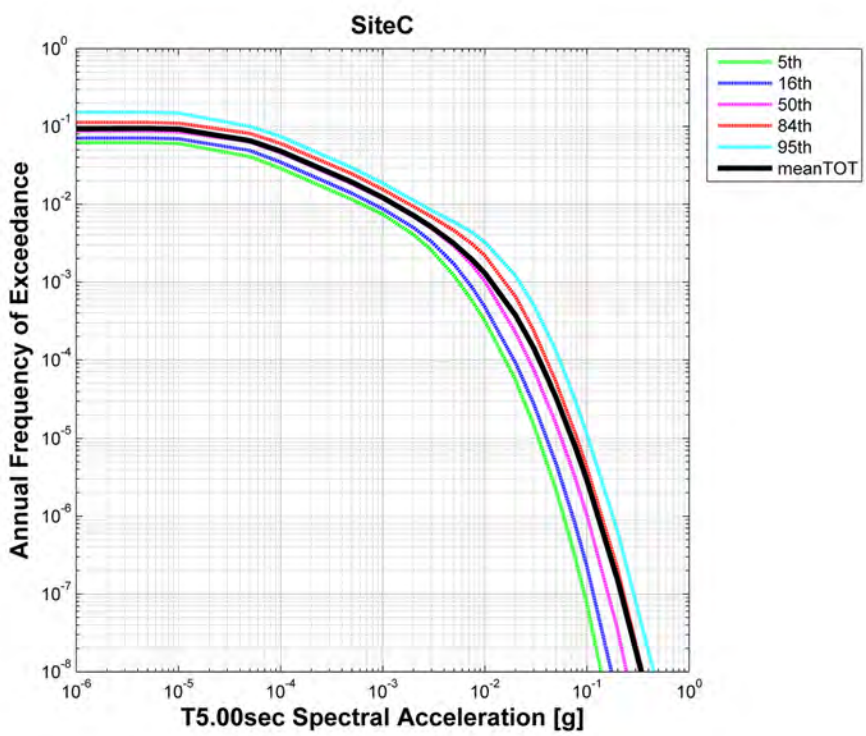

(r)

Figure 10.37. (contd)

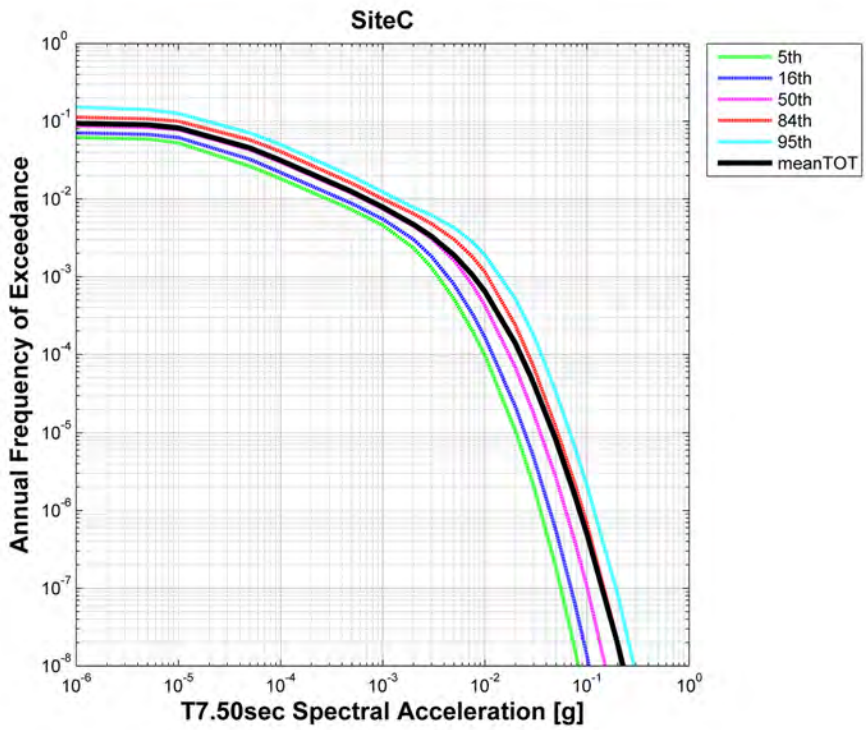

(s)

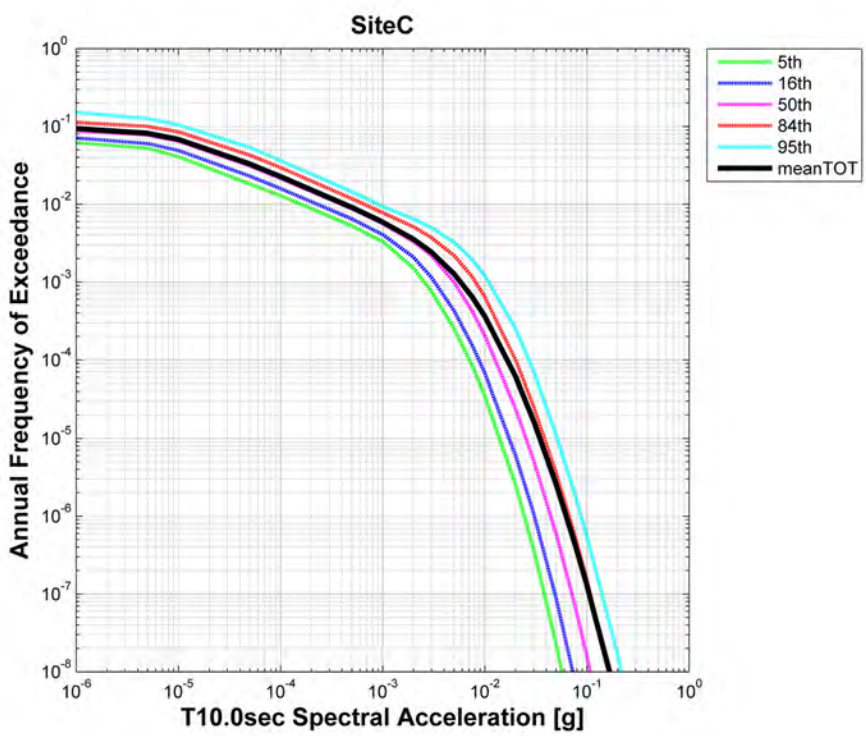

(t)

Figure 10.37. (contd)

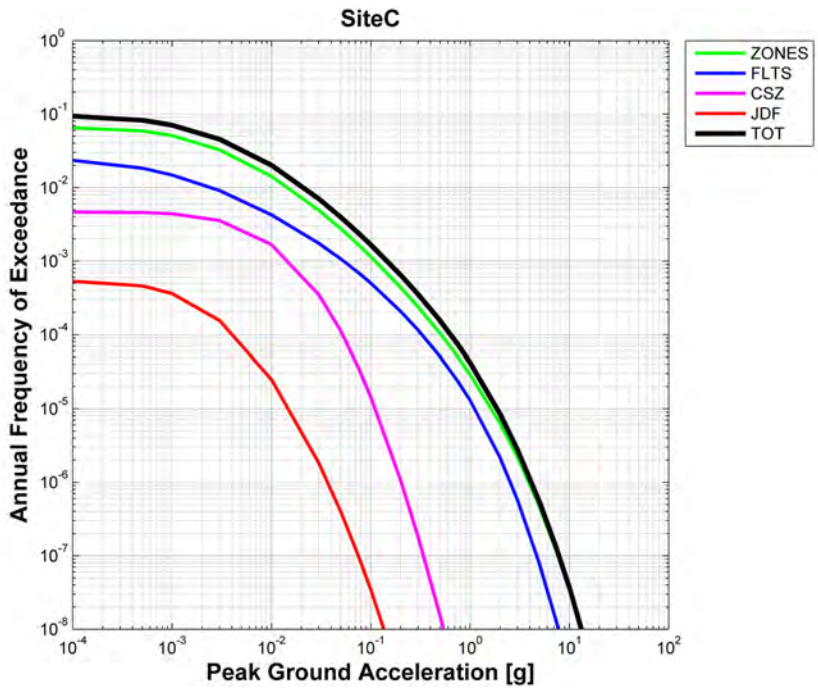

(a)

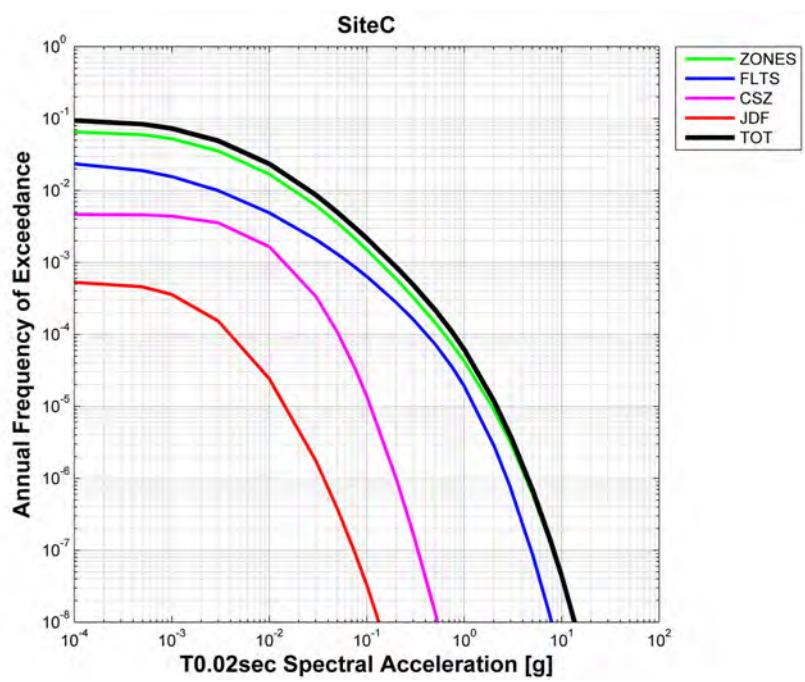

(b)

Figure 10.38. Comparison between the total mean seismic hazard at Site C (black curve) and the contribution of crustal source zones (green curve), faults (blue curve), the Cascadia interface (CSZ - magenta curve), and Cascadia intraslab source (JDF - red curve): a) PGA; b) T 0.02-sec; c) T 0.03-sec; d) T 0.04-sec; e) T 0.05-sec; f) T 0.07-sec; g) T 0.10-sec; h) T 0.15-sec; i) T 0.20-sec; j) T 0.30-sec; k) T 0.40-sec; l) T 0.50-sec; m) T 0.75-sec; n) T 1.0-sec; o) T 1.5-sec; p) T 2.0-sec; q) T 3.0-sec; r) T 5.0-sec; s) T 7.5-sec; t) T 10-sec spectral acceleration.

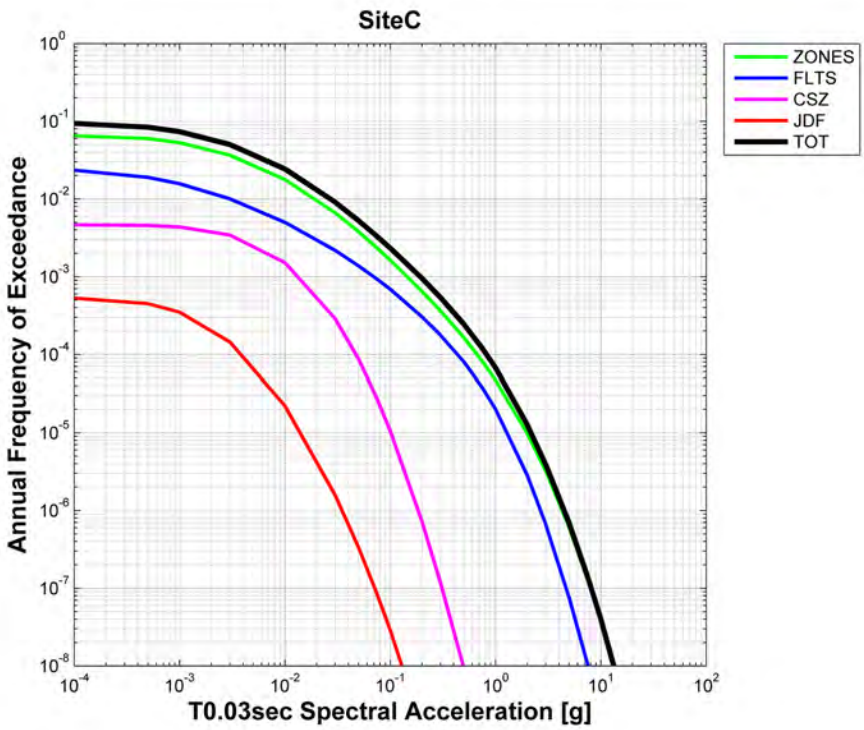

(c)

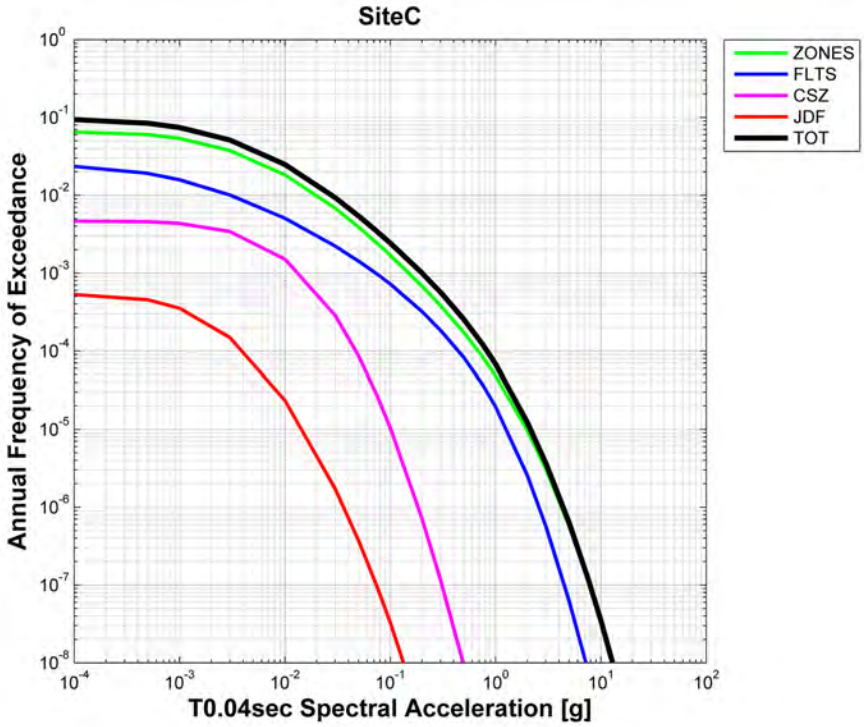

(d)

Figure 10.38. (contd)

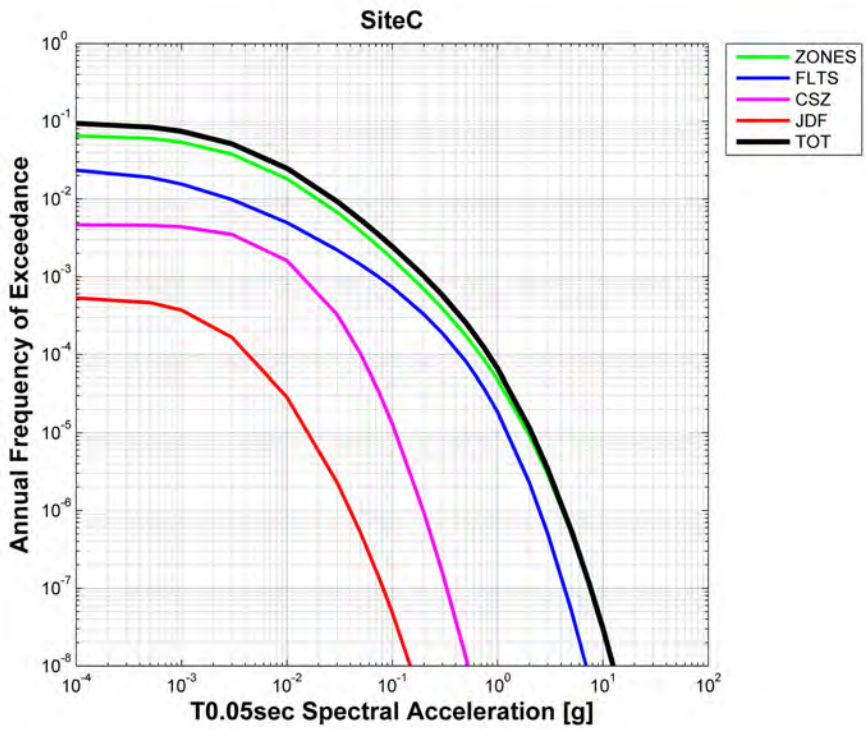

(e)

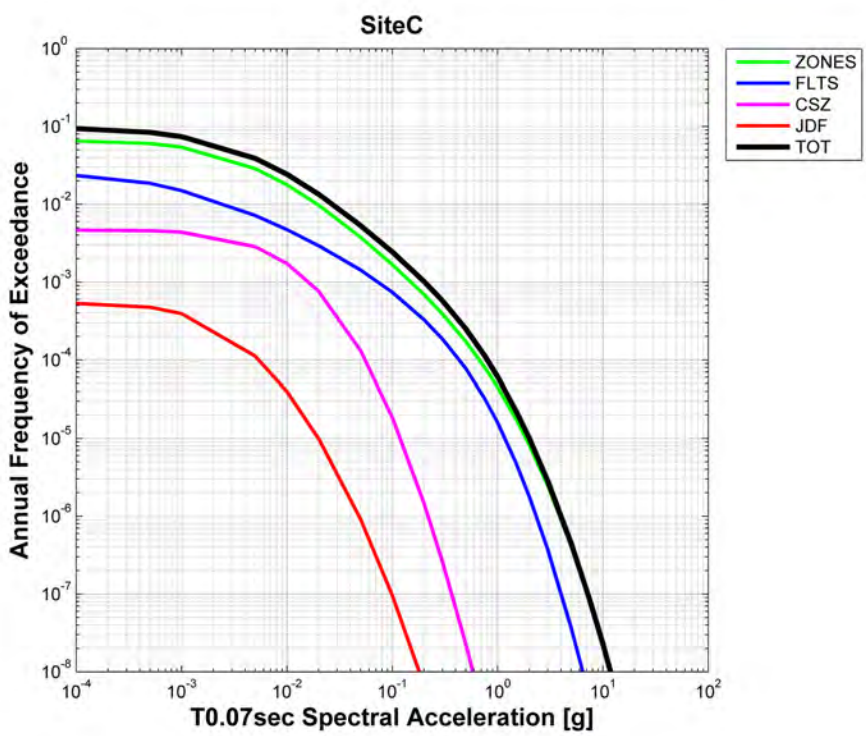

(f)

Figure 10.38. (contd)

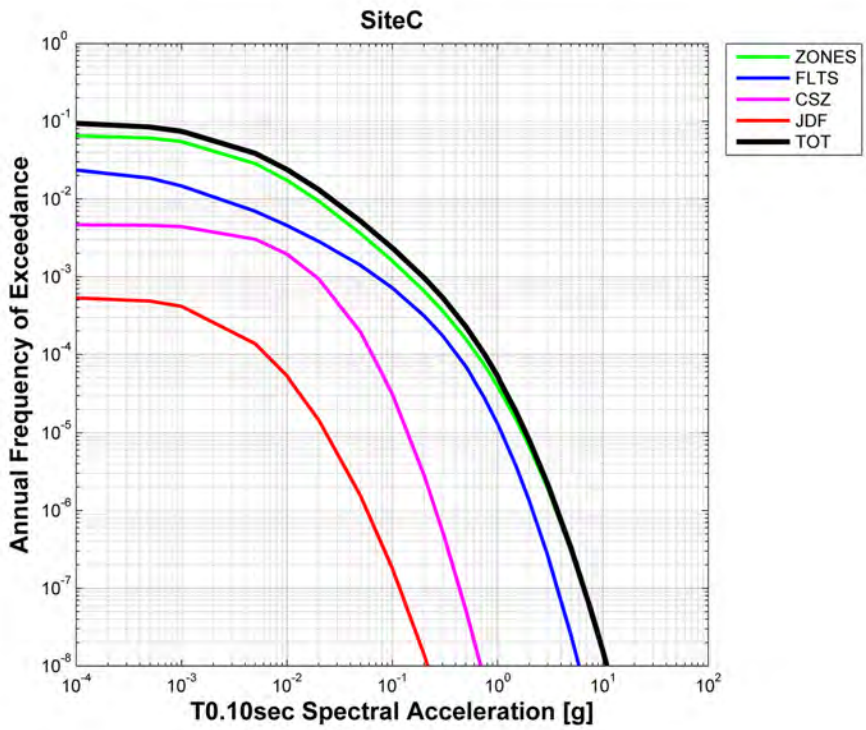

(g)

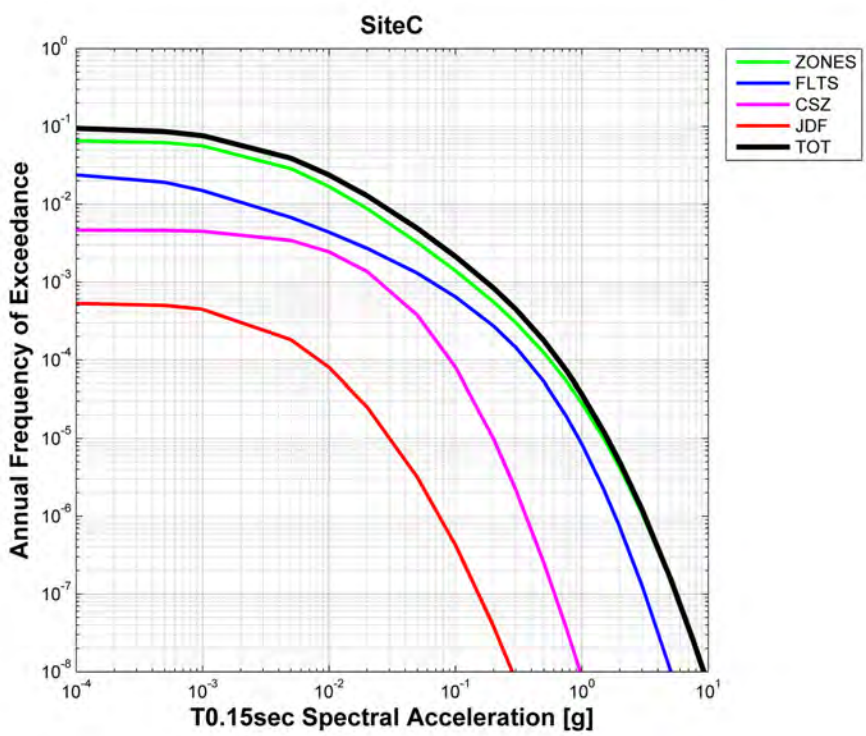

(h)

Figure 10.38. (contd)

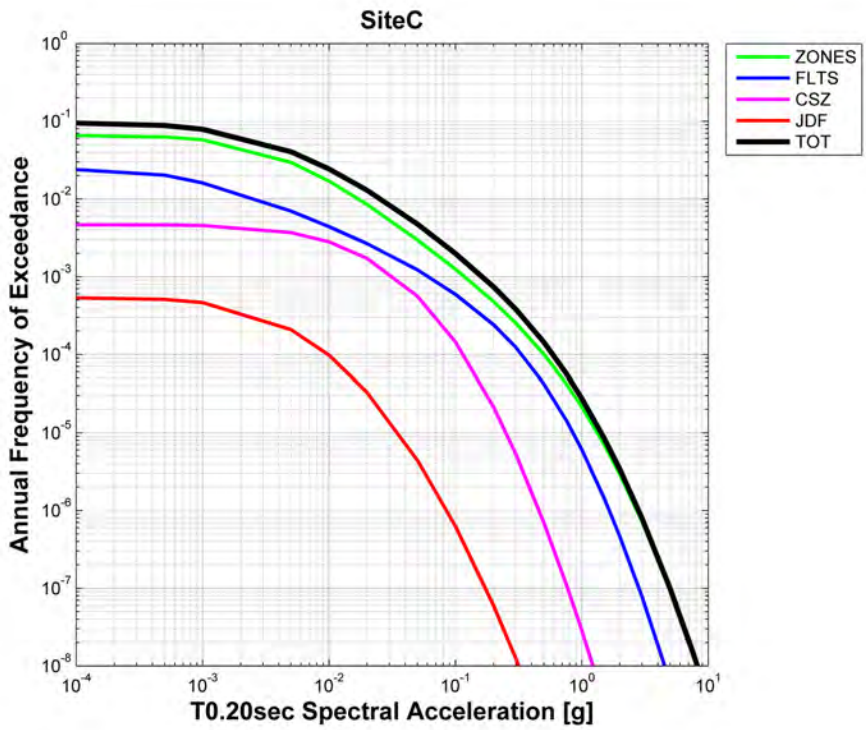

(i)

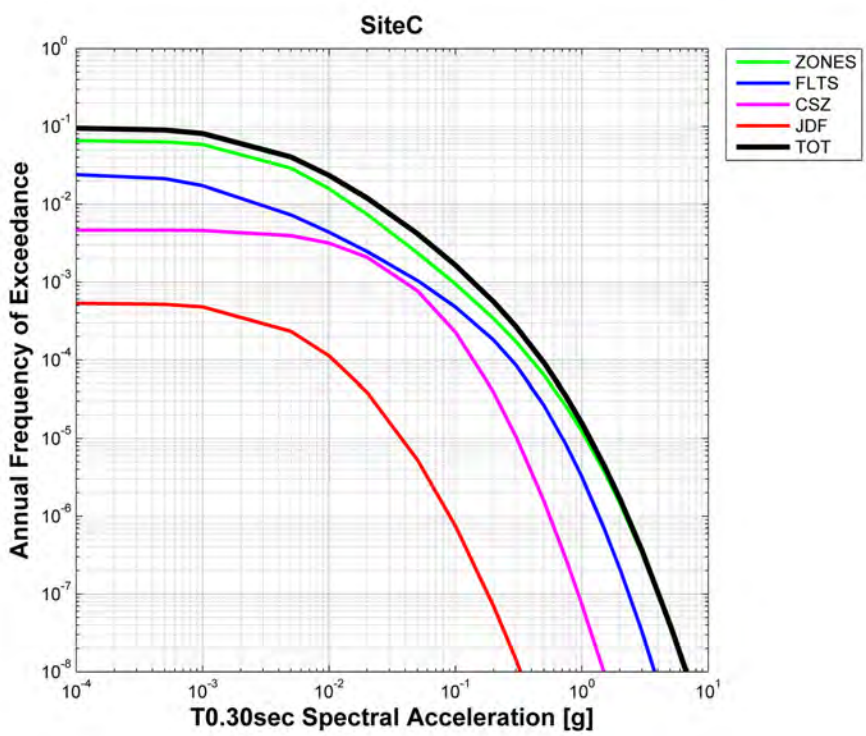

(j)

Figure 10.38. (contd)

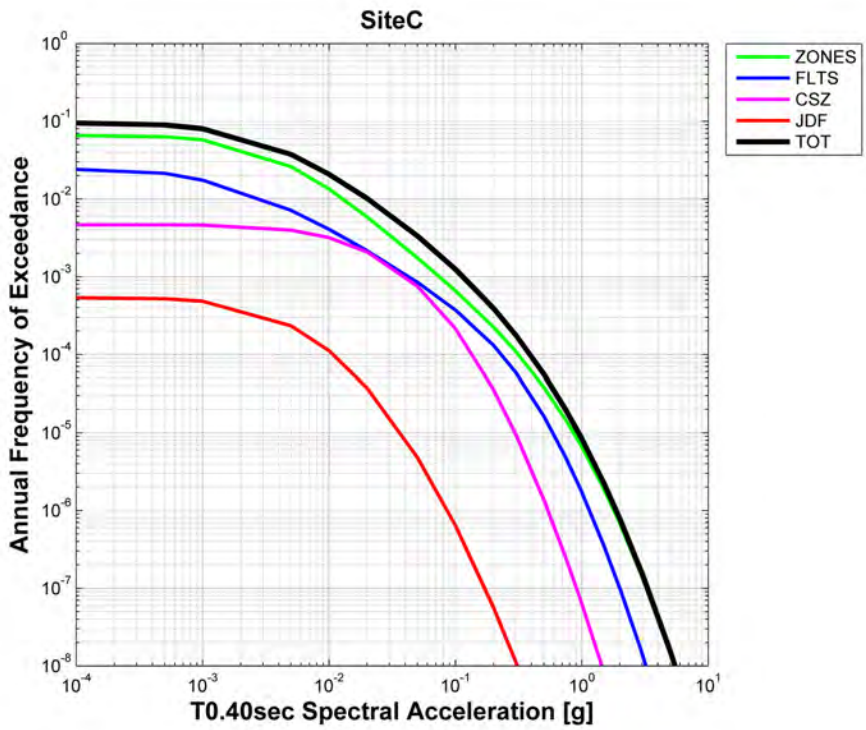

(k)

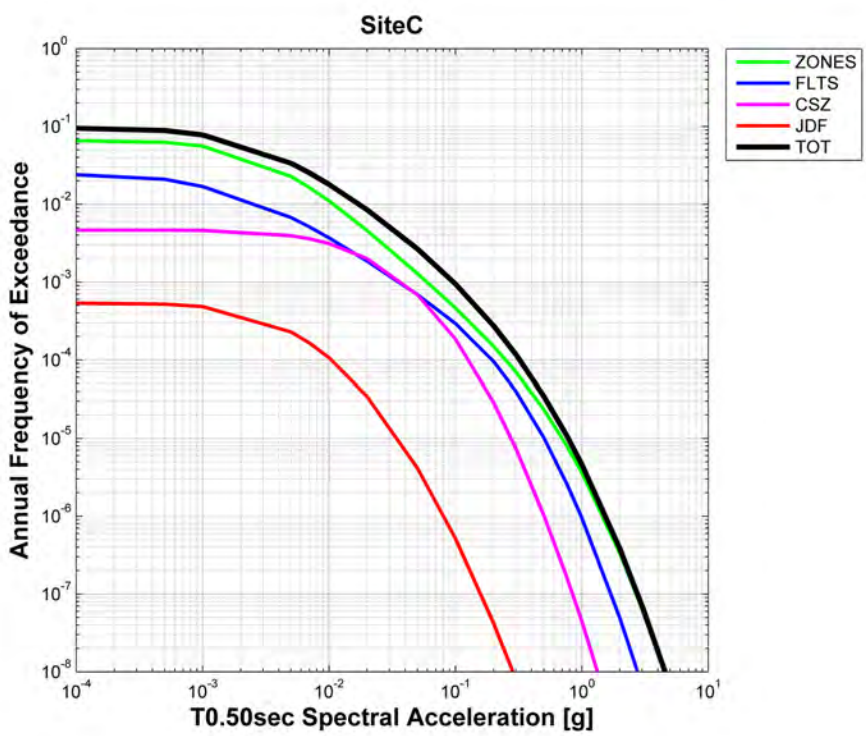

(l)

Figure 10.38. (contd)

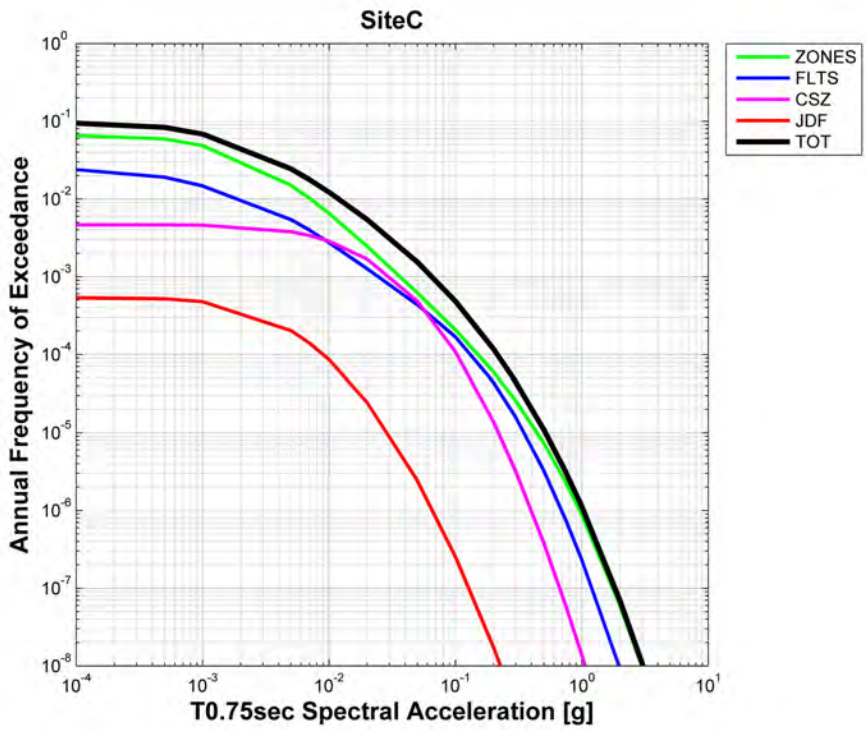

(m)

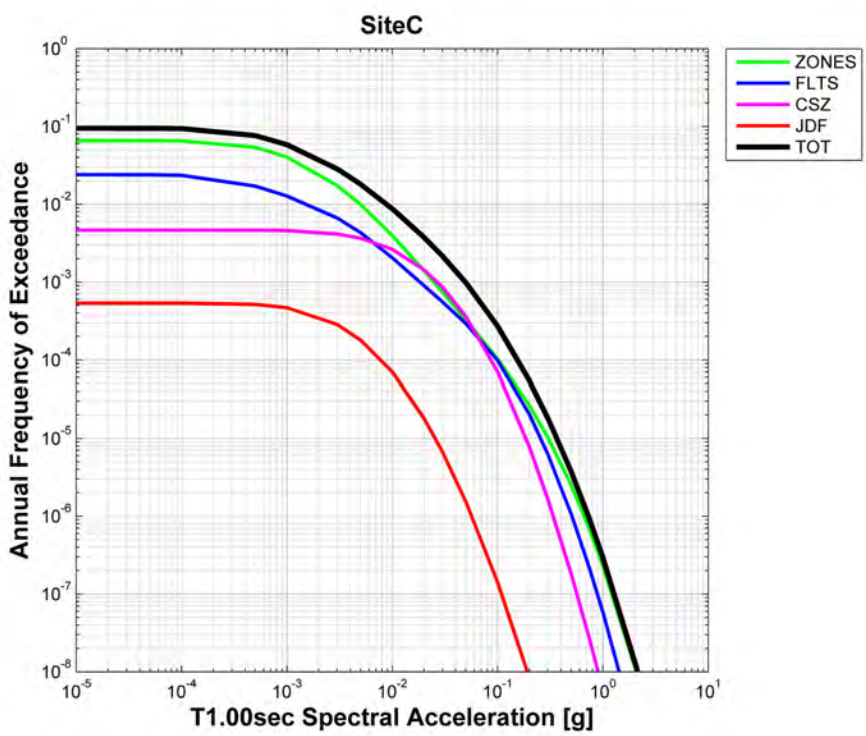

(n)

Figure 10.38. (contd)

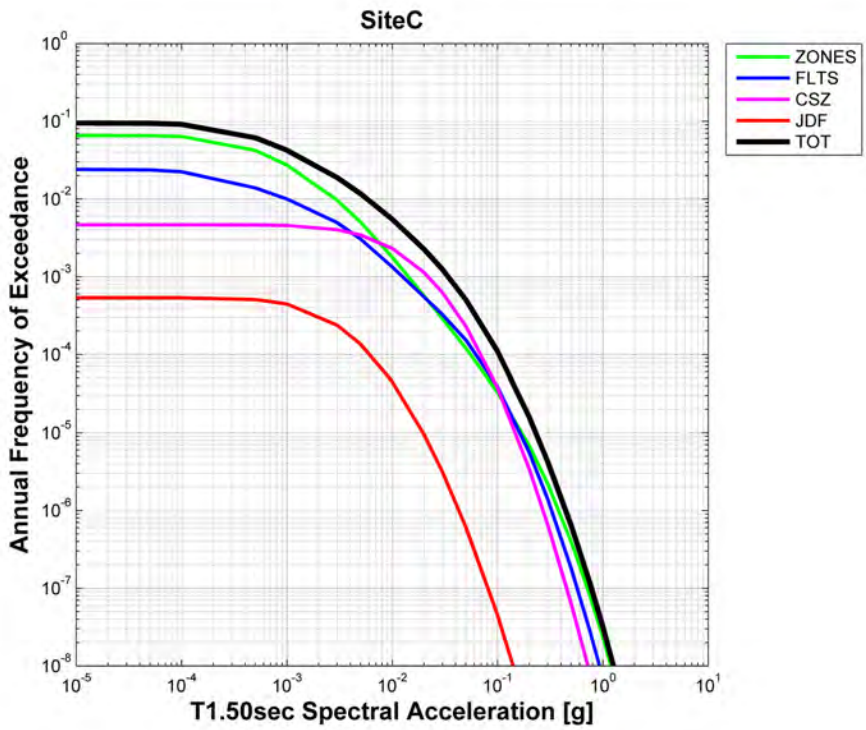

(o)

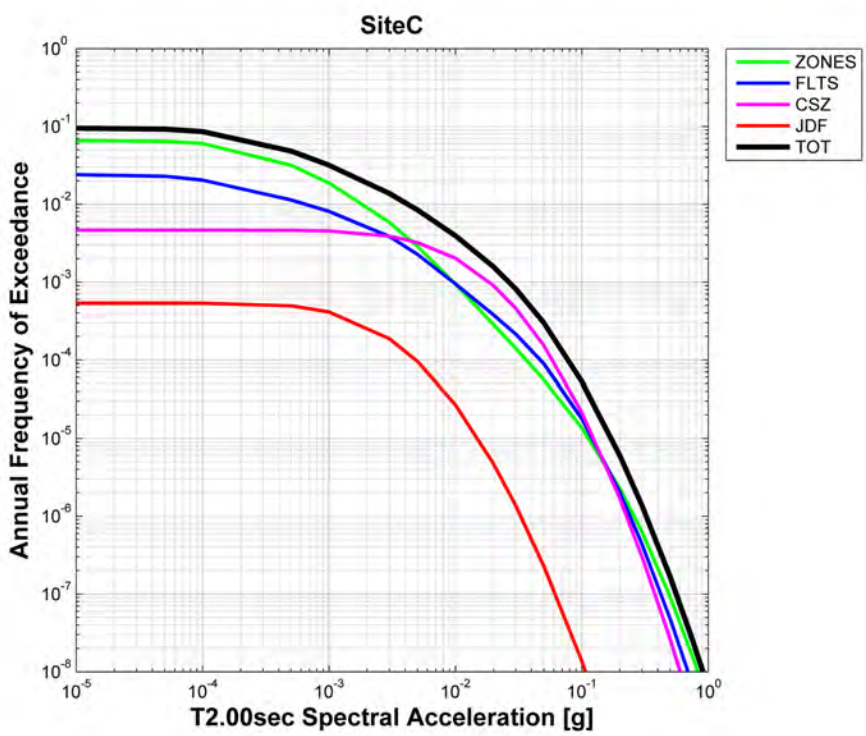

(p)

Figure 10.38. (contd)

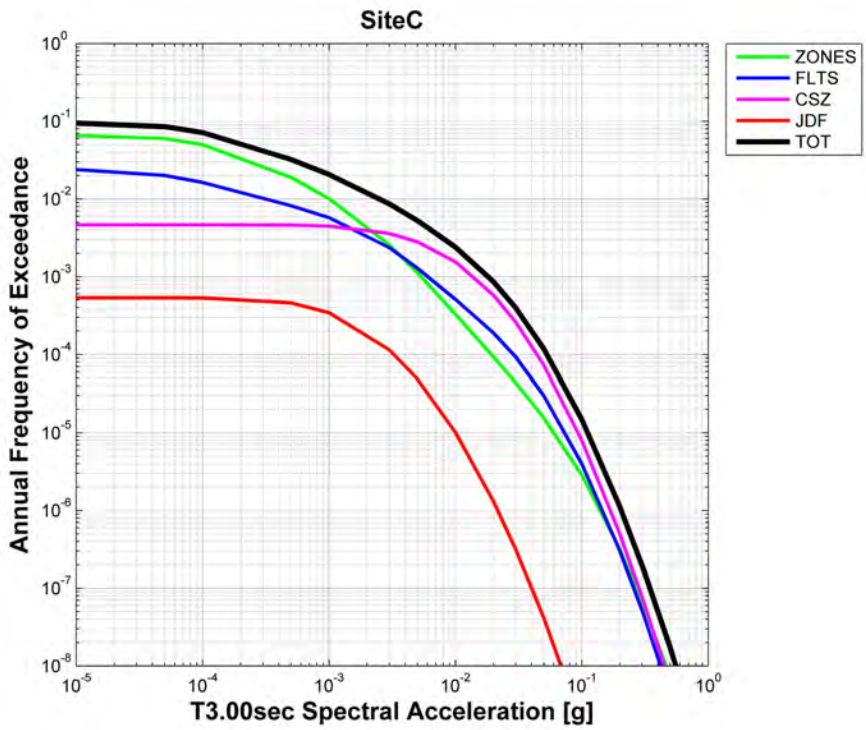

(q)

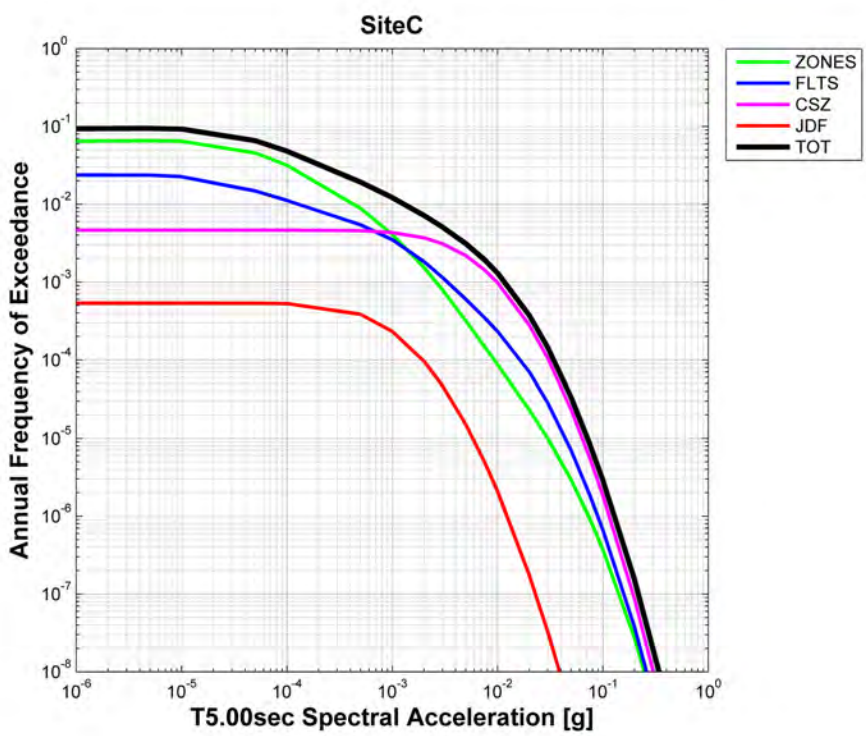

(r)

Figure 10.38. (contd)

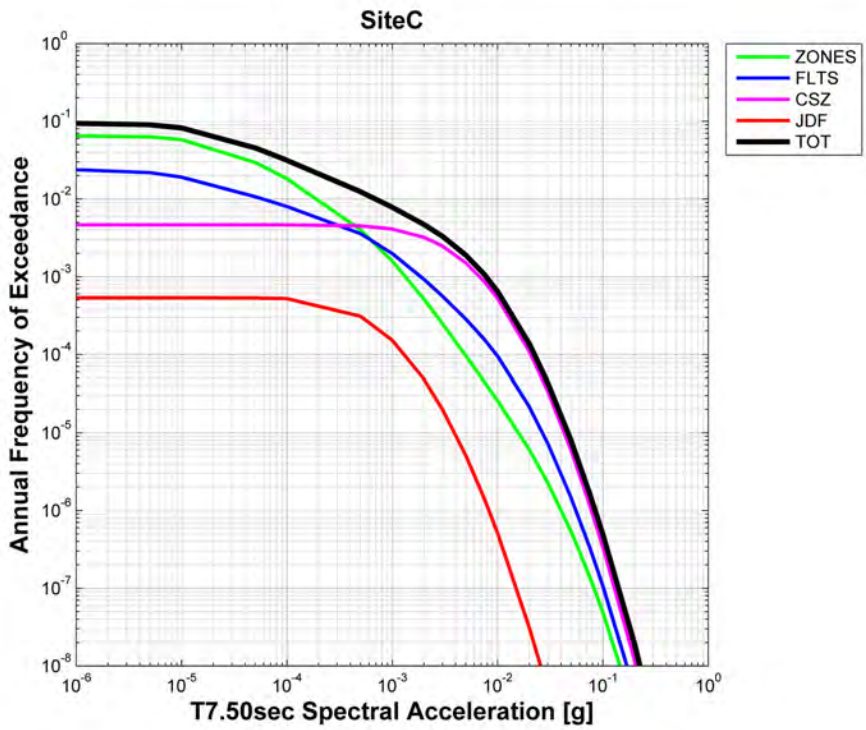

(s)

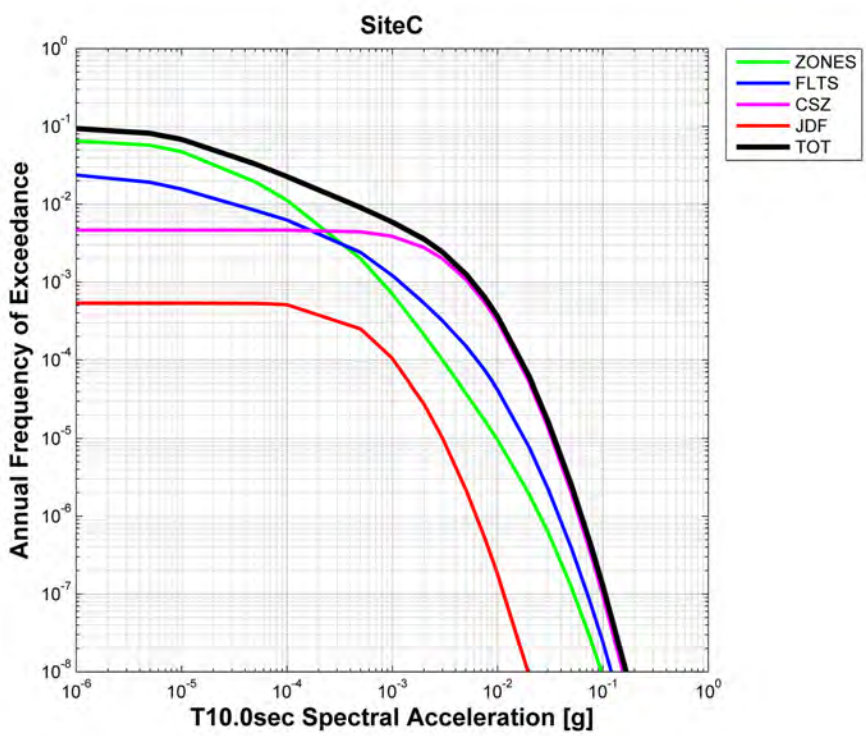

(t)

Figure 10.38. (contd)

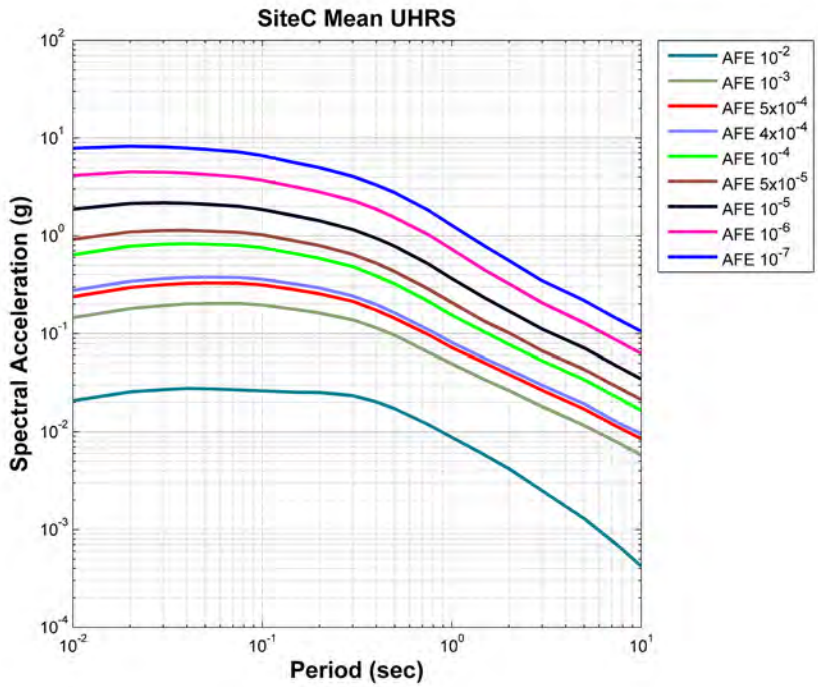

(a)

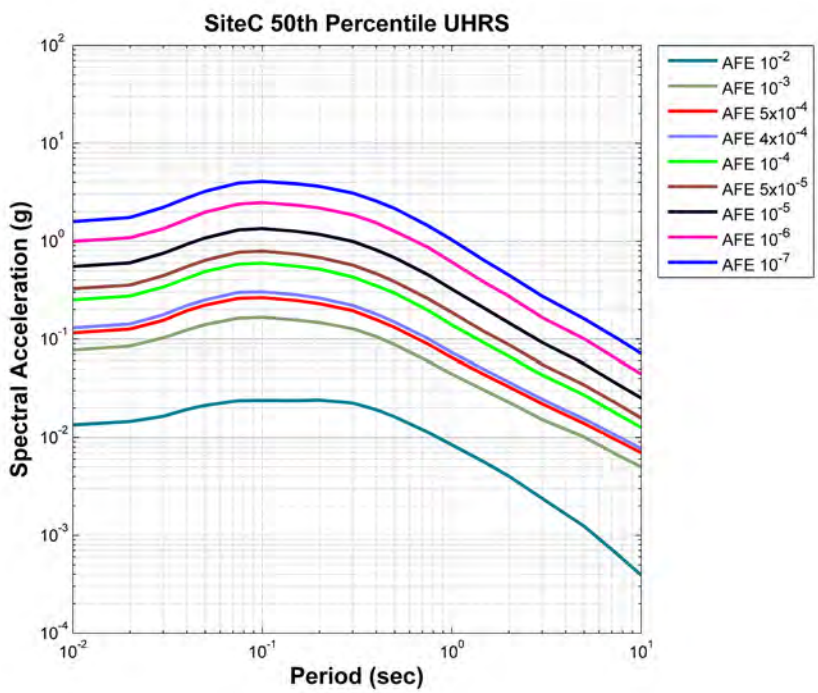

(b)

Figure 10.39. Uniform hazard response spectra at AFEs of 10^{-2}, 10^{-3}, 5×10^{-4}, 4×10^{-4}, 10^{-4}, 5×10^{-5}, 10^{-6}, 10^{-7} (return periods of 100, 1,000, 2,000, 2,500, 10,000, 20,000, 100,000, 1 million, and 10 million years) for: a) mean hazard; b) 50th percentile hazard; c) 84th percentile hazard.

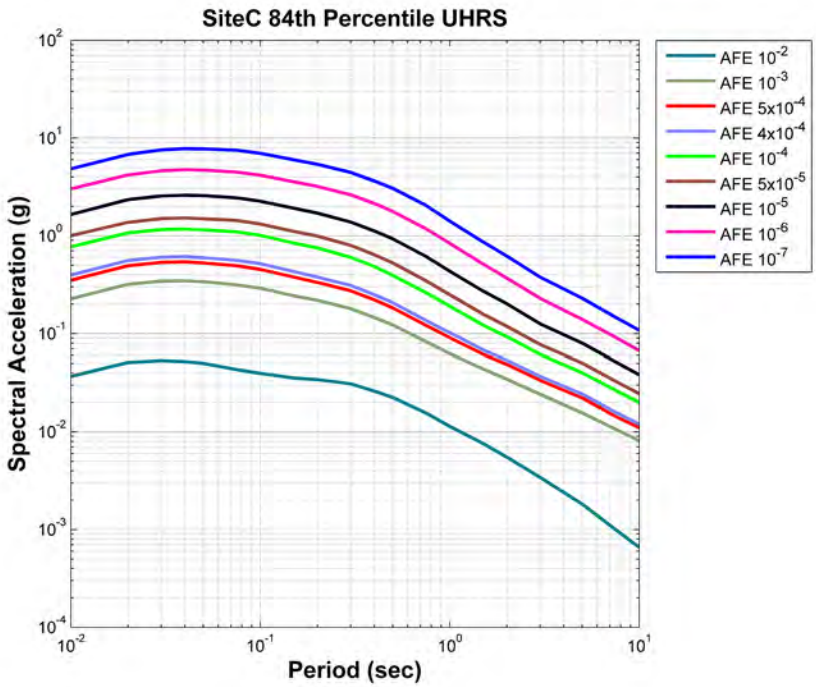

(c)

Figure 10.39. (contd)

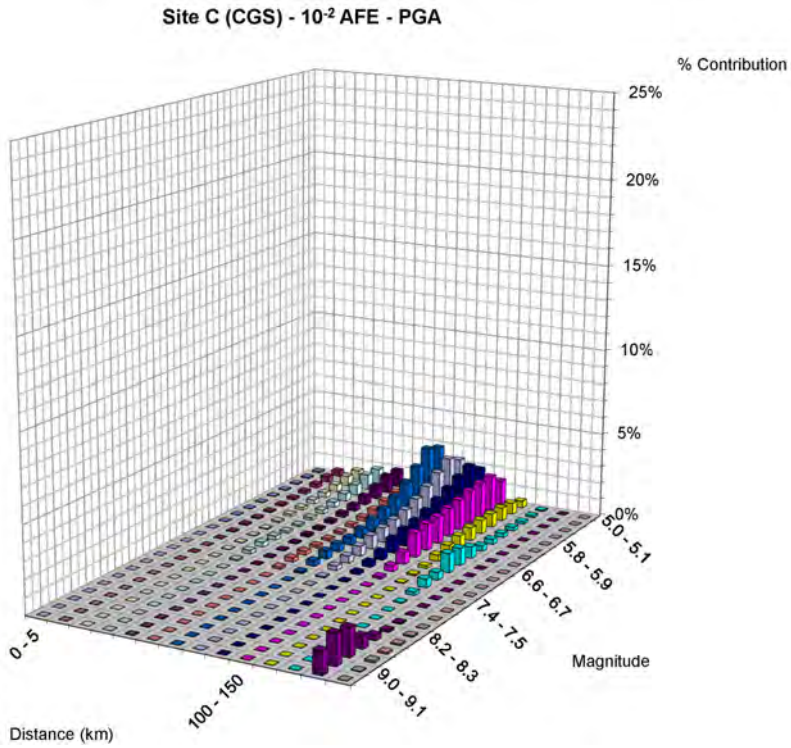

(a)

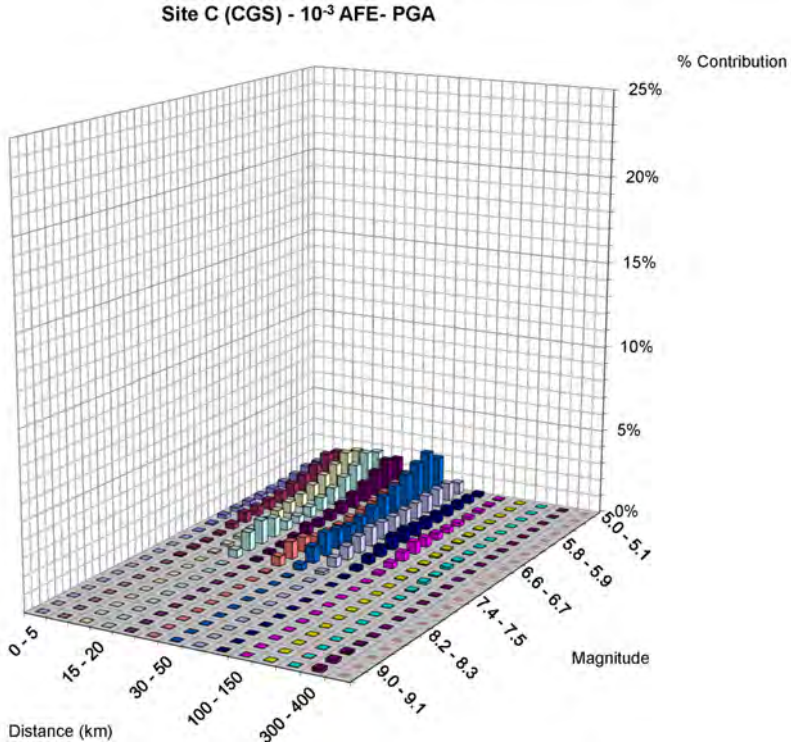

(b)

Figure 10.40. Deaggregation histogram showing magnitude-distance contributions to the total mean hazard at Site C for peak ground acceleration and AFEs of: a) 10^{-2}; b) 10^{-3}; c) 5×10^{-4}; d) 4×10^{-4}; e) 10^{-4}; f) 10^{-5}; g) 10^{-6}; h) 10^{-7}.

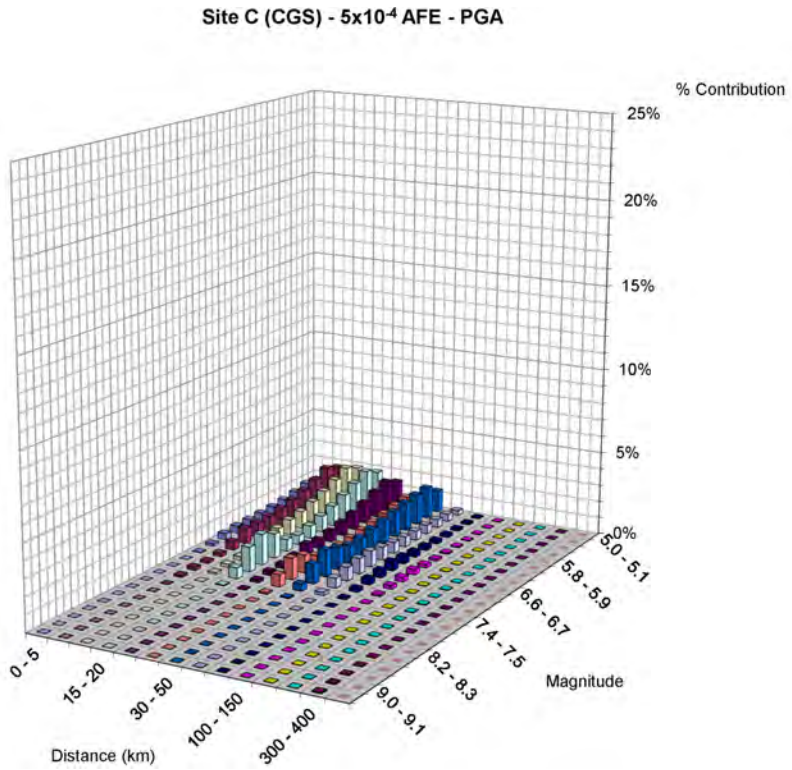

(c)

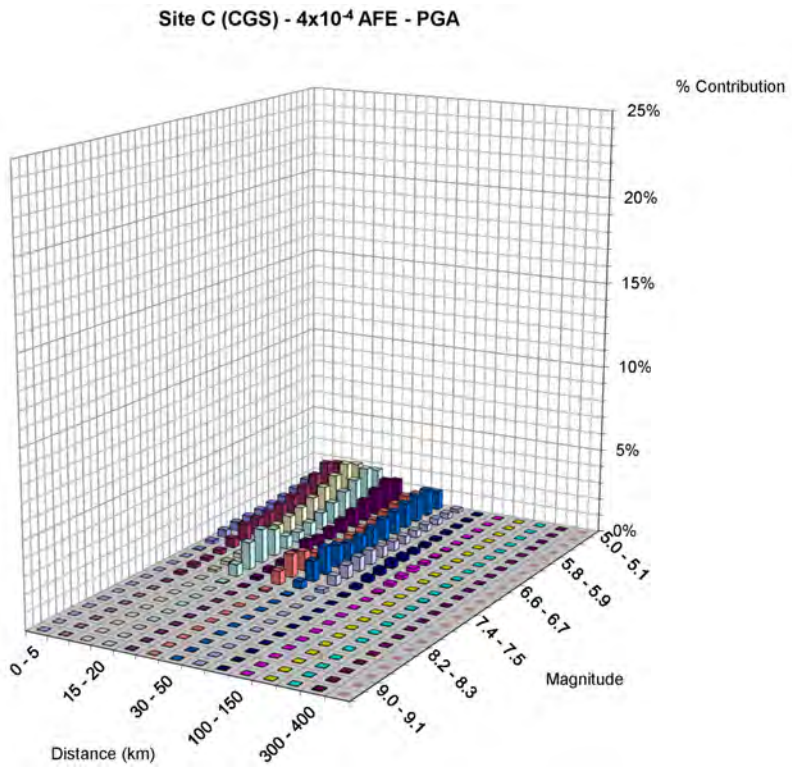

(d)

Figure 10.40. (contd)

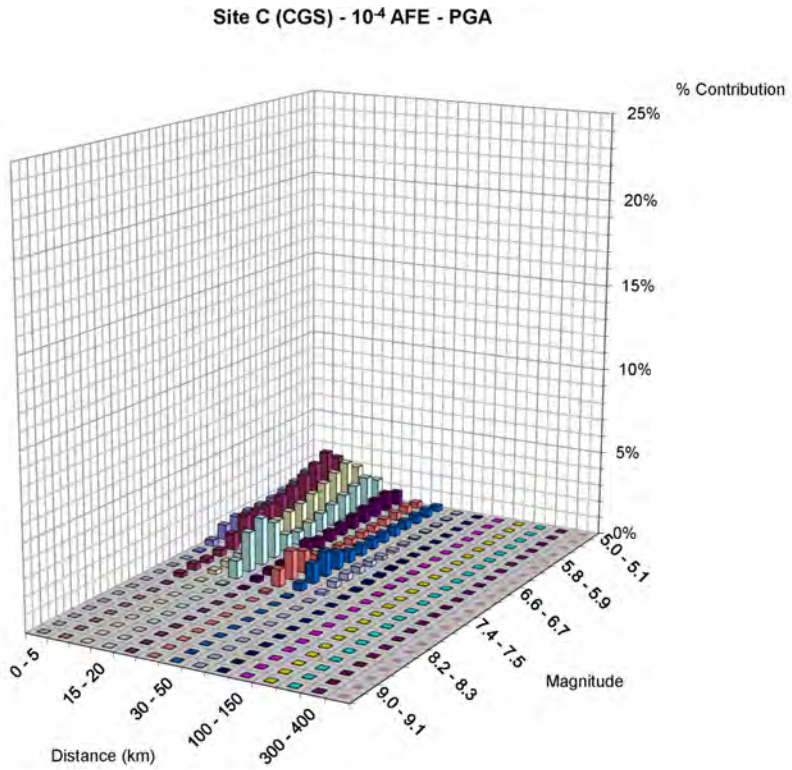

(e)

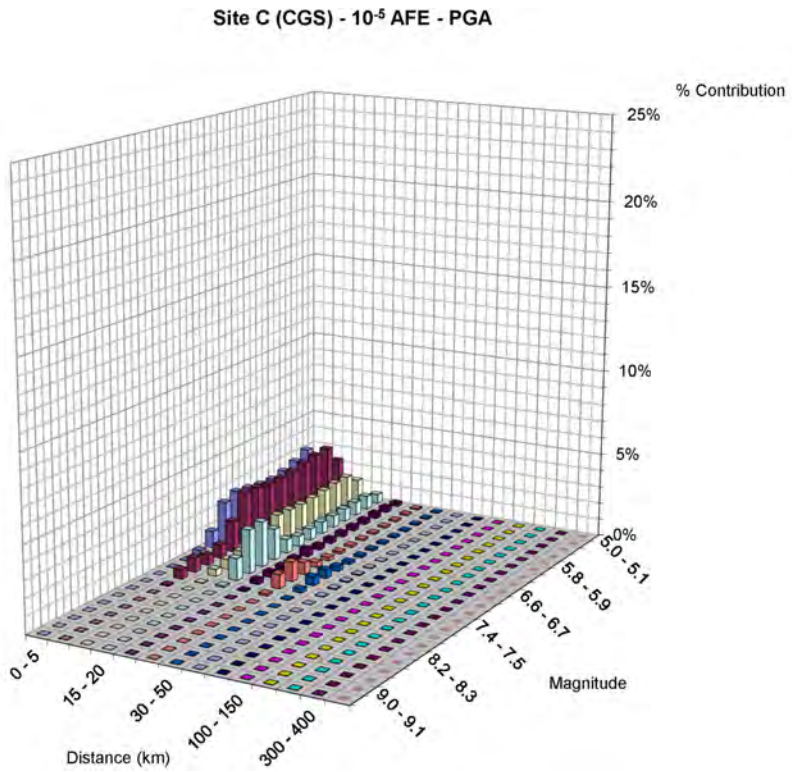

(f)

Figure 10.40. (contd)

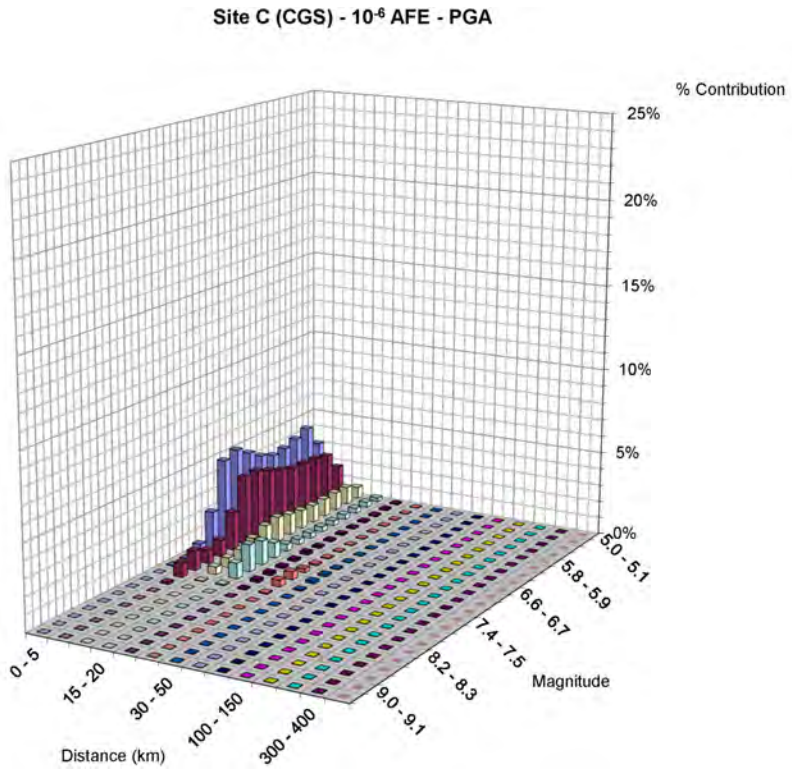

(g)

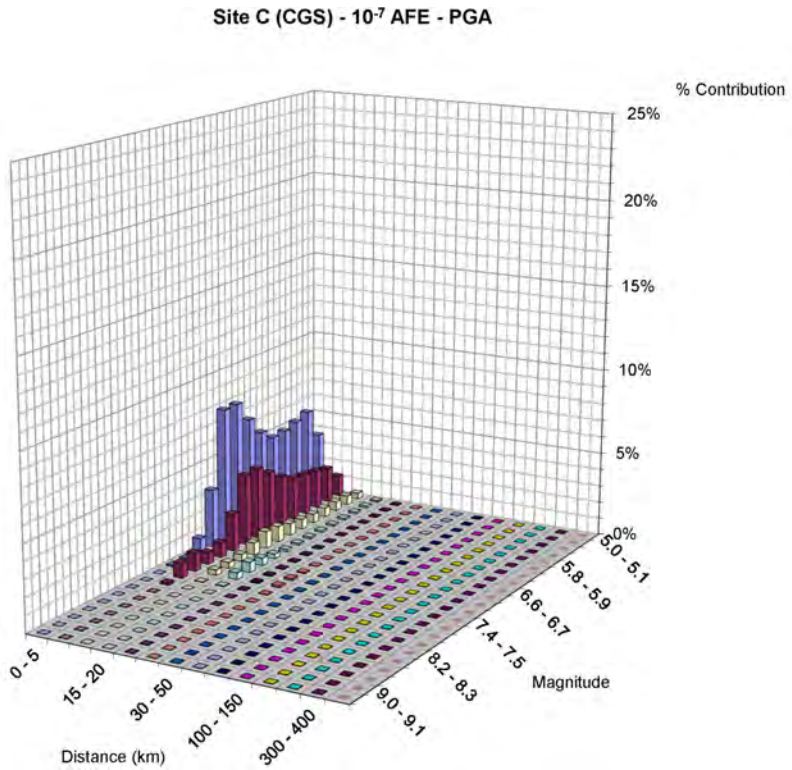

(h)

Figure 10.40. (contd)

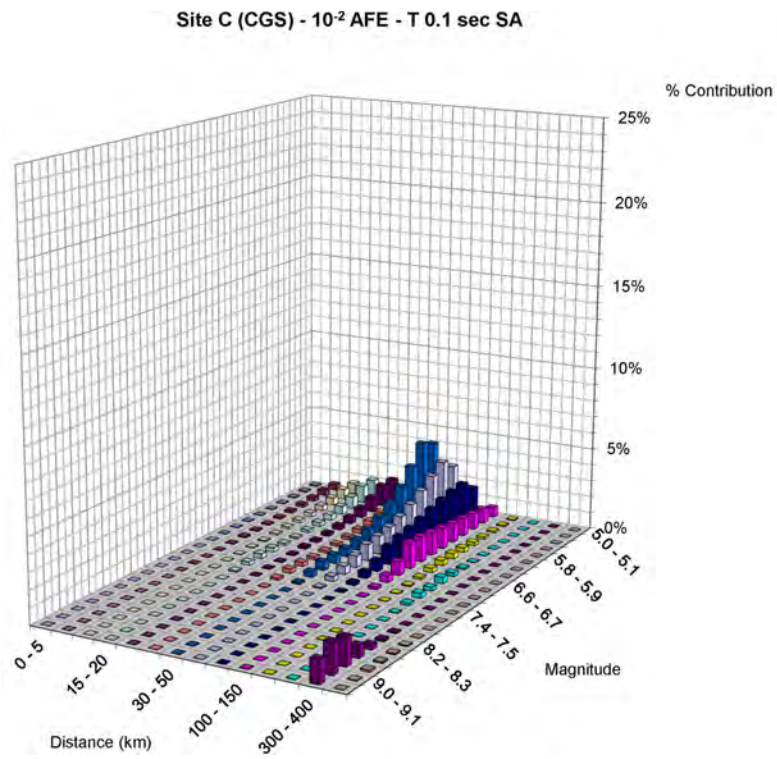

(a)

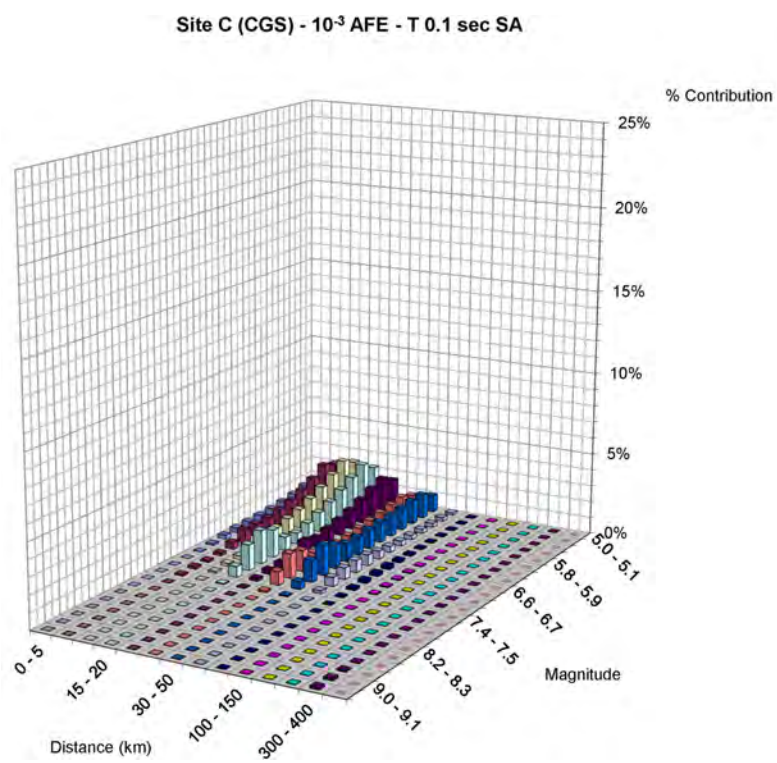

(b)

Figure 10.41. Deaggregation histogram showing magnitude-distance contributions to the total mean hazard at Site C for T 0.1-sec spectral acceleration and AFEs of: a) 10^{-2}; b) 10^{-3}; c) 5×10^{-4}; d) 4×10^{-4}; e) 10^{-4}; f) 10^{-5}; g) 10^{-6}; h) 10^{-7}.

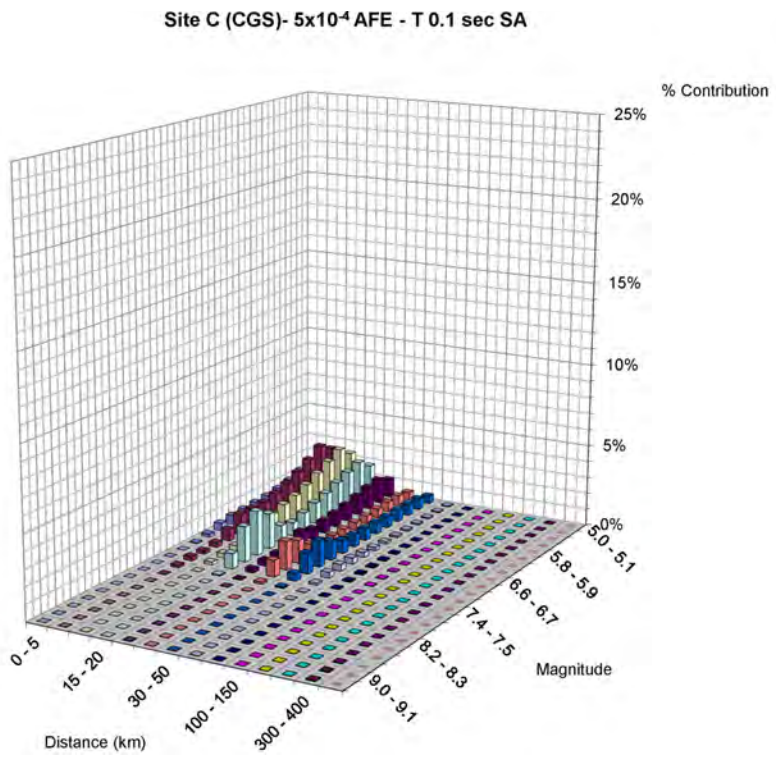

(c)

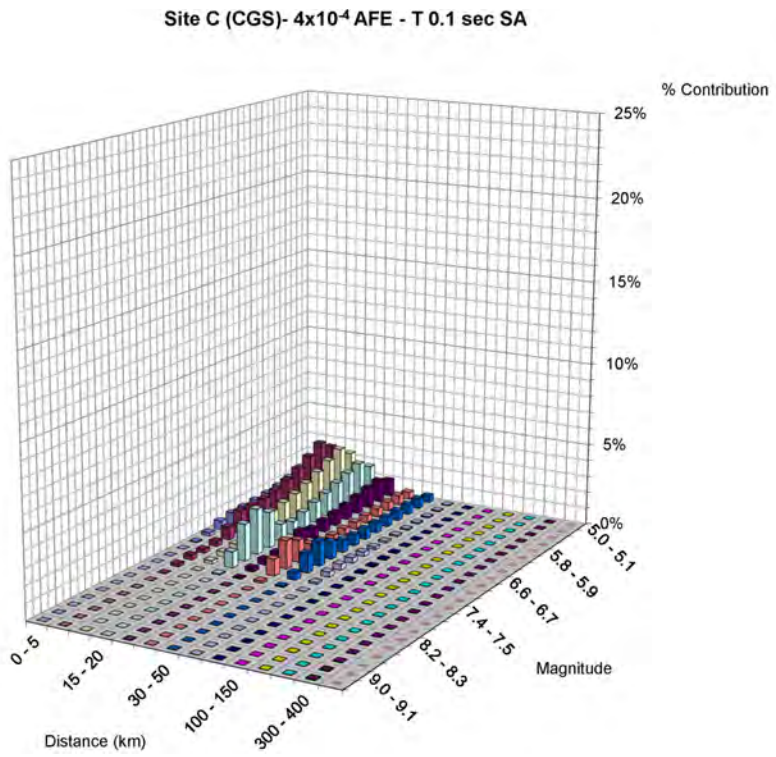

(d)

Figure 10.41. (contd)

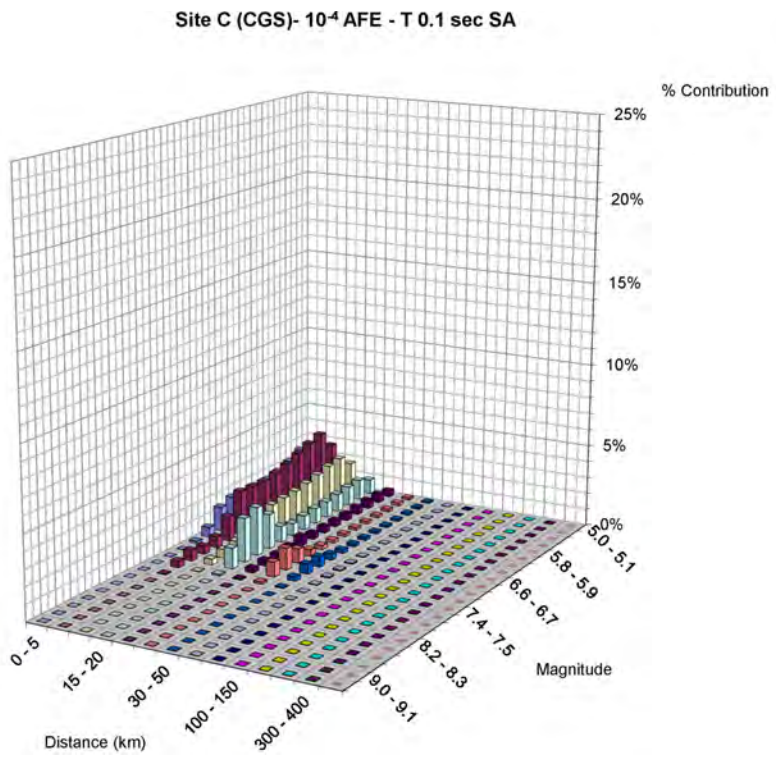

(e)

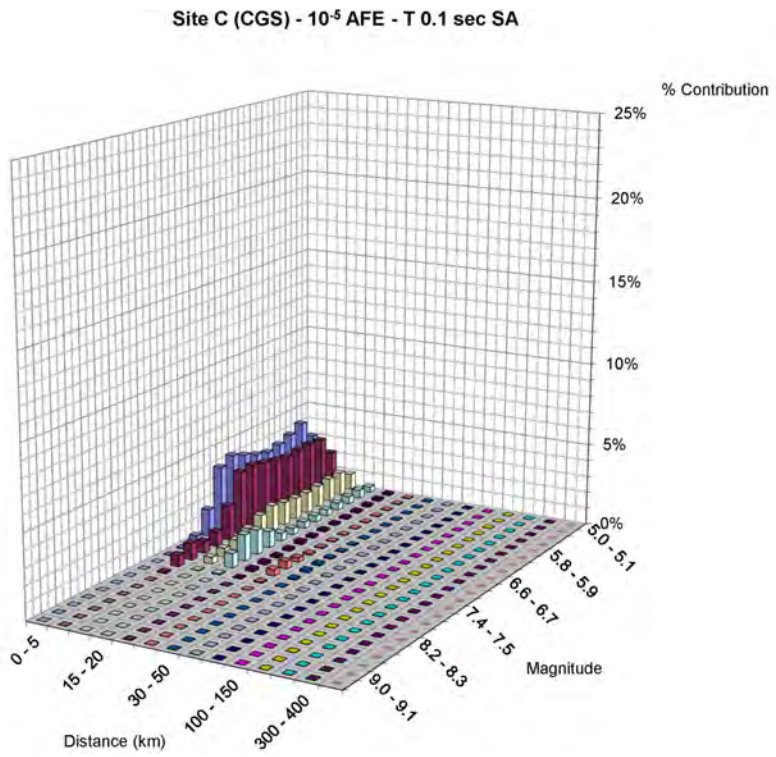

(f)

Figure 10.41. (contd)

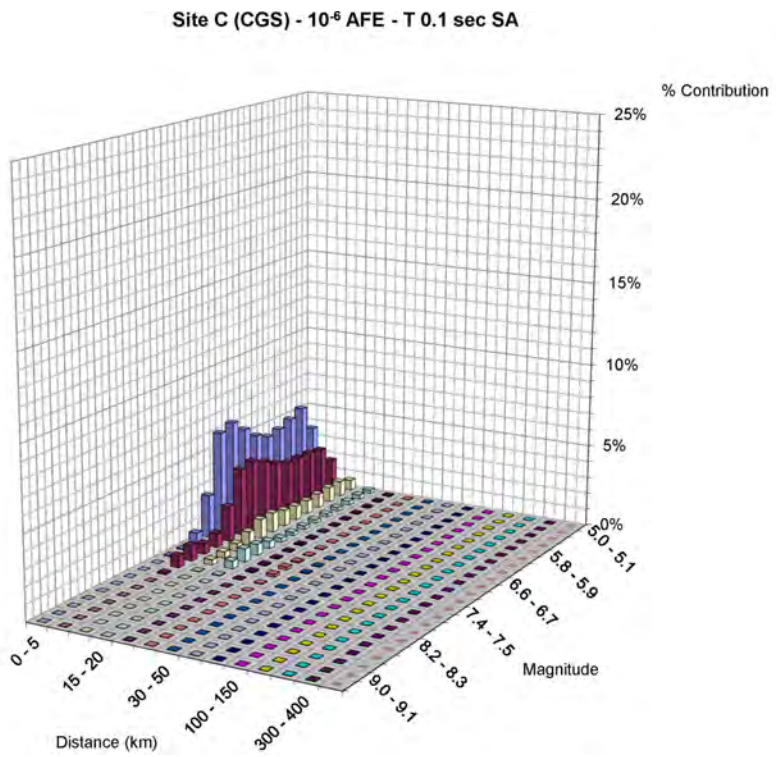

(g)

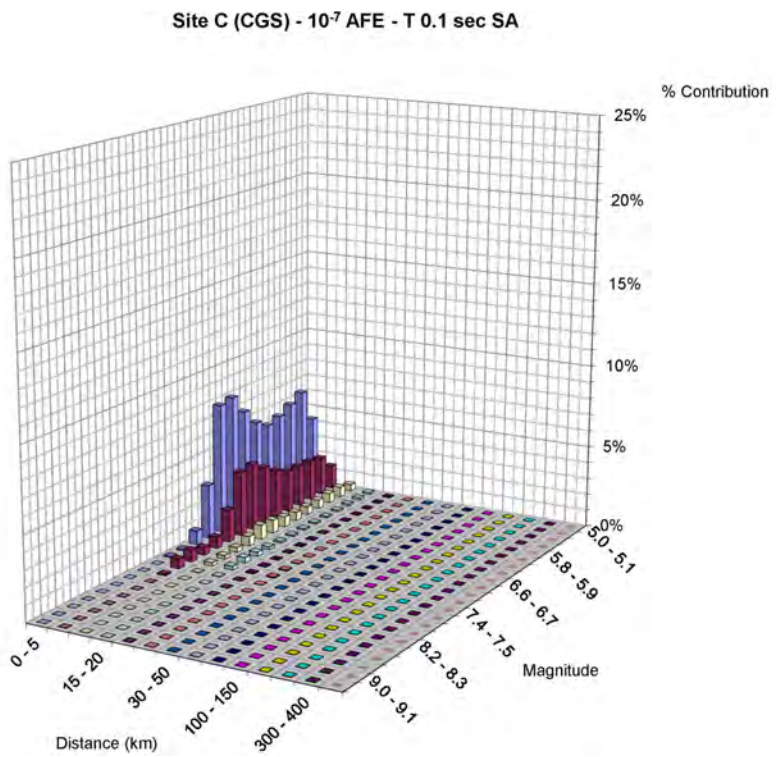

(h)

Figure 10.41. (contd)

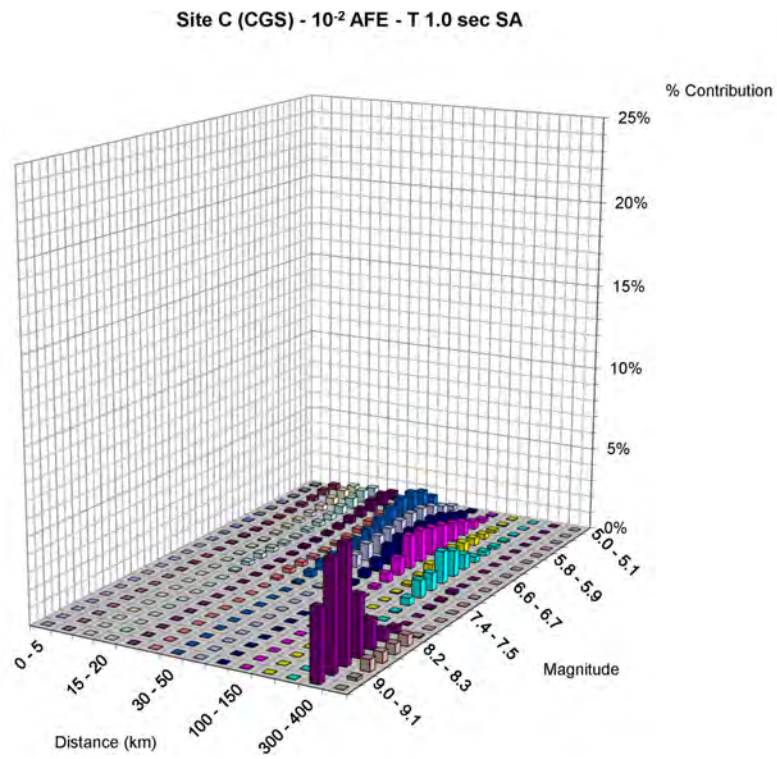

(a)

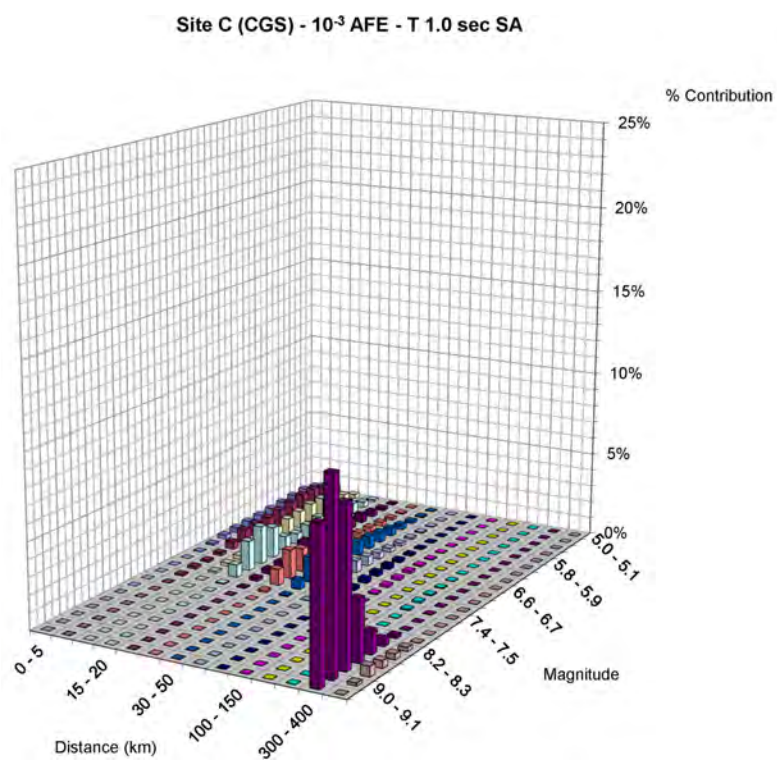

(b)

Figure 10.42. Deaggregation histogram showing magnitude-distance contributions to the total mean hazard at Site C for T 1.0-sec spectral acceleration and AFEs of: a) 10^{-2}; b) 10^{-3}; c) 5×10^{-4}; d) 4×10^{-4}; e) 10^{-4}; f) 10^{-5}; g) 10^{-6}; h) 10^{-7}.

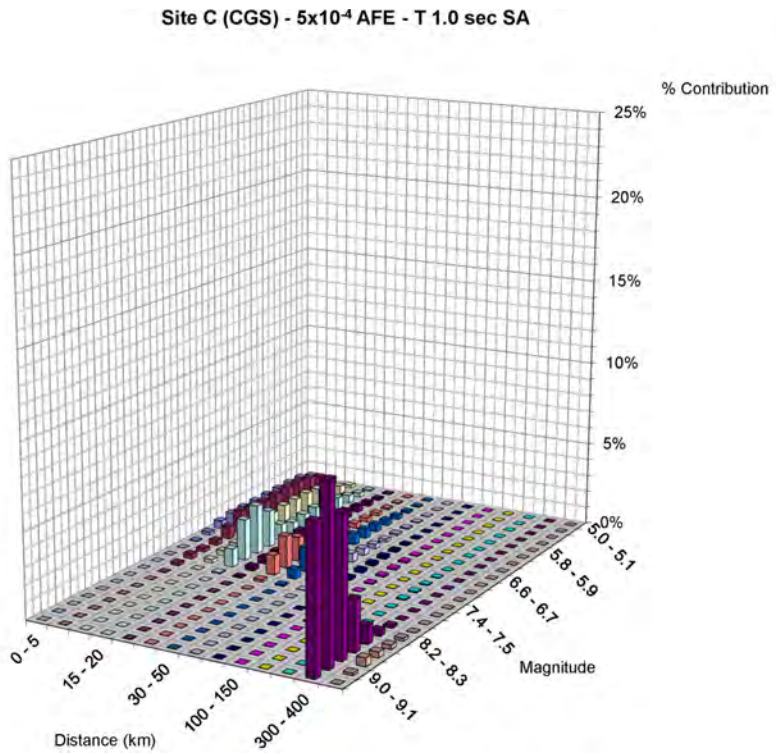

(c)

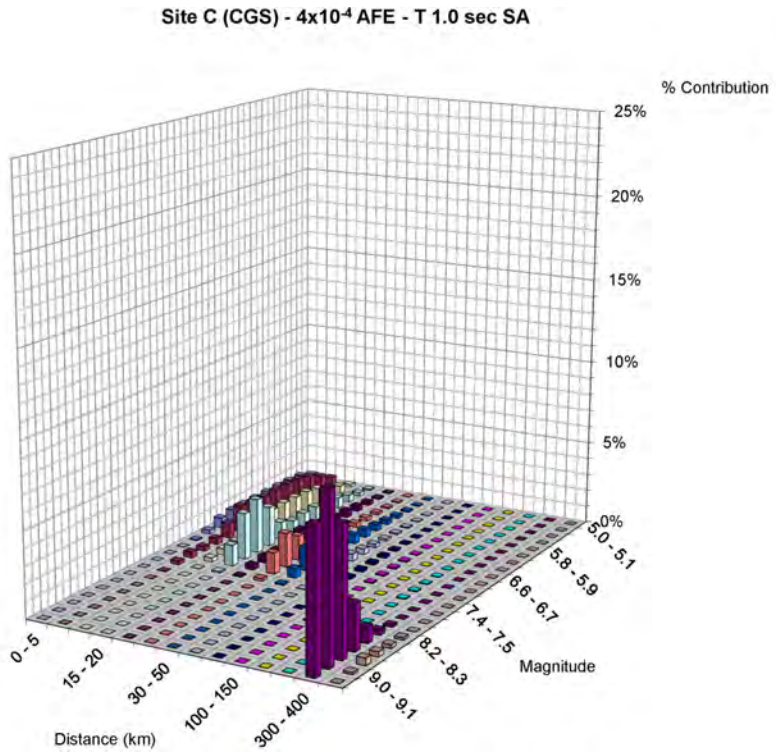

(d)

Figure 10.42. (contd)

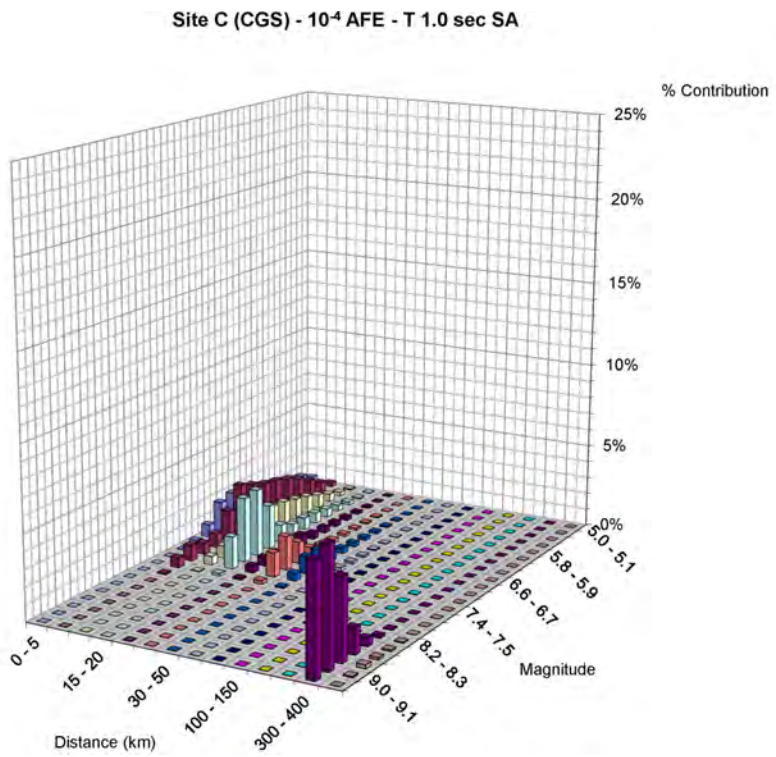

(e)

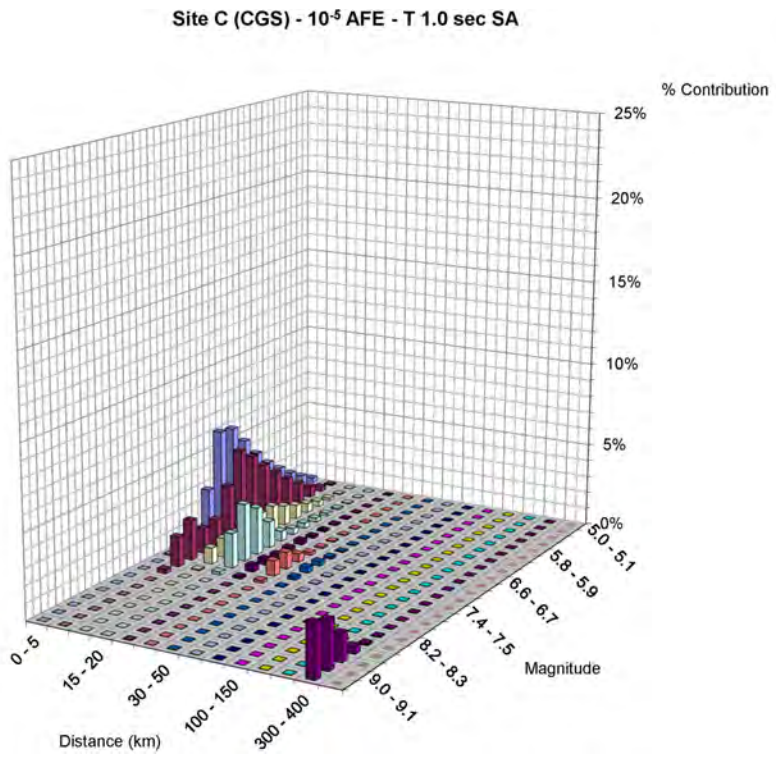

(f)

Figure 10.42. (contd)

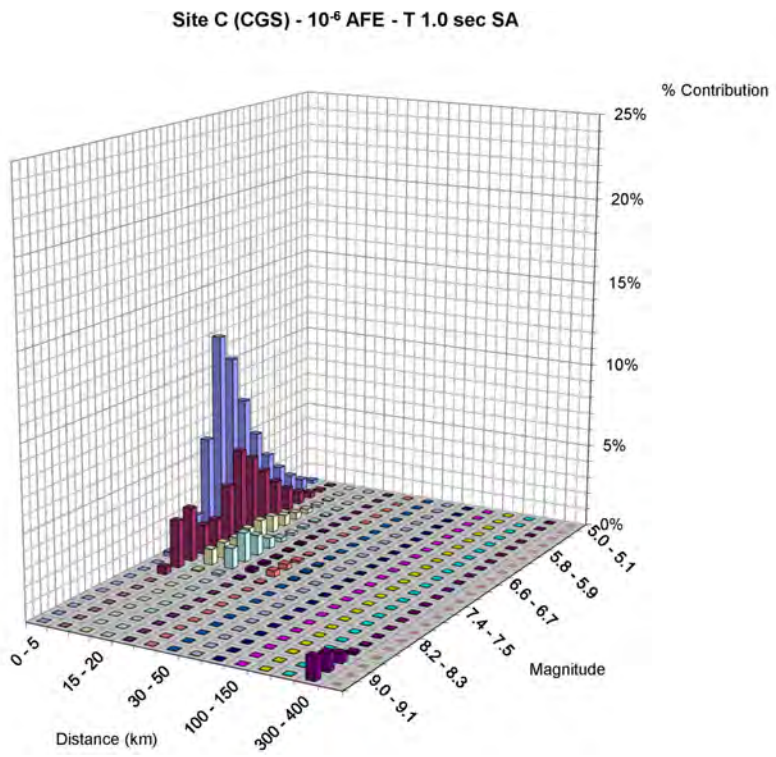

(g)

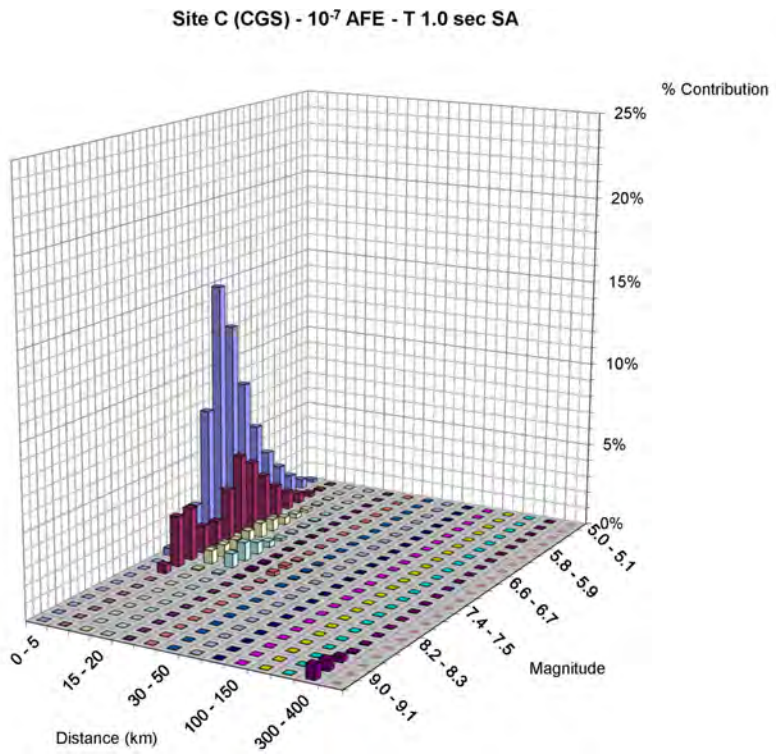

(h)

Figure 10.42. (contd)

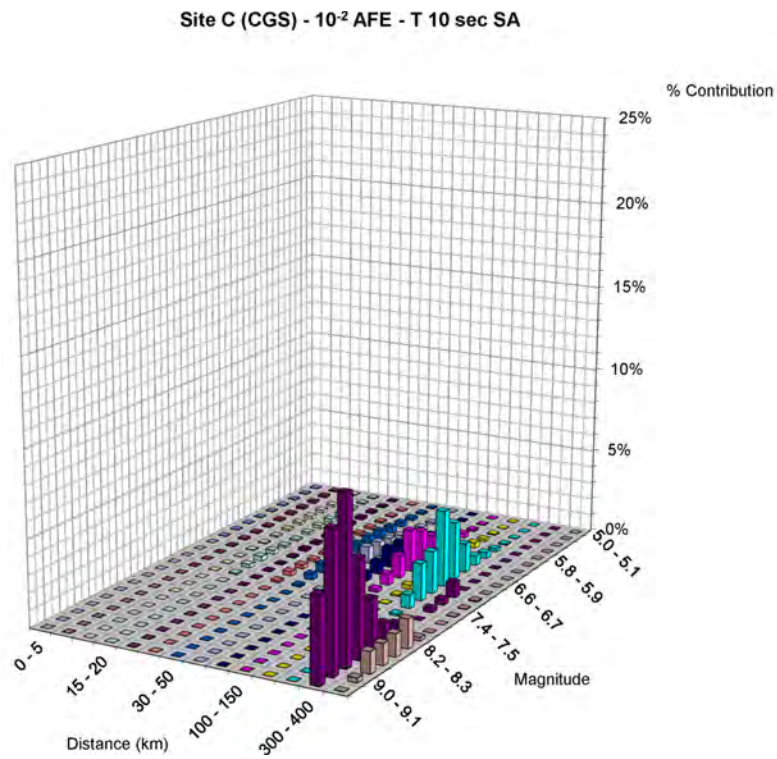

(a)

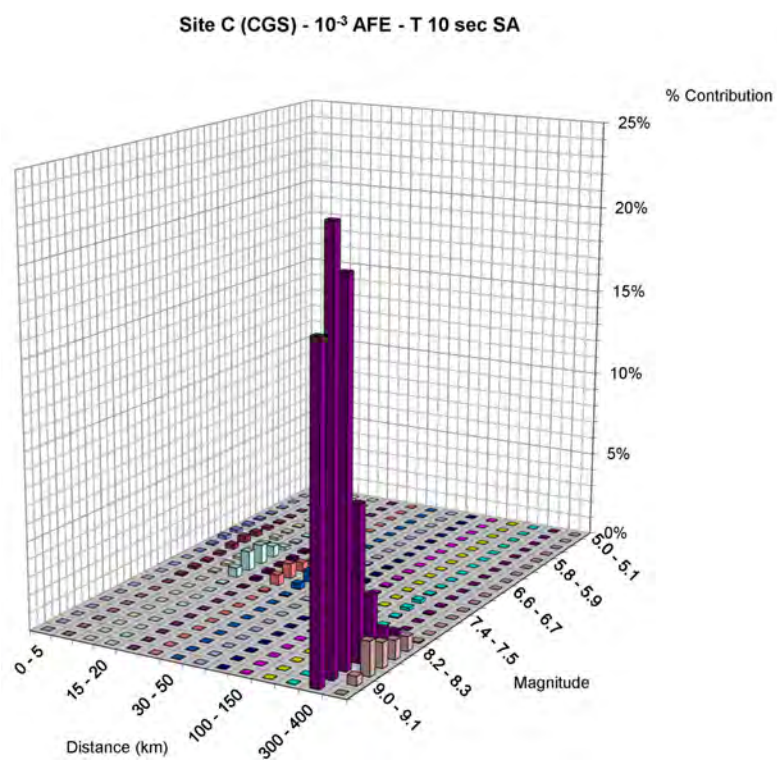

(b)

Figure 10.43. Deaggregation histogram showing magnitude-distance contributions to the total mean hazard at Site C for T 10-sec spectral acceleration and AFEs of: a) 10^{-2}; b) 10^{-3}; c) 5×10^{-4}; d) 4×10^{-4}; e) 10^{-4}; f) 10^{-5}; g) 10^{-6}; h) 10^{-7}.

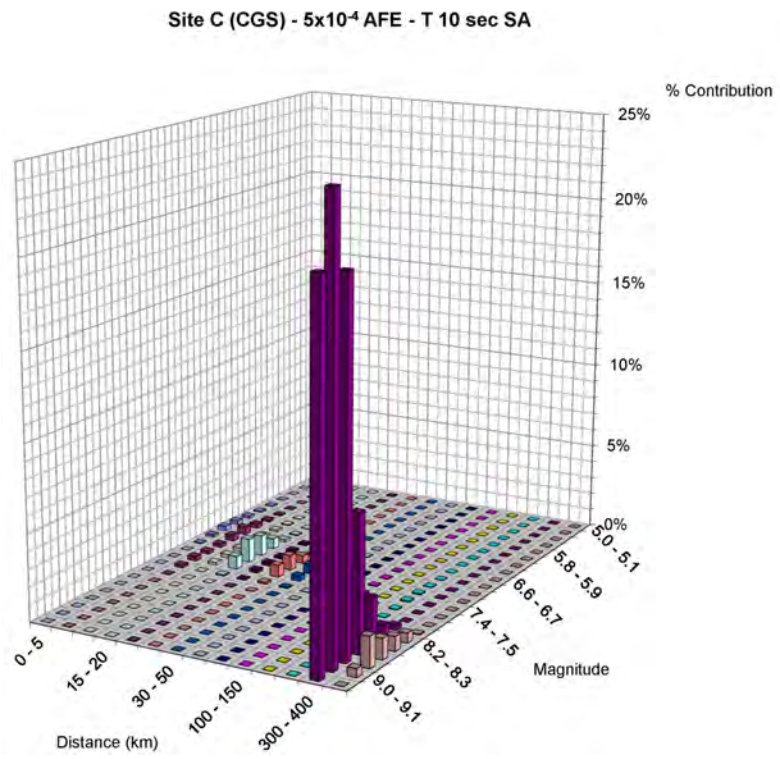

(c)

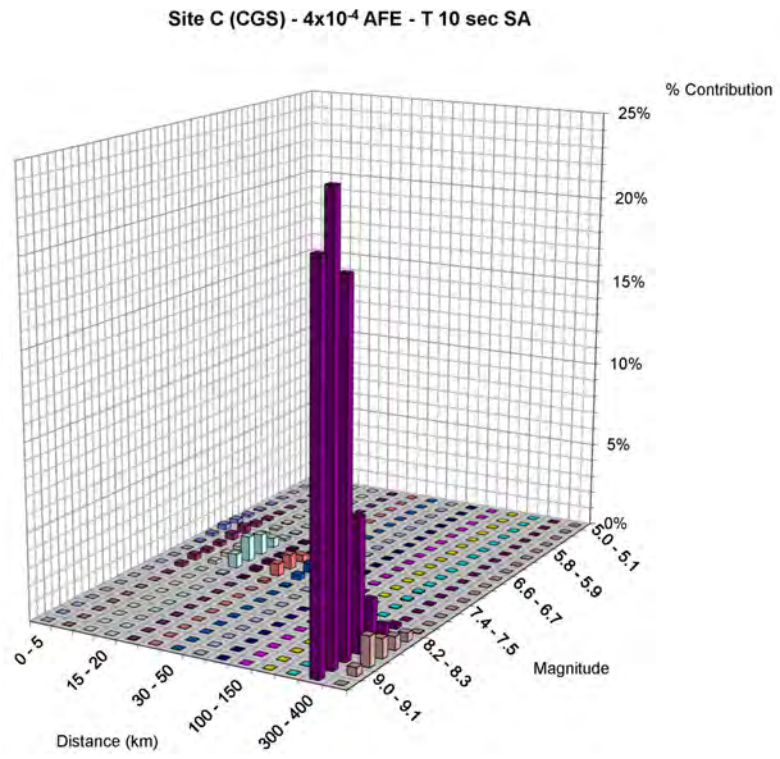

(d)

Figure 10.43. (contd)

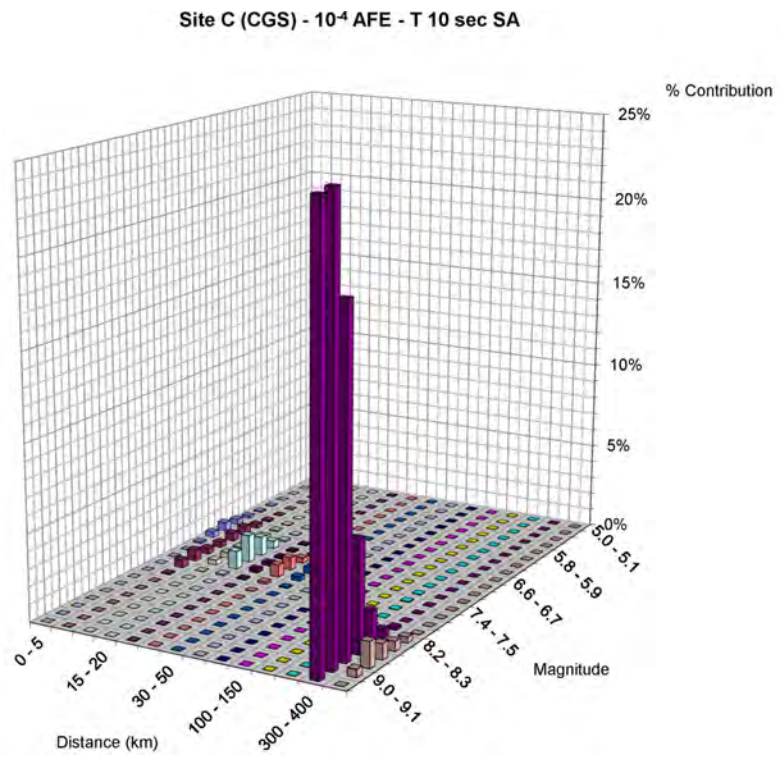

(e)

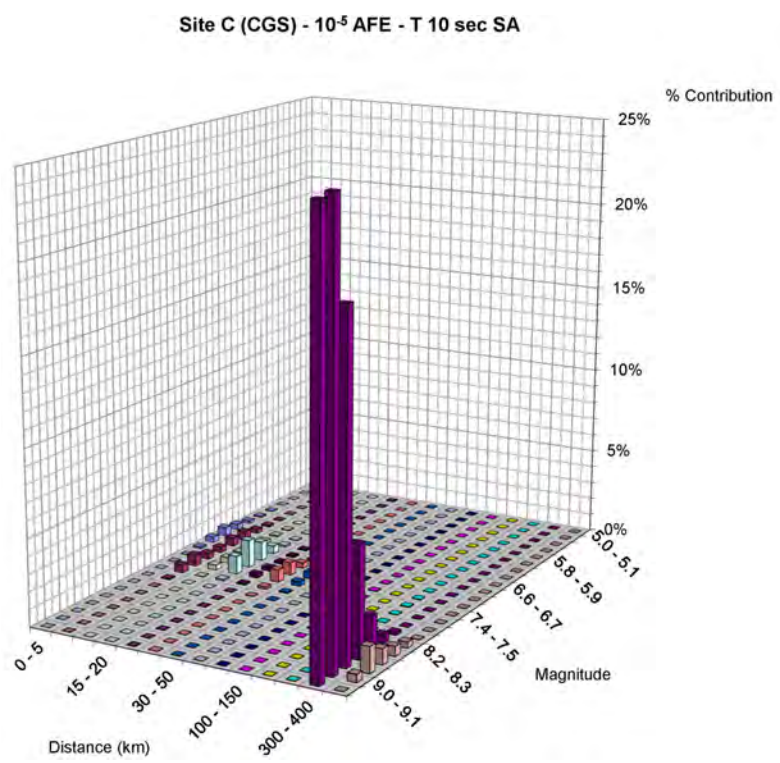

(f)

Figure 10.43. (contd)

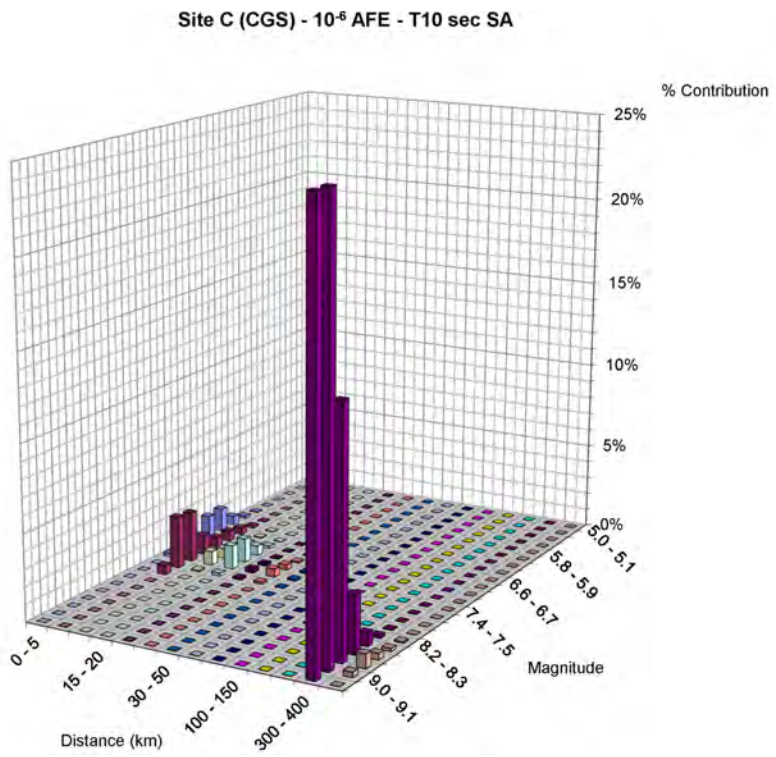

(g)

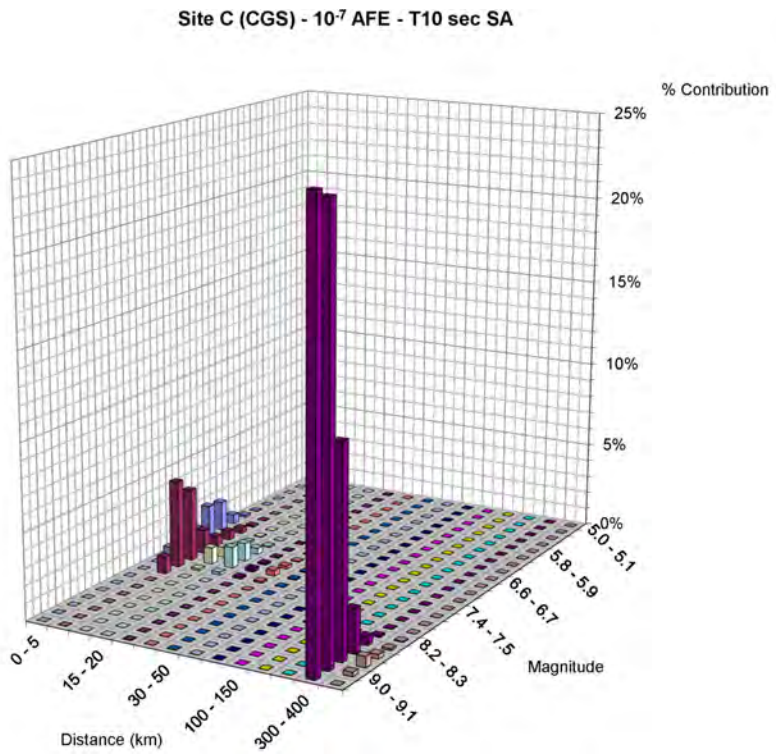

(h)

Figure 10.43. (contd)

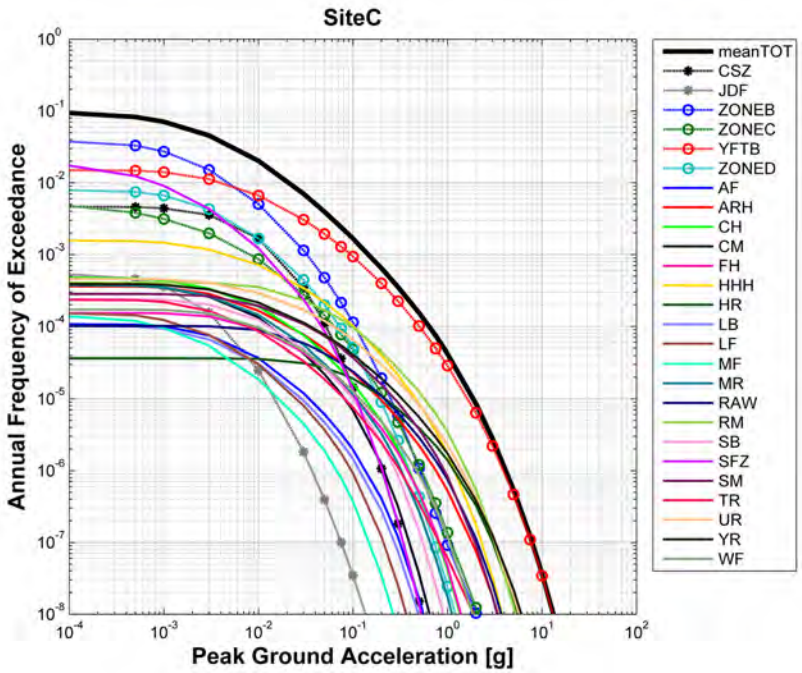

(a)

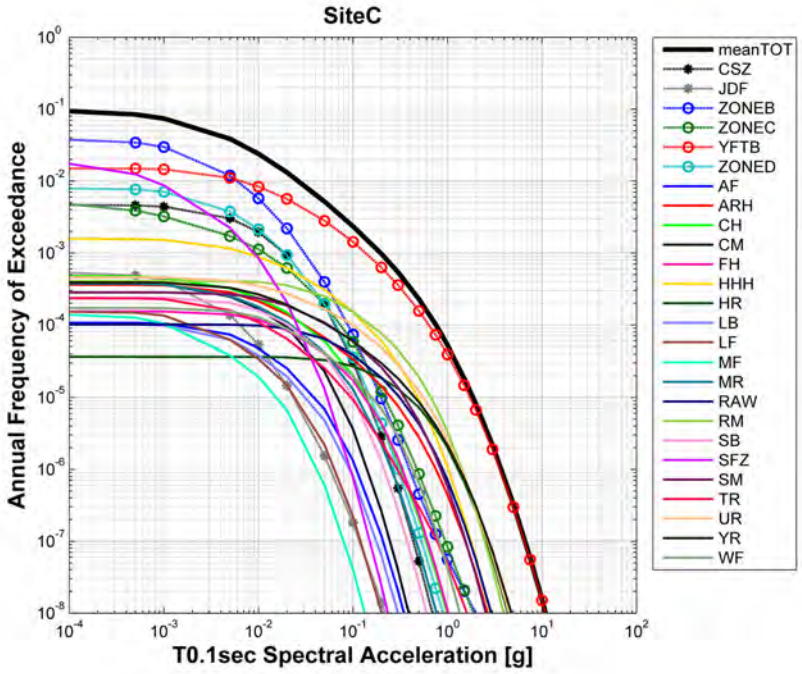

(b)

Figure 10.44. Comparison between the mean hazard curves at Site C obtained for each individual source: subduction sources are shown by dotted star curves; crustal sources by dotted circle curves; and fault sources by solid curves: a) peak ground acceleration; b) T 0.1-sec; c) T 1-sec; d) T 10-sec spectral acceleration. Acronyms used in figures are listed in Table 10.13.

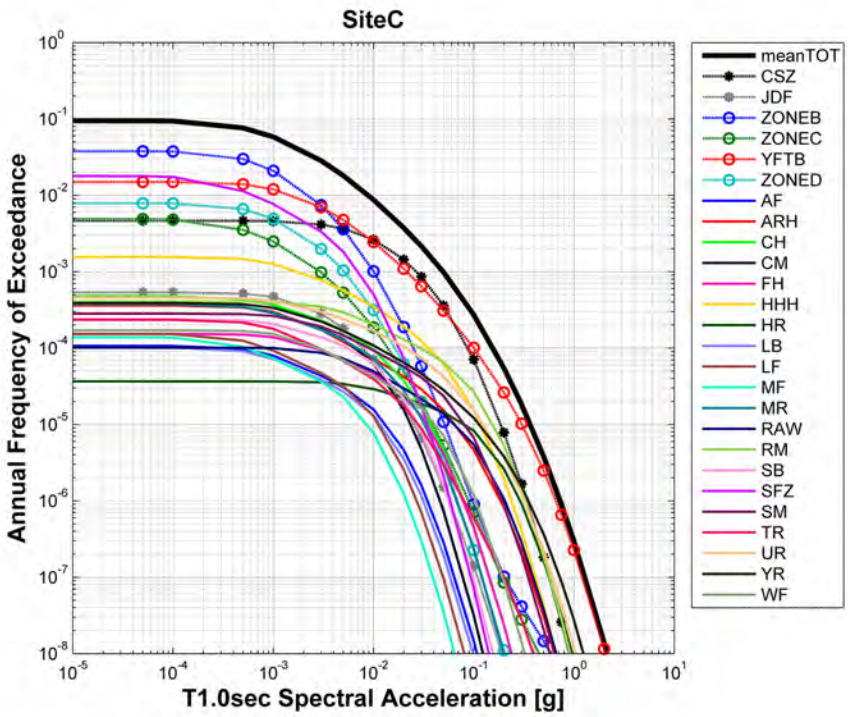

(c)

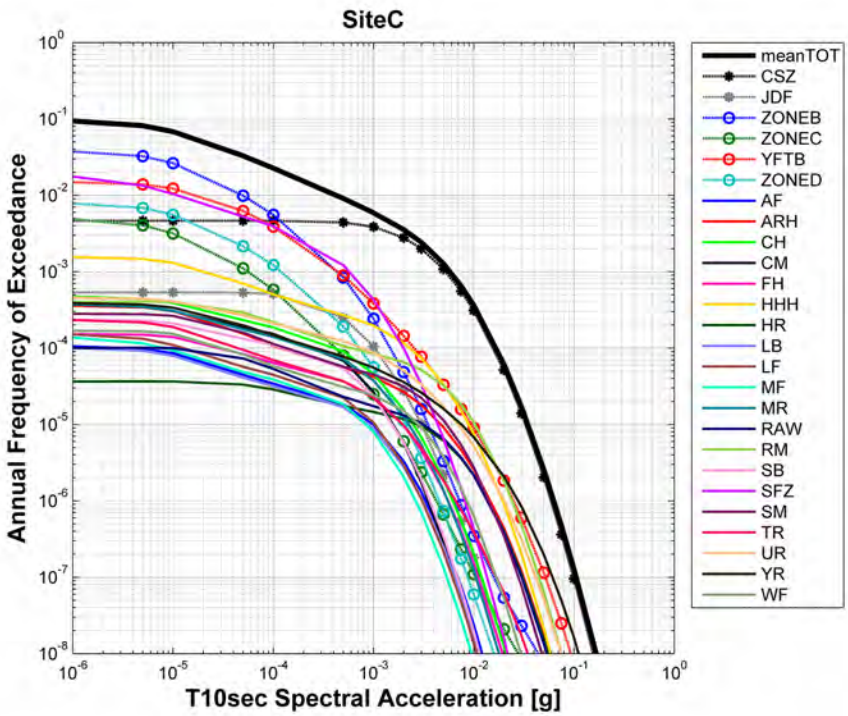

(d)

Figure 10.44. (contd)

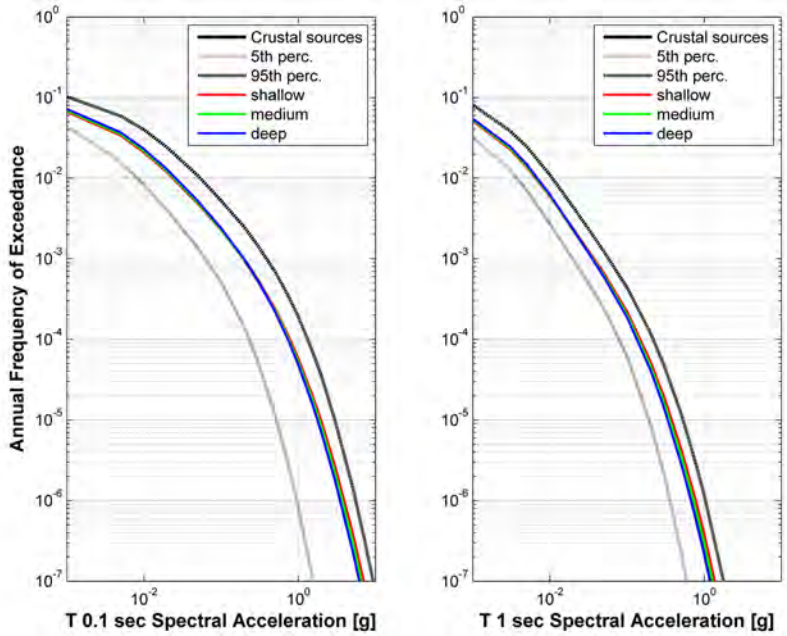

Figure 10.45. Comparison between the total mean crustal sources seismic hazard at Site C (black curve) and the individual contributions at shallow thickness (red curve), medium thickness (green curve), and deep thickness (blue curve) for T 0.1-sec and T 1.0-sec spectral accelerations. The 5th and 95th percentiles of the total crustal hazard are shown by the light and dark grey curves, respectively.

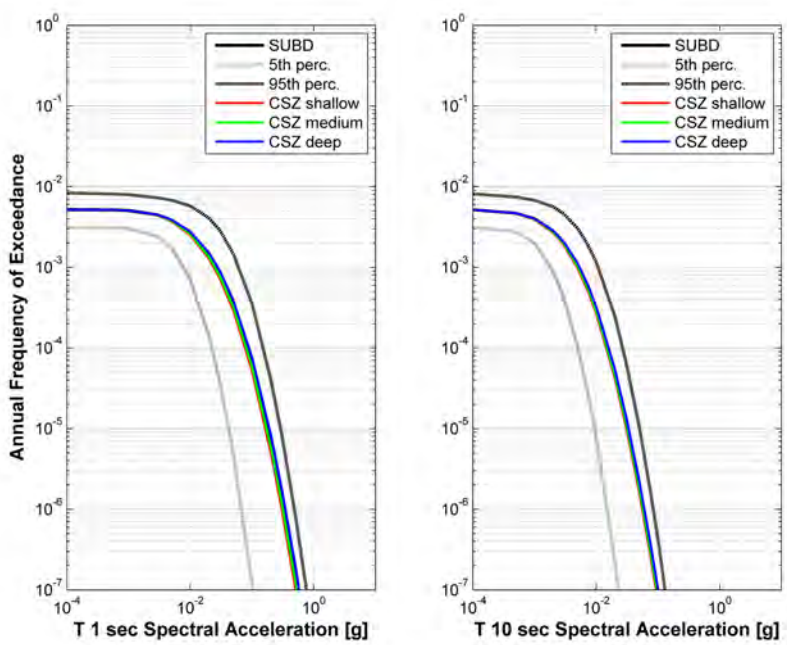

Figure 10.46. Comparison between the total mean CSZ extension seismic hazard at Site C (black curve) and the individual contributions at shallow thickness (red curve), medium thickness (green curve), and deep thickness (blue curve) for T 1.0-sec and T 10-sec spectral accelerations.

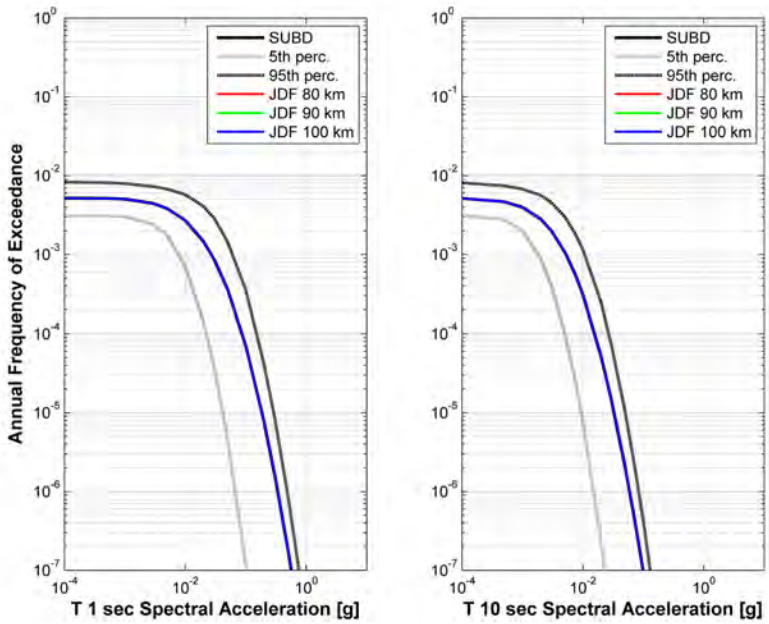

Figure 10.47. Comparison between the total mean JDF extension seismic hazard at Site C (black curve) and the individual contributions at 80 km (red curve), 90 km (green curve), and 100 km (blue curve) for T 1.0-sec and T 10-sec spectral accelerations.

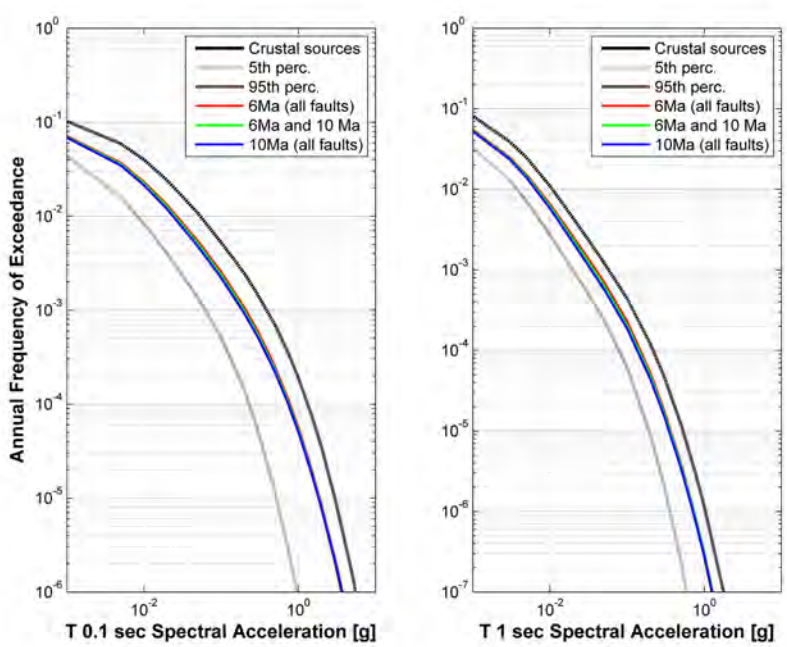

Figure 10.48. Comparison between the total mean crustal sources seismic hazard at Site C (black curve) and the individual start time of deformation contributions at 6 Ma for all faults (red curve), 6 Ma and 10 Ma (green curve), and 10 Ma for all faults (blue curve) for T 0.1-sec and T 1.0-sec spectral accelerations. The 5th and 95th percentiles of the total crustal hazard are shown by the light and dark grey curves, respectively.

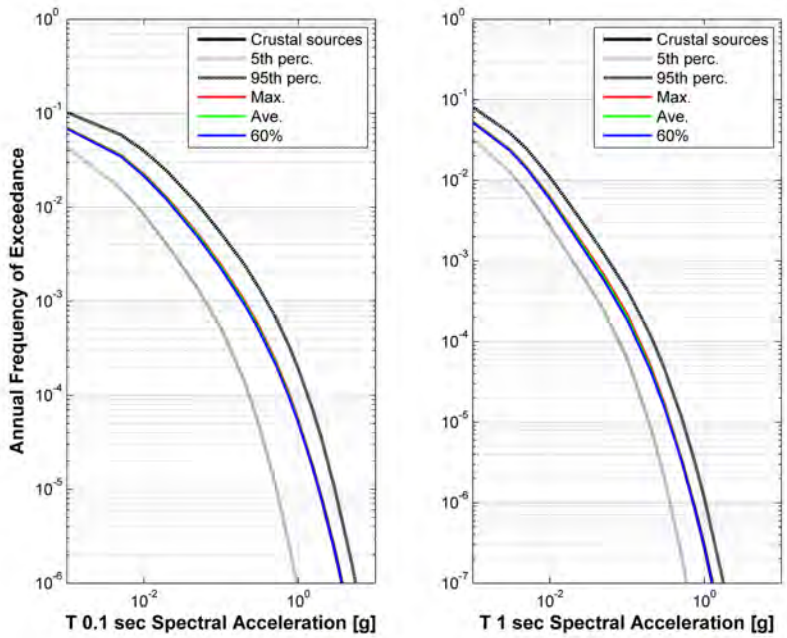

Figure 10.49. Comparison between the total mean crustal sources seismic hazard at Site C (black curve) and the individual basis for fault dip contributions at maximum polygon width (red curve), average polygon width (green curve), and 60% of average polygon width (blue curve) for T 0.1-sec and T 1.0-sec spectral accelerations. The 5th and 95th percentiles of the total crustal hazard are shown by the light and dark grey curves, respectively.

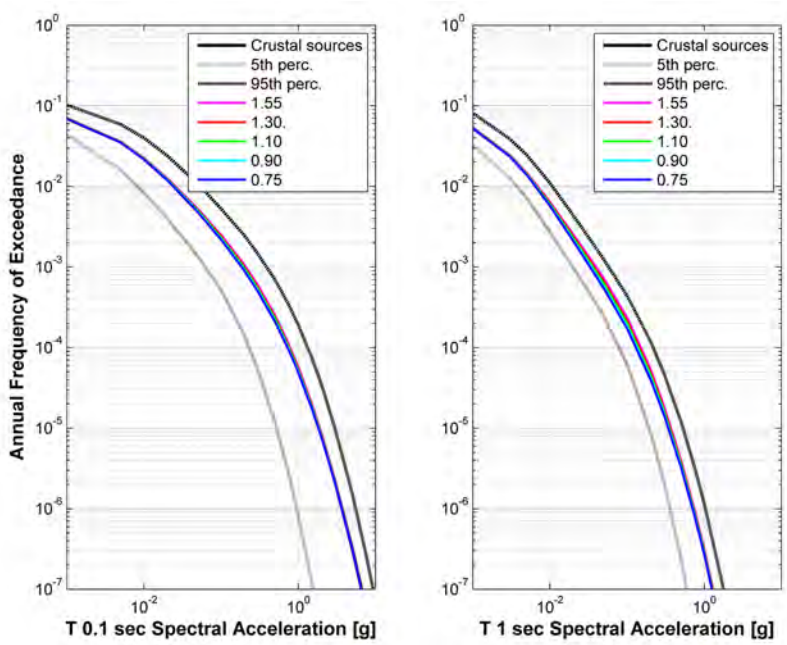

Figure 10.50. Comparison between the total mean crustal sources seismic hazard at Site C (black curve) and the five individual temporal model-scale factor contributions for T 0.1-sec and T 1.0-sec spectral accelerations. The 5th and 95th percentiles of the total crustal hazard are shown by the light and dark grey curves, respectively.

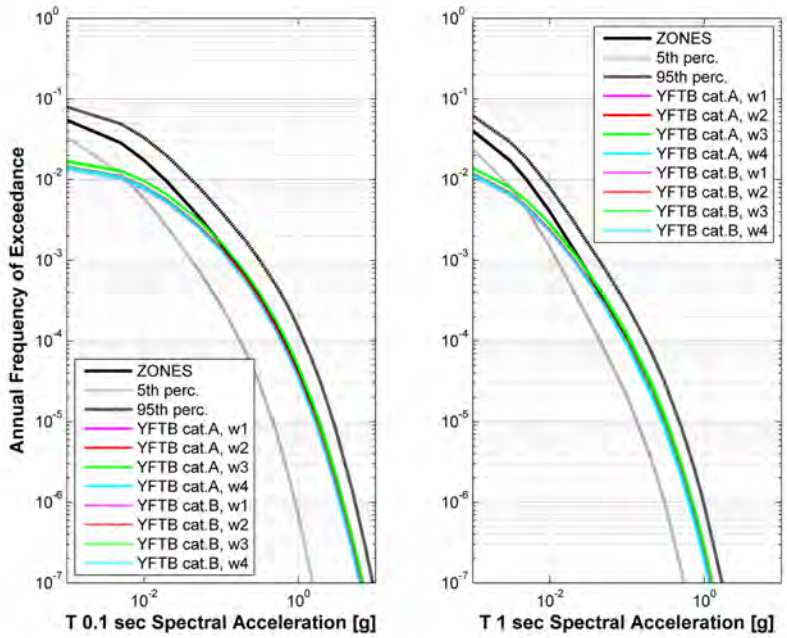

Figure 10.51. Comparison between alternative catalogs and declustering techniques for the YFTB source zone at Site C: a) for T 0.1-sec; b) for T 1.0-sec spectral accelerations. On each plot the black solid curves are the hazard computed from all the background sources (solid curve is the mean, light and dark grey curve show 5th and 95th percentiles, respectively).

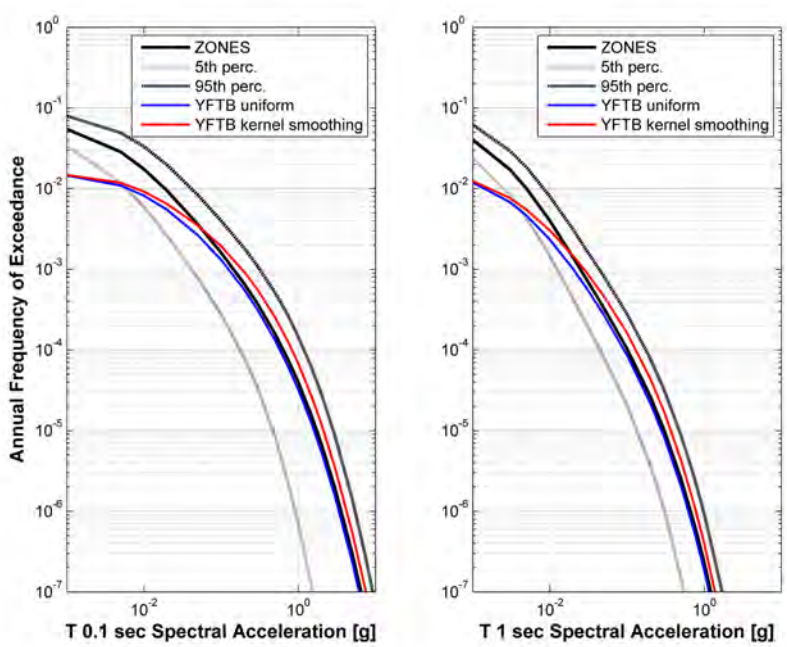

Figure 10.52. Comparison between alternative smoothing techniques for the YFTB source zone at Site C: a) for T 0.1-sec; b) for T 1.0-sec spectral accelerations. On each plot the black solid curves are the hazard computed from all the background sources (solid curve is the mean, light and dark grey curve show 5th and 95th percentiles, respectively).

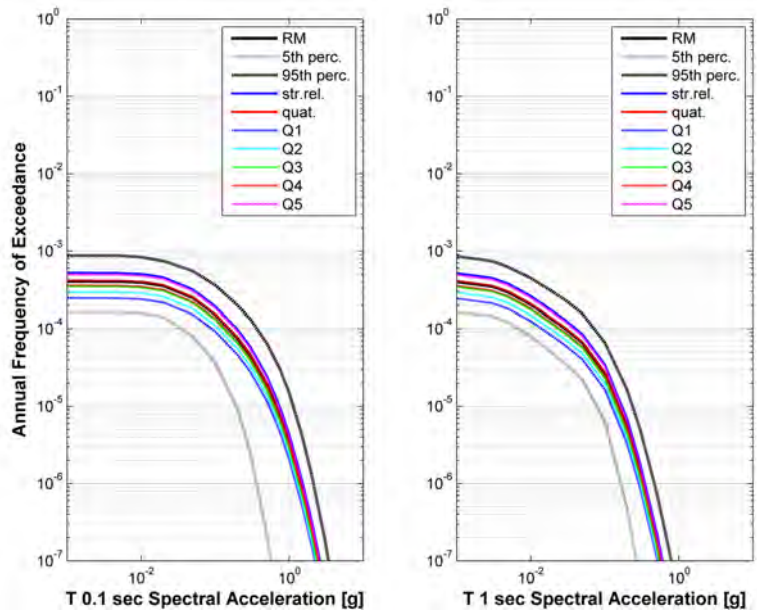

Figure 10.53. Comparison between the total mean Rattlesnake Mountain fault source seismic hazard at Site C (black curve) and the individual contribution of approach to assessing slip rate via use of structural relief (blue solid curve) or quaternary data (red solid curve) for T 0.1-sec and T 1.0-sec spectral accelerations. In addition, the five average quaternary rates are shown by dotted curves. The 5th and 95th percentiles are shown by the light and dark grey curves, respectively.

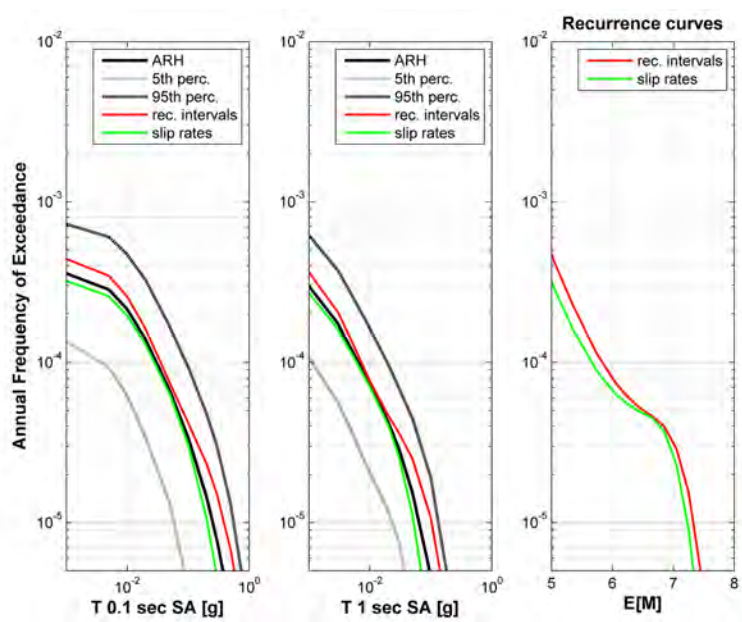

Figure 10.54. Sensitivity analysis for the Ahtanum Ridge-Rattlesnake Hills (ARH) fault at Site C for T 0.1-sec (left) and T 1-sec (middle) spectral accelerations. In both plots the mean seismic hazard for the ARH fault is shown by the black solid curve and its 5th and 95th percentiles by the light and dark grey curves, respectively. The hazard obtained using recurrence intervals is shown by the red curve and using slip rates by the green curve. The recurrence curves are shown for comparison.

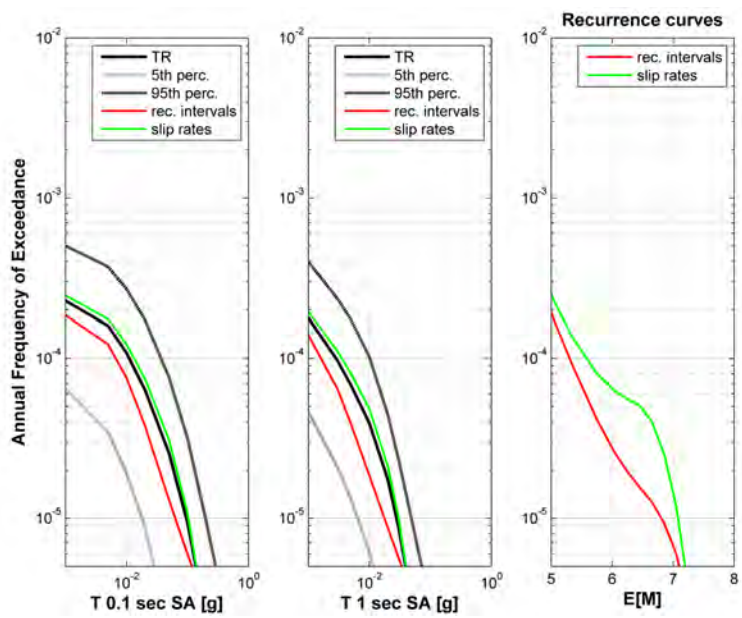

Figure 10.55. Sensitivity analysis for the Toppenish Ridge (TR) fault at Site C for T 0.1-sec (left) and T 1-sec (middle) spectral accelerations. In both plots the mean seismic hazard for the ARH fault is shown by the black solid curve and its 5th and 95th percentiles by the light and dark grey curves, respectively. The hazard obtained using recurrence intervals is shown by the red curve and using slip rates by the green curve. The recurrence curves are shown for comparison.

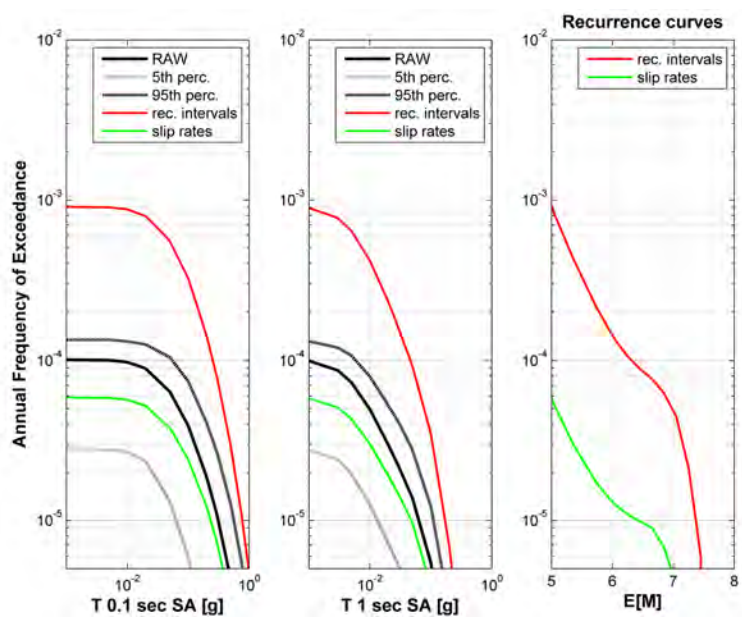

Figure 10.56. Sensitivity analysis for the RAW fault at Site C for T 0.1-sec (left) and T 1-sec (middle) spectral accelerations. In both plots the mean seismic hazard for the ARH fault is shown by the black solid curve and its 5th and 95th percentiles by the light and dark grey curves, respectively. The hazard obtained using recurrence intervals is shown by the red curve and using slip rates by the green curve. The recurrence curves are shown for comparison.

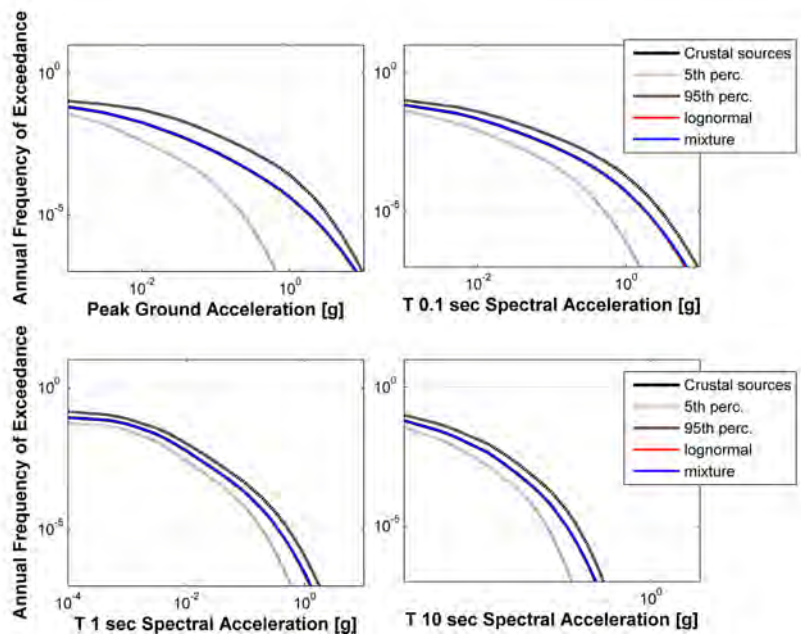

Figure 10.57. Comparison between the total mean crustal sources seismic hazard at Site C (black curve) and the individual contribution from ground motion distribution shape represented by red curve for lognormal model and blue curve for mixture model, for the peak ground acceleration, T 0.1-sec, T 1.0-sec, and T 10-sec spectral accelerations. The 5th and 95th percentiles are shown on each plot by the light and dark grey curves.

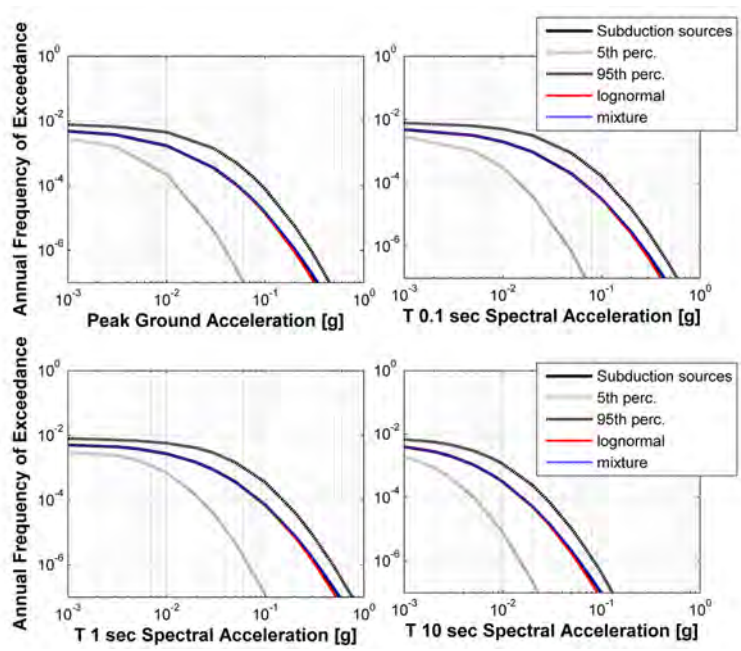

Figure 10.58. Comparison between the total mean subduction sources seismic hazard at Site C (black curve) and the individual contribution from ground motion distribution shape represented by red curve for lognormal model and blue curve for mixture model, for the peak ground acceleration, T 0.1-sec, T 1.0-sec, and T 10-sec spectral accelerations. The 5th and 95th percentiles are shown on each plot by the light and dark grey curves.

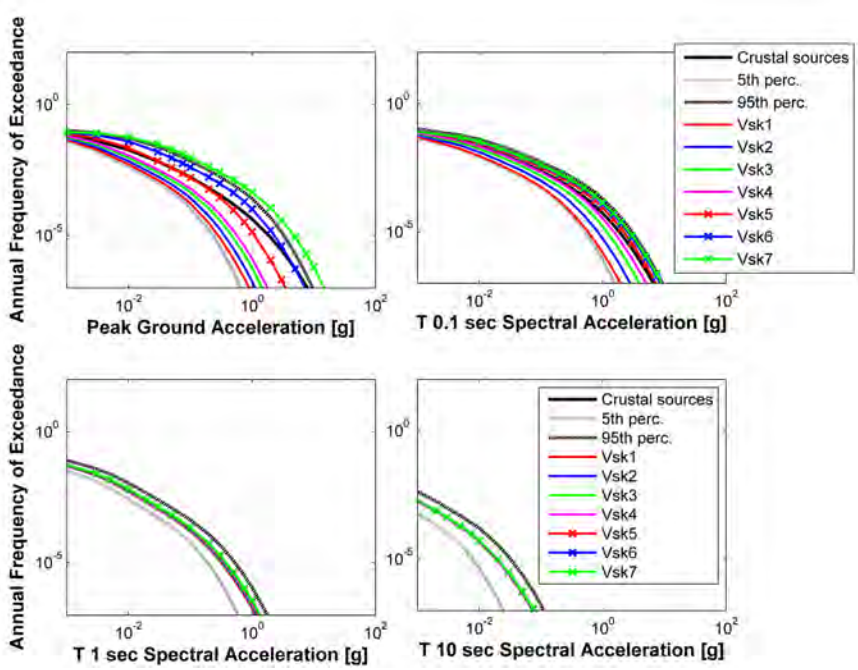

Figure 10.59. Comparison between the total mean crustal sources seismic hazard at Site C (black curve) and the individual contribution from the seven different Vs-kappa adjustment factors, for the peak ground acceleration, T 0.1-sec, T 1.0-sec, and T 10-sec spectral accelerations. The 5th and 95th percentiles are shown on each plot by the light and dark grey curves.

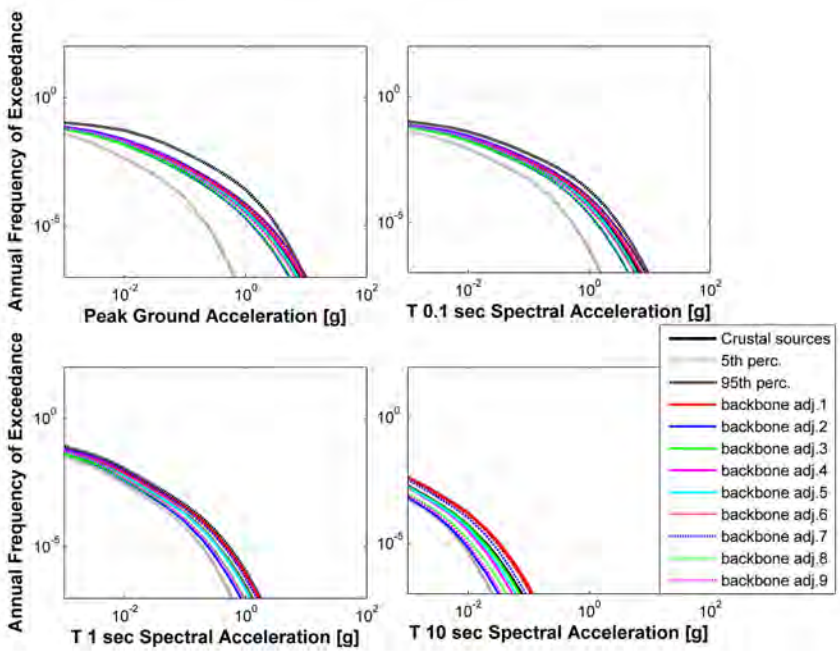

Figure 10.60. Comparison between the total mean crustal sources seismic hazard at Site C (black curve) and the individual contribution from the nine different inherent uncertainty in backbone adjustments, for the peak ground acceleration, T 0.1-sec, T 1.0-sec, and T 10-sec spectral accelerations. The 5th and 95th percentiles are shown on each plot by the light and dark grey curves.

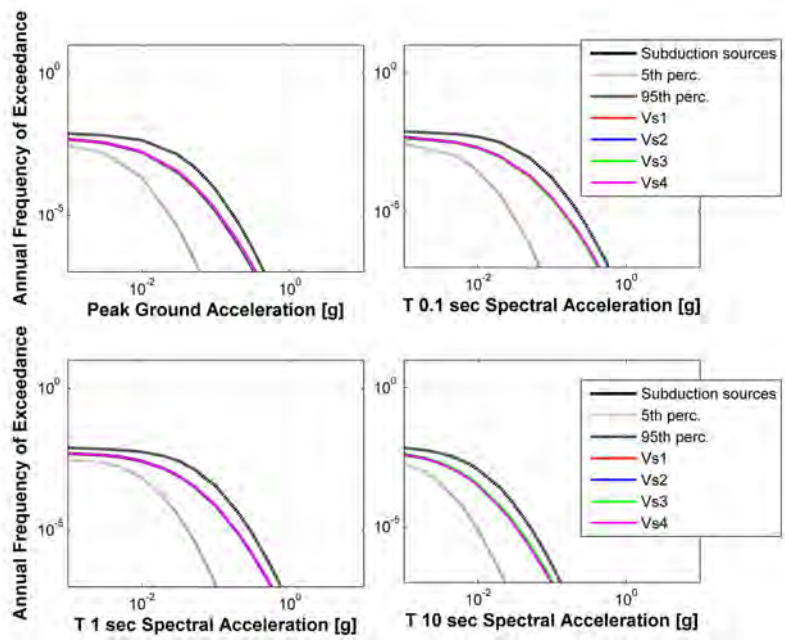

Figure 10.61. Comparison between the total mean subduction sources seismic hazard at Site C (black curve) and the individual contribution from the four different host-to-target Vs adjustment factors, for the peak ground acceleration, T 0.1-sec, T 1.0-sec, and T 10-sec spectral accelerations. The 5th and 95th percentiles are shown on each plot by the light and dark grey curves.

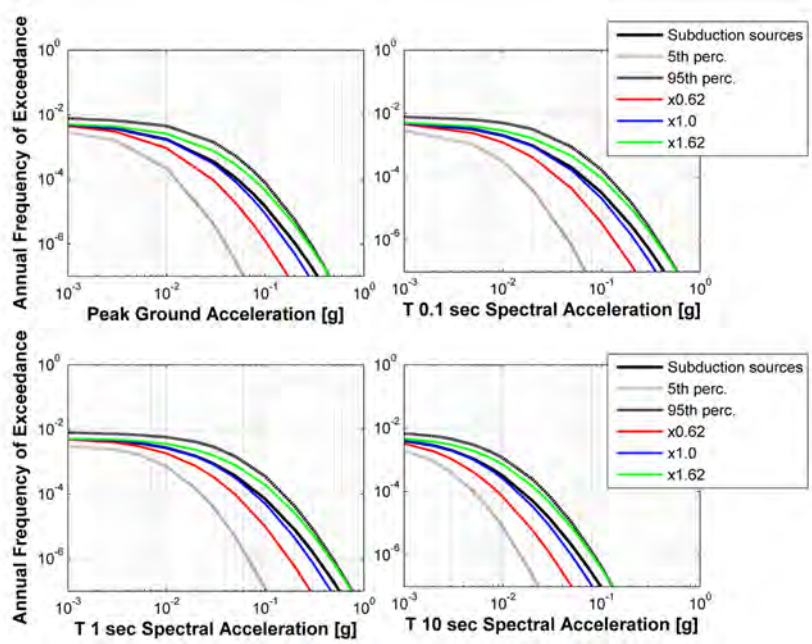

Figure 10.62. Comparison between the total mean subduction sources seismic hazard at Site C (black curve) and the individual contribution from the three different epistemic uncertainty in median factors for the peak ground acceleration, T 0.1-sec, T 1.0-sec, and T 10-sec spectral accelerations. The 5th and 95th percentiles are shown on each plot by the light and dark grey curves.

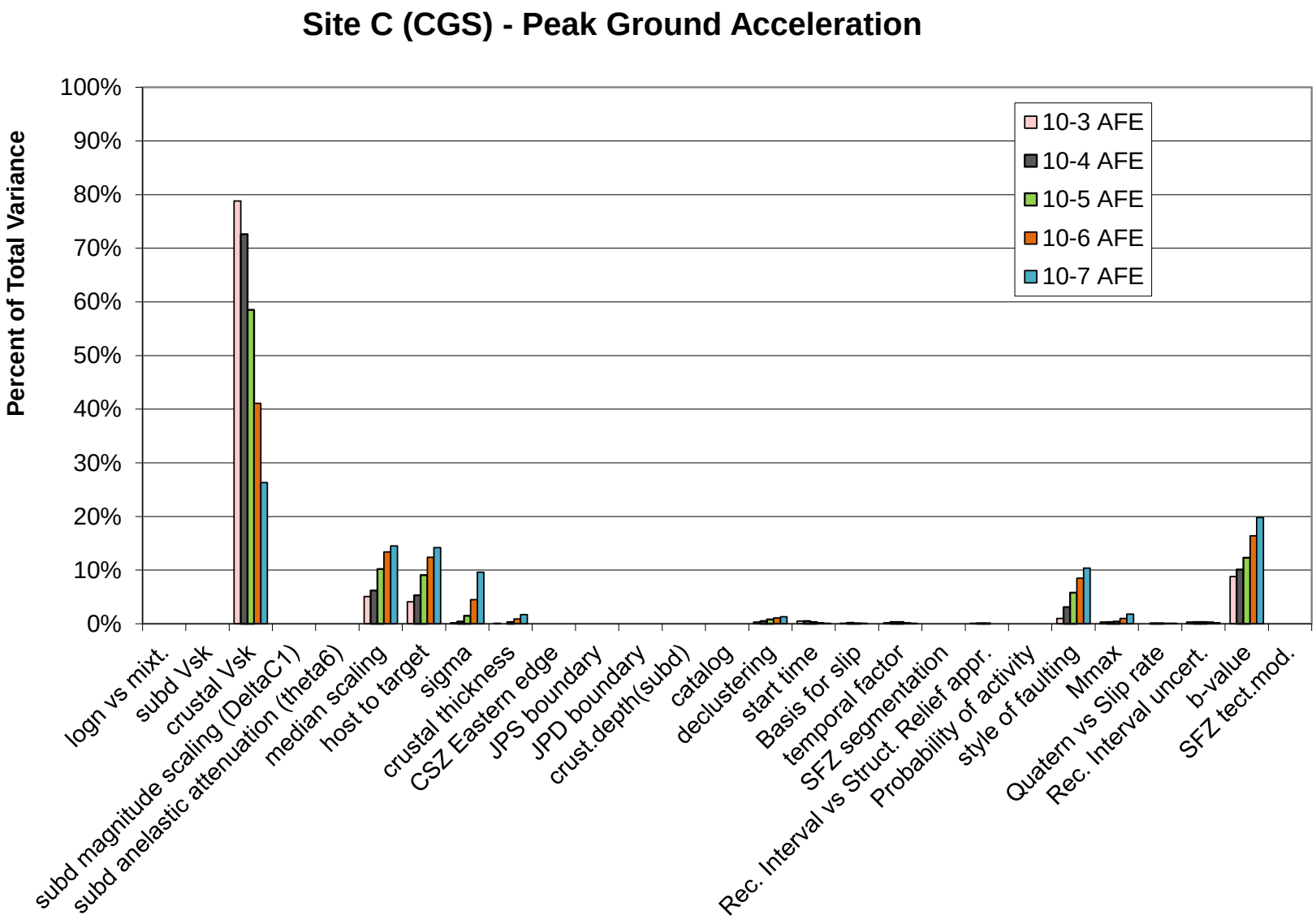

Figure 10.63. Variance contribution histogram at the 10^{-3}, 10^{-4}, 10^{-5}, 10^{-6}, and 10^{-7} annual frequencies of exceedance for peak ground acceleration and Site C.

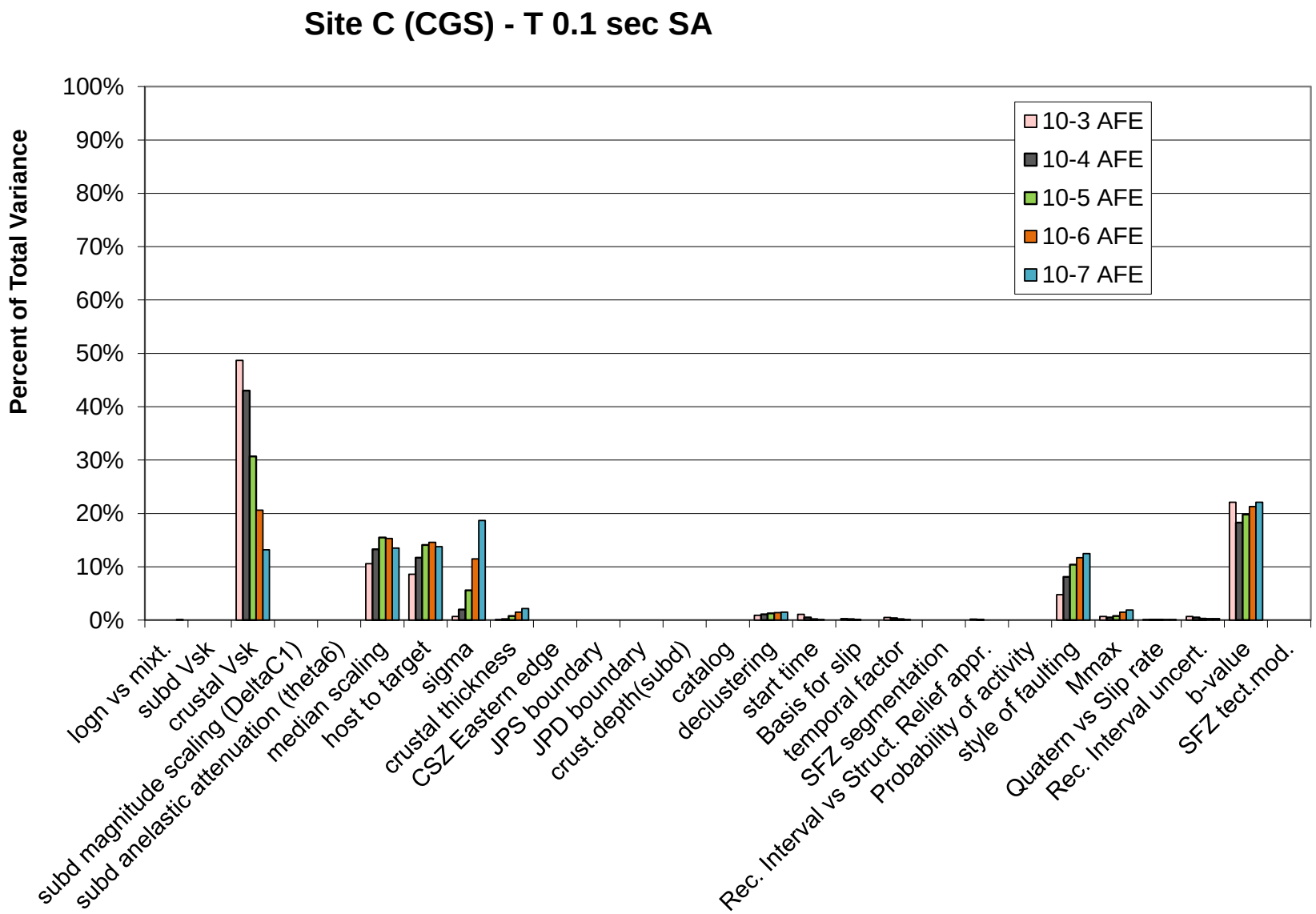

Figure 10.64. Variance contribution histogram at the 10^{-3}, 10^{-4}, 10^{-5}, 10^{-6}, and 10^{-7} annual frequencies of exceedance for T 0.1-sec spectral acceleration and Site C.

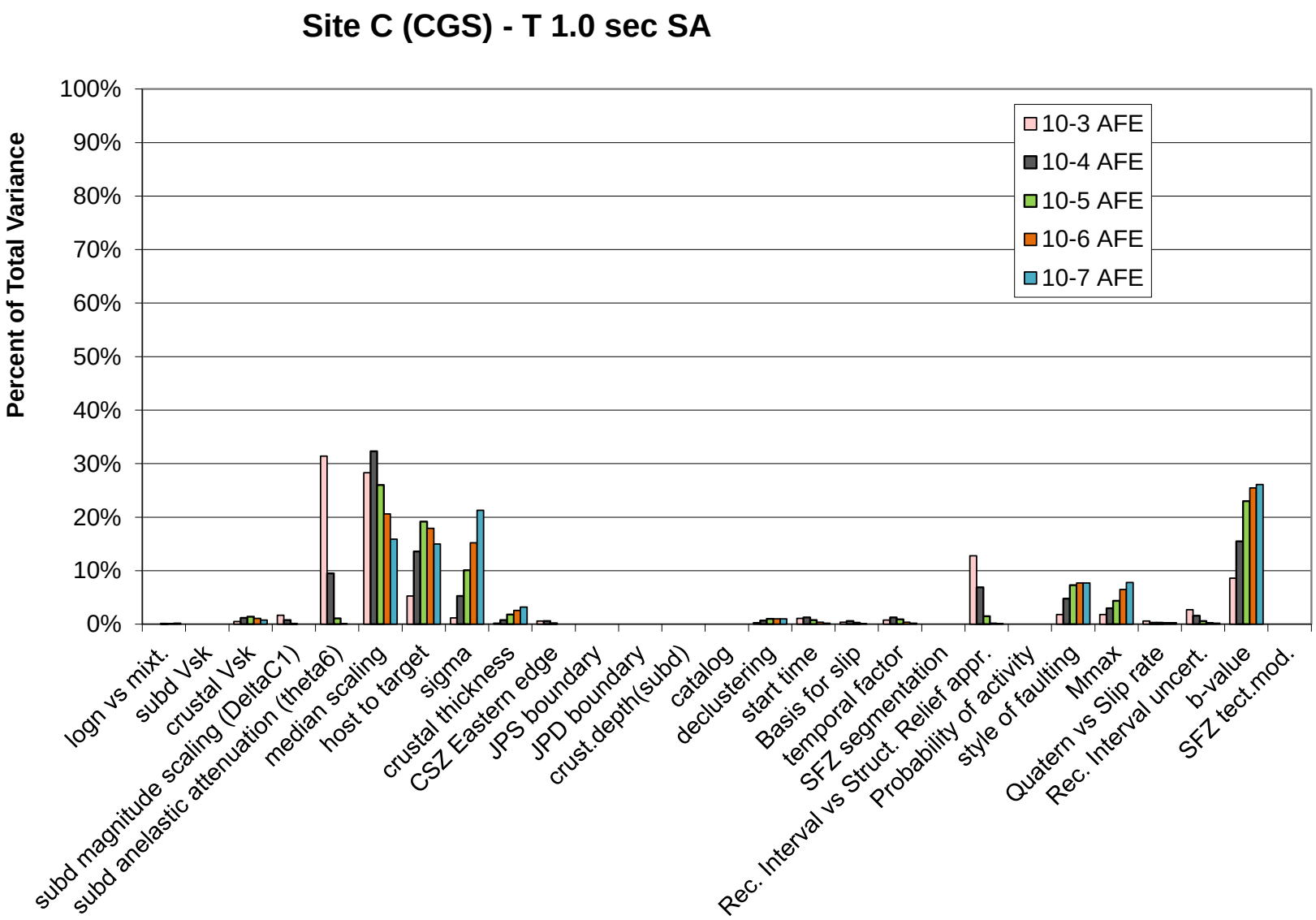

Figure 10.65. Variance contribution histogram at the 10^{-3}, 10^{-4}, 10^{-5}, 10^{-6}, and 10^{-7} annual frequencies of exceedance for T 1.0-sec spectral acceleration and Site C.

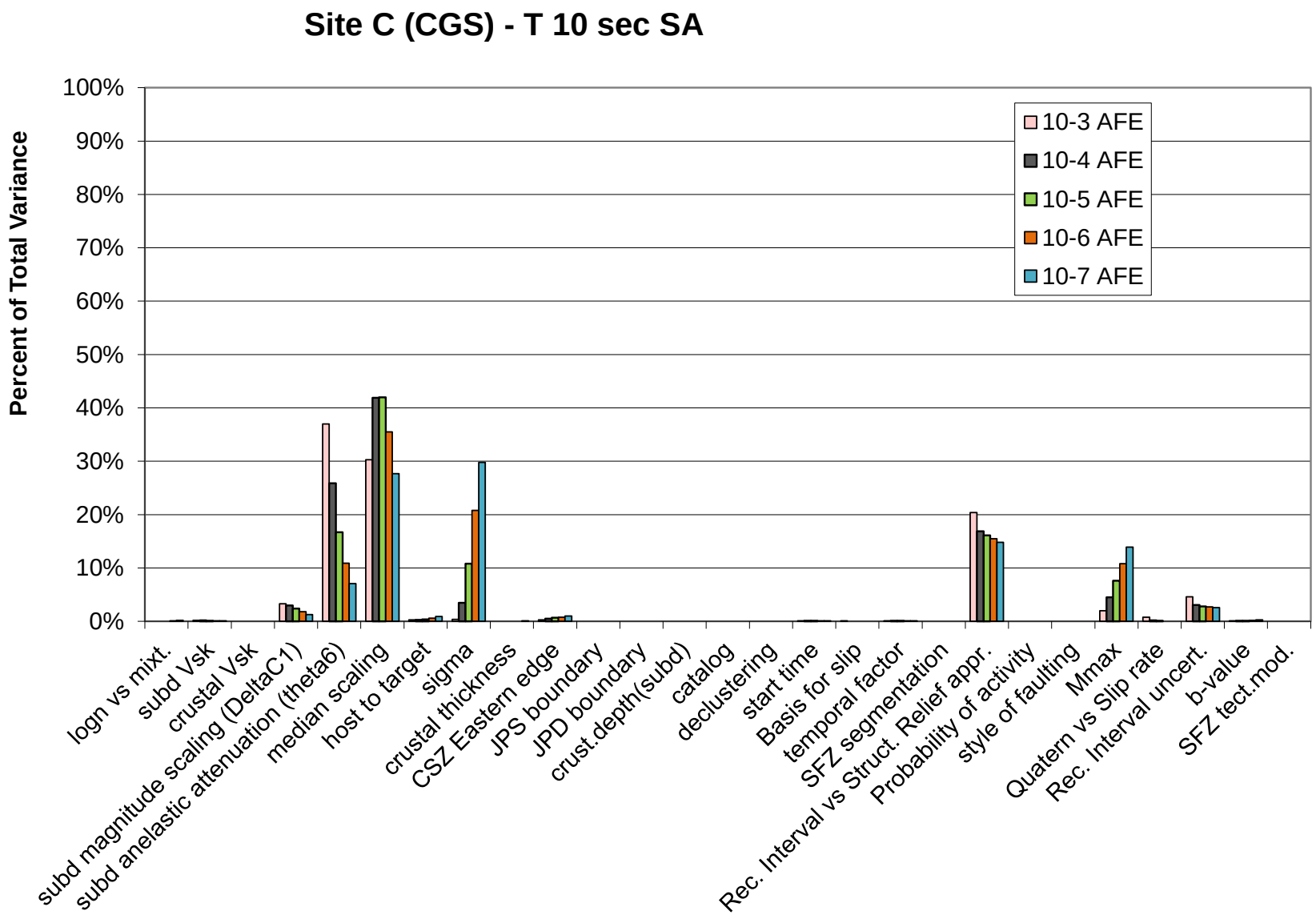

Figure 10.66. Variance contribution histogram at the 10^{-3}, 10^{-4}, 10^{-5}, 10^{-6}, and 10^{-7} annual frequencies of exceedance for T 10-sec spectral acceleration and Site C.

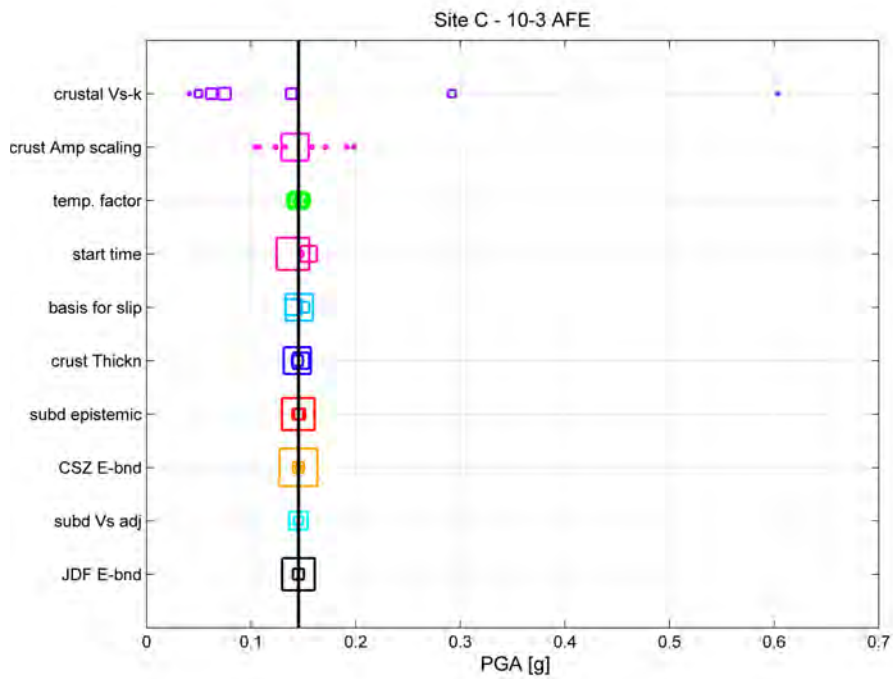

(a)

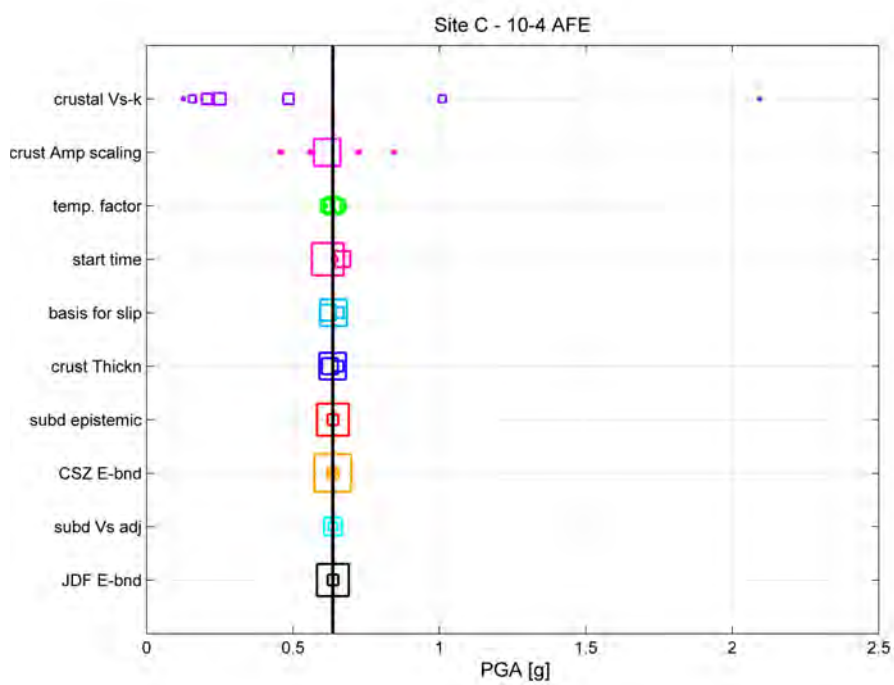

(b)

Figure 10.67. Tornado plots for Site C and peak ground acceleration at AFEs of: a) 10^{-3} (1000 years return period); b) 10^{-4} (10,000 years return period); c) 10^{-5} (100,000 years return period); d) 10^{-6} (1,000,000 years return period); e) 10^{-7} (10,000,000 years return period). The size of the symbols is proportional to the logic-tree weight assigned to each branch.

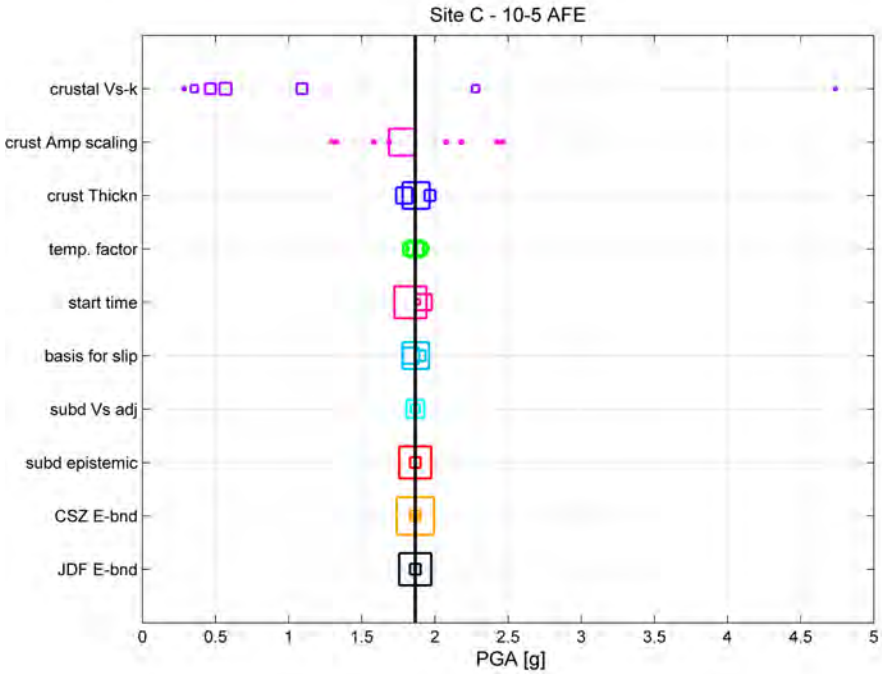

(c)

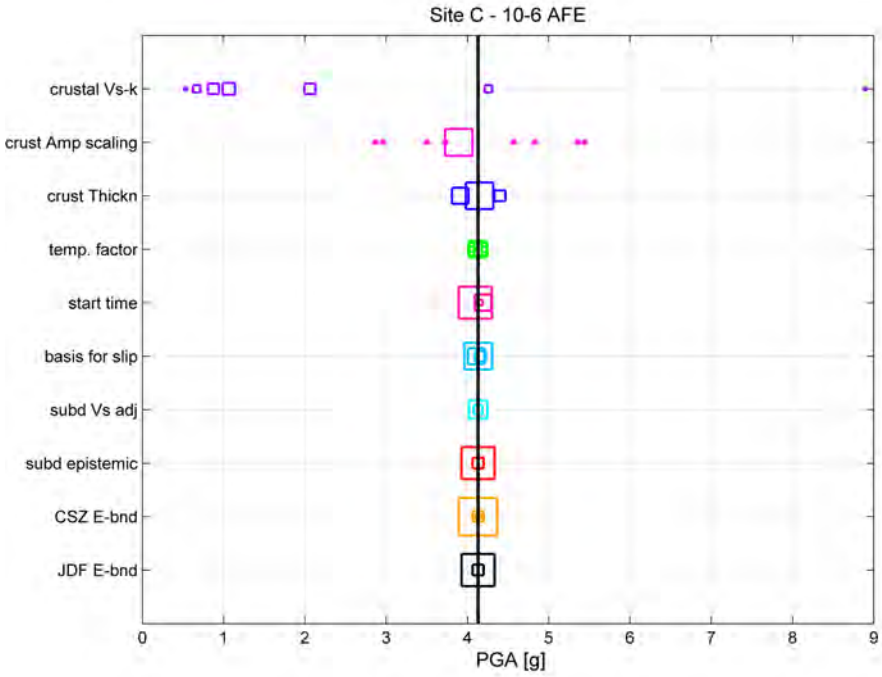

(d)

Figure 10.67. (contd)

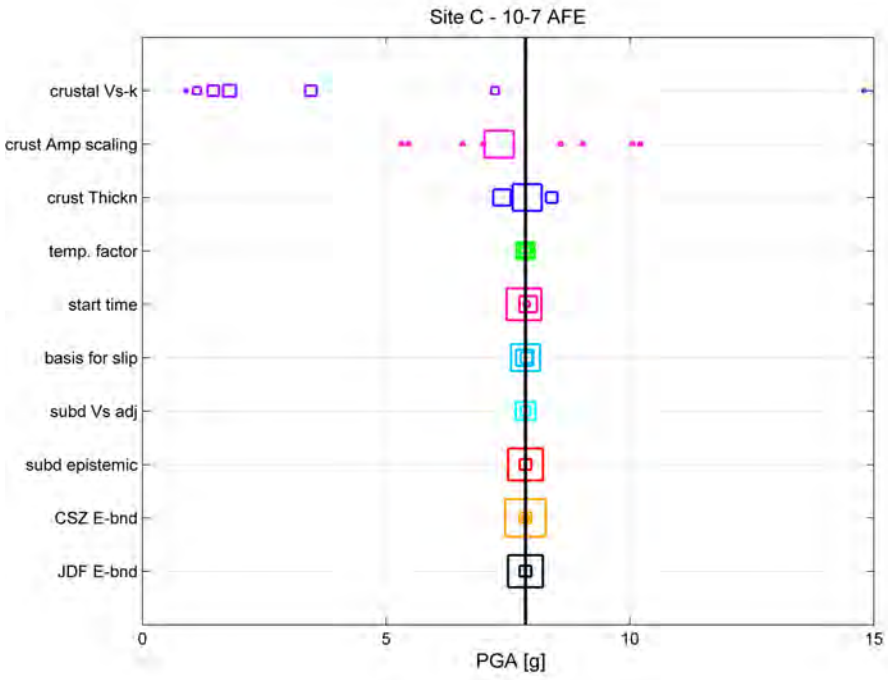

(e)

Figure 10.67. (contd)

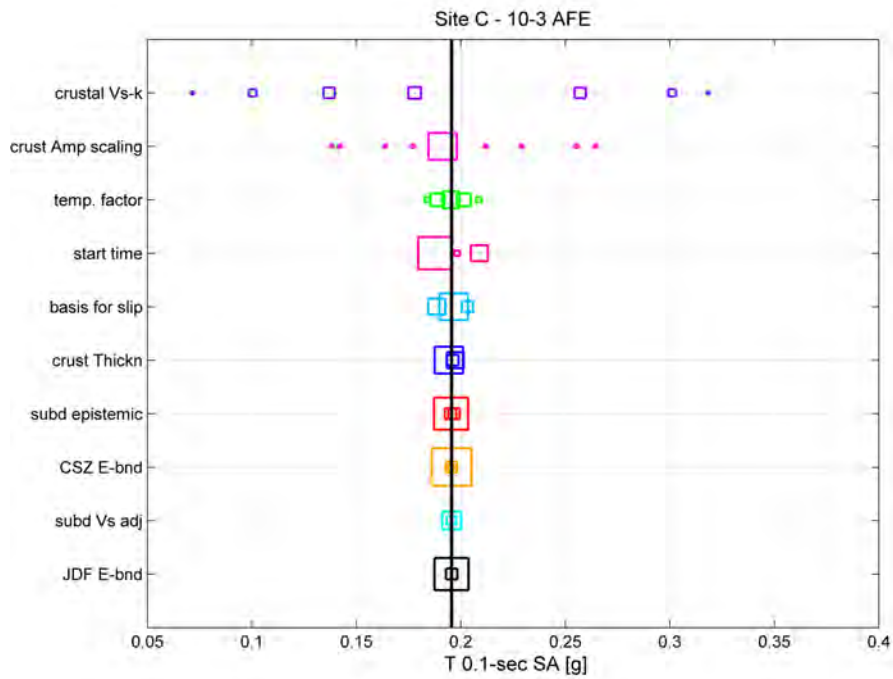

(a)

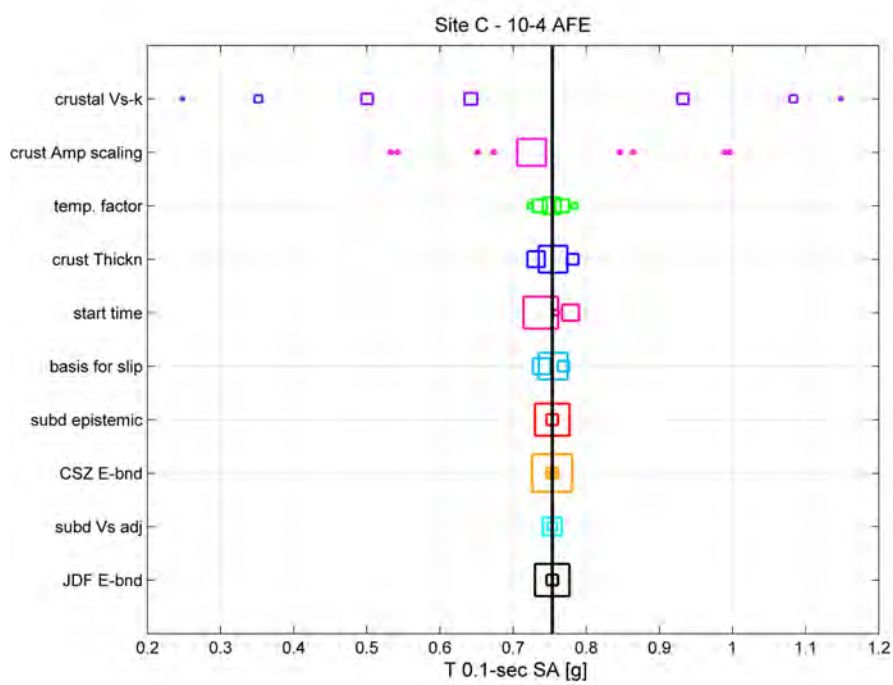

(b)

Figure 10.68. Tornado plots for Site C and T 0.1-sec spectral acceleration at AFEs of: a) 10^{-3} (1000 years return period); b) 10^{-4} (10,000 years return period); c) 10^{-5} (100,000 years return period); d) 10^{-6} (1,000,000 years return period); e) 10^{-7} (10,000,000 years return period). The size of the symbols is proportional to the logic-tree weight assigned to each branch.

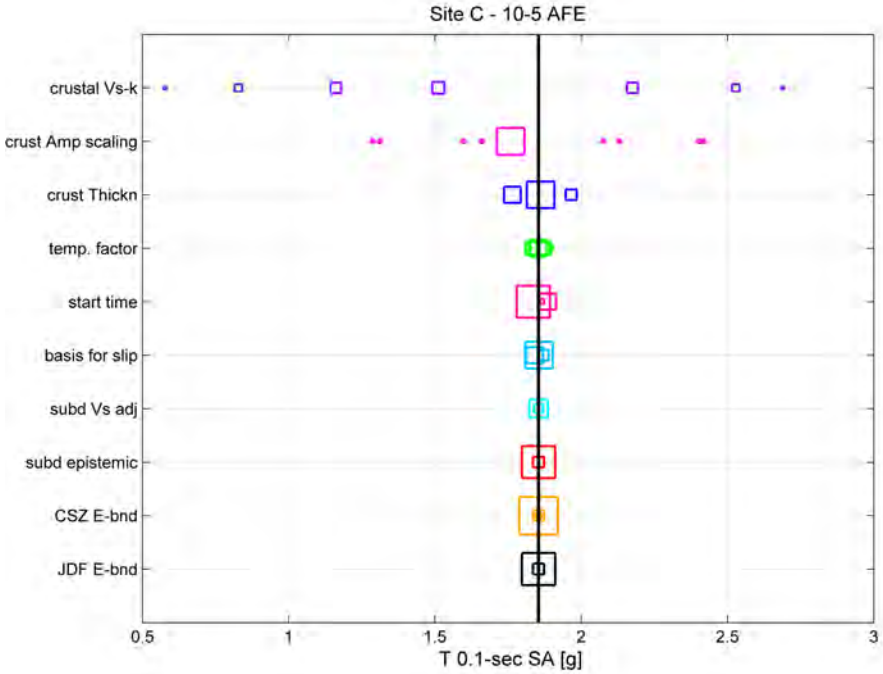

(c)

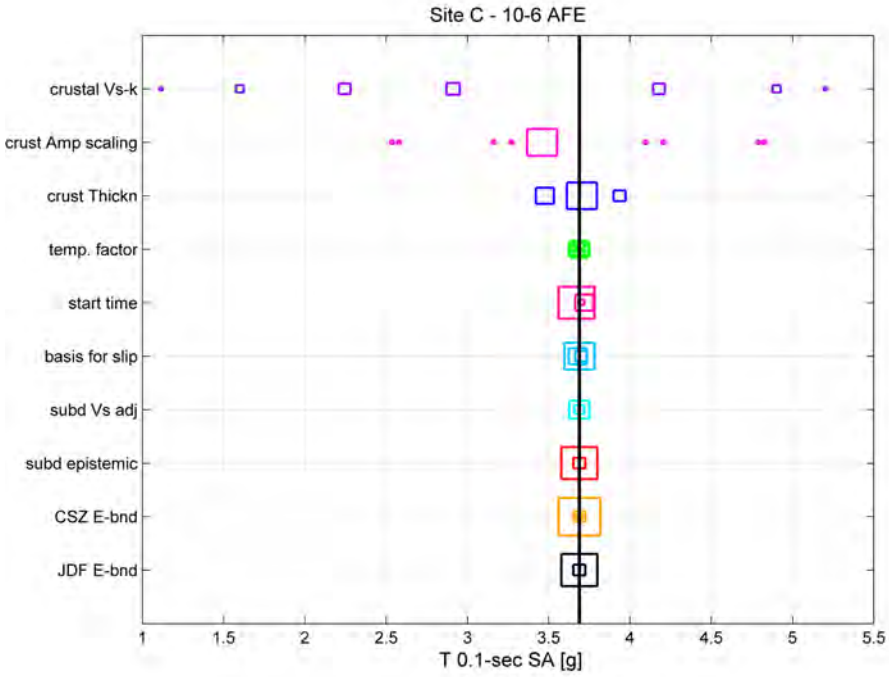

(d)

Figure 10.68. (contd)

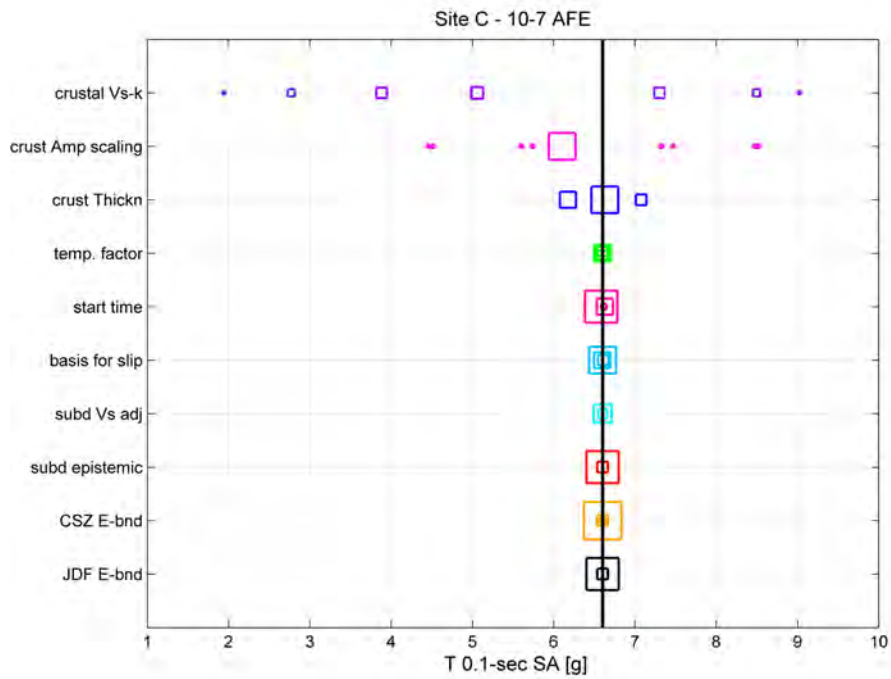

(e)

Figure 10.68. (contd)

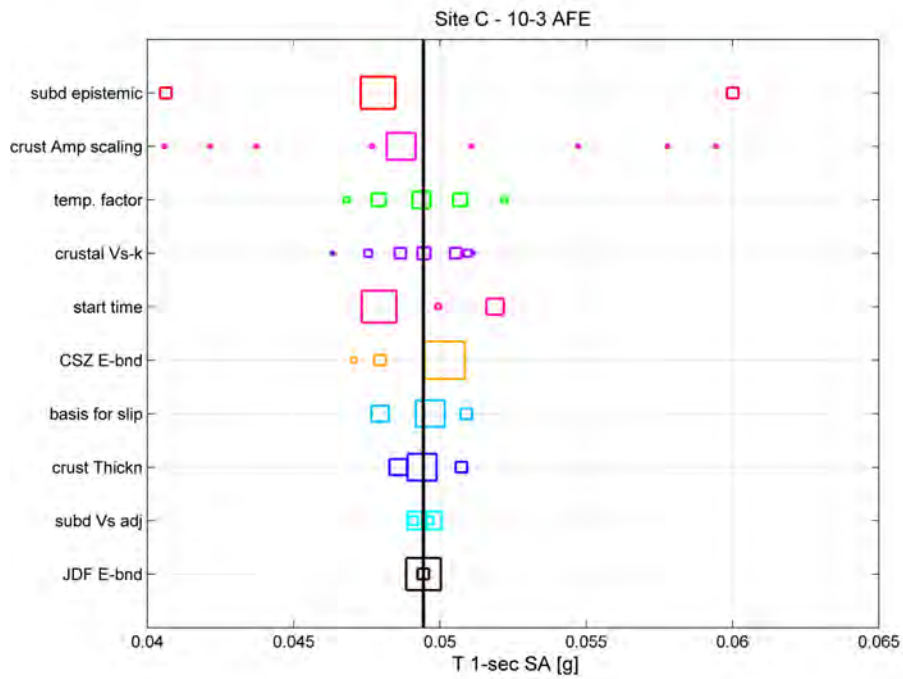

(a)

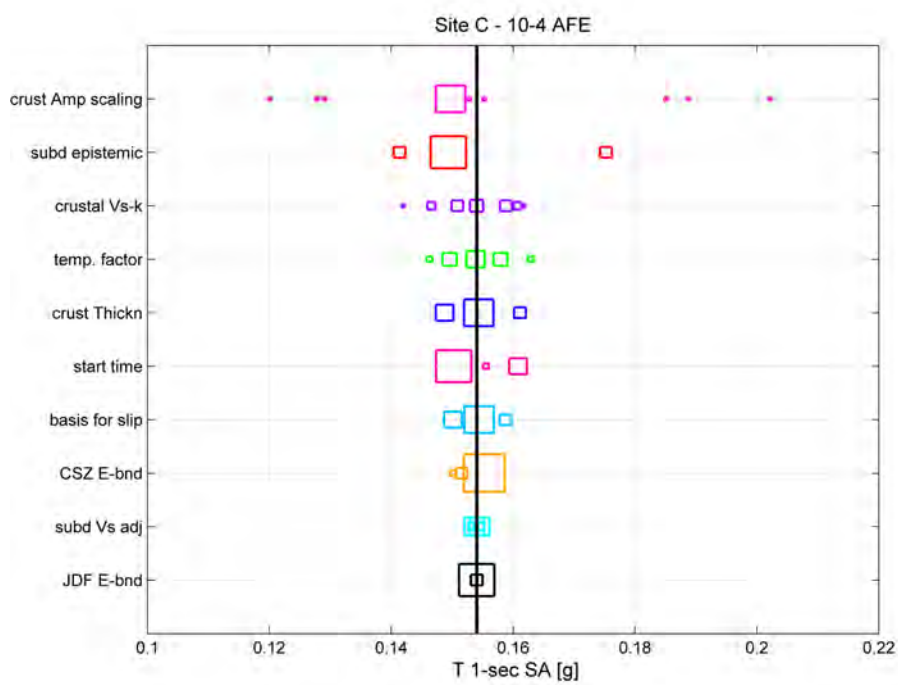

(b)

Figure 10.69. Tornado plots for Site C and T 1.0-sec spectral acceleration at AFEs of: a) 10^{-3} (1000 years return period); b) 10^{-4} (10,000 years return period); c) 10^{-5} (100,000 years return period); d) 10^{-6} (1,000,000 years return period); e) 10^{-7} (10,000,000 years return period). The size of the symbols is proportional to the logic-tree weight assigned to each branch.

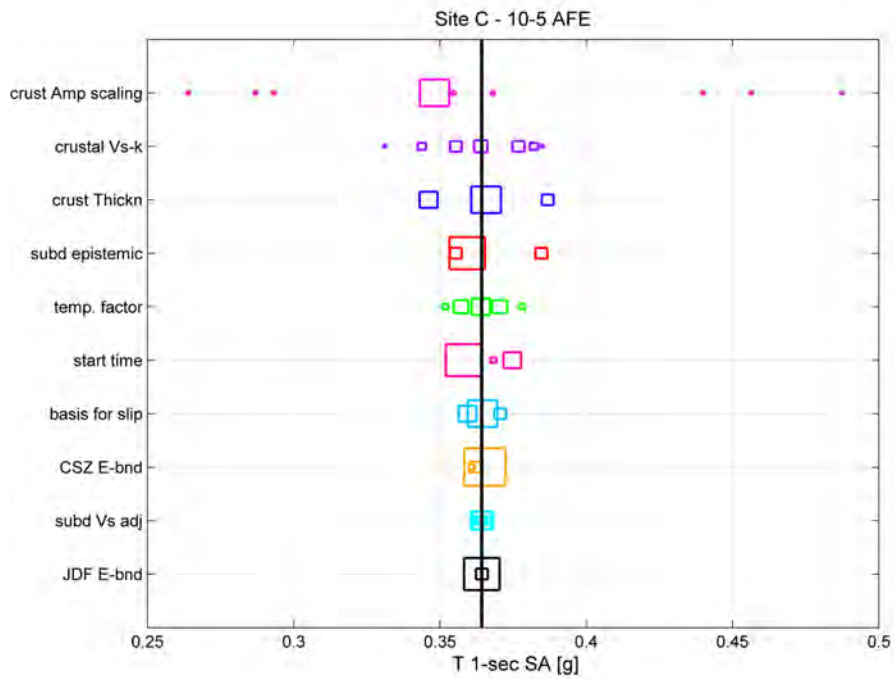

(c)

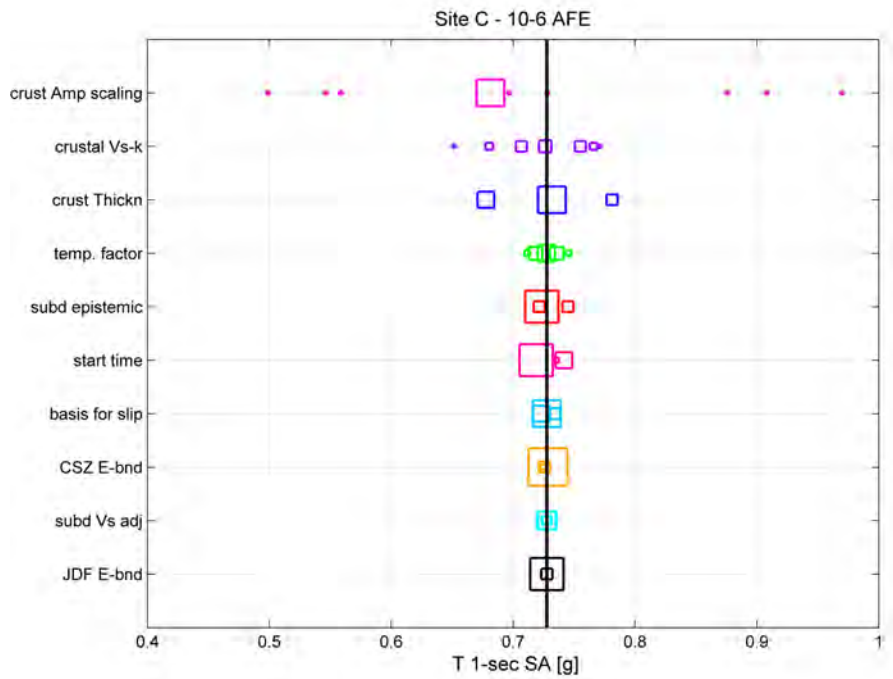

(d)

Figure 10.69. (contd)

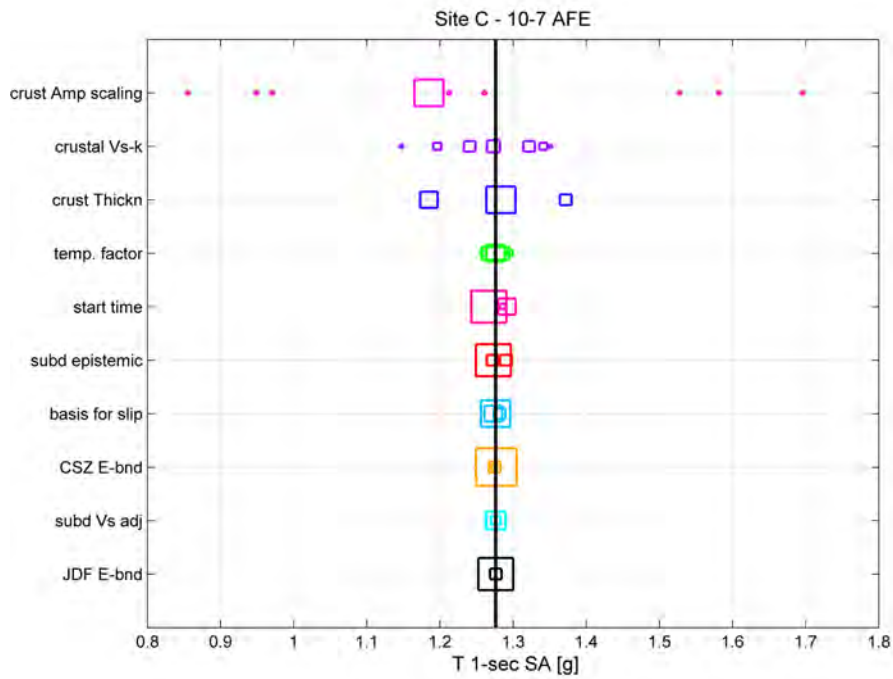

(e)

Figure 10.69. (contd)

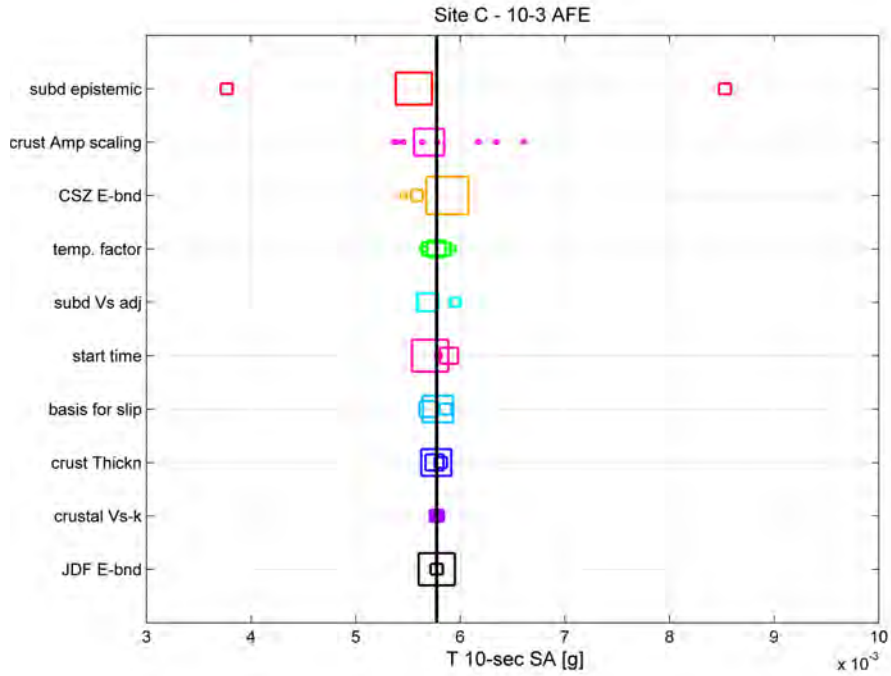

(a)

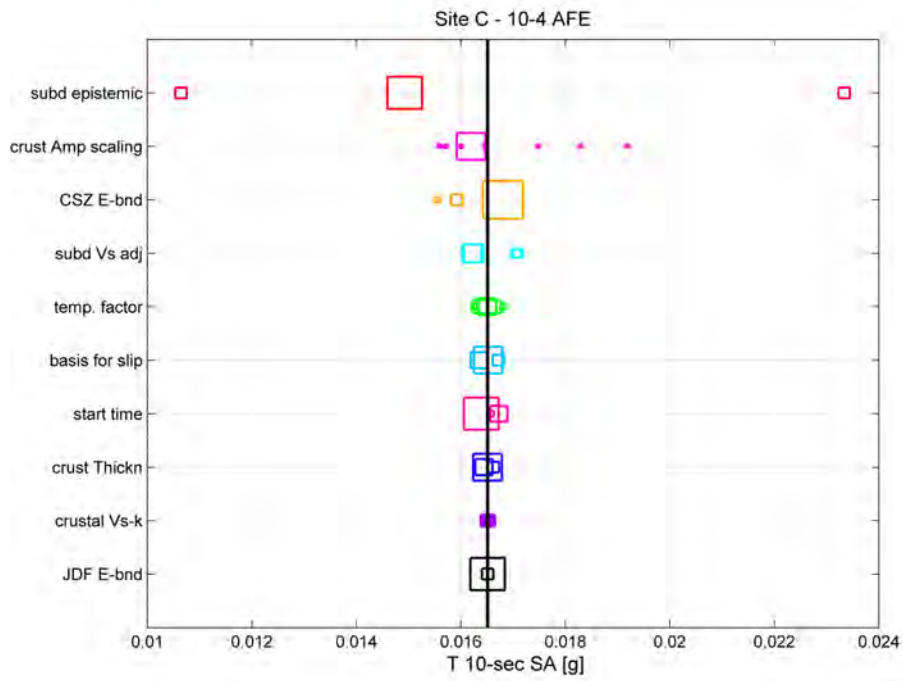

(b)

Figure 10.70. Tornado plot for Site C and T 10-sec spectral acceleration at AFEs of: a) 10^{-3} (1000 years return period); b) 10^{-4} (10,000 years return period); c) 10^{-5} (100,000 years return period); d) 10^{-6} (1,000,000 years return period); e) 10^{-7} (10,000,000 years return period). The size of the symbols is proportional to the logic-tree weight assigned to each branch.

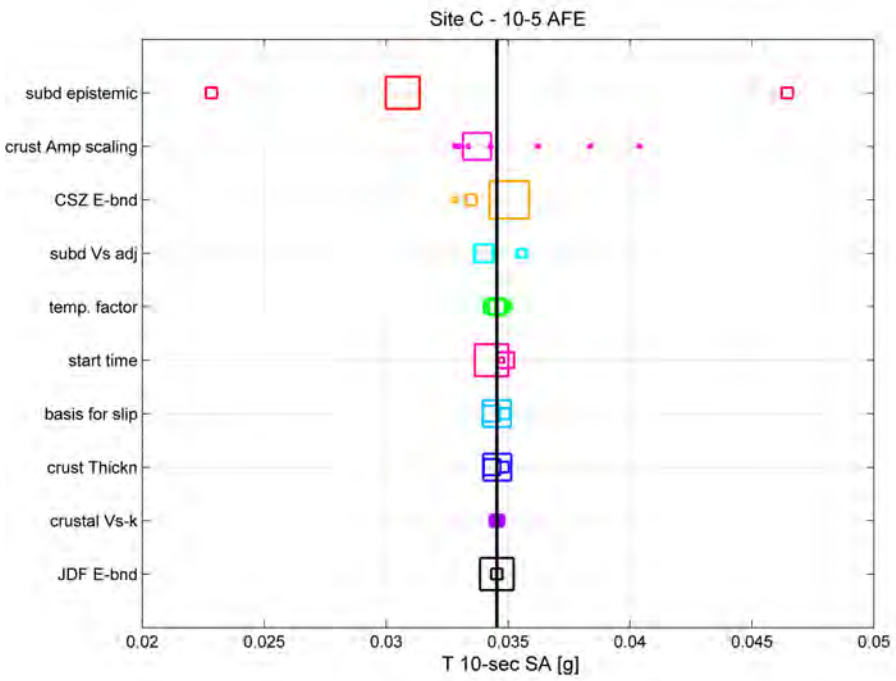

(c)

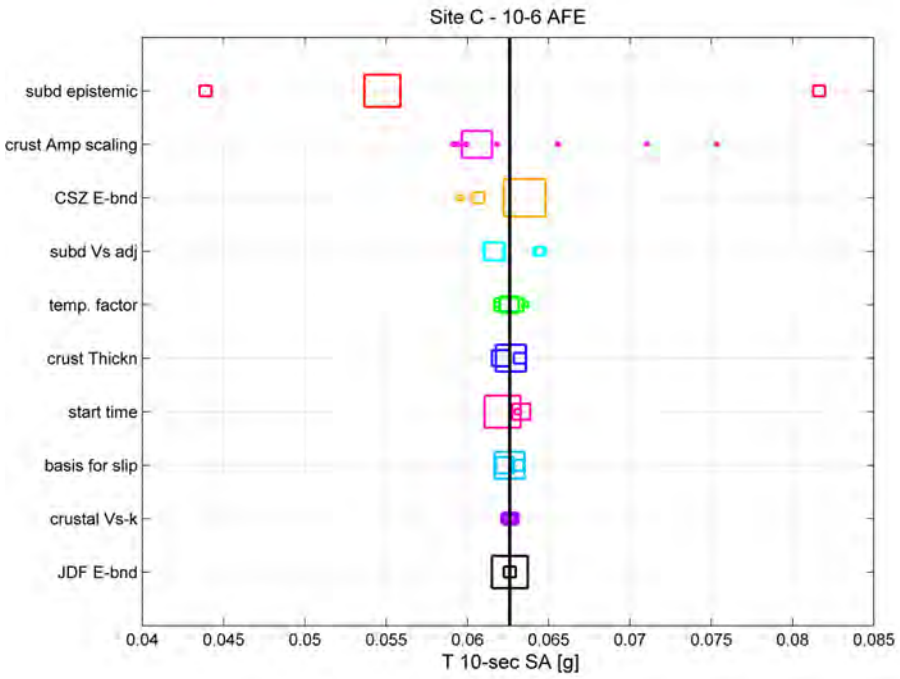

(d)

Figure 10.70. (contd)

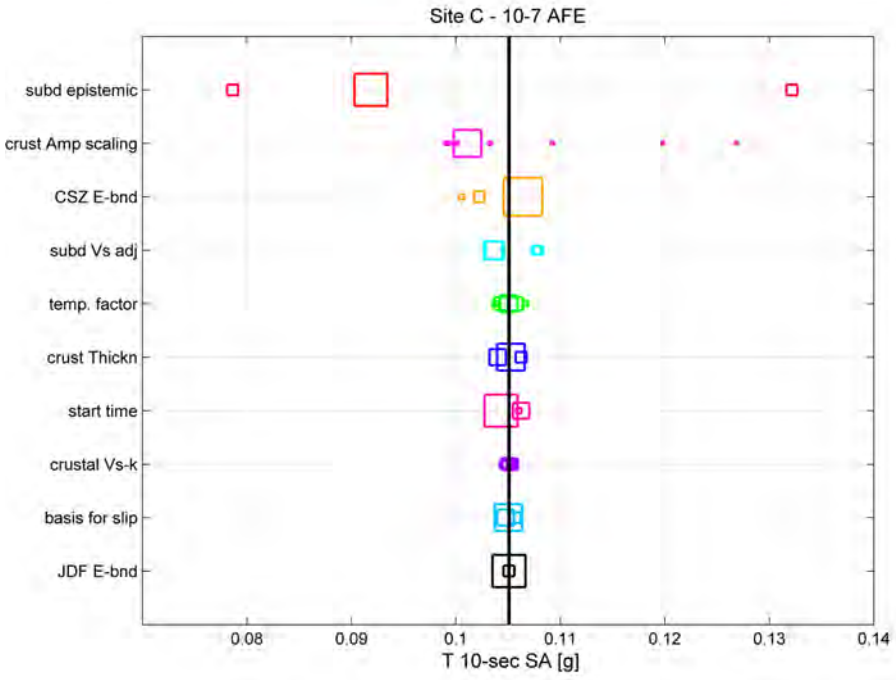

(e)

Figure 10.70. (contd)

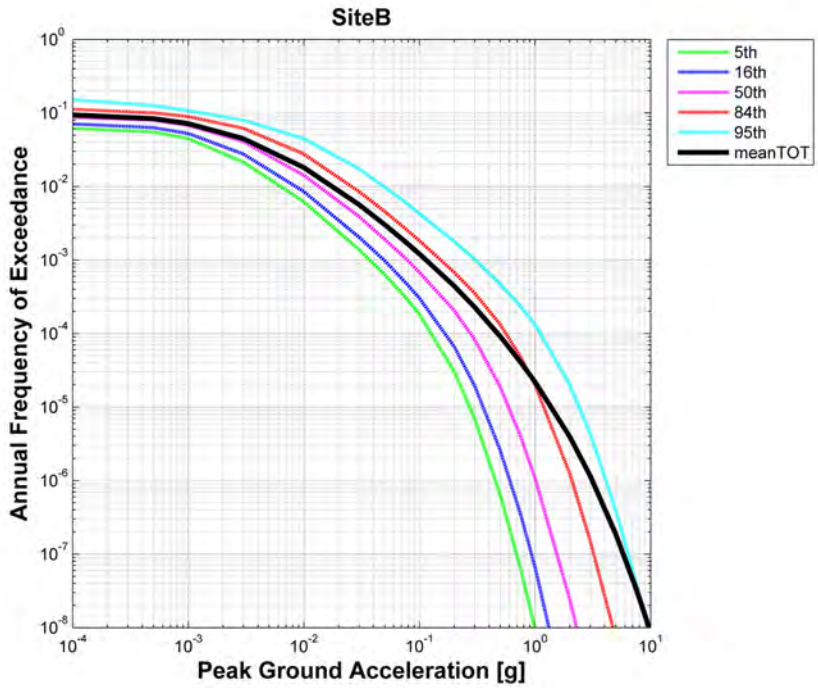

(a)

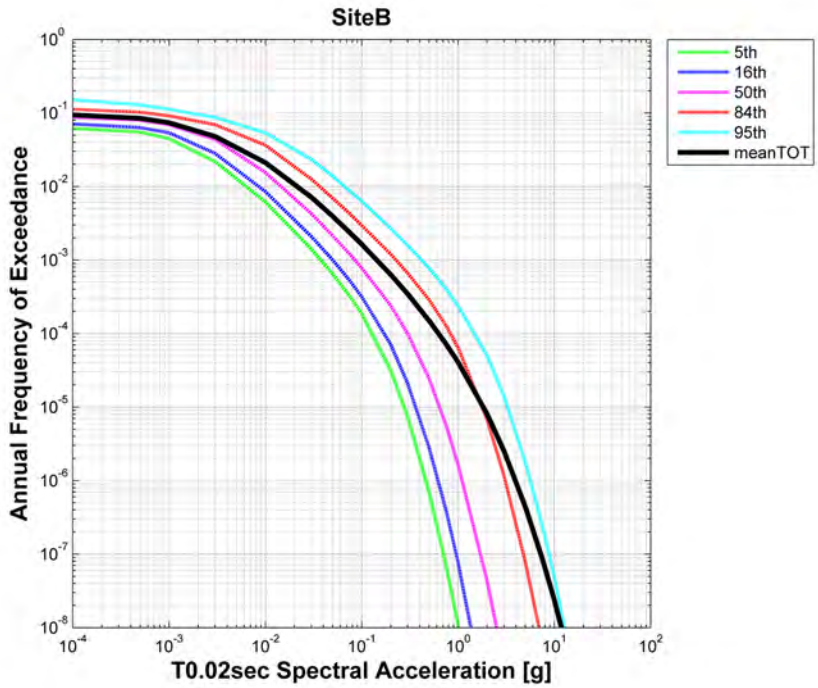

(b)

Figure 10.71. Total mean seismic hazard at Site B and percentiles: a) PGA; b) T 0.02-sec; c) T 0.03-sec; d) T 0.04-sec; e) T 0.05-sec; f) T 0.07-sec; g) T 0.10-sec; h) T 0.15-sec; i) T 0.20-sec; j) T 0.30-sec; k) T 0.40-sec; l) T 0.50-sec; m) T 0.75-sec; n) T 1.0-sec; o) T 1.5-sec; p) T 2.0-sec; q) T 3.0-sec; r) T 5.0-sec; s) T 7.5-sec; t) T 10-sec spectral acceleration.

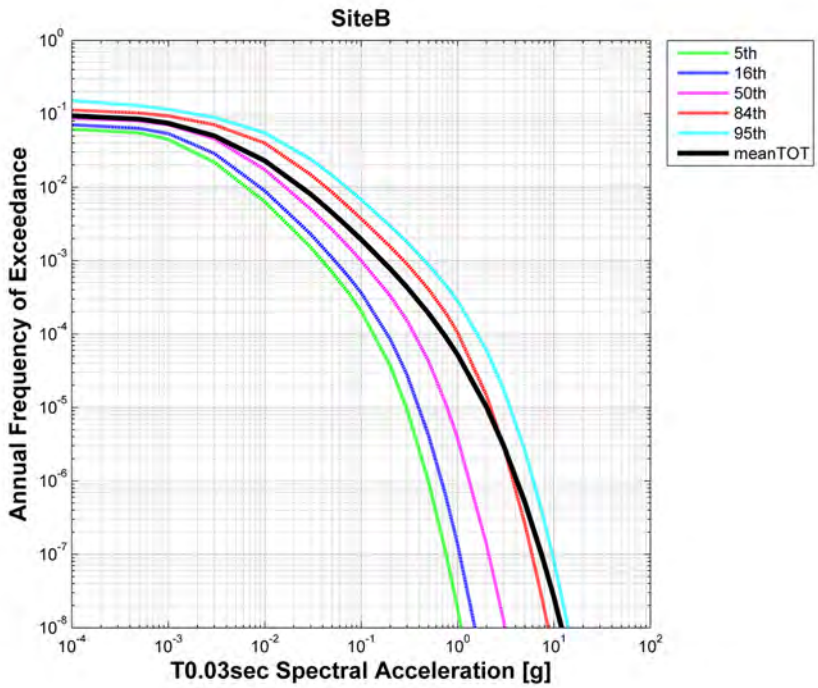

(c)

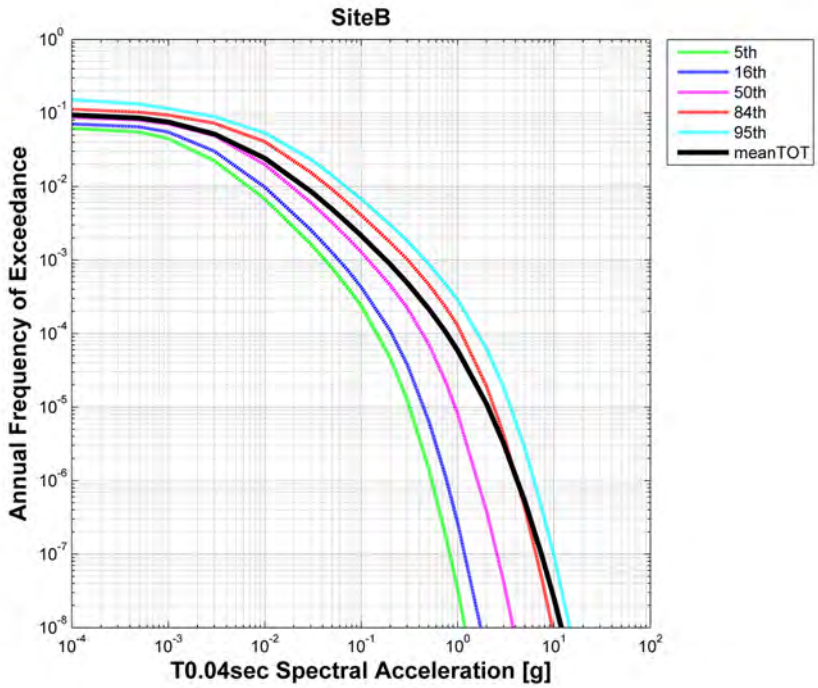

(d)

Figure 10.71. (contd)

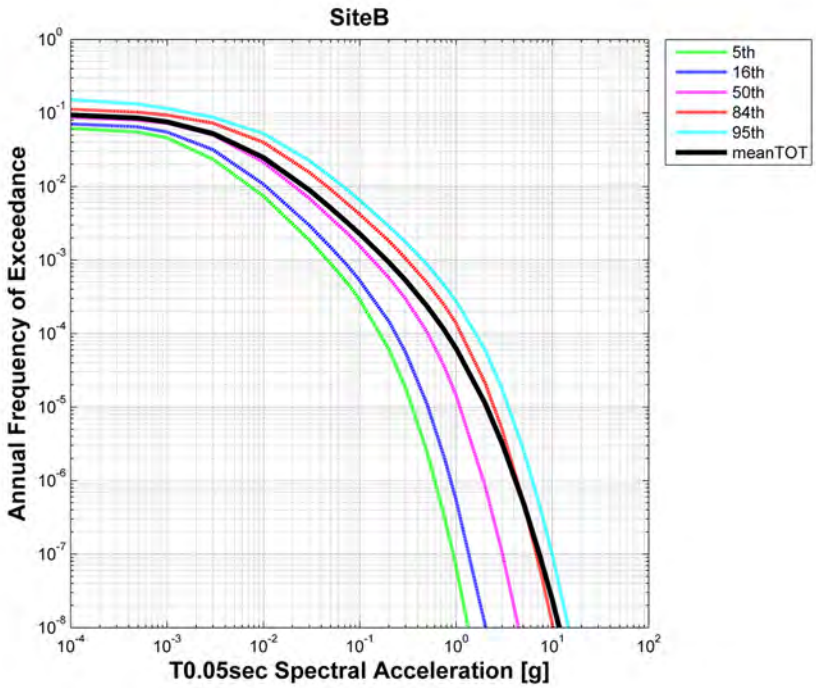

(e)

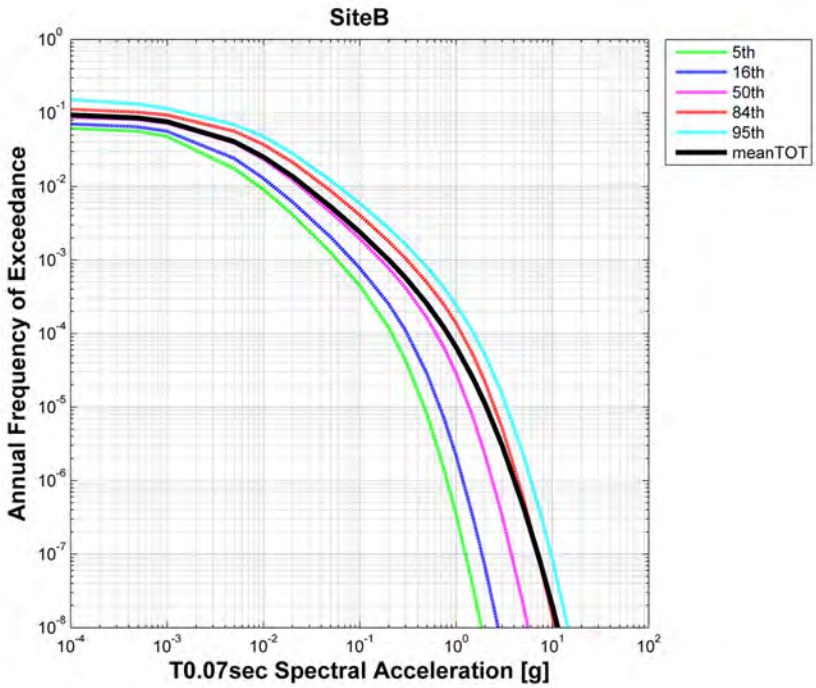

(f)

Figure 10.71. (contd)

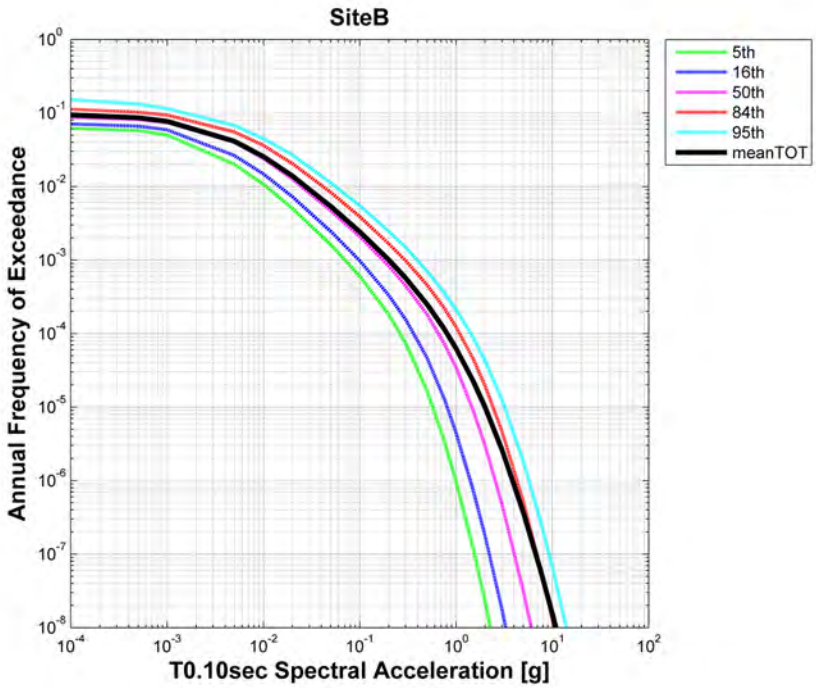

(g)

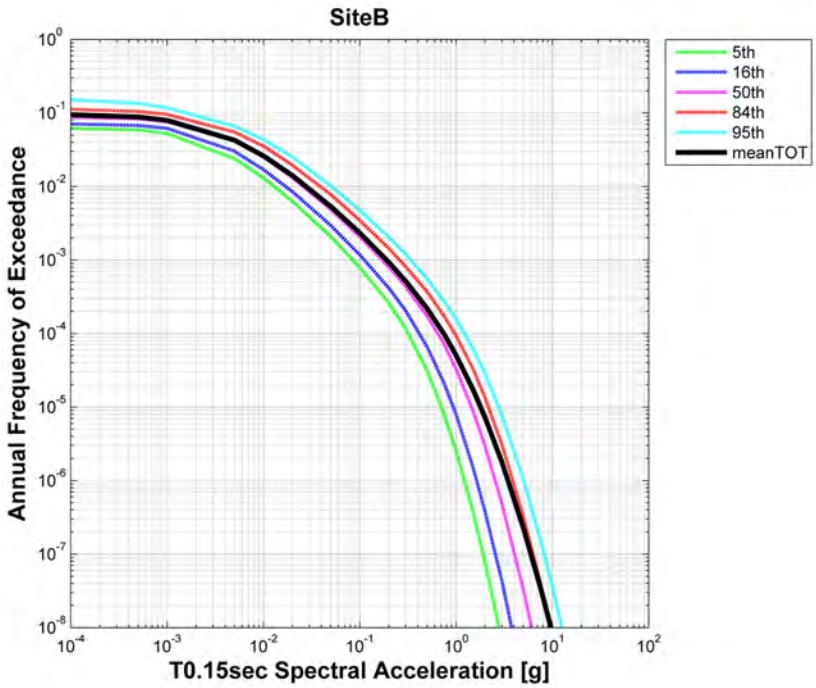

(h)

Figure 10.71. (contd)

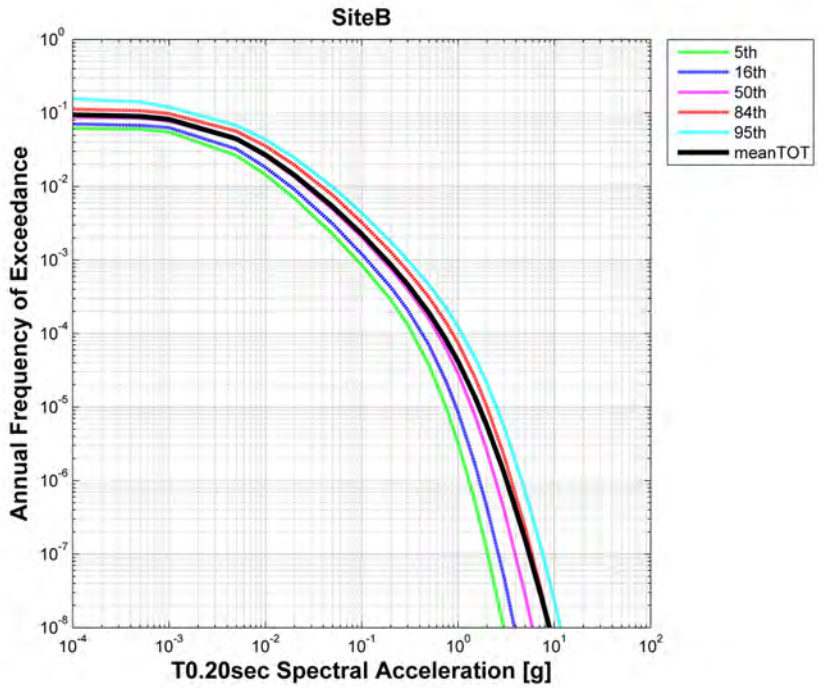

(i)

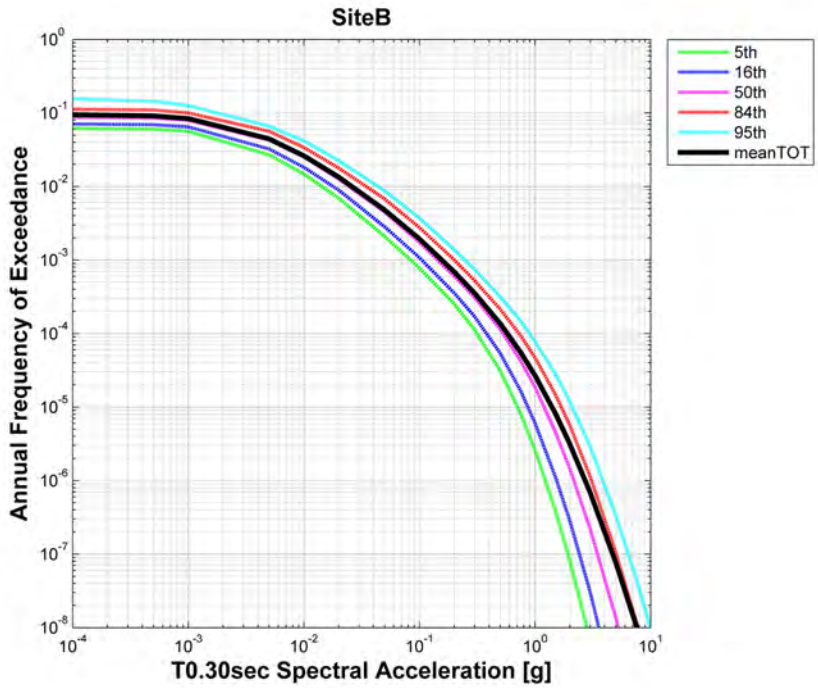

(j)

Figure 10.71. (contd)

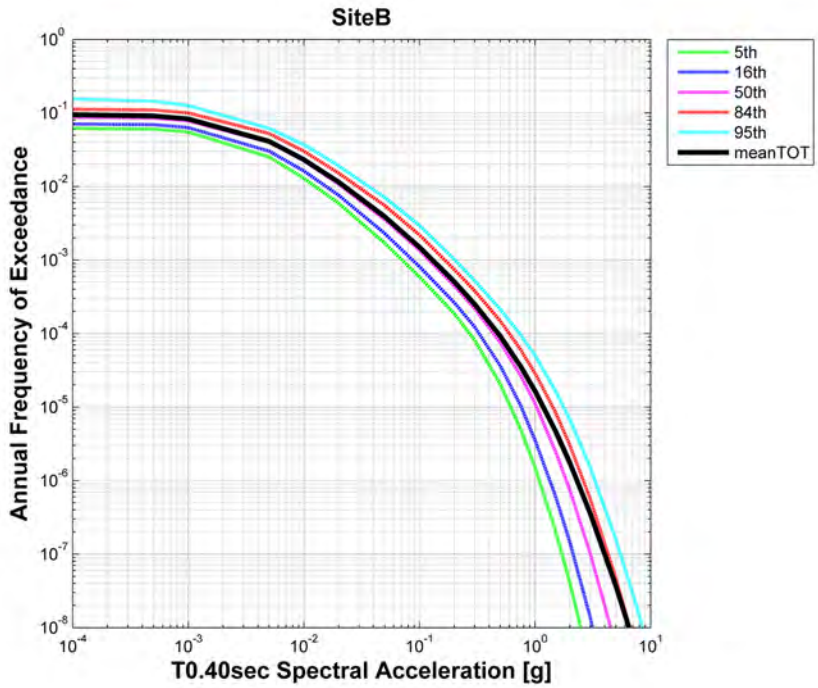

(k)

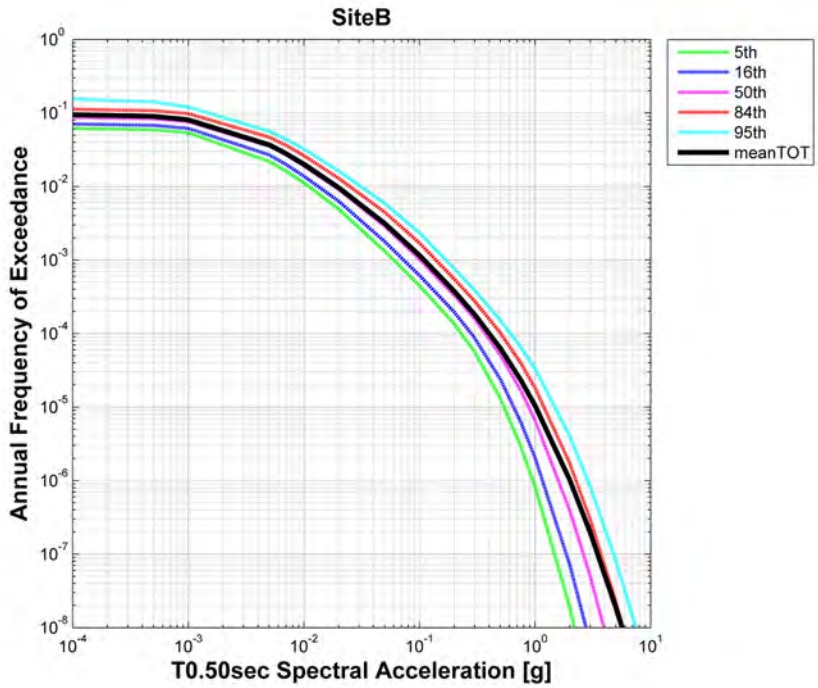

(l)

Figure 10.71. (contd)

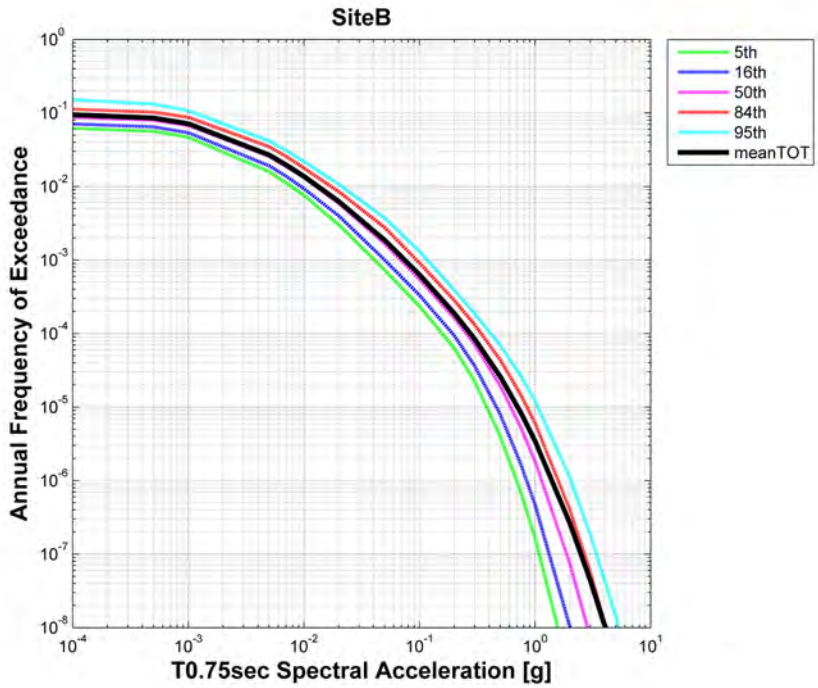

(m)

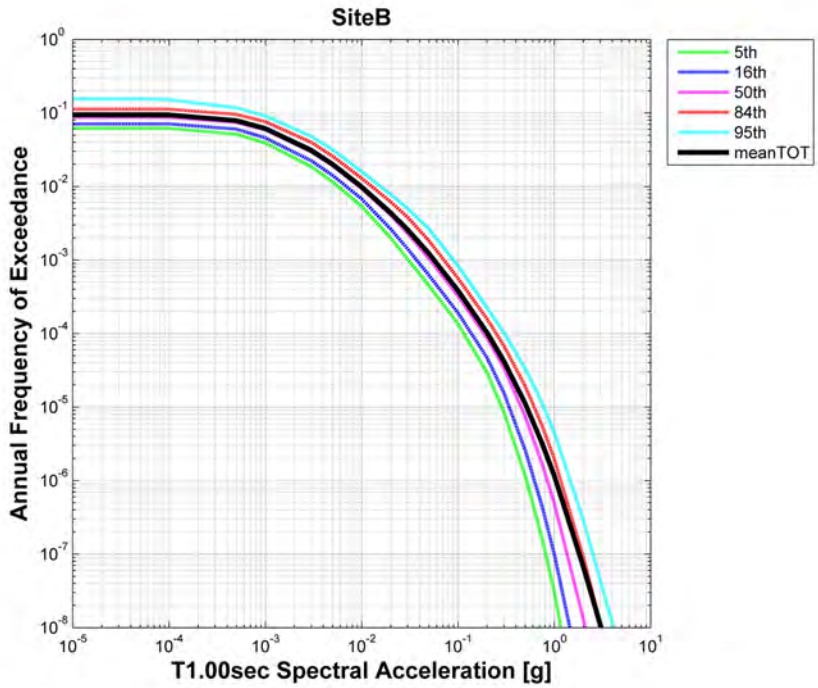

(n)

Figure 10.71. (contd)

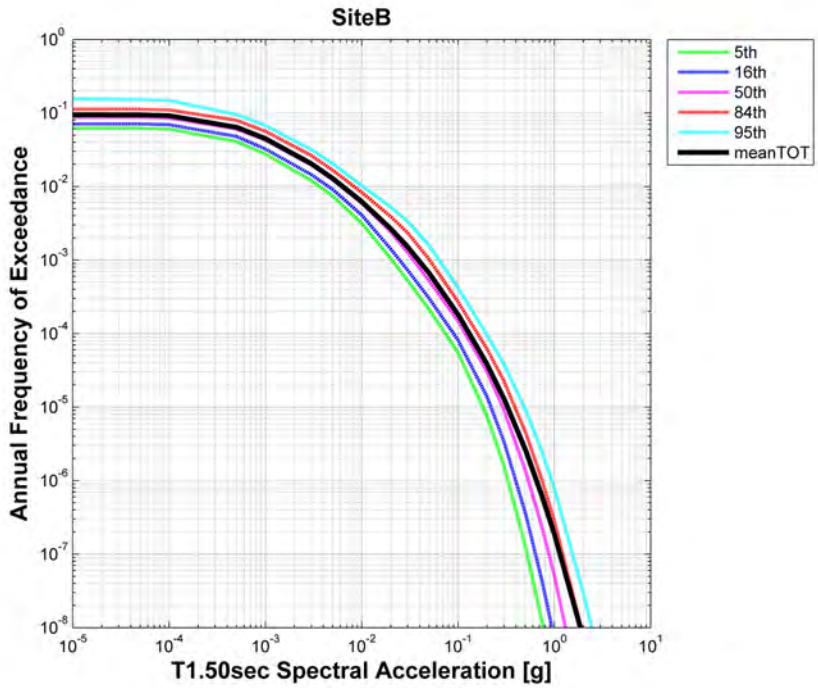

(o)

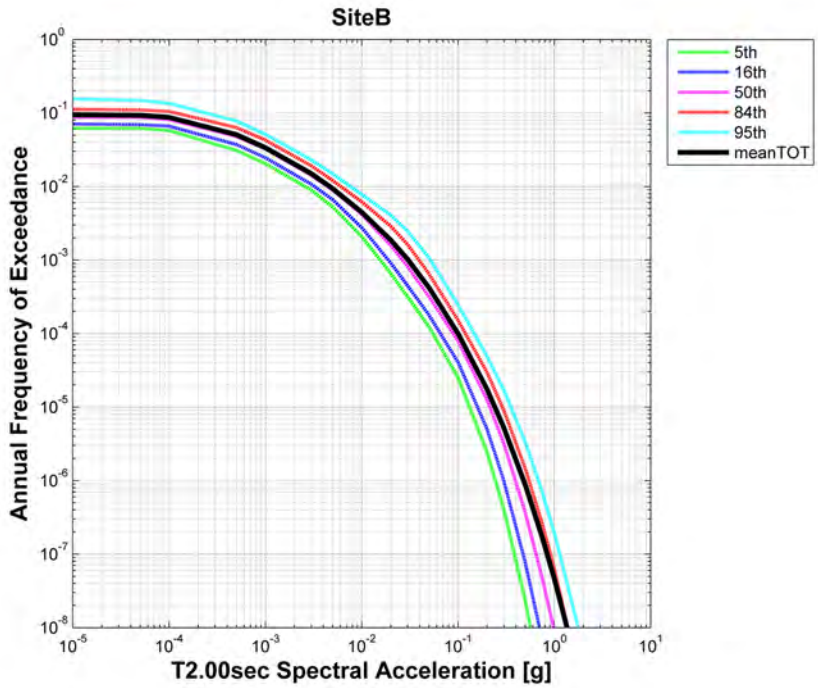

(p)

Figure 10.71. (contd)

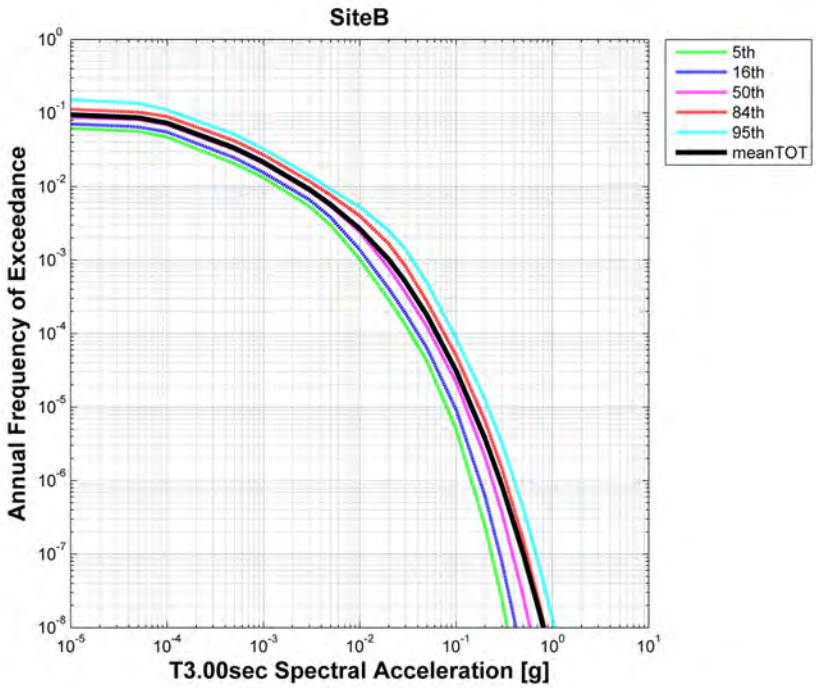

(q)

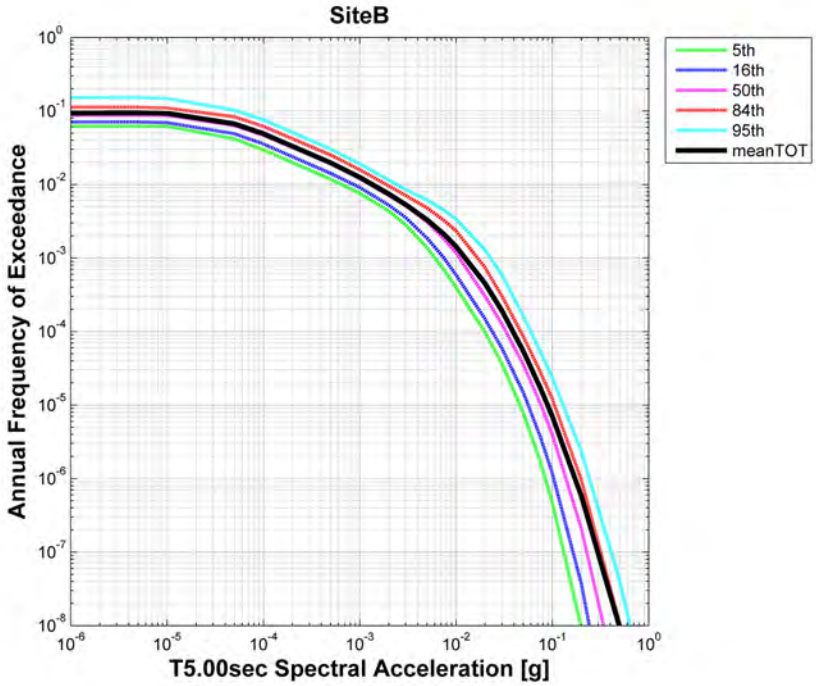

(r)

Figure 10.71. (contd)

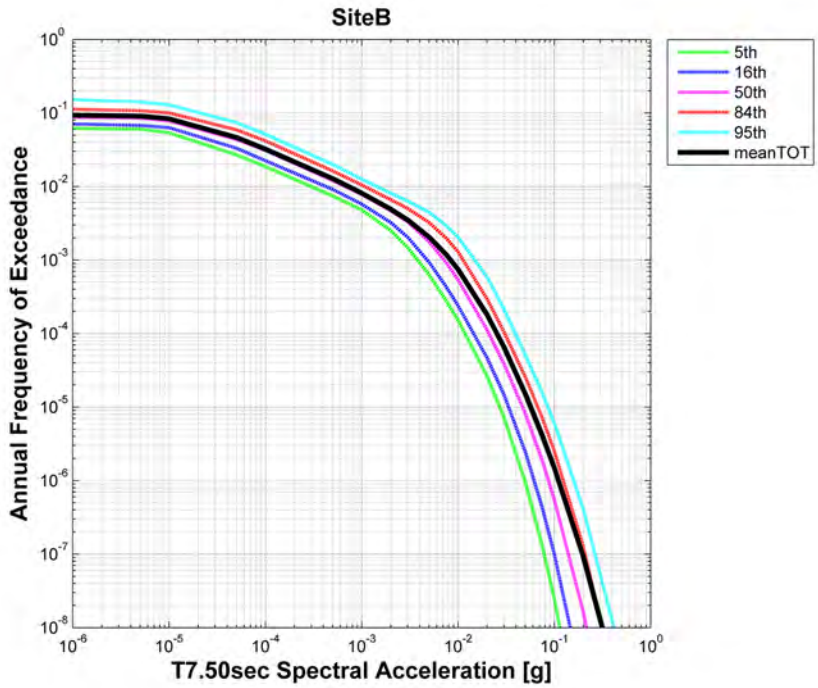

(s)

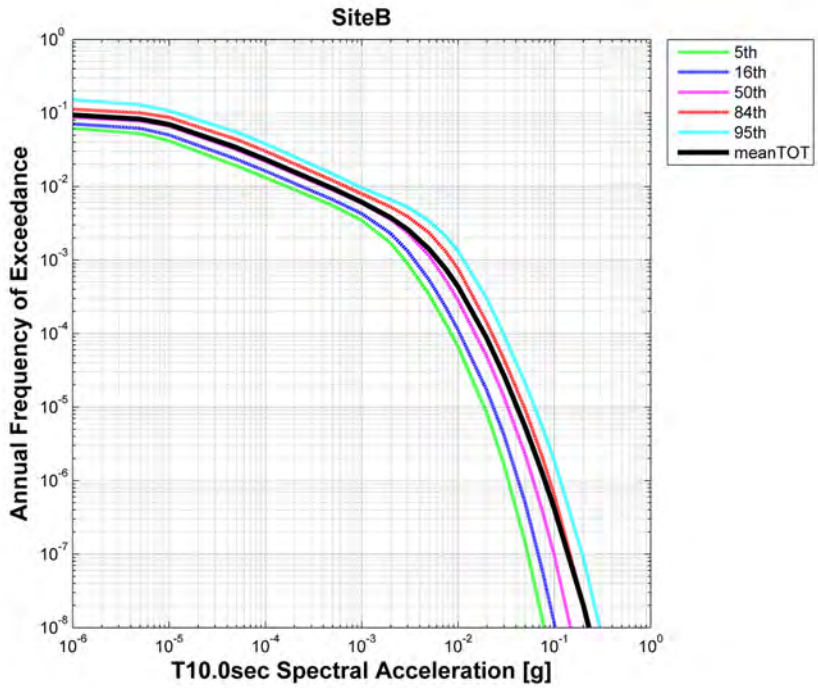

(t)

Figure 10.71. (contd)

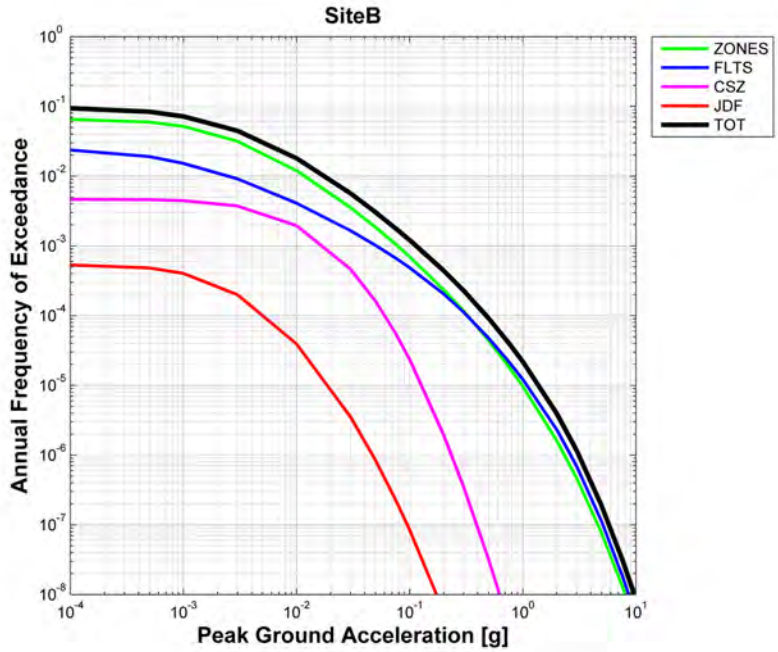

(a)

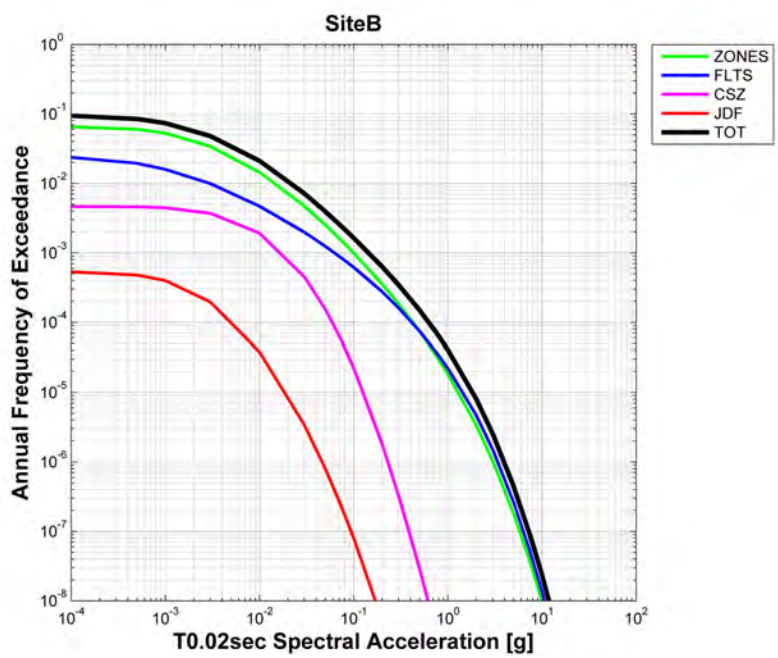

(b)

Figure 10.72. Comparison between the total mean seismic hazard at Site B (black curve) and the contribution of crustal source zones (green curve), faults (blue curve), the Cascadia interface (CSZ - magenta curve), and Cascadia intraslab source (JDF - red curve): a) PGA; b) T 0.02-sec; c) T 0.03-sec; d) T 0.04-sec; e) T 0.05-sec; f) T 0.07-sec; g) T 0.10-sec; h) T 0.15-sec; i) T 0.20-sec; j) T 0.30-sec; k) T 0.40-sec; l) T 0.50-sec; m) T 0.75-sec; n) T 1.0-sec; o) T 1.5-sec; p) T 2.0-sec; q) T 3.0-sec; r) T 5.0-sec; s) T 7.5-sec; t) T 10-sec spectral acceleration.

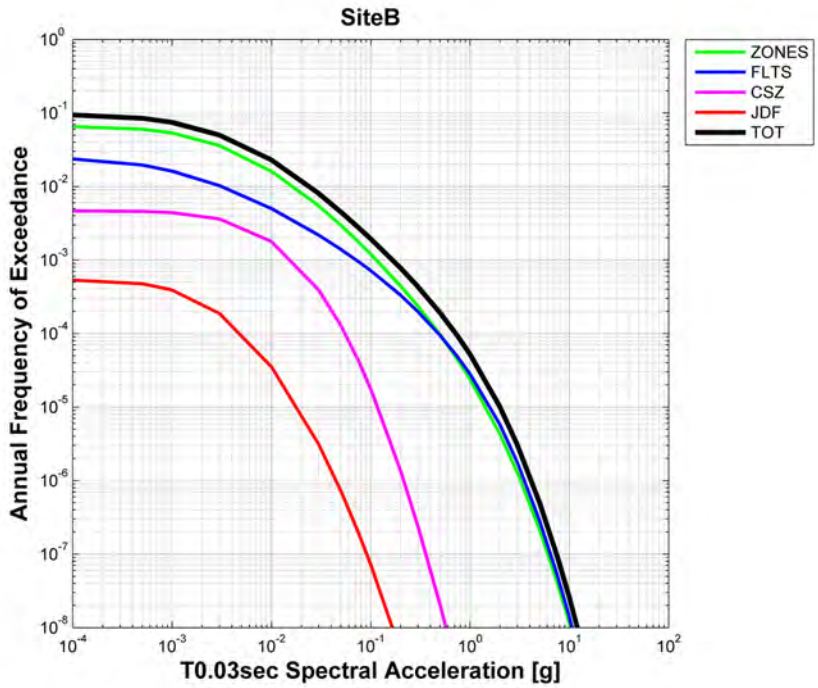

(c)

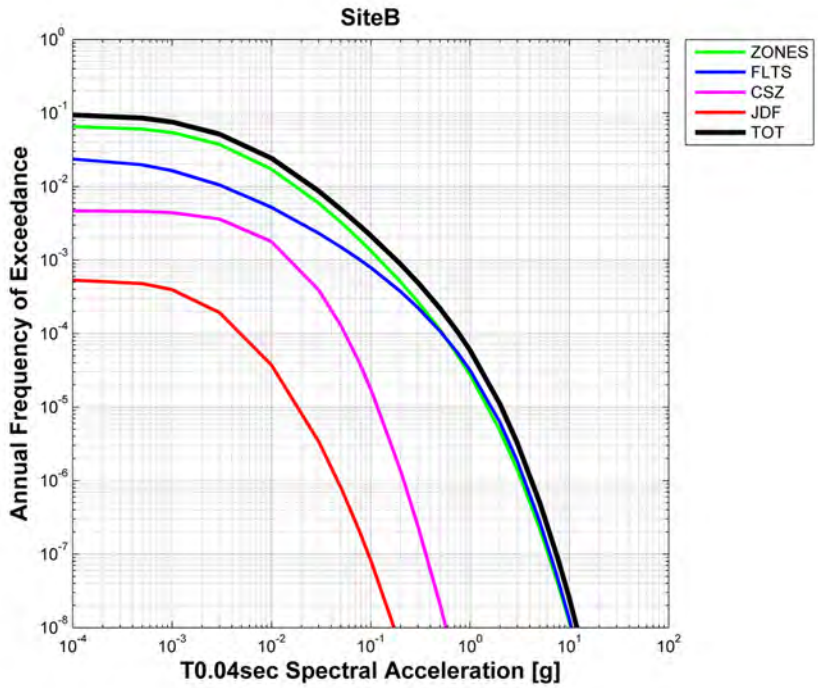

(d)

Figure 10.72. (contd)

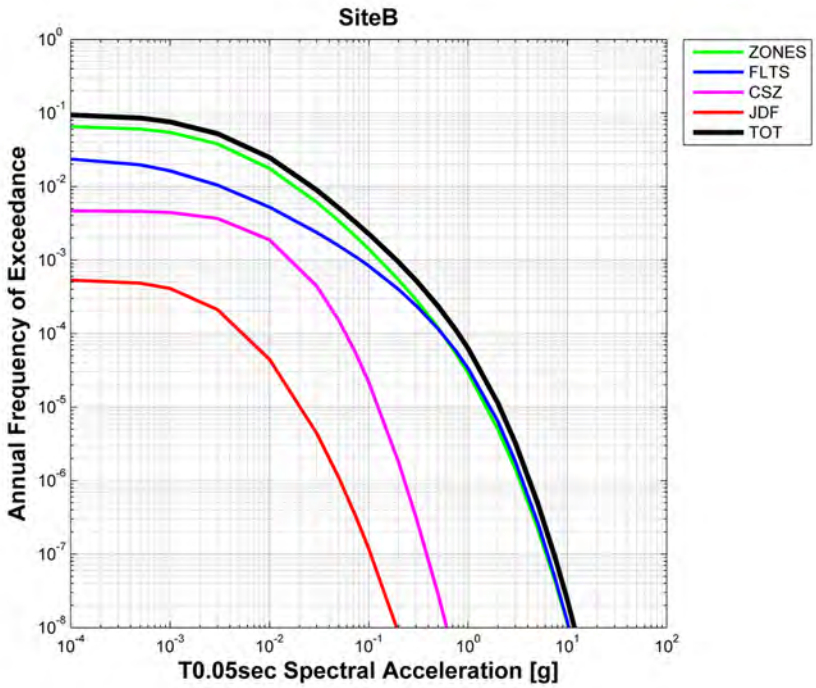

(e)

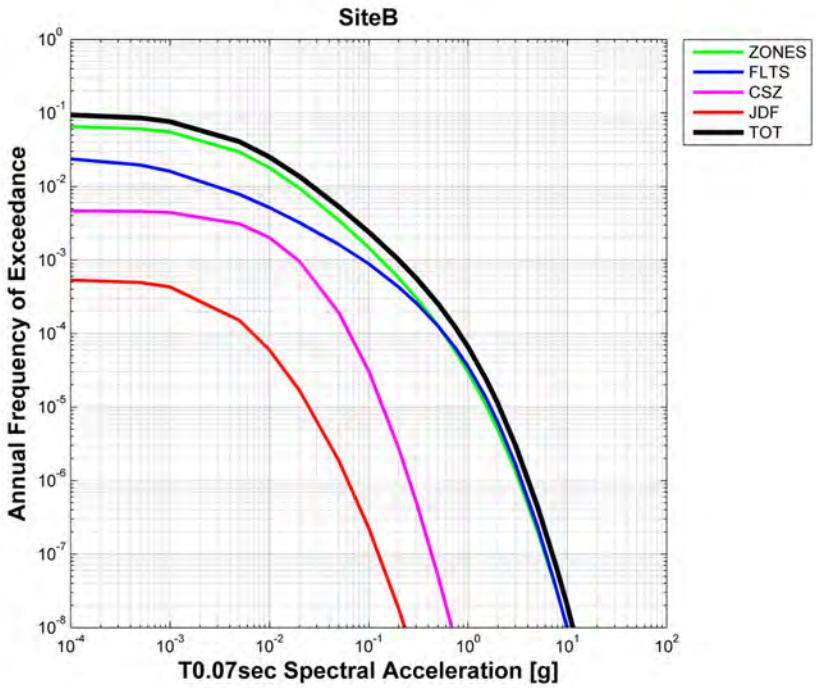

(f)

Figure 10.72. (contd)

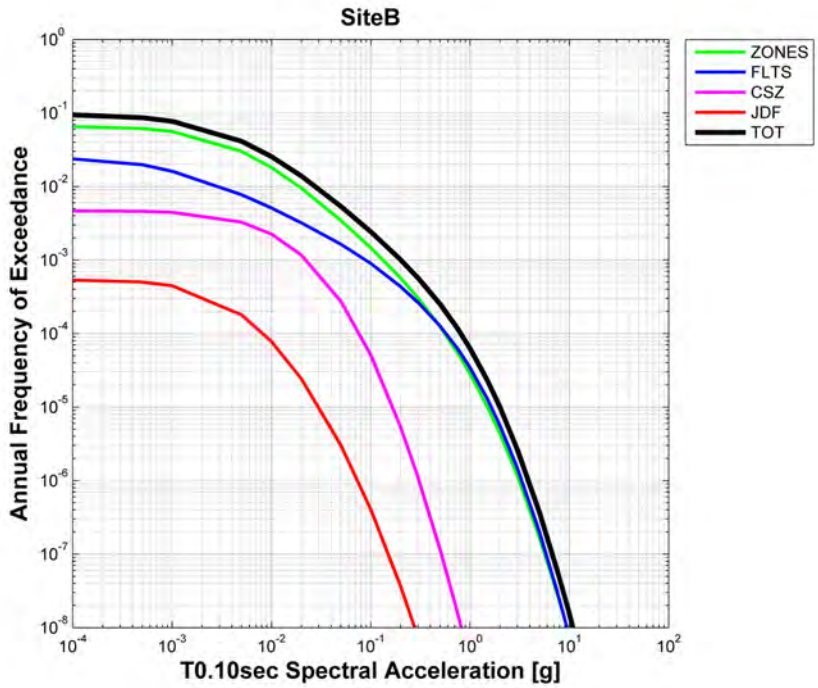

(g)

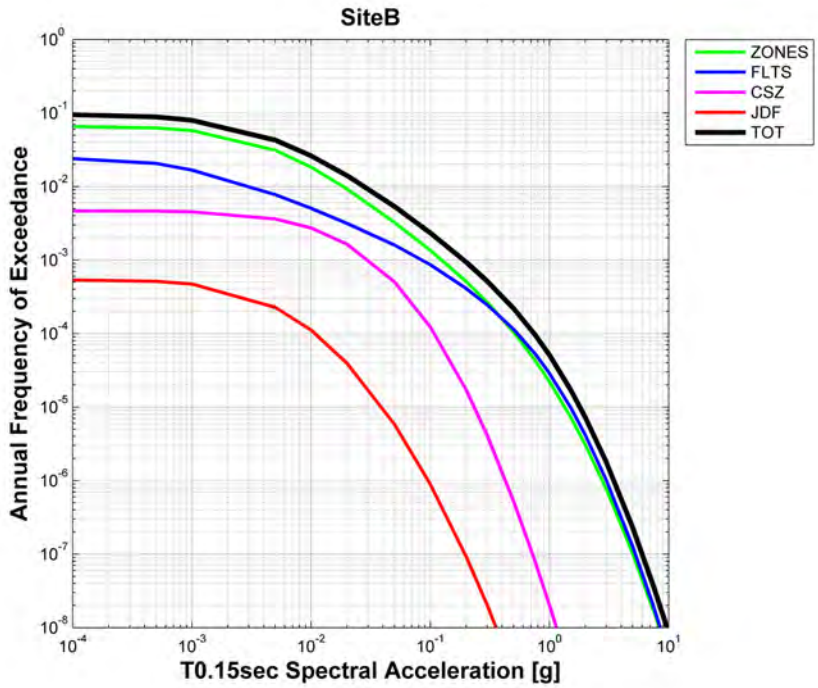

(h)

Figure 10.72. (contd)

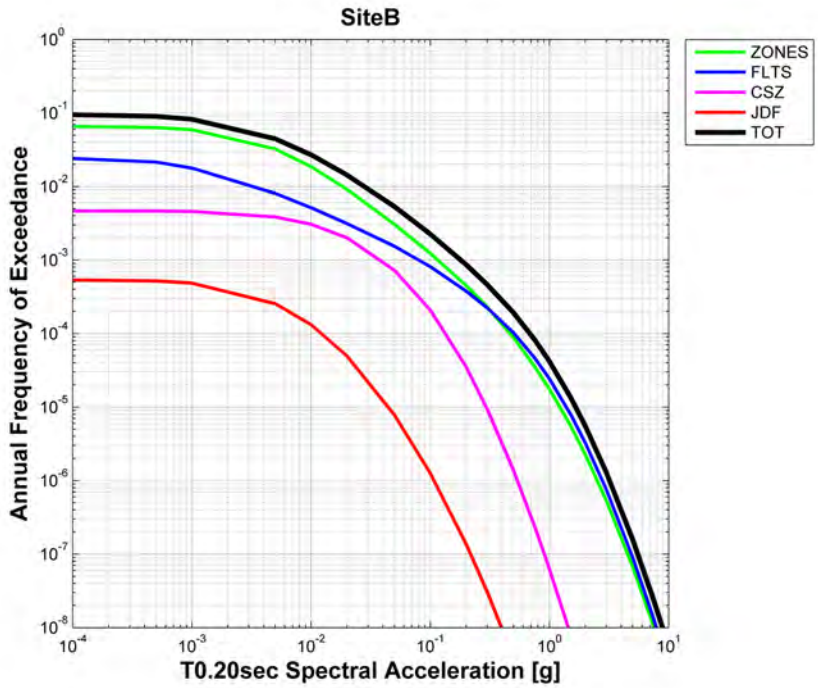

(i)

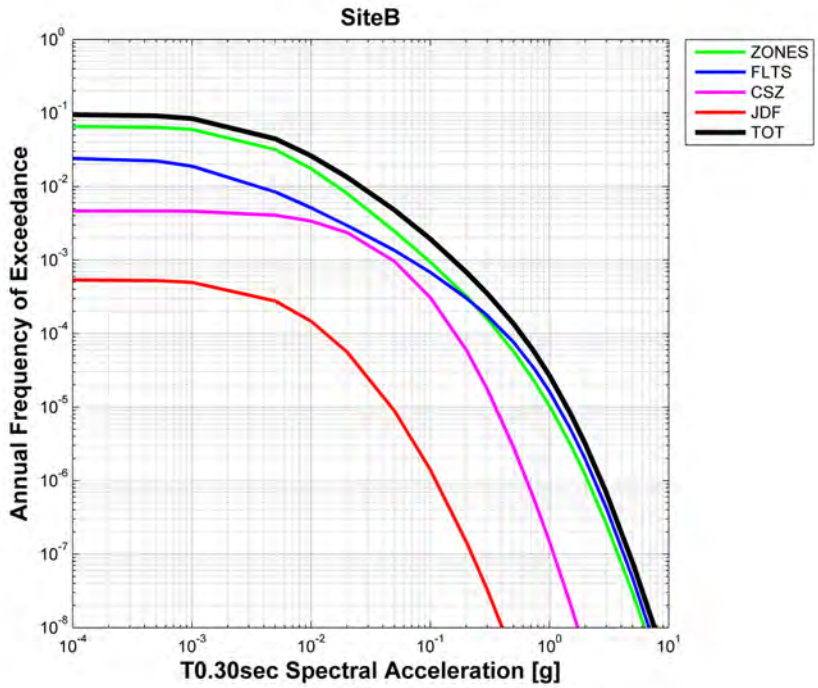

(j)

Figure 10.72. (contd)

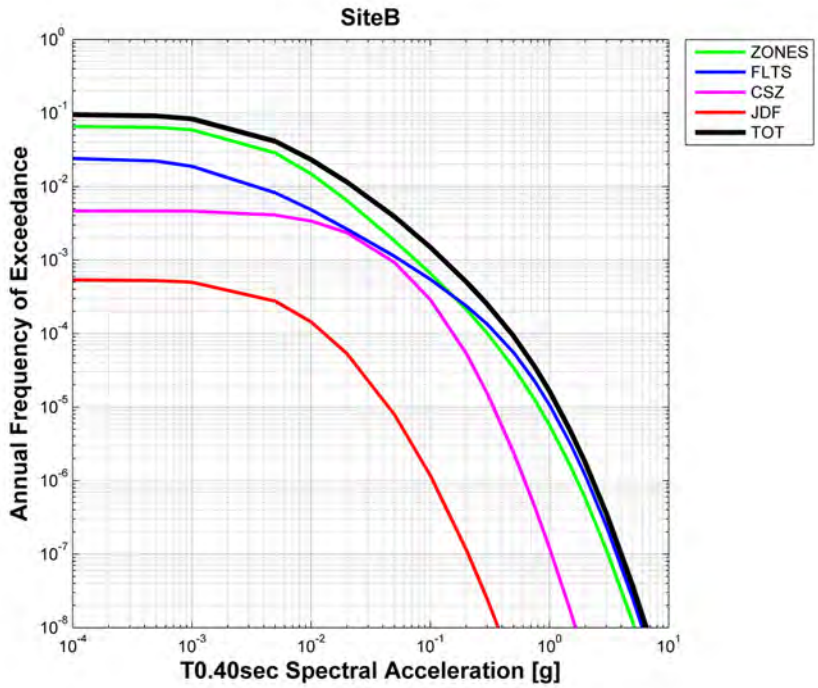

(k)

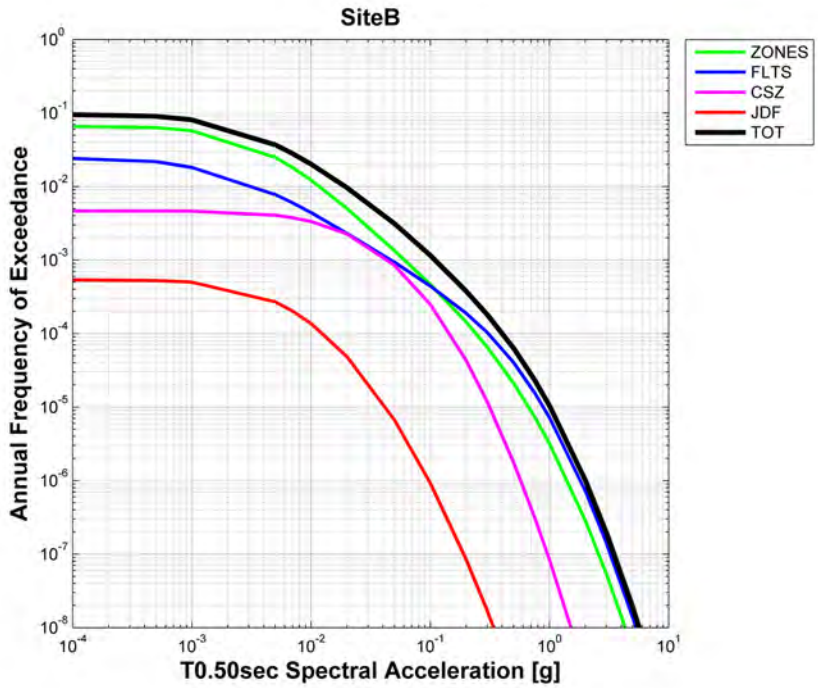

(l)

Figure 10.72. (contd)

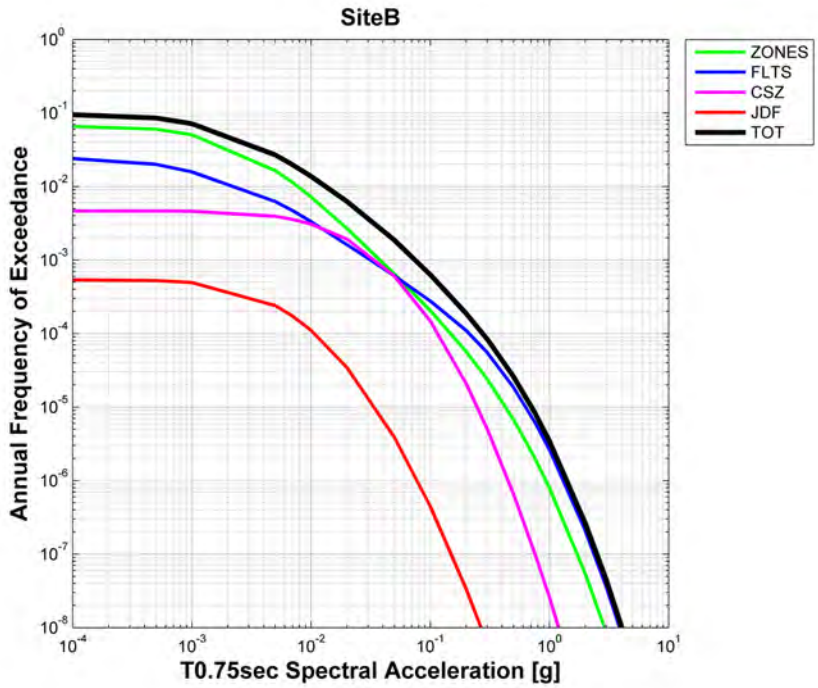

(m)

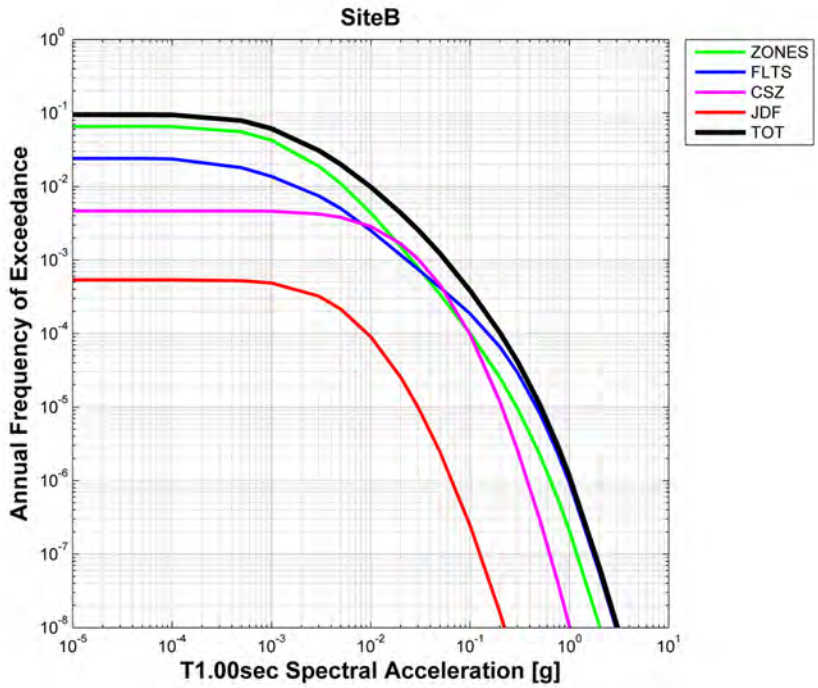

(n)

Figure 10.72. (contd)

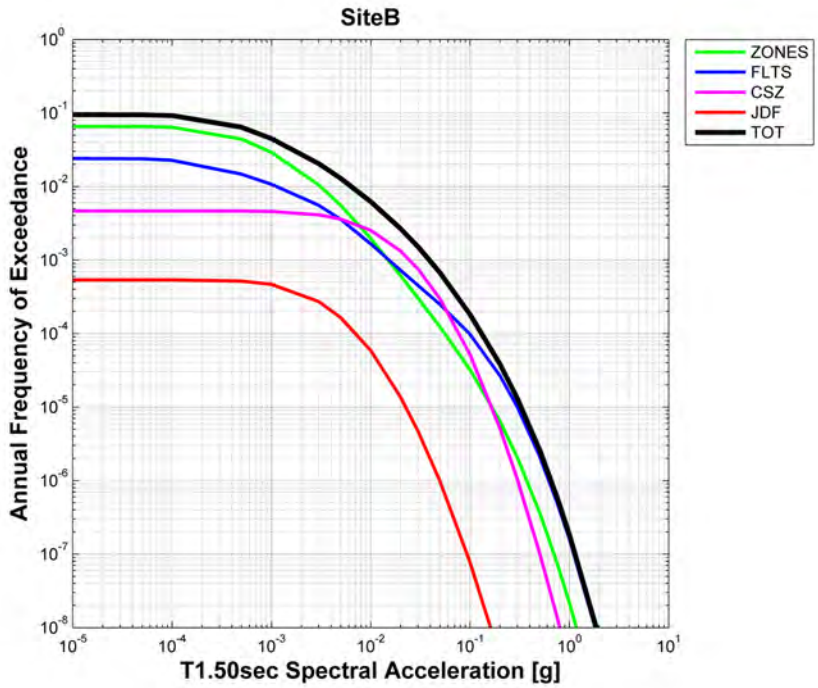

(o)

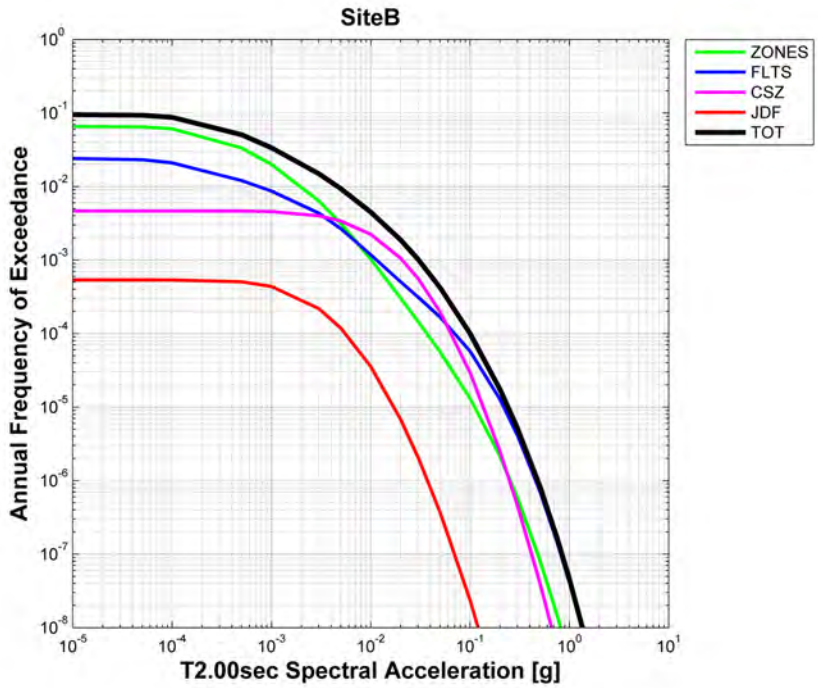

(p)

Figure 10.72. (contd)

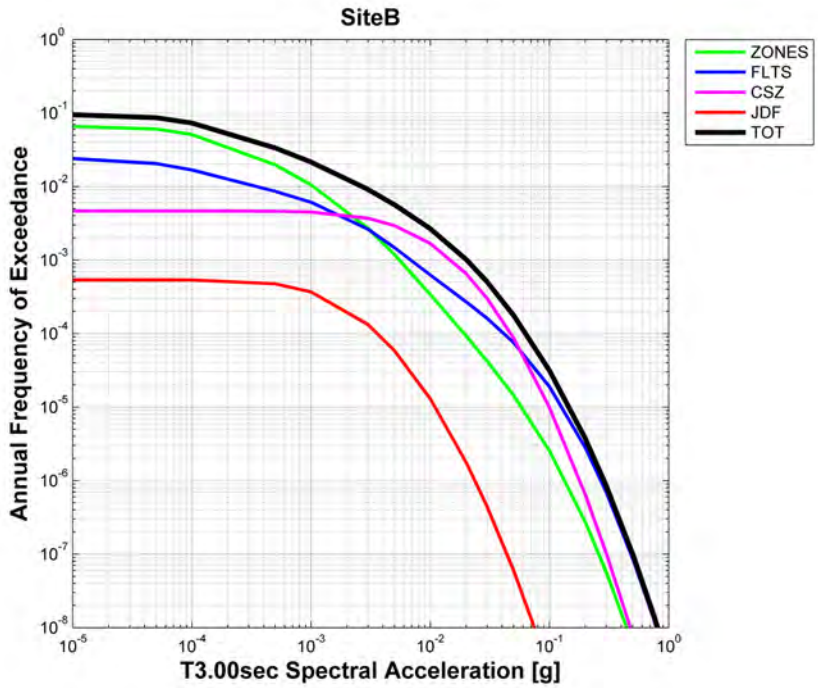

(q)

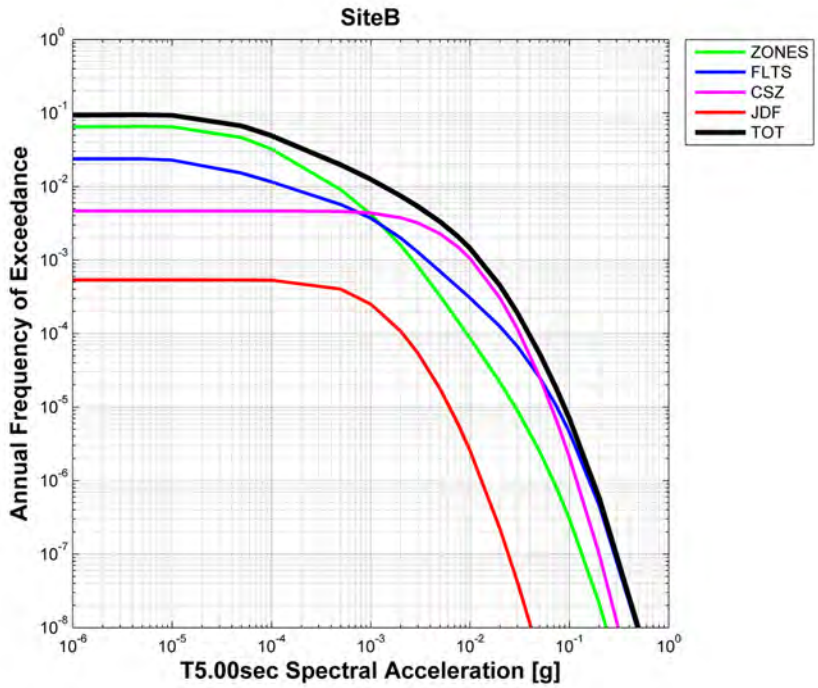

(r)

Figure 10.72. (contd)

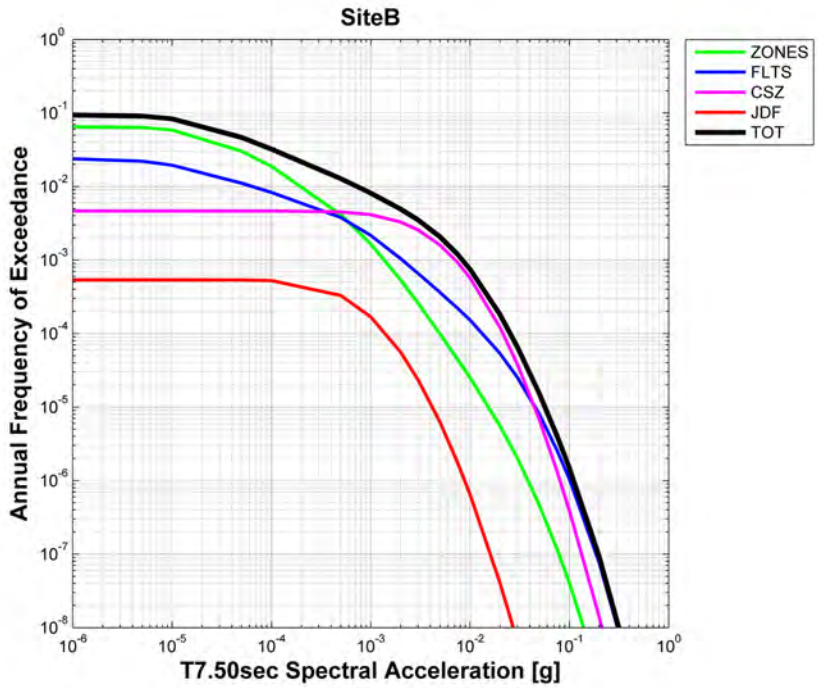

(s)

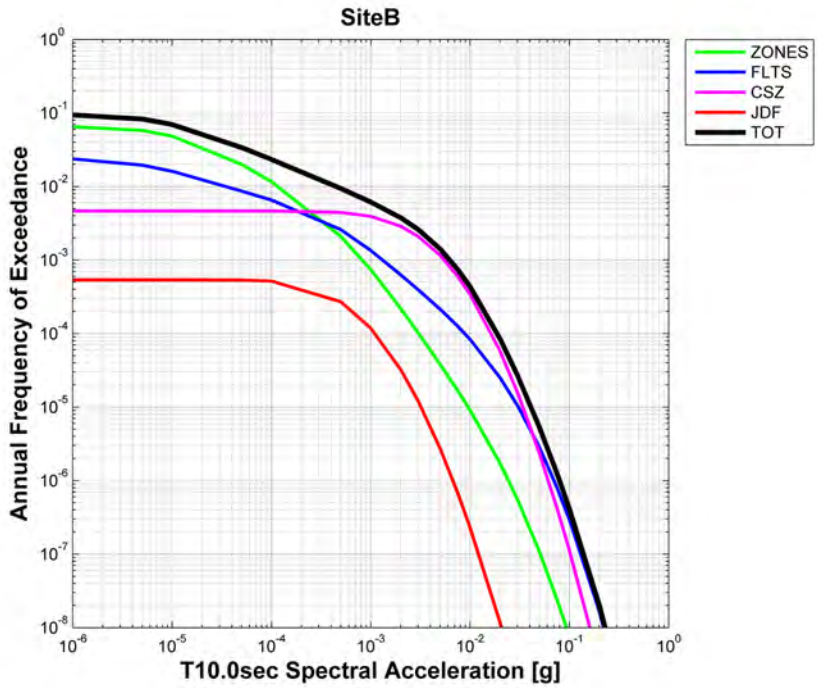

(t)

Figure 10.72. (contd)

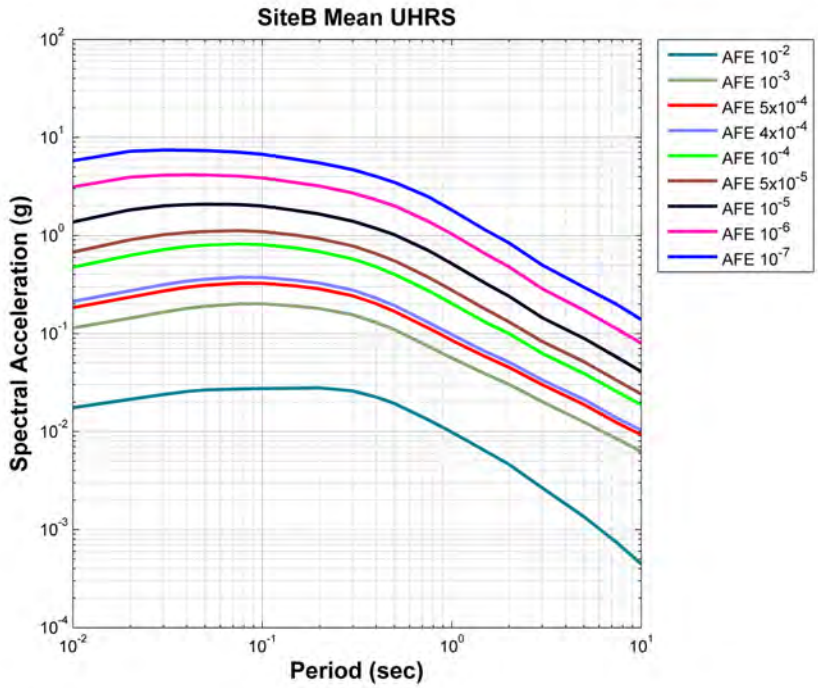

(a)

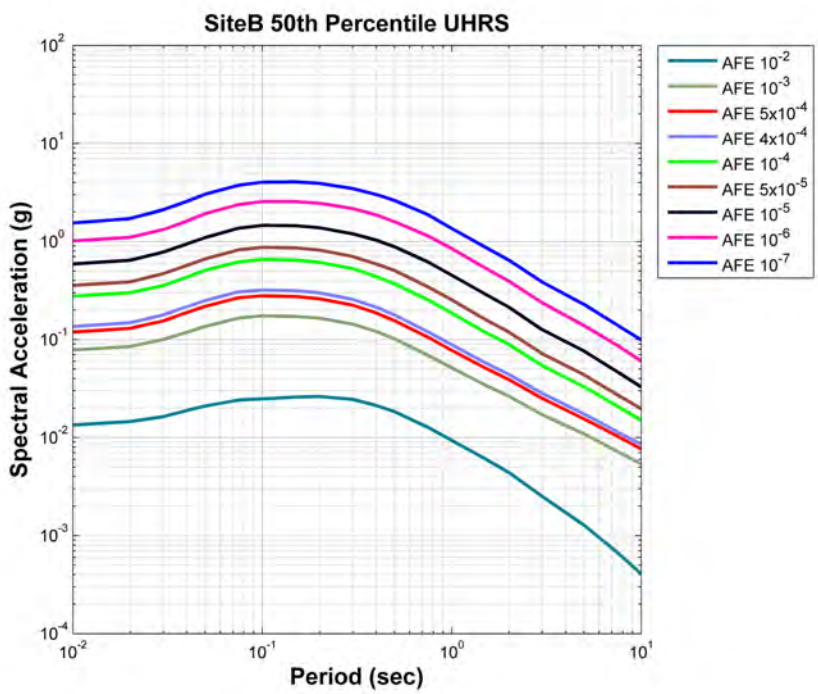

(b)

Figure 10.73. Uniform hazard response spectra at AFEs of 10^{-2}, 10^{-3}, 5×10^{-4}, 4×10^{-4}, 10^{-4}, 5×10^{-5}, 10^{-6}, 10^{-7} (return periods of 100, 1,000, 2,000, 2,500, 10,000, 20,000, 100,000, 1 million, and 10 million years) for: a) mean hazard; b) 50th percentile hazard; c) 84th percentile hazard.

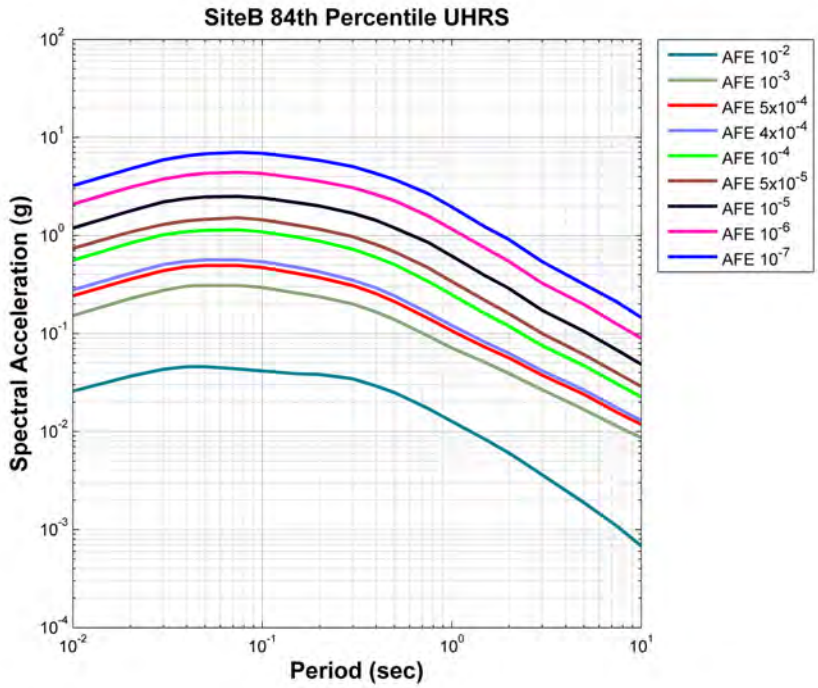

(c)

Figure 10.73. (contd)

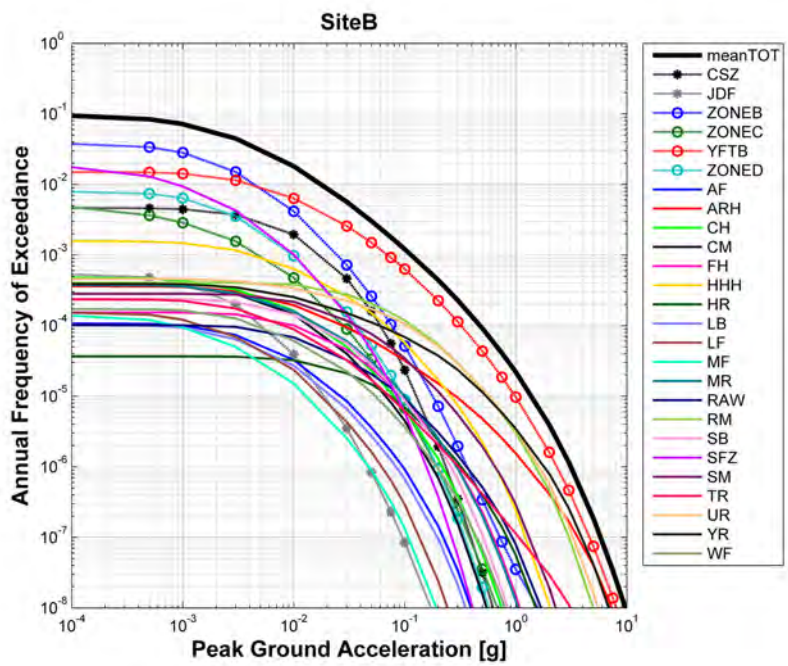

(a)

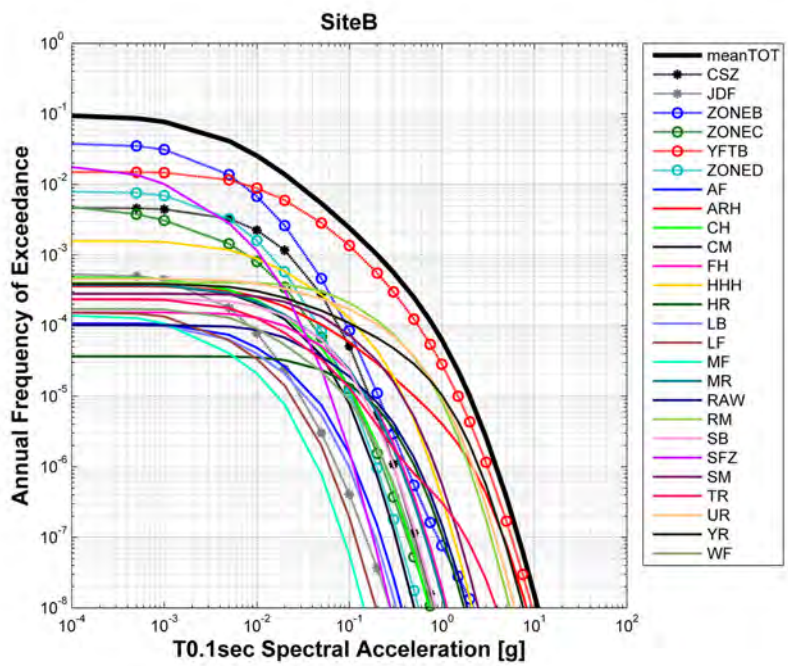

(b)

Figure 10.74. Comparison between the mean hazard curves at Site B obtained for each individual source. Subduction sources are shown by dotted star curves; crustal sources by dotted circle curves; and fault sources by solid curves: a) peak ground acceleration; b) T 0.1-sec; c) T 1-sec; d) T 10-sec spectral acceleration. Acronyms used in figures are listed in Table 10.13.

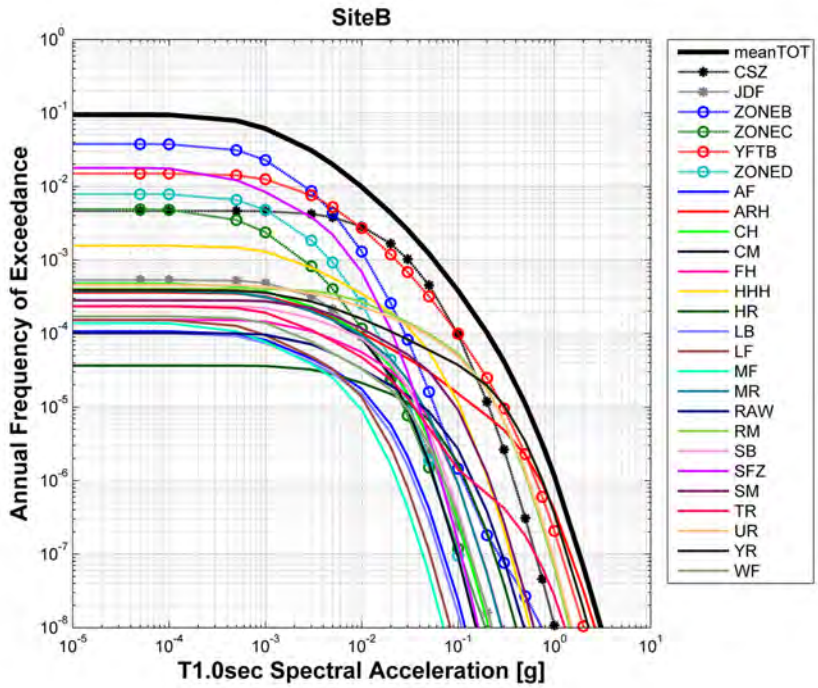

(c)

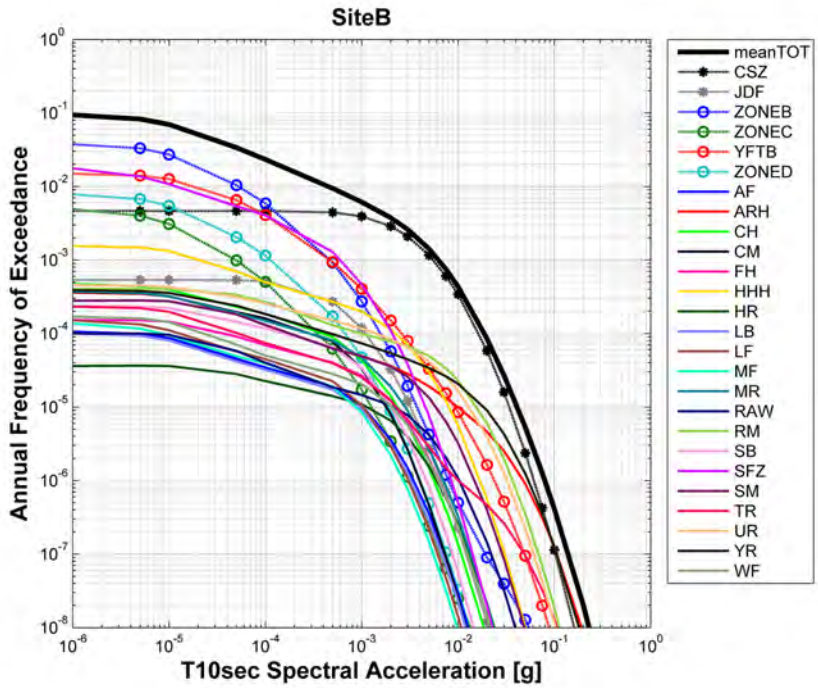

(d)

Figure 10.74. (contd)

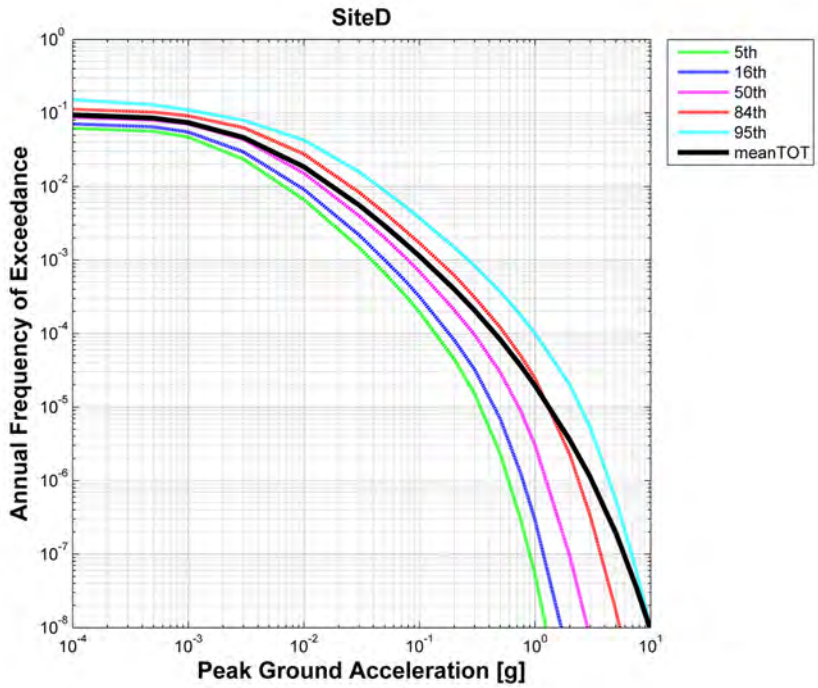

(a)

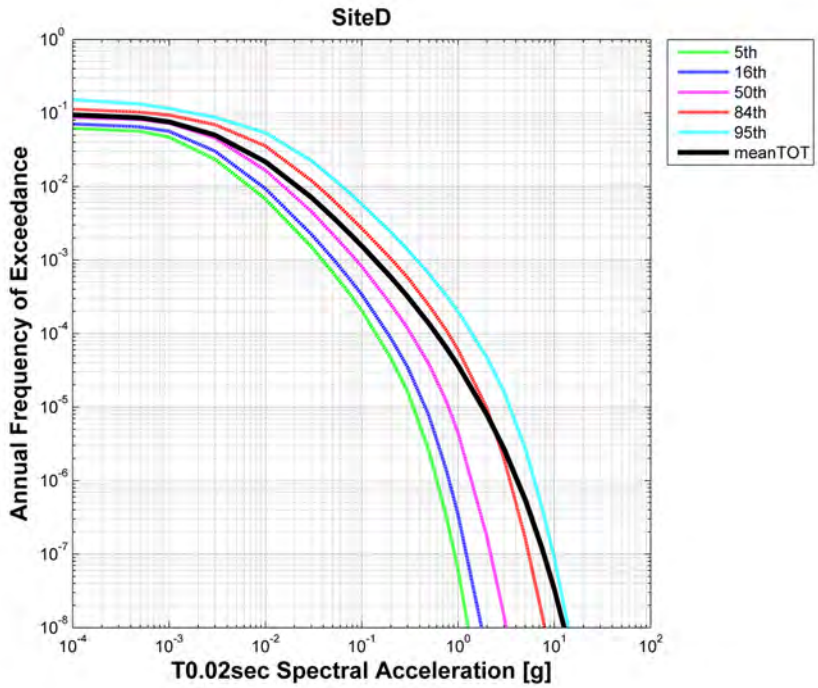

(b)

Figure 10.75. Total mean seismic hazard at Site D and percentiles: a) PGA; b) T 0.02-sec; c) T 0.03-sec; d) T 0.04-sec; e) T 0.05-sec; f) T 0.07-sec; g) T 0.10-sec; h) T 0.15-sec; i) T 0.20-sec; j) T 0.30-sec; k) T 0.40-sec; l) T 0.50-sec; m) T 0.75-sec; n) T 1.0-sec; o) T 1.5-sec; p) T 2.0-sec; q) T 3.0-sec; r) T 5.0-sec; s) T 7.5-sec; t) T 10-sec spectral acceleration.

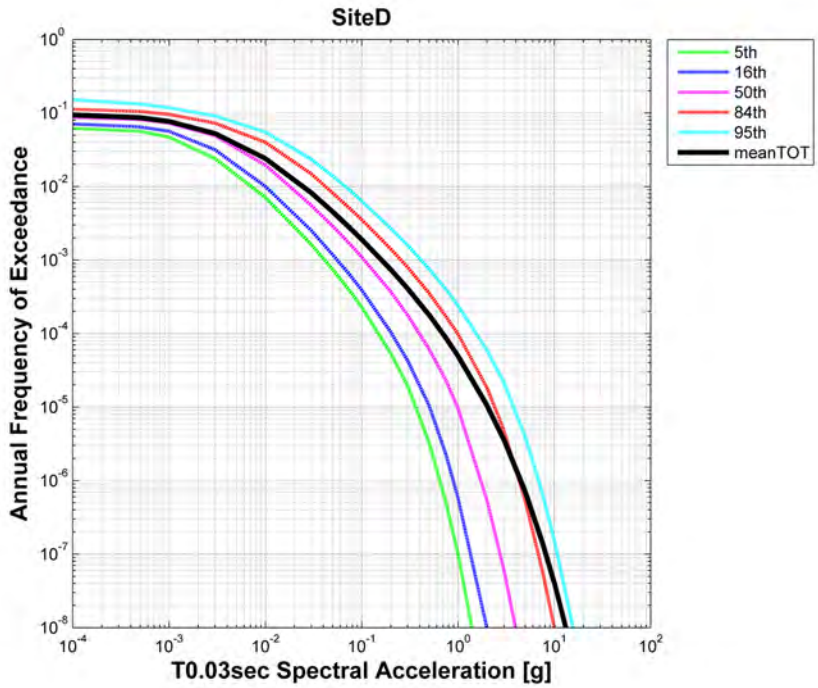

(c)

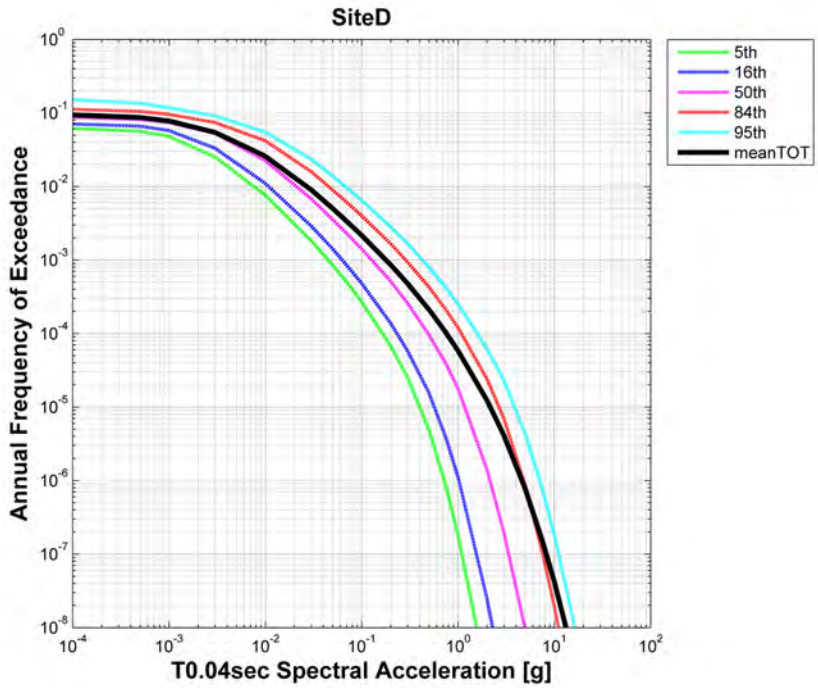

(d)

Figure 10.75. (contd)

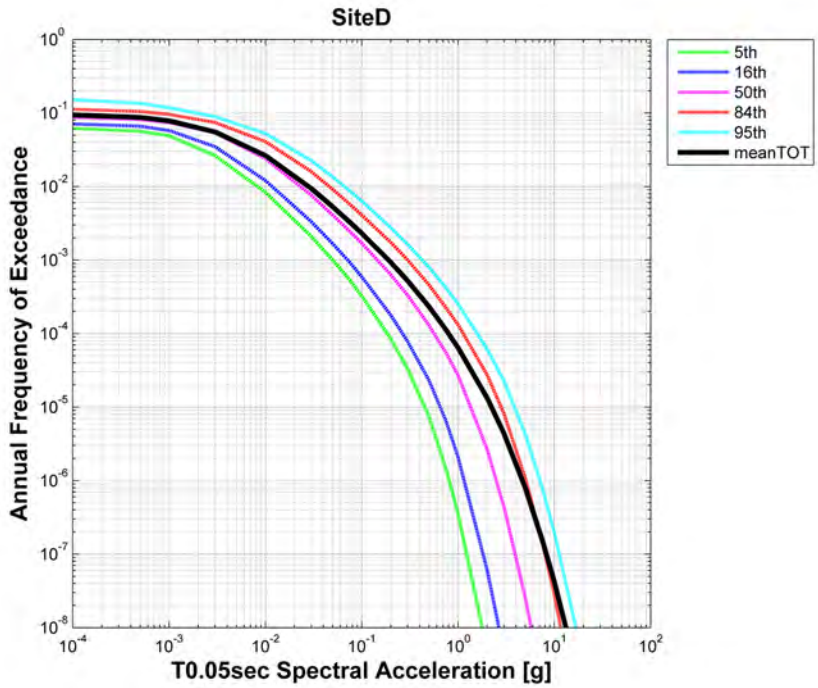

(e)

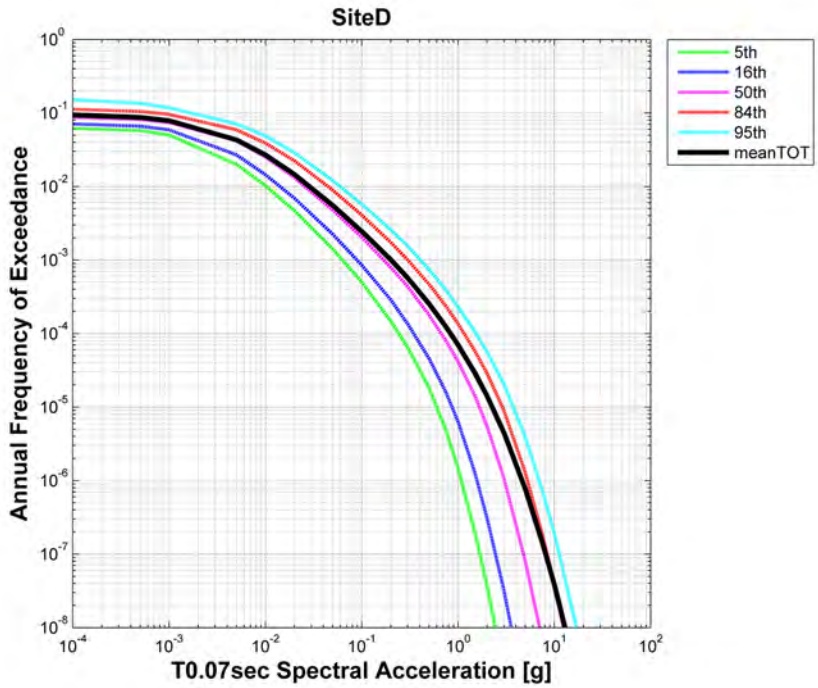

(f)

Figure 10.75. (contd)

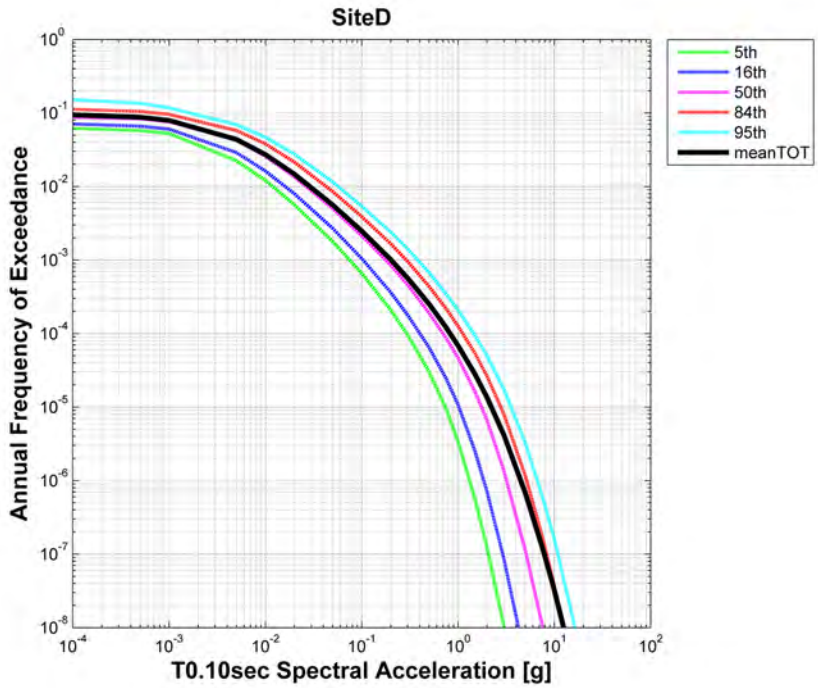

(g)

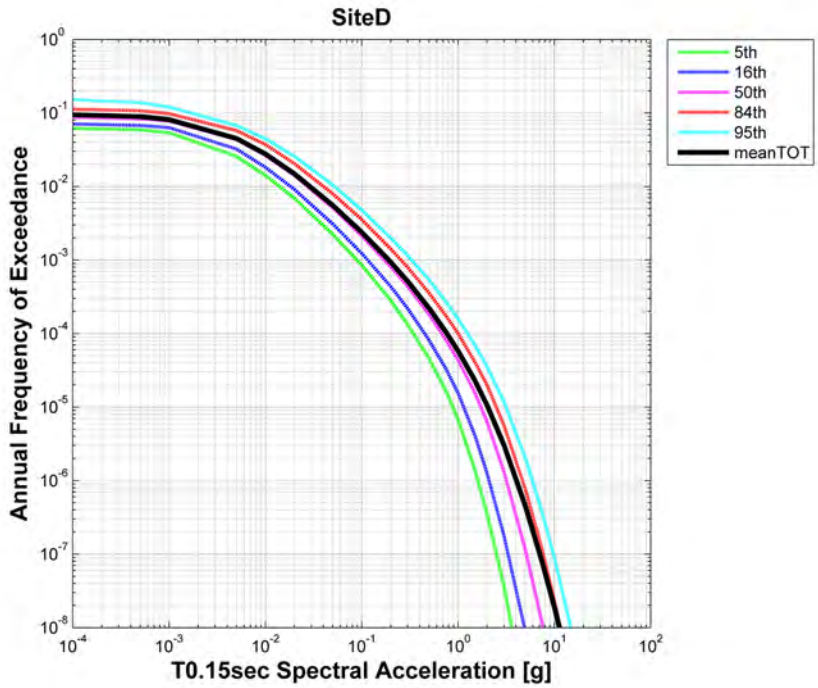

(h)

Figure 10.75. (contd)

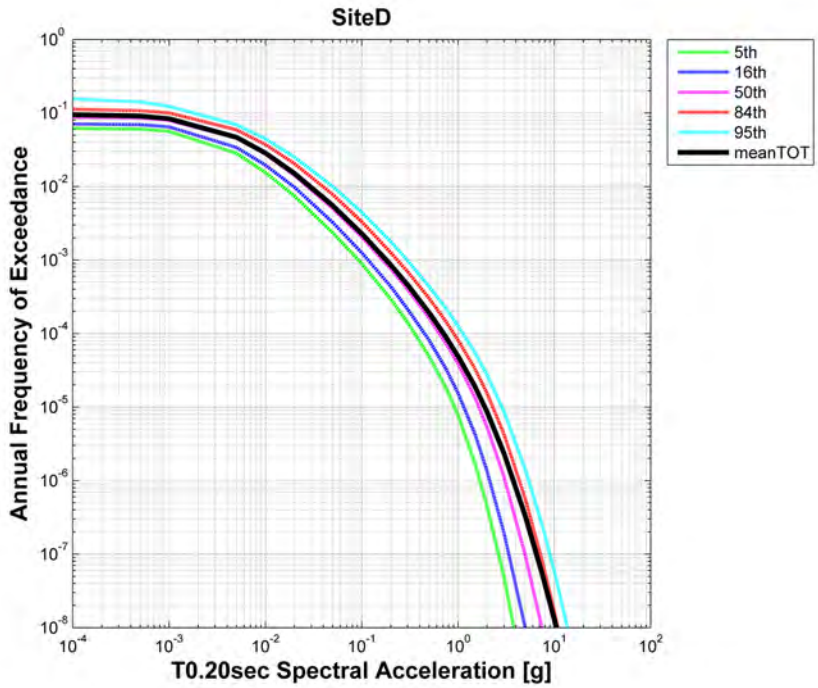

(i)

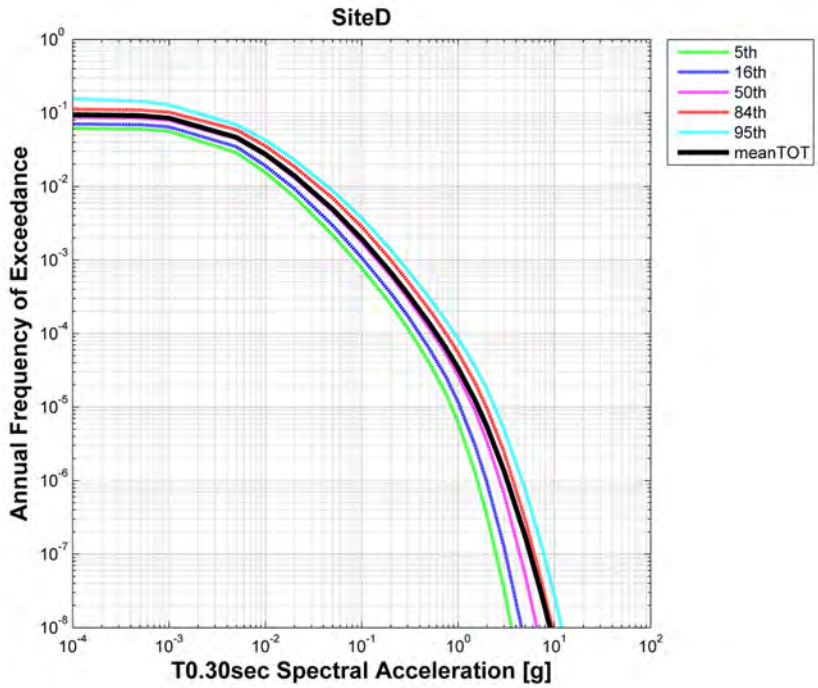

(j)

Figure 10.75. (contd)

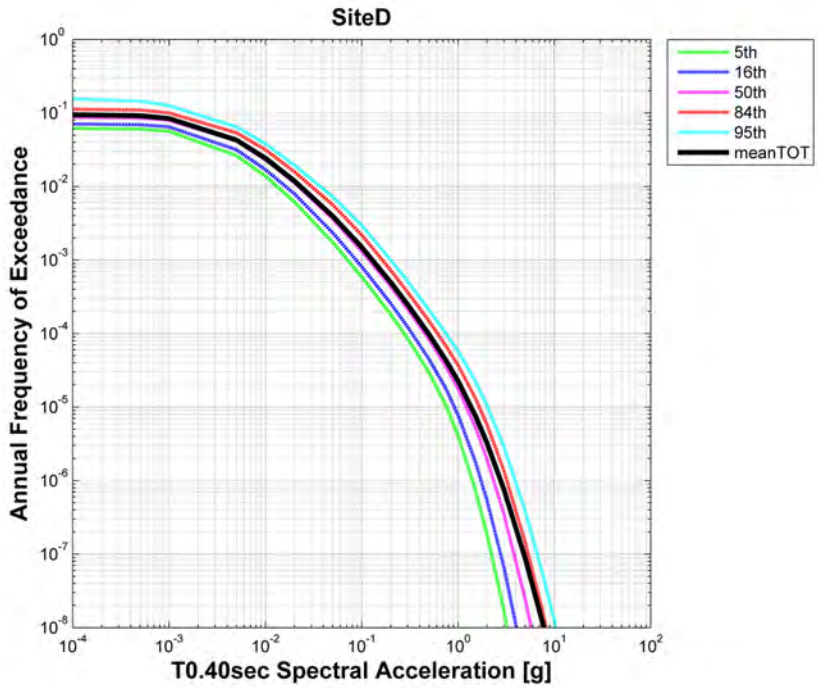

(k)

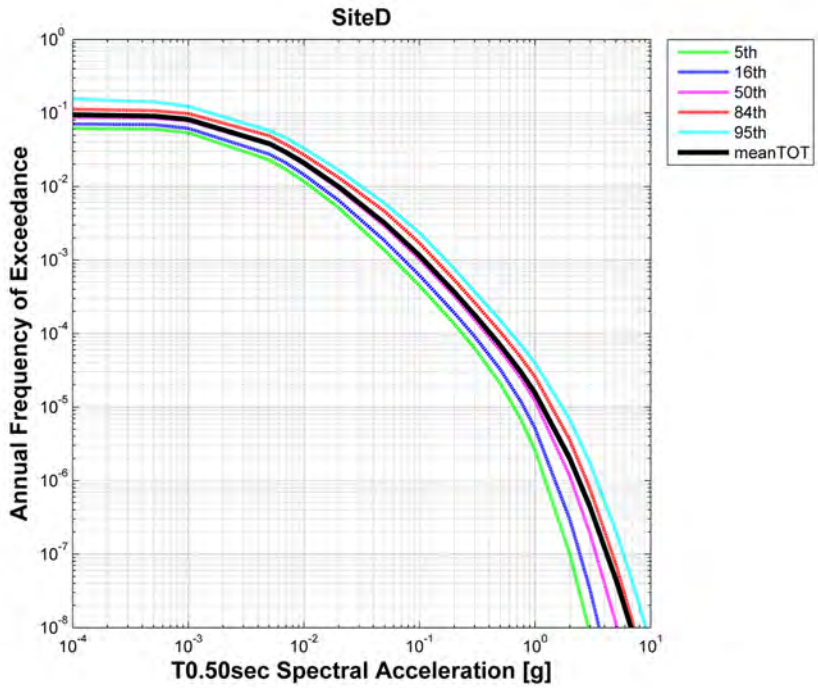

(l)

Figure 10.75. (contd)

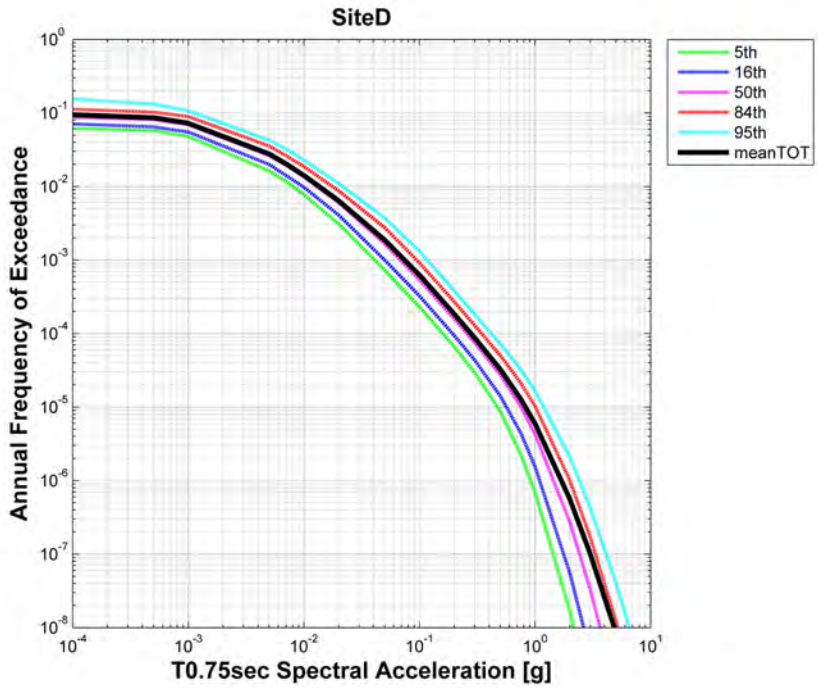

(m)

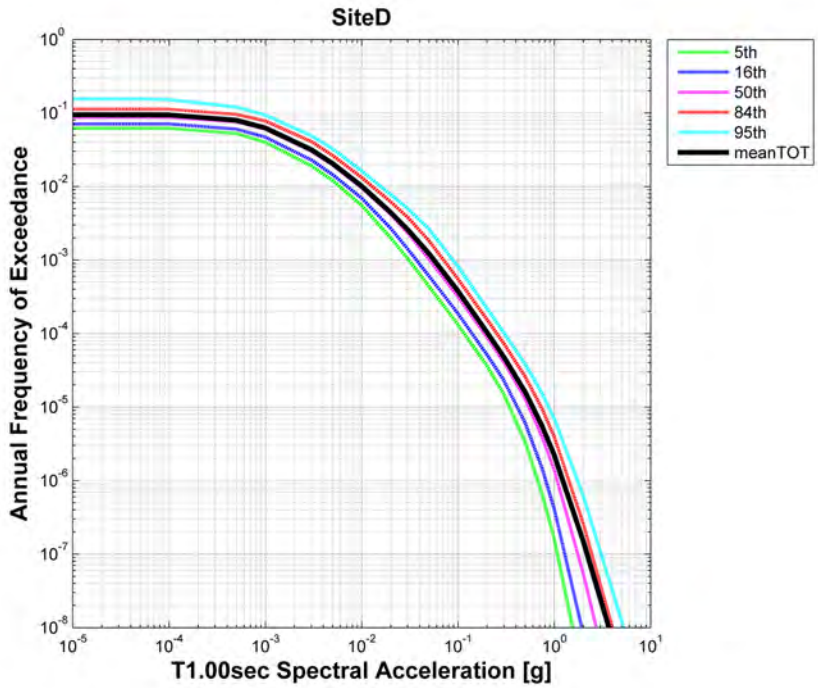

(n)

Figure 10.75. (contd)

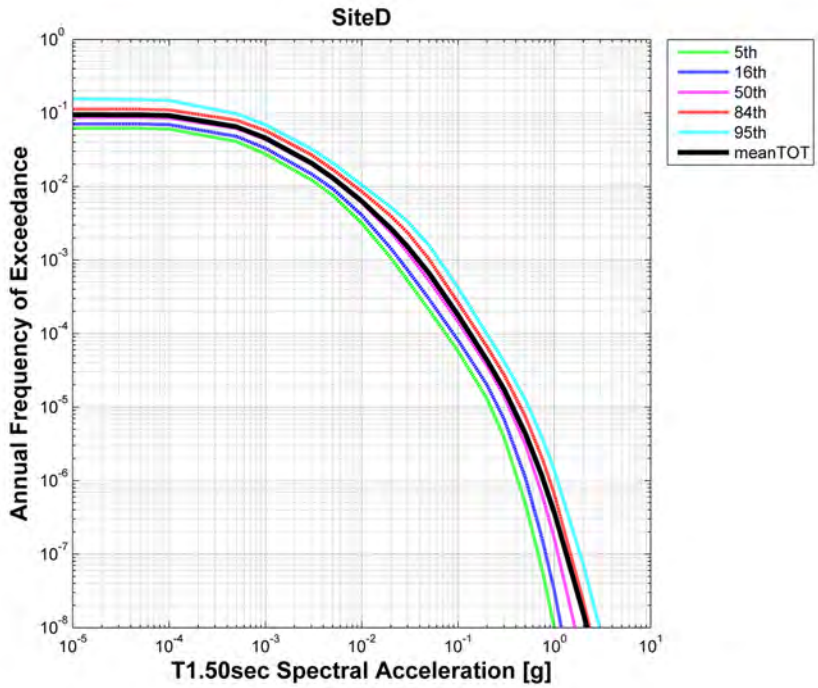

(o)

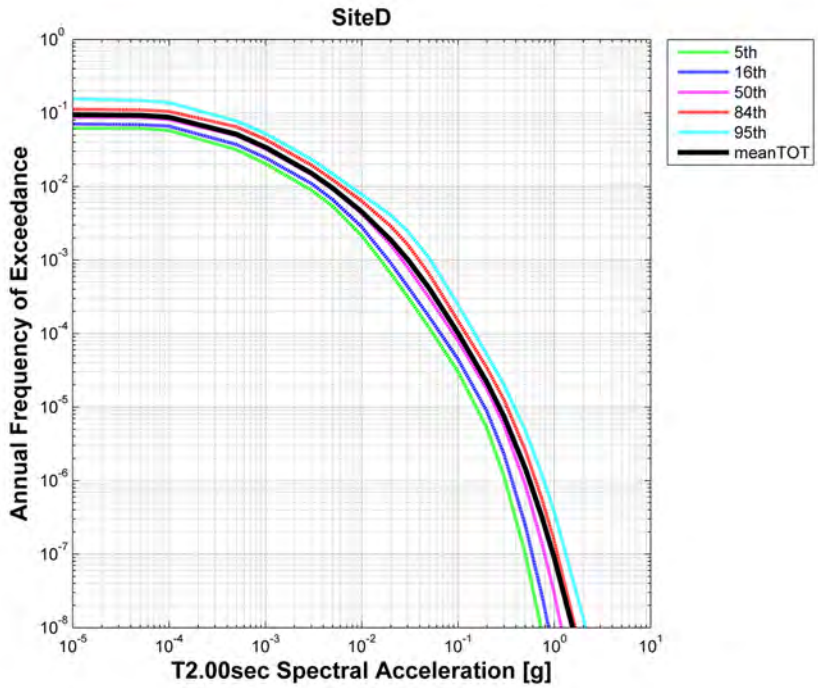

(p)

Figure 10.75. (contd)

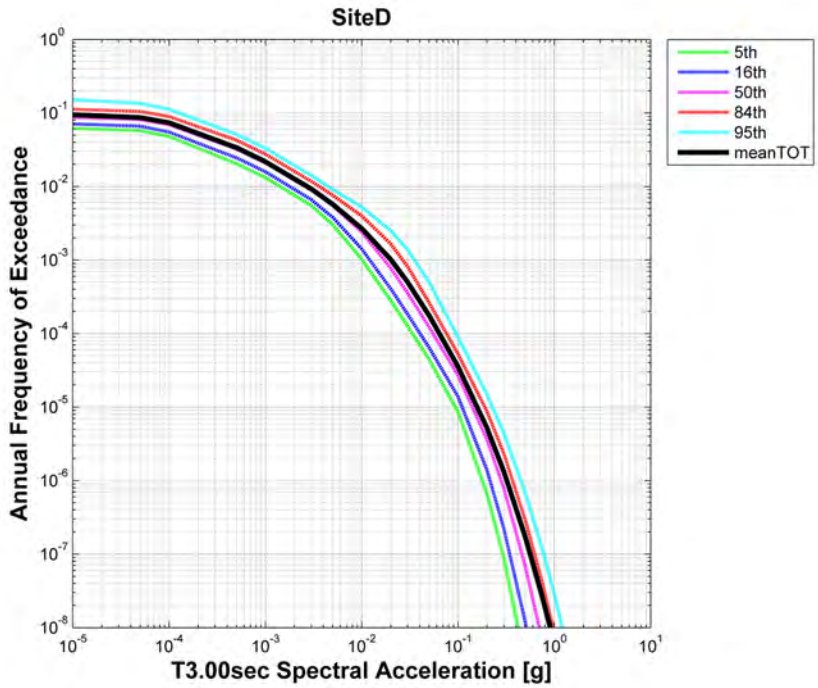

(q)

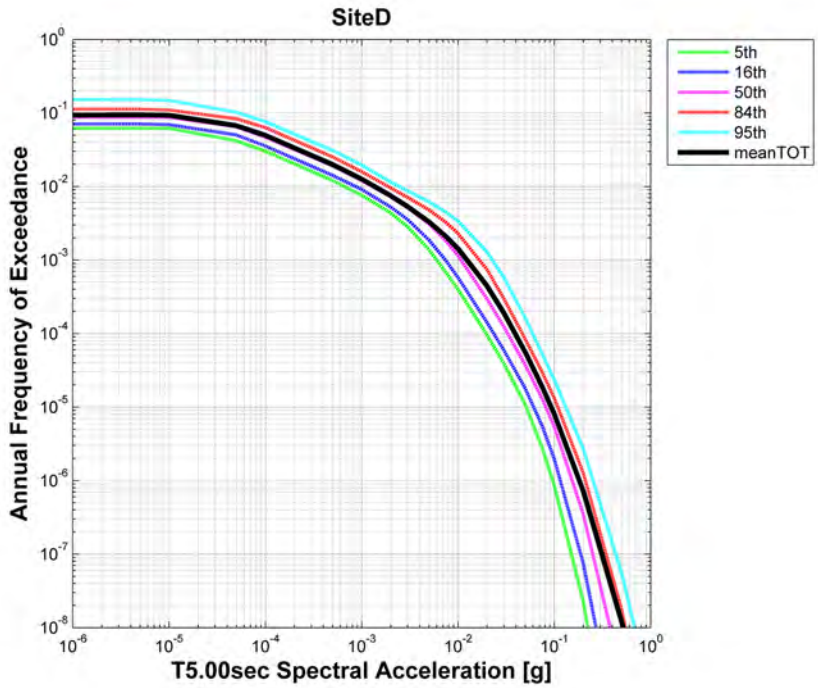

(r)

Figure 10.75. (contd)

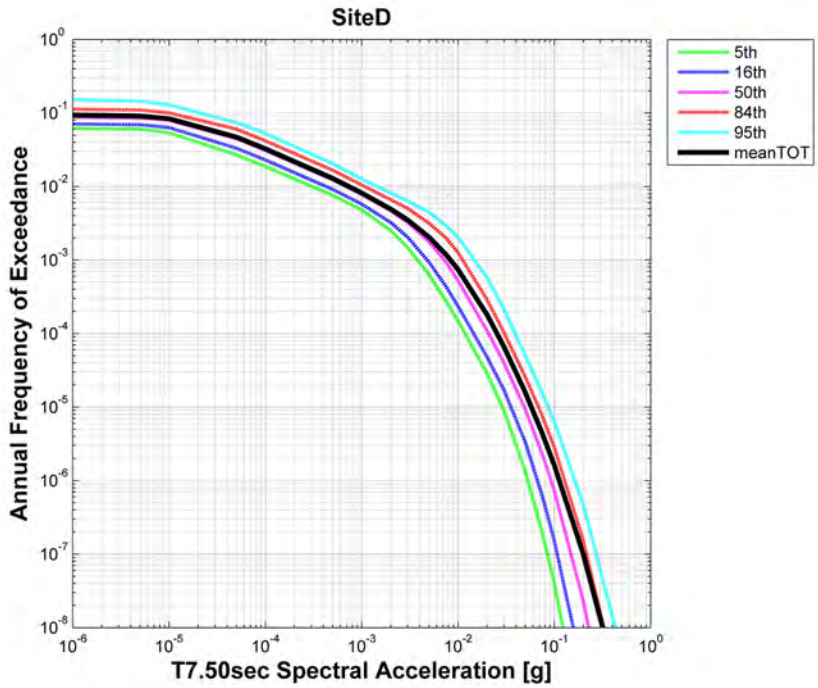

(s)

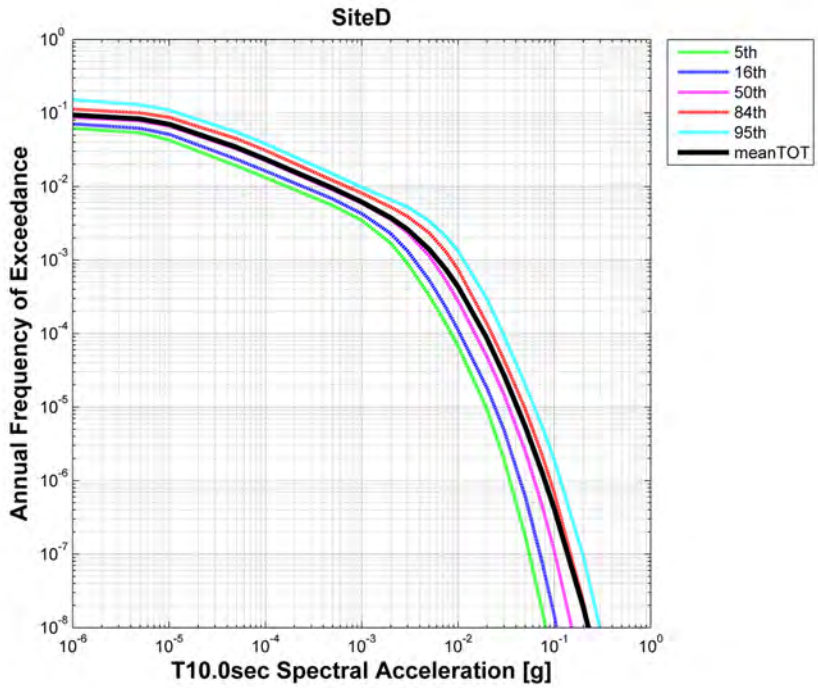

(t)

Figure 10.75. (contd)

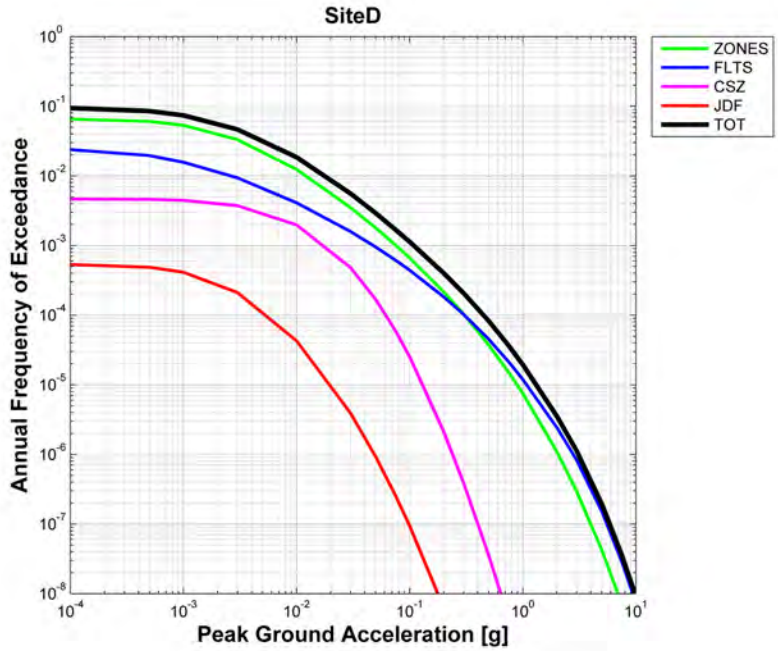

(a)

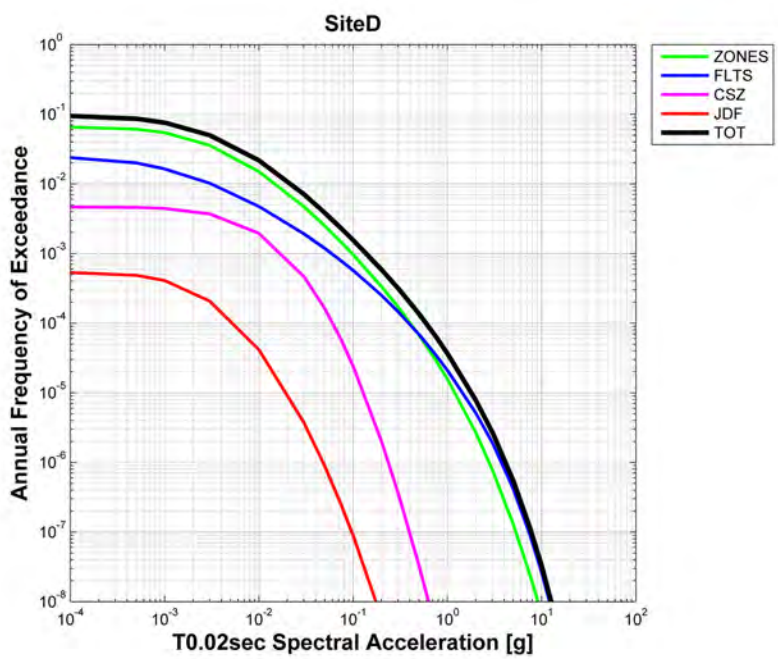

(b)

Figure 10.76. Comparison between the total mean seismic hazard at Site D (black curve) and the contribution of crustal source zones (green curve), faults (blue curve), the Cascadia interface (CSZ - magenta curve), and Cascadia intraslab source (JDF - red curve): a) PGA; b) T 0.02-sec; c) T 0.03-sec; d) T 0.04-sec; e) T 0.05-sec; f) T 0.07-sec; g) T 0.10-sec; h) T 0.15-sec; i) T 0.20-sec; j) T 0.30-sec; k) T 0.40-sec; l) T 0.50-sec; m) T 0.75-sec; n) T 1.0-sec; o) T 1.5-sec; p) T 2.0-sec; q) T 3.0-sec; r) T 5.0-sec; s) T 7.5-sec; t) T 10-sec spectral acceleration.

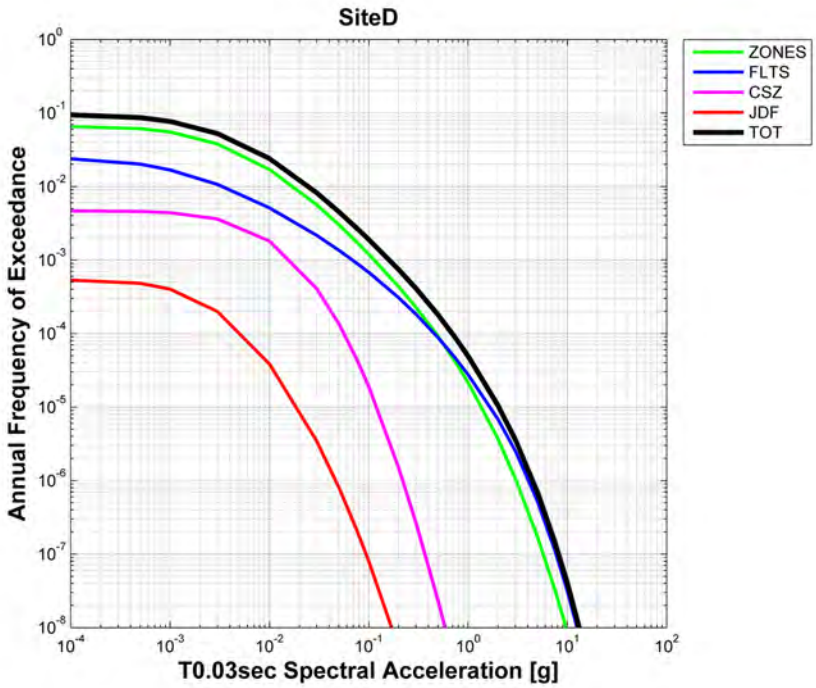

(c)

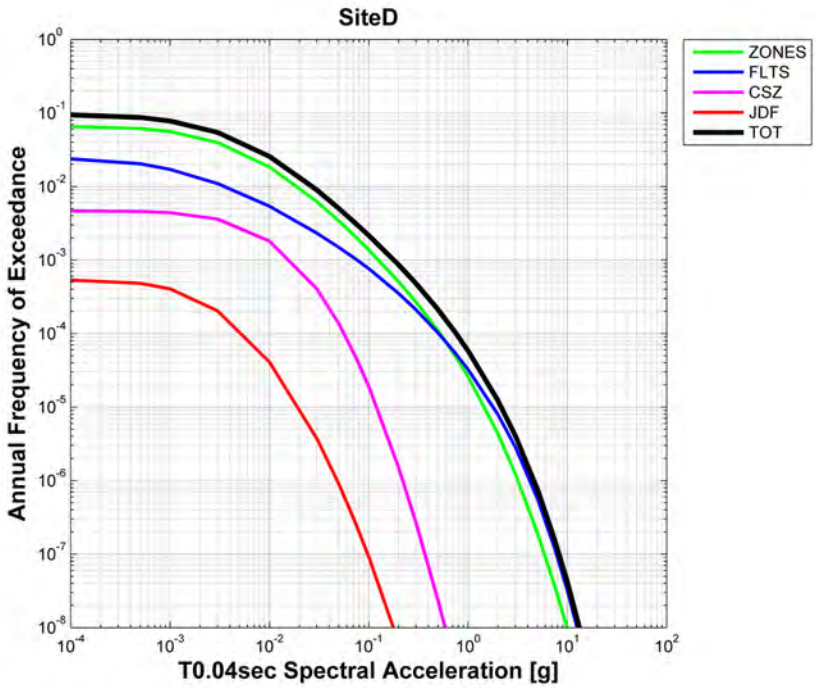

(d)

Figure 10.76. (contd)

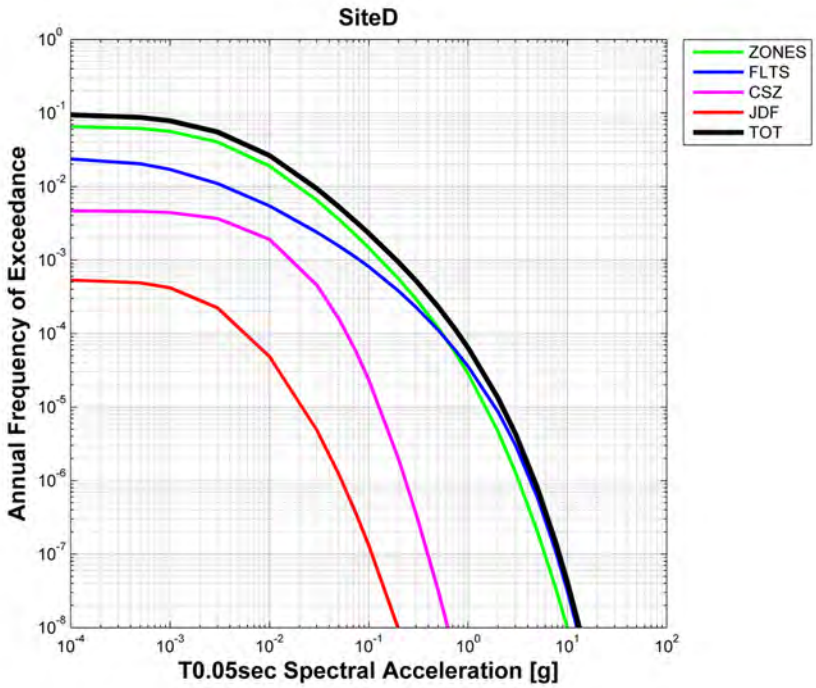

(e)

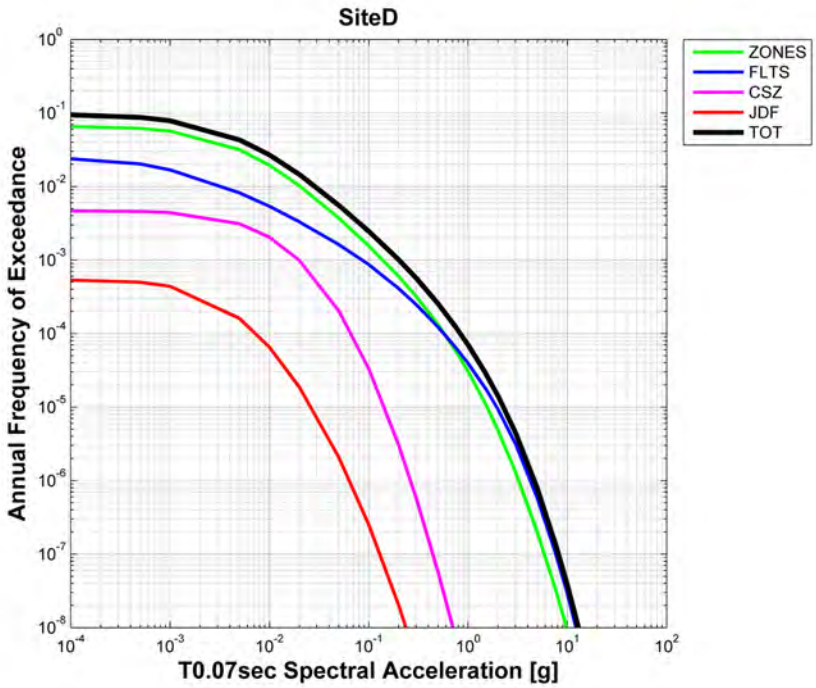

(f)

Figure 10.76. (contd)

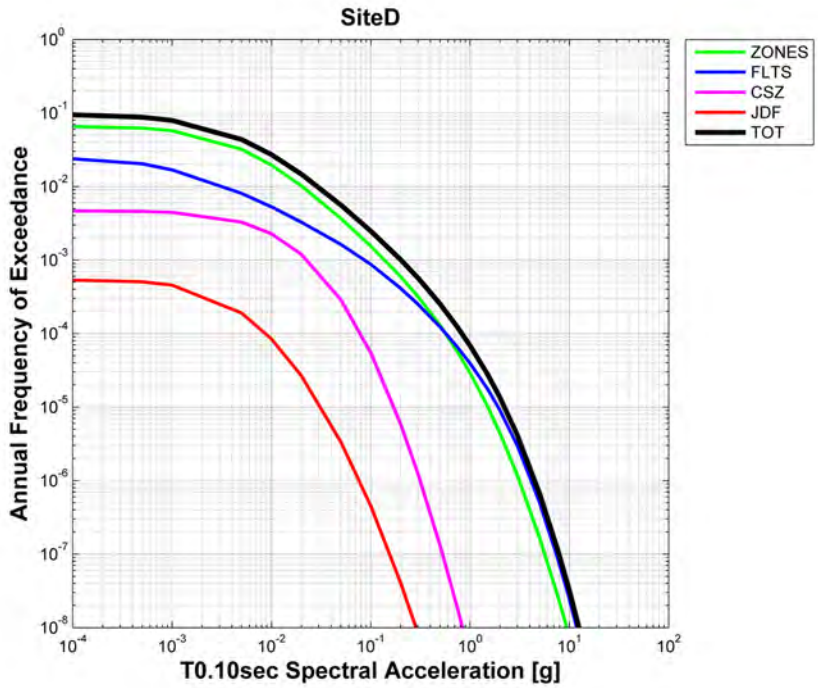

(g)

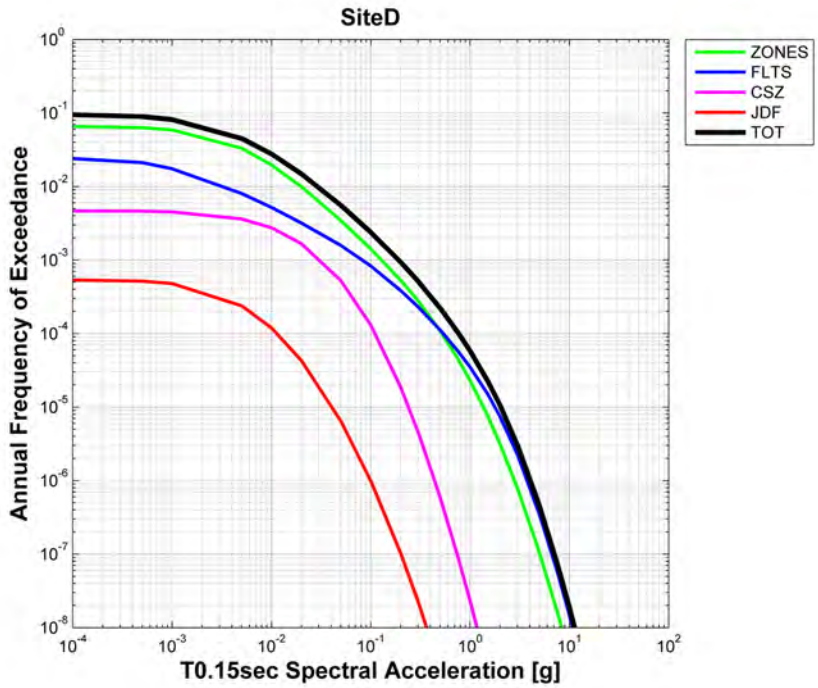

(h)

Figure 10.76. (contd)

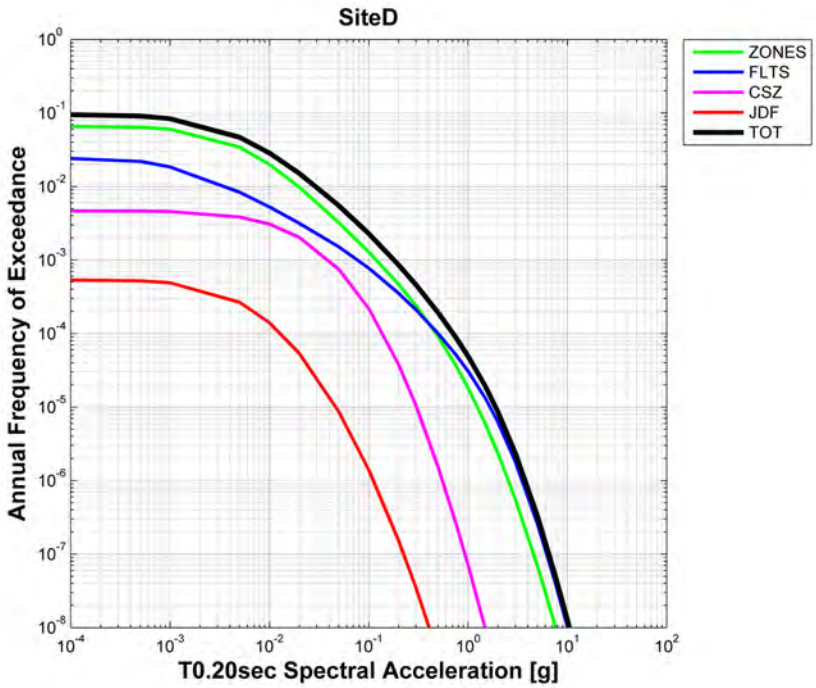

(i)

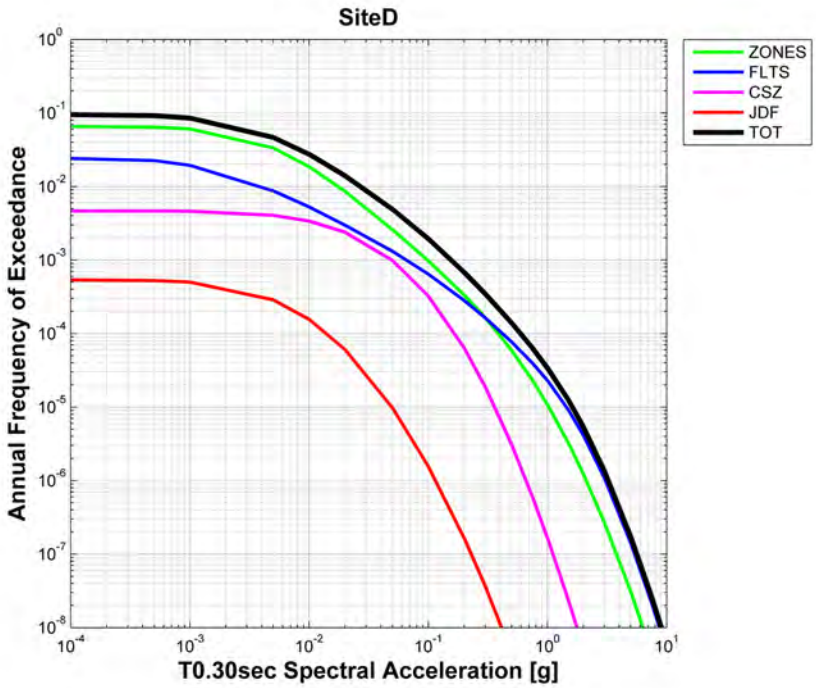

(j)

Figure 10.76. (contd)

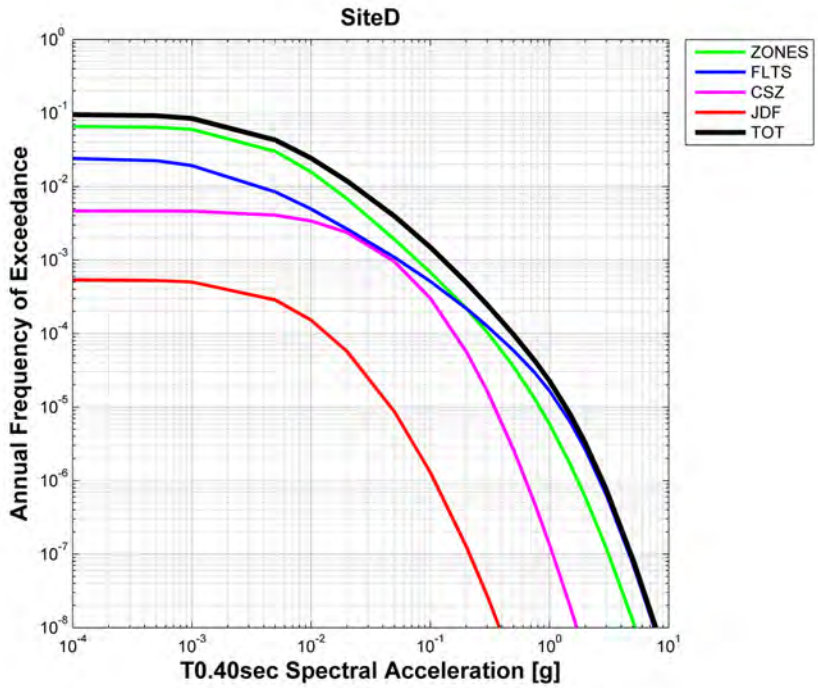

(k)

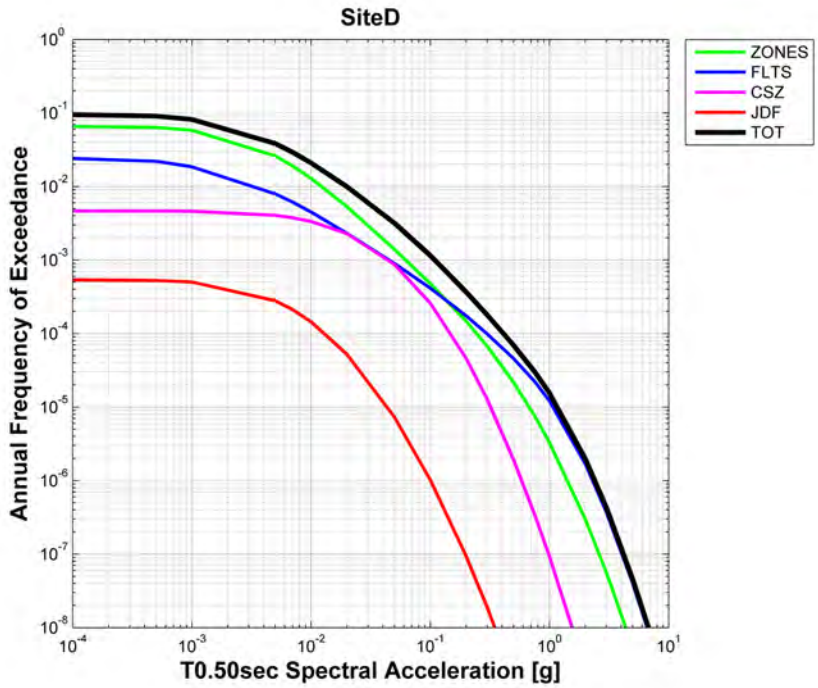

(l)

Figure 10.76. (contd)

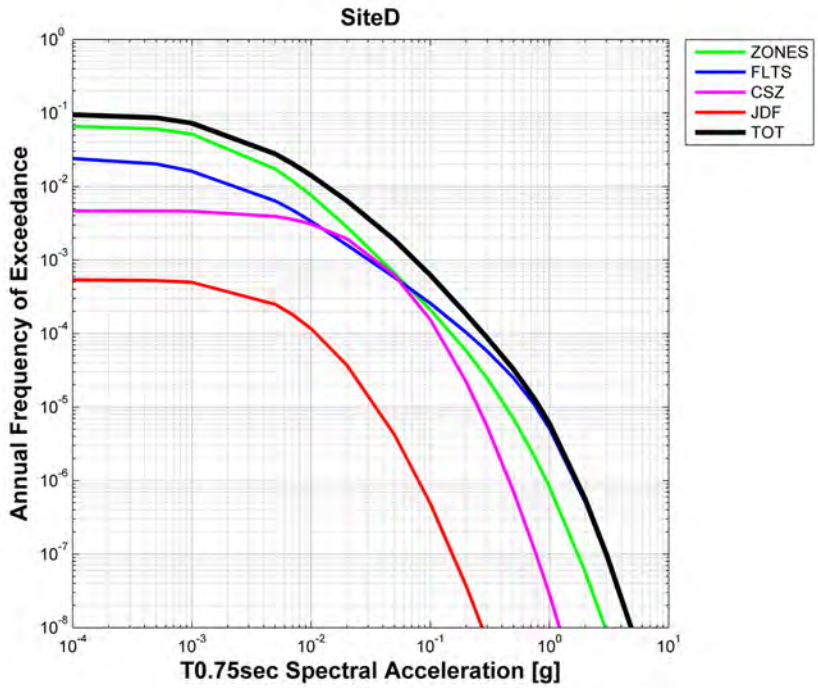

(m)

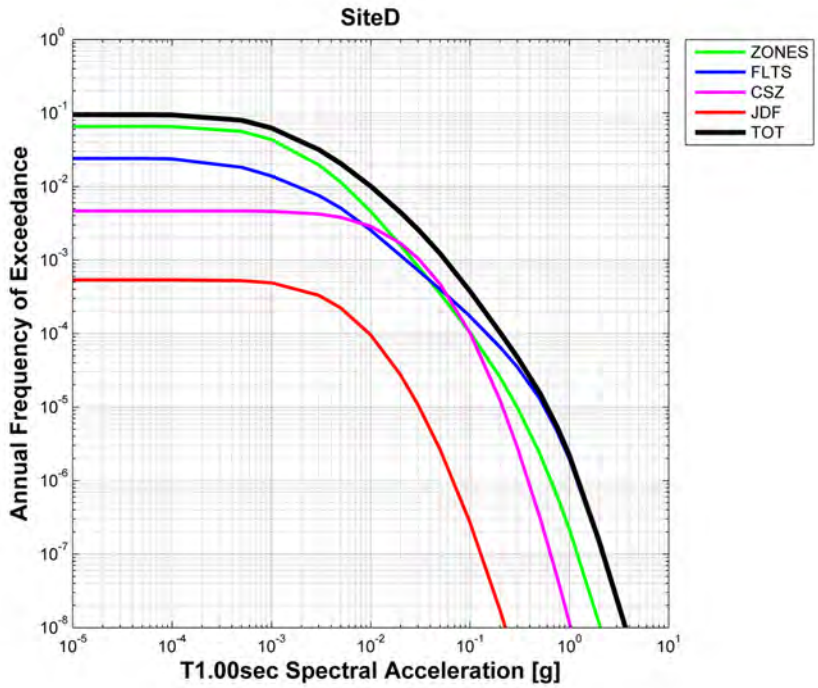

(n)

Figure 10.76. (contd)

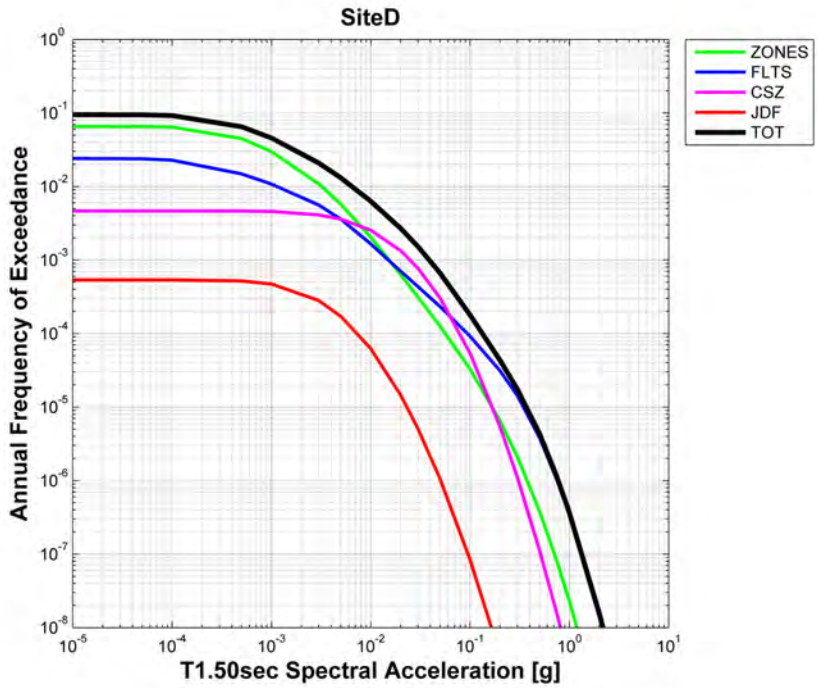

(o)

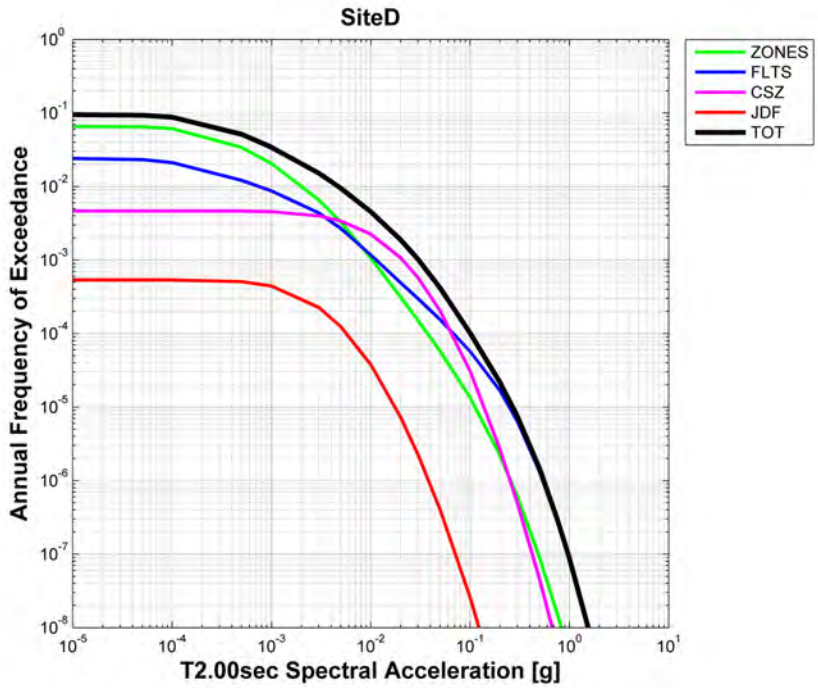

(p)

Figure 10.76. (contd)

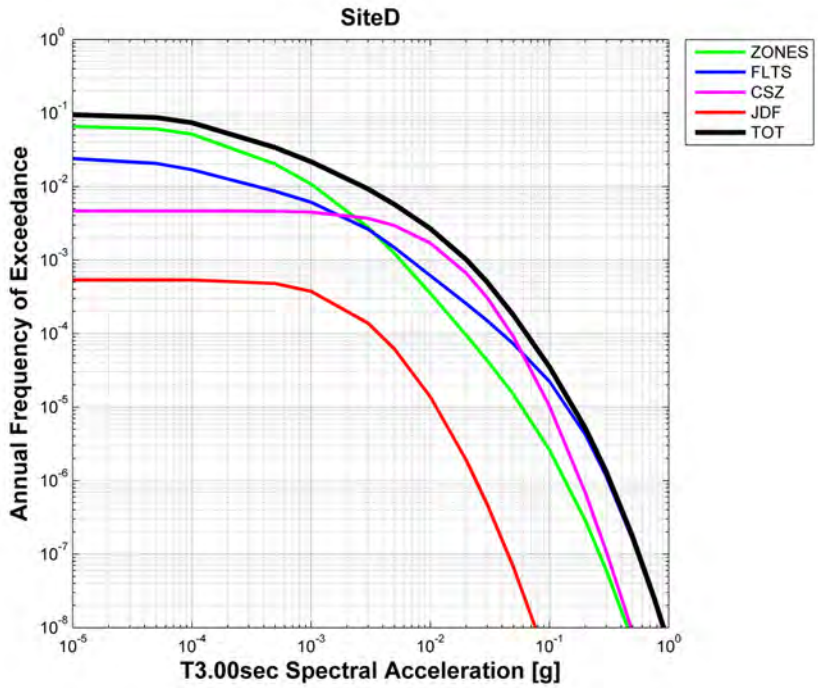

(q)

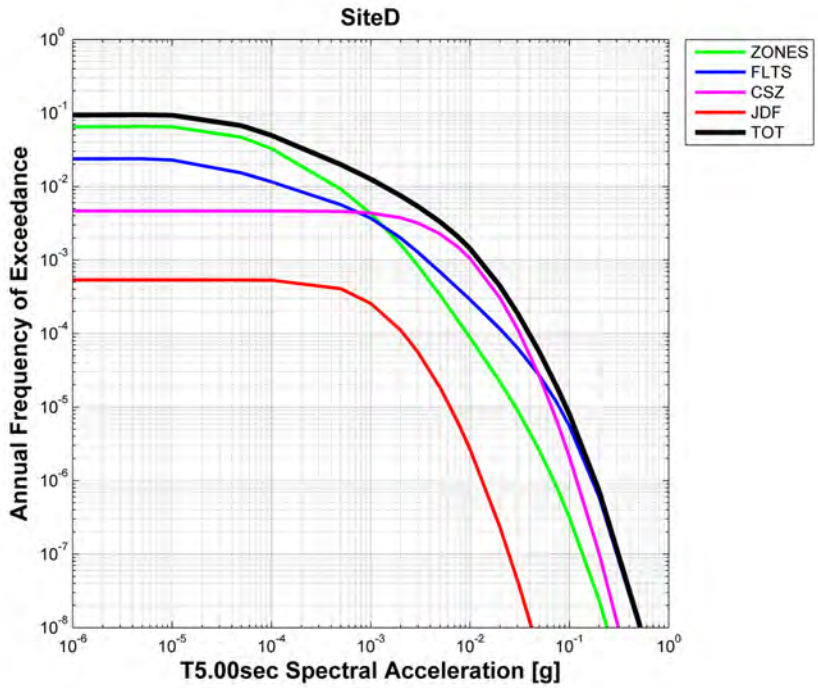

(r)

Figure 10.76. (contd)

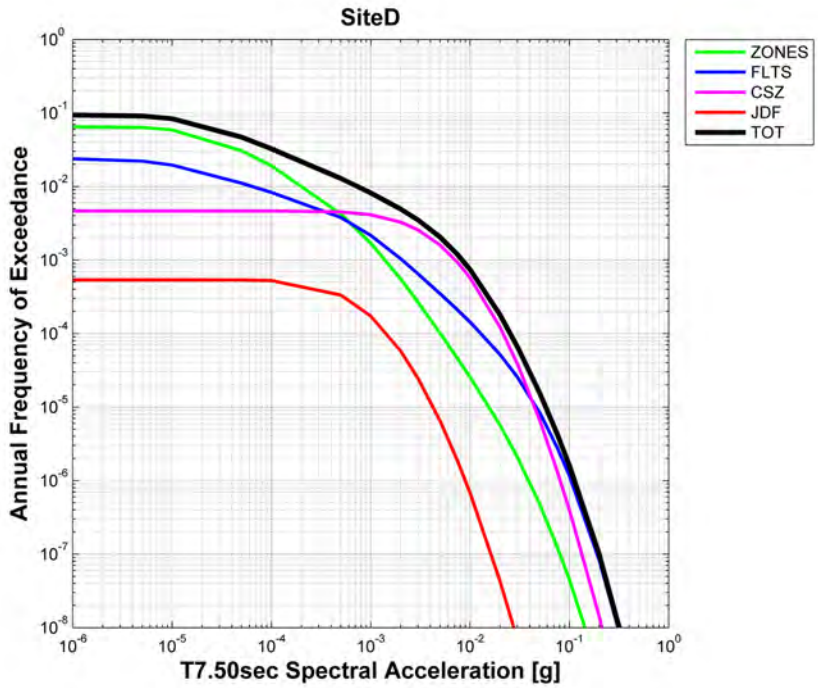

(s)

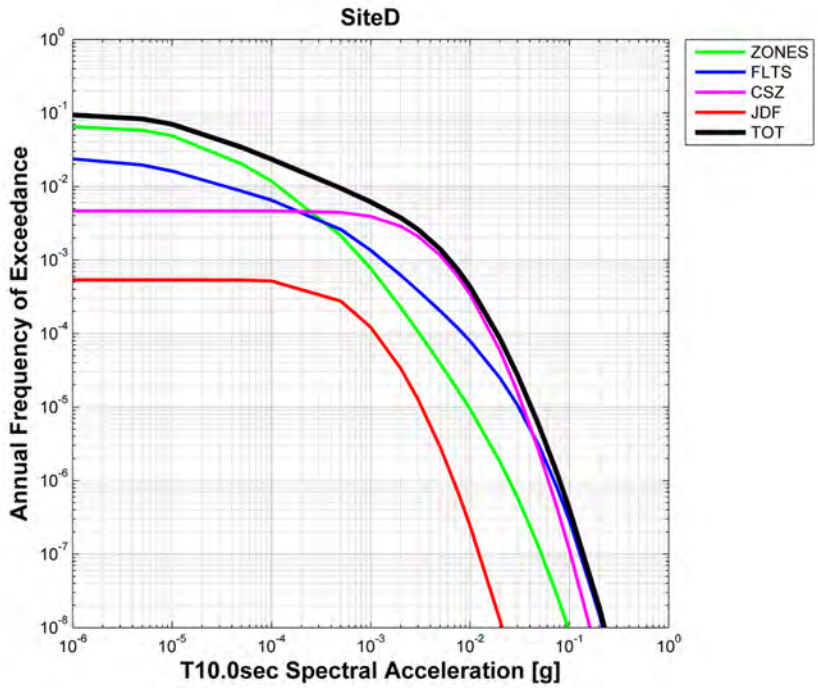

(t)

Figure 10.76. (contd)

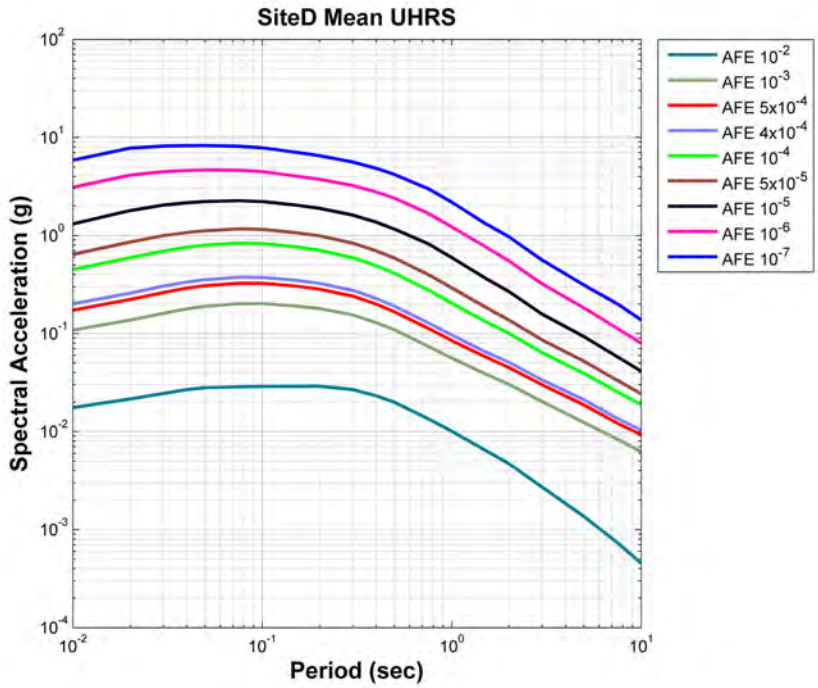

(a)

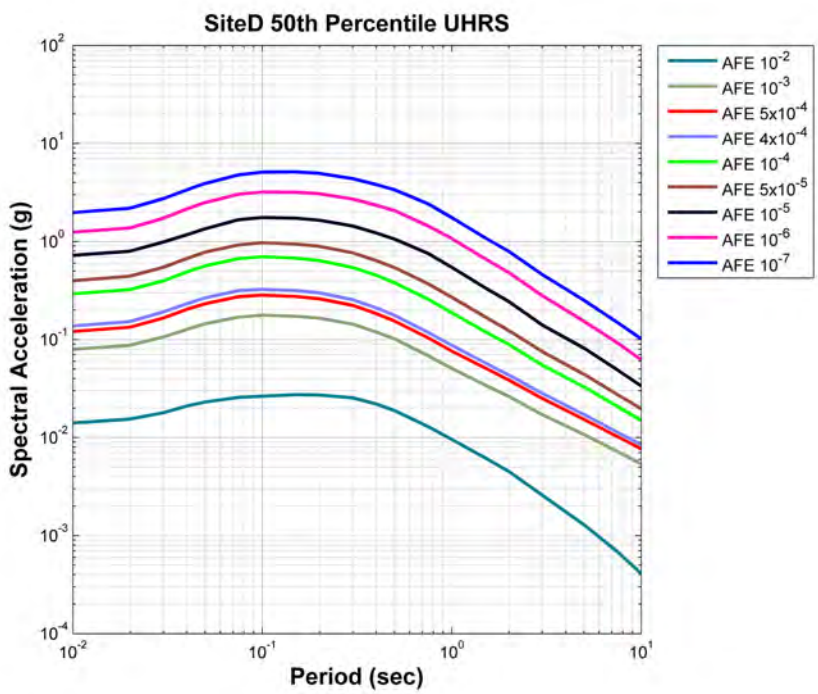

(b)

Figure 10.77. Uniform hazard response spectra at AFEs of 10^{-2}, 10^{-3}, 5×10^{-4}, 4×10^{-4}, 10^{-4}, 5×10^{-5}, 10^{-6}, 10^{-7} (return periods of 100, 1,000, 2,000, 2,500, 10,000, 20,000, 100,000, 1 million, and 10 million years) for: a) mean hazard; b) 50th percentile hazard; c) 84th percentile hazard.

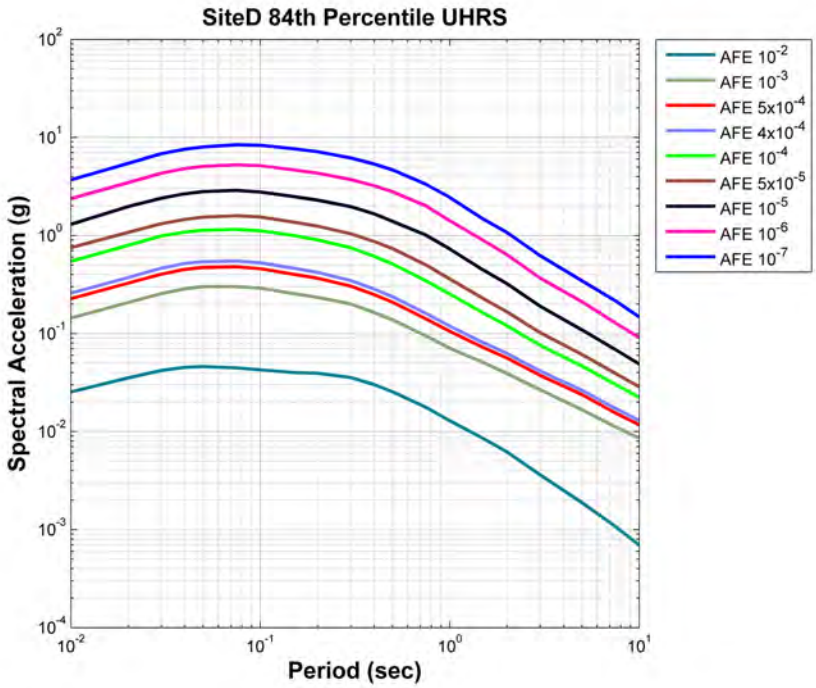

(c)

Figure 10.77. (contd)

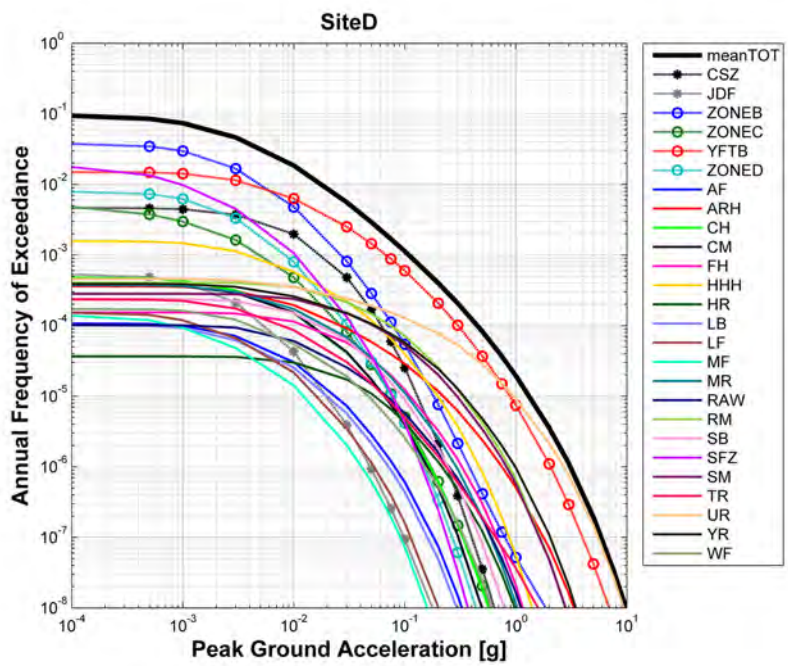

(a)

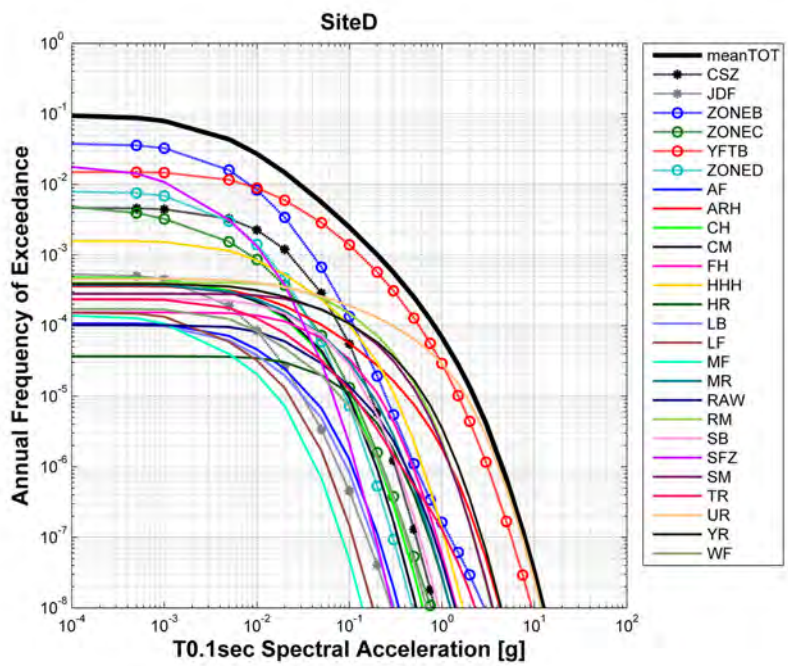

(b)

Figure 10.78. Comparison between the mean hazard curves at Site D obtained for each individual source. Subduction sources are shown by dotted star curves; crustal sources by dotted circle curves; and fault sources by solid curves: a) peak ground acceleration; b) T 0.1-sec; c) T 1-sec; d) T 10-sec spectral acceleration. Acronyms used in figures are listed in Table 10.13 .

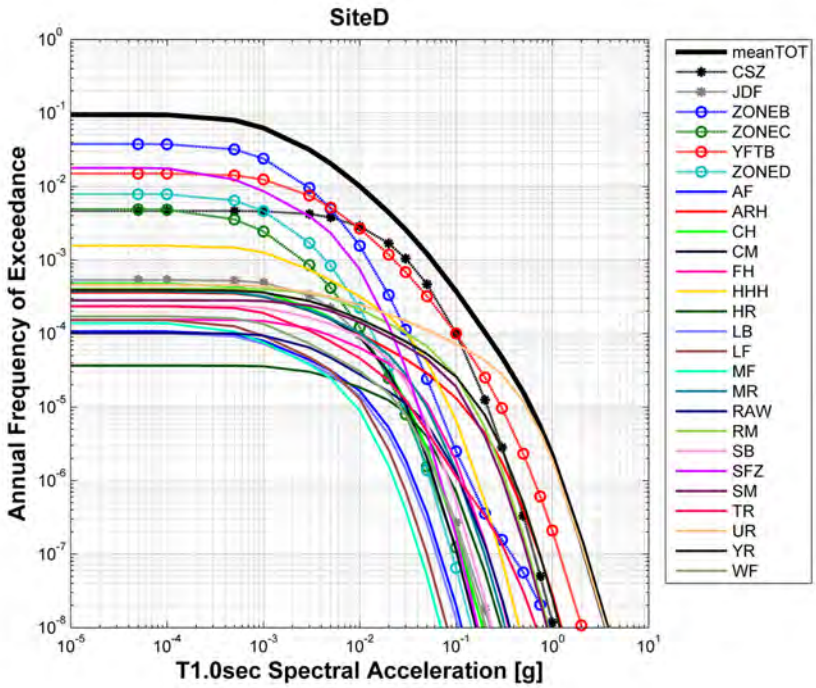

(c)

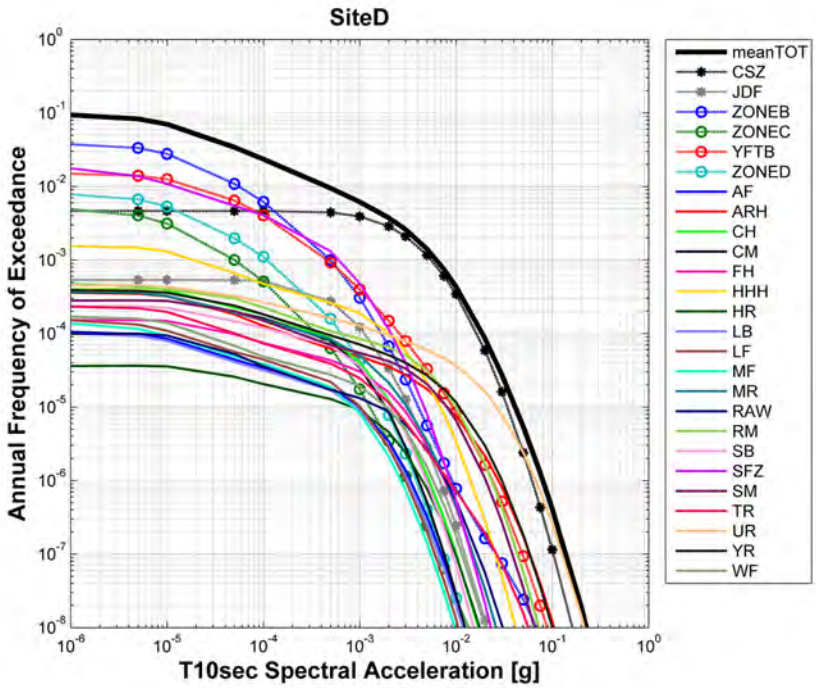

(d)

Figure 10.78. (contd)

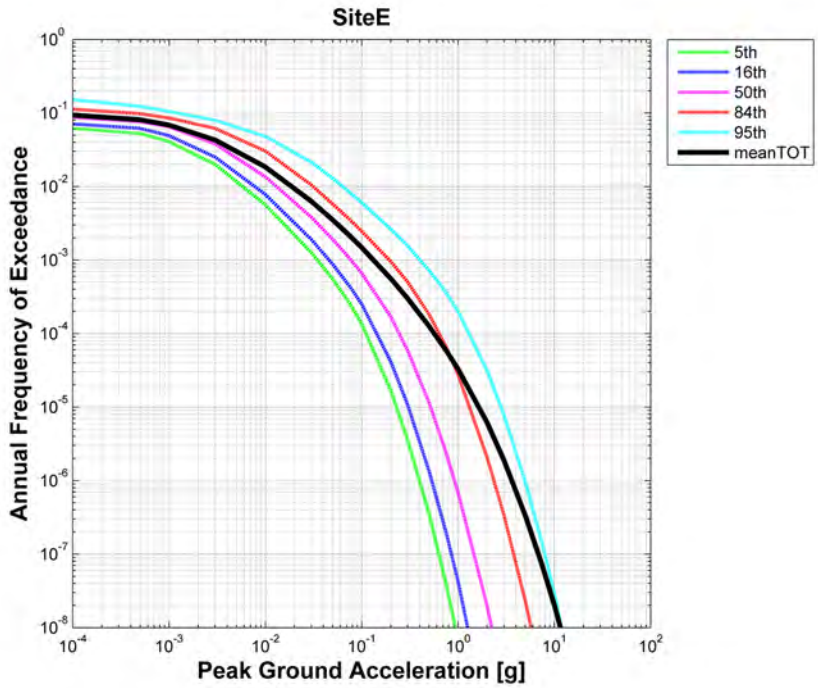

(a)

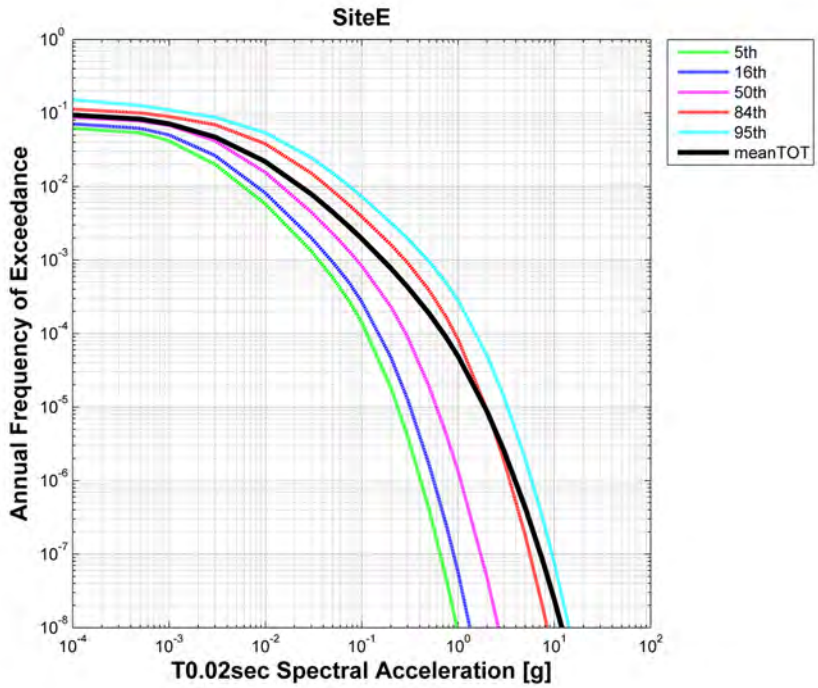

(b)

Figure 10.79. Total mean seismic hazard at Site E and percentiles: a) PGA; b) T 0.02-sec; c) T 0.03-sec; d) T 0.04-sec; e) T 0.05-sec; f) T 0.07-sec; g) T 0.10-sec; h) T 0.15-sec; i) T 0.20-sec; j) T 0.30-sec; k) T 0.40-sec; l) T 0.50-sec; m) T 0.75-sec; n) T 1.0-sec; o) T 1.5-sec; p) T 2.0-sec; q) T 3.0-sec; r) T 5.0-sec; s) T 7.5-sec; t) T 10-sec spectral acceleration.

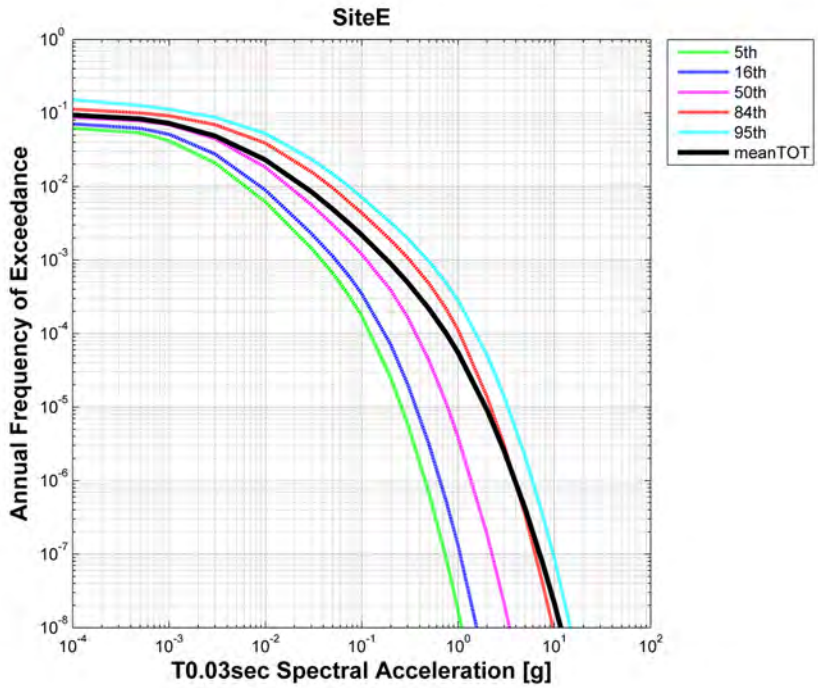

(c)

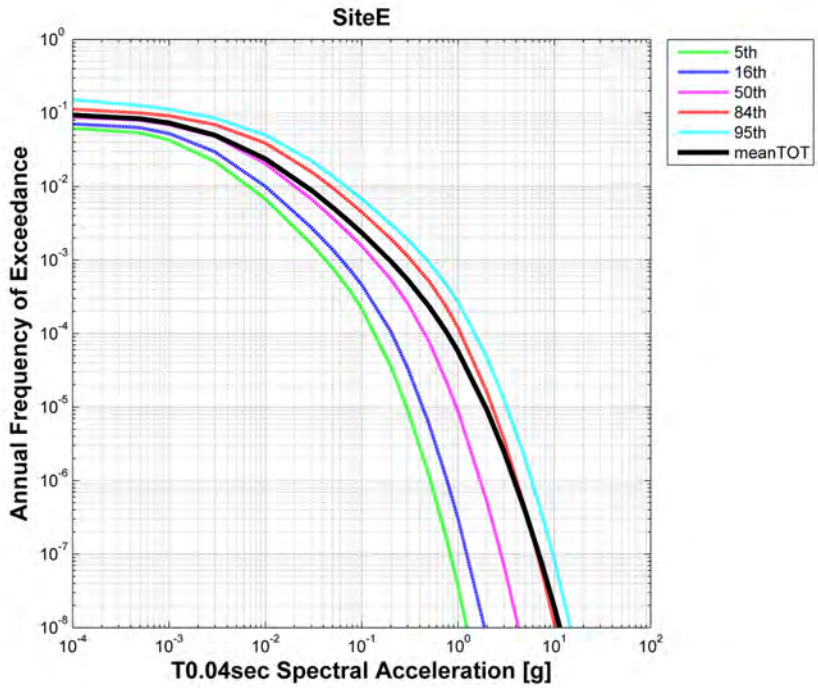

(d)

Figure 10.79. (contd)

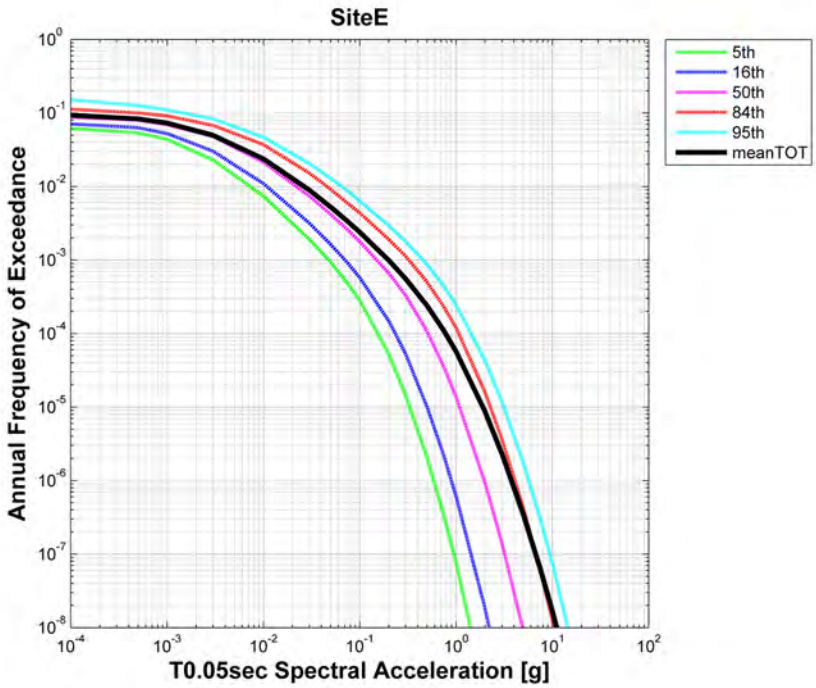

(e)

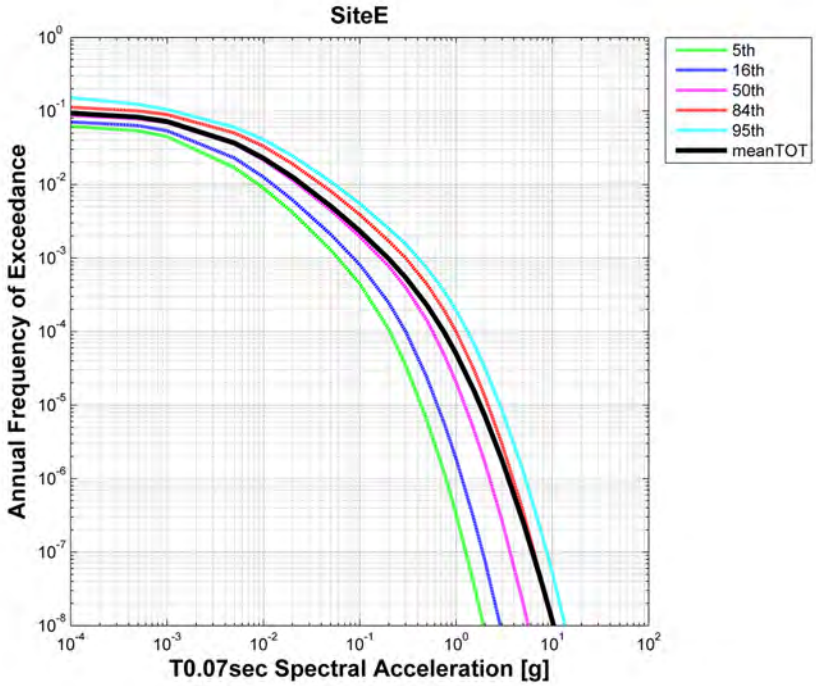

(f)

Figure 10.79. (contd)

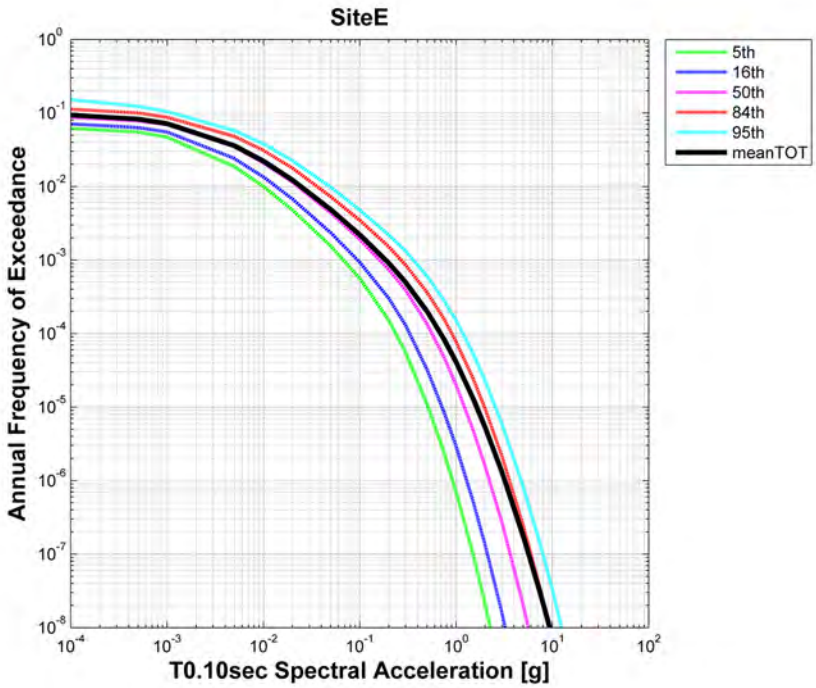

(g)

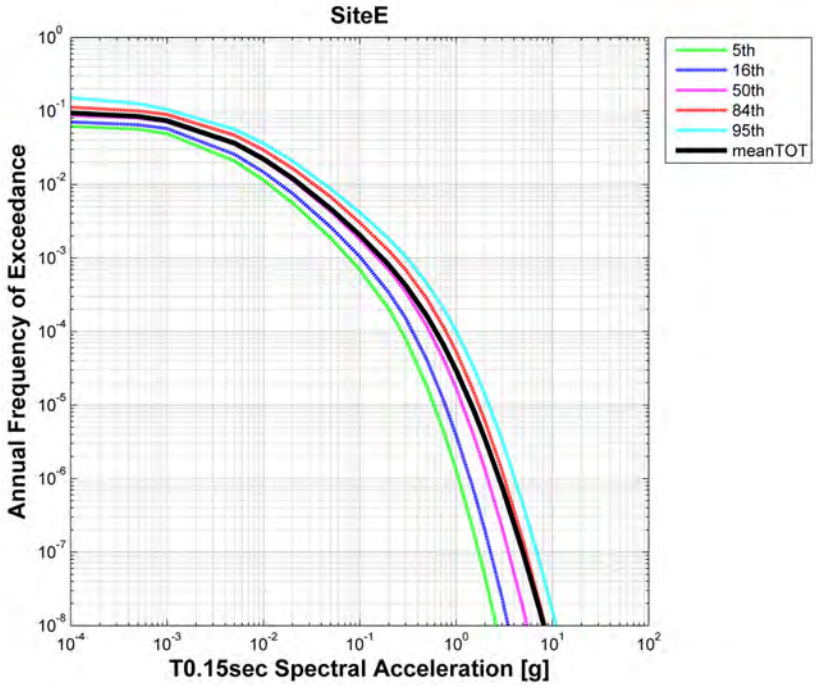

(h)

Figure 10.79. (contd)

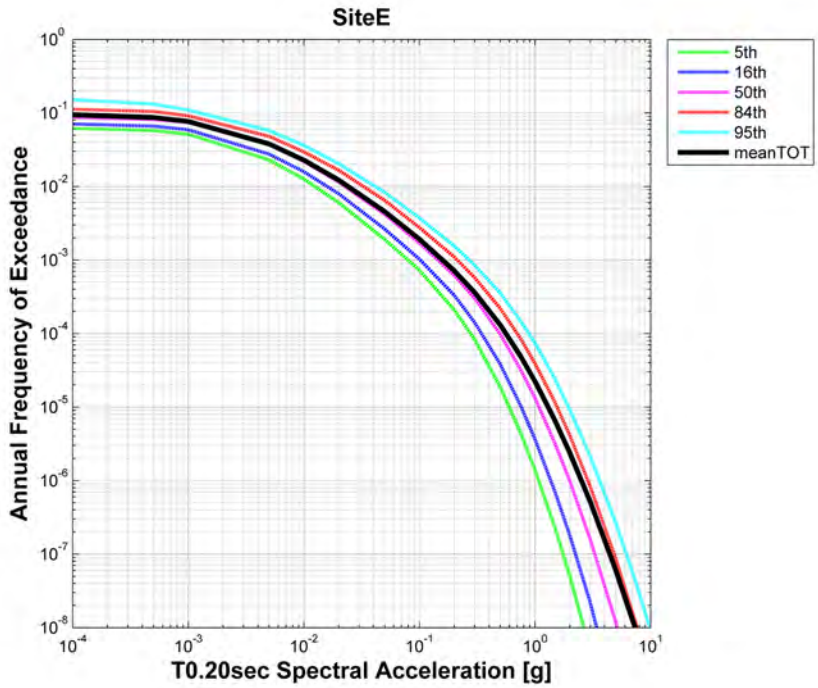

(i)

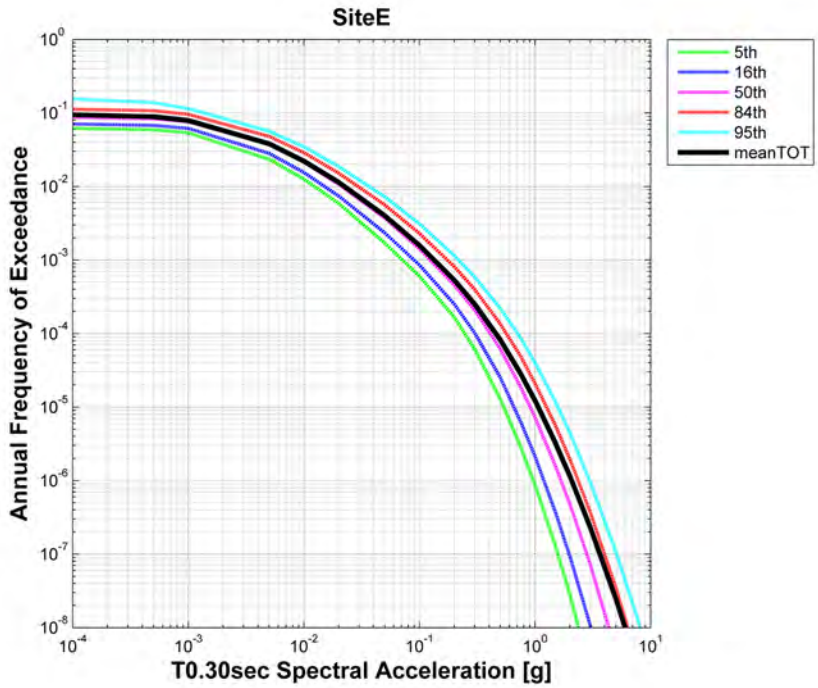

(j)

Figure 10.79. (contd)

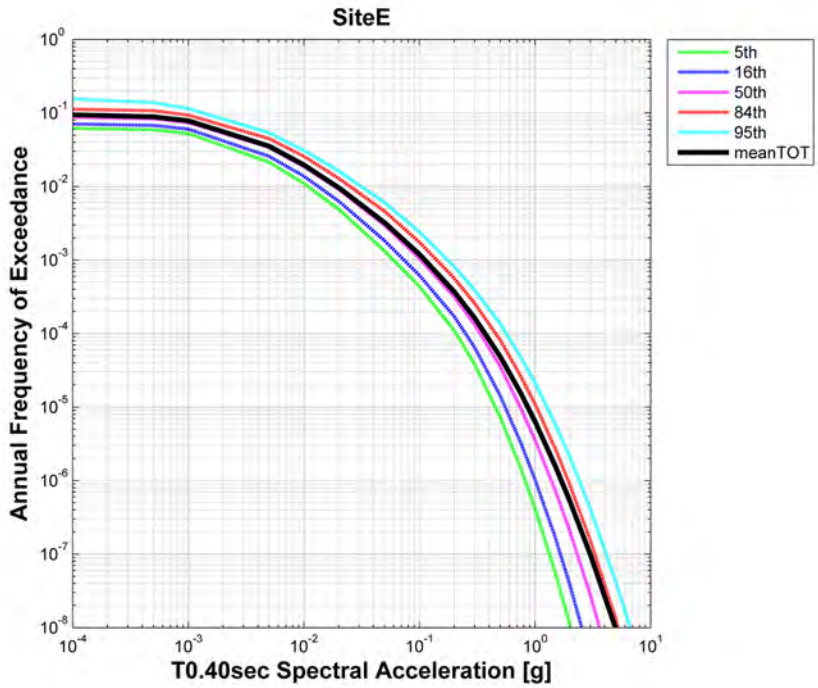

(k)

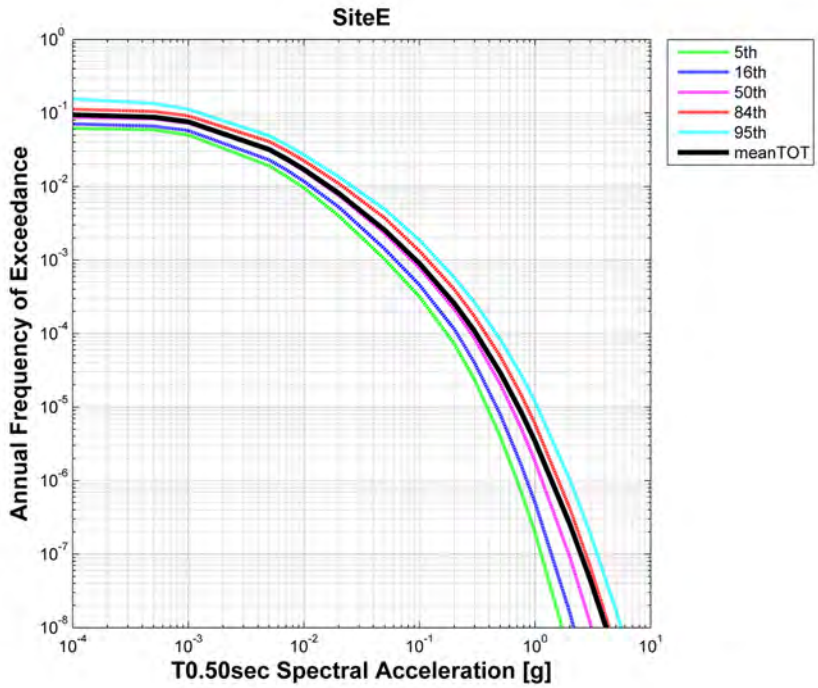

(l)

Figure 10.79. (contd)

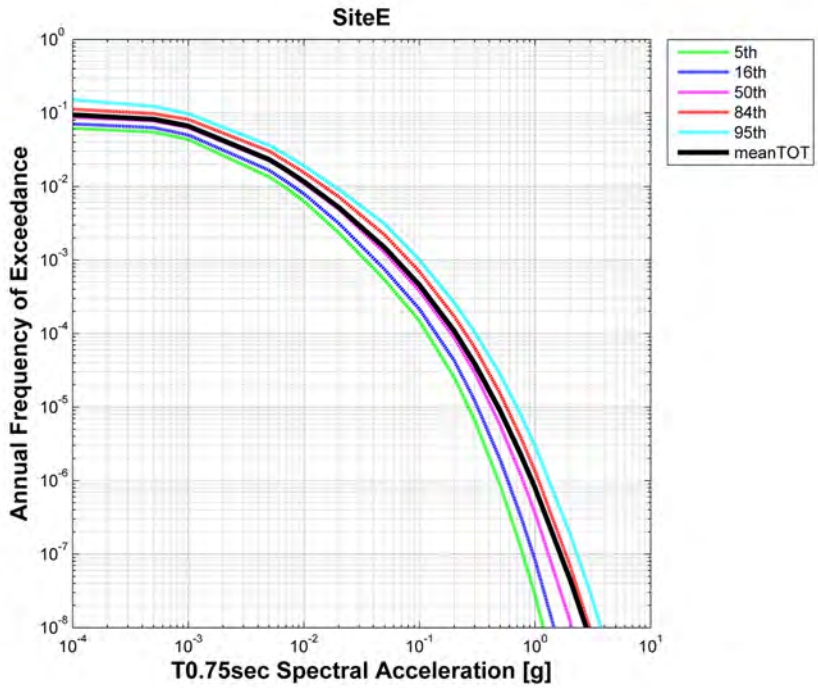

(m)

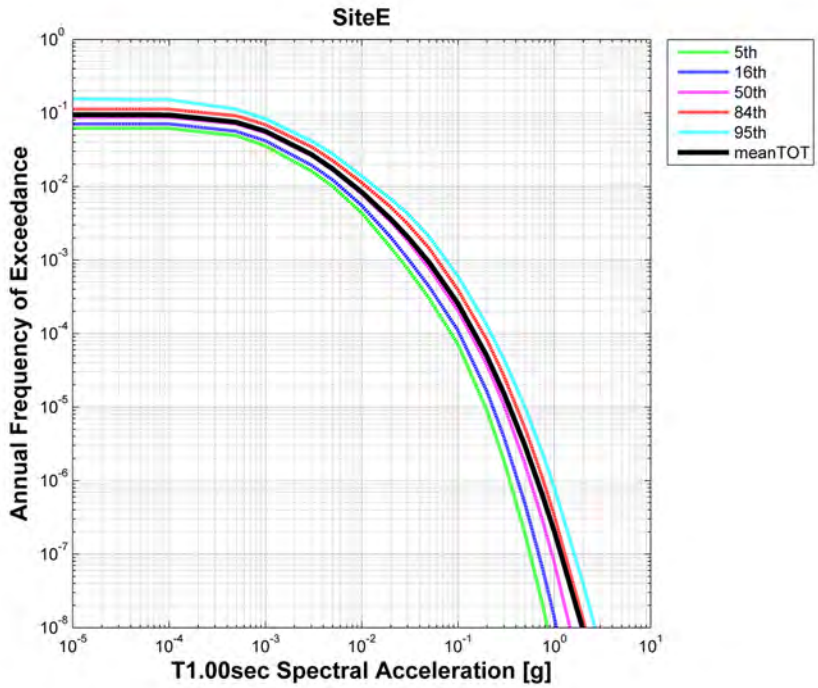

(n)

Figure 10.79. (contd)

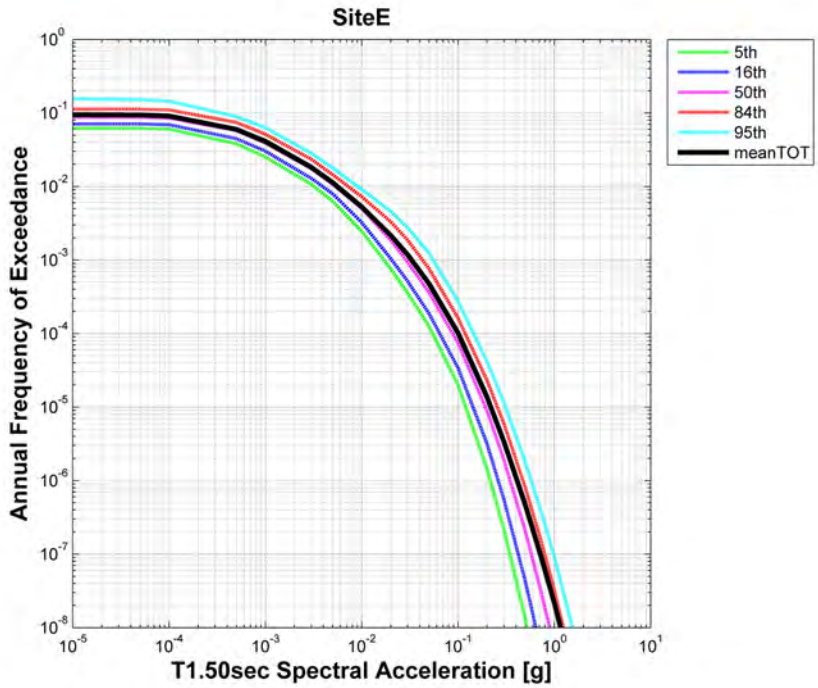

(o)

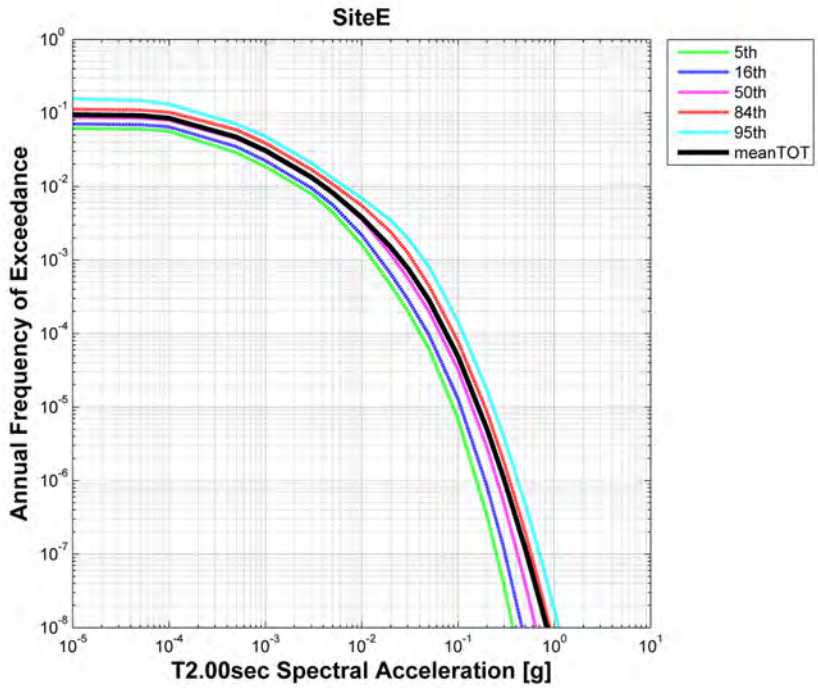

(p)

Figure 10.79. (contd)

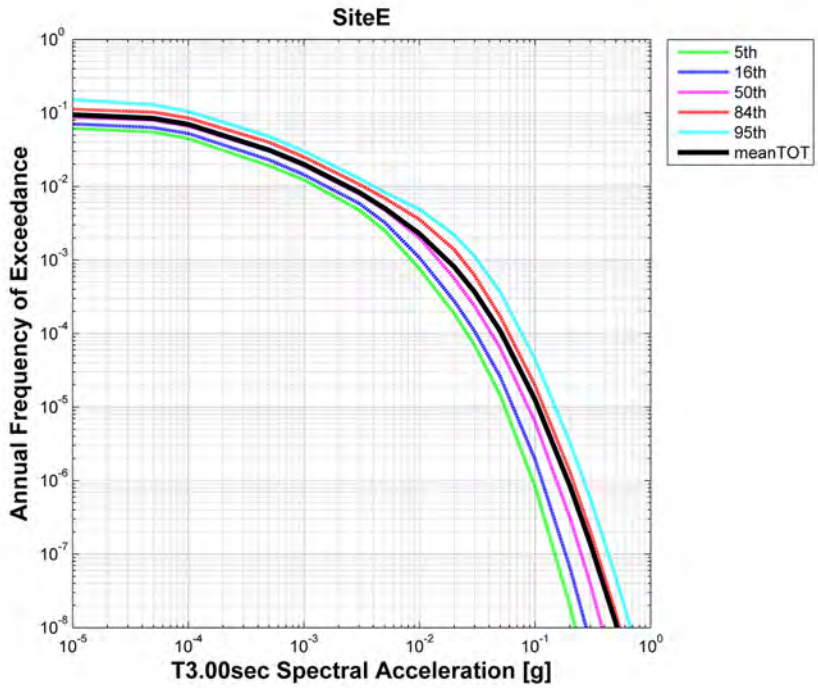

(q)

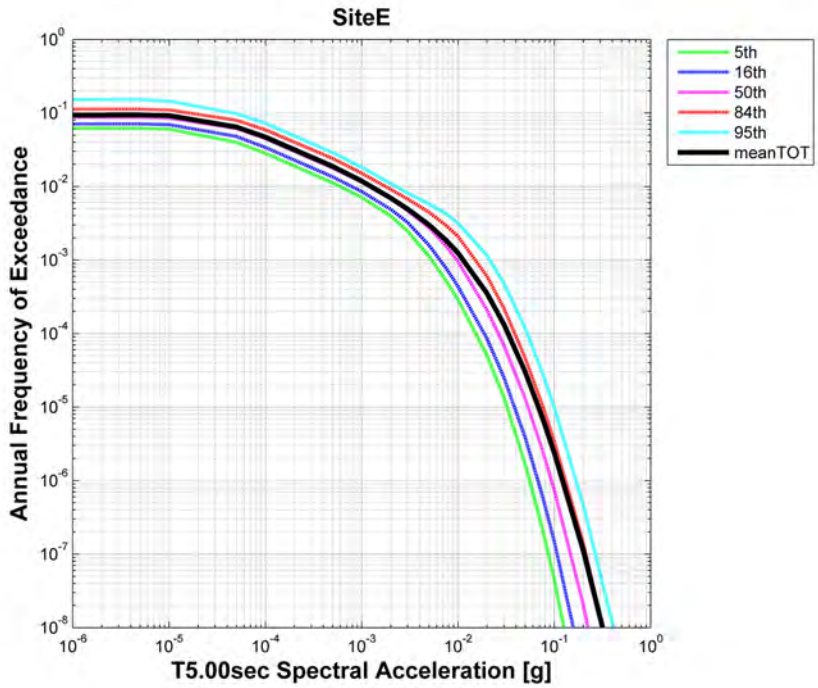

(r)

Figure 10.79. (contd)

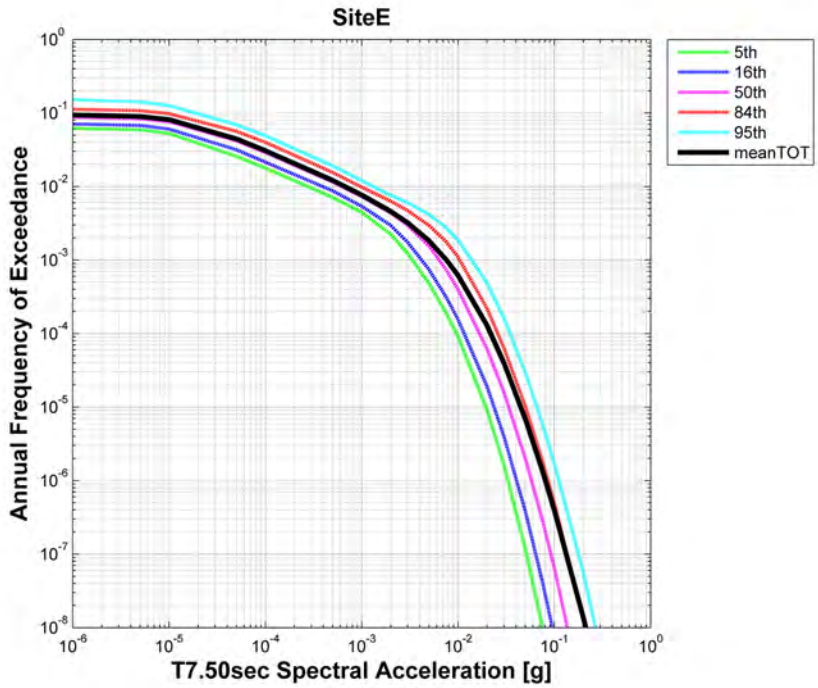

(s)

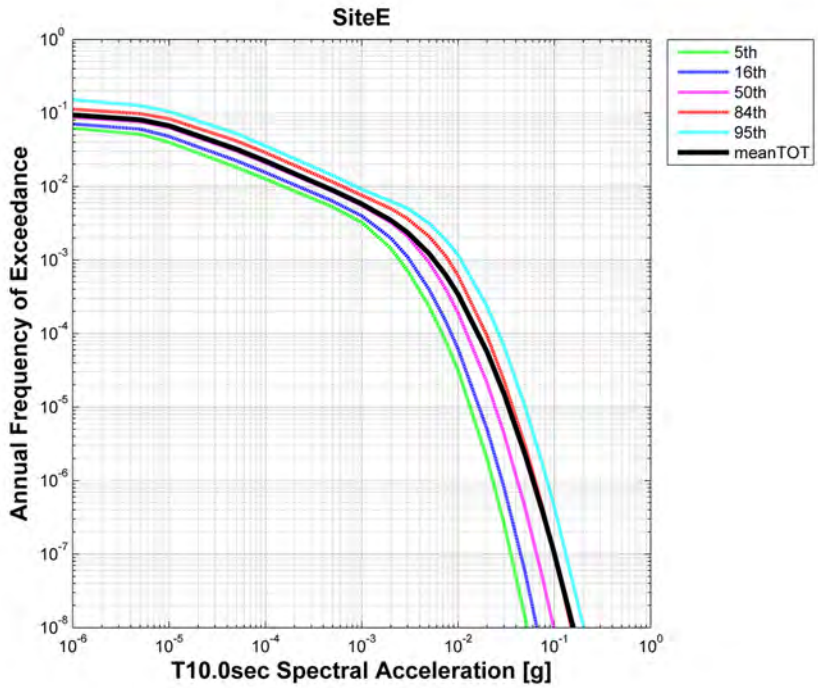

(t)

Figure 10.79. (contd)

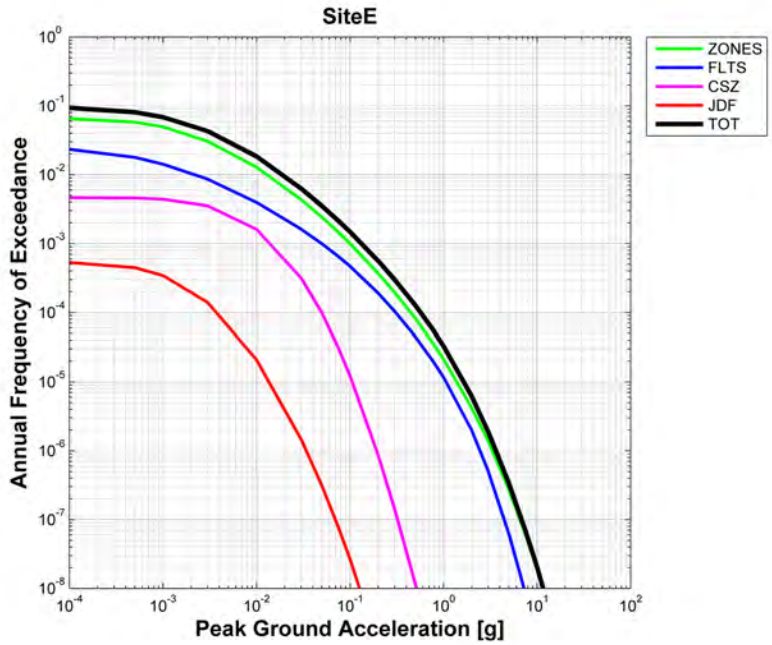

(a)

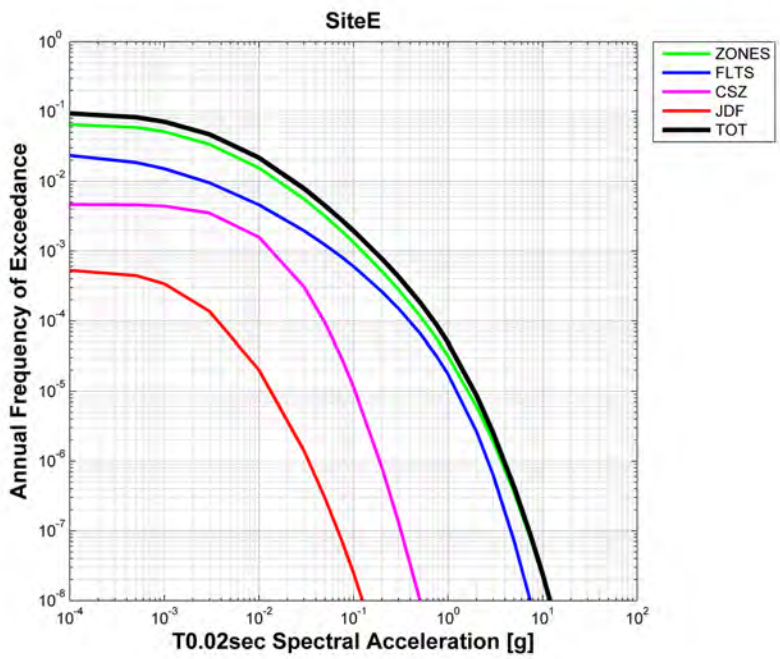

(b)

Figure 10.80. Comparison between the total mean seismic hazard at Site E (black curve) and the contribution of crustal source zones (green curve), faults (blue curve), the Cascadia interface (CSZ - magenta curve), and Cascadia intraslab source (JDF - red curve): a) PGA; b) T 0.02-sec; c) T 0.03-sec; d) T 0.04-sec; e) T 0.05-sec; f) T 0.07-sec; g) T 0.10-sec; h) T 0.15-sec; i) T 0.20-sec; j) T 0.30-sec; k) T 0.40-sec; l) T 0.50-sec; m) T 0.75-sec; n) T 1.0-sec; o) T 1.5-sec; p) T 2.0-sec; q) T 3.0-sec; r) T 5.0-sec; s) T 7.5-sec; t) T 10-sec spectral acceleration.

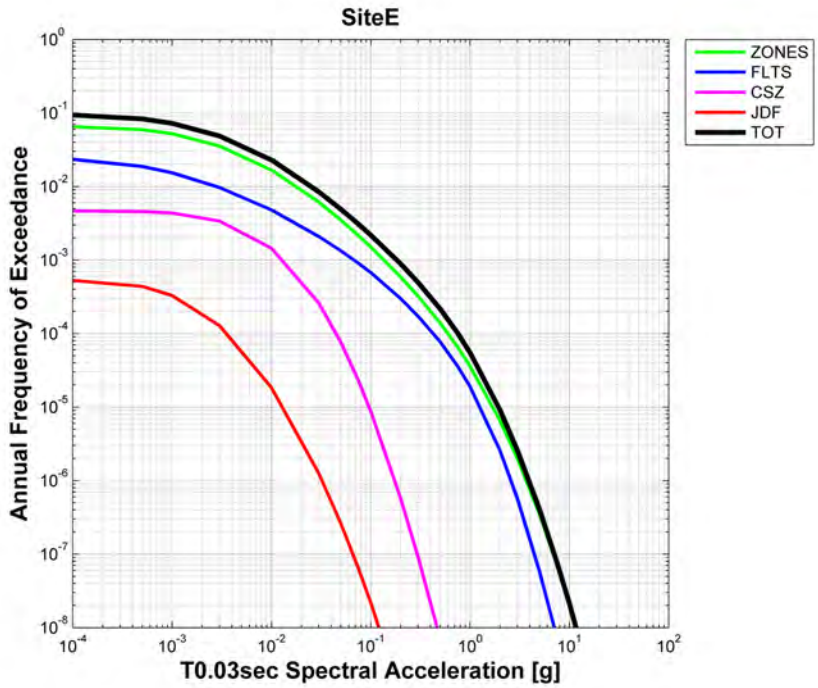

(c)

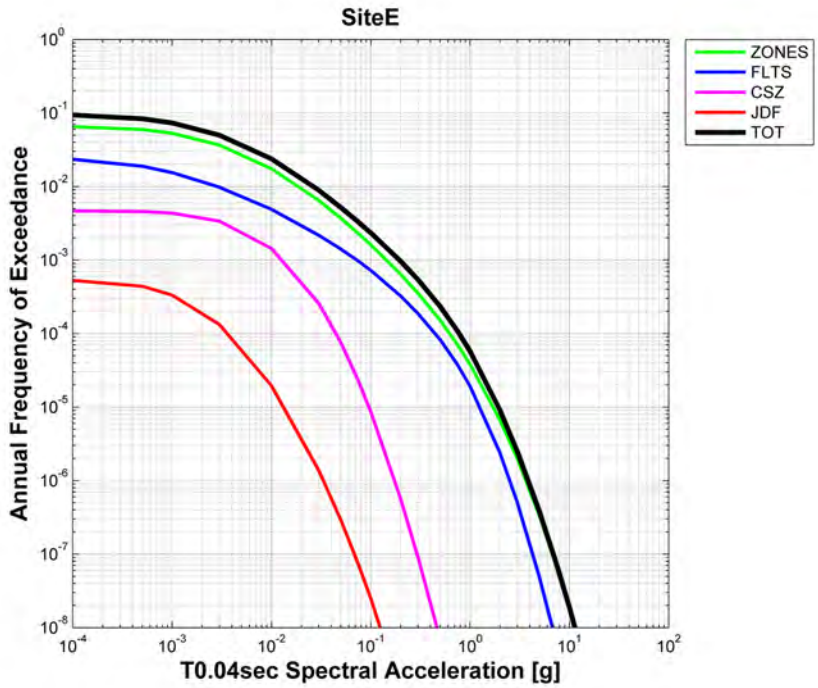

(d)

Figure 10.80. (contd)

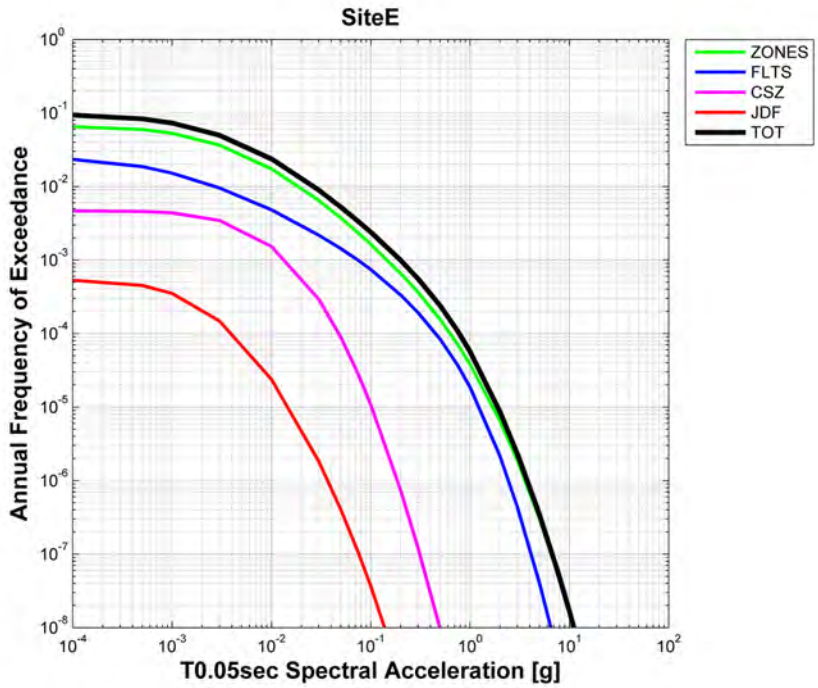

(e)

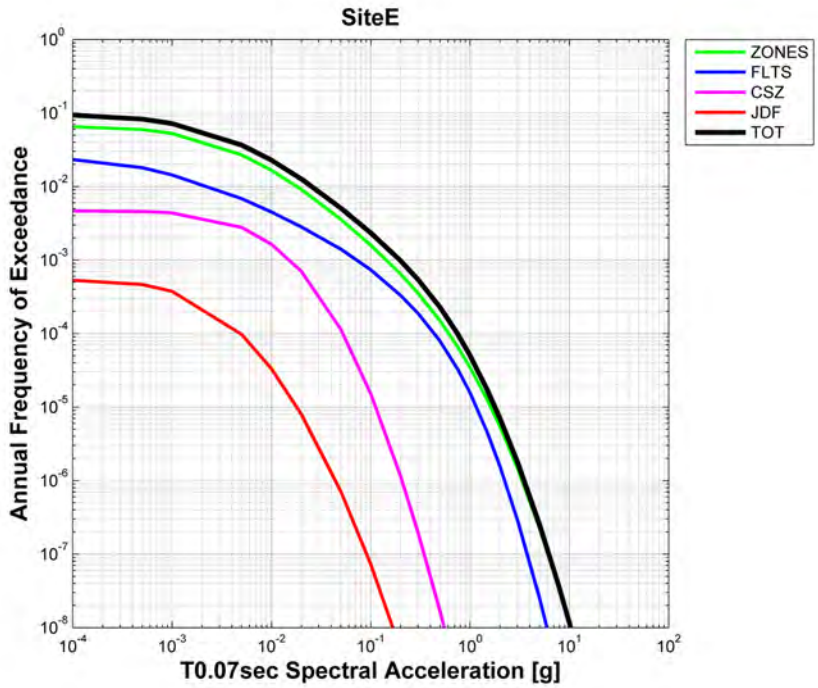

(f)

Figure 10.80. (contd)

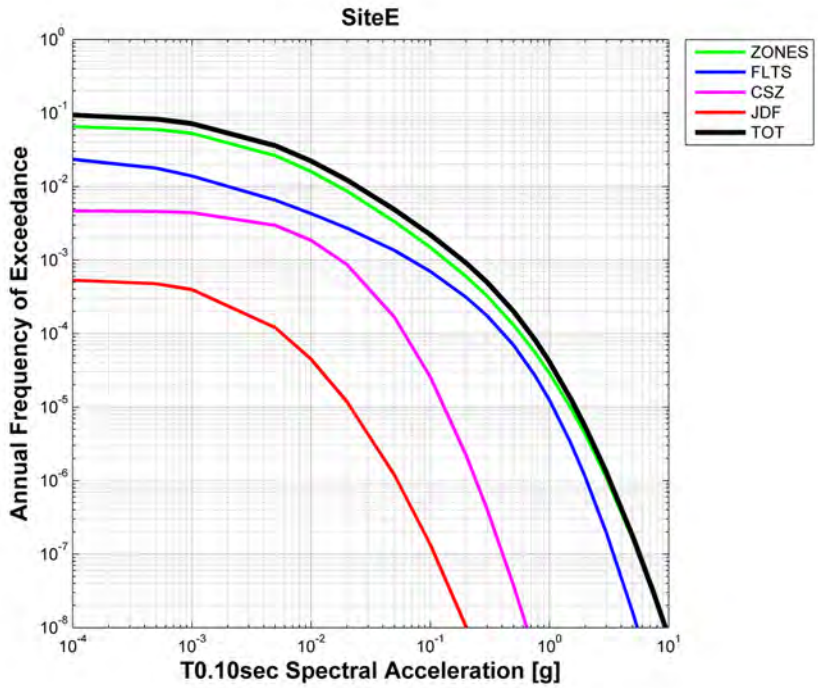

(g)

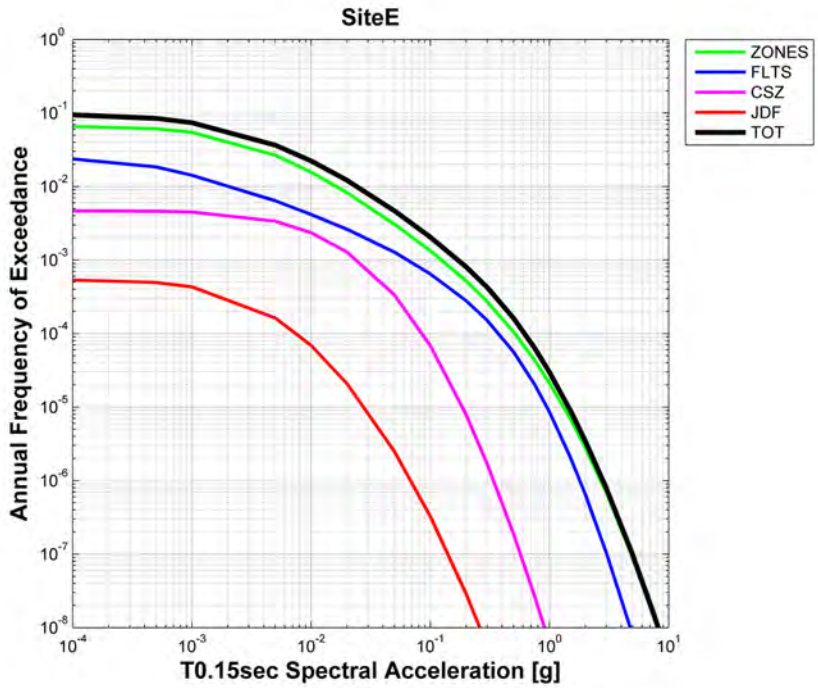

(h)

Figure 10.80. (contd)

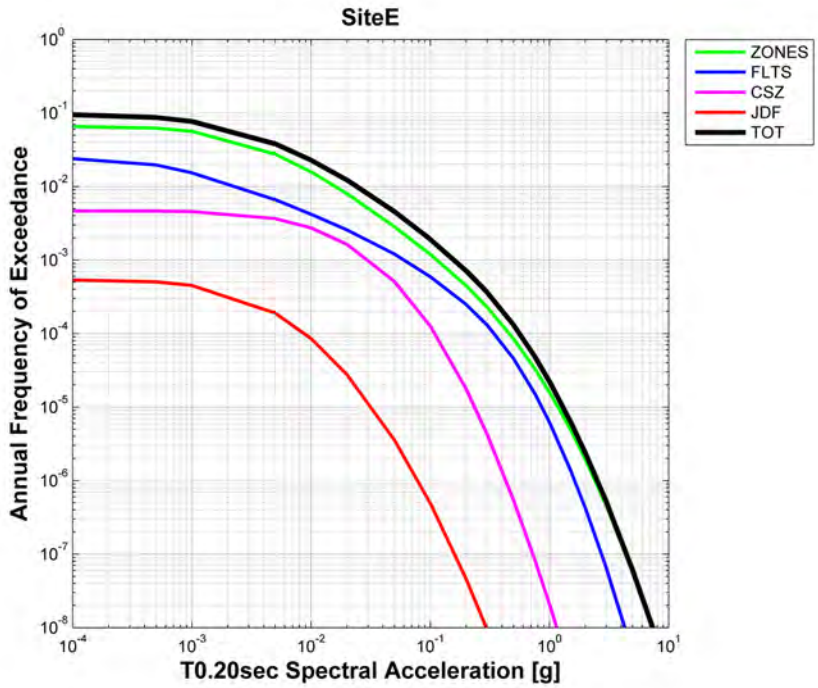

(i)

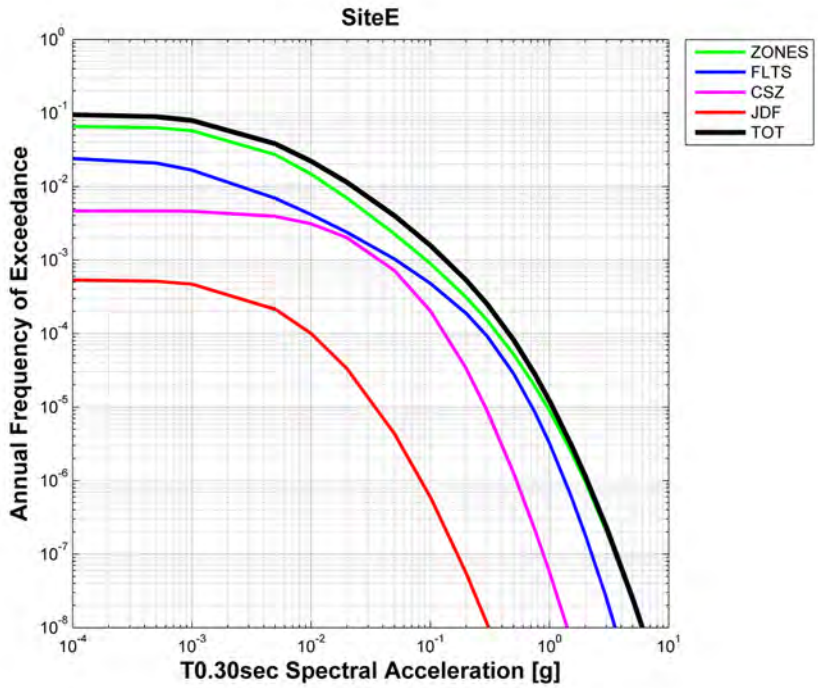

(j)

Figure 10.80. (contd)

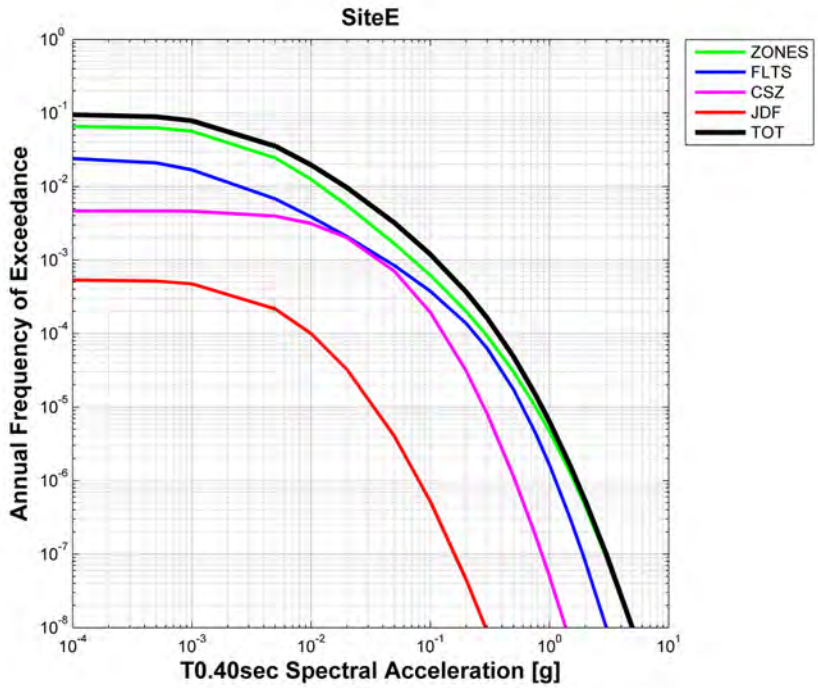

(k)

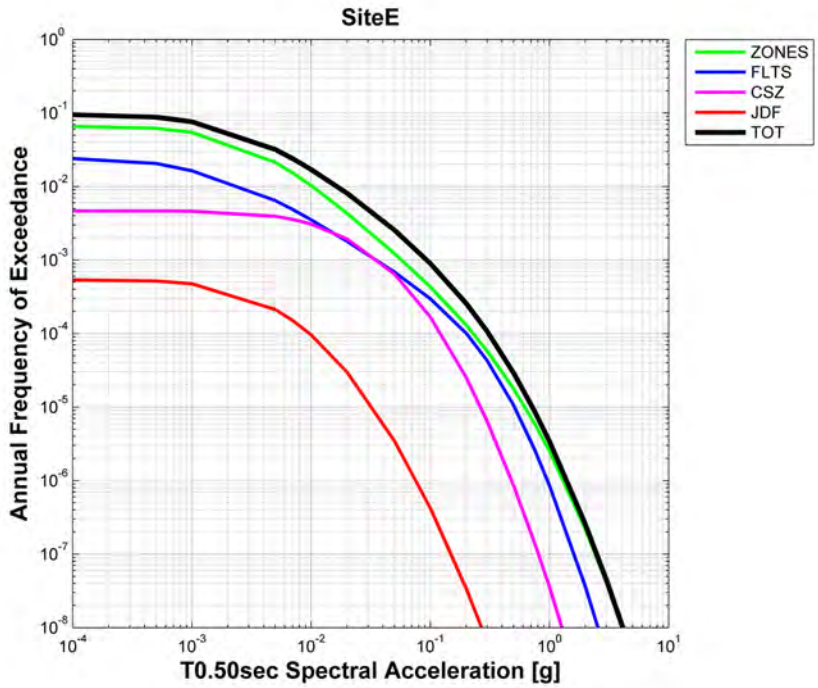

(l)

Figure 10.80. (contd)

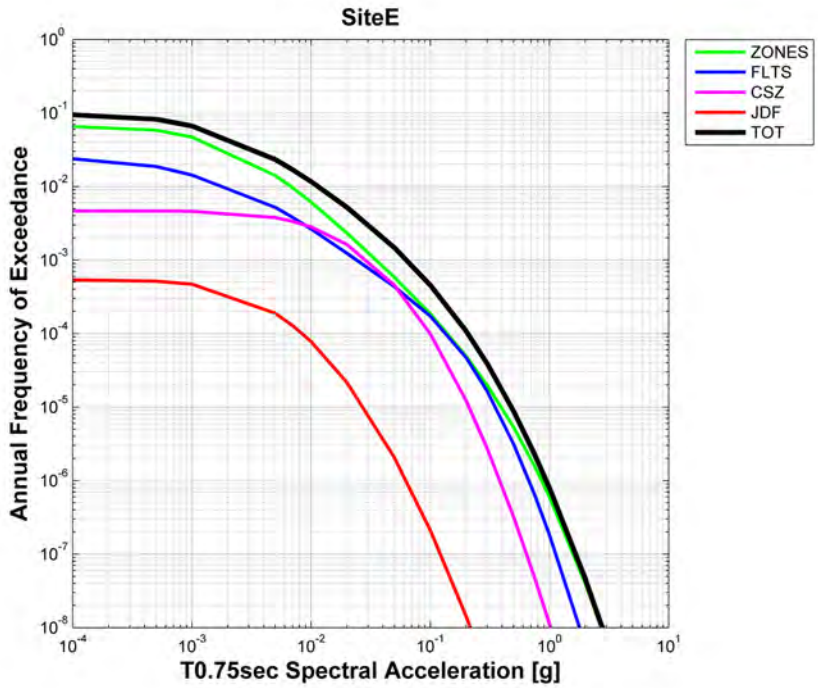

(m)

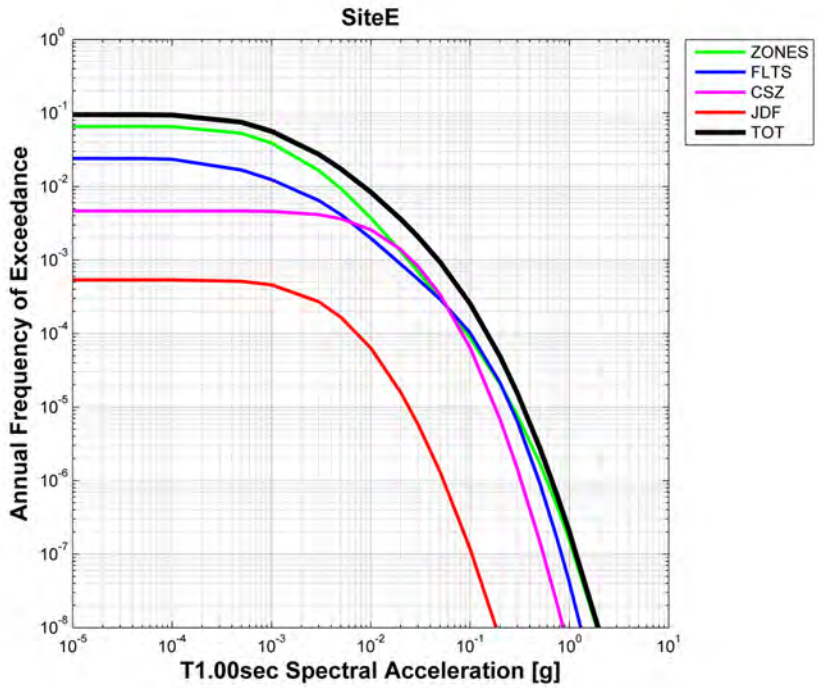

(n)

Figure 10.80. (contd)

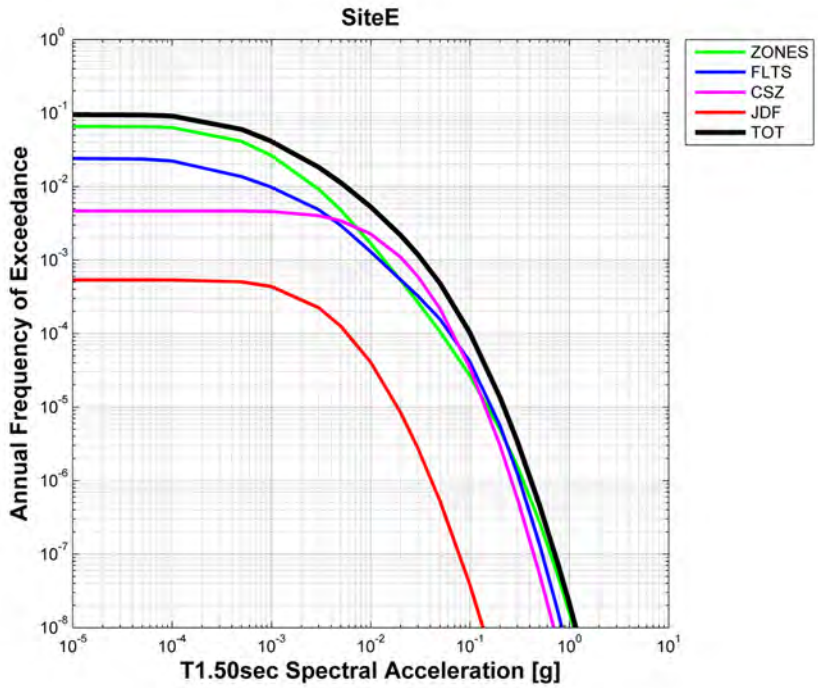

(o)

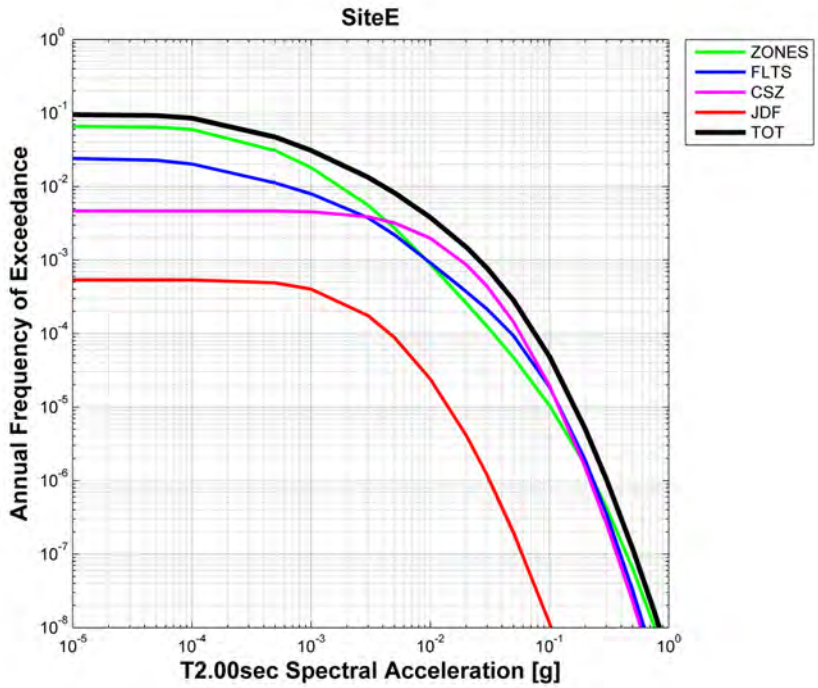

(p)

Figure 10.80. (contd)

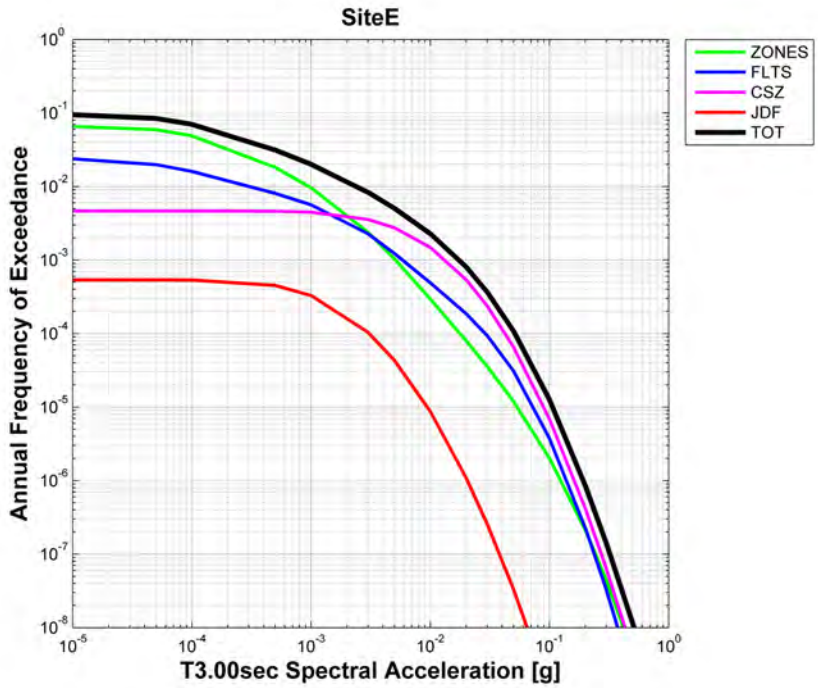

(q)

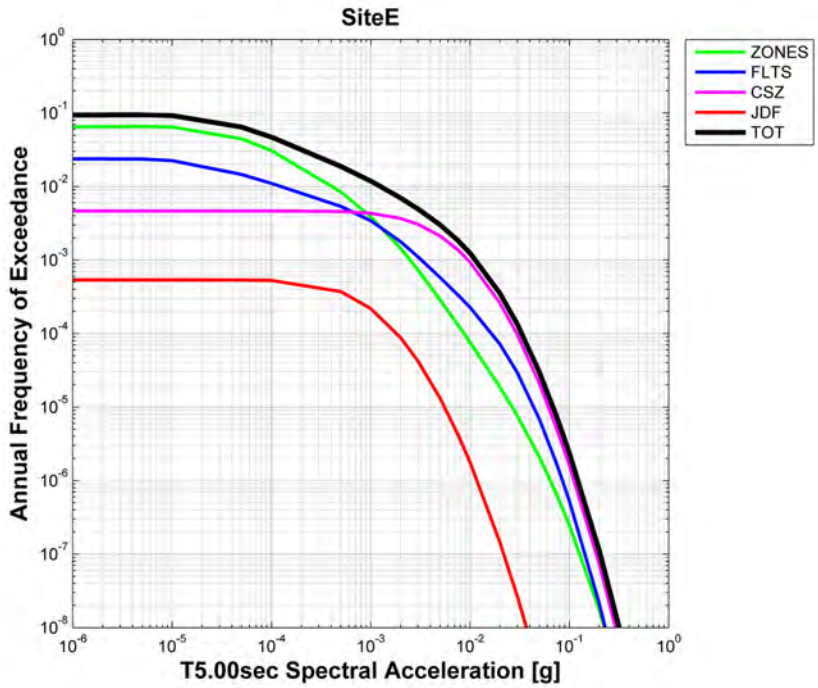

(r)

Figure 10.80. (contd)

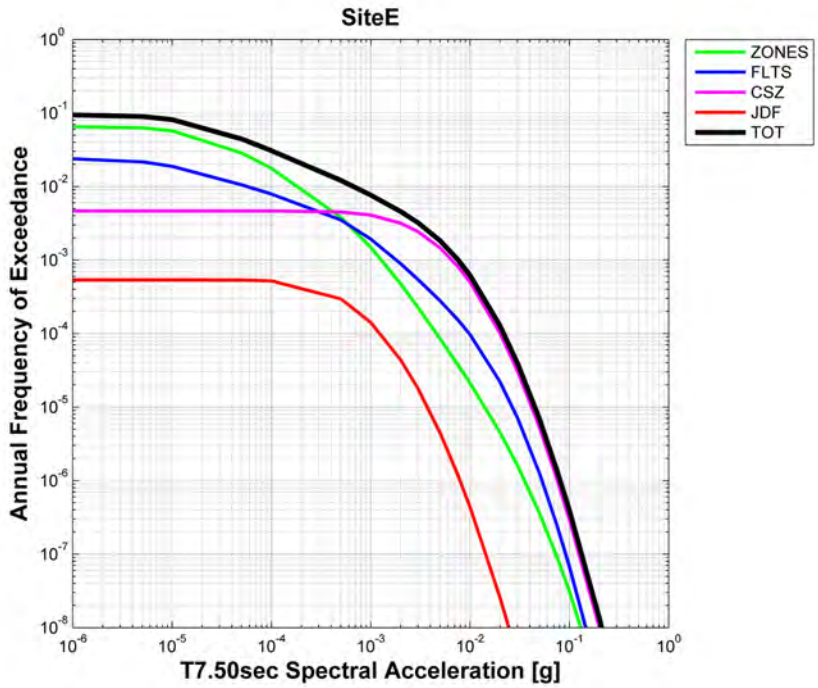

(s)

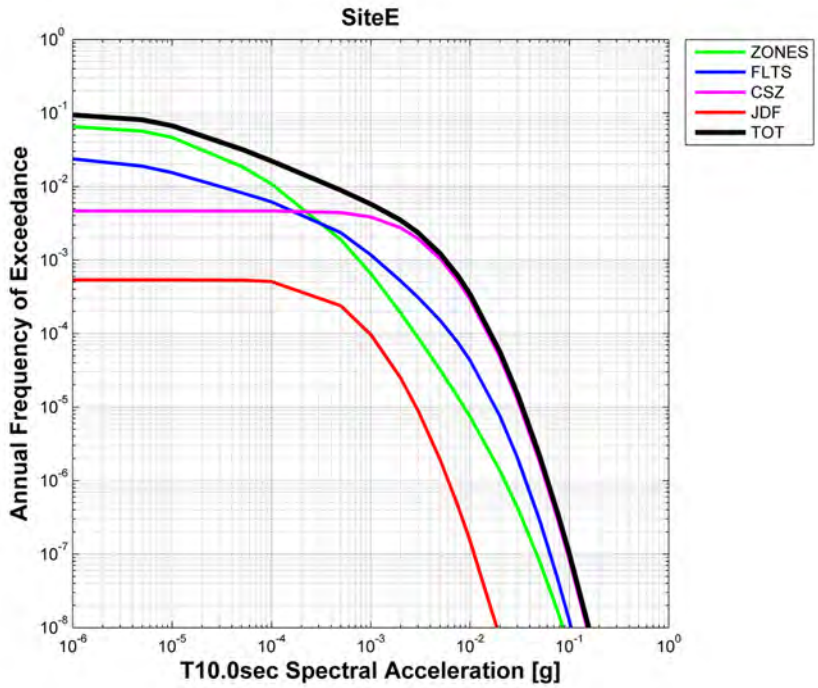

(t)

Figure 10.80. (contd)

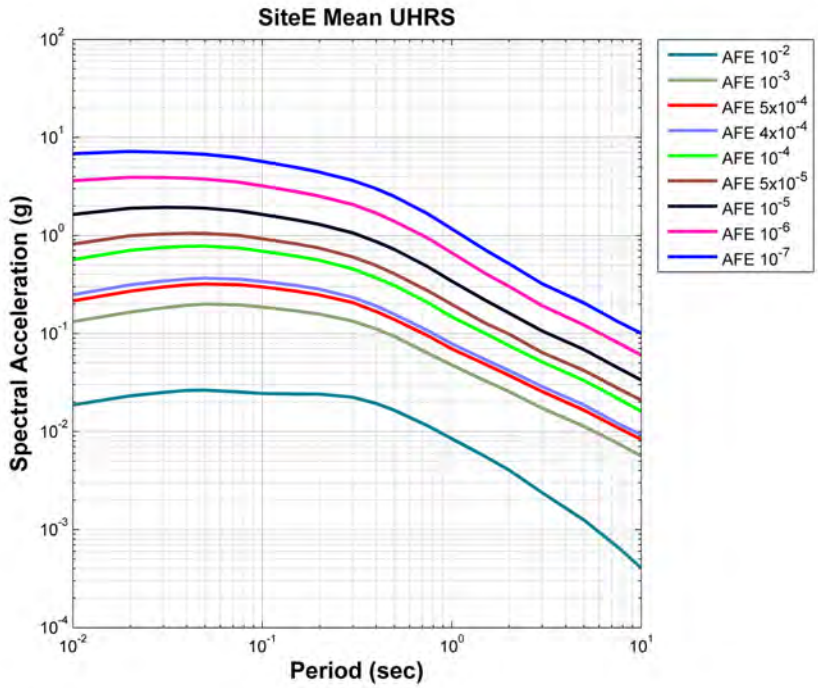

(a)

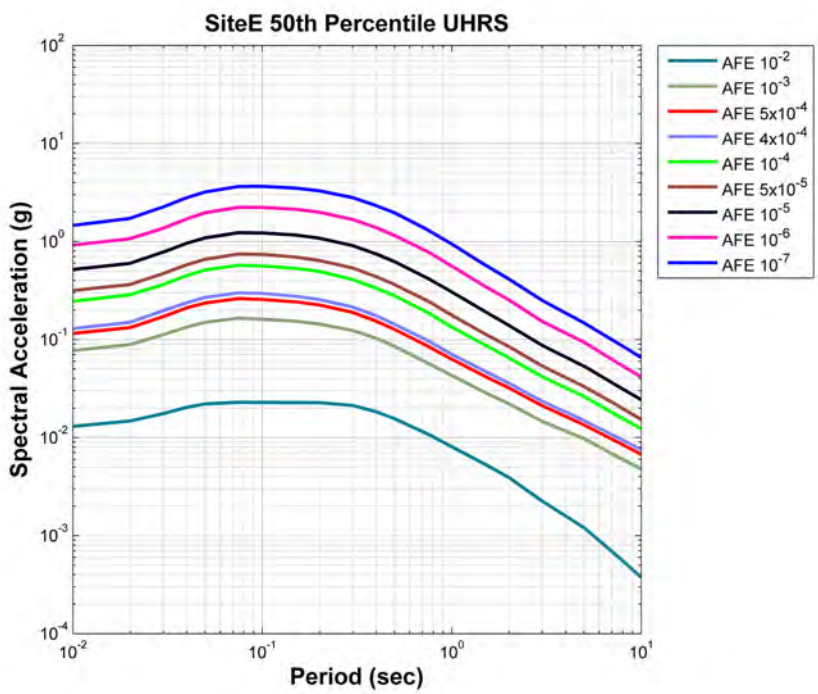

(b)

Figure 10.81. Uniform hazard response spectra at AFEs of 10^{-2}, 10^{-3}, 5×10^{-4}, 4×10^{-4}, 10^{-4}, 5×10^{-5}, 10^{-6}, 10^{-7} (return periods of 100, 1,000, 2,000, 2,500, 10,000, 20,000, 100,000, 1 million, and 10 million years) for: a) mean hazard; b) 50th percentile hazard; c) 84th percentile hazard.

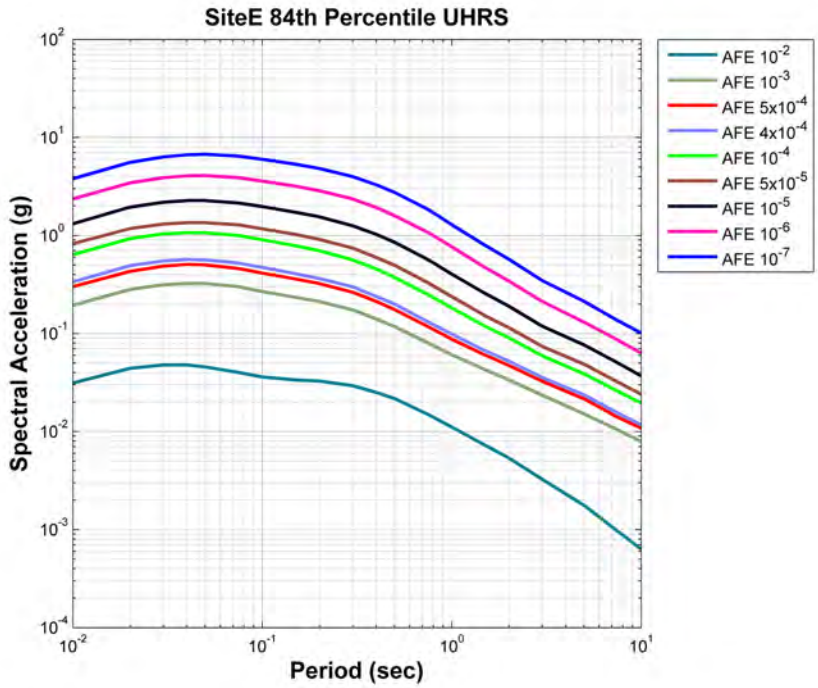

(c)

Figure 10.81. (contd)

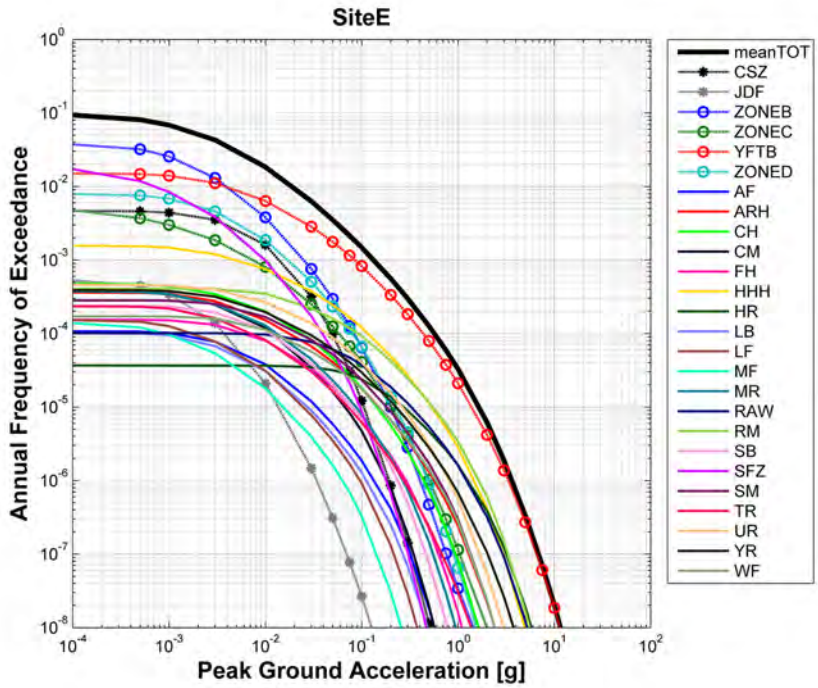

(a)

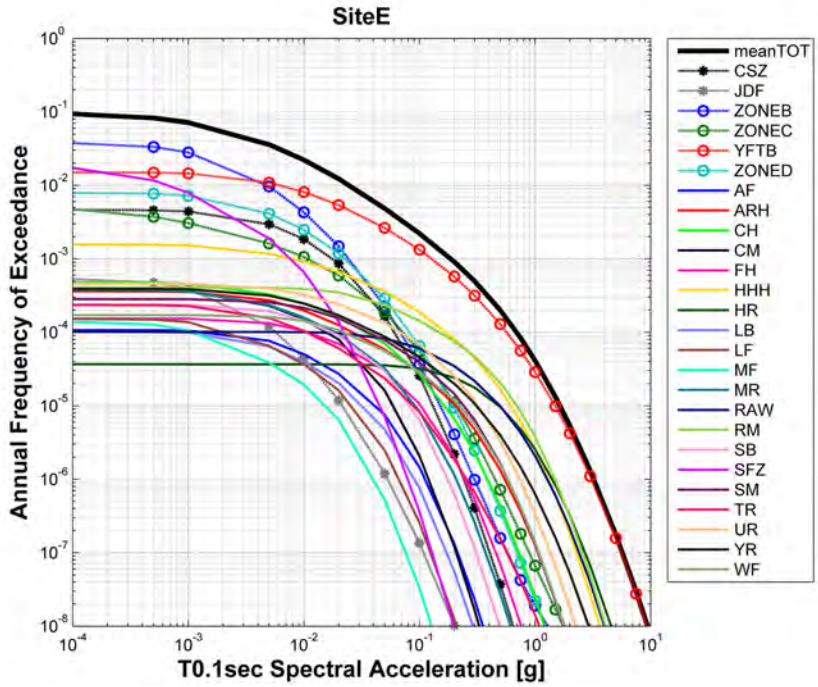

(b)

Figure 10.82. Comparison between the mean hazard curves at Site E obtained for each individual source. Subduction sources are shown by dotted star curves; crustal sources by dotted circle curves; and fault sources by solid curves: a) peak ground acceleration; b) T 0.1-sec; c) T 1-sec; d) T 10-sec spectral acceleration. Acronyms used in figures are listed in Table 10.13.

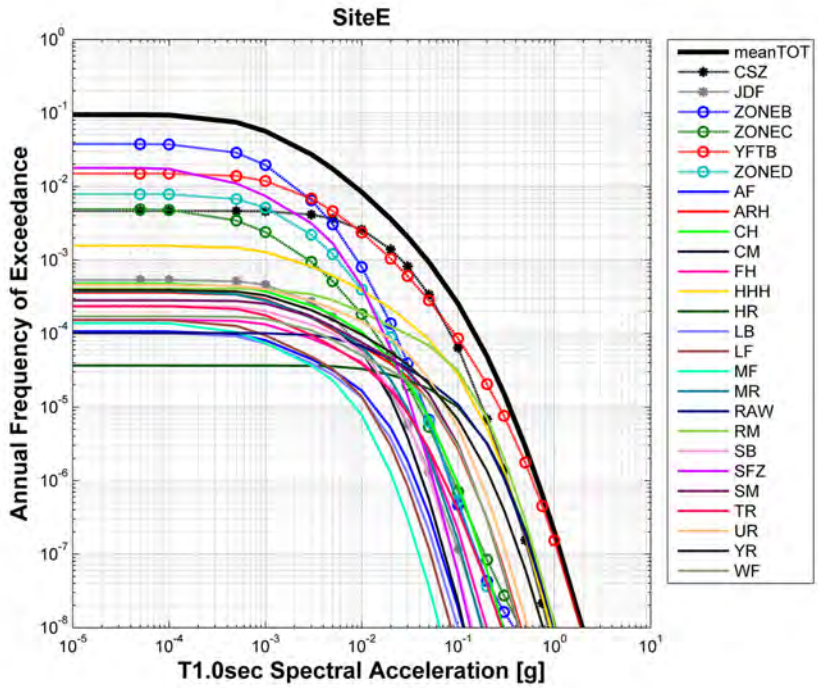

(c)

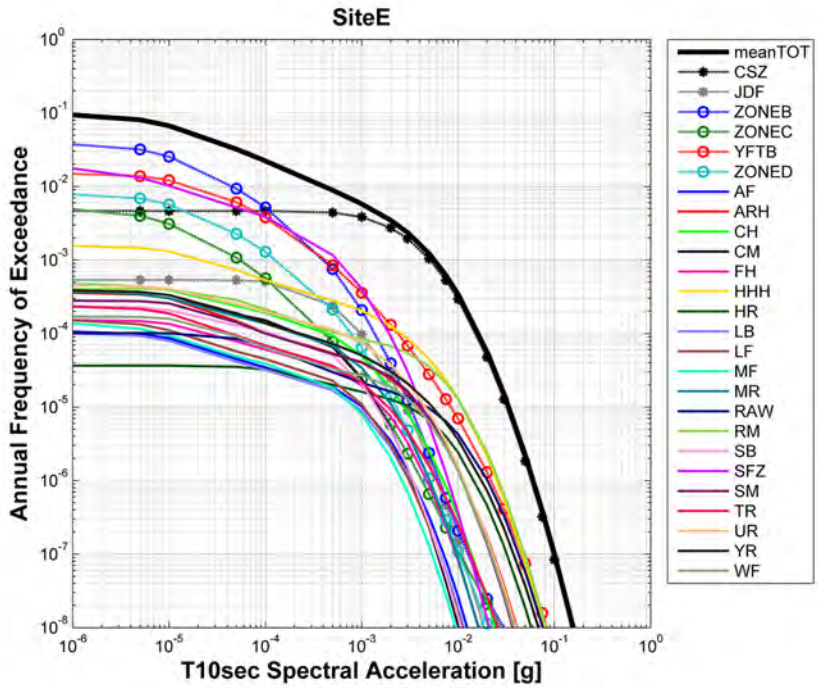

(d)

Figure 10.82. (contd)

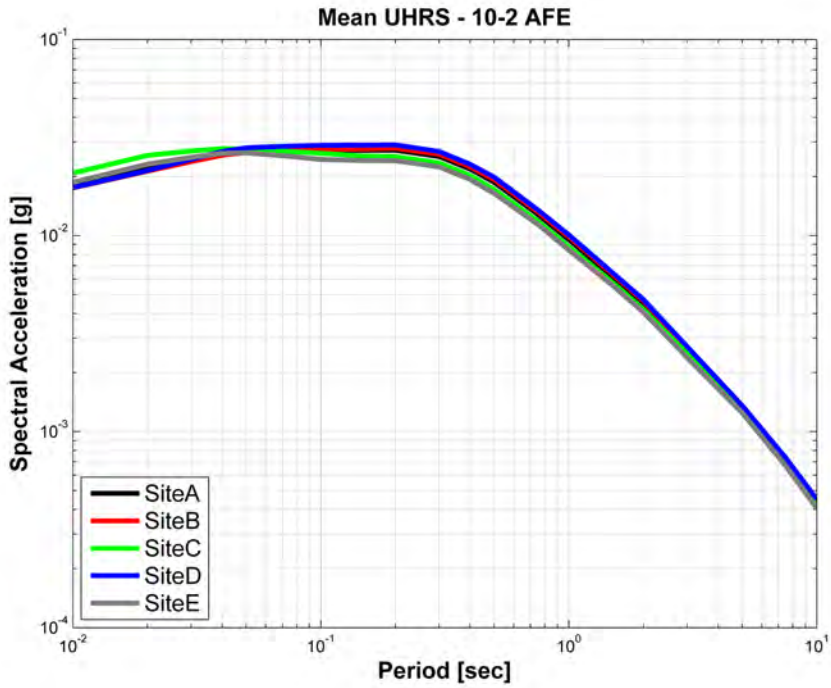

(a)

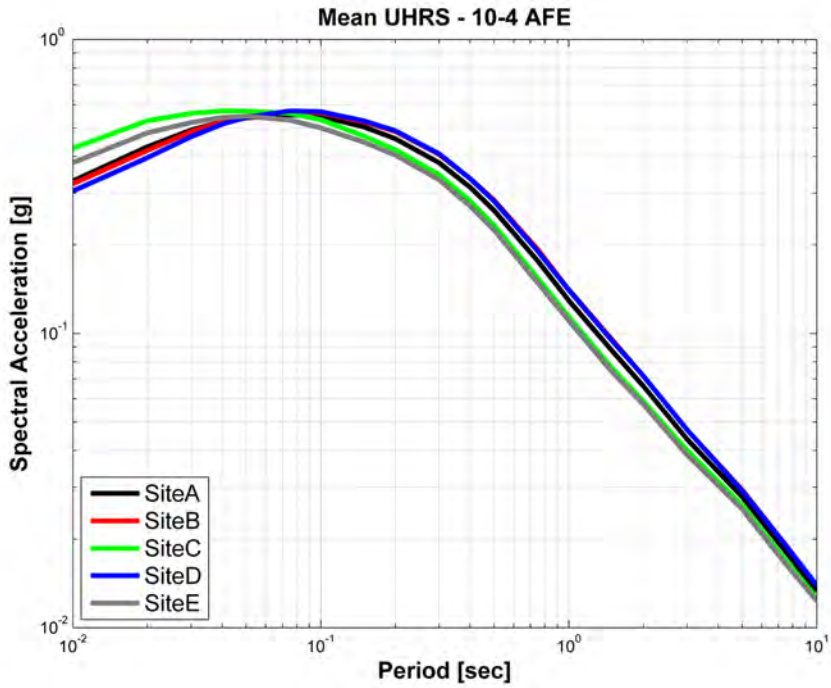

(b)

Figure 10.83. Comparison between the mean UHRS at Sites A, B, C, D, and E: a) 10^{-2} AFE; b) 10^{-4} AFE; c) 10^{-6} AFE.

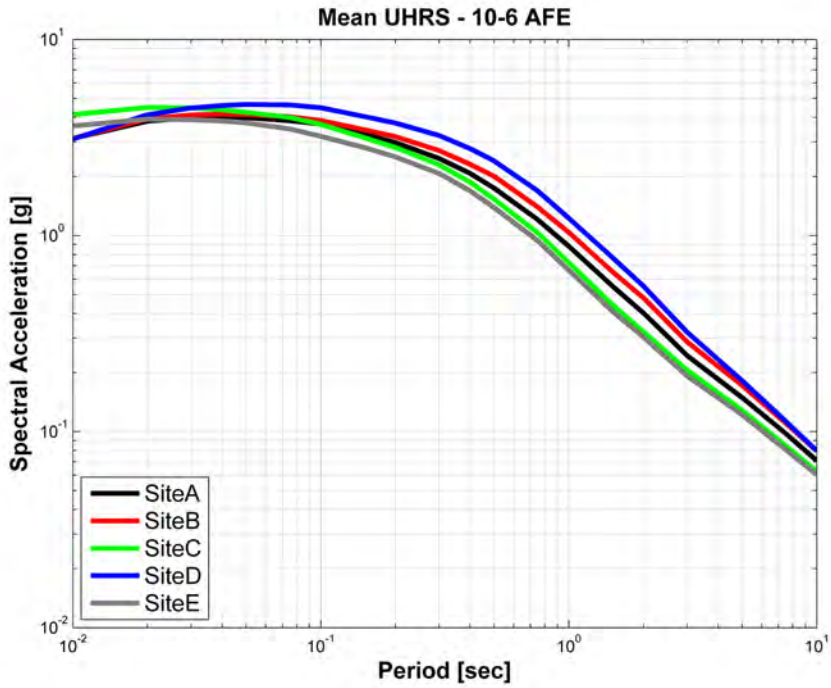

(c)

Figure 10.83. (contd)

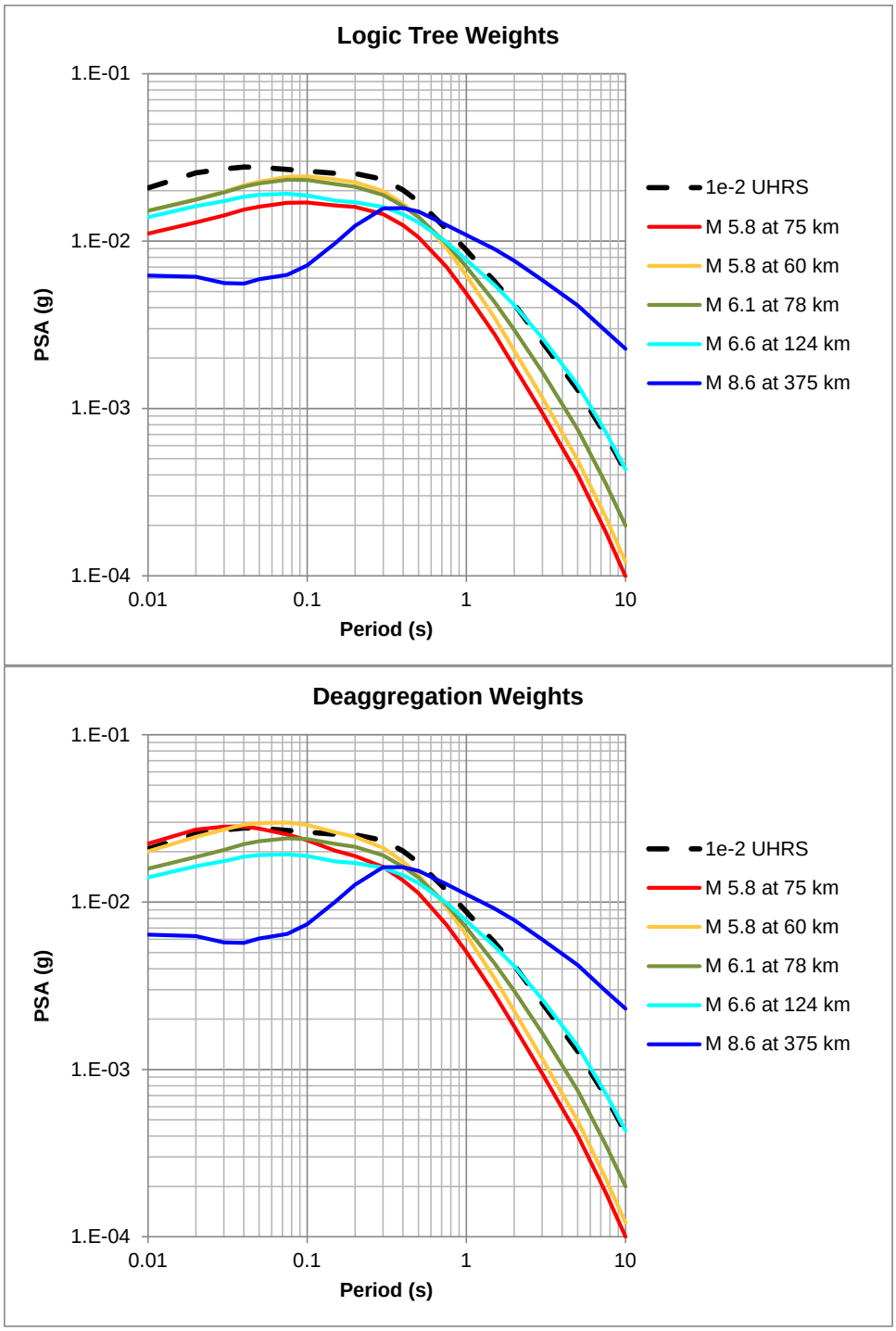

(a)

Figure 10.84. Comparison between the mean UHRS at Site A and weighted median response spectra for scenarios representing the mean magnitude and distance for earthquakes contribution to the hazard at periods of 0.01, 0.1, 1, and 10 s: a) 10^{-2} AFE; b) 10^{-4} AFE; c) 10^{-6} AFE. Weighted median spectra are based on logic-tree weights (top) and deaggregation weights (bottom).

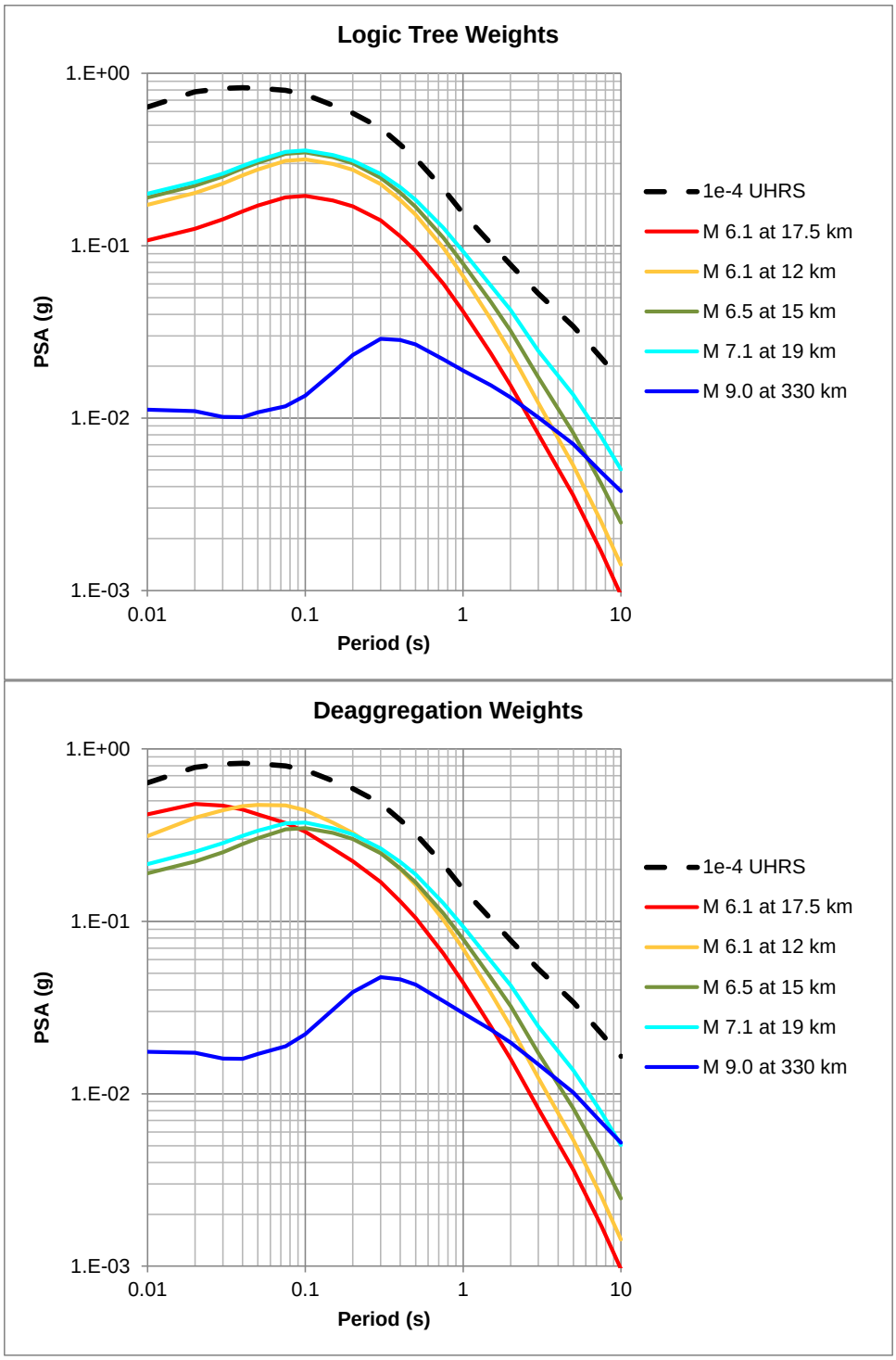

(b)

Figure 10.84. (contd)

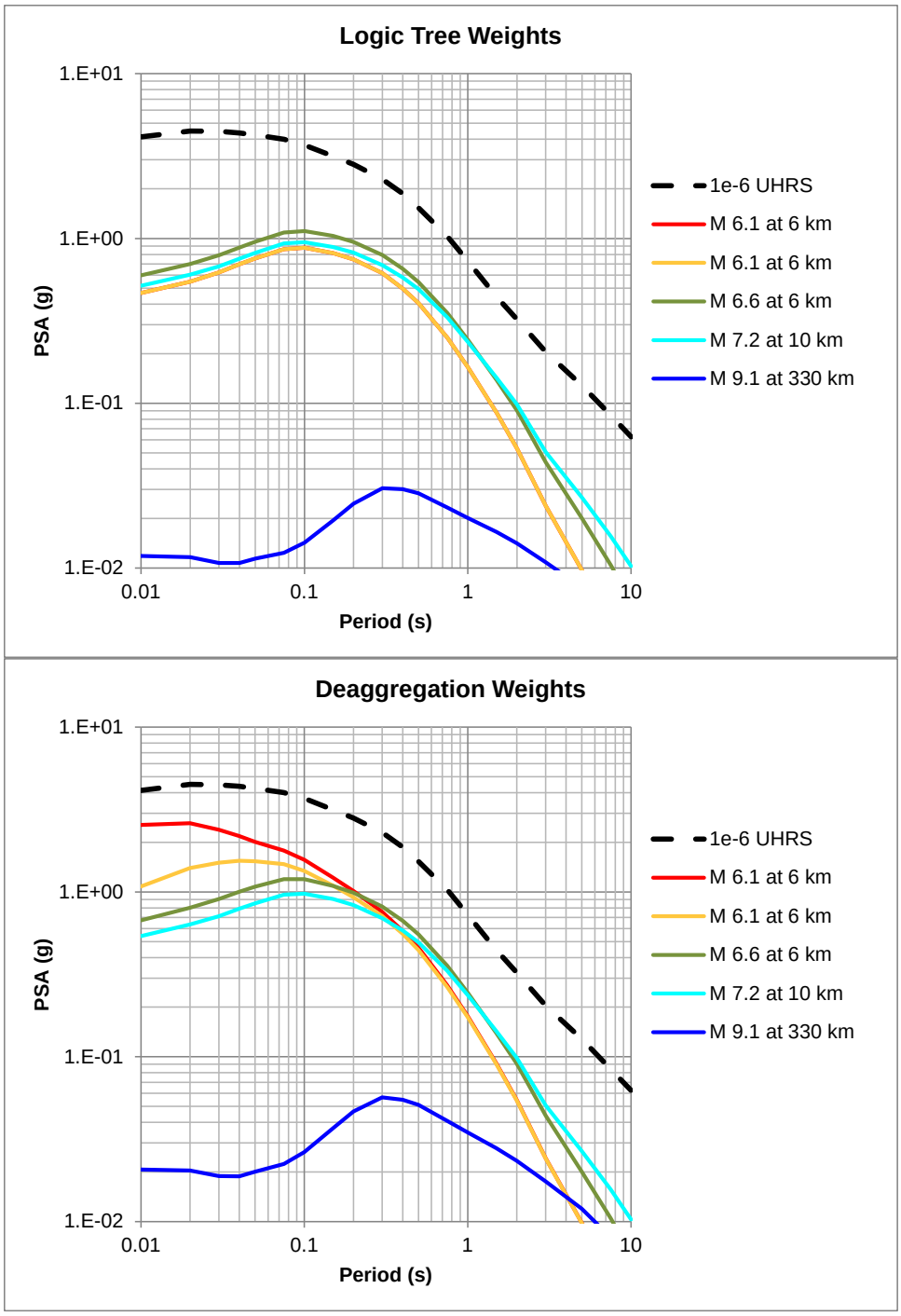

(c)

Figure 10.84. (contd)

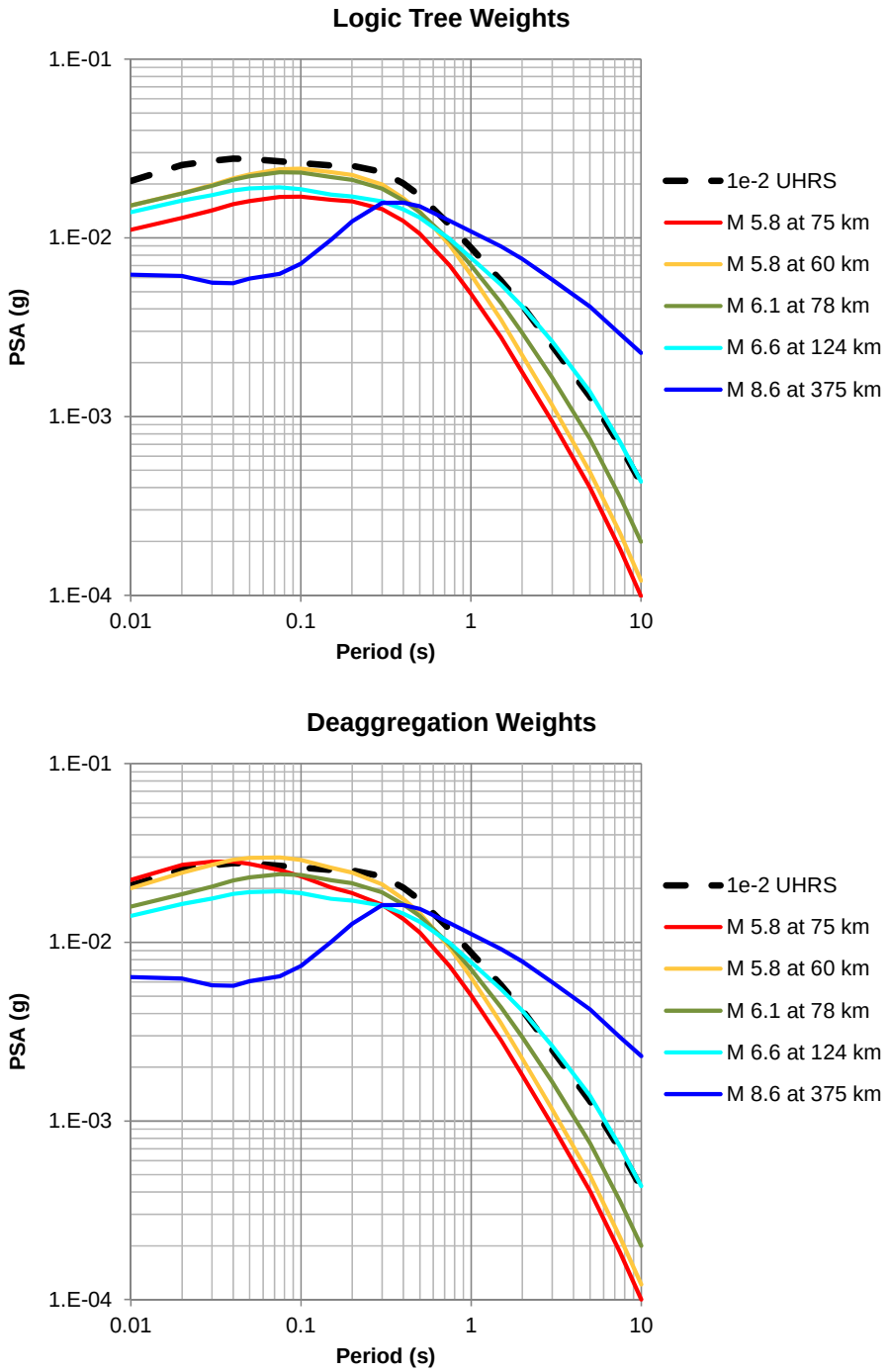

(a)

Figure 10.85. Comparison between the mean UHRS at Site C and weighted median response spectra for scenarios representing the mean magnitude and distance for earthquakes contribution to the hazard at periods of 0.01, 0.1, 1, and 10 s: a) 10^{-2} AFE; b) 10^{-4} AFE; c) 10^{-6} AFE. Weighted median spectra are based on logic-tree weights (top) and deaggregation weights (bottom).

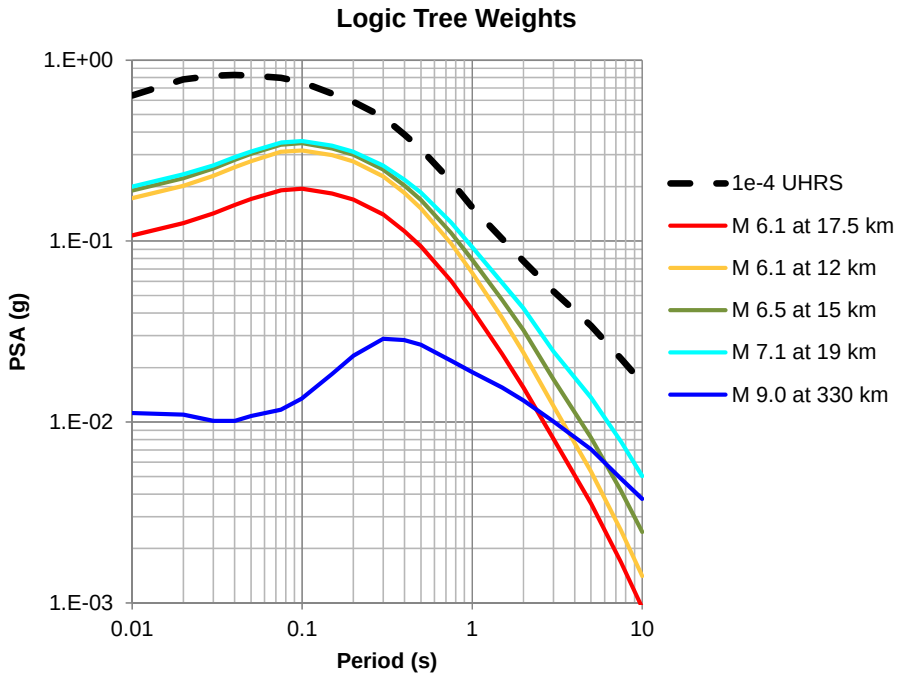

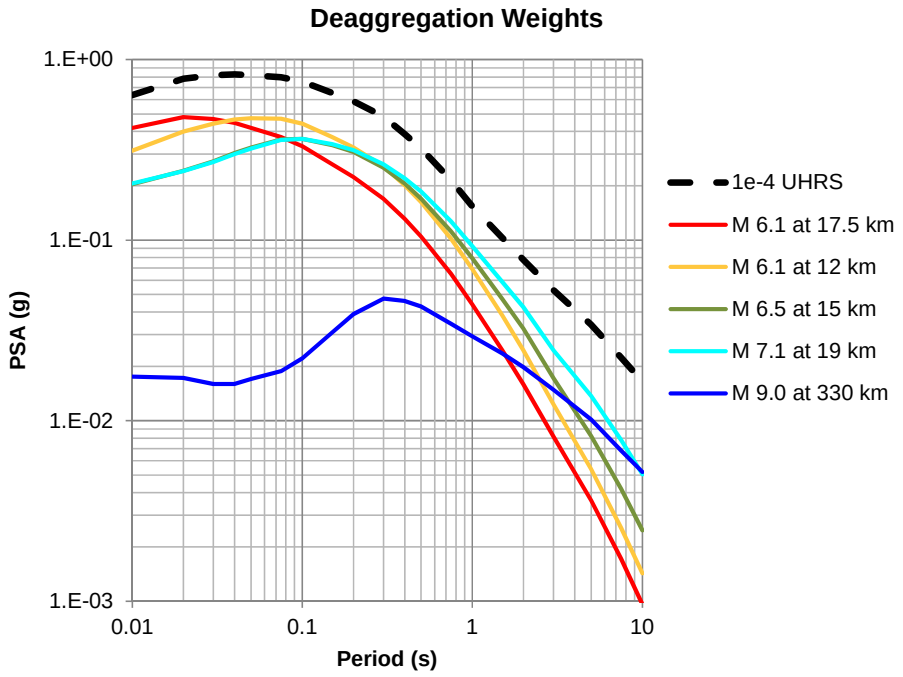

(b)

Figure 10.85. (contd)

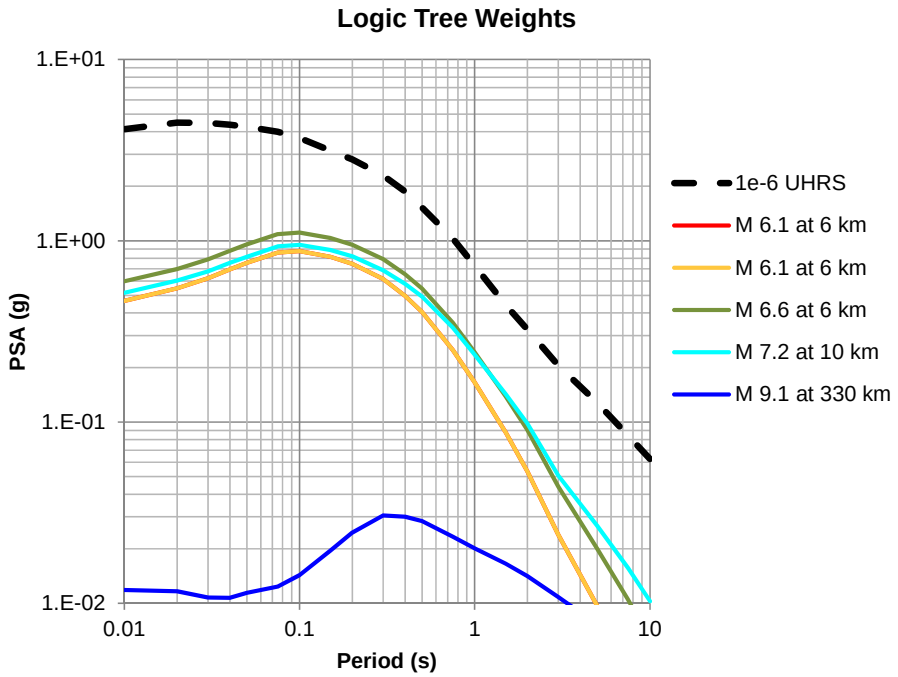

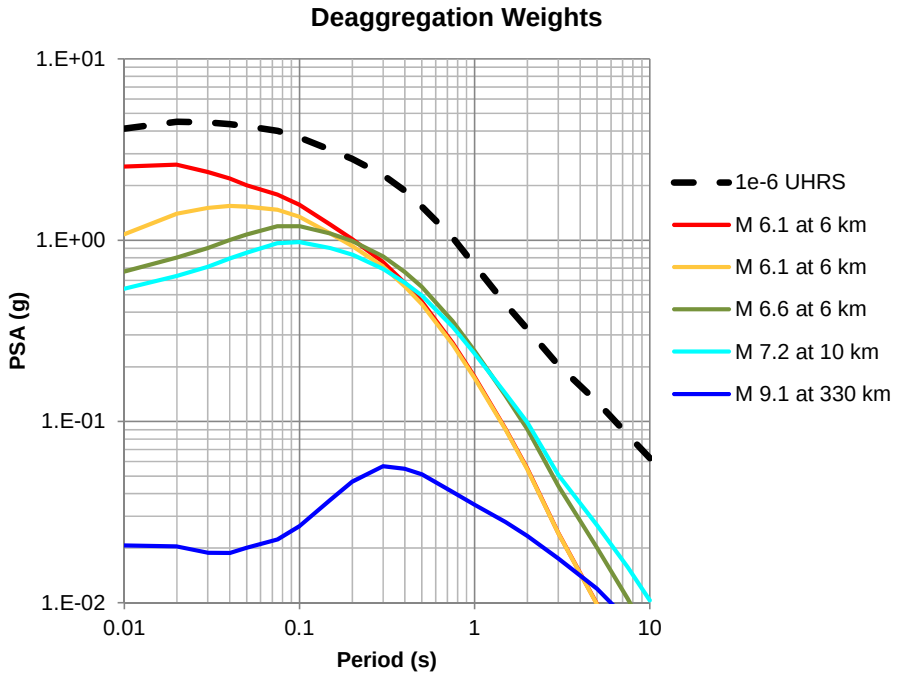

(c)

Figure 10.85. (contd)